STRUCTURALLY REINFORCED CONCRETE PAVEMENTS

AV

ANDERS LOSBERG

teknologie licentiat

AKADEMISK AVHANDLING

SOM MED TILLSTÅND AV CHALMERS TEKNISKA HÖGSKOLA FÖR TEKNOLOGIE DOKTORSGRADS VINNANDE TILL OFFENTLIG GRANSKNING FRAMLÄGGES Å FÖRELÄSNINGS-SALEN FÖR FYSIK, GIBRALTARGATAN 5 B, GÖTEBORG, LÖRDAGEN DEN 28 JANUARI 1961 KL. 10

GÖTEBORG

ELANDERS BOKTRYCKERI AKTIEBOLAG

1960

Contents

Preface

This thesis is the result of an investigation begun in 1945. The problem treated here was actualized this year by the Stockholm Airport Building Committee in connection with the planning of a new airport for the heavy Atlantic traffic at Väsby, north of Stockholm, where the soil conditions were extremely bad. In order to solve the problem of designing a pavement with sufficient bearing capacity in this case, Professor HJALMAR GRANHOLM submitted the idea that the pavement should be designed as a structurally reinforced concrete slab. In my capacity at that time as Research Assistant in Professor Granholm's Department of Structural Engineering at Chalmers University of Technology I was commissioned to take care of an investigation concerning this pavement structure.

I am conscious of the fact that a great deal of time has passed before the result of the investigation has been published, and the publication now presented may have become too comprehensive. During the course of time, however, a great deal of complementary investigation work has been added. It would perhaps have been better to publish the results by degrees, but various requirements and circumstances have made it impossible for me to have enough time for more than preliminary stencilled reports or short summarizing review articles covering part of the investigation work. But when, thanks to the good offices of Professor Granholm, I was provided with the opportunity of spending one year of undisturbed work in the Dept. of Structural Engineering, I took advantage of this possibility to treat all the test material and include it in the publication at the same time as I tried to present the results in a form that would be suitable for practical use in designing work.

Looking back over the long period of work spent on this task, my first feelings of gratitude go to my teacher and former chief, Professor HJALMAR GRANHOLM, *D. Eng.* With never-failing interest he has followed the progress of the investigation, educating me in the methods of research work during planning and discussion of all the theoretical and experimental aspects of the investigation. This work would doubtless never have been fulfilled without his help and encouragement.

Many colleagues have given me valuable assistance during the years. The earliest series of model tests were carried out by Mr. RUNE AXELSSON, *C. E.*, and Mr. OTTO v UNGE, *C. E.*, as a graduation thesis. The later series of model tests were managed by Mr. TOIVO ENNOK with the help of Mr. ILMARI PULKKINEN and Mr. GUNNAR KJELLBERG, *C. E.* Mr. LENNART GARDNER, *C. E.*, and Mr. ERIK ALBERTSSON, *C. E.*, assisted me in the experimental work and test result treatment work concerning the full-scale tests in Gothenburg. During the field tests I had the honour and pleasure of co-operating with the late Mr. STURE JAKOBSSON, *C. E.*, and Mr. LENNART BERNELL, *C. E.*, of the Stockholm Airport Building Committee as well as Mr. NILS ODEMARK, *C. E.*, of the Swedish Road Research Institute. In the final stage of the work valuable help with test result analysis and theoretical calculations was supplied by Mr. RALEJS TEPFERS, *C. E.*, Mr. EMILIS PURINS and Mr. MIODRAG HIBA, *C. E.* Mr. JANIS BUBENKO, *C. E.* helped me with programme and data machine calculations for some of the tables. Mrs. MARIANNE FRÖIER and Mrs. KERSTIN BÖRJESSON typed the manuscript and prepared it for printing. Mrs. INGRID NILSSON prepared the drawings for reproduction and Mr. RICHARD KOOLMAN took the photographs and prepared them for reproduction. Mr. ERIC ELLIOT helped me with the translation of the manuscript.

Contributions to the costs of the investigation have been generously given by the Stockholm Airport Building Committee, the Royal Swedish Air Force's Board of Airfield Buildings and the Royal Board of Civil Aviation as well as Skånska Cement AB, Gullhögens Bruks AB and Smedjebackens Valsverks AB.

To all those, authorities, institutions, industries and private people, named and unnamed, who have contributed to the fulfilment of this investigation, I wish to express my sincere gratitude.

Gothenburg, February 1960.

Anders Losberg.

Notations

A = area of test slab in contact with soil.
A_c = cross-section area of the concrete.
A_r = cross-section area of the reinforcement.
C = $\dfrac{E_s}{(1-\nu_s^2)}$ = soil modulus = modified modulus of elasticity of soil.
D = $\dfrac{Ei}{(1-\nu^2)}$ = flexural rigidity of slab.
D_k = effective rigidity at strengthened edges of slab.
E = modulus of elasticity of slab.
E_c = modulus of elasticity of the concrete.
E_r = modulus of elasticity of the reinforcement (steel).
E_s = modulus of elasticity of the soil.
I = moment of inertia for beam (detail test).
I_k = moment of inertia of edge beam with width b_k.
K = compressive strength of concrete, determined on standard cubes.
$K(x)$ = soil factor according to (22:8 b).
L = length of runway between dilation joints or between cracks in continuous pavement.
M = flexural moment, generally.
M_{ult} = ultimate moment in reinforced concrete beam.
N = normal force, generally.
N_r, N_φ = membrane forces in slab in radial and tangential directions respectively.
N_t = tensile force in pavements due to temperature decrease and shrinkage.
P = total external load on slab.
P_{ult} = ultimate load.
P_M = part of loading on slab admitted by membrane effect.
P_b^{cr} = load at concrete tensile rupture (crack formation) in bottom of slab.
P_b^{yie} = load at yield point in bottom reinforcement of slab.
P_t = load at top surface failure of slab.
P_t^{cr} = load at concrete tensile rupture (commencement of crack formation) in top surface of double-reinforced slab.
P_t^{yie} = load at yield point in top reinforcement of double-reinforced slab.
$P(x)$ = loading factor according to (22:12 b).
$\overline{Q}$ = the resultant of the shear forces in half the failure crack in top of slab.
$\overline{Q}$ = corner forces in the angle between two failure lines.
R = radius of a slab with finite extent.
V = depression volume under slab.
V_p = soil pressure volume under slab.
W = section modulus for beam.

$Z(s)$, $Z(a)$ = functions (series expression) included in expressions for depression (Z_1), soil reaction pressure (Z_2) or moment (Z_3, Z_4) for a slab on soil. An e or k index respectively denotes the corresponding expression for elastic and resilient soil respectively. $Z^0(s)$ represents the expression in question concerning concentrated loading. $Z^m(a)$ represents the values of the function in question in the loading centre with varying relative load distribution a.

$a = \frac{c}{l}$ = relative load distribution, index e and k respectively for elastic and resilient subgrade respectively.

b_k = width of edge beam (edge strip).

c = load distribution radius with circular loading area.

d = distance between loading centres (centres of gravity of loading halves) with twin loading (or distributed double-symmetrical loading area with arbitrary form).

d = mesh width of reinforcement wire fabric.

f = zero point distance from loading centre for assumed linear distribution of the tangential moment in slab.

f_s = coefficient of friction between pavement and soil.

g = weight of test slab per unit area.

g = half the distance between the longitudinal joints.

h = effective thickness or depth of slab or beam.

h_0 = total thickness (height) of slab or beam.

i = moment of inertia of slab per unit width.

k = resilience constant = modulus of subgrade reaction.

$k(s)$ = influence function for soil depression = depression due to a unit load at a distance s from the point.

$l_e = \sqrt[3]{\frac{2D}{C}}$ = elastic radius of rigidity for elastic subgrade.

$l_k = \sqrt[4]{\frac{D}{k}}$ = elastic radius of rigidity for resilient subgrade.

m_r, m_φ = radial and tangential flexural moment in slab per unit width.

$\overset{+}{m}_{\max}$, $\overset{-}{m}_{\max}$ = positive and negative maximum flexural moment respectively in slab per unit width.

m_{int} = moment due to a load on interior of slab.

m_e = moment due to a load on a free edge of slab.

m_e^+, m_e^- = maximum positive and negative flexural moment due to a load on a free edge.

m_e^{sc} = moment due to a load on a semi-circular area on free edge of slab.

m_e^{tg} = moment due to a load tangent to free edge of slab.

m_{ji}^- = maximum negative moment due to a load on a joint intersection.

m_e^- = maximum negative moment due to a load on a free corner.

m, m' = positive and negative ultimate moment respectively on the whole.

m_e, m_e' = ultimate moment with a load on a free edge (joint).

m_c' = negative ultimate moment due to a load on a free corner.

m_{cr}, m_{cr}' = positive and negative flexural moment respectively per unit width at concrete tensile rupture (crack formation).

$m_{y(s)}, m'_{y(s)}$	=	positive and negative flexural moment respectively per unit width at yield point in bottom and top reinforcement respectively.
m_t	=	moment (per unit width) in pavements due to uneven temperature (warp).
$\Delta m'$	=	reduction in neg. ultimate moment due to temperature decrease and shrinkage.
n	=	$\frac{E_r}{E_c}$
p	=	loading acting on slab (distributed over a certain load area) due to external load.
p_s	=	soil reaction pressure.
p_0	=	soil reaction pressure under loading centre or peak value of assumed soil reaction pressure cone.
$\bar{p}$	=	relative reinforcement percentage.
p_{aver}	=	average loading or average soil pressure.
p_c	=	total circumference of the reinforcement in a certain section.
q	=	shear force along failure line.
r	=	distance from loading centre.
r_k	=	distance along the edge between loading centre and negative failure line with a load on a free edge of slab.
r_s	=	radius of circular failure crack in top surface.
r_p	=	radius of zone of slab around loading which has undergone complete plastification.
$\varrho = \frac{r}{l}$	=	distance from loading centre in dimensionless form.
s	=	distance between the centre points of the failure semi-circles with twin loading.
t	=	base radius in soil pressure cone under slab.
t_k	=	half the length along the edge of soil pressure pyramid base area with a load on a free edge of slab.
u	=	radially displacement of points in centre plane of slab.
w	=	depression of slab and soil.
w_0	=	depression under loading centre.
w_{aver}	=	average depression.
w_e	=	depression under a load on a free edge of slab.
w_g	=	depression of test slab in subgrade due to its dead weight.
x	=	distance to neutral layer from the compressed surface in a reinforced concrete section.
x_b	=	bonding stretch along reinforcement beside the cracks.
$\bar{x}$	=	distance from the centre of gravity of the quarter area to the long axis of symmetry with arbitrary, double-symmetrical loading area.
$\bar{x}, \bar{y}$	=	distance from centre of gravity to the free edge or the axis of symmetry at right-angles to the free edge respectively for *half* the loading area with arbitrarily distributed edge loading.
α	=	angle between the assumed straight negative failure line and the positive failure line with a load on a free edge of slab.
γ	=	constant in the soil pressure expression $p_0 = \gamma \cdot \frac{P}{t^2}$
γ_k	=	corresponding constant in the soil pressure pyramid with a load on a free edge of slab, see above.

Δ	= Laplace's operator.
δ	= crack width.
$\varepsilon_r, \varepsilon_\varphi$	= membrane strain in slab in radial and tangential directions respectively.
ε_{sh}	= concrete shrinkage.
μ	= reinforcement percentage.
μ, ν	= constants when calculating the shear forces along slab top surface crack.
ν	= Poisson's ratio for slab.
ν_s	= Poisson's ratio for soil.
Π	= relative pressure distribution according to formula (23:11).
σ_c	= stress in concrete.
$\bar{\sigma}_c$	= the effective average compressive strength of the concrete.
σ_f	= flexural strength of concrete.
σ_f^{stand}	= flexural strength of concrete determined from standard flexure beams.
σ_{mt}	= stresses in pavement due to uneven temperature.
$\sigma_{mt}^b, \sigma_{mt}^t$	= stress due to uneven temperature, in the bottom and top surface respectively.
σ_r	= stress in reinforcement.
σ_r^{cr}	= reinforcement stress in a crack of a continuous pavement.
σ_r^{yie}	= yield point in reinforcement.
σ_t	= pure tensile strength of concrete.
τ_b	= bond stress between concrete and reinforcement.
$\omega = \dfrac{\sigma_f}{\sigma_t}$	= relation between flexural strength and pure tensile strength of concrete.

Abbreviations:

m, cm, mm	= metres, centimetres, millimetres.
kg, t	= kilogrammes, tons.
t m	= ton-metres.
kg/cm^2	= kilogrammes per square centimetres.
b. r.	= bottom reinforcement.
t. r.	= top reinforcement.
srp	= stirrup reinforcement.
∅	= diameter of a reinforcing bar.
e. g. ∅ 6 c/c 150 mm	= reinforcement of bars 6 mm in diameter, spaced with 150 mm from centre to centre.

1. Introduction

The enormous development of road and air traffic in recent decades has made ever-increasing demands on road and airfield pavement. It is primarily the increased wheel load but also the greater traffic intensity that is responsible for these demands.

The pavement of a road or an airfield runway can be said to serve two main purposes, namely:

1. to give the road or runway an even and in other respects suitable surface.

2. to distribute the loads to which it is subjected so as to avoid excessive pressure on the sub-base or the natural soil.

The pavement must also be constructed with a view to keeping down the expenditure for building and maintenance, due respect being paid, however, to the required costs for soil strengthening or sub-base necessary for various types of pavement.

The first-mentioned demand is on the whole satisfied by all types of high-class permanent pavements. The second demand, whereby the pavement has a load-distributing and reinforcing function, is satisfied only by so-called rigid pavements, i. e. pavements made of concrete. It is this demand that has become pre-eminent with the intense increase in traffic during recent years.

Looking back over the short time during which pavement technique has been developed, we find that it is the need for smoothness and good surface properties that first became urgent. This demand was applicable to roads as soon as vehicle speeds became fairly high, and it was primarily non-rigid asphalt pavements that came to be used. The increasing demand for improved load-carrying properties which was the result of road traffic becoming heavier was first satisfied by the improvement and reinforcement of the sub-base rather than by the use of a more rigid pavement with a load-carrying capacity of its own. The first rigid pavements came into use primarily to replace asphalt pavements with a type of pavement that required less maintenance. It was then quite natural that these first concrete pavements should have been constructed of plain concrete.

When gradually the need arose for designing pavements suitable for wheel loads continously increasing, it was a natural development to make these unreinforced concrete pavement slabs thicker and thicker and to design the slabs so as to prevent crack formation under the wheel load. A designing principle of this kind thus led to moderate slab thicknesses on subgrade with fairly good load-carrying properties for the loads exerted by vehicles and aircraft used before the Second World War. But with the enormous traffic development that has taken place in the last few decades the problem entailed by these conservative pavement types has gradually proved too much for the designers. An example of this is the great increase in the weight of aircraft, which was a result of the introduction of jet-propelled aircraft for commercial purposes. The development and the difficulties involved are evident from a report on development and research problems in connection with rigid pavements on military airfields in the United States, supplied by SALE and HUTCHINSON [58]. During the last twenty years or so it has been essential to increase the design criterion for wheel loads from approx. 7 to 120 tons, and it is estimated that within the next five years it will be essential to increase this load to approx. 150 tons. With the design specifications and calculating methods applying to the type of plain concrete pavements mainly used up to now, this would imply a pavement with an unreinforced slab approx. 80 cm thick [18, 50].

It is quite clear that, faced with such a development, designers must elaborate new methods for pavement design. A natural step would appear to be the use of reinforcement as strengthening for a concrete pavement. As far as the present writer has been able to find from published reviews of development and research in the field of pavements [18, 58], reinforcement in concrete pavements has so far been used only to a very small extent with a view to increasing the load-carrying capacity. The reinforcement now more or less regularly used in concrete pavements is chiefly intended, in the event of crack formation, to hold the cracked parts together and prevent the cracks from extending. Reinforcement of this type is normally located in the centre of the slab or nearer the top (see [18, 58]) and does not contribute to the load-carrying capacity since the greatest tensile stresses occur at the bottom of the pavement under the wheel load.

The so-called continously reinforced pavements, which are completely jointless, can be said to form a development of this type of crack reinforcement. In this case the reinforcement has to take up the stresses from temperature decrease and shrinkage due to the completely prevented contraction, this requiring comparatively large amounts of reinforcement. This type of pavement, which has been the subject of many tests in recent years, particularly in the United States (see for example [2]), must still be considered to be in the experimental stage. It is not possible to find any line of thought which attempts to calculate and utilize the reinforcement for admitting flexural stresses due to traffic loading as well.

Another kind of reinforcement in pavements which has been the object of great interest in recent years is pre-stressed reinforcement. Many test roads, notably in Britain, France and Germany, but also in the United States, have been built or are being built, and many different systems are being tested in order to give the pavement slabs pre-stress forces. Summarized accounts of these tests and systems have been supplied by BRINCK [13] and the American Concrete Institute [9], among others. The object of pre-stressed pavements is to give the concrete a higher effective tensile strength by extra external compressive stresses and so to avoid the occurrence of tension cracks; it can therefore be said that the pre-stressed pavement is mainly a further development of the unreinforced type of pavement.[1] Experiences of pre-stressed pavements up to now also show that the costs are generally very high and that there are considerable technical and practical difficulties which have not yet been solved.

Thus, one requirement applicable to all these types of pavements is that no tension failure in concrete must occur in the pavement slab due to the influence of wheel load. I permit myself here briefly to anticipate my treatment in a later section of the problem of the pavement slab. Fig. 1: 1 shows the moment distribution in an elastic slab on soil, which is assumed to function elastically in this case, due to the influence of a fairly concentrated load from a wheel. The figure shows the prominent positive maximum moment which occurs under the wheel in comparison with the small and levelled negative moment which occurs radially at a certain distance round the loading point. It is obvious that a pavement made of plain concrete, which has to take up stresses of this positive maximum moment with the help of the low flexural strength of the concrete only, must be designed in the form of a thick slab as soon as loads become heavy. In addition to this, the thicker and more rigid the pavement is made, the higher the maximum moment will be relative to the load (see Fig. 1: 1).

It would, however, appear to be a natural step, when strengthening the slab, to insert reinforcement in the bottom of the slab to make it function in the same way as flexural reinforcement in a normal reinforced concrete structure, i. e. allow the concrete to crack in the bottom

[1]) The tendency to utilize the pre-stressed reinforcement for admission of flexural stresses is noticeable in French design practice (see for example MELVILLE [51]).

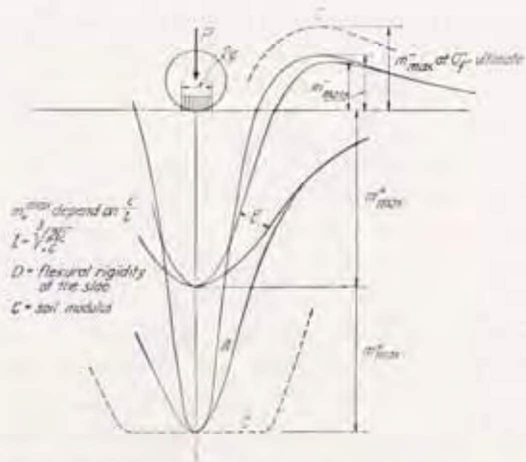

Fig. 1:1. Approximate moment distribution in a reinforced concrete slab on elastic subgrade due to concentrated load.

The curves A och B show the moment distribution according to the elasticity theory when load distribution is small and great respectively (radius of load distribution area = c) in relation to the sradius of elastic rigidity l. The curves C show the moment distribution fundamentally after the slab has passed into plastic stage under the loading centre at commencement of yield in the reinforcement in bottom surface. The lower curve of each kind represents the tangential moment, the upper curve the radial moment.

surface and the reinforcement there to take up the positive moment, while the tensile strength of the concrete at the top takes up the relatively low negative moment. In principle there is, of course, nothing to prevent the insertion of reinforcement also at the top as an extra strengthening procedure and to allow the concrete to crack there as well. Apart from the direct strengthening, the reinforcement also results in a considerable decrease in the flexural rigidity as soon as crack formation develops in the tension zone, this levelling the positive maximum moment as shown in Fig. 1: 1.

The strengthening effect of the reinforcement will be even more advantageous if attention is paid to the function of the reinforced slab in the yielding condition, when loading increases above the value, according to Fig. 1: 1, corresponding to the yield point in the reinforcement. There is then a levelling of moment during continued yield in the bottom crack lines, and the function of the slab can be treated in accordance with the same principles that have been shown to apply for cross-reinforced plates by K. W. Johanssen's yield line theory [31]. This function of a reinforced concrete slab greatly increases the load-carrying capacity and the margin of safety for failure in a pavement of this kind.

It is pavements of this kind, with active so-called *structural* reinforcement, that are treated by the author of the present thesis. As shown by the discussion above, pavements of this kind show great variations in function when compared with conventional plain or crack-reinforced pavements. This applies already in the elastic stage, in which, through continued crack formation at the bottom, the reinforced slab changes its elastic properties successively. It applies even more in the yield stage, after the yield point in the bottom reinforcement has been reached.

Starting from the theories hitherto used for concrete pavements, which are based on the assumption that the pavement functions as an elastic slab on an elastic subgrade, the author attempts to show the extent to which a *reinforced* concrete pavement with this successive crack formation can be calculated according to these theories and also to study the elastic properties of the soil under a pavement of this kind with a relatively low degree of flexural rigidity. This section of the investigation is included in Part 2 of the book. Part 3 concerns the behaviour of the reinforced concrete slab in the yield stage after the yield point in the reinforcement has been passed, and in this part an ultimate strength theory is developed for the pavement. In Part 4 such cases are studied in which the load is located on an edge or on a moment-free joint, and the problem is treated from the points of view both of the elasticity theory and the ultimate strength theory.

In all cases the author has attempted to verify the results of the theoretical presentation by means of tests. These have been of three types, *viz.* tests on test pavements in model scale, tests on full scale slabs under laboratory conditions, and full scale field tests in connection with pavement work in practice. The tests of the two first-mentioned kinds are described in connection with and within the scope of the parts of this paper in which the corresponding theoretical problems have been treated. The field tests carried out in connection with pavement work on airfields have been separately treated in Part 5. In order to clarify the very extensive test material and in order to avoid complicating the presentation with too much detail taken from the test reports, the author has only included summarized test results. He has chosen instead to accumulate the measurement values and more detailed test results in a special test supplement (Part 9), to which reference is made in the cases concerned in connection with test analysis in the other parts of the study.

Apart from wheel load, the pavement is also subjected to stresses due to temperature variations and shrinkage in the concrete. The effect of these, particularly with regard to special problems for *reinforced* concrete pavements has been treated in Part 6.

The various parts of this book thus treat relatively independent problems. For the sake of even greater clarity, the author has therefore generally terminated each part with a section summarizing the results and conclusions. The purely theoretical sections within the various parts generally include a special final summary of formulae.

In a final Part 7 the author has attempted to summarize the limited experience, mainly derived from Swedish airfields with structurally reinforced pavements, and has complemented this presentation with suggestions concerning design specifications of reinforced concrete pavements.

2. Reinforced Concrete Pavements Studied from the Viewpoint of the Theory of Elasticity

21. The Conditions for the Theory. A Short Literary Review

Research workers who have earlier studied the concrete pavement problem from a theoretical viewpoint have, according to the findings of the author, always based their work on the conditions of the elasticity theory.[1] For the slab-soil system, the following conditions have generally been assumed:

1. The slab is completely elastic, isotropic and homogeneous and is of a constant thickness (flexural rigidity). Otherwise, except where specified in the following, the simplified suppositions from which the differential equation of the plate (see 221) is derived have generally been assumed.

2. The soil is completely elastic in accordance with one of the following two different hypotheses concerning its properties:

a) The subgrade is considered to be a flexible bed where the pressure at a certain point is proportional to the degree of depression at the same point while the adjacent unloaded area is not at all affected. The case of an ice-floe floating on water can be mentioned as an example of a subgrade of this type. The soil is thus characterized by a constant of subgrade reaction, a "*resilience constant*"

$$k = \frac{p_s}{w} \tag{21:1}$$

showing the relationship between the intensity of the soil reaction pressure p_s and the deformation of the soil w at the same point. k is known as the modulus of soil reaction ("k-value"). In the following, this type of subgrade is called a "*resilient subgrade*".

[1]) In a paper in Betong 1947 [35] and in stencilled reports, [36, 37, 38, 39] the author has previously dealt with reinforced concrete pavements in plastic ultimate behaviour. The theories of the author have also been referred to and studied by several research workers. See Section 31.

b) The subgrade is considered to be an elastic, isotropic and homogeneous body of semi-infinite extent. It is characterized by a modulus of elasticity E_s and a Poisson's ratio of ν_s which can be included in a constant, the "modified modulus of elasticity".

$$C = \frac{E_s}{(1 - \nu_s^2)} \tag{21:2}$$

C[1]) is described in the following as the "*soil modulus*" and the type of subgrade as "*elastic subgrade*".

3. The slab and the soil are in full contact with one another. No notice is taken of the fact that the slab in a state of deformation under loading can lift from the soil.

In their paper on wheel load stresses in concrete pavements (1949), Bergström, Linderholm and Fromén [4] have produced an exellent review over the current literature at that time in this field. For that reason the author will here only mention the most important papers and those to which he refers when presenting the theory as well as, of course, recent papers of interest for this investigation.

The earliest treatment of the system consisting of a slab on a flexible subgrade was based on the assumption of a resilient subgrade and proceeds from the differential equation[2]) for a thin, elastic plate. Hertz [27] who was the first to deal with the problem, studied the case of the floating ice-floe mentioned above and gave the solution for the effect of a concentrated load on such an ice-floe of infinite extent. An extremely thorough treatment of circular (this including of course also infinite) slabs on a resilient subgrade has been produced by Schleicher [60] who gave the exact solutions for various types of ring symmetrical loading at various boundary conditions, but these solutions are not usually presented in a form that can be utilized in practice. In the case of Westergaard's papers, however, [71, 72, 73, 75, 76, 77] the approximate formulae are intended to be applied directly for the design of plain concrete pavements and they have, indeed, been used to a great extent for this purpose. Apart from the case of the load in the centre of the slab (in point of fact loading on a slab of infinite dimensions), Westergaard has also dealt with the case of loading on a free edge and on a free corner (Westergaard's three basic cases of loading). These last-mentioned cases of loading are treated in more detail in Part 4 later on. In later

[1]) The notation C has been suggested by Schleicher [59] and others.

[2]) See, for example, Timoshenko [66].

papers [74, 76], WESTERGAARD has attempted to correct his formulae with respect to observed poor agreement between theory and test results, while many other research workers have suggested modifications of WESTERGAARD's formulae for the same reason. A review of these is supplied by KELLEY [41].

More recent contributions to the theory concerning slabs on a flexible bed are generally based on the assumption of elastic subgrade. The treatment of this subgrade case is considerably more complicated and general solutions comparable with those of SCHLEICHER mentioned above, dealing with slabs on a resilient subgrade, are not offered in technical literature. Nor have the cases of edge and corner loading been treated.

In the important special case where the slab has infinite dimensions, exact solutions have been provided by HOGG [28], HOLL [29, 30] and BURMISTER [14, 15]. The first two mentioned base their solutions on the differential equation of the plate while the third proceeds from the general elasticity equations. HOLL, whose solution covers the most general conditions concerning the properties of the soil, also implies how the problem is to be solved in the case of a slab with limited dimensions, but the solution he arrives at in this case is not correct and the method described does not appear to be possible in practice.[1]) The slab with limited dimensions has otherwise been dealt with through the use of difference calculating methods by HABEL [26] and BERGSTRÖM [4, 5], whereby HABEL divided up the slab into ten ring elements and BERGSTRÖM divided it up into four ring elements. BERGSTRÖM has developed his method into practical solutions presented in a diagrammatic form.

The solutions suitable for practical use presented above are aimed at load distributions over only *circular* loading surfaces. The effect of twin loading from two circular loading surfaces can generally be obtained by superimposition. Although the load contact surface between a rubber wheel and a pavement surface in general can usually be approximated to a circle, cases can occur where loading surfaces have more complicated forms. In such cases, use can be made of the "influence charts" [57] by PICKETT and RAY. These show the amount of depression and moment on the interior and close to the free edge of a pavement with infinite

---

[1]) A couple of special cases dealing with slabs of limited dimensions have been dealt with by BOROWICKA [11, 12], namely the cases where the whole slab is uniformly loaded and where the slab is influenced by a concentrated load in the centre. Borowicka's solutions do not, however, appear to be completely free from criticism and calculations carried out in accordance with his method are extremely laborious.

DÖLPHER-LARSEN [17] has quoted a method based on the solution for the infinite slab whereby he superimposes a load opposed to the soil pressure from the section outside the circumference of the limited slab. The method does not, however, appear to be possible in practice; the solutions given by Dölpher-Larsen thus include divergent series.

dimensions under the influence of a loading surface distributed arbitrarily. The influence values for a load on the interior of the slab have been calculated according to HOGG [28] (elastic subgrade) and for edge loading according to WESTERGAARD [71] (resilient subgrade).

The conditions forming the basis for these theories and methods consist, to a lesser or greater degree, of simplifications of the actual conditions prevailing in the case of a concrete pavement supported by soil. The assumption that the slab has constant or elastic properties is mainly correct as long as it concerns plain concrete but appears to be particularly doubtful when applied to reinforced concrete slabs, the elastic properties of which change to a great extent as soon as crack formation starts in the tension zone of the concrete. The other component in the system, the soil, has characteristics that are still more difficult to judge. The possibility of utilizing the above-mentioned theories for concrete pavements must thus be judged on the basis of experiments.

The paper of BERGSTRÖM och assoc. [4] mentioned above also includes a detailed and very well produced review of tests carried out by various research workers concerning concrete pavements resting on soil. These tests included only *plain concrete* slabs, with the exception of the tests carried out by the present author himself which are described in more detail later. Discussions of test results in this paper [4] show that both the theories mentioned agree relatively well with the test values obtained concerning deformations and stresses.

In the paper referred to [4], an account is also given of tests carried out by these authors with a circular plain concrete slab lying on clay subgrade (Upplands Väsby). Apart from measurement of depression values and stresses (strains) due to a load on the centre, measurements were also made of the pressure between the slab and the soil at various points by means of pressure-sensitive measuring cells cast into the bottom of the slab, these cells registering in accordance with the inductive principle. The intention of these measurements was primarily to show the properties of the soil since the distribution of soil pressure is quite different according to the two theories while the deformation of the slab and the stress distribution in the slab are comparatively similar. The result of the test showed indubitably closer agreement with the theory for elastic subgrade than with the theory for resilient subgrade.

In later sections of this paper the author will discuss, on the basis of tests carried out with *reinforced* concrete pavements, the applicability of the elasticity theory concerning pavements of this type and thereby return to the question as to which of the two hypotheses concerning the elastic properties of the soil lies closest to actual soil conditions occurring in practice. For this purpose it is first essential to develop the theories for the calculations concerning slabs on soil particularly when the soil is assumed to behave as an elastic subgrade, since the papers referred to above have not in general been developed to practically applicable results as required for the analysis of *reinforced* concrete pavement. The reason for this is that reinforced concrete pavements are usually relatively thin and have a low flexural rigidity and that, in many cases, higher values are obtained concerning the load distribution relative to the rigidity of the slab than those values predicted according to earlier theoretical results since these were primarily aimed at the considerably greater flexural rigidity of plain concrete pavements.

The following presentation of the theory is based to a great extent on the solution to the problem produced by HOLL [29, 30] since this appears to be the most general and, besides, can be applied to both types of subgrade.

22. Theory for Elastic Pavements

221. Basic equation for an elastic pavement of infinite extent

The differential equation for the vertical deformation of an elastic slab can be written, in terms of the polar coordinates,

$$D \cdot \Delta \Delta w(r) = p(r) - p_s(r) \tag{22:1}$$

whereby the usual simplifying assumptions concerning the treatment of elastic slabs are made. In this connection

Δ = Laplace operator

D = flexural rigidity of slab $= \dfrac{E\,i}{1 - \nu^2}$

E = modulus of elasticity of slab

ν = Poisson's ratio for slab

i = moment of inertia of slab per unit width

r = distance from centre of loading

p = load acting on slab

p_s = soil reaction pressure

In the case where the load is radially symmetrical, the Laplace operator then has the form

$$\Delta w(r) = \frac{d^2 w}{dr^2} + \frac{1}{r}\frac{dw}{dr} = \frac{1}{r}\frac{d}{dr}\left(r\frac{dw}{dr}\right) \tag{22:2}$$

In the differential equation the soil reaction pressure between the slab and the soil is not known. If it is assumed that the slab and the soil are permanently in contact with one another, then the surface of the soil has the same deformation as the slab and this soil deformation can be assumed to occur due to the soil reaction pressure operating as an applied load on the surface of the soil.

The connection between the soil pressure and the depression of the soil is a function of the elastic properties of the soil. In order to characterize these generally an influence function is introduced

$$k(s) = k(r,\theta;\, \varrho,\varphi) \tag{22:3}$$

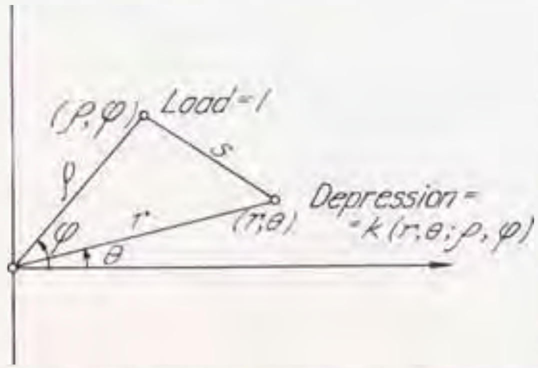

Fig. 22:1. The influence function $k\ (r, \theta; \varrho, \varphi)$ expressing the depression at a point of the subgrade surface with co-ordinates (r, θ) due to a load $= 1$ acting on the subgrade at the point (ϱ, φ).

this showing the depression at a certain point with coordinates ϱ, φ due to a unit load $= 1$ applied to the surface at the point r, θ (see Fig. 22:1). s denotes the distance between both the points. This influence function is, in the case of isotropic soil material, radially symmetrical round the point at which the load is applied, i. e. is a function of only s, and is considered to be known for the soil material in question.

For the two soil types here treated, the influence function has the form

1. Elastic, semi-infinite subgrade

$$k(s) = \frac{1}{\pi C} \cdot \frac{1}{s} \tag{22:4}$$

according to Boussinesq's classical depression formula[1]). C means the modulus of elasticity of subgrade according to the earlier definition (21:2)

2. Resilient subgrade

$$k(s) = \begin{cases} 0 \quad \text{for } s \neq 0 \\ \lim\limits_{\varepsilon \to 0} \dfrac{1}{\pi \varepsilon^2 k} \quad \text{for } s = 0 \end{cases} \tag{22:5}$$

where $k =$ the constant of resilience. This expression follows directly from the definition of k (21:1).

It is now possible to express the degree of depression at a certain point due to the unknown soil reaction p_s by using this influence function $k(s)$.

[1]) See, for example, TIMOSHENKO: Theory of elasticity [65].

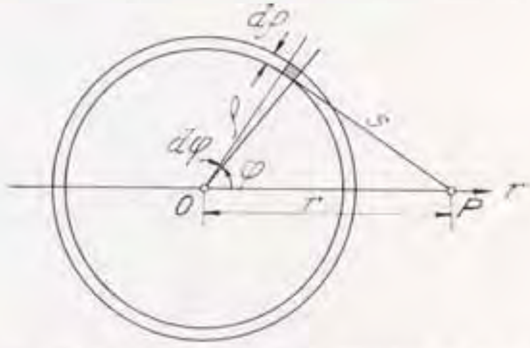

Fig. 22:2. Integration of the influence function according to Fig. 22:1 with a ring-symmetrical load.

Since the load applied to the plate is assumed to be radially symmetrical, the degree of depression is independent of θ and θ can be assumed to be equal to 0, so that the position of the point is only characterized by the distance r from the centre (see Fig. 22: 2). Due to the soil loading $p_s(\varrho)$ on a surface element $d\varrho \cdot \varrho\, d\varphi$, then the depression in P is

$$d\,(dw) = k\,(r;\varrho,\varphi)\; p_s(\varrho)\, d\varrho\; \varrho\, d\varphi$$

and due to the loading from the complete ring-shaped element around O between ϱ and $\varrho + d\varrho$, the depression becomes

$$dw = p_s(\varrho)\; \varrho\, d\varrho \cdot 2 \int_0^{\pi} k(s)\, d\varphi \tag{22:6 a}$$

where the relationship between s and φ is obtained according to the cosine theorem

$$s^2 = r^2 + \varrho^2 - 2\, r\, \varrho \cos \varphi \tag{22:6 b}$$

(see Fig. 22:2).

This expression can be transformed to a Fourier-Bessels integral. According to this transformation an arbitrary function $f(x)$ can be rewritten in the form of a determined integral with an infinite upper limit

$$f(x) = \int_0^{\infty} F(u) \cdot J_0(u\, x)\, u\, du \tag{22:7 a}$$

where the coefficient $F(u)$ is calculated from the integral

$$F(u) = \int_0^\infty f(t)\, J_0(ut)\, t\, dt \tag{22:7 b}$$

J_0 is a Bessels function of the first type and 0 order.[1])

In this way the influence function $k(s)$ can be rewritten

$$k(s) = \frac{1}{2\pi} \int_0^\infty K(u)\, J_0(us)\, u\, du \tag{22:8 a}$$

where

$$K(u) = 2\pi \int_0^\infty k(t)\, J_0(ut)\, t\, dt \tag{22:8 b}$$

If this is introduced into equation (22:6 a) then

$$dw = p_s(\varrho)\, \varrho\, d\varrho \cdot \frac{1}{\pi} \int_0^\infty K(u)\, u\, du \int_0^\pi J_0(us)\, d\varphi \tag{22:9}$$

where s is defined through equation (22:6 b). The last integral in this equation can be integrated according to one of the "addition theorems" for Bessels functions:[2])

$$\int_0^\pi J_0(us)\, d\varphi = \pi\, J_0(ur)\, J_0(u\varrho)$$

The equation then becomes

$$dw = p_s(\varrho)\, \varrho\, d\varrho \cdot \int_0^\infty K(u)\, u\, J_0(ur)\, J_0(u\varrho)\, du \tag{22:10 a}$$

The pressure p_s over the complete soil surface then gives a total depression at a point at a distance r from the centre

$$w(r) = \int_0^\infty p_s(\varrho)\, \varrho\, d\varrho \cdot \int_0^\infty K(u)\, u\, J_0(ur)\, J_0(u\varrho)\, du \tag{22:10 b}$$

Since we have assumed that the slab and the soil are in complete contact at all points, then the expression (22:10 b) also means the deformation surface of the slab. It thus forms a solution to the differential equation of the slab (22:1). If p_s according to equation (22:1) is inserted into the equation (22:10 b),

$$w(r) = \int_0^\infty [p(\varrho) - D \cdot \Delta\Delta\, w(\varrho)]\, \varrho\, d\varrho \cdot \int_0^\infty K(u)\, J_0(ur)\, J_0(u\varrho)\, u\, du \tag{22:11}$$

This forms the equation for the case in question of a slab on soil.

[1]) See, for example, WATSON [70], page 453.

[2]) See WATSON [70], page 367.

For the solution of the equation (22:11) the known applied loading function p is transformed into a Fourier-Bessels integral according to (22:7), so that it is possible to write

$$p(\varrho) = \int_0^\infty P(\varkappa)\, J_0(\varkappa\varrho)\, \varkappa\, d\varkappa \tag{22:12 a}$$

where

$$P(\varkappa) = \int_0^\infty p(t)\, J_0(t\,\varkappa)\, t\, dt \tag{22:12 b}$$

The actual solution to the equation (22:11) itself can also be applied in a similar form

$$w(r) = \int_0^\infty W(\varkappa)\, J_0(\varkappa r)\, d\varkappa \tag{22:13}$$

If these expressions are inserted in the equation (22:11) this becomes

$$\int_0^\infty W(\varkappa)\, J_0(\varkappa r)\, d\varkappa =$$

$$= \int_0^\infty [\varkappa\, P(\varkappa) - D\, \varkappa^4\, W(\varkappa)]\, d\varkappa \int_0^\infty J_0(\varkappa\varrho)\, \varrho\, d\, \varrho \int_0^\infty K(u)\, J_0(ur)\, J_0(u\varrho)\, u\, du \tag{22:14}$$

The last double integral in this expression can be written in the form

$$K(\varkappa)\, J_0(\varkappa r)$$

since this double integral forms a Fourier-Bessels integral transformation (22:7) of the function

$$f(\varkappa) = K(\varkappa)\, J_0(\varkappa r)$$

One then gets

$$\int_0^\infty W(\varkappa)\, J_0(\varkappa r)\, d\varkappa = \int_0^\infty [\varkappa\, P(\varkappa) - D\, \varkappa^4\, W(\varkappa)]\, K(\varkappa)\, J_0(\varkappa r)\, d\varkappa \tag{22:15 a}$$

or

$$\int_0^\infty [W(\varkappa) - \varkappa\, K(\varkappa)\, P(\varkappa) + K(\varkappa)\, D\, \varkappa^4\, W(\varkappa)]\, J_0(\varkappa r)\, d\varkappa = 0 \tag{22:15 b}$$

This expression applies identically for all values of r. The expression in brackets must then be equal to 0 and thus

$$W(\varkappa) = \frac{\varkappa\, K(\varkappa)\, P(\varkappa)}{1 + D\, \varkappa^4\, K(\varkappa)} \tag{22:16}$$

The solution to the equation (22:11) is thus

$$w(r) = \int_0^\infty \frac{\alpha\, P_0(\alpha)\, K(\alpha)}{1 + D\,\alpha^4\, K(\alpha)} \cdot J_0(\alpha r)\, d\alpha \tag{22:17}$$

If this solution is inserted in the differential equation for the slab (22:1) then the expression is obtained for the pressure distribution between the slab and the soil

$$p_s(r) = \int_0^\infty \frac{\alpha\, P(\alpha)}{1 + D\,\alpha^4\, K(\alpha)} \cdot J_0(\alpha r)\, d\alpha \tag{22:18}$$

The expressions (22:17) and (22:18) thus form the general solutions to the problem of a slab on soil, and by calculation together with the insertion in these integrals of the expressions for the subgrade factor $K(\alpha)$ (22:8 b) and the loading factor $P(\alpha)$ (22:12 b) we obtain the solutions for various types of soil and applied loads. The method is naturally not limited to the two types of soil now being considered but any type of soil can be treated in the same way if only the influence function $k(s)$ (22:3) for the type of soil in question can be decided, either theoretically or empirically.

Calculations will now be carried out for the two types of soil in question and for the cases of loading where the load is concentrated or uniformly distributed over a circular surface. The case of elastic, semi-infinite soil will be studied in comparatively great detail, while as far as resilient soil is concerned the author makes a great deal of references to the detailed work of Schleicher [59] and Westergaard [71–76].

222. Elastic, semi-infinite subgrade

222.1 *Concentrated load.*

Subgrade and loading factors. For this type of soil, the subgrade factor is (22:8 b)

$$K(\alpha) = \int_0^\infty 2\,\pi\, t\, \frac{1}{\pi\, C} \cdot \frac{1}{t}\; J_0(\alpha t)\, dt = \frac{2}{C} \cdot \frac{1}{\alpha} \tag{22:19}$$

The loading factor (22:12 b) for a concentrated load will be

$$P(\alpha) = \int_0^\infty \lim_{\varepsilon \to 0} \frac{P}{\pi\, \varepsilon^2}\; t\, J_0(\alpha t)\, dt = \frac{P}{2\,\pi} \tag{22:20}$$

Depression. If the expressions (22:19) and (22:20) are inserted in the equation (22:17), one gets

$$w(r) = \frac{P}{2\pi}\,\frac{2}{C}\int\limits_0^\infty \frac{J_0(\varkappa\, r)}{1 + \varkappa^3\,\dfrac{2\,D}{C}}\,d\varkappa \tag{22:21}$$

In order to get the result in a dimensionless form, the distance from the centre is written as

$$s = \frac{r}{l_e} \tag{22:22}$$

where

$$l_e = \sqrt[3]{\frac{2\,D}{C}} \tag{22:23}$$

is called the *elastic radius of rigidity* and is an expression for the elastic properties of the slab and the soil in the dimension length.[1]) With these notations (22:21) has now the form

$$w(s) = \frac{P\,l_e^2}{2\,\pi\,D}\,s^2\int\limits_0^\infty \frac{J_0(x)}{x^3 + s^3}\,dx \tag{22:24}$$

The depression in the loading centre can be calculated exactly from the integral (22:21) since

$$J_0(\varkappa r) = 1 \qquad \text{where } r = 0$$

The depression w_0 in the centre becomes then

$$w_0 = \frac{1}{3\cdot\sqrt{3}}\cdot\frac{P\,l_e^2}{D} \tag{22:25}$$

The general integral in the equation (22:24) can be presented in the form of a series of powers and log functions.[2]) The first terms are

[1]) The conception elastic radius of rigidity l_e applied in the theory for resilient soil (see page 43), was introduced by SCHLEICHER [60] and has been used by WESTERGAARD [71, etc.], and others. By the introduction of a corresponding notation (22:23) also for elastic soil, the author has managed to present the result in a form that is easily comparable for both the theories. See Section 225.

[2]) The solution of this integral is given by HOGG [28]. Hogg has also calculated the terms in the series (22:26) up to s^8 and given the depression curve for $s < 2.0$.

$$w(s) = \frac{P\,l_e^2}{D} \cdot [(3.979 \cdot 10^{-2}\,s^2 - 107.9 \cdot 10^{-8}\,s^8 + 38.2 \cdot 10^{-14}\,s^{14} -$$

$$- \ldots .)\ln s + 0.19245 - 4.440 \cdot 10^{-2}\,s^2 - 30.07 \cdot 10^{-4}\,s^4 +$$

$$+ 70.74 \cdot 10^{-5}\,s^5 - 83.53 \cdot 10^{-6}\,s^6 + 237.4 \cdot 10^{-8}\,s^8 +$$

$$+ 130.51 \cdot 10^{-10}\,s^{10} - 147.28 \cdot 10^{-11}\,s^{11} + 90.63 \cdot 10^{-12}\,s^{12} -$$

$$- 103.3 \cdot 10^{-14}\,s^{14} - 18.1 \cdot 10^{-16}\,s^{16} + 15.2 \cdot 10^{-17}\,s^{17} -$$

$$- 5.6 \cdot 10^{-18}\,s^{18} + \ldots] = \frac{P\,l_e^2}{D} \cdot Z^0_{1,e}(s) \qquad (22{:}26)$$

The series in the bracket is denoted $Z^0_{1,e}(s)$ whereby the index 0 denotes the load distribution $= 0$, i. e. a concentrated load. The value of this series has been calculated for $s \leq 6$ and has been shown in a diagrammatic form in Fig. 22:5 A, page 50. For higher values of s the series does not converge too well unless still more terms are taken into consideration.

The distribution of pressure can be calculated from (22:18) in the same way as has just been shown for vertical deformation. It is however simpler to insert the series (22:26) in the differential equation for the slab (22:1). The result will be according to (22:1), since the applied load here is singular,

$$p_s(r) = - D \cdot \Delta\,\Delta\, w(r)$$

or with dimension-free variable

$$p_s(s) = - \frac{D}{l_e^4} \cdot \Delta\,\Delta\, w(s) = - \frac{D}{l_e^4}\left(\frac{1}{s}\,\frac{d}{ds}\left\{s\,\frac{d}{ds}\left[\frac{1}{s}\,\frac{d}{ds}\left(s\,\frac{dw}{ds}\right)\right]\right\}\right) =$$

$$= - \frac{P}{l_e^2} \cdot \Delta\,\Delta\, Z^0_{1,e}(s) \qquad (22{:}27)$$

and insertion of the series gives

$$p_s(s) = \frac{P}{l_e^2}\,[(24.86 \cdot 10^{-4}\,s^4 - 107.9 \cdot 10^{-10}\,s^{10} + \ldots .)\ln s + 0.19245 -$$

$$- 1.5918 \cdot 10^{-1}\,s^1 + 4.829 \cdot 10^{-2}\,s^2 - 40.18 \cdot 10^{-4}\,s^4 -$$

$$- 83.53 \cdot 10^{-6}\,s^6 + 144.4 \cdot 10^{-7}\,s^7 - 130.5 \cdot 10^{-8}\,s^8 +$$

$$+ 258.6 \cdot 10^{-10}\,s^{10} + 90.6 \cdot 10^{-12}\,s^{12} - 122.3 \cdot 10^{-13}\,s^{13} +$$

$$+ 52.1 \cdot 10^{-14}\,s^{14} - \ldots] = \frac{P}{l_e^2} \cdot Z^0_{2,e}(s) \qquad (22{:}28)$$

The pressure p_0 under the loading centre is, quoted exactly

$$p_0 = \frac{1}{3\sqrt{3}} \frac{P}{l_r^2} \tag{22:29}$$

The distribution of pressure is shown in diagrammatical form in Fig. 22:6 A, page 51 for values $s \leq 4$. For higher s-values the series does not converge too well but it can be seen that if the asymptote values of J_0 for large-scale argument are inserted in the integral expression for (22:18),

$$J_0(r) \approx \sqrt{\frac{2}{\pi r}} \cos\left(r - \frac{\pi}{4}\right)$$

the pressure decreases very rapidly as s increases and that it is less than 0 the whole time. This also applies concerning the depression.

The flexural moments tangentially and radially are calculated in the usual way from the derivatives of vertical deformation

$$\left.\begin{aligned} m_r &= -D\left(\frac{d^2w}{dr^2} + \nu \frac{1}{r}\frac{dw}{dr}\right) \\ m_\varphi &= -D\left(\nu \frac{d^2w}{dr^2} + \frac{1}{r}\frac{dw}{dr}\right) \end{aligned}\right\} \tag{22:30}$$

At the centre point due to symmetry $m_r = m_\varphi$, and thus

$$m^+_{\max} = -D\frac{1+\nu}{2}\left(\frac{d^2w}{dr^2} + \frac{1}{r}\frac{dw}{dr}\right)_{r=0} = -D(1+\nu)\left(\frac{d^2w}{dr^2}\right)_{r=0} \tag{22:31}$$

By derivating the series for (22:26) one gets

$$\begin{aligned} D\frac{d^2w}{dr^2} = P\,[&(0.07958 - 60.42\cdot 10^{-6}s^6 + 69.5\cdot 10^{-12}s^{12}\ldots\ldots)\ln s + \\ &+ 0.03056 - 3.608\cdot 10^{-2}s^2 + 14.15\cdot 10^{-3}s^3 - 25.06\cdot 10^{-4}s^4 + \\ &+ 116.72\cdot 10^{-6}s^6 + 117.46\cdot 10^{-8}s^8 - 162.01\cdot 10^{-9}s^9 + \\ &+ 119.64\cdot 10^{-10}s^{10} - 177.7\cdot 10^{-12}s^{12} - 43.4\cdot 10^{-14}s^{14} + \\ &+ 41.34\cdot 10^{-15}s^{15} - 16.0\cdot 10^{-16}s^{16} + \ldots] = P\cdot Z^0_{3,e}(s) \end{aligned} \tag{22:32}$$

$$D\,\frac{1}{r}\,\frac{dw}{dr} = P\,\big[(0.07958 - 8.632\cdot 10^{-6}\,s^{6} + 5.35\cdot 10^{-12}\,s^{12}\ldots)\ln s -$$
$$- 0.04902 - 1.203\cdot 10^{-2}\,s^{2} + 3.537\cdot 10^{-3}\,s^{3} -$$
$$- 5.012\cdot 10^{-4}\,s^{4} + 17.91\cdot 10^{-6}\,s^{6} + 13.05\cdot 10^{-8}\,s^{8} -$$
$$- 16.20\cdot 10^{-9}\,s^{9} + 10.87\cdot 10^{-10}\,s^{10} - 14.08\cdot 10^{-12}\,s^{12} -$$
$$- 2.893\cdot 10^{-14}\,s^{14} + 2.584\cdot 10^{-15}\,s^{15} -$$
$$- 1.00\cdot 10^{-16}\,s^{16} + \ldots\big] = P\cdot Z^{0}_{4\varrho}(s) \qquad (22{:}33)$$

The series (22:32) and (22:33)[1]) are calculated and stated in the form of curves in Fig. 22:7, page 52 for values of $s \leq 6$. For higher values of s more terms are necessary but it can be seen that the expression goes rapidly towards 0 as s increases.

The flexural moments radially and tangentially become, expressed in these series:

$$\left.\begin{aligned} m_r &= -\,P\,[Z^{0}_{3\varrho}(s) + \nu\,Z^{0}_{4\varrho}(s)] \\ m_\varphi &= -\,P\,[Z^{0}_{4\varrho}(s) + \nu\,Z^{0}_{3\varrho}(s)] \end{aligned}\right\} \qquad (22{:}34)$$

Since ν is a small quantity (in the case of reinforced concrete ν is usually put as being equal to 0), then the distribution of the radial moment can be made apparent to a great extent by the $Z^{0}_{3\varrho}$ curve while the tangential moment largely follows the $Z^{0}_{4\varrho}$ curve (Fig. 22:7).

The moment values at the centre point can be obtained by derivating the integral (22:21) and inserting the result in the equation (22:31). An infinitely large value is thus obtained, this also being shown by the series (22:32; 22:33). This depends on the fact that the elementary slab theory used here does not apply close to the point at which the load is applied. In practice, however, load distribution is always so great that the elementary theory can be used also for the area under loading.

The maximum negative moment occurs, as shown in Fig. 22:7 at a distance $s \approx 1.9$ from the point where the load is applied and is

$$m^{-}_{\max} = -\,0.0195\cdot P \quad \text{for } \nu = 0 \text{ (reinforced concrete)}$$
$$m^{-}_{\max} = -\,0.0165\cdot P \quad \text{for } \nu = 0.15 \text{ (plain concrete)}$$

[1]) In the paper by HOGG [28] mentioned, the terms up to s^{8} in these series have been calculated and curves for values of $s \leq 2$ have been drawn.

222.2. *Distributed load*

Only the case where the load is uniformly distributed over a circular surface will be considered. This load distribution does not naturally agree with that resulting in practice by the pressure from a rubber wheel since in this case the load contact surface is generally more or less extended. Both theoretical and experimental analysis have shown, however, that the influence of this deviation from the circular distribution of loading is small[1]) and that the calculations for the distributed load in the majority of cases can be based on the assumption that the pressure contact surface is circular and that the uniformly distributed load corresponds to the air pressure in the wheel. In principle the methods given below can naturally be applied to load contact surfaces with arbitrary shape[2]) and load distribution.

The loading factor. If the pressure from the wheel (thus = air pressure in wheel) = p, then the load distribution radius c thus can be calculated from

$$p = \frac{P}{\pi c^2} \tag{22:35}$$

The loading factor for this case of loading will thus be, according to (22:12 b)

$$P(\alpha) = \frac{P}{\pi c^2} \cdot \int_0^c t\, J_0(\alpha t)\, dt = \frac{P}{\pi c} \frac{J_1(\alpha c)}{\alpha} \tag{22:36}$$

Depression. By inserting this expression and the expression (22:19) for the soil factor in the equation (22:17) an expression is thus obtained for the depression of the soil caused by a distributed load

$$w(r) = \frac{P}{\pi c} \frac{2}{C} \int_0^\infty \frac{J_0(\alpha r) \cdot J_1(\alpha c)}{\alpha\,(1 + \alpha^3 l_e^3)}\, d\alpha \tag{22:37}$$

The integral (22:37) is difficult to calculate. The depression at the centre point is obtained in a simpler way from the earlier calculated series Z^0_{1e} (22:26) for the depression of the soil due to a *concentrated* load if it is observed that this expression is simultaneously the influence function for the depression at the centre point of the slab due to a concentrated

[1]) See, for example, Bergström and assoc. [4], page 48.

[2]) See Pickett-Ray [57].

load at a certain distance from this point. The depression in the centre caused by ring-shaped distributed loading on the area element between r and $r + dr$ is thus

$$dw = \frac{P}{\pi c^2} \, 2 \pi r \, dr \, \frac{l_e^2}{D} \, Z_{1e}^0 \left(\frac{r}{l_e} \right)$$

and from the complete loading on the load distribution surface the depression in the centre thus is

$$w_0 = \frac{2 P l_e^2}{D c^2} \int_0^c r \, Z_{1e}^0 \left(\frac{r}{l_e} \right) dr$$

If the load distribution radius is written in a dimension-free form by the introduction of the notation

$$a_e = \frac{c}{l_e} = \text{relative load distribution} \tag{22:38}$$

one gets

$$w_0 = \frac{2 P l_e^2}{D a_e^2} \int_0^{a_e} s \, Z_{1e}^0(s) \, ds \tag{22:39}$$

which through integration gives the series

$$w_0 = \frac{P l_e^2}{D} (0.1925 - 0.0272 \, a_e^2 + 0.0199 \, a_e^2 \ln a_e \ldots) \tag{22:40}$$

Only the first terms have been included here since the load distribution is rarely so great that the other terms have any influence (formula (22:40) applies for $a_e \leq$ about 1.5). The values for depression in the centre have been calculated and have been shown in a diagrammatic form in Fig. 22:5 B page 50 for a relative load distribution $a_e \leq 6$, in which case more terms have naturally been included when intergrating (22:39).

In order to obtain the remaining appearance of the depression curve in the case of distributed loads one can proceed in a corresponding way to that recently given for the calculation of the centre point value and thus start from the curve for a concentrated load regarded as an influence function. Fig. 22:3 shows the calculating method and integration is carried out here numerically by a suitable division of the loading surface

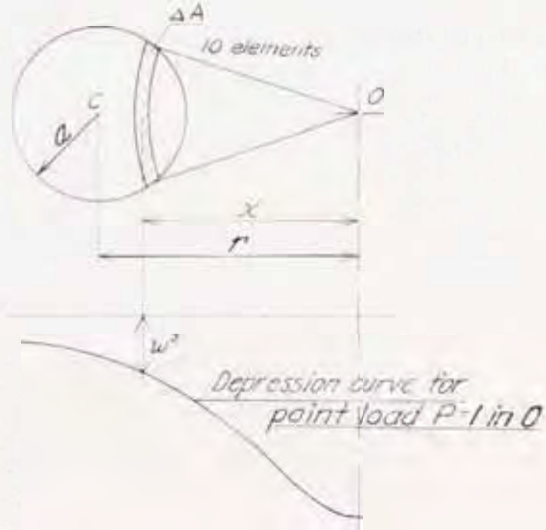

Fig. 22:3. Calculation of the depression due to a circularly distributed load $p = \frac{P}{\pi c^2}$ with the help of the depression curve for a concentrated load. The depression in the point O due to the load $p\,\Delta A$ on a curved element ΔA with the centre point at O is = the depression under the element due to the same load $p\,\Delta A$ at O $= p\,\Delta A\,w_x^\circ$. The depression at O due to the entire distributed load will thus be

$$w_r = \sum_{n=1}^{10} p\,\Delta A\,w_x^\circ$$

into curved elements with a centre point at the point O, the depression of which is to be calculated. In this way the depression curves for several different values of the relative load distribution radius have been obtained. For calculation, the loading surface has been divided up into ten elements. The result is shown by the curves in Fig. 22:5 A, page 50. The diagram shows that the depression outside the load distribution surface coincides to a great extent with the depression curve for a concentrated load.

The distribution of pressure in the case of circular load distribution is obtained from (22:18)

$$p_z = \frac{P}{\pi c} \cdot \int_0^\infty \frac{J_0(\alpha r) \cdot J_1(\alpha c)}{1 + \alpha^3 l_e^3}\, d\alpha \tag{22:41}$$

The calculation of this integral is also troublesome and it is simpler to calculate the distribution of pressure from the pressure distribution curve Z^0_{2e} (22:28) for a concentrated load, considered as an influence function, in the same way as described above concerning the depression.

The pressure p_0 in the loading centre point is thus obtained from the expression

$$p_0 = \frac{2\,P}{l_e^2\, a_e^2} \int\limits_0^{a_e} s\, Z^0_{2e}(s)\, ds \tag{22:42}$$

and after integration the series

$$p_0 = \frac{P}{l_e^2}\,(0.1925 - 0.1061\, a_e + 0.0242\, a_e^2 + \ldots\ldots) \tag{22:43}$$

is obtained, whereby only the first terms have been included (applies when $a \leq$ about 1.5). The soil pressure at the centre of loading has been calculated for several values of the relative distribution of loading and shown by the curve in Fig. 22:6 B whereby more terms of the series have been included in series (22:43).

The distribution of pressure has otherwise been calculated for various different values of the relative load distribution a_e in accordance with the method quoted above for the calculation of the depression curves. The result is shown in Fig. 22:6 A page 51. It can also be seen that the pressure distribution curves become rapidly similar to the pressure distribution curve for a concentrated load as soon as they pass outside the edge of load distribution. Compared with the depression, however, the influence of load distribution on the pressure close to the centre is of more significance.

Flexural moment. When calculating the moment under the loading centre it is simplest to start from the integral expression (22:37) for the depression and insert this expression in the expression (22:31) for the moment at the loading centre. One thus obtains

$$\left(\frac{d^2 w}{dr^2}\right)_{r=0} = -\frac{P}{2\,\pi\, c}\,\frac{2}{C}\int\limits_0^{\infty}\frac{\varkappa\, J_1(\varkappa c)}{1 - \varkappa^3\,\dfrac{2\,D}{C}}\, d\varkappa \tag{22:44}$$

This expression is identical with the expression for $\dfrac{1}{r}\,\dfrac{dw^0}{dr}$ where w^0 is the integral (22:21) for the depression in the case of a concentrated load if r is replaced by c. The moment at the centre in the case of a distributed load thus can be obtained from the series (22:33) and the corresponding curve in Fig. 22:7 if s is replaced by a_e and thus is obtained

$$m^{+}_{\max} = - P\,(1 + \nu)\, Z^0_{4e}(a_e) \tag{22:45}$$

When calculating the values of the tangential and radial moments at points outside the loading centre a procedure can be used which is similar to that used for the calculation of the depression and the soil pressure. As earlier the loading surface is divided into a suitable number of curved area elements (see Fig. 22:4). The moment contributions from the various points along each such curved element cannot be added up directly since the moment is a vectoral magnitude and the load from the various elements dA in the curved elements gives moment values at the point O which turn at right angles to or along the radius between O and the element in question. This is also the reason why it is not possible to calculate the moment at the centre point by integrating in the same way as in the earlier determination of the depression and the soil pressure at the centre point.

From the load on the given area element dA in Fig. 22:4 in a certain curved element ΔA of the loading surface, the figure shows that an elementary contribution dm_r is obtained to the radial moment m_r at the point O

$$\begin{aligned} dm_r &= dm^{\vartheta}_r \cos^2\vartheta + dm^{\vartheta}_{\varphi} \sin^2\vartheta = \\ &= -\left[(Z^0_{3e} + \nu\, Z^0_{4e}) \cos^2\vartheta + (Z^0_{4e} + \nu\, Z^0_{3e}) \sin^2\vartheta\right] p\, dA \end{aligned} \tag{a}$$

whereby the expression (22:34) is applied and Z^0_{3e} and Z^0_{4e} are the series (22:32) and (22:33) for the calculation of the moment due to a concentrated load. From the loading on the complete curved element ΔA, integration over the length of the curve gives a moment contribution

$$\begin{aligned} \Delta m_r &= - \int\limits_{-\alpha}^{+\alpha} \left[(Z^0_{3e} + \nu\, Z^0_{4e}) \cos^2\vartheta + (Z^0_{4e} + \nu\, Z^0_{3e}) \sin^2\vartheta\right] pr\, \Delta r\, d\vartheta = \\ &= - pr\, \Delta r \left\{\left[(\alpha + \tfrac{1}{2}\sin 2\alpha)\, Z^0_{3e} + (\alpha - \tfrac{1}{2}\sin 2\alpha)\, Z^0_{4e}\right] + \right. \\ &\quad \left. + \nu\left[(\alpha + \tfrac{1}{2}\sin 2\alpha)\, Z^0_{4e} + (\alpha - \tfrac{1}{2}\sin 2\alpha)\, Z^0_{3e}\right]\right\} \end{aligned} \tag{b}$$

In the same way when calculating the tangential moment it is found that

$$\begin{aligned} \Delta m_{\varphi} &= - pr\, \Delta r \left\{\left[(\alpha + \tfrac{1}{2}\sin 2\alpha)\, Z^0_{4e} + (\alpha - \tfrac{1}{2}\sin 2\alpha)\, Z^0_{3e}\right] + \right. \\ &\quad \left. + \nu\left[(\alpha + \tfrac{1}{2}\sin 2\alpha)\, Z^0_{3e} + (\alpha - \tfrac{1}{2}\sin 2\alpha)\, Z^0_{4e}\right]\right\}. \end{aligned} \tag{c}$$

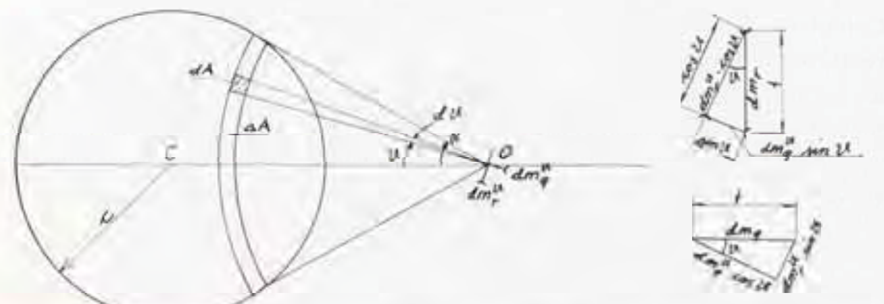

Fig. 22:4. Calculation of the flexural moment in the slab due to a circularly distributed load $p = \frac{P}{\pi c^2}$. From the load on the surface element dA is obtained at the point O, at right angles to and parallel with the connecting line between dA and O respectively, the moment components dm_r^ϑ and dm_φ^ϑ which can be calculated as the moments of a concentrated load from the expressions (22:32), (22:33) and (22:34) or from the corresponding curves in Fig. 22:7. The contribution of these "elemental moments" to the radial and tangential flexural moments respectively at the point O due to the circularly distributed load P are obtained if tringular slab elements is considered at the point O with one side $= 1$ at right angles to or parallel with the radius OC and the other sides parallel with the moment components dm_r^ϑ and dm_φ^ϑ. The equilibrium equations of these triangular elements give

$$dm_r = dm_r^\vartheta \cos^2\vartheta + dm_\varphi^\vartheta \sin^2\vartheta$$

$$dm_\varphi = dm_r^\vartheta \sin^2\vartheta + dm_\varphi^\vartheta \cos^2\vartheta$$

The contribution from the complete arc element ΔA is obtained by integrating over the arc, and the moments m_r and m_φ of the complete loading surface by adding up the contributions from the 10 arc elements.

The moment due to the complete loading P is obtained by adding up the expressions (b) and (c) for all the curved elements.

If (b) and (c) are compared with the expressions (22:30) and (22:34) for the moment due to a concentrated load it can be seen that the derivative expressions in the case of a distributed load, which correspond to (22:32) and (22:33) in the case of concentrated load, can be thus calculated:

$$D\,\frac{d^2w}{dr^2} = P\sum_0^n -\frac{r\,\Delta r}{\pi c^2}\left[\left(\alpha + \tfrac{1}{2}\sin 2\alpha\right)Z_{3e}^0 + \left(\alpha - \tfrac{1}{2}\sin 2\alpha\right)Z_{4e}^0\right] = P\cdot Z_{3e} \qquad \text{(d)}$$

$$D\,\frac{1}{r}\,\frac{dw}{dr} = P\sum_0^n -\frac{r\,\Delta r}{\pi c^2}\left[\left(\alpha + \tfrac{1}{2}\sin 2\alpha\right)Z_{4e}^0 + \left(\alpha - \tfrac{1}{2}\sin 2\alpha\right)Z_{3e}^0\right] = P\cdot Z_{4e} \qquad \text{(e)}$$

Calculations have been carried out for several different values of the relative load distribution and distance from the centre of loading, whereby as before, the loading surface has been divided up into ten curved elements. The result has been presented as curves for Z_{3_ϱ} and Z_{4_ϱ} and these are shown in Fig. 22:7, page 52. Through these curves it is thus possible to calculate the moments, namely:

$$\left.\begin{aligned} m_r &= - P\,(Z_{3_\varrho} + \nu\, Z_{4_\varrho}) \\ m_\varphi &= - P\,(Z_{4_\varrho} + \nu\, Z_{3_\varrho}) \end{aligned}\right\} \qquad (22{:}46)$$

It becomes apparent by the Z_{4_ϱ}-curves which approximately correspond to the distribution of the tangential moment, that this moment is, on the whole, only influenced by the load distribution within its own zone while the moment curve outside the edge of the load distribution surface rapidly approaches the corresponding curve for a concentrated load. This does not, however, apply to the moment curves Z_{3_ϱ} (approximately corresponding to the distribution of the radial moment), the complete appearance of which is influenced by the load distribution. In the case of increased load distribution the negative moment maximum is displaced outwards to a point outside the edge of the loading surface, and its value decreases rapidly with increased load distribution. The value of $m^-_{\max}$ has been calculated from the various curves and has been marked in on a special diagram in Fig. 22:7.

223. Resilient subgrade

Subgrade factor. With this type of soil, the subgrade factor (22:8 b) is

$$K(\varkappa) = \lim_{\varepsilon \to 0} \int_0^{\varepsilon} \frac{2\pi}{k}\,\frac{J_0(\varkappa t)}{\pi\,\varepsilon^2}\, t\, dt = \frac{1}{k} \qquad (22{:}47)$$

Concentrated load. If this expression (22:47) together with the loading factor (22:20) for a concentrated load is inserted in the equation (22:17) then the expression for depression in this case becomes

$$w(r) = \frac{P}{2\pi} \int_0^{\infty} \frac{\varkappa}{k + D\,\varkappa^4}\, J_0(\varkappa r)\, d\varkappa \qquad (22{:}48)$$

It can be shown that this integral is identical with the solution obtained by Herz [27] when he proceeded directly from the differential equation of the slab, in which the loading term in the case of resilient subgrade can be directly expressed by the depression, thus

$$D \cdot \Delta\Delta\, w(r) = p(r) - k \cdot w(r) \tag{22:49}$$

The solution for the slab of infinite dimensions can be written in the form[1])

$$w(s) = -\frac{P\, l_k^2}{8\, D}\, \frac{4}{\pi}\, \text{kei}\, s = \frac{P\, l_k^2}{D}\; Z_{1k}^0(s) \tag{22:50}$$

whereby it is written in a dimension-less form in the same way as in the theory for elastic subgrade with the help of the elastic radius of rigidity[2]), which here has the form

$$l_k = \sqrt[4]{\frac{D}{k}} \tag{22:51}$$

The depression at the loading centre w_0 becomes

$$w_0 = \frac{P\, l_k^2}{8\, D} \tag{22:52}$$

The depression function Z_{1k}^0 is shown in Fig. 22:8 A, page 53

The distribution of pressure between the slab and the soil is in this case

$$p_s(s) = k\, w(s) = \frac{P}{l_k^2}\; Z_{1k}^0(s) \tag{22:53}$$

and is thus also represented by the function Z_{1k}^0 and the diagram in Fig. 22:8 A.

The flexural moments m_r and m_φ are calculated in the usual way according to the equation (22:30) and (22:31) and are thus obtained through derivatives of the expression (22:50) for depression. These derivatives are shown in Fig. 22:9 with the notations of $Z_{3k}^0 = D\, \frac{d^2 w}{dr^2}$ and $Z_{4k}^0 = D\, \frac{1}{r}\, \frac{dw}{dr}$. Also in this case the value of the moment in the loading point becomes infinitely large. The maximum negative moment

---

1) Concerning the Bessel function kei see note 1, page 45, and Mc Lachlan [49].

2) In this form the solution was given by Schleicher [60] who thereby introduced the conception of elastic radius of rigidity as an expression for the elastic properties of the slab and the soil with this type of soil. See page 32, note 1.

occurs as shown in Fig. 22:9 at a distance $s \approx 1.5$ from the load point and is:

$$m^-_{max} = -\,0.025\,P \text{ for } \nu = 0$$

$$m^-_{max} = -\,0.022\,P \text{ for } \nu = 0.15$$

The influence of load distribution. In the case where the load is uniformly distributed over a circular loading surface with radius c, then solutions can be obtained in the same way as earlier by inserting the expressions for the subgrade and loading factors in the equation (22:17). Due to the difficulties involved in solving this integral it is easier to come to results in another way.

The values of depression and moment at the centre point are obtained easiest in exactly the same way as the corresponding expression (22:40) and (22:45) concerning the type of soil earlier considered. By starting with the depression curve (22:50) for a concentrated load and here replacing the Bessels function kei with a corresponding series expression in powers and logarithmic functions[1]), integration over the loading surface will result in the formulae

$$w_0 = \frac{P\,l_k^2}{8\,D}\,(1 - 0.2174\,a_k^2 + 0.8440\,a_k^2 \ln a_k \ldots) \qquad (22:54)$$

$$m^+_{max} = P\,(1 + \nu)\,(0.04901 - 0.07958 \ln a_k + 0.0781\,a_k^2) \qquad (22:55)$$

where a_k is the load distribution radius c expressed in a dimension-less form through the relationship

$$a_k = \frac{c}{l_k} \qquad (22:56)$$

These expressions are identical with Westergaards formulae for depression and moment [72]. These formulae only concern relatively limited values of load distribution ($a_k <$ about 1.0), since only the first terms in the series have been included. In Fig. 22:8 B and Fig. 22:9 the curves for w_0 and m have been marked in for values of $a_k < 5.0$, more accurate methods having been used for this calculation (see below).

In order to calculate the values of depression and moment in the points outside the loading centre it is simplest to start from the general solution of the differential equation (22:49), which solution has been carried out by Schleicher [60]. For this particular case (slab of infinite dimensions) one can write

---

[1]) See note 1), page 45.

$$\left.\begin{aligned} w(s) &= \frac{P}{\pi a_k^2} \frac{l_k^2}{D} (1 - c_1 \cdot \operatorname{ber} s - c_2 \cdot \operatorname{bei} s) \qquad 0 < s < a_k \\ w(s) &= \frac{P}{\pi a_k^2} \frac{l_k^2}{D} (c_3 \cdot \operatorname{ker} s + c_4 \cdot \operatorname{kei} s) \qquad s > a_k \end{aligned}\right\} \quad (22{:}57)$$

where the integration constants c_1, c_2, c_3 and c_4 are determined from the boundary conditions at the dividing line between the loaded and unloaded zones.[1]) The moment is obtained in the usual way by derivation of the equation (22:57) according to the expressions (22:30). In this way the depression and moment distribution at several values of relative load distribution have been calculated (also for the case where the load distribution $= 0$). The result is shown by the diagrams in Fig. 22:8 A and 22:8 B, page 53 and Fig. 22:9 page 54. It becomes apparent from Fig. 22:8 A that the depression (and thereby also the pressure distribution) outside the load distribution surface rapidly approaches the corresponding curve for a concentrated load in the same way as was the case with the corresponding curves for the elastic subgrade. The same applies to the tangential moment as shown in Fig. 22:9 while the distribution of the radial moment on the whole is strongly influenced by the load distribution in the same way as in the case of the corresponding moment curves for the type of subgrade earlier considered.

In the same way as with the elastic subgrade (see page 39, equation (22:44) and (22:45)), it can be shown that the curve $Z_{4k}^0 = \frac{1}{r} \frac{dw^0}{dr}$, concerning a concentrated load, also represents the relationship between the moment in the loading centre and the relative load distribution in the case of a distributed load, thus

$$m_{\max}^{+} = - P\,(1 + \nu)\, Z_{4k}^0(a_k) \qquad (22{:}58)$$

The value of $m_{\max}^{-}$ for various load distributions have been calculated from the curves and marked in on a special diagram in Fig. 22:9.

---

[1]) Concerning the meaning of the Bessels functions ber, bei, ker and kei introduced by KELVIN, reference is made to MC LACHLAN [49]. SCHLEICHER [60] has written the solutions (22:50) and (22:57) with his own function notations

$$Z_1(x) = \operatorname{ber} x \qquad Z_3(x) = -\frac{2}{\pi} \operatorname{kei} x$$

$$Z_2(x) = -\operatorname{bei} x \qquad Z_4(x) = -\frac{2}{\pi} \operatorname{ker} x$$

In both [49] and [60] the functions and their respective derivatives are tabled, and these tables have been used by the author when making calculations for the diagram in Fig. 22:8 A and B and Fig. 22:9.

224. Slabs with finite extent

The results hitherto quoted concern slabs with *infinite* dimensions. With the cases occurring in practice, however, slabs with *finite* extent must naturally be considered. It appears however probable that even slabs with relatively moderate extent can be dealt with according to the theory for slabs of infinite extent, the degree of approximation being sufficiently good.

As far as slabs on elastic subgrade are concerned, this question can be studied with the help of the results obtained by Bergström on the bases of his difference method [4, 5] (see page 23). Bergström thereby divides the slab into four ring elements, the inner of which has the same extent as the centre loading surface, and he makes the soil pressure under each of these elements constant. The depression of the soil under each element can then be written according to the expression for soil depression under constant loading given by Schleicher [59] and the deformation of the slab can be expressed by means of the differential equation of the plate (22:1), which can easily be solved on the assumption that the loading is of this simple step form. If these deformations are assumed to be similar in the centre of the elements, a sufficient number of equations is obtained to calculate the unknown soil pressure under each element. Bergström has carried out calculations for $\nu = 0.15$ (plain concrete) and given the result in the form of diagrams showing the soil pressure under the elements as well as the depression and the moment at the centre, these diagrams showing the connection curves between these magnitudes and the radius of the slab in the case of various load distributions relative to the radius of the slab.

By comparing the results for slabs with increasing radius, Bergström has shown that the depression and moment at the loading centre rapidly approaches the corresponding values for a slab of infinite dimensions, while the convergency is not so good concerning soil pressure. The conditions can however be observed more clearly if the values according to Bergström's curves are re-written through the same parameter for the slab as earlier used by the author, namely the elastic radius of rigidity

$$l_e = \sqrt[3]{\frac{2\,D}{C}}$$

The results are shown as curves of the same type as for the slab of infinite dimensions used to demonstrate the distribution of soil pressure under the slab as well as depression and moment at the loading centre (Fig. 22:5 B as well as Fig. 22:6 A and 22:7). The pressure distribution curves in this form can also be checked and adjusted in a simple way by a numerical calculation of the pressure volume, since

$$P = \int^{A} p_s \, dA$$

The result is shown by the Figures 22:10, 22:11 and 22:12, and by way of comparison the corresponding curves for the slab of infinite extent have been inserted. The figures show that the variations between the conditions in the case of small and infinitely large slabs are great, at least as far as pressure distribution and depression are concerned, but it also becomes apparent that these variations decrease very rapidly as the radius of the slab increases. Even with a relative slab radius $\frac{R}{l_e} = 3.0$ agreement with the slab of infinite dimensions is very good, and with a relative slab radius $= 5.0$, practically exact. Concerning the flexural moment at the centre point the agreement with the slab of infinite dimensions is good even with a relative slab radius $= 1.5$ and perfect with a relative slab radius $= 3.0$.

In the case of resilient subgrade it is possible to obtain exact solutions also for slabs with finite radii from the differential equation of the slab (22:49). The case has been considered by SCHLEICHER [60]. For the sake of simplicity the slab here is considered only to be influenced by a concentrated load in the centre in which case the depression can be written

$$w(s) = \frac{P}{2\pi} \frac{l_k^2}{D} (d_1 \operatorname{ber} s + d_2 \operatorname{bei} s - \operatorname{kei} s) \qquad (22:59)$$

The integration constants d_1 and d_2 are determined from the boundary conditions at the free edge of the plate where flexural moments and shearing forces are equal to zero. The moments are obtained by derivation of (22:59) according to the expressions (22:30).

In this way the depression curves and the distribution of moment for various radii of a finite slab have been calculated. The result is shown in Fig. 22:13 and 22:14, page 58 and 59. In the same way as earlier it can be shown that the curves for m_φ in Fig. 22:14 also represent the connection between the moment in the centre of the slab and the relative load distribution. Figs. 22:13 and 22:14 show that the depression and moment distribution, as slab radius increases, rapidly approach the corresponding values for the slabs of infinite dimensions. With a relative slab radius $\frac{R}{l_k} = 5$ agreement is practically complete except in the zone nearest the free slab edge.

It may be possible to imply that the depression and moment distribution in the case of slabs with finite extent on *elastic* subgrade show similar agreement with the corresponding values for slabs of infinite dimensions. The fact that there is good agreement concerning the values at the loading centre for depression and moment as well as for the soil pressure distribution has been shown above.

The investigations in this section of the paper thus show that concerning slabs with finite radii, good approximation can be obtained by applying the formulae valid for slabs of infinite extent. Agreement is good concerning depression and soil pressure where the slabs have a radius greater than about $3\,l$ and they are practically exact concerning flexural moment with a plate of a radius greater than about $3\,l$ and depression and soil pressure with plates with a radius greater than about $5\,l$. Agreement is not quite so good only in the zones nearest the edge.

225. **Summary of results**

The most important of the formulae arrived at in this previous section, namely the expressions for depression, soil pressure and moment at the loading centre, have been placed together in Table 22:1 below. The formulae, which actually concern slabs of infinite extent, can be used as shown in 224 without any larger errors occurring also in the case of finite slabs where the load is fairly far from the edge. In the table the corresponding formulae for both the types of soil considered have been set up beside each other and have been rewritten in such a way that they can be easily compared. In the series expressions so many terms have been included that the degree of error is less than approx. 1 %, where the distribution of load is equal to the relative radius of stiffness. In the series terms ${}^{10}\log$ have been introduced instead of ${}^{e}\log$.

The diagrams showing the results of the calculations in the previous sections have been collected on the following pages, 50—59, Fig. 22:5—22:14.

If the formulae in Table 22:1 for resilient and elastic subgrade are compared, it will be found that from a purely formal point of view there are large similarities. This applies particularly to the formulae for the flexural moment at the loading centre, in which case the formulae are practically identical. This shows that the relative radius of stiffness expressed in the way suggested by the author is a comparable fundamental magnitude for both the theories.

If the curves for the same magnitude for both the theories of soil are

TABLE 22:1. Formulae for depression, soil pressure and flexural moment in the loading centre concerning an elastic slab on resilient as well as elastic subgrade.

	Resilient subgrade	Elastic subgrade
Elastic radius of rigidity	$l_k = \sqrt[4]{\frac{D}{k}}$	$l_e = \sqrt[3]{\frac{2D}{C}}$
Rel. load distribution	$a_k = \frac{c}{l_k}$	$a_e = \frac{c}{l_e}$
Centre depression	$w_0 = \frac{P l_k^2}{8 D} [1 - a_k^2 (0.217 - 0.367 \, {}^{10}log \, a_k)]$	$w_0 = \frac{P l_e^2}{3\sqrt{3} \cdot D} [1 - a_e^2 (0.144 - 0.238 \, {}^{10}log \, a_e)]$
Centre soil pressure	$p_0 = \frac{P}{8 l_k^2} [1 - a_k^2 (0.217 - 0.367 \, {}^{10}log \, a_k)]$	$p_0 = \frac{P}{3\sqrt{3} \cdot l_e^2} [1 - 0.552 \, a_e + 0.126 \cdot a_e^2)]$
Centre moment	$m_{max}^{+} = - P (1 + \nu) [0.1833 \, {}^{10}log \, a_k - 0.0490 - 0.0078 \, a_k^2]$	$m_{max}^{+} = - P (1 + \nu) [0.1833 \, {}^{10}log \, a_e - 0.0490 - 0.0120 \, a_e^2]$

compared it is found that the pressure distribution curves show the greatest differences. In the case of elastic soil, the pressure distribution curve is more concentrated under the loading centre and the soil pressure decreases more rapidly with increased distance from the centre than the pressure distribution does in the case of resilient subgrade. If, for the sake of comparison, the vertical deformation is taken as being similar according to both the theories, then the soil pressure under the loading centre in the case of elastic subgrade is $\frac{64}{27}$ greater than in the case of Herz. The curve for depressions and moment do not show any great differences and, particularly the moment distribution curves according to the two theories are, in the neighbourhood of the loading centre, practically identical.

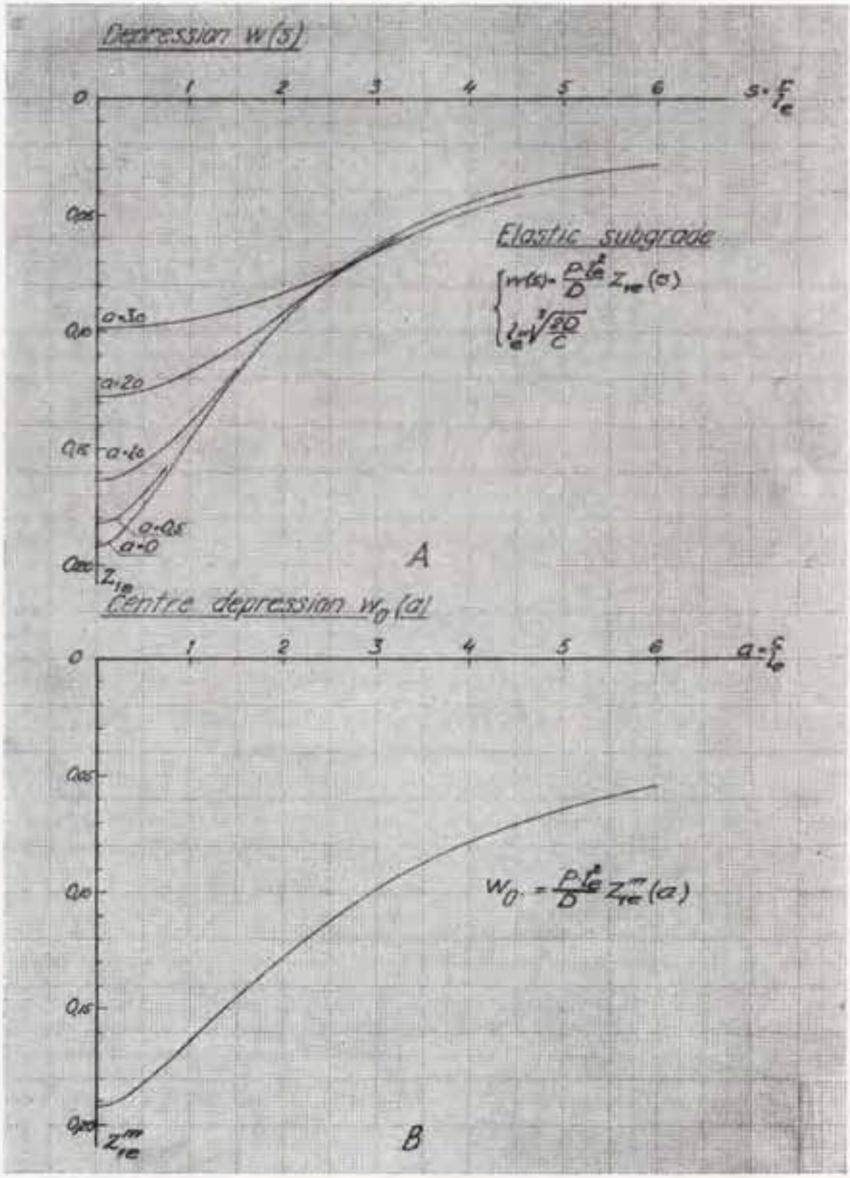

Fig. 22:5 A. The depression curves for an elastic slab of infinite extent on *elastic* subgrade with various relative load distribution $a_e = \frac{c}{l_e}$. The lower curve for $a = 0$ consists of the function Z_{1e}^0 (22:26), which, as influence curve for the depression at a certain point due to a concentrated load, has been utilized to calculate the other curves. See Fig. 22:3.

Fig. 22:5 B. The depression in the *loading centre* for an elastic slab of infinite extent on *elastic* subgrade with various load distribution $a_e = \frac{c}{l_e}$.

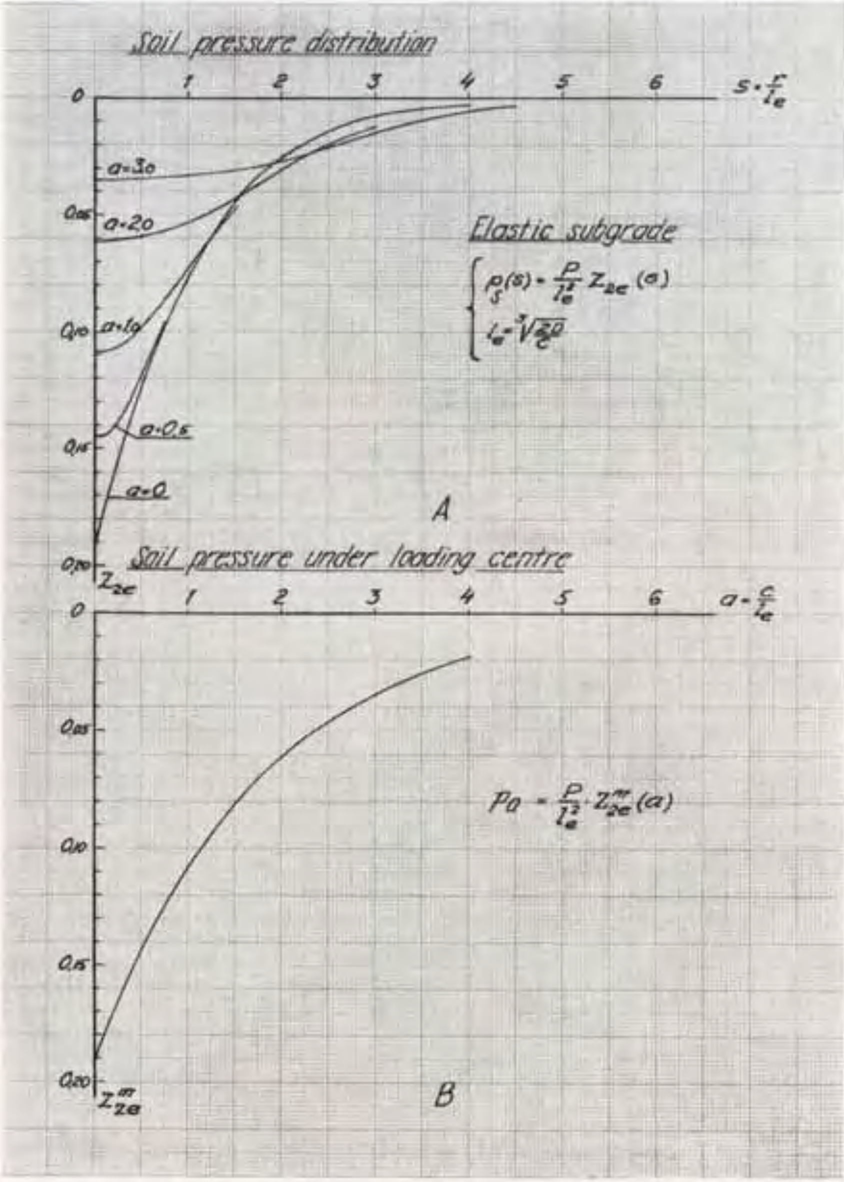

Fig. 22:6 A. The distribution of soil pressure under an infinite elastic slab on *elastic* subgrade with various relative load distribution $a_e=\dfrac{c}{l_e}$. The lower curve for $a=0$ consists of the function Z_{2e}^0 (22:28) which, as influence curve for the soil pressure due to a concentrated load, has been utilized to calculate the other curves.

Fig. 22:6 B. The soil pressure in the loading centre for an elastic slab of infinite extent on *elastic subgrade* with various relative load distribution $a_e=\dfrac{c}{l_e}$.

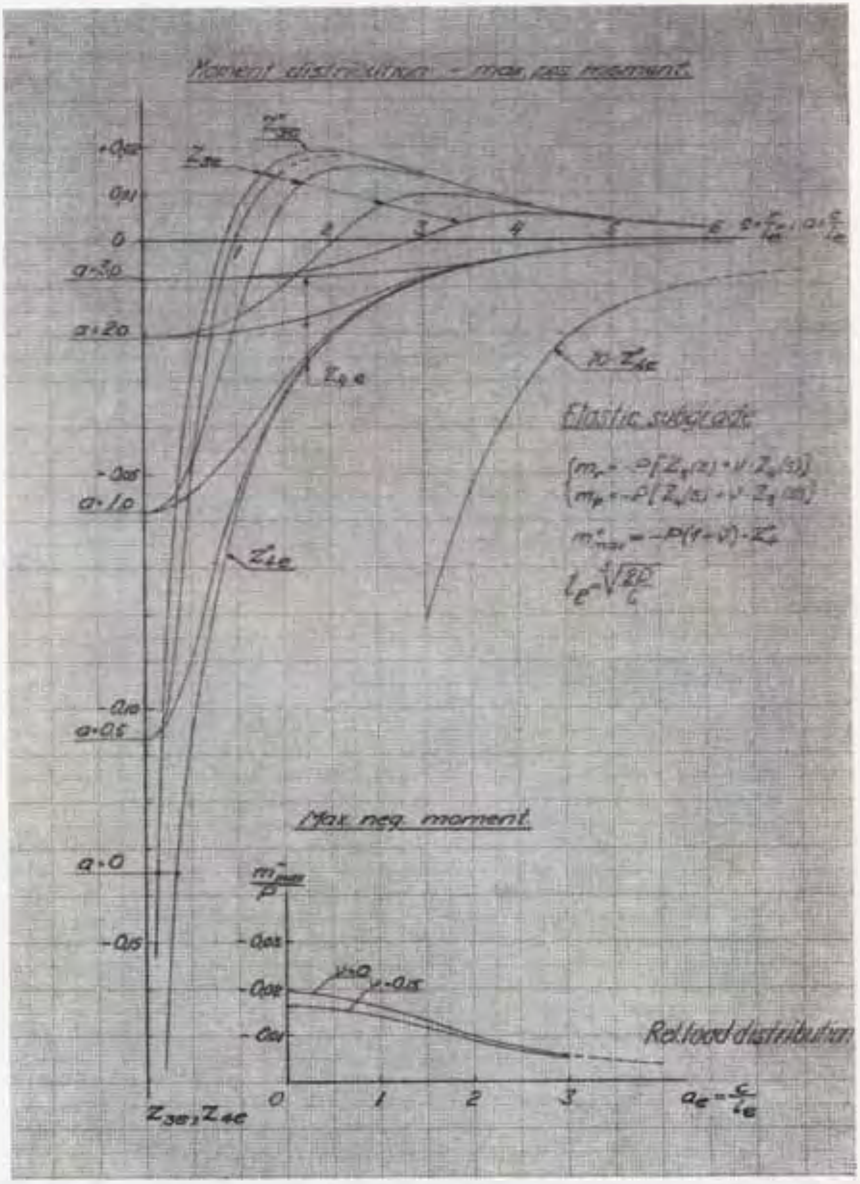

Fig. 22:7. The flexural moment in an elastic slab of infinite extent on *elastic* subgrade for various values of the relative load distribution $a_e = \frac{c}{l_e}$. The collection of curves Z_{3e} represents $D \frac{d^2w}{dr^2}$ and the collection of curves Z_{4e} represents $D \frac{1}{r} \frac{dw}{dr}$. Since ν is small (~ 0 for reinforced concrete), then the Z_3-curves represent on the whole the distribution of the radial moment and the Z_4-curves represent the distribution of the tangential moment. The Z^0-curves furthest out in both the curve collections apply to the concentrated load ($a = 0$) and represent the series (22:32) and (22:33), these curves have been used when calculating the other curves.

The curve Z^0_{4e} also represents the maximum flexural moment in the loading centre as a function of the relative load distribution a_e.

In the lower diagram, the values for the maximum radial top surface moment is compiled for $\nu = 0$ (the peak values of the Z_3-curves) and $\nu = 0.15$.

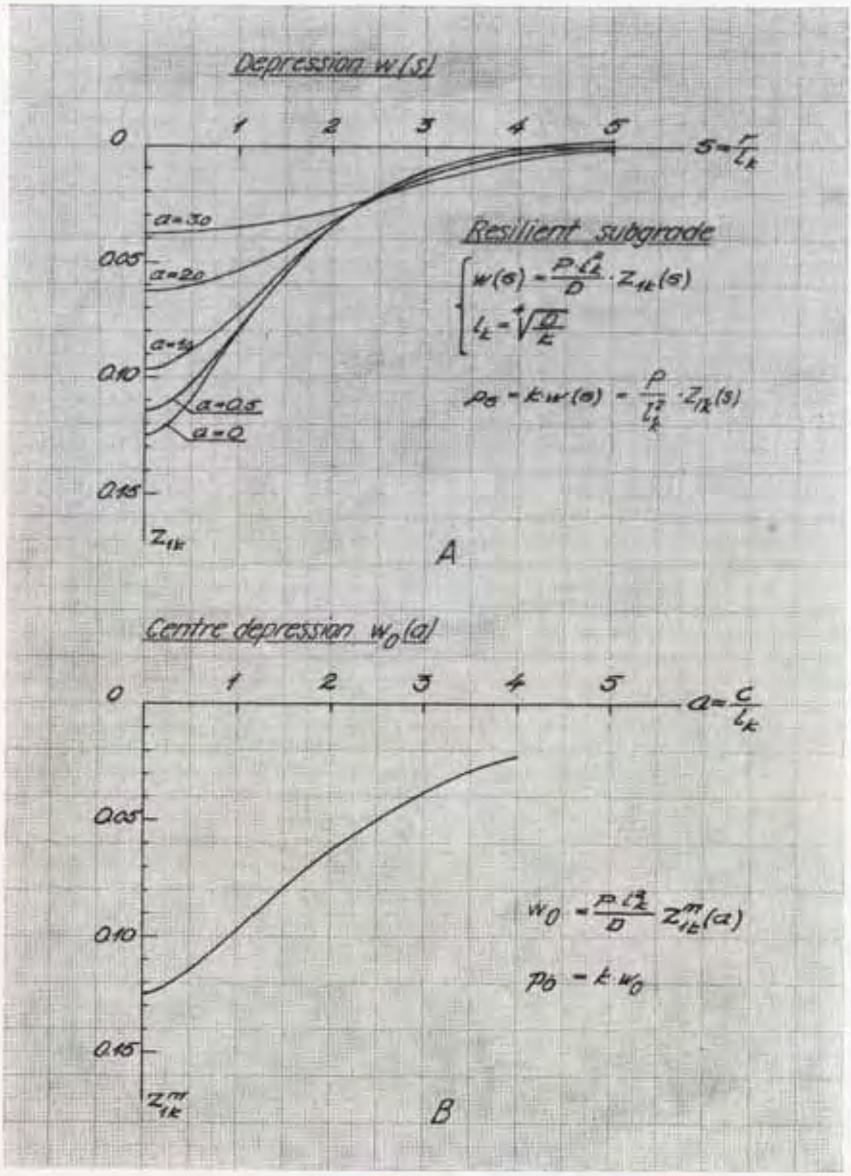

Fig. 22:8 A. The depression curves for an elastic slab of infinite extent on *resilient* subgrade with various relative load distribution $a_k = \frac{c}{l_k}$.

Fig. 22:8 B. The depression in the loading centre of an elastic slab of infinite extent on *resilient* subgrade with various relative load distribution $a_k = \frac{c}{l_k}$.

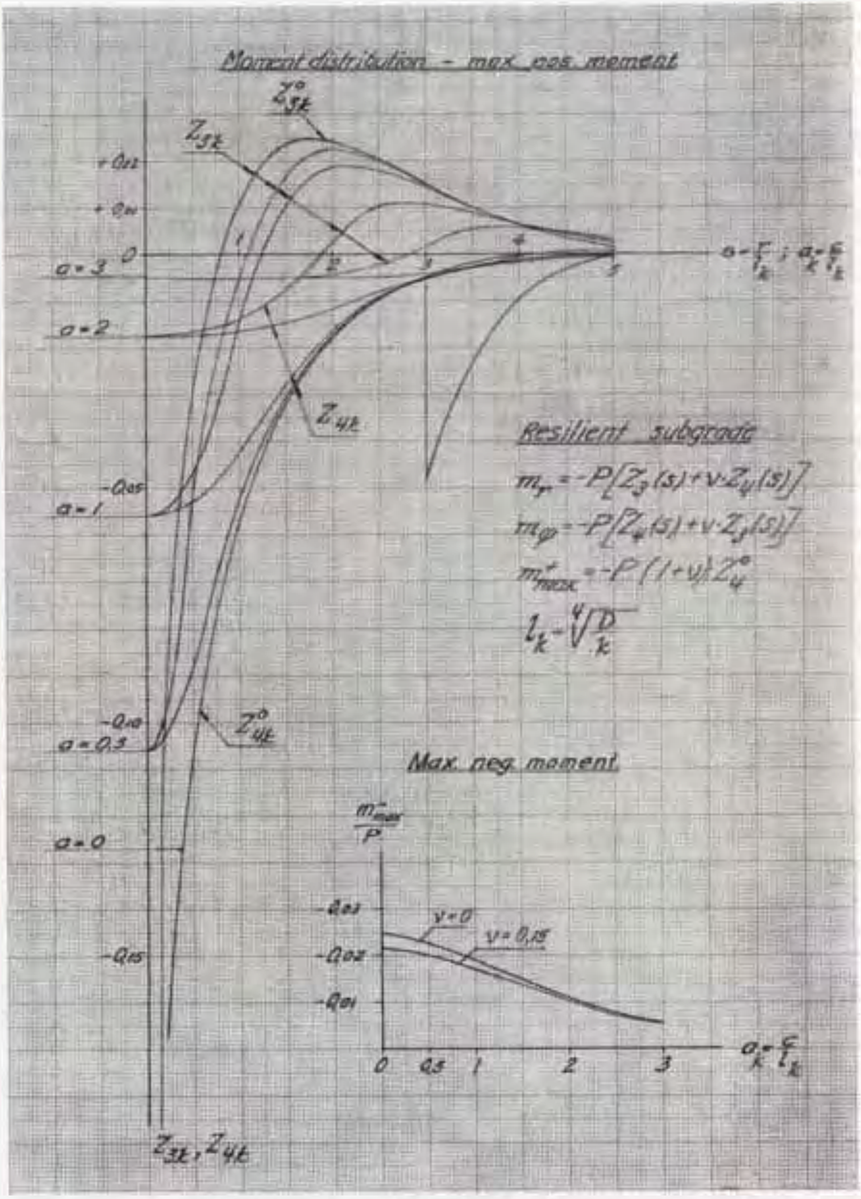

Fig. 22:9. The flexural moment in an elastic slab of infinite extent on *resilient* subgrade with various values of the relative load distribution $a_k = \frac{c}{l_k}$. The collection of curves $Z_{3k} = D \frac{d^2w}{dr^2}$ shows, on the whole, the distribution of the radial moment while the collection of curves $Z_{4k} = D \frac{1}{r} \frac{dw}{dr}$ shows, on the whole, the distribution of the tangential moment.

The Z^0_{4k} curve also represents the maximum flexural moment in the loading centre as a function of the relative load distribution a_k.

In the lower diagram, the values for the maximum negative top surface moment have been compiled for $\nu = 0$ and $\nu = 0.15$.

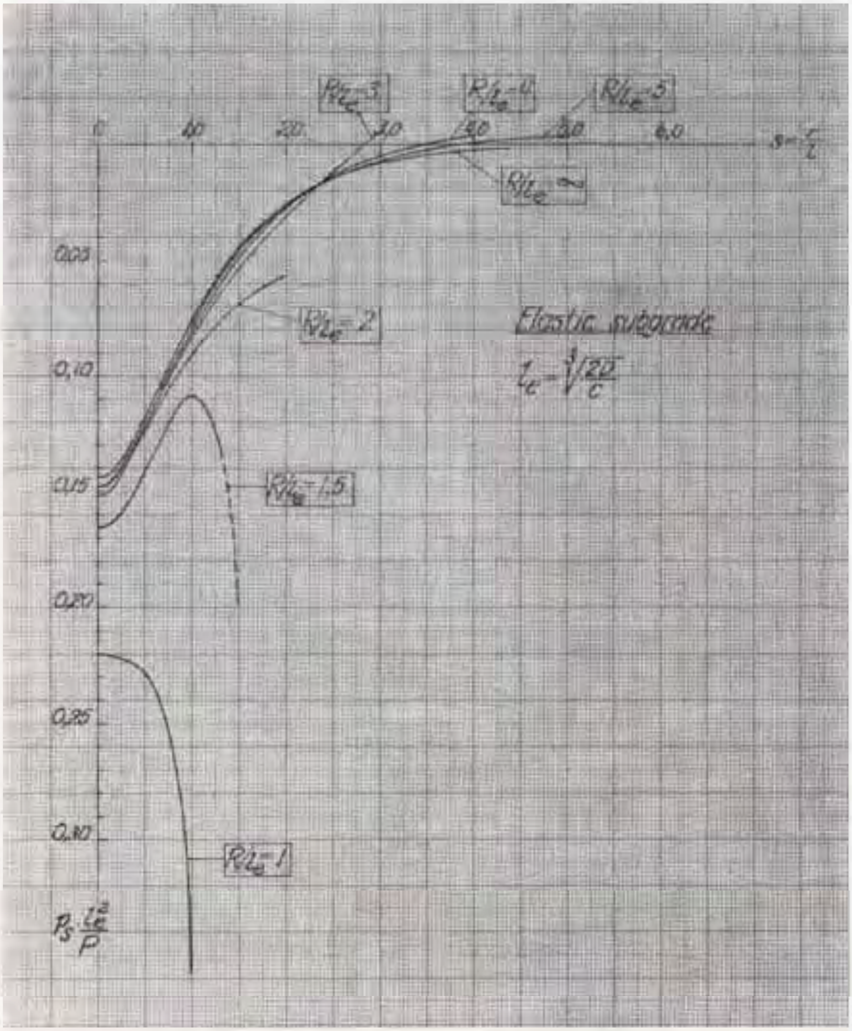

Fig. 22:10. The soil pressure distribution under slabs with finite radius R on *elastic* subgrade, influenced by uniformly distributed load in the centre with relative load distribution $a_e = \frac{c}{l_e} = 0.5$. The Poisson's ration for the slab $\nu = 0.15$. For comparison, the corresponding curve for the slab of infinite extent is shown.

The pressure distribution curves are arrived at on the basis of the values obtained according to Bergströms difference method [5] and adjusted so as to give a correct pressure volume.

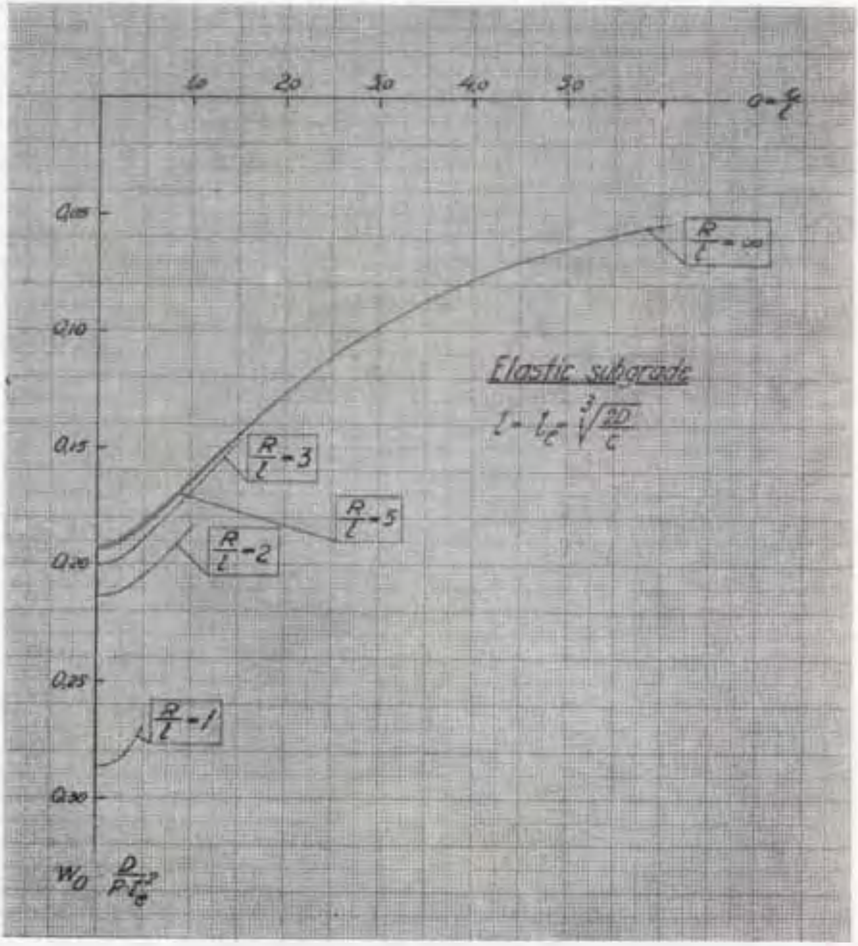

Fig. 22:11. The depression in the loading centre under the slabs with finite radius R on *elastic* subgrade with various relative load distribution $a_e = \frac{c}{l_e}$. The Poisson's ratio for the slab $\nu = 0.15$. For comparison, the corresponding curve for the slab of infinite extent is shown.

The curves are arrived at on the basis of the values according to BERGSTRÖM [5].

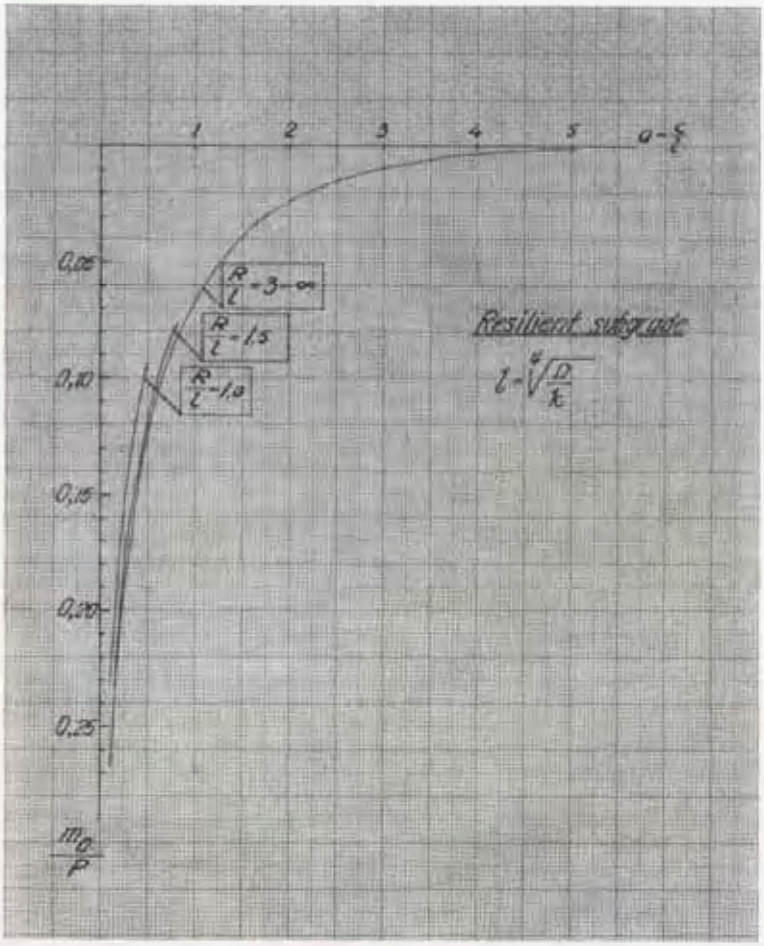

Fig. 22:12. The flexural moment in the loading centre for slabs with finite radius R on *elastic* subgrade with various relative load distribution $a=\frac{c}{l}$.

The Poisson's ratio for the slab = 0.15. For comparison, the corresponding curve for the slab of infinite extent is shown.

The curves are arrived at on the basis of the values according to BERGSTRÖM [5].

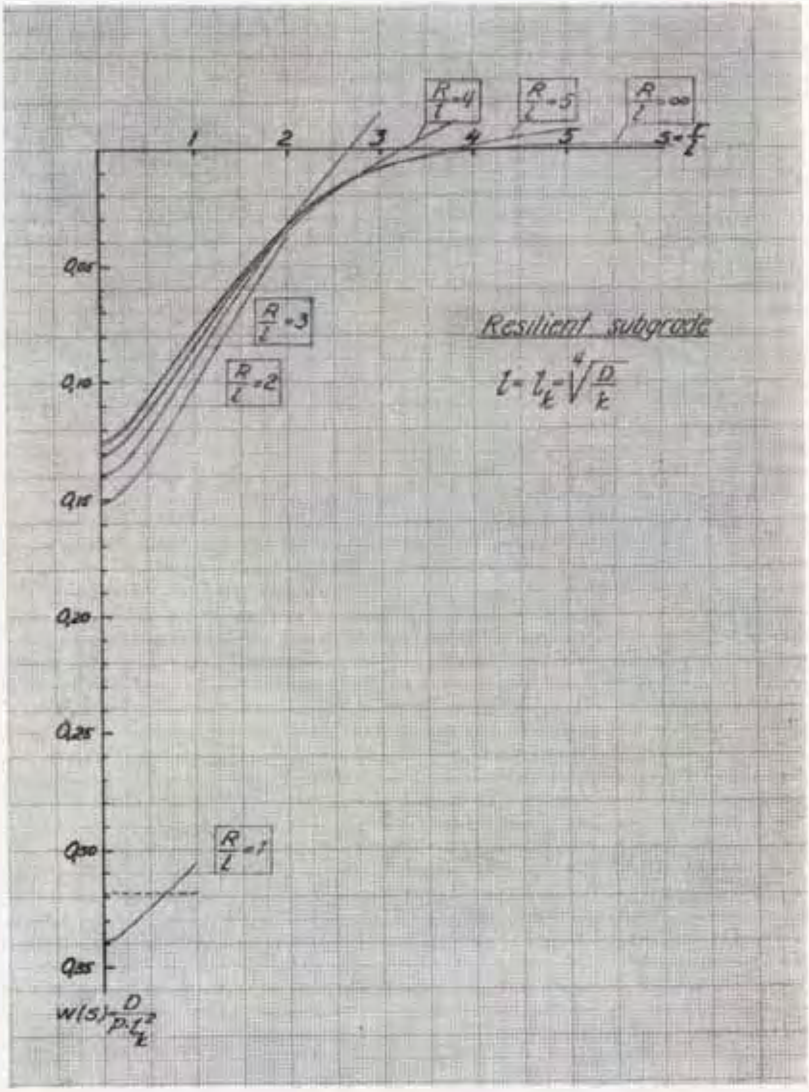

Fig. 22:13. The depression curves for slabs with finite radius R on *resilient* subgrade, under the influence of a concentrated load in the centre. The curves apply for a Poisson's ratio of $\nu=0$ for the slab. For comparison, the corresponding curve for a slab of infinite extent is shown.

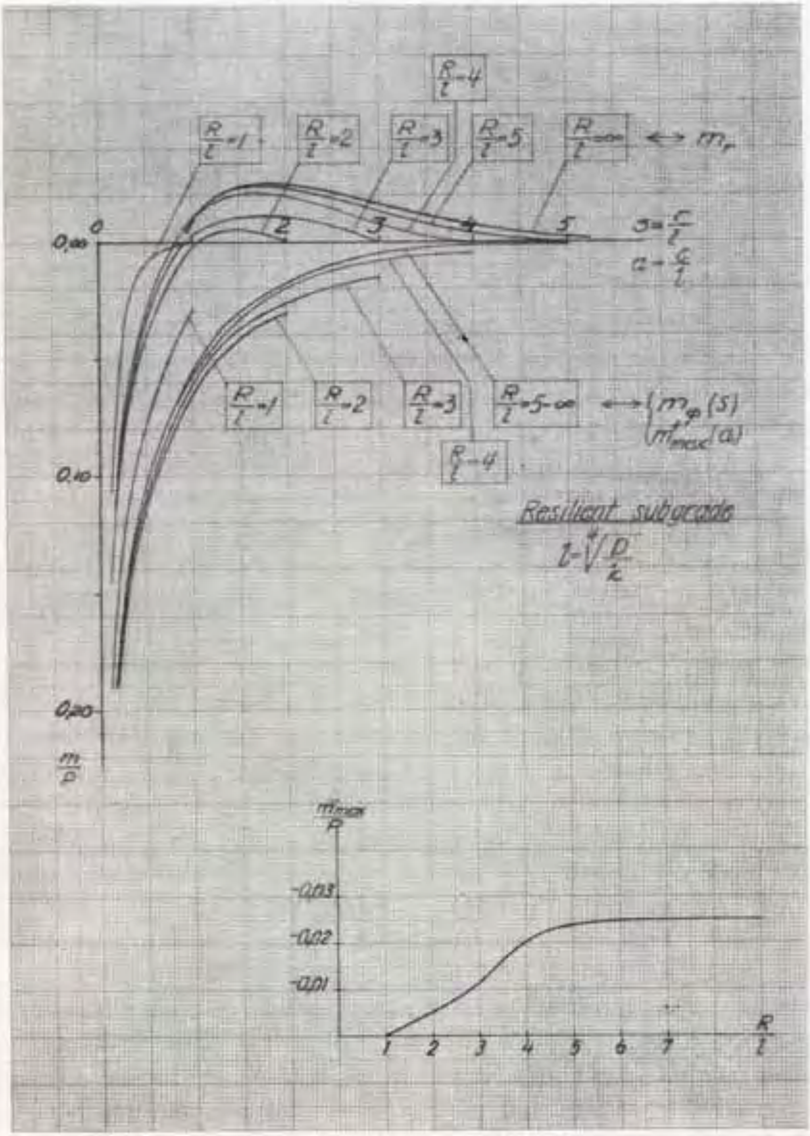

Fig. 22:14. The flexural moment in slabs with finite radius R on *resilient* subgrade, under the influence of a concentrated load in the centre. The curves apply for a Poisson's ratio $\nu=0$ for the slab. The upper curves represent the radial moment m_r and the lower represent the tangential moment m_φ.

The latter curves also give the *maximum moment* in the loading centre as a function of the relative load distribution $a=\frac{c}{l}$. For comparison, the corresponding curves for a slab of infinite extent are shown.

At the bottom is shown the values for the maximum negative moment as a function of $\frac{R}{l}$.

23. General Viewpoint on the Tests and on the Analysis of Test Results

231. Review of tests

The theories previously considered assume that the properties of both the slab and the soil are ideally elastic. The fact that this is by no means the case for a reinforced concrete slab on natural soil has already been mentioned. In order to be able to judge the suitability of the theories when applied to reinforced concrete pavements and to be able to study the behaviour of reinforced concrete pavements on the whole under loading, extensive testing is necessary.

The tests with reinforced concrete pavements which have been carried out by the author or in which he has collaborated have been of three different types.

The more systematic study of various types of reinforced concrete pavement under various conditions has been carried out with the help of *model tests* (series M) on a laboratory scale. The test slabs have been octagonal or circular in form with a diameter of 2.5 to 3.5 metres, with bottom reinforcement or, in some cases, double reinforcement of welded and annealed wire fabric. As an elastic subgrade the author has used high porosity wood fibre board with varying thickness and softness.[1])

Since it is naturally doubtful whether the result from such model tests can be applied to the conditions existing in practical concrete pavement constructions, and since particularly the properties of the subgrade during the model tests and in the case of concrete pavements on soil are completely dissimilar, the author has studied two test slabs on a full scale tested under laboratory conditions. These have been laid on natural soil, in this case clay soil (Gothenburg clay) to some considerable depth. During these tests, preferably called the *Gothenburg tests* (series G), particular emphasis has been laid on the study of soil pressure at the type of subgrade in question.[2])

It is primarily these two series of tests that the author has utilized

---

[1]) An account concerning certain of these tests has earlier been supplied in a stencilled report from the Department of Structural Engineering at Chalmers University of Technology [37].

[2]) An account of these tests has earlier been supplied in stencilled reports from the Department of Structural Engineering, Chalmers University of Technology [36, 38].

when discussing the suitability of the elasticity theory on reinforced concrete pavements and they will therefore be considered within the range of this part of the book (Section 24 and 25). The model tests have here primarily been used to show if and to what extent *the reinforced concrete pavement* can be considered as being an elastic slab within the meaning of the theory, and the Gothenburg tests have served as a basis for a discussion concerning *the characteristics of natural soil* compared with the assumed soil characteristics in accordance with the two soil hypotheses considered.

The author has also had opportunities to study a number of test slabs which have been laid out in connection with planned pavement work on airfields. These test slabs have thus been laid out under the conditions applying for the respective pavement work and have been supported on soil of the same type as that concerned in the planned pavement. The programme for these test series has been made up by the author in close co-operation with the Stockholm Airport Building Committee and tests have been carried out in co-operation with the Swedish State Road Institute as well as the Stockholm Airport Building Committee, these institutions having described certain of the tests in their own reports [8, 47, 48, 53].[1]) These tests are discussed later on in this book in a separate Part 5.

For the analysis of the various tests according to the theories it is primarily essential to determine suitable values for the material constants included in the formulae, namely the flexural rigidity of the slab $D = E\,i/(1 - \nu^2)$ and the constant for the elastic characteristics of the soil, the resilience constant k or the soil modulus $C = E_s/(1 - \nu_s^2)$. As a matter of fact, this is one of the greatest difficulties in the test analysis since the slab and the soil have far from ideally elastic characteristics and the so-called "constants" thus vary. These difficulties will now be discussed in more detail and the methods used by the author in this connection will be explained.

232. Determining the flexural rigidity and the ultimate moments of the slabs

As has already been pointed out, the difficulties in finding a suitable value of the flexural rigidity of the slab are particularly great in the case of a *reinforced* concrete pavement. Such a pavement slab can be

[1]) For the most recent of these test series concerning test slabs on the ready graded subbase for the east-west runway at Arlanda airport, the author has issued an account in the form of a stencilled report from the Department of Structural Engineering, Chalmers University of Technology, [39].

considered to be elastic and isotropic only in the case of very small stresses before the concrete in the tension zone has cracked (Stage I). As soon as the formation of cracks starts, the flexural rigidity decreases to a great extent, and since the crack formation zone in the case of increasing loading gradually increases from the centre and outwards, the elastic properties of the plate alter continuously during the complete test.

At a certain load the slab can be said to be divided into different zones with completely different elasticity characteristics. In the vicinity of the loading centre the concrete has developed tension cracks in the bottom surface and is in the so-called Stage II (or in the case of higher loading in failure Stage III with the reinforcement at the yield point). Outside this central zone there is a region where the moment changes sign and the stresses in the slab are very small, where it can be assumed that the concrete is completely uncracked. For slabs with reinforcement in both top and bottom surfaces there is, outside this, a further zone with tension cracks in the upper surface, and still further from the centre the moment has decreased so much that the concrete is once more completely without cracks. The various zones overlap one another continuously and the zone limits become displaced as the loading increases. It is obvious that under such conditions it is particularly difficult to determine an average value for the flexural rigidity of the slab, a value which can be used when applying the theories which assume that the slab is elastic and isotropic and has a constant flexural rigidity.

The elastic properties of a concrete pavement can be best studied in detail by the means of special flexural tests on strips of the slab which are tested as simply supported beams. Such slab strips, known hereinafter as *detail tests*, have in practically all the test series been made simultaneously with the test slabs. In some of the field tests, these detail tests have instead been sawn out of undamaged parts of the test pavement. These detail tests have been generally test loaded with two concentrated loads as shown in Fig. 23:1 whereby a region is obtained between the loading points with a constant flexural moment and thus a constant curvature. This curvature can be obtained from measurements of the deflection of the centre point relative to the loading points or points between these. The test results give curves showing the relationship between the moment and the deflection or the moment and the curvature of the type shown in Fig. 23:1. The first relatively straight part represents Stage I, the condition in which the concrete slab is before cracks start forming in the tension zone. When the formation of cracks commences the curve changes form and gradually assumes the form of a straight line which corresponds to the deformation of a slab with a tension zone cracked right through, Stage II. Finally, when

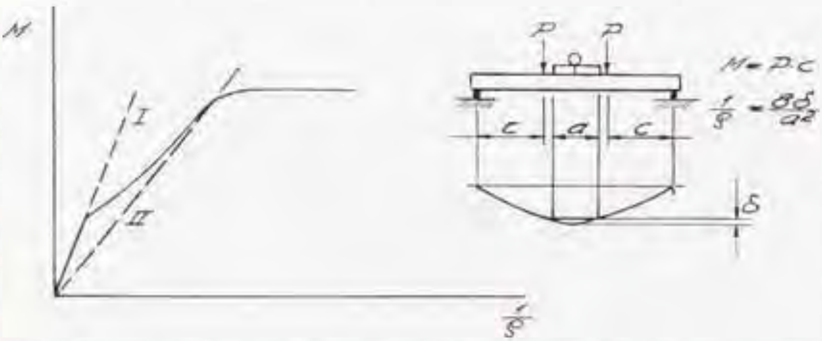

Fig. 23:1. Flexural tests on slab strips, so-called detail tests. The slab strips have been test-loaded with two concentrated loads as shown in the figure and the flexural deformation δ has been measured over a distance a between the points at which the loads are acting. Since the moment and thereby the curvature over this distance is constant, the curvature $\frac{1}{\varrho}$ (ϱ = radius of curvature) can be calculated from δ through the chord theorem. The figure shows a typical relationship curve $M - \frac{1}{\varrho}$ for a single-reinforced slab. The inclination of the curve secant gives the flexural rigidity of the slab for various loadings, while $EI = M/\frac{1}{\varrho}$. The secants marked in correspond to EI in Stage I and Stage II.

the reinforcement begins to yield, there is a more or less horizontal part of the curve corresponding to the ultimate moment (Stage III).

The inclination of the first part of the curve corresponds to the flexural rigidity of the test slab in Stage I. The modulus of elasticity of the concrete when subjected to low loading can be calculated from this value. The inclination of the curve secant at the yield point corresponds roughly to the flexural rigidity in Stage II with the tension zone cracked right through, and this value corresponds to the value obtained in a theoretical calculation of the flexural rigidity of the section based on the moment of inertia for Stage II. The section of the curve after the beginning of tension crack formation represents higher values of the flexural rigidity depending on the fact that the tension zone is still partly operative and is only gradually eliminated as the cracks grow up towards the neutral layer.

Flexural tests of this type give thus some idea how the flexural rigidity varies with varying loading and between different zones in the test pavement. During very low loading before the tension cracks have begun to form under the loading centre, the flexural rigidity applying to the slab corresponds to the Stage I part of the curve in Fig. 23:1. As a suitable limiting value for flexural rigidity in the case of high loading it should be possible to use the secant modulus value at the point corresponding to yield, thus the theoretical Stage II value as shown in Fig. 23:1. As has been earlier mentioned it is naturally only in the central sections that the slab reaches up to or even exceeds this stage, but it appears to be these zones in the slab that make the greatest contribution to the deformation of the slab. It has therefore been considered reasonable during the test analysis to carry out calculations in general for two different values of the flexural rigidity, partly for the Stage I value for low loads and partly for the Stage II value for loads in the neighbourhood of failure, and these values have been determined from flexural tests on slab strips as described above. This reasoning can, however, not be used in the case of very thin slabs which require a large degree of deformation before the tension zone can be considered to be cracked right through. In these tests values of flexural rigidity taken from the intermediate sections of the deformation curve have also been used.

The ultimate moment of the slab under flexure with the reinforcement in the tension zone is obtained, as mentioned above, from the upper horizontal part of the deformation curve from detail tests as shown in Fig. 23:1. The ultimate moment for negative moments in the slab have been decided by similar flexural tests on slab strips which have been tested with the upper surface in the tension zone.

In the tests where it was possible to determine the thickness of the test slabs (primarily the model tests), the result of the flexural tests on the detail test specimens has been corrected with respect to any differences that may occur in total thickness h_0 or effective thickness h between the test slabs and the detail tests belonging to them. The flexural rigidity in Stage I has here been calculated proportional to h_0^3 and the flexural rigidity in Stage II proportional to h^2 while the ultimate moment in Stage I (negative ultimate moment in the case of single-reinforced slab) has been calculated proportional to h_0^2 and the ultimate moment in Stage II and III has been calculated proportional to h.

233. Investigation of the elastic properties of the subgrade

According to both the theories under consideration the soil is assumed to have ideal elastic properties characterized by a constant k or C if the subgrade is considered to be resilient or elastic respectively.

Particularly in the case of full scale tests on natural soil, the difficulties in determining a suitable value for these constants is considerable. The properties of natural soil are, in point of fact, far from ideally elastic. It is a well-known fact that when the surface of the soil is subjected to loading, the degree of depression obtained is more or less dependent on the time factor. In the case of unloading, a great deal of the deformation proves to be of a permanent character. The curve showing the relationship between deformation and loading is generally far from linear and the above-mentioned plastic deformation properties increase as a rule as the loading is increased. Soil material of different types, friction and cohesion material, have quite different properties in these and other respects. Furthermore the assumption made in the case of elastic subgrade, that the soil material is isotropic and homogeneous to infinite depth, generally only applies to a very small extent concerning natural soil.[1])

When determining the constants k or C it should in principle be most correct to start from a simple soil loading test without any connection with the loading test on the test slab. The best known of such tests is the so-called k-value determination which, following the American prototype, has become more or less standardized for Swedish conditions by the Swedish State Road Institute [53]. In this test the soil is loaded with a circular rigid slab usually with a diameter of 40 cm and the depression of the plate is measured at a load usually of 5 tons. Through repeated loading and unloading it is usual to eliminate the permanent deformation, and the result of the test, the k-value, is calculated from the *elastic* depression due to the 5 tons load. This test gives naturally a certain impression of the supporting capacity of the soil and its rigidity towards deformation, but according to the impression gained by the author it cannot be considered a basis for the design of pavements and to an even smaller extent it can be used for the analysis of loading tests on test pavements. In this connection due respect must also be taken to the permanent deformation since it is naturally the *total* deformation of the soil which determines the degree of depression of the pavement and thus also the stresses in the slab. It appears therefore to be most correct to start out from the deformation occurring during the first test loading on the pavement subbase after this has been fully compressed.

The k-values arrived at through these tests or similar tests are, however, generally very dependent on the size of the test slab. This is, actually,

---

[1]) The influence of limited depth in the case of elastic subgrade has been considered by BERGSTRÖM [4] (page 149), whereby he maintains that soil with a comparatively great depth over a hard bottom functions as a subgrade with infinite depth, but with a more reduced C-value, while the subgrade with a diminishing depth shows an increased tendency to function as a resilient subgrade. The affect of layered subgrade in its simplest case (two or three layers) has also been studied by BERGSTRÖM [4] (page 152), who has shown that the layered subgrade can be considered to function as an isotropic subgrade with an average modulus C_{aver}, the value of which does not only depend on the C-value of the soil layers but also on the stiffness of the concrete pavement. ODEMARK [53] has considered the same case and has produced the expression for C_{aver} in a diagrammatic form which is very convenient for practical calculations.

5

an argument for the fact that the soil behaves as an elastic, isotropic subgrade, since, in accordance with Boussinesq's well-known formula [65] the following applies to determine the depression of a rigid slab with radius R and a loading q_0 uniformly distributed over the surface:

$$w = \frac{q_0}{C} \cdot \frac{\pi R}{2} \tag{23:1}$$

If the definition of k (21:1) is inserted here, the relationship is obtained

$$k = \frac{2C}{\pi R} \tag{23:2}$$

this showing that k is inversely proportional to the diameter $2R$ of the rigid slab if C is assumed to be constant. This relationship has been corroborated by several loading tests with rigid slabs on clay soil but the relationship is less regular where the soil consists of friction material.[1])

It should thus be possible to use this method for a direct determination of the C-value whereby a series of slabs of varying diameters should preferably be used. In application to test slabs on natural soil however, tests of this type are not particularly reliable since the soil does not always definitely have the same properties at the places where the main test slab is placed and where the detail test is carried out. Apart from this the loading conditions on the soil in both the cases are not comparable.

For the model tests which have been carried out, a test of this type can be considered to be more reliable however. For these tests the subgrade consisted of a bed of porous wood fibre board and had thus comparatively constant characteristics. It is also clear that a subgrade of this type cannot be considered to be anything else than a resilient subgrade since it has a very moderate thickness, 10–20 cm, and rests on a concrete floor. It should thus in these tests be possible to obtain the k-value directly through test loading on a cut-out part of the subgrade and such tests have actually been carried out.

During tests on natural soil the k-value should obviously be determined preferably through testing with a test slab of the same size and shape as the main test and this should also give the best result in model tests with respect to possible unevenness in the artificial subgrade. This can be carried out by analysis of the values of depression during the actual main tests without it being necessary to refer to any relationship according to the theory. From an equilibrium equation for the complete slab we obtain

---

[1]) See Bergström and assoc. who in the paper referred to [4] discussed these questions in Section 121, page 8.

$$P = \int_A p_s\, dA = \int_A k\, w\, dA = k \int w\, dA = k\, w_{\text{aver}}\, A$$

where

$$p_s = k \cdot w = \text{the soil pressure}$$

and

$$w_{\text{aver}} = \frac{1}{A} \int_A w\, dA = \text{average depression},$$

whereby integration is carried over the section A of the surface of the slab against which the subgrade pressure is effective, thus not over that part of the surface which lifts from the subgrade. If the "average loading" is written

$$p_{\text{aver}} = \frac{P}{A}$$

we obtain

$$k = \frac{p_{\text{aver}}}{w_{\text{aver}}} \tag{23:3 a}$$

or, written directly

$$k = \frac{P}{\int_A w\, dA} = \frac{P}{V} \tag{23:3 b}$$

Here the integral $V = \int_A w\, dA$ means the depression volume. This can be calculated through numerical integration according to Guldin's rule by measuring the values of the depression of the slab at various points, thereby however not including (or as a particular correction removing) that part of the deformation curve showing lifting over the subgrade. In this connection respect should be taken to the fact that the subgrade, due to the weight of the slab, has a certain initial reaction. When the edges of the slab lift, this reaction is decreased and becomes zero, as soon as the lift is similar to or greater than the depression $w_g = \frac{g}{k}$ corresponding to the weight g. When calculating the depression volume corresponding to the applied load P, the volume lying under the lifted section of the slab up to w_g thus should be considered *negative* (see Fig. 23:2).

This method of determining the k-value of the subgrade can actually

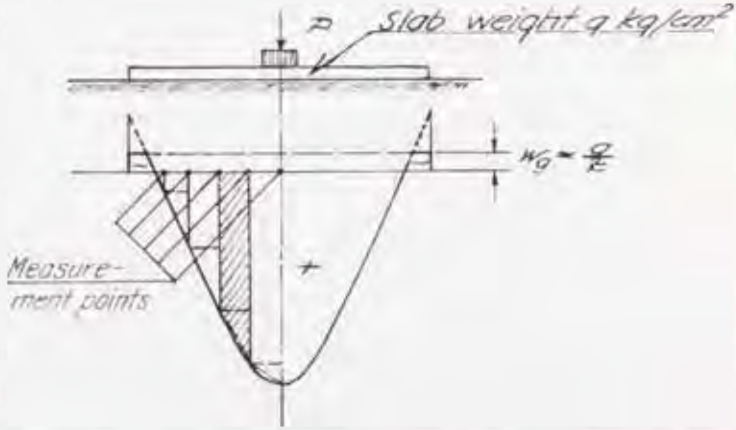

Fig. 23:2. Calculation of the depression volume. The test values for depression — generally the average values of the depression measurements along four radii — are used to obtain the depression line for each loading step, and the depression volume is calculated according to Guldin's rule, whereby the the surface is divided up into rectangular and triangular elements, those corresponding to the slab edge lifting being calculated as negative. The value w_g = the depression due to the slab's dead-weight g.

be applied only in the cases where the test slabs are circular, thus in the model tests and the Gothenburg tests. Attempts to use the method also in other field tests where the test slabs had square or rectangular forms have given less satisfactory results.

In order to be able to use the theory for elastic subgrade for a test where the properties of the subgrade have been studied according to the above mentioned method, the k-value determined in this way should be able to be "translated" to the corresponding C-value. BERGSTRÖM has suggested [4], that one should compare the maximum vertical deformation obtained due to a concentrated load according to both the theories. By writing the expressions (22:25) and (22:52) for these deformations as being equal one obtains

$$k = 0.166 \sqrt[3]{\frac{C^4}{D}} \quad \text{or} \quad C = 3.84 \sqrt[4]{D\,k^3} \qquad (23:4)$$

These formulae are based, however, on the assumption that both the theories will give an equally correct value of vertical deformation in the centre or, more correctly stated, the constant C must be modified so that this condition is satisfied. This method of determining the C-value can obviously *not* be suitable if the analysis of the tests in question concerns the application of the elasticity theory to reinforced concrete pavements and to decide which of the two hypotheses concerning subgrade corresponds best to the actual soil characteristics.

SCHLEICHER [61] shows a possibility of getting more directly at the C-value with a method which, analogous with the k-value calculation shown above, is based on the average depression of the test slab. The depression at an arbitrary point at a distance r from the loading centre can, according to (22:4) and (22:6 a) be written (see Fig. 22:2)

$$w(r) = \int_0^R p_s(\varrho)\, \varrho\, d\varrho \cdot 2 \int_0^\pi \frac{1}{\pi C} \frac{d\varphi}{s} \tag{23:5}$$

where R is the radius of the slab and $p_s(\varrho)$ is the soil pressure at a distance ϱ from the loading centre. The last integral can be rewritten in the form of an elliptical integral and one thus obtains (see SCHLEICHER [59])

$$w(r) = \frac{4}{\pi C} \left[\int_0^r \frac{\varrho}{r} p_s(\varrho)\, K\left(\frac{\varrho}{r}\right) d\varrho + \int_r^R p_s(\varrho)\, K\left(\frac{r}{\varrho}\right) d\varrho \right] \tag{23:6}$$

where K is the complete elliptic integral

$$K(k) = \int_0^{\frac{\pi}{2}} \frac{d\,\Phi}{\sqrt{1 - k^2 \sin^2 \Phi}} \tag{23:7}$$

The expression is rendered dimension-less by inserting

$$r = R\, r'\,;\ \ \varrho = R\, \varrho' \tag{23:8}$$

as well as

$$p_s(\varrho) = p_{\text{aver}}\, \Pi(\varrho) = p_{\text{aver}}\, \Pi(\varrho') \tag{23:9}$$

where p_{aver} = average soil pressure defined through the equation

$$P = \int_A p_s\, dA = \int_0^R p_s(\varrho) \cdot 2\,\pi\, \varrho\, d\varrho = p_{\text{aver}}\, A \tag{23:10}$$

and Π = the relative pressure distribution which, according to (23:9) and (23:10), shall be selected with such an ordinate scale that

$$\int_0^1 2\, \Pi(\varrho')\, \varrho'\, d\varrho' = 1 \tag{23:11}$$

If instead of the radius R, the surface A of the slab is inserted, one obtains

$$w(r) = p_{\text{aver}} \frac{\sqrt{A}}{C} \; \Omega(r') = \frac{P}{C\sqrt{A}} \; \Omega(r') \tag{23:12}$$

where

$$\Omega(r') = \frac{4}{\pi\sqrt{\pi}} \left[\int_0^{r'} \frac{\varrho'}{r'} \, \Pi(\varrho') \, K\left(\frac{\varrho'}{r'}\right) d\varrho' + \int_{r'}^{1} \Pi(\varrho') \; K\left(\frac{r'}{\varrho'}\right) d\varrho' \right] \tag{23:13}$$

The average depression will then be

$$w_{\text{aver}} = p_{\text{aver}} \; \frac{\sqrt{A}}{C} \; \Omega_{\text{aver}} = \frac{P}{C\sqrt{A}} \; \Omega_{\text{aver}} \tag{23:14}$$

where the average value function

$$\Omega_{\text{aver}} = \int_0^1 \Omega(r') \, 2\, r' \, dr' \tag{23:15}$$

is a function of only the relative pressure distribution Π.

Schleicher [61] has calculated the average value function Ω_{aver} for several different pressure distributions Π (see Fig. 23:3), and has shown that the value of Ω_{aver} is only influenced to a very slight extent by the distribution of soil pressure. For the two theoretical limiting cases of an infinitely stiff slab and a slab with a flexural rigidity equal to zero loaded with concentrated load (i. e. Boussinesq's classic basic case) is obtained according to well-known expressions for depressions (see, for example, Schleicher [59]), when comparing with equation (23:14), as shown in Fig. 23:4

for an absolutely stiff slab

$$w_{\text{aver}} = w = \frac{P}{2\,C\,R} = \frac{P}{C\sqrt{A}} \; \frac{\sqrt{\pi}}{2}; \quad \Omega_{\text{aver}} = \frac{\sqrt{\pi}}{2} = 0.89 \tag{a}$$

for a slab with a flexural rigidity $= 0$

$$w_{\text{aver}} = \frac{1}{\pi R^2} \int_0^R w(r) \, 2\,\pi\, r \, dr = \frac{2\,P}{\pi R^2} \; \frac{1}{C} \int_0^R dr = \frac{2\,P}{\pi\, C\, R} = \frac{P}{C\sqrt{A}} \; \frac{2}{\sqrt{\pi}}$$

$$\Omega_{\text{aver}} = \frac{2}{\sqrt{\pi}} = 1.13 \tag{b}$$

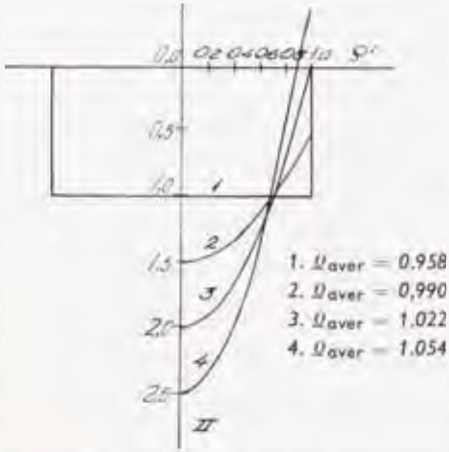

Fig. 23:3. The average value function Ω_{aver} shown for various cases of load distribution according to a calculation made by SCHLEICHER [61]. The influence of the form of the load distribution curve is strikingly small.

Even between these cases of extreme pressure distribution the variation of Ω_{aver} is thus relatively small.

With the slabs studied in this paper which have a relatively low degree of flexural rigidity, there may be a pressure distribution which approximately corresponds to the curves 3 or 4 in Fig. 23:3, and one can therefore assume the average value function $\Omega_{\text{aver}} = 1$. The error should in this

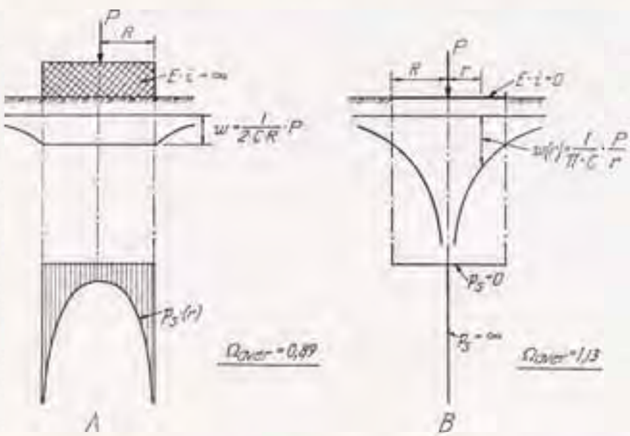

Fig. 23:4. Depression and pressure distribution under a circular slab with radius R in the two extreme cases when the slab is infinitely rigid (Fig. A) and where the flexural rigidity of the slab = 0 (Fig. B).

case not be more than a very few percent. Under such conditions the C-value can be calculated from the expression

$$C = \frac{p_{\text{aver}}}{w_{\text{aver}}} \sqrt{A} \tag{23:16 a}$$

with an error which is definitely of less significance than other sources of error. If the expression for k according to (23:3 a) is inserted here, one obtains the relationship between C and k

$$C = k \cdot \sqrt{A} \tag{23:16 b}$$

By the insertion of (23:3 b) this gives

$$C = \frac{P}{\int\limits_A w\, dA} \sqrt{A} = \frac{P}{V} \sqrt{A} \tag{23:16 c}$$

The depression volume

$$V = \int^A w\, dA$$

can be calculated from the test values in the way stated above. As a principle one can here select the area A arbitrarily (see Fig. 23:4 B), if one merely knows the deformation of *the soil* within A. With this type of subgrade there are also depressions even outside the zone where the soil pressure operates (see Fig. 23:4). The tests, however, only give the deformation of *the slab*, and for that reason V should be calculated within the region where the slab and the soil are in contact. This is assumed to coincide with the surface of the slab up to the limit where, according to the measurements, the edge lifts, a supposition that should be more or less correct. In the case of edge lifting, the central zone will be subjected to extra loading by the weight of the lifted edge zone and when calculating one should thus actually increase the load P by a correction corresponding to the weight of the lifted edge zone. The result will be practically the same if instead the depression volume is corrected for the opposed resilience of the soil in the same way as in the k-value determination according to Fig. 23:2. It is thus possible in this way to use the result for the k-value determination when calculating C and thus use the formula (23:16 b), where A means the contact area estimated with a radius as above.

The method has been used on the two circular slabs in the Gothenburg tests. Concerning the other field tests with rectangular slabs it is difficult to calculate the value of the depression volume to any great accuracy.

Apart from the methods with direct loading on the unpaved soil which, as already mentioned, give unreliable values for test analysis, the only remaining possibility in these tests is to determine the soil constant from the deformation of the test slabs under loading by applying the elasticity theory results. In this connection it is simplest to use the formulae for the depression under the loading centre. One can often neglect the influence of load distribution and use the centre depression formulae for concentrated loading

$$w_0 = \frac{1}{3\sqrt{3}} \frac{P\, l_e^2}{D} \tag{23:17}$$

or

$$w_0 = \frac{1}{8} \cdot \frac{P\, l_b^2}{D} \tag{23:18}$$

whereby directly from the test values w_0 on the centre depression one obtains the elastic radius of stiffness, from which C or k can be calculated. Where the load distribution influence has significance, one can gradually correct the approximate value from (23:17) or (23:18) by using the more complete formulae for depression under the loading centre in Table 22:1 or the corresponding diagram in the Figures 22:5 b and 22:8 b whereby one commences from the approximate value of l according to (23:17) or (23:18) when calculating the relative load distribution $\alpha = \frac{c}{l}$. In general it is sufficient with only one correction of this type. A disadvantage with the method is that the flexural rigidity D of the slab is included in the formulae for depression so that faults or doubts in determination of D will influence the result.

Where tests are to be used for the study of the application of the elasticity theory to reinforced concrete pavements, the last-mentioned method of determining the soil constant cannot be considered to be completely satisfactory since in the determination — at least to a certain extent — that theory is utilized, the suitability of which is to be verified. In the relatively few tests where this method alone has been used, the author has always been particularly anxious to carry out comparisons between theory and tests from so many separate aspects as possible.

On the other hand, in cases where the result of test is to be used for the determination of necessary *data for designing* a pavement, then the method of determining the soil constant in question is free from criticism, and it is naturally better, the more the test pavement is similar to the final pavement. In such cases BERGSTRÖM's relationship formula (23:4) between k and C is naturally completely correct; in fact, it is obtained by writing the expressions of w_0 according to (23:17) and (23:18) as being identical.

234. Influence of membrane stresses

Particularly the thin model slabs show, when testing with higher loading, vertical deformations between the edge and the middle which are of the same magnitude as the thickness of the slab, and in such cases the membrane effect in the slab may imply an increase in the ultimate load which is by no means inconsiderable. It is thus essential, when judging test results, to attempt to estimate the influence of the membrane stresses on the ultimate load value.

An approximate calculation of this influence can be carried out according to a principle stated by FÖPPL [19][1]) whereby the loading is considered as being divided up into one part which is held up only by "the normal slab effect", i. e. the flexural stresses, and one part P_M, which is held up by the membrane stresses in the plane of the slab.

The energy principle[2]) is used when calculating P_M. The strain energy of the membrane stresses radially and tangentially N_r and N_φ can, in a circular elastic plate with radius R, be written

$$V_M = \frac{1}{2} \int_0^{2\pi} \int_0^R (N_r \varepsilon_r + N_\varphi \varepsilon_\varphi)\, r\, dr\, d\varphi =$$

$$= \frac{\pi E h}{1 - \nu^2} \int_0^R (\varepsilon_r^2 + \varepsilon_\varphi^2 + 2 \nu \varepsilon_r \varepsilon_\varphi)\, r\, dr \qquad (23:19)$$

If this expression for the tensions is inserted

$$\left.\begin{aligned} \varepsilon_r &= \frac{du}{dr} + \frac{1}{2} \left(\frac{dw}{dr}\right)^2 \\ \varepsilon_\varphi &= \frac{u}{r} \end{aligned}\right\} \qquad (23:20)$$

where u and w are the displacements of a point in the centre plane of the slab radially and at right angles respectively to the plane, one obtains

---

[1]) Quoted work [19], part I, page 224.

[2]) See, for example TIMOSHENKO, [66] page 329.

$$V_M = \frac{\pi E h}{1 - \nu^2} \int_0^R \left[r \left(\frac{du}{dr}\right)^2 + \frac{1}{4} r \left(\frac{dw}{dr}\right)^4 + r \frac{du}{dr}\left(\frac{dw}{dr}\right)^2 + \right.$$

$$\left. + \frac{u^2}{r} + 2 \nu u \frac{du}{dr} + \nu u \left(\frac{dw}{dr}\right)^2 \right] dr \tag{23:21}$$

In this expression suitably chosen function expressions for u and w are inserted, care being taken to ensure that the boundary conditions for the slab are satisfied.

That part of the applied load which is carried up by the membrane stresses can thus be obtained according to the principle of virtual energy, thereby considering that the plate is given a virtual deformation giving an increase δw_0 of the maximal vertical deformation,

$$\int^{A} p_M \; (\delta w)_{\delta w_0} \; dA = \frac{\partial V_M}{\partial w_0} \delta w_0 \tag{23:22}$$

whereby p_M includes both the load component P_M as well as that part of the subgrade pressure maintaining equilibrium with P_M.

When applying this on the test slabs it is difficult to find a suitable function relationship for the vertical deformation w. It is therefore considered suitable to utilize directly the test values for depression at a loading step in the vicinity of the ultimate load and to use difference calculation. The slab is divided into elements as shown in Fig. 23:5, and if the test values at the chosen load (w_{I} to w_{V} as shown in the figure) are denoted w_{test}, then the corresponding values at the ultimate load can be calculated as

$$w = \frac{w_0}{w_{\mathrm{V}}} \cdot w_{\mathrm{test}} \tag{23:23 a}$$

and the derivative between the element boundaries

$$\frac{dw}{dr} = \frac{w_0}{w_{\mathrm{V}}} \cdot \frac{\Delta w_{\mathrm{test}}}{\Delta r} \tag{23:23 b}$$

whereby w_0 denotes the centre depression at the ultimate load.

For the tension component u a simple function relationship

$$u = C_1 r + C_2 r^3 \tag{23:24}$$

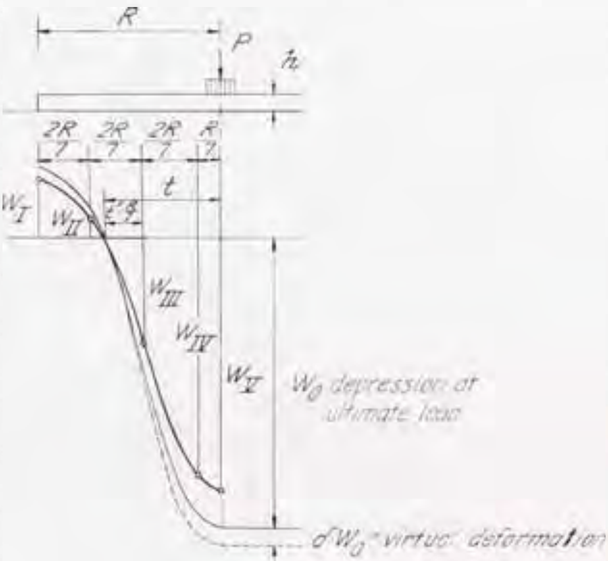

Fig. 23:5. Element sub-division when calculating the membrane stresses. w_I to w_V are the average values of the depression values measured along the four radii and w_0 is the estimated centre depression at the ultimate load. In the calculation of the various quantities required, the depression curve is assumed to be made up of straight lines between the depression values.

is applied where C_1 and C_2 are determined so that the boundary conditions are satisfied.[1])

The energy expression (23:21) can, for a simpler calculating procedure, be divided up into three terms

$$V_M = V_{M_1} + V_{M_2} + V_{M_3} \qquad (23:25)$$

where

$$V_{M_1} = \pi E h \int_0^R \left[r \left(\frac{du}{dr} \right)^2 + \frac{u^2}{r} \right] dr \qquad (23:25\text{ a})$$

$$V_{M_2} = \frac{1}{4} \pi E h \int_0^R r \left(\frac{dw}{dr} \right)^4 dr \qquad (23:25\text{ b})$$

[1]) Calculations for some of the slabs have been made also for a more correct but more laborious function relationship for u

$$u = C_1 r + C_2 r^2 + C_3 r^3$$

(according to NADAI [52] page 298 or TIMOSHENKO [66], page 333). The difference in the correction term P_M is less than 10 %, i. e. 1—2 % of P.

$$V_{M_3} = \pi E h \int_0^R r \frac{du}{dr} \left(\frac{dw}{dr}\right)^2 dr \tag{23:25 c}$$

where ν in the expression (23:21) has been put equal to zero. If the expressions (23:23) and (23:24) for the tension components are inserted here and the integrals are divided up into parts between the element boundaries, after simplification one obtains:

$$V_{M_1} = \pi E h \left(C_1^2 R^2 + \tfrac{5}{3} C_2^2 R^6 + 2 C_1 C_2 R^4\right) \tag{23:26}$$

$$V_{M_2} = \pi E h \frac{1}{R^2} \frac{49}{16} \frac{w_0^4}{w_V^4} \left(3 \varDelta w_{II-I}^4 + 2 \varDelta w_{III-II}^4 + \varDelta w_{IV-III}^4 + 2 \varDelta w_{V-IV}^4\right) \tag{23:27}$$

$$V_{M_3} = \pi E h \frac{w_0^2}{w_V^2} \left(C_1 W_1 + C_2 R^2 W_2\right) \tag{23:28}$$

where, in the expression for V_{M_3}, have been introduced the notations

$$\left.\begin{aligned} W_1 &= 3 \varDelta w_{II-I}^2 + 2 \varDelta w_{III-II}^2 + \varDelta w_{IV-III}^2 + \tfrac{1}{2} \varDelta w_{V-IV}^2 \\ W_2 &= \tfrac{1}{49}\left(333 \varDelta w_{II-I}^2 + 102 \varDelta w_{III-II}^2 + 15 \varDelta w_{IV-III}^2 + \tfrac{3}{4} \varDelta w_{V-IV}^2\right) \end{aligned}\right\} \tag{23:29}$$

C_1 and C_2 are determined so that the boundary condition at a free edge is satisfied

$$\left[\frac{du}{dr} + \frac{1}{2}\left(\frac{dw}{dr}\right)^2\right]_{r=R} = 0 \tag{23:30}$$

giving the relationship

$$C_1 + 3 C_2 R^2 + \frac{49}{8 R^2} \frac{w_0^2}{w_V^2} \varDelta w_{II-I}^2 = 0 \tag{23:31}$$

If, through (23:31), C_1 is eliminated from the equations (23:26) and (23:28), then C_2 can be determined from the theorem of the minimum of strain energy

$$\frac{\partial V_M}{\partial C_2} = 0 \tag{23:32}$$

and in this way one obtains the expressions

$$
\left.\begin{aligned}
C_1 &= -\frac{9}{28}\,\frac{1}{R^2}\,\frac{w_0^2}{w_V^2}\left(3\,W_1 - W_2 - \frac{49}{9}\,\Delta\,w_{II-I}^2\right)\\
C_2 &= \frac{3}{28}\,\frac{1}{R^4}\,\frac{w_0^2}{w_V^2}\left(3\,W_1 - W_2 - \frac{49}{2}\,\Delta\,w_{II-I}^2\right)
\end{aligned}\right\} \qquad (23:33)
$$

The calculations are facilitated with the new notations

$$
\left.\begin{aligned}
\Delta\,W_1 &= \tfrac{12}{49}\,(9\,\Delta\,w_{II-I}^2 + 16\,\Delta\,w_{III-II}^2 + 11\,\Delta\,w_{IV-III}^2 + \tfrac{97}{16}\,\Delta\,w_{V-IV}^2)\\
\Delta\,W_2 &= \tfrac{1}{3}\,(-\,705\,\Delta\,w_{II-I}^2 - 110\,\Delta\,w_{III-II}^2 + 53\,\Delta\,w_{IV-III}^2 + \tfrac{187}{4}\,\Delta\,w_{V-IV}^2)\\
\Delta\,W_3 &= \tfrac{49}{16}\,(\tfrac{19}{4}\,\Delta\,w_{II-I}^4 + 2\,\Delta\,w_{III-II}^4 + \Delta\,w_{IV-III}^4 + 2\,\Delta\,w_{V-IV}^4)
\end{aligned}\right\} \qquad (23:34)
$$

and

$$
\Delta\,W = \tfrac{3}{56}\,(\Delta\,W_2 \cdot \Delta\,w_{II-I}^2 - \Delta\,W_1^2) + \Delta\,W_3 \qquad (23:35)
$$

after which the energy expression (23:25) can be written

$$
V_M = \frac{1}{R^2}\,\pi\,E\,h\left(\frac{w_0}{w_V}\right)^4 \cdot \Delta\,W \qquad (23:36)
$$

When calculating the energy of the external forces, respect must also be taken to the pressure from the subgrade which, it is assumed in the usual way, can be written

$$
p_s = k \cdot w
$$

Of p_s one part p_M is considered to maintain equilibrium against that part of the external load P_M carried up by the membrane stresses.

According to the principle of virtual energy (23:22) is thus obtained

$$
\frac{\partial\,V_M}{\partial\,w_0}\,\delta\,w_0 = P_M\,\delta\,w_0 - \int_0^t p_M\;\delta\,w\;dA \qquad (23:37)
$$

where integration can be carried out over the surface (with radius t) of the subgrade which is in contact with the slab (see Fig. 23:5). One can write

$$
p_M = \frac{P_M}{P}\,p = \frac{P_M}{P}\;k\;w \qquad (23:38)
$$

and

$$
\delta\,w = \delta\,w_0 \cdot \frac{w}{w_0} \qquad (23:39)
$$

and one then obtains

$$\frac{\partial V_M}{\partial w_0} = P_M - \frac{P_M}{P} \; k \; \frac{2\pi}{w_0} \int_0^l w^2 \, r \, dr \tag{23:40}$$

When calculating the integral, division is made as earlier into elements between the depression values $w_I - w_V$ and the depression curve is assumed to be linear between the measuring values (see Fig. 23:5). In this way one obtains

$$\int_0^l w^2 \; r dr = \frac{w_0^2}{w_V^2} R^2 \; W_p \tag{23:41}$$

where

$$\left.\begin{aligned} W_p &= \tfrac{1}{588} [w_V^2 + 2\, w_V \, w_{IV} + 15 \, w_{IV}^2 + 16 \, w_{IV} \, w_{III} + 20 \, w_{III}^2 + \\ &\quad + w_{III}^2 \, t' \, (12 + t')] \\ t' &= 2 \cdot \frac{w_{III}}{w_{III} - w_{II}} \end{aligned}\right\} \tag{23:42}$$

If the expression for the derivative $\dfrac{\partial V_M}{\partial w_0}$ in (23:37) is inserted according to the equation (23:36), then the ultimate load correction P_M due to the membrane stresses is obtained in the final form

$$P_M = \frac{4\pi}{1 - 2\pi \, R^2 \; \dfrac{k}{P} \dfrac{w_0}{w_V^2} \; W_p} \left(\frac{w_0}{w_V}\right)^3 \frac{E\,h}{R^2} \; \frac{\Delta W}{w_V} \tag{23:43}$$

For the calculation it is only necessary to calculate the constants ΔW according to (23:34) and (23:35) as well as W_p according to (23:42) for a load in the vicinity of the ultimate load.

Calculations carried out on model slabs show that the expression (23:43) can normally be approximated as

$$P_M = \psi \cdot \frac{E\,h}{R^2} \left(\frac{w_0}{w_V}\right)^3 \frac{(w_V - w_I)^4}{w_V} \tag{23:44}$$

where ψ is fairly constant and can be written $= 1{,}5 - 2{,}0$.

In the expression (23:43) for the membrane stress correction is included the modulus of elasticity of the slab E. This constant is included in the original equation (23:19) by writing

$$N = \sigma^M h_0 = \varepsilon^M \frac{E\, h_0}{1 - \nu^2} \approx \varepsilon^M E\, h_0 \tag{23:45}$$

where σ^M is the stress supplement due to the membrane strain ε^M. Hereby is assumed a homogeneous section and uniform strain distribution over the whole transverse section. As a matter of fact, when subjected to the loads at which the membrane stress correction has any significance, the slab is completely cracked in the bottom of the central region as well as, in the case of the top reinforced slabs, also in a large region on the top of the slab. For a section cracked in this way in Stage II one can approximately write the expression (23:45) thus

$$N = \sigma_c^M x + \sigma_r^M A_r = \varepsilon^M (E_c x + E_r A_r) = \varepsilon^M \cdot E_c (x + n \mu h) \tag{23:46}$$

where σ_c^M and σ_r^M are stresses in the concrete and reinforcement due to membrane tension and x the active compression zone depth. μ is the percentage of reinforcement. If one puts $n = 15$, the "reduced modulus of elasticity" E_{II}^M for the membrane stress calculation at Stage II corresponding to E in the expression (23:45) can thus be estimated from the expression:

$$E_{\text{II}}^M = E_c \left(\frac{x}{h} + 15\, \mu \right) \frac{h}{h_0} \tag{23:47}$$

For various values of the reinforcement percentage μ one obtains

$\mu = 1\ \%$	$E_{\text{II}}^M = 0.51\, E_c$
0.8	0.45
0.6	0.39
0.4	0.31
0.2	0.22

If the section reaches a state of failure with the reinforcement at yield point, the reduction will naturally be even greater.

It is thus obvious that the expression for the membrane stress energy is powerfully influenced if the slab is cracked to any greater extent, and when estimating the correct value one should actually divide up the slab into different zones with different moduli of elasticity. In order to study the effect of different types of crack formation, the author has carried out such a calculation of the membrane stress energy. In this connection the expression

$$(\varepsilon_r^2 + \varepsilon_\varphi^2)\, r \tag{23:48}$$

in the membrane energy integral (23:19) ($\nu = 0$) has been estimated with the help of the expressions (23:20), (23:24) and (23:33), whereby the slab has been divided up into differences according to the previous presentation. The result of the calculation for one of the top-reinforced model slabs (slab MII:13) is shown in Fig. 23:6. The calculation has been carried out for partly a load somewhat under the crack formation load for the top surface and partly a load when the top reinforcement is close to the yield point. The areas Y in the figure under the curves for the function (23:48) represent the membrane stress energy within different concentric zones of the model slab and by dividing up the areas in a suitable way and multiplying with the suitable values of the modulus of elasticity one can come to a fairly correct estimation of the membrane stress energy in a partly cracked slab. In this way, in the example shown in the figure, a reduced membrane stress correction P'_M, has been obtained which has a value of 0.98 P_M at the *lower* load with limited crack formation under the centre but only approx. 0.40 P_M at the *higher* load with crack formation also in the top surface whereby comparison has been carried out with a P_M-value calculated for the unreduced E_c-value (Stage I) over the complete slab.

It is thus obvious that a moderate crack formation zone in the vicinity of the centre of the slab will influence membrane stress energy only to a very slight extent and that in such cases it may be allowable to use the value of the modulus of elasticity for the concrete in Stage I. On the other hand there is a very powerful reduction in the membrane stress energy for example in the case of a top-reinforced slab with crack formation in the top surface or a slab with extended crack formation in the bottom surface. In such cases a calculation carried out in accordance with the method quoted would mainly prove to be unreliable.

In normal cases of slabs with moderate deformation and crack formation only in the bottom surface in the vicinity of the centre, one can thus use the modulus of elasticity for Stage I when estimating the membrane stress correction according to equation (23:43). In this way correction calculations in the following test result analysis have been carried out. For the top-reinforced slabs with thoroughly cracked top surfaces and for other slabs with exceptionally large flexural deformation and where crack formation in the bottom surface can be considered as being extensive, then the correction values calculated in this

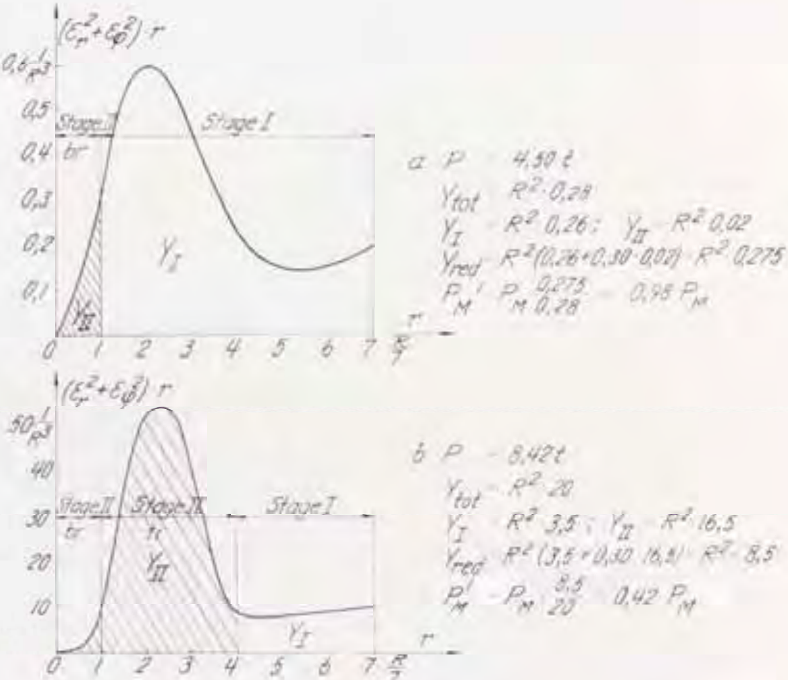

Fig. 23:6. Estimation of the influence of the membrane stresses due to crack formation in the top and bottom surfaces of slab MII:13. The data for the slab: $R=175$ cm, $h=5{,}4$ cm, top and bottom reinforcement consisting of 3.4/50 mesh.

The figure shows the variations in the function $(\varepsilon_r^2+\varepsilon_\varphi^2)\,r$ for the membrane stress energy at the two loads

a) $P=4.50$ tons — immediately before crack formation in the top

b) $P=8.42$ tons — yield point in the top reinforcement with extensive crack formation in the top.

The area under the curves represents the membrane stress energy (equation 23:19). By comparison with the strain measurements (see Fig. 24:23), the boundaries for the crack zones can be estimated, and the different surface areas Y_I and Y_{II} are multiplied by the respective moduli of elasticity, whereby E_{II} is put as being equal to $0.30\,E_I$ ($\mu=0.37$ ‰, equation 23:47). The area thus reduced

$$Y_{red}=Y_I+0.30\,Y_{II}$$

gives the reduced membrane stress correction

$$P_M'=P_M\cdot\frac{Y_{red}}{Y_{tot}}$$

where P_M is calculated for a modulus of elasticity $=E_I$ over the whole slab. The total area under the curves in the figure has been checked by means of the formulae (23:35) and (23:36); the area should have the same value as the constant ΔW in (23:35).

way must be judged as being too unreliable for use. It should, however, be pointed out that also in the case of more "normal" slabs, crack formation can have a more or less significant effect. From this point of view the case shown in fig. 23:6a may belong to the more favourable. Especially in the case of slabs where the membrane stress effect as described above is large compared with the total loading, the P_M-value should be utilized with care and used more to explain any possible deviations between the test results and theoretical values than as a pure correction to the test loading.

The flexural deformation of the slab is also influenced by the membrane stresses, and in a comparison between the test result obtained and the theoretical depression value, one should compare the values according to the theory for a load $(P - P_M)$ with the test values at a load P. Due to the difficulties in establishing reliable values for the correction P_M, the author has abstained from making such a correction in the depression calculations. When judging the test results concerning vertical deformation at higher loading steps one should thus bear in mind the fact that the membrane stress effect here causes a decrease in the test values (or a corresponding increase in the theoretical values).

24. Model Tests (Series M)

241. Review of tests

As has already earlier been mentioned, most of the loading tests with reinforced concrete slabs on elastic subgrade have been carried out as model tests in the Structural Engineering Laboratories at Chalmers University of Technology, Gothenburg. These tests can be divided into two subsidiary series. The first of these, Series MI, which was carried out during 1945, was of a more preparatory character and was intended to show the influences of various subgrades and various forms of load distribution. Only deformation measurements were carried out during these tests. The later and larger test series, Series MII, was carried out during the years 1948—49, and the purpose here was to clarify the influence of various design of the pavement itself such as various thickness, various degree of flexural strength in the concrete as well as various types of reinforcement (Series MII A). The last-mentioned series of tests also included tests with twin loading, mobile load and repeated loading (Series MII B). In the tests in Series MII also measurements of deformation as well as measurements of tensions in the top surface of the test slabs were carried out. The test slabs in the first series of tests were octagonal, 2.5 m across and approx. 3 cm thick, while the tests slabs in the last-mentioned series of tests were completely circular with a diameter of 3.5 m and a thickness of 4—5 cm. The last of the slabs in Series MII was in half-scale with a thickness of 8 cm (Series M II C).

Table 24:1 provides a review of the test programme and includes data for the test slabs in both the series.

242. Performance of test slabs

The elastic subgrade for the test slabs consisted of porous wood fibre board which was laid directly on the floor of the laboratory. During the first tests in the Series MI two layers of so-called high-porosity Kramfors board of this type were used. This board is manufactured by casting fibre pulp. This bed was replaced after each test, and by using board of varying degrees of hardness a certain variation in the resilience of the subgrade could be obtained. When the later test series

TABLE 24:1. Series M. Review of the test programme and data for the slabs.

Test Programme			Test slabs, data									
Main Series	Sub-series	Aim of test	Test no.	Diam cm	Thickness cm	Reinforcement ⌀/square mm br	Reinforcement ⌀/square mm tr	K[1]) kg/cm²	σ_f[1]) kg/cm²	cement kg/m³/ water-cement ratio	Subgrade, approx. k-value kg/cm³	Load distribution plate diam cm.
M I		Thickness, subgrade and load distribution varied	1	240	2.0	1.8/22.5		149		240/1.10	0.3	10
			2	250	3.2	3.0/50		125		240/1.10	0.1	10
			3	250	3.1			214		310/0.86	0.3	10
			4	250	3.1			134		275/1.05	0.05	20
			5	250	2.8			200		300/0.86	0.3	20
			6	250	3.2			112		230/1.23	0.6	20
			7	250	3.0			100		250/0.98	0.2	40
M II A	a:1 a	Reinforcement in bottom varied	1	350	4.10	2.5/50		378	39	300/0.58	0.3	40
	a:1 b		8		4.44	2.5/50		184	31	230/0.83		
	a:2		2		4.52	3.4/50		215	34	240/0.78		
	a:3		3		4.36	5.0/50		194	30	240/0.80		
	b:1	Concrete (tensile strength) varied	4		4.36	3.4/50		74	16	160/1.25		
	b:2		5		4.26			147	27	190/1.00		
	b:3		6		4.42			318	32	290/0.65		
	c 1:1	br const. tr varied	9		5.62	3.4/50	2.5/100[2])	139	25[3])	175/1.10		
	c 1:2		7		5.10		2.5/50[2])	257	35	290/0.65		
	c 1:3		11		5.78		3.4/50	102	21	175/1.20		
	c 2:1	$m+m'=$ constant	12		5.56	5.0/50	— [3])	72	20.5[3])	175/1.30		
	c 2:2		10		5.59	4.2/50	3.1/50	90	20	175/1.10		
	c 2:3		13		5.42	3.4/50	3.4/50	75	19	175/1.30		
M II B	a:1	Twin load	14	350	5.53	3.4/50		168	32.2	230/0.83	0.3	40
	a:2		15		5.63			155	30.4	230/0.83		2 st ⌀ 28 c/c 42
	a:3		16		5.38			178	29.8	230/0.83		2 st ⌀ 28 c/c 84
	b:1	Repeated load	17		5.23	3.4/50		177	36.6	230/0.83		40
	b:2		18		5.11			190	29.0	230/0.83		
	b:3		19		5.20			156	28.6	230/0.90		
	c	Mobile load	20		5.30	3.4/50		175	29.2	230/0.90	0.5	40 in 3 points
M II C		Half-scale test	21	350	8.05	5.0/50		153	28.8	230/0.90	0.5	40

[1]) Average value of 4 tests in series M I, 3 tests in series M II. [2]) Top reinforcement was here without function due to excessively high value of concrete flexural strength. The slab functions completely as a single-reinforced slab. [3]) The tensile strength of the concrete broken by insertion of concentric cardboard rings.

was carried out, manufacture of board of the above-mentioned type had ceased and it was necessary to use normal pressed wood fibre board instead. Since this were considerably harder, a thicker bed was used consisting of four layers of these board plates. There was quite a variation in hardness between the different plates and when the bed was made up, the plates were combined so that any inequalities in the different layers were cancelled out as much as possible, and the result was a bed with a comparatively constant resilience.

This was examined by test-loading directly on the bed with a rigid plate, placed at various points. The result is shown in Figure 24:1. This bed was used for all of the 21 test slabs in this series. After each test, the top surface of the bed was levelled by means of a thin layer of fine sand. A control testing of the bed after about half the test series was completed was carried out in the same way as the control before the commencement of testing and showed that the reilience constant (k-value) of the bed was unchanged on the whole.

The test slabs were cast on the flat form bottom on the laboratory floor and, after hardening, they were lifted over on to the bed. The reinforcement in the MI:1 plate consisted of annealed iron netting and in all the other slabs of welded wire fabric. This wire fabric was made of cold-drawn steel wire, but since it was desirable that the reinforcement should have a significant yield strength, the reinforcement fabric was annealed before use by heating it up to about 700° C. Tensile tests showed the wires to have properties identical with that of soft carbon steel. The reinforcement was laid out and attached in a simple way directly to the bottom of the mould, so that it was partially visible on the bottom surface of the slab. Due to the closely spaced welded intersections, however, fully satisfactory bond was obtained in spite of this. In casting the slabs with double reinforcement, the top surface mesh was fitted on carriers at the correct height before casting was started.

Simultaneous with the casting of each test slab, slab strips were also cast. These strips were used as detail tests to determine flexural rigidity and ultimate strength, as has already been described in Section 232. These strips were made with the same thickness and the same reinforcement as the main test slab and the width was generally 30 cm. For every slab in the first series of tests three of these detail tests were cast, one of these being of plain concrete while the two others were reinforced with strips of wire fabric which was clipped from two edges at right angles to each other of the same mat of wire fabric as was used in the test slab in question. In the later series four detail test strips were cast for each slab, two of these being reinforced with strips taken from one wire direction and two with strips taken from the

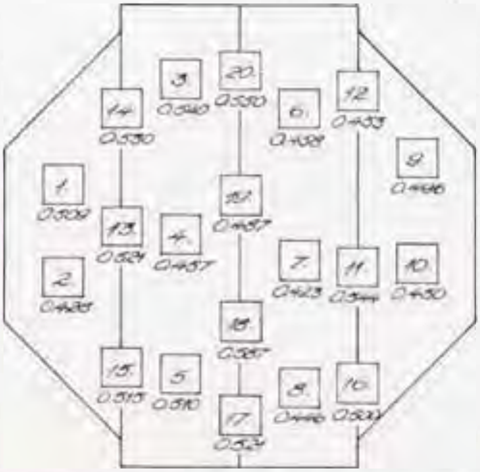

Fig. 24:1. Testing the artificial subgrade for the slabs in the MII series. The bed consisted of four layers of approx. 50 mm thick porous wood fibre board. The bed was tested at 20 points by means of a steel plate 30 × 30 cm, which was loaded with $P = 217$ kg. The depression δ of the plate in the bed was measured by means of dial gauges placed at the centre of two opposite sides. The k-values obtained in kg/cm³ were calculated from

$$k = \frac{P}{900 \cdot \delta_{\text{aver}}}$$

and are shown under the respective measuring points.

other wire direction of the wire fabric. The longitudinal reinforcement was placed in the same layer as the wires in the corresponding direction of the reinforcement mesh in the main test unit.

The concrete consisted of quick-hardening cement and sand for the slabs in the first series and standard cement, pea-sized gravel and sand for the slabs in the later series (the proportions of gravel: sand were approx. 3:4). The consistency of the concrete was maintained at approx. 4° VB. The amount of cement and water- cement ratio for the concrete in the various slabs is shown in Table 24:1, page 85. The compressive strength of the concrete was checked by means of test cubes and, in case of the later series, also standard beams for testing flexural strength. The test values are shown in Table 24:1. Three wires from both the directions of the mesh for each slab were clipped and tension tested. There was often a considerable difference in the strength between the wires from the two directions.

When casting was carried out the concrete was stamped by the use of a wooden stamp. The surface was levelled against the edges of the mould and evened carefully with a steel levelling tool. During the hardening period, the surface was maintained moist by the use of saw-dust. The slabs in Series MI which were made of quick-hardening cement, were tested when they were about 10 days old, the slabs in Series MII were tested at an age of 2—3 weeks. Detail test strips and standard tests were tested on the same day or the day following the main test.

243. Test devices, test procedures and test results

Fig. 24:2 shows the principle of the loading device. The load was imposed on the centre of the slab via a circular load distribution plate by means of a jack which was attached upside-down to an I-beam. This went transversely over the slab and, outside the edges of the slab, it was attached to the floor by means of iron straps and floor bolts. The load was measured through the pressure in the jack hydraulic fluid by means of a precision manometer. The plunger in the jack was well ground into the cylinder and had also been turned backwards and forwards during the test in order to eliminate plunger friction. A thin, pressure-equalizing wood fibre plate was laid between the load distributing plate and the concrete slab during testing.

Fig. 24:3 and 24:4 show photographs of the test slab and the test devices during both the first series of tests.

During the test loading the depression of the surface of the slab at various points was determined by the help of normal dial gauges. These were placed along two diameters at right angles to each other and were attached to special measuring beams fitted outside the edges of the slab (see Fig. 24:3 and 24:4). The location of the measuring points varied somewhat for the various slabs. The interval between them was closer along one of the diameters; in Series MI generally 20 cm, in Series MII 25 cm. Along the other diameter, the interval was generally double the size. Fig. 24:5 shows examples of the normal location of the instruments.

In the MI series no measurements were made of the depression at

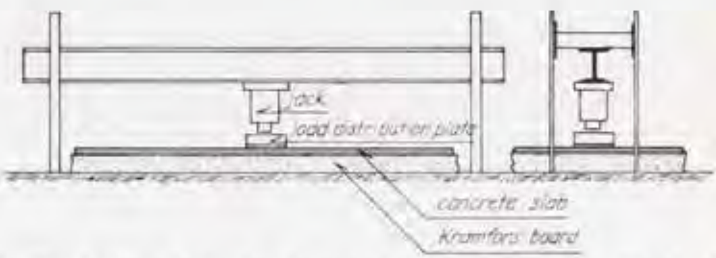

Fig. 24:2. The loading device for the test slabs in the M series. Sketch of layout.

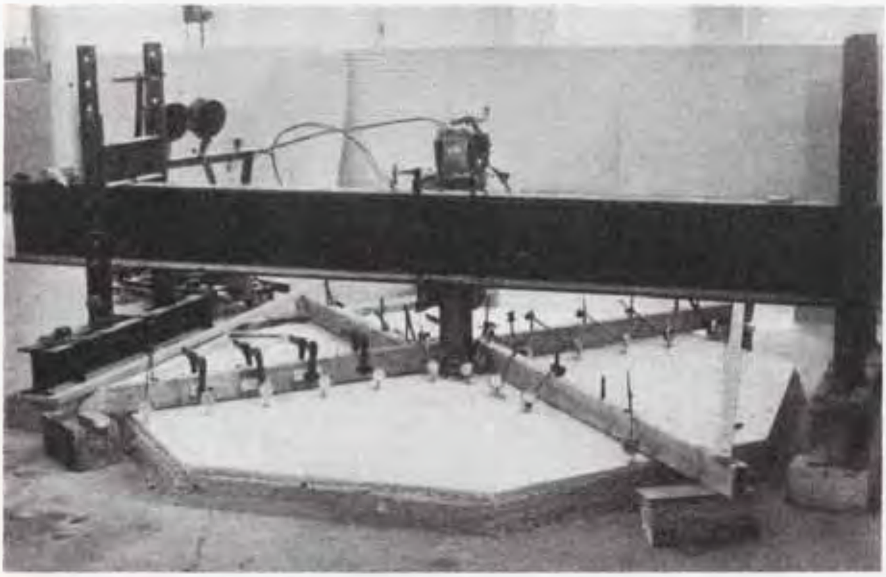

Fig. 24:3. A test slab in the MI series, ready for testing. The dial gauges for depression measurements are in position.

Fig. 24:4. A test slab in the MII series, ready for testing. The dial gauges and strain gauges are in position. Notice the "tunnel" under the jack in which the curvature gauge in Fig. 24:6 was located.

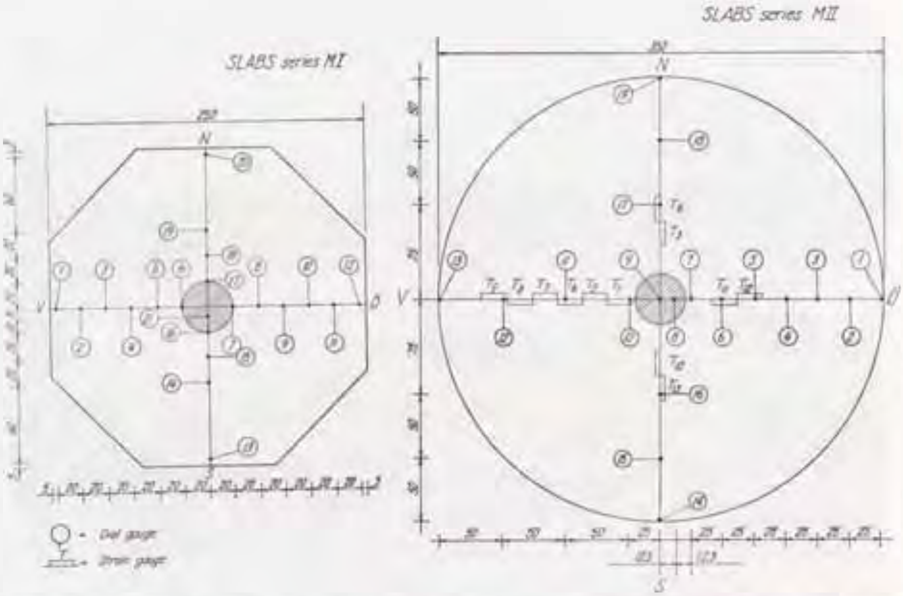

Fig. 24:5. The location of the dial gauges for depression measurements and the strain gauges for strain measurements on the test slabs in the MI and MII series respectively. On the slabs in the MII series, the location of the strain gauges was varied slightly (the exact location is shown by the sketches in the result diagrams,) but the figure shows the most usual location.

the centre point but this was estimated with the aid of the depression at the points close to the edge of the loading plate. In the MII series the depression at the centre point was measured as well as at a further point under the loading plate by means of a special "curvature gauge" as shown in Fig. 24:6. The measuring points on the dial gauges were taken down through holes in the loading plate and the actual "measuring bridge" was taken through a "tunnel" between the jack and the loading plate. This device registered depressions at these points under the loading plate relative to the legs of the measuring bridge (base 50 cm) and by measuring the depression at the points where these legs rested outside the edge of the loading plate, it was possible to calculate the absolute movement at the centre point. The device also provides the possibility of calculating the curvature in the central zone of the slab, whereby the deformation line of the slab in the centre is considered to correspond to a 4-grade parabola according to the method shown in Fig. 24:7.

Measurements of tension in the top surfaces were also carried out on the slabs in Series MII. The actual purpose of these measurements

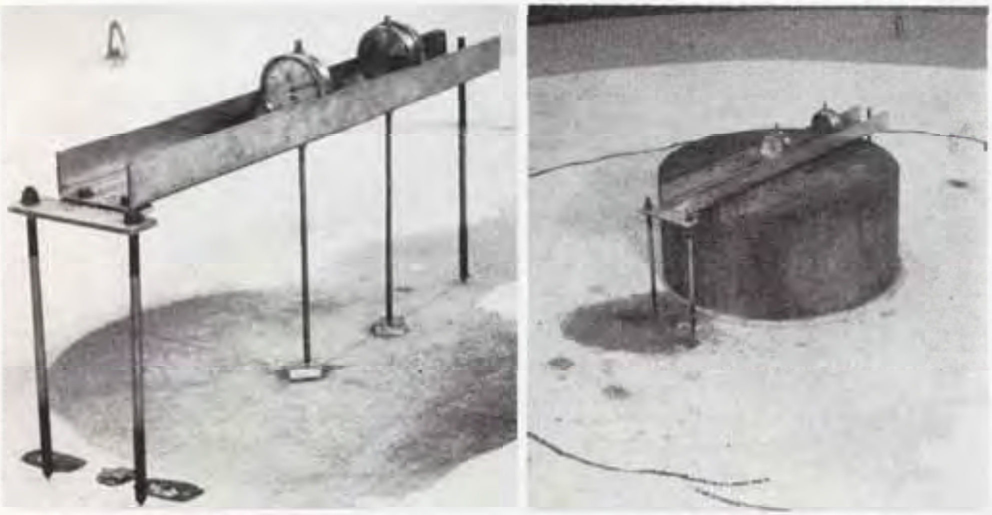

Fig. 24:6 A and 24:6 B. The curvature gauge for measurement of the deformation of the slab in the centre. The two dial gauges with extended points measured the depression of the slab relative to the legs of the measuring bridge (Fig. 24:6 A). The points passed through holes in the loading plate (Fig. 24:6 B).

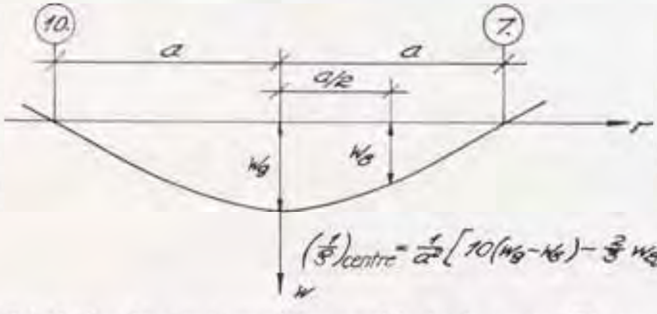

Fig. 24:7. Calculating the curvature of the test slabs in the centre. The measuring bridge in Fig. 24:6 was used to obtain the relative depressions w_8 and w_9 in relation to the measuring points 7 and 10. If the equation of the depression line in the centre zone is approximated to a fourth grade function

$$w = p\,r^4 + q\,r^2$$

where the coefficient

$$q = \frac{1}{2\,a^2}\left[10\,(w_9 - w_8) - \frac{2}{3}\,w_9\right]$$

then the curvature in the centre will be

$$\left(\frac{d^2 w}{dr^2}\right)_0 = \left(\frac{1}{\varrho}\right)_0 = 2\,q,$$

that is to say

$$\left(\frac{1}{\varrho_0}\right) = \frac{1}{a^2}\left[10\,(w_9 - w_8) - \frac{2}{3}\,w_9\right]$$

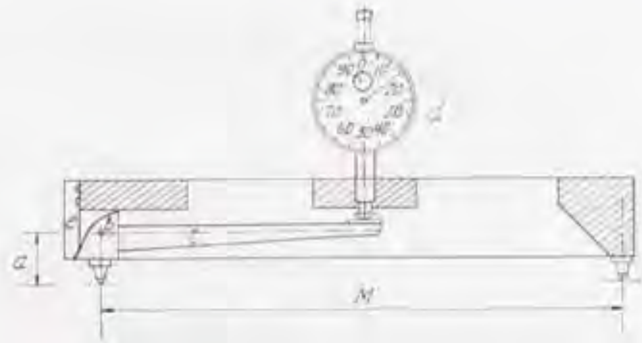

Fig. 24:8. The strain gauge used for strain measurements on the top surface of the slab, MII series. The movable edge a consists of one arm of a right-angle lever, hinged at b, the longer arm l of which transfers its movement to a dial gauge d. The lever arms have a ratio of approx. 5:1 and the measuring base M is 20 cm, so that a movement of 1 mm on the dial gauge corresponds to a strain of 1 ‰. e is a spring which retains the levers in contact with the dial gauge.

was to register crack formation in the top surface which makes its presence obvious through uneven movements in the strain gauge which is placed over a developing crack. The gauges used, the design and application of which are shown in Fig. 24:8 and 24:9, had a relatively long measuring base, 20 cm, and were usually placed within the zone where the deformation of cracks could be expected. It is therefore not generally possible from these tension measurements to derive any definite information concerning the distribution of moments along the radius of the slab, and test analysis in this respect has only been carried out in special cases.

The seven slabs in Series MII B (see Table 24:1), which all had the same reinforcement and concrete of the same composition, were used for an investigation of the influence of varying conditions of loading. On three of the slabs (subsidiary Series MII B:a) the influence of twin loading was studied, one of these slabs was serving as a comparison slab with a single load, (load distribution = 40 cm) while both the other slabs had the load distributed over two circular surfaces with the same total area (diameter = 28 cm) and with the distance between centres of 42 and 84 cm respectively. The loading and measuring devices are shown in Fig. 24:10. Of the other four slabs in Series MII B (subsidiary Series MII B:b) three were tested by repeated loading and unloading and one (MII B:a) by subjecting it to a mobile load. A more detailed description of these tests is given in Section 331 in connection with a discussion of the ultimate load.

The loading was increased in steps of about 100—200 kg. and all

Fig. 24:9. Fitting the strain gauges on the top surface of the slab. The strain gauges were fitted overlapping by means of steel bows which were attached by synthetic resin adhesive (kaurit) to the surface of the slab. The measuring edges rested on small steel plates, also attached by adhesive to the surface of the concrete. The figure also shows how the depression dial gauges were fitted to the measuring beam.

Fig. 24:10. The loading and measuring devices when testing with twin loads. The figure shows how the depression and strain were measured at the centre of the slab by means of curvature gauges and strain gauges placed between the two loading plates.

the measuring instruments were read off at each step. During the tests a certain time scheme was followed as far as possible: increase of load during one minute and constant loading during four minutes, the gauges being read off during the last minute.

During the higher loading steps, observations of crack formation and the failure procedure in the top surface were made. In order to facilitate such observations, the top surface of the slab was painted white with a white-wash made of chalk. At a certain loading value, a circular crack was observed on the surface of the slab. Usually a smaller part of the crack was discovered first, but during the time a loading step was imposed, the crack generally developed along a complete circumference approx. concentric with the loading plate. In the case of the top-reinforced slabs and also with some of the single-reinforced slabs several circular cracks appeared with further increased loading, usually with lesser radii than the first crack. The cracks were marked in as they appeared and were later drawn or photographed on the termination of the tests. Fig. 24:11 shows the crack pattern for some of the test slabs.[1])

The values of the loads when the first crack was discovered have been introduced in Table 24:4 in Section 245:1 together with the values of the crack loads and the loads at which the reinforcement in the top of the double-reinforced slabs began to yield, objectively decided by analysing the results of the tension gauge readings for the slabs in Series MII (see Section 245:1).

In the MI test series the loading was increased until stamping out failure occurred in the part of the pavement round the edge of the loading plate or in certain cases along the inner circular crack. This caused large degree of deformation in the wood fibre bed so that it was necessary to replace this after each test. In the MII series, where the bed was used for all the tests, loading was therefore not taken up to this stamp-out failure level but was generally taken only a few loading steps over the load at which the first circular crack occurred or, in case of top-reinforced slabs, until the top-reinforcement bars were judged to have reached the yield point.

The results of the depression and tension measurements are shown and analysed in Section 245.[2])

After this test had been completed, the slab was lifted up from the

[1]) All the crack patterns are shown in the test result supplement, Section 921.

[2]) Complete test results in the form of diagrams of the depression lines for the two diameters at right angles along which the gauges were located as well as centre depression and curvature diagrams and diagrams of the tension measurement values are contained in Section 922 of the test result supplement.

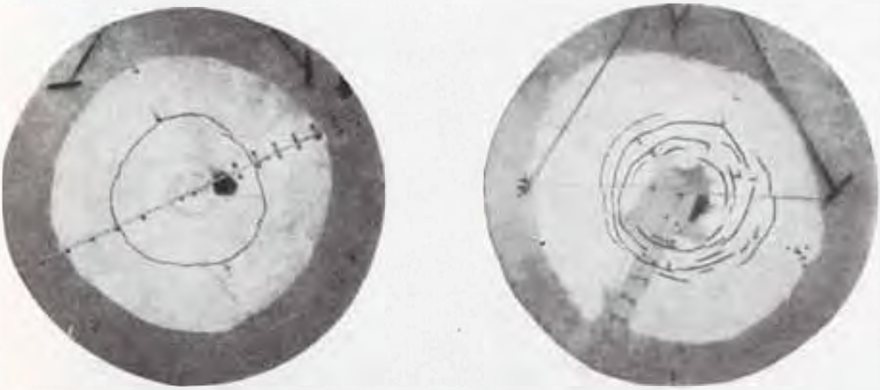

Fig. 24:11. The test slabs MII:2 (single-reinforced) and MII:7 (double-reinforced) photographed after test loading with the circular crack formation marked in.

subgrade and broken so that the thickness could be checked. Measurements of this were carried out at about 30 points along the circular crack and inside it, so that both the total thickness of the slab and the position of the reinforcement was measured. The results of these measurements are introduced in Table 24:2 in a following section.

244. Material constants for slabs and subgrade

244.1. *Determination of the ultimate moment and the flexural rigidity*

The elasticity and strength properties of the test slabs have, as already described, been determined with the help of the detail tests (page 86), these consisting of slab strips, cast at the same time as the test slabs. The test device is shown in Fig. 24:12, 24:13 and 24:14. These detail tests have generally been loaded by means of two linear loads, and deformation has been measured by means of a *curvature gauge* on a measuring length between the loading points, inside which zone the moment and the curvature were constant, all following the method shown in Fig. 23:1, page 63. When testing the detail tests in MII series, the *tensions* of the tension side of the test strips were also measured by means of strain gauges of the same type as those used during the main test (see Fig. 24:13).

Of the three detail tests for each test slab in the MI series, two were reinforced and these were tested with the reinforcement in the tension zone, corresponding to the positive moment in the main test, while the third plain concrete detail test was subjected to testing by flexure corresponding to the negative moment in the main test. Of the four

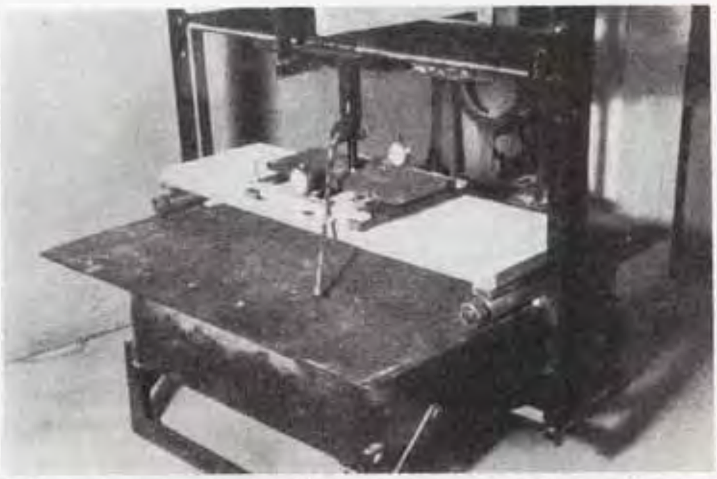

Fig. 24:12. Device for testing the detail test strips belonging to the test slabs in Series MI. The slab strip is laid on the pan level of sliding weight scales and the loading, which is transferred from a frame attached to the base of the scales by means of a screw jack, is measured on the sliding weight scales. The deformation is measured by means of a curvature gauge as shown in Fig. 24:6. The weight of the slab itself must be included in the calculation of the ultimate moment.

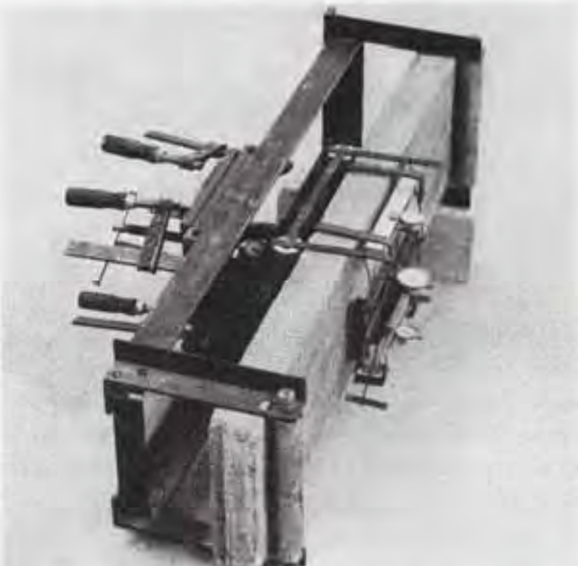

Fig. 24:13. Test device for detail test strips belonging to the test slabs in the MII series. The slab strip is laid on rollers attached to an L-girder frame and the load is applied by means of a screw jack between the frame and a load distribution beam with two rollers against the slab strip. The loading is measured by means of a ring dynamometer as shown in Fig. 24:14 placed between the jack and the load distribution beam. While testing was carried out, the complete device was laid on its side, so the weight of the slab itself had no effect.

Fig. 24:14. A ring dynamometer of the type used in the test device shown in Fig. 24:13. The dynamometer was calibrated repeatedly between the tests.

detail tests, belonging to each test slab in the MII series, two with reinforcement taken from both directions of the reinforcement mesh were tested with positive moment and the other two with negative moment. Each detail test unit was generally utilized for several tests in such a way that the uncracked parts on each side of the crack zone were tested again for failure so that in the MI series in most cases one of the halves has been tested for positive and the other for negative ultimate moment, while in the MII series both the halves of a detail test have been loaded with a moment of a direction opposed to that of the moment of loading on the original testing. During these latter tests on "half-strips" no deformation or tension measurements were carried out, only flexural loading to failure; the test device is shown in Fig. 24:15. These last-mentioned types of test provided the possibility of a more definite reliability when judging the ultimate moment values (generally six tests). These show comparatively large variation, even if respect is taken to variation in the thickness of the test slab strips and the position of the reinforcement, these dimensions having been carefully measured at the section of rupture after each test. Variation was particularly large concerning the negative ultimate moment values (tensile strength of the concrete).

The values for deformation and tension measurements carried out on the detail test units have been accumulated into curvature and tension

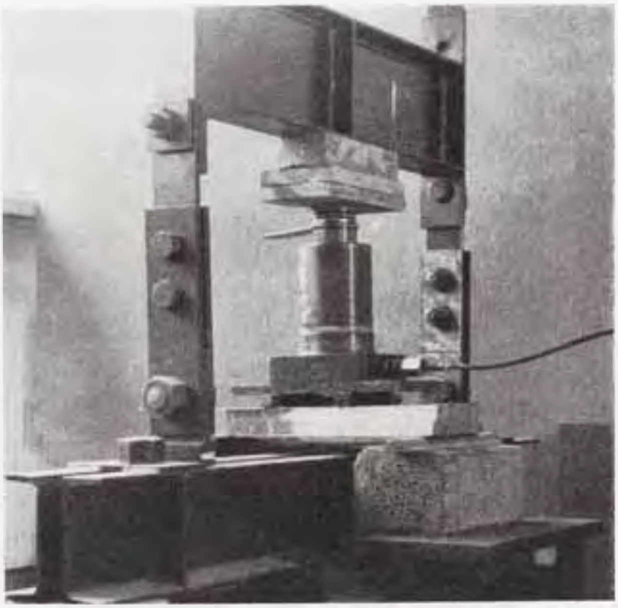

Fig. 24:15. Test device when testing the "half-slabs" on each side of the failure section after testing the detail test strips in the device shown in Fig. 24:13. The loading was applied through two loading rollers from a hydraulic jack. The ultimate moment here must be corrected with respect to the dead-weight of the slab.

diagrams of the type shown in Fig. 24:16.[1]) From these diagrams the required test results can be obtained.

The results of the tests with negative moment were particularly irregular and difficult to judge in the case of many of the double-reinforced slab strips. This depends upon the fact that the top reinforcement selected was too weak, so that the ultimate moment, when the yield point in the top reinforcement was reached, was only insignificantly over (in the case of slab MII:7 even under) the moment when tension rupture of the concrete itself occurred and, as has already been pointed out, these slabs function more as single-reinforced slabs. In order to be able to discuss the slabs also from this point of view, when analysing the results, the moment at tension rupture in the concrete has also been estimated from the result curves of the curvature and tension measurements for loading of negative moment (see Fig. 24:16). Also the tensions in the top surface, when crack formation began and when the yield point in the top reinforcement had just been reached, have been calculated from the result curves for the tension measurements. These tension values

[1]) Curvature and tension diagrams for all the detail tests are shown in the test result supplement, Section 922.

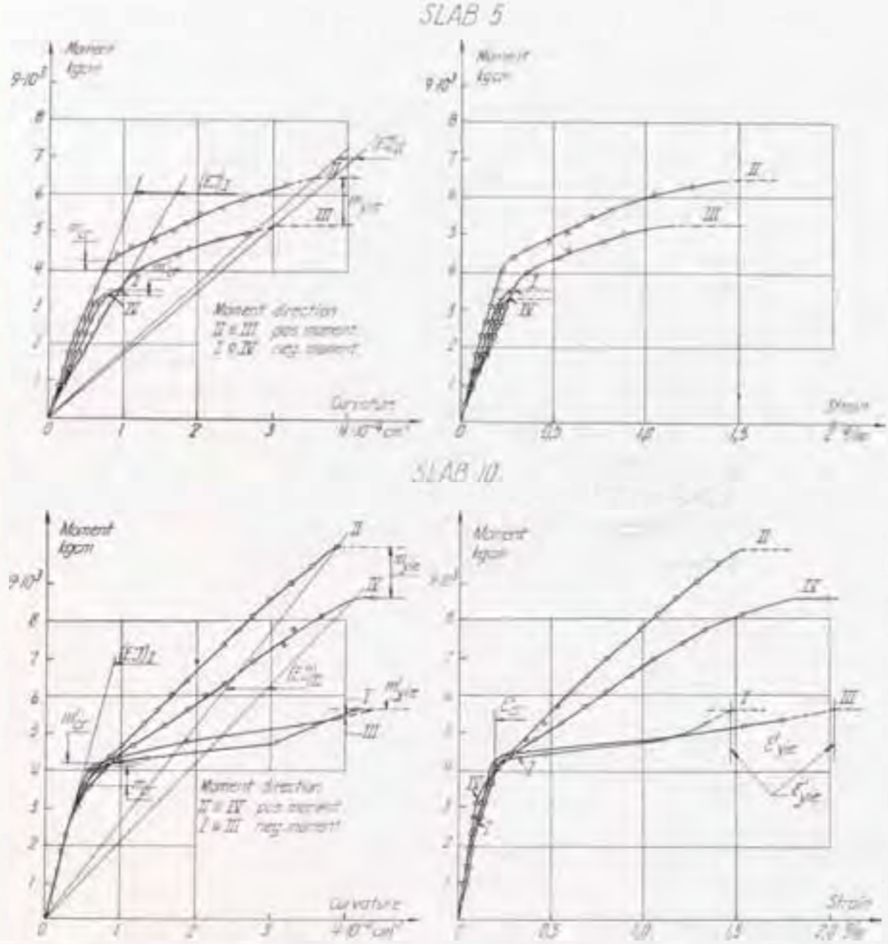

Fig. 24:16. Curvature and strain diagrams for the four detail tests from slab MII:5 (single-reinforced) and slab MII:10 (double-reinforced) respectively. The secant lines have been drawn in on the diagrams, these being used to calculate the flexural rigidity, as well as the moment values at crack formation and reinforcement yield together with the corresponding strain values (for negative moment), all of which are marked in.

have been utilized when determining the loads during the main tests with the double-reinforced slabs corresponding to concrete tension failure in the top surface or reinforcement yield point in the top reinforcement, whereby comparisons have been made with the corresponding tension measurements in the main tests. The results of the test loadings for negative moment of the slab strips belonging to the double-reinforced slab MII:9 could not be used, since, during the main tests, the tensile strength in the top surface of the test slab was broken by means of concentric cardboard slip rings laid in, but corresponding slips were, by mistake, not laid in in the corresponding slab strips. For this particular slab, the negative ultimate moment and the corresponding tension in the top surface have been estimated by calculation from the yield strength of the reinforcement bars.

The moment values for the tension rupture of the concrete have, in the same way, also been determined for positive moment loading in order to provide data for the study of the test slabs when crack formation started in the bottom surface (Stage I) (see Fig. 24:16).

The results from all the tests with the detail test units have been collected in Table 24:2.[1]) The figures, shown there for each slab, are thus average values of the results of the tests on the detail test units and half-strips of these belonging to slab in question. The values of the flexural rigidity in Stage I and Stage II have been calculated according to the principles discussed in Section 232 and all the test results have been corrected for differences in thickness and position of reinforcement between the detail test unit and the main test in the way described in the same section.

In the table theoretically calculated values for Ei have also been introduced. For this calculation, the values $n = 10$ for stage I and $n = 15$ for Stage II have been used and the tension zone in the later case has been assumed to be completely inactive. By comparison with the test values it shows that agreement is relatively good.

244:2. *Discussion of the properties of the subgrade and determination of the subgrade constant*

During the model tests the subgrade consisted, as already mentioned, of a bed of high-porosity wood fibre board which was laid directly on the hard concrete floor in the laboratory. The thickness of the bed in the MI series was about 10 cm and in the MII series about 20 cm.

It is obvious that a bed of this type should behave almost as a resilient subgrade. It is obviously unreasonable in the case of a 10—20 cm thick bed on a hard bottom to use a theory based on an assumption of an elastic subgrade of infinite depth. It can, however, be pointed out that the property of the theoretical resilient bed, whereby loading on one point does not cause any depression at adjacent points, cannot be completely satisfied in the case of a bed made of board.

In order to clarify the properties of wood fibre board as a flexible subgrade, reference is briefly made below to some of the results from an examination of the use of board as a vibration-damping layer in concrete

[1]) The complete result is shown in the test result supplement, Section 922.

Slab			Dimensions, reinforcement				Test results from detail tests, re-calculated for main test dimensions								Calculated values	
Litt.		Test number	Total thickness h_u cm	Effect. thickness aver. h cm	Reinforcement ⌀ square mm		Ultimate moment kgcm/cm				Ultimate strains in top surface ‰		Flexural rigidity kgcm²/cm		Flexural rigidity kgcm²/cm	
							at yield point		at concrete failure							
Main series	Sub series				br	tr	in bottom m_{yie}	in top m'_{yie} (neg)	in bottom m_{cr}	in top m'_{cr}	ε'_{cr}	ε'_{yie}	$(Ei)_I$	$(Ei)_{II}$	$(Ei)_I$ $n=10$	$(Ei)_{II}$ $n=15$
M I		1	2.0	1.8	1.8/22.5		44			22				$0.34 \cdot 10^5$	$1.56 \cdot 10^5$	$0.45 \cdot 10^5$
		2	3.2	2.8	3.2/50		138			36				1.3	6.6	2.1
		3	3.1	2.7	3.2/50		112		[3])	59				1.7	6.0	1.9
		4	3.1	2.7	3.2/50		109			46				1.9	6.0	1.9
		5	2.8	2.4	3.2/50		104			35				1.7	4.4	1.4
		6	3.2	2.8	3.2/50		130			40				1.5	6.4	2.1
		7	3.0	2.6	3.2/50		102			34				1.4	5.4	1.8
M II A	a	1	4.10	3.88	2.5/50		206		148	135			$16.5 \cdot 10^5$	$6.4 \cdot 10^5$	$12.5 \cdot 10^5$	$2.2 \cdot 10^5$
		8	4.44	4.21	2.5/50		157		135[2])	135			17.5	4.8	15.9	2.6
		2	4.52	4.14	3.4/50		222		148	135			17.1	6.0	17.6	4.1
		3	4.36	3.58	5.0/50		337		142	131			19.8	6.0	17.0	5.2
	b	4	4.36	4.07	3.4/50		195		98	86			11.8	4.0	15.8	4.0
		5	4.26	3.94	3.4/50		198		140	115			14.3	6.0	14.5	3.6
		6	4.42	4.03	3.4/50		235		180	180			18.2	7.6	16.2	3.8
	c:1	9	5.02	5.31	3.4/50	2.5/100[2])	269	100[4])	160		0.26	1.68[4])	28.0	8.1	33.0	7.0
		7	5.10	4.80	3.4/50	2.5/50[1])	283		196	216[1])			28.0	11.7	25.0	5.7
		11	5.78	5.30	3.4/50	3.4/50	293	253	170	164	0.20	1.03	35.0	8.1	35.8	7.7
	c:2	12	5.56	4.84	5.0/50	[2])	418	0	139	0[2])			23.3	9.4	34.2	10.5
		10	5.59	5.13	4.2/50	3.1/50	345	202	146	164	0.20	1.73	28.0	9.3	33.0	9.2
		13	5.42	4.96	3.4/50	3.4/50	260	220	133	137	0.18	1.40	28.0	7.2	29.4	6.2
M II B	a	14	5.53	5.00	3.4/50		277		198	209			$31.0 \cdot 10^5$	$8.6 \cdot 10^5$	$31.6 \cdot 10^5$	$6.5 \cdot 10^5$
		15	5.63	5.15	3.4/50		299		215	218			27.5	8.2	33.0	6.6
		16	5.38	4.98	3.4/50		303		200	207			31.5	9.5	29.0	6.1
	b	17	5.24	4.82	3.4/50		280			190			26.5	9.6	26.6	5.7
		18	5.11	4.62	3.4/50		271			173			30.0	7.9	24.5	5.2
		19	5.20	4.80	3.4/50		270			176			22.5	7.7	26.0	5.5
	c	20	5.30	4.80	3.4/50		264			189			31.5	6.8	27.5	5.4
M II C		21	8.05	7.38	5.0/50		768		~400	410			$105 \cdot 10^5$	$28 \cdot 10^5$	$100.0 \cdot 10^5$	$26.5 \cdot 10^5$

1) Top reinforcement without function due to high tensile strength, slab considered as single-reinforced; m'-value stated thus concerns concrete failure. 2) Tensile strength of concrete broken by insertion of concentric cardboard rings. 3) The moment at concrete tension failure in the bottom for these slabs in Series M I has been put $= m'_{cr}$ for concrete tension failure at negative moment. 4) The values have been estimated from the reinforcement yield point and yield tension.

Fig. 24:17. Test device when testing plain concrete slab strips on elastic subgrade. The size of the test beam was 260 × 30 × 6.4 cm and the subgrade consisted of high-porosity wood fibre board.

slabs.[1]) This investigation included the test loading of two slab strips of plain concrete on a subgrade consisting of two layers of board of the same type as those used during the MI series. The loading consisted of a concentrated linear load in the centre and the depression was measured at several points along the centre line of the slab strip. The test device is shown in Fig. 24:17. After the slabs had failed, this taking place exactly under the loading line, the flexural rigidity and flexural strength were determined by testing both the slab halves, these being test-loaded as simply supported beams. The k-value of the wood fibre bed was determined partly through a test on a recessed section of the bed and partly from the average degree of depression during the main tests.

The slab strips can be considered as being beams on a flexible subgrade. Since the beam material in this case was plain concrete then the elastic properties of the beam can be considered to be comparatively good (Stage I). The equation for such a beam can, if the subgrade is considered to be resilient, be written

$$EI \frac{d^4 y}{dx^4} = - k\, b\, y \tag{24:1}$$

where EI = the flexural rigidity of the beam, b = the width of the beam.

[1]) Kramforsplattan som vibrationsdämpande mellanlägg i betongplattor. (The Kramfors board as a vibration-damping layer in concrete slabs.) Stenciled report from the Department of Structural Engineering, Chalmers University of Technology, Gothenburg, 1945.

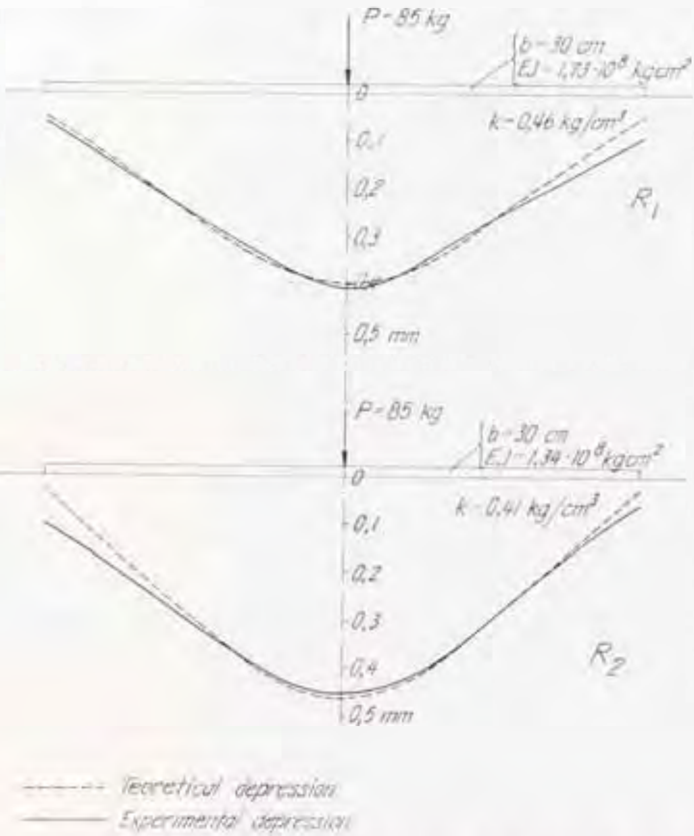

Fig. 24:18. Deflection curves for the slab strips as shown in Fig. 24:17 with a load of 85 kg. For comparison, the theoretically calculated elastic lines are shown.

This equation can, in the case of the existing loading and boundary conditions, be easily solved exactly and the solution can be used for the calculation of the vertical deformation and the moment in the various sections of the test beams. Fig. 24:18 shows the result of the vertical deformation measurements compared with the theoretical elastic lines with a load of 85 kg and in Table 24:3 the average depression figures have been calculated as well as the central moment and the corresponding ultimate loads together with the test results obtained. The results show that particularly good agreement prevails between theory and practice. This shows, that a subgrade of porous board has, on the whole, properties that correspond to those of a resilient subgrade. In the analysis of the model test result, *only* this theory will thus be considered.

The k-values for the model tests in the MI series have been determined partly through tests on recessed sections of the bed and partly by

TABLE 24:3. Flexural testing of plain concrete strips on a subgrade of high-porosity wood fibre board as shown in Fig. 24:17 and 24:18.

Test beam	Thickness in failure section, cm	Material constants			Deflection in centre at $P=85$ kg according to		Ultimate load, kg	
		k kg/cm³	EI kg cm²	σ_f kg/cm²	test	theory	In main test	According to theoret. max. mom. at σ_f
R_1	6.25	0.46	$1.73 \cdot 10^8$	34.7	0.41	0.40	260	298
R_2	6.35	0.41	$1.34 \cdot 10^8$	35.2	0.45	0.46	290	320

calculation of the average depression (depression volume) in the main tests according to the formulae (23:3) in the way described by the author in Section 233.

For the k-value determination on cut-out sections of the bed, a test surface of 20×30 cm was used and during test loading, the load was distributed over the complete surface by means of a thick concrete plate. The test device is shown in Fig. 24:19. The co-relation between the depression, calculated from the average value of the depression of the four corners, and the load are given in the form of diagrams,[1]) some typical examples of which are shown in Fig. 24:20 A. One can see, that the k-value, which forms the secant modulus to the curves, increases somewhat when the slab is compressed but the degree of constancy

Fig. 24:19. k-value determination on cut-out sections of the subgrade material in the MI series, high-porosity wood fibre board. The loading device was the same as that used for the deflection tests as shown in Fig. 24:12 and the depression was measured by means of four dial gauges in the corners of the concrete load distribution plate.

[1]) All the diagrams for the k-value determinations for slabs in the MI series are shown in the test result supplement, Section 922.

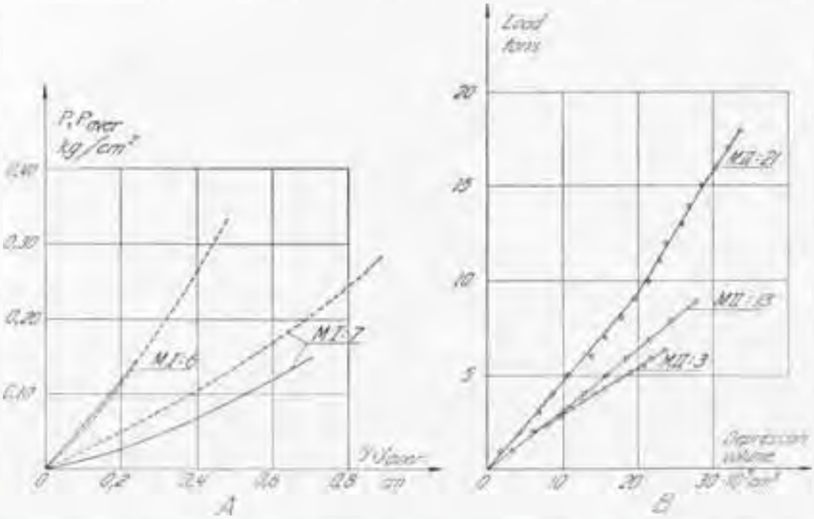

Fig. 24:20 A. Relationship curves between loading and deformation for the subgrade material of wood fibre board for the slabs 6 and 7 in series MI. The unbroken curves have been obtained from the average depression during the main tests, while the broken ines have been obtained from the tests on the cut-out sections of the subgrade material (with the test device shown in Fig. 24:19).

Fig. 24:20 B. Curves showing the relationship between the load and the depression volume for the slabs 3, 13 and 21 in series MII. Observe that the bed, which consists of the same plates of wood fibre board for all the tests, becomes less resilient as more tests are carried out, this depending on the successive permanent compression of the material composing the bed.

in k is comparatively satisfactory. The k-value determinations from the main tests are shown as relationship curves between the average depression and the average loading, and some curves of this type for the MI series have also been marked in on Fig. 24:20 A[1]). The good agreement between the curves according to both the methods further corroborates that the wood fibre board can be considered as being a good resilient subgrade.

In the MII series, the k-value determinations have been carried out only according to the last-mentioned of the methods quoted above, that is to say by calculation of the depression volume from the main tests. Some of the result curves, showing the relationship between the depression volume and the load, are shown in Fig. 24:20 B[1]). The curves have a more linear appearance than in the case of the MI series depending on the fact that the bed was considerably thicker. In the case of the slabs MII: 15 and :16, tested with twin load, the calculation could not be carried out

[1]) See note 1, previous page.

since the depression volume is unsymmetrical, and the *k*-value has been estimated with the aid of the corresponding values for the slabs which were tested immediately before these two in question. It should be pointed out that the same bed material in the MII series was used for all the slabs, and the *k*-value determinations also show that the properties of the subgrade alter only to a slight extent between the various tests. The gradual successive increase in the *k*-value of the bed depends on the remaining permanent compression of the wood fibre board.

In order to study the properties of the bed in the case of a higher degree of compression, as can be considered to occur just under the centre of the tests slab, several test were also made on cut-out sections of the bed material. In these cases result curves were obtained of the same type as the curves in Fig. 24:20 A and in the case of a high degree of compression of the board the *k*-value increased considerably.

The *k*-values used for the theoretical analysis of the model test results have been obtained from the average depression curves for the main tests. These values obviously give the best impression of the average characteristics of the bed. For each slab generally two *k*-values have been calculated from secants to the average depression curves, viz. at a load corresponding to the failure of the concrete in the bottom surface at the centre of the plate and at a load corresponding to a failure in the top surface. The *k*-values estimated in this way and used for the analysis of test results have been introduced in the Tables 24:5—24:8 in the following section.

245. **Test results, treatment and theoretical analysis**

245.1. *General. Determinations of failure loads*

In the previous section it has been shown that the *subgrade* of wood fibre board functions mainly as a *resilient subgrade*. An analysis of the test results according to the theory for elastic slabs on resilient subgrade should thus clarify to which extent a *reinforced concrete pavement* with its varying elastic properties behaves as an *elastic slab* according to the assumptions made in the theory. The test results and the theory should thereby be compared with respect to depression as well as moments and ultimate loads.

The depression measurements on the various slabs can be best shown by compiling the measuring values as *depression lines* for the two diameters at right angles along which measurement has been carried out. Fig. 24:21 shows an example of the depression lines for one of the slabs.[1])

[1]) The depression lines for all the slabs are shown in the test result supplement, Section 922.

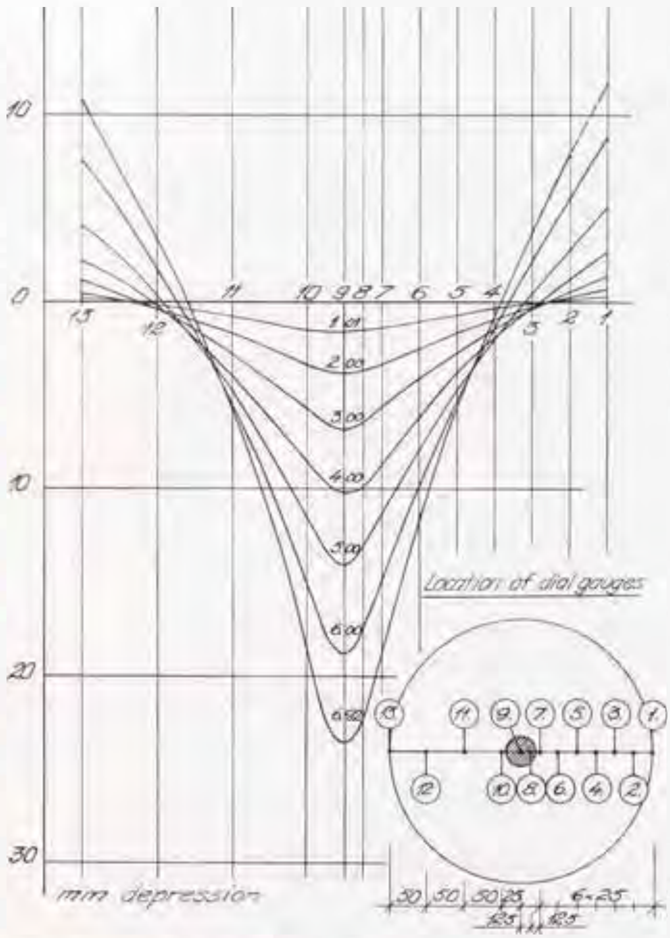

Fig. 24:21. The depression lines for one of the two measuring diameters at right angles on the slab MII : 8 for part of the loading steps. The load is shown in tons at the top of the respective curves.

This figure shows that the edge of the slab lifts to a comparatively great extent from the subgrade, and the same thing applies more or less to all the slabs. This should not be forgotten when judging the theoretical test analysis since, according to the assumptions made in the theory, the slab and the subgrade must be in contact over the entire surface.

The measurements of depression nearest the centre of the slab by means of "curvature gauge" (Fig. 24:6) makes it possible to calculate the curvature of the slab at the centre according to the method stated in Fig. 24:7. These curvature values can be utilized to estimate the *moment* at the centre In this case the curvature values in question are compared

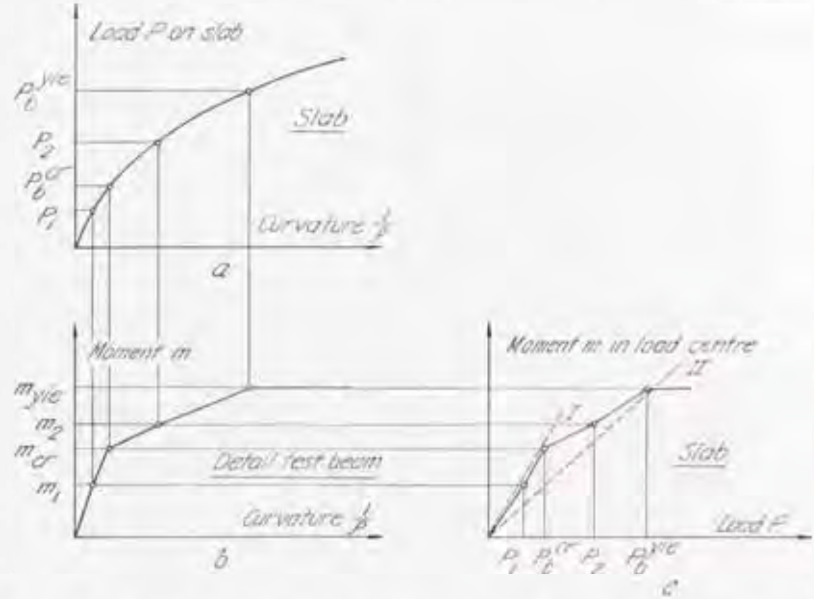

Fig. 24:22. Method for drawing the relationship curves $P - m_{\max}^{+}$ for the test slabs. By comparison between the curvature graphs a, obtained from the curvature measurements in the main tests (see Fig. 24:7), and the curves b from the tests on the appropriate detail tests beams (Fig. 24:16), it is possible to obtain the value of the moment in the loading centre for different loads P_1, P_2 (curve c) as shown in the figure. Vice versa, the loads P_b^{cr} and P_b^{yie} causing crack formation and bottom reinforcement yield respectively can be obtained from the ultimate moment values m_{cr} and m_{yie} determined in the detail tests.

The figure also includes assumed lines I and II for the moment value according to the theory, calculated for the slab constants in Stage I and Stage II respectively.

with the results of the curvature measurements on the associated detail test strip (see Fig. 24:16), whereby the the last-mentioned curvature values have been corrected for variations in thickness between the main test slab and the detail test unit. Fig. 24:22 shows the method resulting in relationship curves between the loading and the moment in the centre for the different test slabs.[1]) It is obvious that the method is comparatively unreliable since the loads are indirectly estimated through a comparison between the curvature measurements. Especially for the circular slabs where the curvature is obtained from the differences between the $\frac{1}{100}$ mm graduated dial gauges (see Fig. 24:7), the result, especially in the case of small loads, is influenced to a great extent by the deficiencies in the measuring devices, such as the initial resistance to movement of the dial gauges.

[1]) All these diagrams are shown in the test result supplement, Section 922.

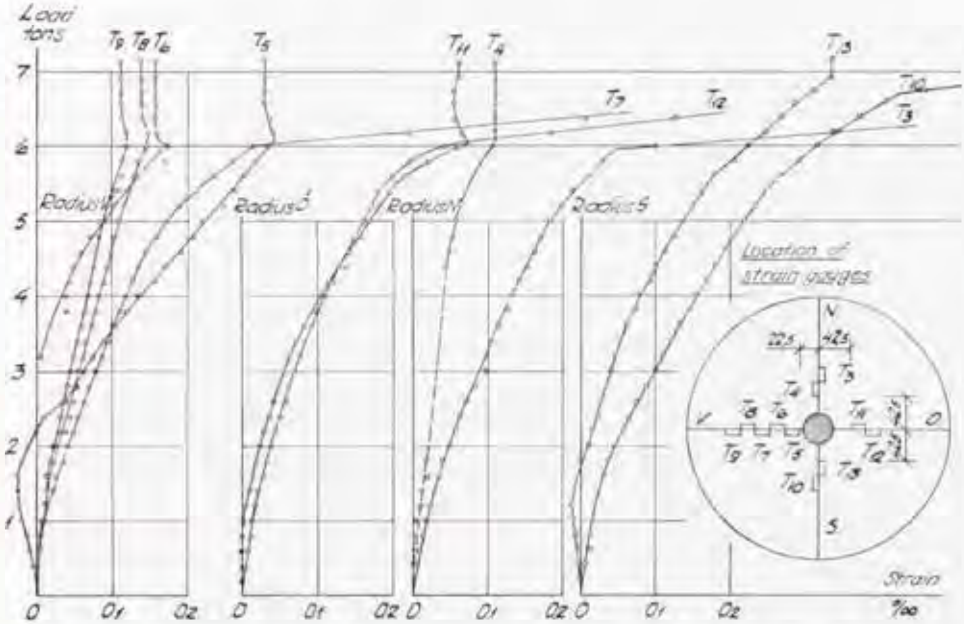

Fig. 24:23. The strains along the four measuring radii for the slab MII:14 (single-reinforced). The annular crack appeared between the measuring points on the gauges T_3, T_7, T_{10} and T_{12}, and the break-off point on the curves representing the movements of these gauges clearly shows the load causing a crack, which can thus be accurately estimated even if it lies between two loading steps. The resulting crack load has been calculated as the average value of the four loads estimated in this way.

These curves can be used to estimate the loads at the beginning of the crack formation P_b^{cr} and at the beginning of yield in the reinforcement under the loading centre P_b^{yie}, being the loads corresponding to the moment values at crack formation m_{cr} and yield point m_{yie} according to Table 24:2 (see Fig. 24:22). The load values obtained in this way have been introduced in the Tables 24:6—24:8 together with the corresponding theoretical values (see below).

The ultimate loads in the case of failure in the top surface due to crack formation P_t^{cr} or, in the case of the double-reinforced slabs, when the yield point in the top reinforcement is reached P_t^{yie} can be objectively fixed for the slabs in the MII series by an analysis of the measurement values for the tension gauges which were fitted on the top surface. Fig. 24:23 shows the collected tension measurements for one of the slabs. In this case of the single-reinforced slabs, as shown in the figure, crack formation was indicated through a very rapidly increasing gauge reading, when a crack occurred between both the edges of one of the gauges, and through such an analysis of the strain gauge movements (see Fig. 24:23) then the load causing the first cracks could thus be determined with a fair degree of accuracy. In the case of the double-reinforced slabs no such clearly marked discontinuity in the movements of the strain gauges were noticeable when the first crack occurred, but the intention of the tension measurements on these slabs was actually to try to decide when the top reinforcement reached the yield point. The estimation of the load in question has been carried out so that the tension measurements on the slab have been compared with the corresponding measurements carried out on the detail test strips from these slabs (Section 244:1). Here the tension in the top surface at the negative ultimate moment for the detail test unit has been re-calculated to the corresponding failure-tension value for the main test, respect having been taken to differences in slab thickness and the position of the top reinforcement between the detail test unit and the main test unit. The corresponding loads have then been obtained from the tension measurement curves for the main tests. An estimation of this type must however be comparatively unreliable, partly due to the fact that the movements of the tension gauges are strongly influenced by crack formation in the concrete and the number of cracks and the position between the edges of the gauges, partly due to the fact that top reinforcement has been selected so small and in certain cases located so far under the top surface that the negative moment at the yield point for the top reinforcement generally lay insignificantly over (in certain cases even under) the moment at the commencement of crack formation. The double-reinforced slabs have therefore largely functioned as single-reinforced slabs, and in order to be able to consider them as such slabs in the following test analysis, also the load at the first formation of top surface cracks has been estimated from the discontinuity in the tension measurements, which has also been compared with the corresponding measurements on the test slab strips (see Table 24:2), belonging to the slabs in question. The determination of load causing cracks in the case of these double-reinforced slabs is considerably more unreliable than in the case of the single-reinforced slabs. In the case of slab MII:9 with a very weak top reinforcement, the tensile strength of the concrete had been broken by rings of cardboard slip which had been inserted concentrically in the top surface of the slab, so that in the case of this slab it was not possible to obtain any loading value corresponding to concrete failure.

No tension measurements were carried out on the slabs in the MI series, but the author has attempted to determine the load causing cracks objectively through analysis of the depression measurements at the points laying nearest to the circular crack. The relationship curves

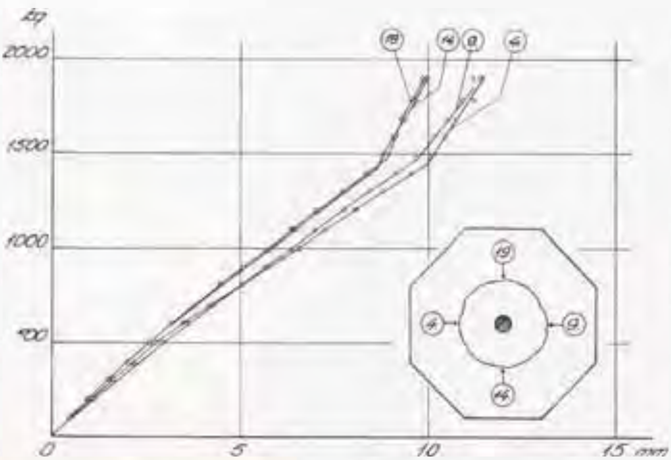

Fig. 24:24. Estimation of the crack load for slab MI:4 through analysis of the depression values for the measuring points close to the annular crack. The clearly defined break-off points on the four depression curves indicate the crack formation at the respective measuring radii. The crack load is calculated as the average value of the four loads estimated in this way.

between the load and the depression at these points showed that, at least with some of the slabs, there is a clearly marked break-off point at a load corresponding to the failure load. This obviously depends upon the fact that the crack functions as a hinge and thus alters the moment distribution and deformation in the adjacent zones of the slab. Fig. 24:24 illustrates such a case. Also with the slabs in the MII series the determinations of the load causing cracks have been carried out as far as possible according to this method, whereby good agreement has been reached with the values according to the tension measurements. It was shown that the crack was first noticed by a visual inspection at a rather heavier load than that which, according to the methods described, could be objectively estimated, but the difference was generally comparatively small and lay within the limits of one loading step.

The results of the various determinations of crack loadings are shown in Table 24:4, and, in the case of top-reinforced slabs, also the estimated loads for the yield of the top reinforcement have been introduced in the table. The table finally shows the assumed loads for top failure of the slabs. These have been determined as the average value for the various observations, little or no respect having been taken to the unreliable values (marked in the table by means of brackets).

For the theoretical analysis of the test values, the test results were compared with the corresponding theoretical values of the moment, Load values according to strain gauges, dial gauges close to cracks and visual observation. The values in brackets represent unreliable estimations of the depression measurements.

Series	Slab no.	Loads for failure in top surface according to: strain gauges, measuring radius E	W	S	N	Average value	dial gauge close to crack, meas. radius E	W	S	N	Average value	Visual observation	Assumed ultimate load
M I	1						670	650	670	610	650	635	650
	2							(1420)	1410			1630	≦1630
	3						1510	(1550)	1540	1600	1570	1770	1570
	4						1430	1455	1380	1465	1435	1580	1440
	5						1550	1670	1460	1660	1590	1640	1590
	6											1670	≦1670
	7						1730	(1750)	1760	(1880)	(1750)	1835	≦1830
M II	1		4650				4750	4700	4750	(5200)	4730	5000	4700
	2		4800				4950	4800	—	(4800)	4850	5000	4850
	3		4400				4600	4200	—	4400	4400	4380	4400
	4				2150		2650	2650	2800	2150	2550	3000	2550
	5		4000				4400	4000	4600	3800	4200	4000	4200
	6		6550				6300	6500	6520	6300	6400	—	6400
	7[1])		5670[1])				6050	5670	—	6150	5950	6920	5950
	8	5200	4900	5200	5150	5110	—	4600	5200	—	—	5400	5100
	9[2])	—	7950	8800	8350	8370[2])							8370[2])
	10	9500	8800	9000	9800	9200[3])							9200[3])
		6200	6200	6600	6200	6300[4])							6300[4])
	11	7600	7600	7700	—	7630[3])	top- reinforced slabs						7600[3])
		4700	4800	5000	4900	4900[4])							4900[4])
	12[5])	6300	—	5500	5850	5900[5])							5900[5])
	13	~8800	~8600	~8500	~8700	~8600[3])							8650[3])
		5000	4400	5000	4000	4600[4])							4600[4])
	14	6060	6020	6700	5950	6180	5900	6000	6750	6050	6170		6180
	15	9400	8900	9400	8400	9030							9030
	16	11320	10840	10840	—	11000						11320	11000
	17	7050	6800	6920	6900	6920	7050	6750	—	6920			6920
	18	6800	6550	6900	6600	6710							6700
	19	7140	7000	7220	6650	7000						6920	7000
	20	(7400)	7400	7300	7200	7320	7600	7600	7200	7300	7420		7330
	21	16000	16000	16000	15200	15800						16000	15800

[1]) Top reinforcement without effect, slab functions entirely as a single- reinforced slab. [2]) Load at yield point in top reinforcement, calculated for top reinforcement strain at yield point. [3]) Load at yield point in top reinforcement, estimated by comparison with detail tests. [4]) Load at formation of first top surface crack, estimated from discontinuity in strain gauges and through comparison with strain readings for detail tests.

crack and yield loads and depression values, these having been calculated according to the theory for elastic slabs on a resilient subgrade. The slab and the subgrade have been assumed to be completely elastic with a flexural rigidity value D and a resilience constant k according to Section 244. The values of the constants used in the calculations and the corresponding values of the elastic radius of stiffness l and the relative load distribution $a = \frac{c}{l}$ are introduced in the test result Tables 24:5—24:8 in the following sections. When applying these, a flexural rigidity value according to Stage I and a corresponding k-value should be used in the case of low loading, while the corresponding values for Stage II should be used in the case of higher loading.

The theoretical flexural moment in the centre of the slab has been compared with the test values by taking the theoretical relationship lines $\frac{P}{m}$, calculated from Diagram 22:9, and inserting them in the moment diagram according to Fig. 24:22. From this the theoretical loads P_b^{cr} and P_b^{yie}, corresponding to the formation of cracks and yield in the bottom surface under the loading centre, have been calculated for the corresponding moment values according to Table 24:2.

Furthermore, the theoretical values of P_t in the case of failure in the top surface (circular crack or reinforcement yield) according to table 24:4 have been compared with the corresponding test values. In this connection respect has been taken to the correction for the membrane effect, estimated in accordance with the methods in Section 234, page 74. (In the case of the lower loads P_b^{cr} and P_b^{yie} the membrane stress correction has no significance whatsoever). The theoretical failure values have been calculated from the diagram for the maximum negative moment in Fig. 22:14 and Fig. 22:9, $\nu = 0$, whereby the values according to Fig. 22:14 (concentrated load on slabs with finite radii) have been corrected for the influence of load distribution estimated in accordance with Fig. 22:9 for slabs of infinite extent.

For some of the slabs curves, in accordance with the theory and tests, of the moment distribution along the radius of the slab have been constructed for certain loadings, whereby the test values have been obtained by comparison between the tension measurements along the slab radius and the corresponding measurements of the detail test unit according to the same method as shown in Fig. 24:22. In the usual way correction has been made for difference in slab thickness between the main test slab and the detail test unit. The corresponding theoretical moment curves have been obtained by using the diagram in Fig. 22:9 for the central zone and, for the values nearest the edge where the influence of the load distribution can be assumed to be very small, by using the corresponding diagram in Fig. 22:14.

Comparison has been made between the theoretical and experimental depression values in the loading centre for the loads P_b^{cr}, P_b^{yie} and P_t defined above. The theoretical depression values have been calculated according to the formula in Table 22:1 and diagram in Fig. 22:8 B; calculations have been made for Stage I and Stage II. The corresponding theoretical relationship $P - w_0$ has been marked in on the test curves concerning the depression in the centre.[1])

For some of the slabs comparisons have also been made between the theoretical and experimental values concerning the depression lines for the diameter. The theoretical lines have been obtained by adapting the formulae (22:57) for the central zone or the corresponding diagram in Fig. 22:8 A and 22:8 B, concerning a slab of infinite extent, and for the edge zone the formula (22:59) and the diagram in Fig. 22:13 for a slab with finite extent under the influence of a concentrated load in the centre. This method should be permissible, since the influence of load distribution, as has earlier been shown, rapidly decreases outside the loading zone.

The compiled results of the tests are shown in the following Sections 245:2—4 and in Tables 24:5—24:8. These tables contain, apart from the experimental and theoretical results, also information concerning the test slabs and the constants and data necessary for calculation. A final section 245:5 is used to discuss the result of the model tests in their entirety.

245:2. *Test slabs, series MI*

No measurements of the depression in the centre were made on the slabs in the MI series. When making out the depression lines the values for the depression in the centre have been estimated according to exterpolation from the measuring points lying nearest to the centre.[2]) For a calculation of curvature and thus the moment in the centre these values can naturally *not* be used.[3])

---

[1]) Test result supplement, Section 922.

[2]) Test result supplement, Section 922.

[3]) BERGSTRÖM has, in his paper [4], produced a calculation for curvature and moment in the loading centre of the slabs in the test series MI (page 99 in the paper quoted). BERGSTRÖM states that he has calculated his test values from the depression lines supplied by the author in the preliminary test report [37] Judging by the test account made above a calculation of this type is altogether unreliable. BERGSTRÖMS "test values" have been quoted by BERNELL [8]. In this paper, BERNELL has analysed these and other tests from the viewpoint of the theory of elasticity, utilising methods, notations, formulae and diagrams of the author [38] without crediting the source.

TABLE 24:5. Series M I. Centre loading on test slabs.

Comparison between test results and elasticity theory.
Diameter 250 cm, bottom-reinforcement: slab 1, mesh 1.8/22.5; other slabs, mesh 3.2/50.

Series M I.	test no.	1	2	3	4	5	6	7
DATA FOR THE TEST SLABS								
Thickness, total h_s	cm	2.0	3.2	3.1	3.1	2.8	3.2	3.0
effective h	cm	1.8	2.8	2.7	2.7	2.4	2.8	2.6
Load distribution radius c	cm	5	5	5	10	10	10	20
Flexural rigidity, Stage II Ei	kgcm	$0.34 \cdot 10^5$	$1.3 \cdot 10^5$	$1.7 \cdot 10^5$	$1.9 \cdot 10^5$	$1.7 \cdot 10^5$	$1.5 \cdot 10^5$	$1.4 \cdot 10^5$
Resilience constant k	kg/cm³	0.27	0.13	0.33	0.053	0.34	0.54	0.16
Elastic radius of rigidity l	cm	18.5	31.6	26.8	43.5	26.6	23.0	30.6
Relative load distribution $\alpha = \frac{c}{l}$		0.28	0.16	0.19	0.23	0.38	0.43	0.65
Ultimate moment	kgcm/cm							
at bottom reinf. yield m		44	138	112	109	104	130	102
at top concrete failure m'		22	36	59	46	35	40	34

RESULTS: {F from tests, T from theory		1 F	1 T	1 F/T	2 F	2 T	2 F/T	3 F	3 T	3 F/T	4 F	4 T	4 F/T	5 F	5 T	5 F/T	6 F	6 T	6 F/T	7 F	7 T	7 F/T
Load at top surface failure P_t^{cr}	tons	0.65			1.63			1.57			1.44			1.59			1.67			1.83		
membrane stress corr. P_M	tons	0.07			(0.67)			0.09			(1.30)			0.23			0.09			0.42		
corr. test load/theor. load	tons	0.58	0.95	0.61		1.86		1.48	2.59	0.56		4.95		1.36	1.62	0.84	1.58	1.78	0.89	1.41	2.00	0.71
Centre depression at P_t^{cr}	cm	0.72	0.80	0.90	1.80	1.50	1.20	0.86	0.82	1.05	2.29	1.76	1.30	1.01	0.79	1.28	0.72	0.68	1.06	1.33	1.33	1.00

Comparison between tests and theory for these slabs have thus only concerned the load P_t in the case of top surface failure (circular crack) and the depression in the loading centre. The results are shown in Table 24:5. Slabs 2 and 4 have exceptionally large flexural deformation (soft subgrade), and the crack formation in the bottom surface can be judged to be so extensive that the calculated values for the membrane stress correction in these cases would appear to be much too high so these values have not been included when making a comparison between test and theory.

The result shows that the agreement between the test values and the values calculated according to the elasticity theory for the load causing failure in the top surface is not particularly good; in any case the F/T ratio shows vast spread. The centre depression values according to test and theory, however, show fairly satisfactory agreement.

245:3. *Test slabs, series MII A and C, slabs with single load*

For these slabs the comparisons between test and theory have also included loads and depression values at commencement of crack formation as well as at the yield point in the bottom surface under the loading centre. The theoretical depression values at the yield load P_b^{yie} have been calculated for slab data both at Stage I and Stage II in order to clarify the function of the slab at this phase of loading, when only a very limited zone in the centre of the slab is completely cracked, while the other zones in the slab are still in the uncracked stage. The calculation of the corresponding load has however only been carried out on the basis of data for Stage II, while the moment (stresses) in the centre of the slab depend, to a large extent, only on the deformation of the slab in the cracked centre zone, while the depression in the centre is determined by the elastic characteristics and the deformation of the slab on the whole.

The results for the *single-reinforced* slabs are shown in Table 24:6. These values show that there is good agreement between the experimentally estimated and theoretically calculated loads at the crack formation and at the yield point in the bottom surface under the loading centre P_b^{cr} and P_b^{yie} respectively, particularly with respect to the degree of unreliability in the estimation of the test loads, discussed in 245:1. Agreement, on the other hand, is less good concerning the ultimate loads P_t^{cr} in the case of concrete failure in the circular crack in the top surface, particularly with respect to the fact that the determination of the test values (crack load) is here considerably more accurate. The experimental and theoretical values for depression show, on the whole, fairly satisfactory agreement, and it should be pointed out that the

TABLE 24:6. Series M II, sub-series A, a and b, and sub-series C, single-reinforced slabs with single load. Centre loading on test slabs. Comparison between test results and elasticity theory.
Diameter 350 cm, load distribution radius $c = 20$ cm.

Series M II, sub-series	:A							:C
litt. / test no	a:1 a 1	a:2 2	a:3 3	b:1 4	b:2 5	b:3 6	a:1 b 8	21
DATA FOR THE TEST SLABS								
Thickness, total h_o cm	4.1	4.5	4.4	4.4	4.3	4.4	4.4	8.1
effective, h cm	3.9	4.1	3.6	4.1	3.9	4.0	4.2	7.4
Bottom reinforcement mesh	2.5/50	3.4/50	5.0/50	3.4/50	3.4/50	3.4/50	2.5/50	5.0/50
Flexural rigidity Ei kgcm								
Stage I	$16.5 \cdot 10^5$	$17.1 \cdot 10^5$	$19.8 \cdot 10^5$	$11.8 \cdot 10^5$	$14.3 \cdot 10^5$	$18.2 \cdot 10^5$	$17.5 \cdot 10^5$	$105 \cdot 10^5$
Stage II	$6.4 \cdot 10^5$	$6.0 \cdot 10^5$	$6.0 \cdot 10^5$	$4.0 \cdot 10^5$	$6.0 \cdot 10^5$	$7.6 \cdot 10^5$	$4.8 \cdot 10^5$	$28 \cdot 10^5$
Resilience constant k kg/cm^3								
Stage I	0.27	0.25	0.26	0.25	0.27	0.37	0.34	0.44
Stage II	0.22	0.24	0.26	0.25	0.27	0.30	0.30	0.52
Elastic radius of rigidity l cm								
Stage I	49.8	51.0	53.0	46.6	48.0	47.0	47.6	70.0
Stage II	41.4	39.8	40.0	35.6	38.7	40.0	35.6	48.2
Relative load distribution $a = \frac{c}{l}$								
Stage I	0.40	0.39	0.38	0.43	0.42	0.43	0.42	0.29
Stage II	0.48	0.50	0.50	0.56	0.52	0.50	0.56	0.42
Ultimate moment kgcm/cm								
at bottom concrete failure m_{cr}	148	148	142	98	140	180	135	~400
at bottom reinf. yield m_{yie}	206	222	337	195	198	235	157	768
at top concrete failure m'_{cr}	135	135	131	86	115	180	135	410

RESULTS: {F from tests, T from theory}	F	T	F/T	F	T	F/T	F	T	F/T	F	T	F/T	F	T	F/T	F	T	F/T	F	T	F/T	F	T	F/T
Load in tons																								
at bottom concrete failure P_b^{cr}	1.0	1.06	0.9	1.0	1.03	1.0	0.9	0.98	0.9	0.6	0.75	0.8	0.91	1.03	0.9	1.5	1.35	1.1	1.0	0.99	1.0	2.6	2.42	1.1
at bottom reinf. yield P_b^{yie}	1.9	1.89	1.0	2.2	2.08	1.1	3.3	3.17	1.0	1.7	1.99	0.9	1.91	1.92	1.0	2.4	2.21	1.1	1.4	1.60	0.9	7.1	6.50	1.1
at top concrete failure P_t	4.70			4.85			4.40			2.55			4.20			6.40			5.10			15.80		
membrane stress corr. P_M	1.59			0.75			0.39			0.12			0.44			1.30			1.19			1.14		
corr. test load – theoretical load	3.11	6.92	0.45	4.10	6.75	0.61	4.01	6.59	0.61	2.43	4.20	0.58	3.76	5.65	0.67	5.10	9.00	0.57	3.91	6.44	0.61	14.6	27.7	0.53
Centre depression in cm																								
at test load P_b^{cr}	0.18	0.17	1.1	0.20	0.18	1.1	0.18	0.15	1.2	0.16	0.14	1.1	0.23	0.17	1.3	0.26	0.21	1.2	0.20	0.15	1.3	0.16	0.14	1.1
at test load P_b^{yie} Stage I	0.47	0.33	1.43	0.58	0.39	1.49	0.89	0.54	1.65	0.56	0.36	1.55	0.52	0.35	1.48	0.48	0.33	1.45	0.31	0.21	1.48	0.55	0.39	1.41
at test load P_b^{yie} Stage II		0.59	0.80		0.60	0.97		1.01	0.88		0.60	0.93		0.54	0.96		0.58	0.83		0.41	0.76		0.69	0.80
at test load P_t	1.96	1.45	1.35	1.68	1.33	1.26	1.32	1.34	0.99	0.95	0.91	1.04	1.40	1.19	1.18	1.84	1.54	1.20	1.70	1.51	1.13	1.84	1.53	1.20

depression at the yield point P_b^{yie} shall obviously be calculated *according to Stage II* — corresponding calculations concerning Stage I do not agree anywhere near so well with the test results.

The results concerning the *double-reinforced* slabs are shown in Table 24:7. In this connection it should be remembered that the top reinforcement in the case of slab MII:7 was so weak, that the tensile strength in the concrete gave a higher failure moment than the reinforcement, thus being completely worthless, as well as the fact that in the case of slabs MII:9 and 12, the strength of the concrete was quite broken — the last-mentioned of these slabs had no top reinforcement whatsoever and is included in this series in order to complete it with a slab with a negative ultimate moment $m' = 0$. For the other slabs, calculations have been made for loads both at the commencement of crack formation and at reinforcement yield at the top surface P_t^{cr} and P_t^{yie} respectively.

Concerning the membrane stress correction P_M it is obvious that the calculated values at the last-mentioned load are completely unreliable (see fig. 23:6 b); these corrections have not been included when comparing with the theoretical values.

As shown by the results, there is relatively good agreement between the experimentally estimated and theoretically calculated loads at crack formation and yield in the bottom surface, P_b^{cr} and P_b^{yie}. In the cases where agreement is less good, the reason for this appears to lie in the unreliable results of the curvature measurements in the centre of the slab. Concerning the loads at crack formation and yield in the top surface P_t^{cr} and P_t^{yie}, the agreement between test and theory is less satisfactory. It should, however, be pointed out that the test value determination here is less accurate than in the case of single-reinforced slabs, since the failure loads in question have been estimated by comparison between the tension measurements on the top surface of the slab and on the detail test unit (see 245.1).

Concerning the depression values, as in the case of the single-reinforced slabs the depression at the load P_b^{yie} should be calculated in accordance with Stage II, and thereby good agreement is obtained with the test values. In the case of the lower load, P_b^{cr}, agreement for some of the slabs is not so good, but this can depend upon the fact that the bed of wood fibre board which was used for the complete test series gradually developed a deepening towards the centre due to permanent compression, and this was filled by a loosely laid layer of fine sand. This could imply that the slab during the first loading steps had a higher degree of depression in the centre before the thicker sand layer there was sufficiently compressed. For higher loads the agreement concerning

Series M II:A	litt. test no	c 1:1 7¹)	c 1:2 9³)	c 1:3 11	c 2:1 12³)	c 2:2 10	c 2:3 13
DATA FOR THE TEST SLABS							
Thickness, total, h_0	cm	5.1	5.6	5.8	5.6	5.6	5.4
effective h	cm	4.8	5.3	5.3	4.8	5.1	5.0
Reinforcement mesh							
bottom		3.4/50	3.4/50	3.4/50	5.0/50	4.2/50	3.4/50
top		2.5/50¹)	2.5/100²)	3.4/50	— ³)	3.1/50	3.4/50
Flexural rigidity Ei	kgcm²/cm						
Stage I		$28.0 \cdot 10^5$	$28.0 \cdot 10^5$	$35.0 \cdot 10^5$	$23.3 \cdot 10^5$	$28.0 \cdot 10^5$	$28.0 \cdot 10^5$
Stage II		$11.7 \cdot 10^5$	$8.1 \cdot 10^5$	$8.1 \cdot 10^5$	$9.4 \cdot 10^5$	$9.3 \cdot 10^5$	$7.2 \cdot 10^5$
Resilience constant k	kg/cm³						
Stage I		0.31	0.33	0.24	0.23	0.29	0.30
Stage II		0.31	0.33	0.29	0.26	0.31	0.32
Elastic radius of rigidity l	cm						
Stage I		55.0	54.0	61.8	56.3	55.8	55.0
Stage II		44.0	39.5	42.0	43.6	42.6	38.0
Relative load distribution $\alpha = \frac{c}{l}$							
Stage I		0.36	0.37	0.32	0.36	0.36	0.36
Stage II		0.45	0.51	0.48	0.46	0.47	0.52
Ultimate moment	kgcm/cm						
at bottom concrete failure m_{cr}		196	160	170	139	146	133
at bottom reinf. yield m_{yie}		283	269	293	418	345	260
at top concrete failure m'_{cra}		216	— ⁴)	164	—	164	137
at top reinf. yield m'_{yie}		— ¹)	~ 100²)	253	0³)	202	220

RESULTS: {F from tests, T from theory}	c 1:1 F	T	F/T	c 1:2 F	T	F/T	c 1:3 F	T	F/T	c 2:1 F	T	F/T	c 2:2 F	T	F/T	c 2:3 F	T	F/T
Load in tons																		
at bottom concrete failure P_b^{cr}	— ²)	1.30	—	1.25	1.10	1.1	0.5	1.07	0.5	0.5	0.93	0.5	0.9	0.98	0.9	0.7	0.89	0.8
at bottom reinf. yield P_b^{yie}	— ²)	2.50	—	2.6	2.56	1.01	2.0	2.68	0.75	2.3	3.74	0.62	2.5	3.10	0.81	2.1	2.51	0.84
at top concrete failure P_t^{cr}	5.95			—			4.9			—			6.3			4.6		
membrane stress corr. P_M	0.71			—			1.04			—			0.74			0.28		
corr. test load — theor. load	5.24	12.20	0.43	—	—	—	3.86	8.68	0.45	—	—	—	5.56	8.76	0.64	4.32	6.61	0.65
at top reinf. yield P_t^{yie}	—	—	—	8.4	4.95	1.7	7.6	13.40	0.57	5.9	0		9.2	10.80	0.85	8.6	10.61	0.81
Centre depression in cm																		
at test load P_b^{cr}	0.22	0.16	1.4	0.18	0.15	1.2	0.09	0.06	1.5	0.10	0.08	1.2	0.15	0.12	1.2	0.11	0.09	1.2
at test load P_b^{yie} Stage I	0.51	0.31	1.64	0.47	0.31	1.52	0.51	0.26	1.96	0.59	0.37	1.59	0.51	0.33	1.55	0.44	0.27	1.63
at test load P_b^{yie} Stage II		0.48	1.06		0.58	0.81		0.50	1.02		0.54	1.09		0.56	0.91		0.48	0.92
at test load P_t^{cr}	1.55	1.14	1.36	—	—	—	1.48	1.23	1.20	—	—	—	1.70	1.41	1.20	1.20	1.05	1.14
at test load P_t^{yie}	—	—	—	2.70	1.86	1.45	2.66	1.90	1.40	1.90	1.38	1.38	2.84	2.07	1.37	2.62	1.96	1.33

¹) $m'_{cr} > m'_{yie}$ — tensile strength too high — so that top reinforcement is *completely without function*. The slab behaves as a single-

depression with the theoretical values is fairly good approximately up to the top surface crack load P_t^{cr}, but at P_t^{yie} the relationship is generally worse. This could depend on the fact that the top reinforcement, as earlier discussed, is weak in relation to the tensile strength of the concrete itself so that after the formation of cracks in the top surface the slab has a very low flexural rigidity and therefore a greater degree of depression than that given by the theory.

The figure 24:25 shows examples of relationship curves according to tests and theory between load and depression as well as load and moment in the loading centre[1]). These show clearly that the theory gives separate linear relationship curves for Stage I and Stage II, while the test curves show that the slabs gradually change their elastic properties as the loading increases. Concerning the moment curves (Fig. 24:25) this gradual alteration occurs particularly in the section between the load P_b^{cr} at the commencement of crack formation and the load P_b^{yie} at the yield point; over this load there is naturally no agreement whatsoever between the theory and the tests. Concerning the depression curves, the test curves show that there is a decreasing gradient during the whole loading procedure and it is obvious that it is not possible to get more than a very approximate agreement between the test values and the theoretical values. It should be reminded that the depression figures have not been corrected for the influence of the membrane stresses; a correction of this kind would imply that the depression values for the highest loading steps would be even higher.

In order to further illustrate the relationship between tests and theory, the test results and the theoretical depression and moment distribution along the radius have been compared for some of the slabs, and the results are shown by figures 24:26 A, B and C. The depression and moment curves in question have been shown for load steps in the neighbourhood of the crack and yield loads for top and bottom. For a load P_2 (see the fig.) in the vicinity of P_b^{yie} the theoretical curves have been calculated for the slab and subgrade constant values for both Stage I and Stage II.

The figures show relatively good agreement between test and theory concerning the depression lines, and for the load P_2 the curves according to Stage II show the best agreement. The conformity in the vicinity of the edge is not so good and this naturally depends on the fact that the test slabs have lost contact with the subgrade at the edge and that the soil pressure there is thus equal to zero while the theory assumes that the soil pressure in such a zone should be negative. This must

[1]) These curves for all the slabs are given in the test result supplement, Section 922.

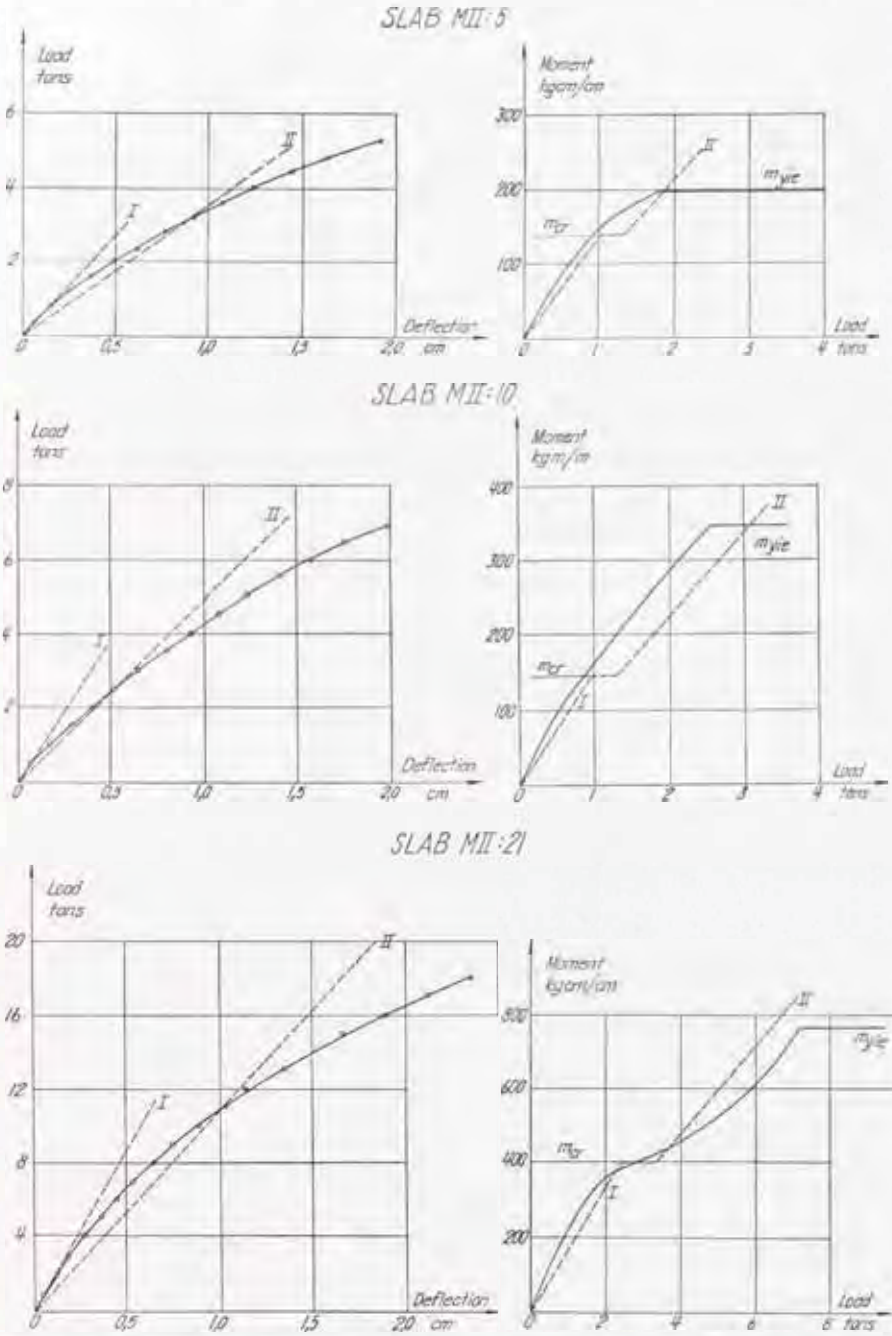

Fig. 24:25. Moment and depression in the centre according to tests (unbroken lines) and theory (broken lines) for three of the model slabs in the MII series. The test curves for the centre moment have been obtained according to the method illustrated in Fig. 24:22. The theoretical curves have been calculated with the help of the diagrams in Fig. 22:9 (moment) and Fig. 22:8 (depression), whereby calculations have been carried out for the constant values for the slab and the subgrade at Stage I (with $\nu = 0.15$) and Stage II ($\nu = 0$). No corrections have been made for the influence of the membrane stresses (on the depression).

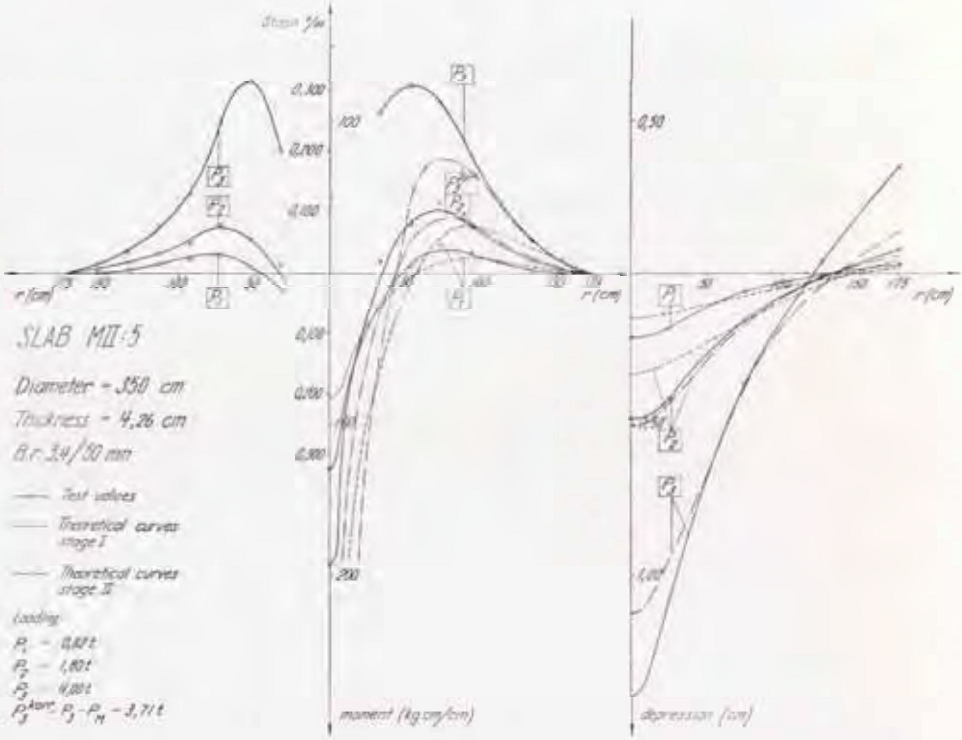
SLAB MII:5
Diameter = 350 cm
Thickness = 4,26 cm
B.r. 3,4/50 mm
Test values
Theoretical curves stage I
Theoretical curves stage II
Loading:
P1 = 0,82 t
P2 = 1,80 t
P3 = 4,00 t
P3 korr = P3 - PH = 3,71 t
moment (kg cm/cm)
depression (cm)
r (cm)

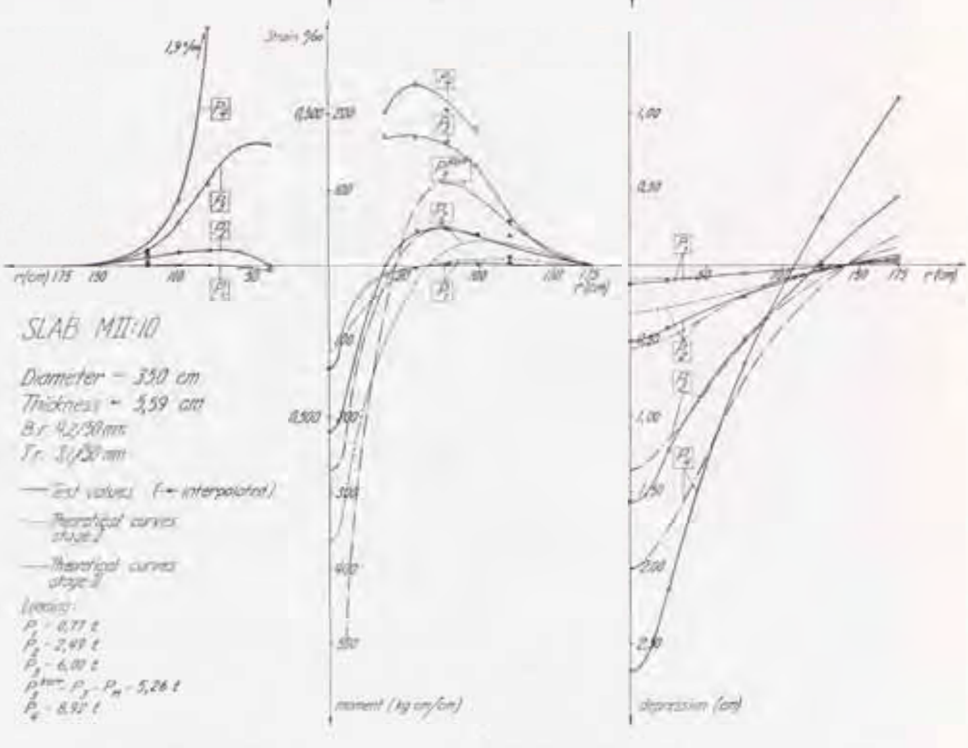
SLAB MII:10
Diameter = 350 cm
Thickness = 5,59 cm
B.r. 4,2/50 mm
Tr. 3,1/50 mm
Test values (+ = interpolated)
Theoretical curves stage I
Theoretical curves stage II
P1 = 0,77 t
P2 = 2,49 t
P3 = 6,00 t
P3 korr = P3 - PH = 5,26 t
P4 = 8,92 t
moment (kg cm/cm)
depression (cm)
r (cm)

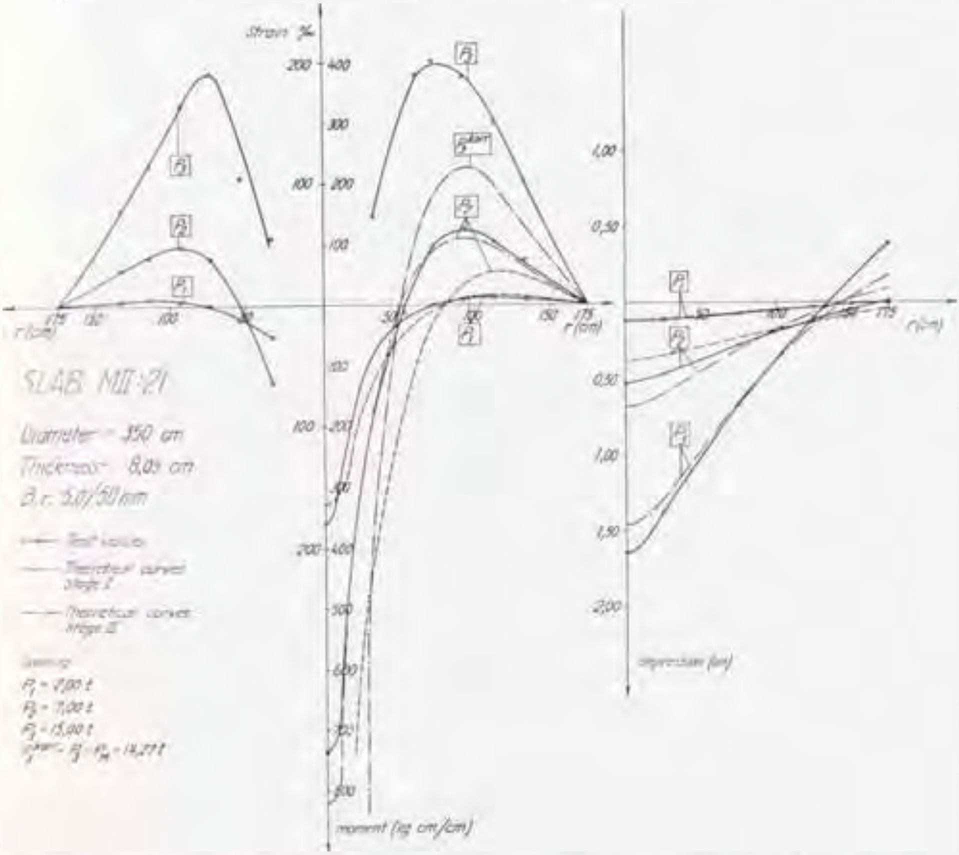

Fig. 24:26 A, B and C. The radial moment m_r and the depression along the radius according to test and theory for three of the model slabs in the MII series (5, 10 and 21). The curves have been drawn for the loads P_1 and P_2 in the neighbourhood of the loads corresponding to the commencement of crack formation P_b^{cr} and bottom reinforcement yield P_b^{yie} respectively, as well as P_3 in the neighbourhood of the load for the top surface failure P_t^{cr} (for the double-reinforced slab 10 also for a load P_4, corresponding to the yield point in the top reinforcement P_t^{yie}).

The test values for the moments have been obtained by comparison between the strain measurements along the slab radius in the main test and the corresponding strain measurements in the detail tests (generally the average values from the two detail tests with the bottom reinforcement in the compression zone, see Fig. 24:16). In some cases, and particularly at the lowest load, obvious irregularities in the strain measurements have been evened out by means of interpolation between the adjacent values. The strain measurements used have been drawn in on the figures in the form of strain diagrams.

The theoretical moment values have been obtained with the help of the diagrams in Fig. 22:9 (slab of infinite extent with distributed load) which has given values in the neighbourhood of the centre, and Fig. 22:14 (slab of finite radius and concentrated load) which has given the values in the neighbourhood of the edge.

The test curves of the depression consist of the average curves of the depression lines for all four radii along which depression was measured.

The theoretical curves for the depression and moment have been calculated for the constant values for slab and subgrade at Stage I ($\nu = 0.15$) for the loads P_1 and P_2, as well as for Stage II ($\nu = 0$) for the loads P_2 and P_3. For the last-mentioned load, correction has been made for the membrane stress effect. See also 245:1, page 113.

mean that the theory will give a smaller degree of edge lifting than in the tests, and this is also shown in the figures.

Concerning the moment distribution curves the agreement is fairly good for loads up to P_b^{gis} (load P_2 in the figure), but at the last-mentioned load, however, only for moment curves according to Stage II. At higher loads the moment in the top surface increases much more rapidly than according to the theory. This is also completely in agreement with what can be expected with respect to the fact that the moment under the loading centre will remain constant when the loading exceeds the yield point load and that the conditions in the slab thus deviate more and more from the assumptions made in the elasticity theory.

Considering the choice of the flexural rigidity value for the slab it is obviously that the Stage I value can be used only in the case of such small loads that the slab is *completely* uncracked. With fairly extensive crack formation in the bottom surface under the loading centre then calculations with a flexural rigidity value according to Stage II give much more correct results concerning both the depression and the moments, not only in the cracked central zone but also over the *complete* slab.

245.4. *Test slabs Series MII:B, slabs with twin load*

This series also includes a comparison slab with a single load. These slabs are otherwise identical and the two loading surfaces for the twin load with a distance between centres of 42 and 84 cm respectively have the same total surface as the extent of the single load. Other data concerning the slabs is shown in Table 24:8.

For analysis of the test results concerning the twin load slabs MII:15 and 16 the theoretical curves concerning depression and moment distribution along both the diameters at right angles have been constructed with the help of the corresponding diagram for single load in Figures 22:8 and 22:13, 22:9 and 22:14 respectively, these being used as influence lines. When marking in the moment curves for the diameters at right angles to the axis through the twin load centres, the moment values for the tangential and radial moments have been obtained by vectoral addition of the values from the Z_3 and Z_4 curves in Fig. 22:9. Respect has been taken to finite slab radius in such a way that the distance from the nearest loading point to the edge of the slab has been considered to correspond to the radius of the slab when calculating the value from the diagrams 22:14 and 22:13 respectively for moment distribution and depression in the vicinity of the slab edge. The curves obtained are shown in Figures 24:27 A and B.

Based on these curves, the theoretical values for the loads at the beginning of crack formation and at yield in the bottom surface as well as concrete failure in the top surface, and for corresponding depression in the centre, have been calculated and are shown together with the test results in Table 24:8. It should be pointed out that the theoretical values of the loads at the crack formation and at yield point in the bottom surface in the case of slab 16 have been calculated from the values for both the maximum moment (under the loading surface) and the centre point moment. As shown in Fig. 24:27 B, there is a very rapid variation of the moment within the zone between the concentrated loads for this slab and it is probable that the measurements carried out with curvature gauge at the centre point have given a kind of average value of the moment between the load points. The test load also lies between both the theoretical values.

The influence of the membrane stresses on the ultimate load P_t has, in the usual way, been calculated for slab MII:14; for both the slabs with the twin load a calculation of this kind cannot be carried out due to the fact that the depression volumes are not ring symmetrical, so that the corresponding membrane stress correction values have been estimated with the help of the value for slab 14 and the interpolation formula (23:44).

The result according to the table shows that the agreement between the tests and the theoretical loads at the beginning of crack formation and yield in the bottom surface is good, as in the previous tests, while the agreement between the test and the theory concerning top surface ultimate load is not so good. Concerning the depression values, agreement between the tests and theory is satisfactory and as usual it can be established that when calculating the depression at the bottom surface yield point then the slab rigidity for Stage II should be used.

The results are illustrated further by curves according to test and theory for centre depression and centre moment for the twin load slabs in Fig. 24:28 as well as by the test values concerning moment and depression marked in in Fig. 24:27 A and B. The last-mentioned moment values have been obtained in the usual way by comparing the tension measurements on the detail test unit and the main test. The theoretical curves at the load in the neighbourhood of P_b^{gir} has, as earlier, been calculated for constant values according to both Stage I and Stage II and it can also be maintained here that the flexural rigidity of the slab at this load should be calculated for Stage II.

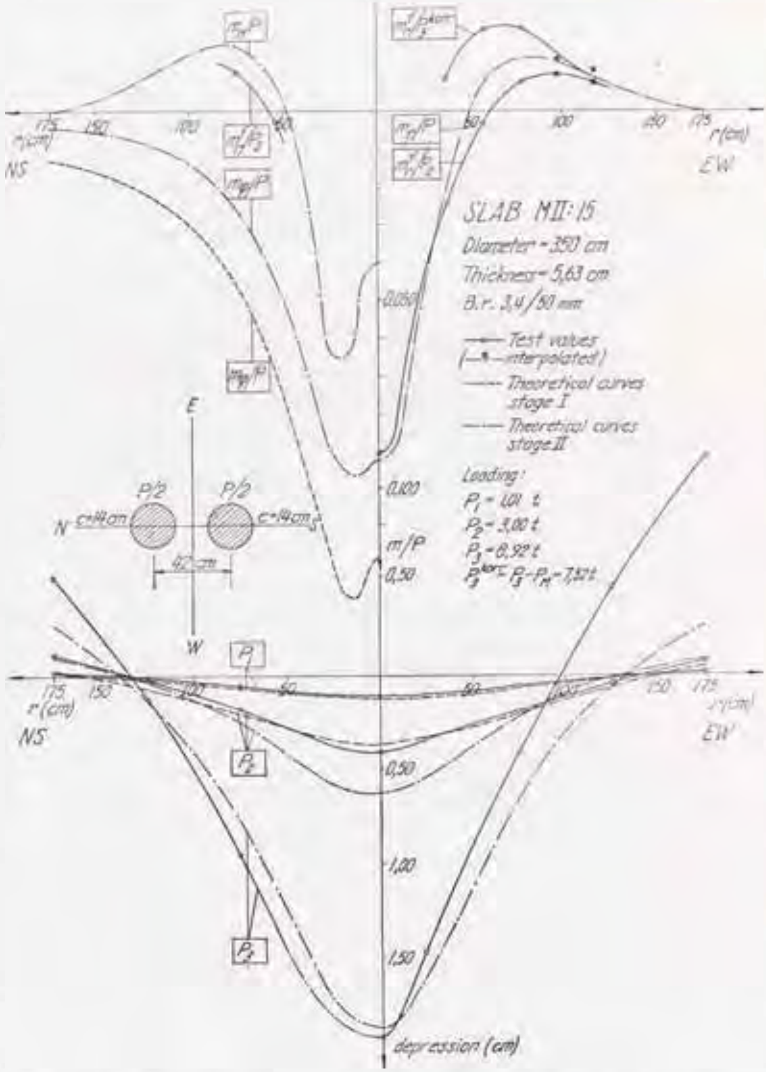

Fig. 24:27 A and B. Diagrams showing the distribution of the radial and tangential moment m_r and m_φ respectively as well as the depression lines along a slab radius through the centres of the loading points (NS) and radius (EW) at right-angles to this for the twin-loaded slabs MII:15 and 16.

The theoretical moment curves, calculated for the constants at Stage I ($\nu = 0.15$) and Stage II ($\nu = 0$) according to Table 24:8 have been drawn dimension-free with the ordinate $\frac{m}{P}$ for convenient use in the theoretical analysis work. The moment curves have been

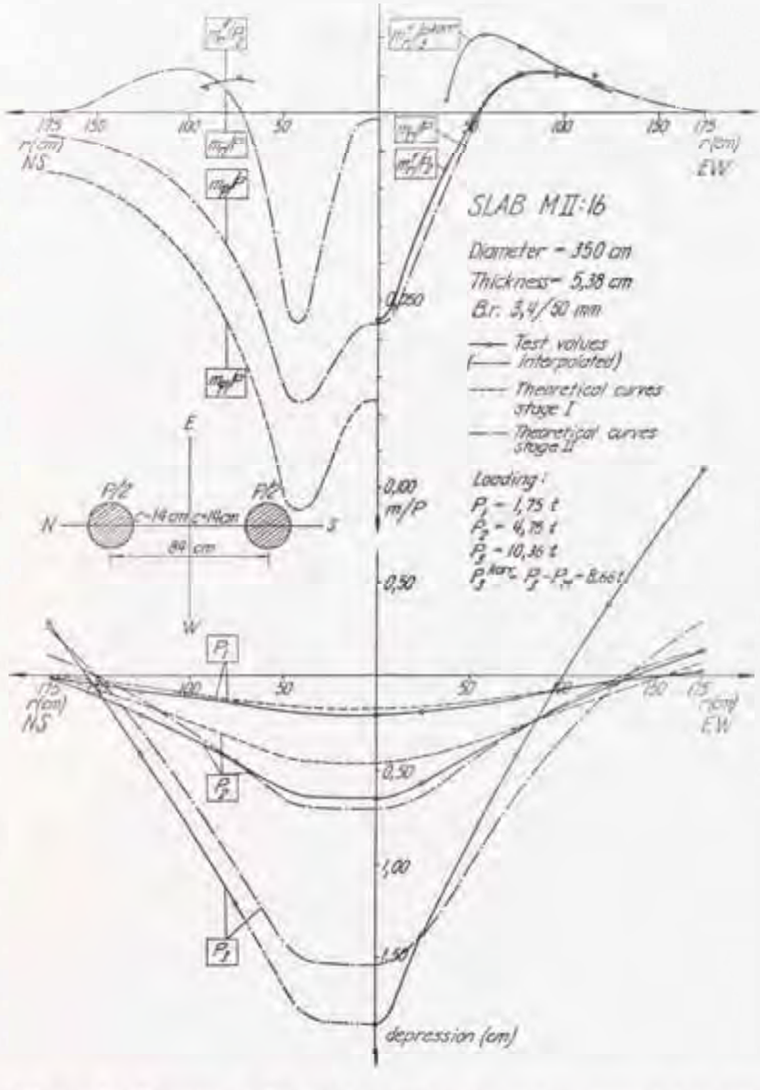

obtained from the diagrams in Fig. 22:9, whereby the various curve points have been obtained by super-imposition of the moment values from each of the loading points; for the points on the radius EW at right-angles to the loading axis, the projections of m_r and m_φ values at right-angles to and parallel with EW respectively have been added. For values in the neighbourhood of the slab edges, the moment values have been taken from the diagram 22:14. As comparison, the test values $\frac{m_r^{\text{test}}}{P}$ for the moment, obtained as shown in Fig. 22:26, have been drawn in for the loading steps indicated in the figures.

TABLE 24:8. Series M II sub-series B: a, slabs with *twin load*. Centre loading on test slabs. Comparison between the test results and the elasticity theory.
Diameter 350 cm, bottom reinforcement mesh 3.4/50.

Series M II B	litt. / test no	a:1 14			a:2 15			a:3 16		
DATA FOR THE SLABS										
Thickness, total h_0	cm	5.5			5.6			5.4		
effective h	cm	5.1			5.2			5.0		
Flexural rigidity Ei	kgcm²/cm									
Stage I		$31.0 \cdot 10^5$			$27.5 \cdot 10^5$			$31.5 \cdot 10^5$		
Stage II		$8.6 \cdot 10^5$			$8.2 \cdot 10^5$			$9.5 \cdot 10^5$		
Resilience constant k	kg/cm³									
Stage I		0.25			0.28¹)			0.28¹)		
Stage II		0.28			0.30¹)			0.30¹)		
Elastic radius of rigidity l	cm									
Stage I		59.5			56.0			58.0		
Stage II		41.4			40.8			42.2		
Load distribution radius c										
actual dim. cm		20			2 × 14			2 × 14		
relative measure Stage I		$0.34\ l$			$0.25\ l$			$0.24\ l$		
relative measure Stage II		$0.48\ l$			$0.34\ l$			$0.33\ l$		
Dist. between loading centres										
actual measure d	cm				42			84		
relative measure Stage I					$0.75\ l$			$1.45\ l$		
relative measure Stage II					$1.03\ l$			$2.00\ l$		
Ultimate moment	kgcm/cm									
at bottom concr. failure m_{cr}		198			215			200		
at bottom reinf. yield m_{yie}		277			299			303		
at top failure m'_{cr}		209			218			207		
RESULTS: {F from tests / T from theory		F	T	F/T	F	T	F/T	F	T	F/T
Load in tons										
at cracks in bottom P_b^{cr}		1.1	1.27	0.87	1.5	1.74	0.86	< 2.0	1.9 – 2.6²)	1.05 – 0.7
at bottom reinf. yield P_b^{yie}		2.1	2.54	0.83	3.4	3.15	1.08	5.0	3.9 – 5.4²)	1.28 – 0.9
at failure in top P_t		6.18			9.03			11.0		
membrane stress corr. P_M		1.55			1.4¹)			1.7¹)		
corr. test load – theor. load		4.63	10.89	0.43	7.63	12.8	0.60	9.30	18.8	0.50
Centre depression in cm										
at test load P_b^{cr}		0.18	0.15	1.20	0.17	0.18	0.94	0.23	0.20	1.15
at test load P_b^{yie} Stage I		0.42	0.28	1.50	0.48	0.42	1.14	0.69	0.49	1.41
at test load P_b^{yie} Stage II			0.48	0.88		0.72	0.67		0.75	0.92
at test load P_t		1.95	1.41	1.38	2.00	1.91	1.05	2.00	1.65	1.21

¹) Interpolated between values for adjacent slabs.
²) The lower value apply to m_{max} (under the loading centres), the later m_{centre} (in slab centre).

245.5. *Discussion of test results*

In the previous section comparisons have been made between the test results and the corresponding theoretical values of depression and moment (or loads at certain crack and ultimate moment values). In judging the results obtained, it may be important to know partly the degree of accuracy to be expected in the theoretical calculation

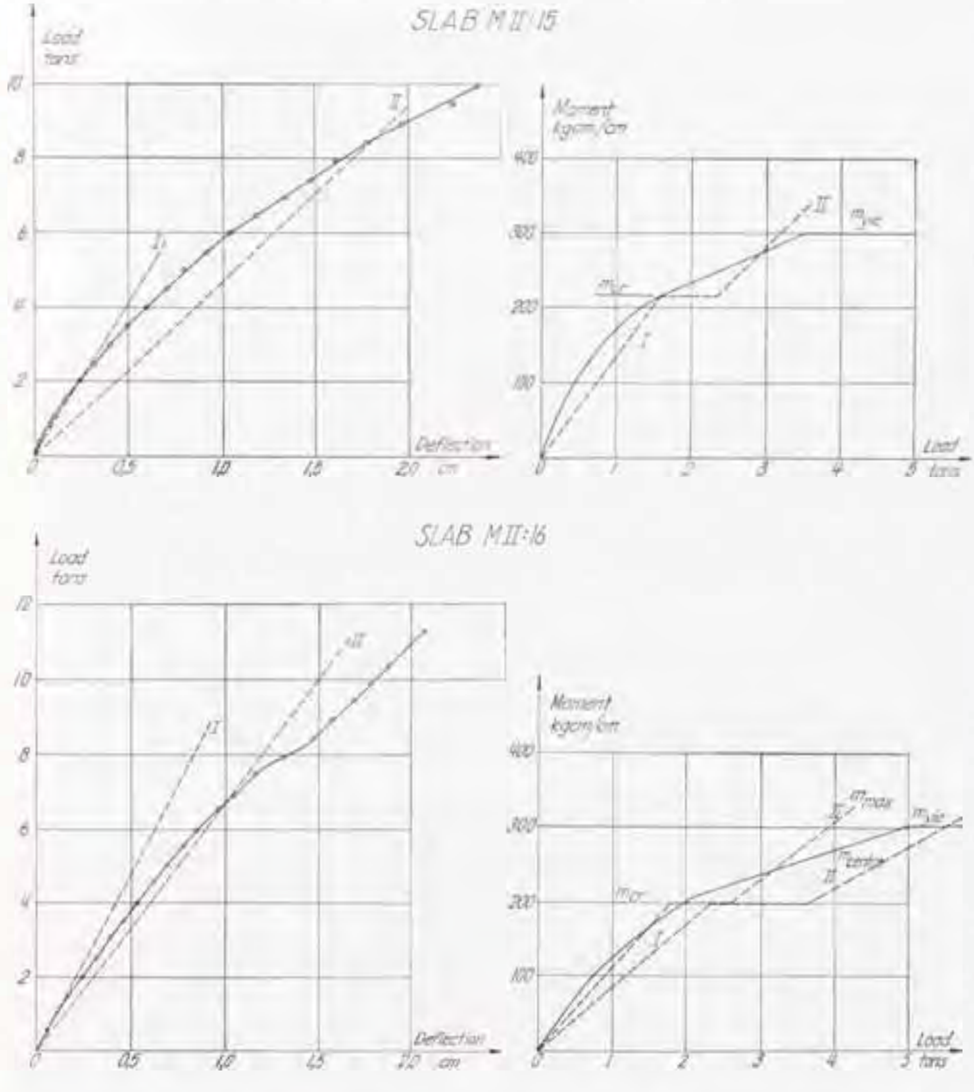

Fig. 24:28. Moment and depression in the centre (halfway between the loads) for the twin loaded slabs MII:15 and 16. The test curves for the centre moment have been obtained according to the method shown in Fig. 24:22. The theoretical curves (broken lines) have been obtained from the centre point values for the corresponding theoretical curves in Fig. 24:27; the curves for the constant values at both Stage I and Stage II have been drawn in. In the moment diagram for slab 16, the theoretical curves for both the centre point moment and the maximum moment (under the loading point) have been drawn in; since the moment m_{φ} within the zone between the measuring points varies very rapidly (see Fig. 24:27 B), it is probable that the curvature gauge in the centre point, which had a measuring base of 50 cm, has given a sort of average value of the moment in the centre zone.

and partly the degree of accuracy to be obtained from the test values.

Concerning the moments and characteristic loads respectively, the result is influenced to a comparatively small extent by the unreliable factors in the constants D and k for the slab and the subgrade. Variation in these constants has only a very weak influence on the relative load distribution a. On the other hand the characteristic loads are directly influenced by unreliabilities in the moment values. This can be seen from an estimation of the maximum error in the calculation of a loading value for bottom surface failure through differentiating the expression (22:55) for the maximum moment

$$dm = (m)_{P=1}\ dP + P\ (0{,}080 - 0{,}156\ a^2)\ \frac{da}{a} \qquad (24:2)$$

where da can be obtained by taking out the logarithm and differentiation of

$$a = \frac{c}{l} = c \sqrt[4]{\frac{k}{D}}$$

One thus obtains

$$\frac{dP}{P} = \frac{dm}{m} - \frac{P}{m}\ (0{,}080 - 0{,}156\, a^2)\ \frac{1}{4} \left(\frac{dD}{D} - \frac{dk}{k} \right) \qquad (24:3)$$

or, for values of relative load distribution a within the actual values between $0{,}3$ and $0{,}6$

$$\frac{dP}{P} \approx \frac{dm}{m} - 0{,}1 \left(\frac{dD}{D} - \frac{dk}{k} \right) \qquad (24:4)$$

When estimating the reasonable maximum deviations in the constant values respect should be taken to the unreliability involved in the determination of the flexural rigidity D. Determination of the k-value which is based on the average depression should be, however, comparatively reliable for this type of subgrade material. As reasonable values for the maximum percentual deviations we can assume

$$\frac{dD}{D} = \pm 30\,\%; \quad \frac{dk}{k} = \pm 10\,\%$$

Concerning variation in m it should be pointed out that from the tests we have determined the associated values m and P, but that the relationship is based on a very inaccurate indirect comparison between the curvature measurement in the main test and the detail tests. It does not seem unreasonable to consider this deviation as going up to about 30 %. With maximum deviation values assumed in this way one thus obtains according to (24:4)

$$\frac{dP}{P} = \pm 0{,}30 \pm 0{,}1\ (\pm 0{,}30 \pm 0{,}10)$$

or a maximum variation between the theoretical and test load values of approx. 35 %.

With respect to this the agreement between the test and the theory considering the loads and the moment at failure in the bottom surface appears to be surprisingly good. The deviation in general is within 10 %. The large deviations existing in certain individual cases can be easily explained as the influence of the faults in the test values discussed above.

Concerning the load at failure in the top surface (by negative moment) the theoretical value is even less influenced by variations in the relative distribution of the load than in the cases discussed above (see Fig. 22:9), and assumed variations in D and k can be considered to have no influence at all on the theoretical ultimate load. The ultimate moment values $m^-_{max} = m'$, on the other hand, and the ultimate test load P_t are here determined through independent tests. The ultimate moment is determined as the average value of, in general, six flexural tests on detail test strips and the maximum deviation is (apart from a few stray results) below ± 10 %. To this must thus be added the degree of unreliability in the ultimate load determination which, in the case of the single-reinforced slabs where tension measurements were carried out or where depression measurements close to the crack gave clear indication (see Table 24:4), can be assumed to be only a few percent, while in the case of the slabs where the load causing crack formation was determined by visual inspection or, as in the case of the top-reinforced slabs, from estimation from the stress measurements, a larger degree of unreliability must be assumed, reasonably not more than 10 %. Thus, the maximum deviations may be approx. ± 10 % for slabs with accurate ultimate load determination and approx. ± 20 % for the other slabs between test loads and theoretically calculated loads in the case of top surface failure, *if the elasticity theory is applicable*.

The results of the tests show, however, deviations in this respect which for many slabs are considerably greater and where dispersion in the value of the relationship between the test load and the theoretical load is very great. It can thus be confirmed that *the elasticity theory cannot be adapted for calculation of the ultimate top surface load P_t.* It is easy to explain that this actually is the case since the central zone of the slab has assumed a plastic character at these loading values. The fact that this influences the moment values not only in the central zone but throughout the complete slab is clearly shown by the test curves in the Figures 24:26 and 24:27.

Concerning the depression, when calculating the theoretical values one has to reckon with a considerably larger influence of the unreliability in the constants D and k for slab and soil. Since the depression in the loading centre can be written

$$w_0 = P \frac{l^2}{D} Z_1^m,$$

where the function Z_1^m is only slightly influenced by alterations in the relative load distribution a (see Fig. 22:8) and can be considered in this connection as being constant, we get from differentiation

$$\frac{dw}{w} = 2\frac{dl}{l} - \frac{dD}{D} = \frac{1}{2}\left(\frac{dD}{D} + \frac{dk}{k}\right) \tag{24:5}$$

When estimating reasonable deviations in the test values used for the flexural rigidity D one should consider the condition that the elastic properties of the slab vary from the centre to the edge and are completely changing during the whole loading procedure and that, for example, the depression in the centre point is the result of deformations from the complete slab with its complicated variations of elastic characteristics. At lower load values, for example up to the yield point in the centre of the slab, then a lower value of the deviation in D is motivated and, by adapting the values earlier used

$$\frac{dw}{w} = \frac{1}{2}\,(\pm\,0{,}30 \pm 0{,}10) = \text{max. } 20\ \%$$

With higher loading up to failure in the top surface the variations in the "effective flexural rigidity" depend on the extent of the plastic region in the centre of the slab. Deviations of up to 100 % do not appear to be unreasonable.

Under such conditions one cannot expect any particularly good agreement between the theoretically and experimentally determined values (the last-mentioned can naturally be obtained with a very good degree of accuracy). The calculations in the foregoing have been carried out for constant D-values concerning partly Stage I for the complete slab and partly Stage II for the complete slab. The test curves for the depression at the centre point, as an example. (Fig. 24:25 and 24:28), have, generally speaking, a fairly good relationship to begin with when compared to the theoretical Stage I curve, but at higher loads they approach more and more the stage II curves and at the highest loads give somewhat (in a few cases significantly) larger depression than this curves. The result appears to be characteristic for a slab which is subjected to increasingly extensive crack formation and, in the case of higher loads, the assumption of a plastic character in the central zone. The fairly good agreement between test and theory in spite of this, even in the case of higher loads, appears to depend on the fact that the plastic section around the centre of the slab is of comparatively limited extent and does not influence the degree of depression of the slab on the whole to any great extent.

By way of summary it can be said that a reinforced concrete slab on a resilient bed can very well be treated in accordance with the elasticity theory up to a loading corresponding to the yield point at the loading centre. In this connection one should reckon with slab constants according to Stage II for at least this final phase. In the case of higher loads the same theory can, it appears, still be used fairly well for deformation calculations. *For the calculation of the definite ultimate load with failure in the top surface of the slab, however, the elasticity theory is not suitable.*

25. Gothenburg Tests (Series G)

251 Review of tests

The model tests previous described were intended to show to what extent reinforced concrete pavements could be treated according to the theory for elastic slabs on an elastic subgrade. The artificial subgrade of wood fibre board had relatively good elastic properties and functioned on the whole as a resilient bed.

In order to be able to judge how the type of pavement in question behaves under the conditions occurring with a subgrade of *natural* soil and particularly under the conditions existing for the then topical air-field project at Upplands Väsby north of Stockholm, the model tests were supplemented during the spring of 1945 and the winter 1945—46 with full scale tests consisting of two reinforced concrete slabs with a diameter of 7 metres, cast on a suitable clay subgrade in Gothenburg. The soil consisted here of relatively loose clay (so-called Gothenburg clay) to some considerable depth and the conditions in this respect were similar to those of the Väsby project.

In this part of the investigation, one of the most important tasks was thus to study the elastic properties of the subgrade material and attempt to judge which of the two earlier discussed types of subgrade nearest corresponded to the natural soil material. Particular emphasis has therefore been made in the tests to arrive at the actual pressure distribution between the slab and the subgrade, since according to the theoretical analysis it is just in the question of pressure distribution that both the theories show the greatest differences.

The original programme was to test only *one* slab which was bottom-reinforced in the normal way (slab G1). The measurements of the pressure between the slab and the ground thereby carried out were, however, very incomplete, although the method used appeared to give promising results. It was also considered valuable to let the investigation also concern a double-reinforced slab (G 2), in which case considerably more extensive measurements of the subgrade pressure were carried out.

Both the slabs were cast on the same subgrade surface. After the first slab had been tested it was broken up and removed, and the top

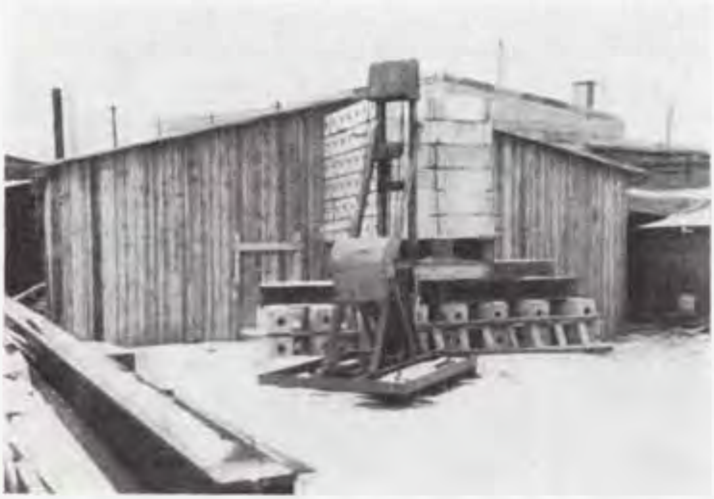

Fig. 25:1. The test house round slab G2. The house was built at winter-time and warmed by means of electric heaters so that the slab could be tested during the winter. Part of the loading device projects through the end wall.

clay layer was taken off before the second slab was cast. When the slab G 2 was manufactured the reinforcement was allowed to stick out round the edge (see Fig. 25:7). After the slab had been tested by loading in the centre further concrete was cast all around the circumference so that it became square with dimensions 8×8 metres, and the four edges were strengthened in different ways. The slab thus completed was utilized for loading tests with a load on a free edge. These tests are reviewed elsewhere (Section 43).

The experiments with the test slab G 2 were carried out during the winter, since it was considered essential that the test results should be used in the planning of the Väsby airfield the following spring. In order to prevent the effect of frost in the ground and to be able to complete casting and measuring work in the prevailing cold weather, a provisional test house was built round the slab and this house had well insulated walls. See Fig. 25:1. The test house was warmed up during the complete experiment time with the help of electric heaters.

252. Performance of test slabs

At the testing place, the subgrade consisted of a layer of clay about 30 m thick, resting on a hard base. The clay was relatively wet with a shear strength in the surface layer of approx. 1.0 ton/m². Before the slabs were cast, the surface of the subgrade was removed so as to expose the clay, and the surface was carefully levelled with sand.

Both the slabs in this test series were circular with a diameter of 7 metres and a total thickness of 15 cm. The reinforcement and performance in general are shown in Fig. 25:2. The main reinforcement consisted of deformed bar ⌀ 8 Ks 40,[1]) and as shear reinforcement in the centre of slab G 2 (see Fig. 25:2) ⌀ 6 Ks 40 was used. The composition of the concrete was standard cement: sand: gravel: water = 1:4:4:1.2, and the consistency was about 4° VB. The compressive strength of the concrete was checked by means of cubes which were tested together with the main test; for slab G 1 14 test cubes were cast and the average compressive strength was 238 kg/cm², for slab G 2 16 cubes were cast of which the average compressive strength was 230 kg/cm², (the maximum deviation was ± 35 kg/cm²).

During casting the concrete was stamped down with a wooden stamp and the surface was levelled with the edge of the mould by means of an alignment plank; the surface was not specially smoothed off. After casting was complete the concrete was watered and was kept covered with moist sawdust during about 15 days.

At the same time as the test slabs were manufactured, slab strip beams were also made, used as detail tests for the determination of the ultimate moment and the flexural rigidity. For slab G 1, three detail test beams were made with dimensions 15×40×250 cm and for slab G 2 four detail test beams were made with dimensions 15×60×250 cm. The detail test beams were reinforced in the same way as the slabs they belonged to and in both cases test beams were carried out, which had longitudinal reinforcement both in the upper and lower layer. The surface was smoothed off in the same way as with the circular slabs.

The slab G 1 was tested when it was 53 days old. The test load was distributed over a plate with a diameter of 40 cm, but this showed itself to be altogether too small so that stamp-out failure was obtained round the edge of the loading area, long before any tendencies to moment failure in the top could be noticed. Since this test (loading 1) did not give any information concerning the normal ultimate strength, the slab was repaired for renewed testing (loading 2). Thereby the centre section around the stamp-out cracks was broken up to a diameter of about 1.20 m, since it was noticed that the reinforcement had taken with it the concrete in the bottom of the slab quite a long way out. The edge of the hole was made in the form of an incline so that the new casting would

[1]) Deformed reinforcement bars with a yield point of 4 000 kg/cm².

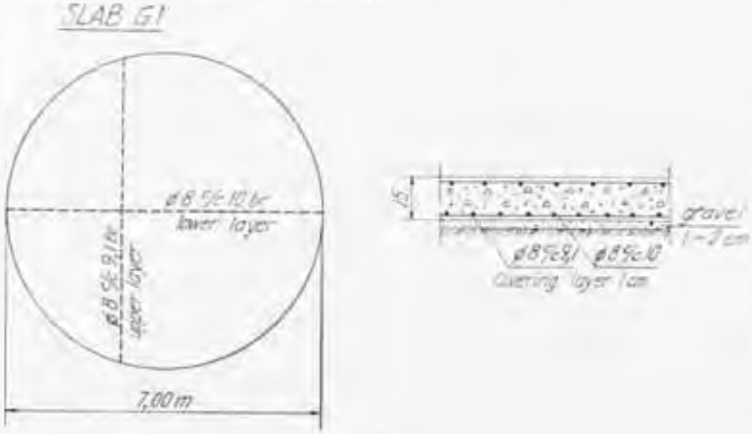

A

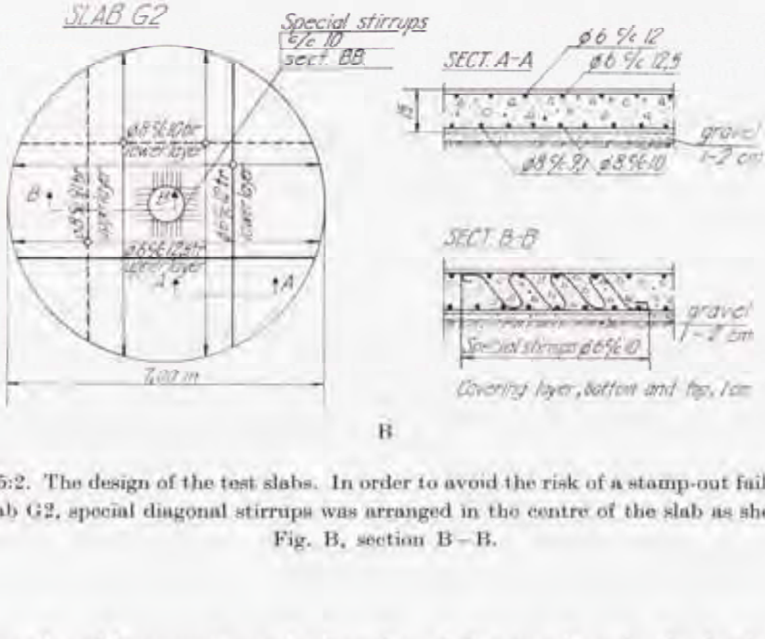

B

Fig. 25:2. The design of the test slabs. In order to avoid the risk of a stamp-out failure on the slab G2, special diagonal stirrups was arranged in the centre of the slab as shown in Fig. B, section B – B.

rest on the old concrete, and after the reinforcing bars in the broken-up surface were carefully suspended and the subgrade carefully levelled with gravel and sand, the hole was filled with concrete of the same type previous used for the rest of the slab. The slab was then tested again after a further 18 days whereby a load distribution plate with a diameter of 80 cm was used. By this test normal moment failure was obtained with circular failure crack in the top surface long way outside the newly cast section.

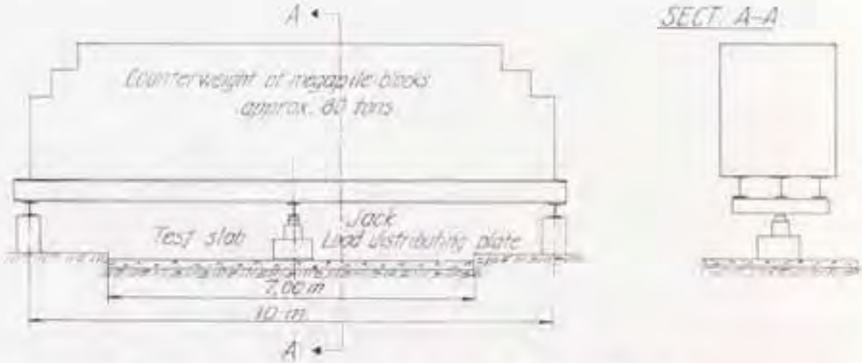

Fig. 25:3. A diagrammatic sketch of the loading device.

253. Test devices, test procedure and results

253:1. *The loading device*

Fig. 25:3 shows the loading device in principle. The slabs were loaded at the centre point by means of a 100-ton hydraulic jack and as backing for the jack a beam system consisting of three DIP 32 beams which were 10 metres long was used. These were arranged with their end supports on wooden beds on the ground outside the edge of the concrete slab. Concrete pile stumps with a weight of 80 tons were stacked up on the beams. The arrangement of the loading device is shown in Fig. 25:4.

The loading was transferred to the centre of the slab with the help of load distributing plates which, during the first loading of slab G 1, consisted of a cylindrical wooden block with a diameter of 40 cm, while in the other tests it consisted of a cylindrical concrete unit with a diameter of 80 cm. This concrete unit had a diametrical channel in the bottom in which a curvature measuring bridge was located in order to determine the movement of the centre point. A thin pressure-equalizing wood fibre sheet was laid between the load distribution cylinder and the concrete slab. The device is shown in Fig. 25:6.

253.2. *Measuring devices*

During the test loading, the following measurements were carried out:

a) The flexural deformation of the slabs was measured with the help of dial gauges located along two diameters at right angles to each other.

b) Strains in the top surface were measured on slab G 2 with the help of strain gauges located along the radius.

c) The pressure between the slab and the subgrade was measured with the help of subgrade pressure gauges which, in the case of slab G 1,

Fig. 25:4. The test slab G1 with the loading device. The photograph shows the slab after the second loading and after final stamp-out failure had occurred.

were located in the neighbourhood of the centre, half-way between the centre and the edge and at the edge itself, while in the case of slab G 2 they were located closer after one of the radii where the dial gauges were fitted.

The location of the various gauges is shown in Fig. 25:5.

About 30 dial gauges were used to measure the flexural deformation; the number of gauges used and the location varied between the different tests as shown in Fig. 25:5. They were located along two diameters at right angles with one another and generally at intervals of 50 cm. They were fitted against measuring beams which were supported on the edges of the slab as shown in Fig. 25:6 and 28:8. The gauges thus registered the deformations of the slab relative to the beam support points on the edges of the slab, and the readings must thus be corrected for the movement of these points relative to the surrounding subgrade. These movements were measured with the help of four dial gauges, attached to iron bars, which were driven down inside a tube going down to a depth of 6—7 metres in the ground and the gauges were thus fixed in the ground under these tubes, see Fig. 25:7. It can definitely be considered, that the ground at this depth under the edges of the slab must be uninfluenced by the test loading. The eventual movements of the measuring beam supports, relative to the edges of the slab, were checked by means of four dial gauges which were attached to the ends of the beams and measured against the edge of the slab.

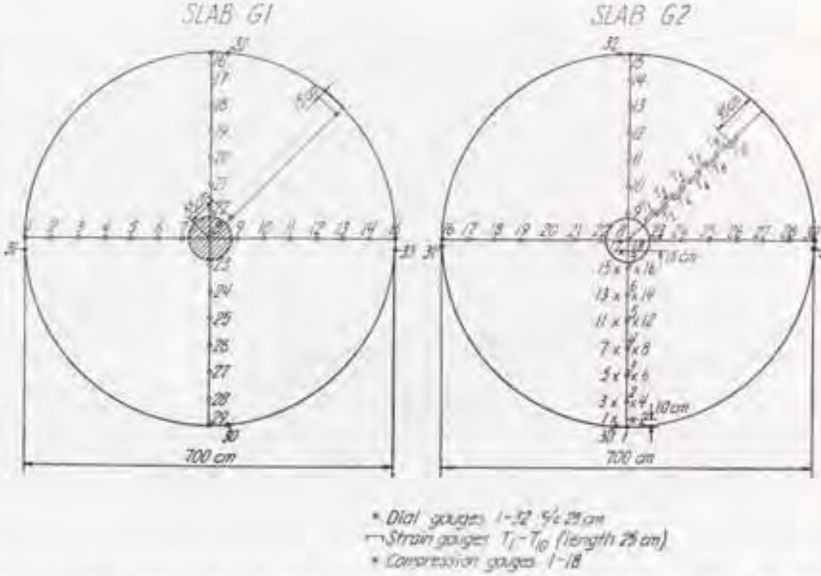

Fig. 25:5. The location of the measuring equipment for both the test slabs. For slab G 1, only the location of the gauges for loading 2 is shown, in the case of loading 1 no deformation was measured in the centre.

When test loading was carried out with the 80 cm load distributing cylinder, the movements in the centre of the slab were measured under the loading surface with the help of a curvature measuring bridge of the same type as that used in the model tests. The measuring bridge was placed in a tunnel in the bottom surface of the load distributing cylinder and it registered the movements of the centre point relative to the support points of the measuring bridge beside the dial gauge points nearest outside the edge of the load distributing cylinder.

In the case of slab G 2 the strains in the top surface of the slab were measured by means of 10 strain gauges which were located close together along one radius. See Fig. 25:8. The strain gauges were of the same type as those used for indicating cracks in the model tests but had a measuring length of 25 cm and were of a more robust design. See Fig. 25:9. The points of the gauges were placed against small steel plates attached to the surface of the concrete slab with shellac, and a punch mark had been made in the steel plates to fix the measuring points. No strain measurements were carried out during the test with slab G 1.

For the measurement of the pressure between the slab and the subgrade a type of acoustic pressure cell was used which has been designed at Chalmers University of Technology, Department of Structural Engineering in co-operation with *D. Eng.* Per W. Brüel who was

Fig. 25:6

Fig. 25:7

Fig. 25:6. The arrangement of the measuring beams at the load distributing cylinder. The through beam lies beside the jack and forms the support for the other two beams. It can be seen from the photograph that one of these, the end being in the form of a yoke, straddles the jack. The photograph also shows the 80 centimetre load distribution cylinder made of concrete with the channel in the bottom, in which the curvature gauge is placed.

Fig. 25:7. Measuring the movement of the slab edge. The gauge is attached to the upper end of an approx. 8 metre long bar which has been driven down into a tube, itself about 6 metres deep in the ground. Notice the reinforcement sticking out from the circumference of the slab (slab G2), this being used for the later casting of the four slab edges tested later.

Fig. 25:8. The location of the strain gauges on slab G2.

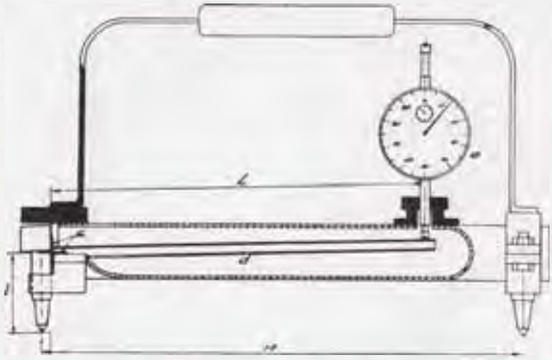

Fig. 25:9. Schematic diagram of the strain gauges used. The movable (left-hand) point forms one arm l of a right-angle lever, the other arm d of which influences the dial gauge e. Its readings thus amplify the movement of the point by a factor $\frac{d}{l}$, c is a hinge consisting of two crossed steel springs. Measuring base $M = 25$ cm.

then head of its Acoustic Laboratory. The design if the gauges is shown in Fig. 25:10 and 25:11. The pressure sensitive surface of the gauge consists of a circular membrane and between this and a fixed tension head a thin piano wire is stretched. If the membrane is influenced by a pressure it will be bent inwards whereby the tension of the wire will decrease. The wire will then have a lower natural frequency. The frequency is measured by means of two electro-magnets attached close to the wire. One of these is connected to a frequency generator and the frequency is set so that it agrees with the natural frequency of the wire. The wire will then start vibrating and induce a current in the other electro-magnet so that a reading will be obtained on a valve volt-meter which is connected in. It is thus possible to measure a difference in pressure on the membrane by measuring the natural frequency of the wire before and after the difference in pressure. Before being used, the gauges must be calibrated and use is here made of a device with communicating tubes where a quicksilver pressure is allowed to influence the membrane. Only a very small deformation of the membrane is necessary to influence the frequency of the wire so that it is not worth worrying about the fact that this membrane deformation should locally influence the subgrade pressure under the surface of the membrane. The gauge magnet system is surrounded by a protective casing with a watertight screw union against the lower part of the gauge, and the inner part of the gauge is protected against condensation moisture by placing a small beaker filled with hygroscopic salt inside the protective casing. (see Fig. 25:10).

Fig. 25:10

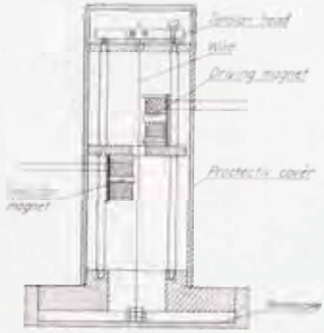

Fig. 25:11

Fig. 25:10. Photograph of a pressure measuring cell with the protective cover screwed off. The cover has a water-tight screw union with a gasket and the interior of the unit is protected from condensation water by means of hygroscopic salt in a small tube (visible in the photograph under the lower magnet).

Fig. 25:11. Schematic diagram of an acoustic pressure gauge. In practice both the electromagnets have their axes at right-angles so that their magnetic fields would not interfere with each other.

The pressure cells were cast in the test slabs so that the surface of the membrane was level with the bottom of the concrete slab and in contact with the subgrade. Fig. 25:12 shows some of the gauges before they were cast in. While casting was being carried out extra care was taken to insure that the gauges were not moved from their positions and to insure that they did not receive any extra loading when the actual concrete was laid out.

When the slab G1 was made, the acoustic pressure gauges had not reached the end of the experimental stage. They only contained, for example, one magnet which was used both to drive and measure. The use of the pressure gauges in this test was mainly to be considered as a section of the experimental work with them. Only three gauges were cast into the slab, and for the sake of comparison some pressure gauges of inductive type as designed at the Swedish Cement- and Concrete Research Institute[1]) were also cast into the slab at the same

[1]) These inductive gauges are described in more detail in the earlier cited work [4] by Bergström, etc.

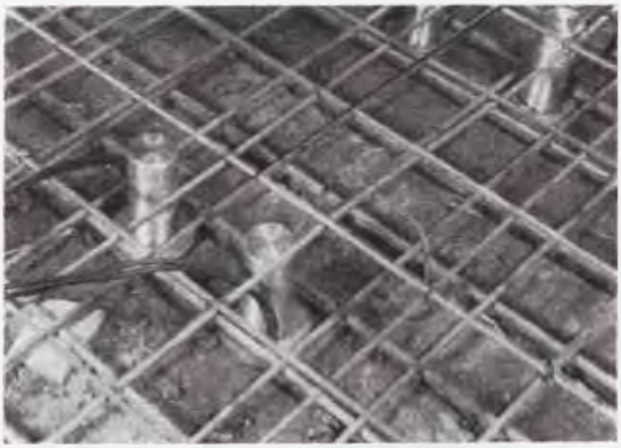

Fig. 25:12. Some of the pressure gauges before slab G2 was cast. Before being placed on the ground, large stones were removed and a layer of finely-screened sand was laid out, after which the surface was moistened and levelled off carefully. When being placed in position, the gauges were pressed lightly down into the subgrade.

distance from the centre and close beside the acoustic gauges. The inductive gauges, however, produced results which were very difficult to interpret and these results have not been included in this description.

On slab G2, 16 acoustic pressure gauges were used located along the radius where the dial gauges 1—8 were fitted (see Fig. 25:5), in pairs beside one another under each dial gauge. Two pressure gauges were also used in the test which were not cast in but lay loose on top of the slab. These were connected in at every series of reading before and after measurements on the cast-in pressure gauges. It became obvious that these gauges did not give fully constant readings on the frequency generator and this can depend on the fact that certain displacements in the frequency scale took place during the procedure of the test. This has been taken into consideration in the analyses of the values obtained in such a way that the frequency values for the different gauges at a certain loading step are corrected with a quantity equal to the average value of the alteration in frequency of both the control gauges.

One thing which became apparent during both tests was the fact that most of the gauges registered various differing initial pressures in excess of that which can have been caused by the weight of the slab itself. This apparently depends on the fact that the gauges have been somewhat pressed down into the subgrade during the casting process.

In the calculation of the pressure value readings for the various loading steps, this initial value has been considered to correspond to a pressure equal to zero.

253.3. *Test procedure and results*

The loading was applied in loading steps which in the case of the slab G1 was approx. 2.5 tons and in the case of slab G2 4.5 tons. The load was measured with the help of a manometer which showed the pressure of the hydraulic oil in the jack. The time interval between each increase of loading was approx. 8 min. total. Of this 3 min. was used to increase the load and 2 min. to maintain it constant during which time the greater part of the creep in the subgrade was allowed to proceed. Finally 3 min. was allowed to read off the instruments. The reading off of the pressure gauges on slab G2, which took a longer time, began as soon as the actual load increase was completed. When testing slab G2 an off-loading to zero was carried out at the loading step 36.2 tons. The reason for this was that a fault occurred in the oil pump. Loading was recommenced again after about two hours.

During the higher loading steps, the surface of the slab was carefully inspected in order to discover any eventual cracks. In order to facilitate this, the centre part of the upper surface of the slab was covered with chalk powder.

During loading 1 of slab G1 a stamp-out failure was obtained round the loading surface at 38.9 tons. No crack formations had been observed in the top of the slab up till this load so that it can be assumed that no moment failure occurred in the top surface during this test. During loading 2 after the plate had been repaired in the middle and when a larger load distribution surface was used, moment failure was normally obtained in the form of annular cracks in the top which were discovered at 54.9 tons. The load increase was continued until a stamp-out failure occurred round the loading surface at 64 tons.

In the case of slab G2, which was top reinforced, crack formation occurred more successively. The final failure through stamp-out round the loading surface occurred at 68.5 tons. The crack diagrams for both the slabs are shown in Fig. 25:13.

The result of the depression, strain and pressure measurements as well as other test results are analyzed and discussed in the following Section 255[1]).

[1]) The complete results concerning the measurement values are shown in the result supplement, Section 93.

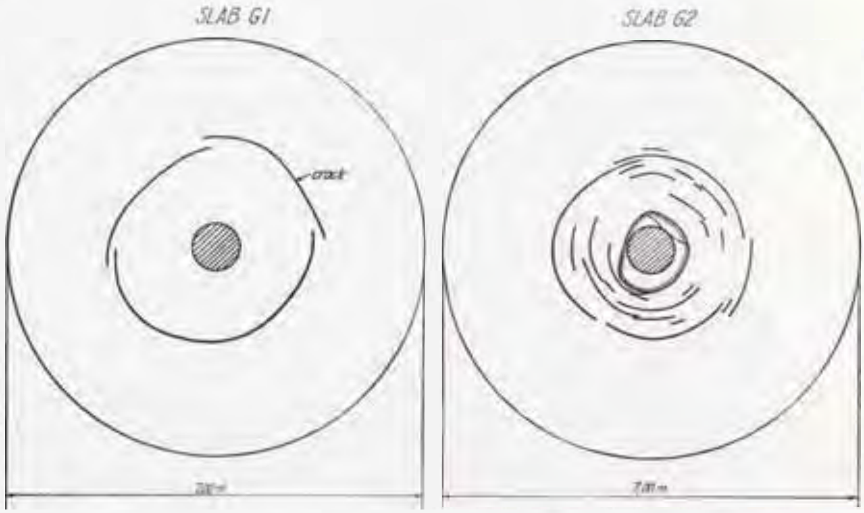

Fig. 25:13. Crack patterns after failure in the top surface. For slab G2, the final stamp-out crack around the loading surface has been specially marked.

254. Material constants for the slabs and the subgrade

254.1. *Ultimate moment and flexural rigidity of the slabs*

The ultimate moment and the flexural rigidity of the test slabs has as usual been determined with the help of the detail test beams which were cast simultaneously with the test slabs. These have been tested simply supported with two concentrated loads. The deformation under loading has generally been measured by means of curvature gauges within the space between the loading points. In the case of two of the detail test beams from slab G1, the total horizontal deflection at the centre point was measured instead.

The detail test beams from slab G1 were all tested with the reinforcement in the tension side. Two of the beams were tested together with loading 1 while the third beam was tested together with loading 2 of the circular slab. After the detail test beams had been tested to failure, the parts of the beams which lay outside the failure cracks were utilized for failure tests for negative moment with the reinforcement in the tension zone.

Of the four detail test beams belonging to slab G2, two of them were tested with the largest reinforcement (= the bottom reinforcement in the circular slab) in the tension side and two with the least reinforcement (= top reinforcement in the slab) in the tension side. These tests thus represent the deflection of the test slab for positive and negative moment in both the main directions of the reinforcement. Due to the fact that the reinforcing bars in both the layers in the top and bottom of the slab respectively had somewhat different distances (see Fig. 25:2), then the four detail tests with respect to the reinforcement corresponded to somewhat different beam widths during deflection in Stage II; respect has here been taken to that in the calculation of the ultimate moment and the flexural rigidity. Apart from the curvature measurements, measurements were also carried out concerning the strains on the tension and compression sides, strain gauges being used here of the same type as in the main tests. The strain gauges on the tension side were located so that it was possible to study the influence of crack formation between the extensometer pointers. These measurements were arranged so that it was possible to compare the result from the test beams with the result from the strain measurements on the top of the circular slab.

The result of the tests is summarized in Table 25:1[1]).

Fig. 25:14 shows the curvature and strain diagrams calculated from the average values of the measurement results from the detail tests belonging to slab G2. From the curvature diagram for positive deflection, the flexural rigidity has been calculated for Stage I and Stage II (the secant modulus at the commencement of crack formation or the yield point respectively), and the average values have been introduced in Table 25:1. The test values show good agreement with the theoretically calculated flexural rigidity values for Stage I ($n = 10$) and Stage II ($n = 15$), which have been also introduced in the table. In the same way the values for ultimate moment given in the table concerning positive and negative flexure have been obtained from the corresponding test beam values. Based on the result curves for curvature and strain measurements, the moment at concrete tension failure for positive and negative deflection have also been calculated and introduced in the table. In all these calculations, corrections have been made for moment in the detail test beams due to their own weight, and also the curvature and strain curves have been corrected for this influence when compared with the corresponding measurements during the main test which is carried out in the test analysis in the next section (see Fig. 25:14).

The strain diagrams have also been used to estimate the values of the strain on the tension side at the beginning of crack formation and at the yield point in the reinforcement. In this connection most attention has been taken to the strain gauges between whose points one crack has appeared since generally speaking in the main test only one crack

[1]) The tests are fully reported in the form of curvature and strain diagrams in the result supplement, Section 93.

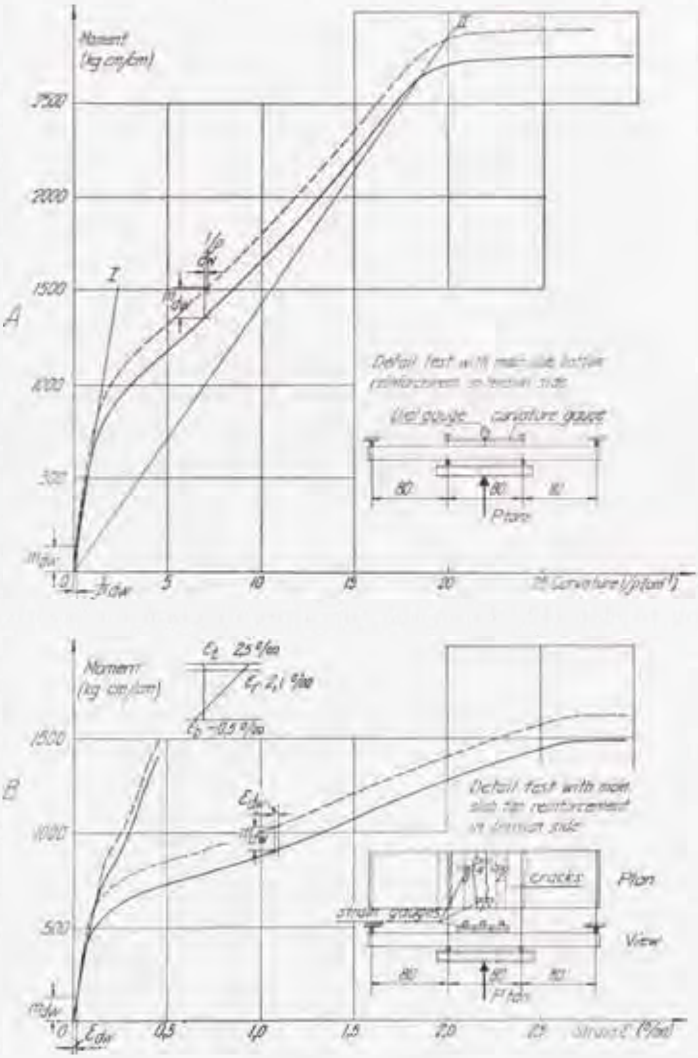

Fig. 25:14. Curvature for positive flexion (Fig. A), and strain values on the tension side for negative flexion (Fig. B), calculated as average values of the measurements on the test slab G2 detail test beams. The figure also includes the correction for the influence of the weight of the unit (broken line); the correction can be obtained as a displacement of the origin corresponding to the dead-weight moment. In the curvature diagram, secants have been inserted, according to which the flexural rigidity for low and high loading have been calculated. Beside the strain diagrams is shown how the strains in the tensile reinforcement have been calculated (introduced into Table 25:1) as well as how the strain gauges were located and how the tension cracks occurred for one of the beams (the unbroken lines correspond to the yield cracks).

TABLE 25:1. Series G. Detail tests.

Summary of flexure tests. The results shown are made up of the average values from the number of tests indicated.

Detail test from slab Reinforcement	G 1 Single reinforcement		G 2 Double reinforcement	
Direction of moment	pos.	neg.	pos.	neg.
Average of (number of tests)	3	3	2	2
Moment at first concrete crack kgcm/cm	940		900	680
Ultimate moment kgcm/cm	3300	950	2900	1620
Strain in tension side ‰				
at first concrete crack			0,15 à 0,20	0,15 à 0,20
at yield point on the surface			2,2	2,5
in reinforcement			1,9	2,1
Flexural rigidity Ei acc. to test kgcm²/cm				
when crack formation begins	$60 \cdot 10^6$		$70 \cdot 10^6$	$70 \cdot 10^6$
at yield point	$16 \cdot 10^6$		$14 \cdot 10^6$	$9 \cdot 10^6$
Theoretically calculated Ei kgcm²/cm				
for stage I	$63 \cdot 10^6$		$70 \cdot 10^6$	
for stage II	$13 \cdot 10^6$		$13 \cdot 10^6$	

appeared within the measuring range of every strain gauge[1]). It can be pointed out that the first crack generally became visible at a considerably higher loading than that at which crack formation should have commenced according to the strain and curvature diagram. These strain value readings in the case of slab G2 have been utilized when determining the loads in the main test which correspond to the tension concrete failure or the yield point in the top reinforcement (see 255:2).

254.2. *Subgrade constants*

Since the intention of this test series was, among other things, to discuss the properties of the subgrade from the point of view of the theory for elastic as well as for resilient subgrade, determinations have been made both of the modulus of soil reaction k and the modified modulus of elasticity C. In this calculation the methods have been used as already discussed in Section 233 and which are based on the depression measurements from the main tests and the calculated values of the depression volume obtained from them (equations (23:3) and (23:16), respectively). The calculations for some of the loading steps are summarized in Table 25:2 and for slab G2 the result is shown in Fig. 25:15.

[1]) The location of the gauges and the crack formation during strain measurements on the test beams are marked in on the diagram in the result supplement.

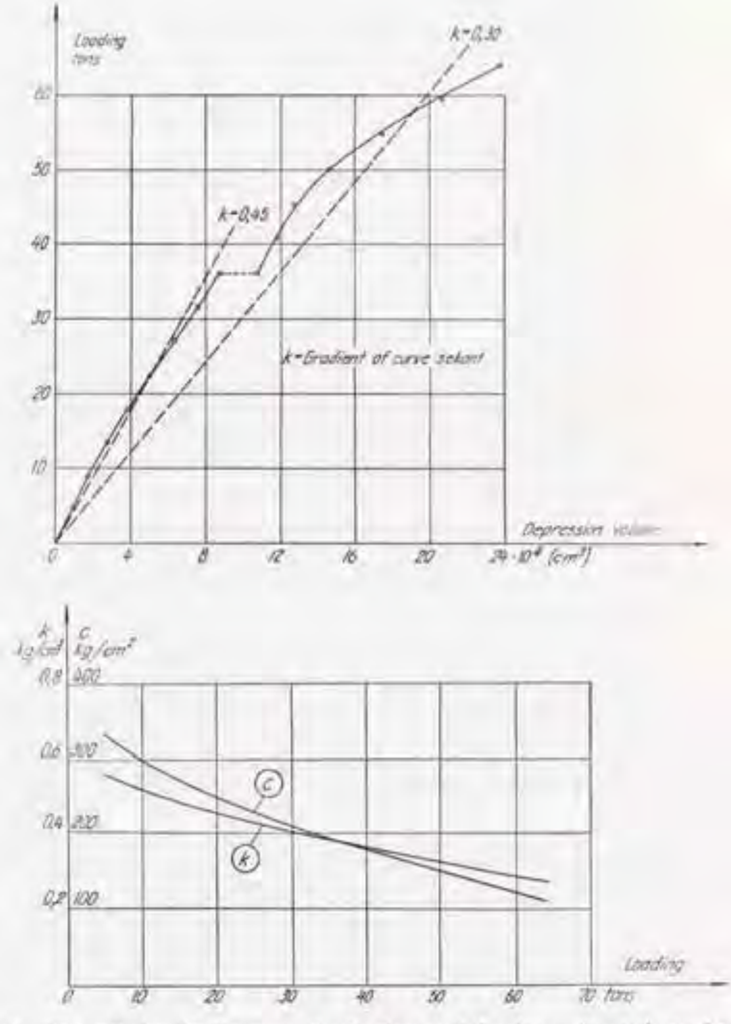

Fig. 25:15. The relationship between the loading and the depression volume for the slab G2 as well as the variation in the subgrade constants k and C for various loading. The secant lines inserted in the upper diagram represent the values of k and C used in the test analysis.

It is obvious that the properties of the subgrade vary to a great extent depending on the extent of the deformation. Fig. 25:15 shows how the subgrade constants decrease with increased loading, i. e. increased deformation. The modulus of elasticity of the subgrade C alters most and this should in itself imply that the elastic subgrade is the least correct of both the discussed hypotheses for the properties of the soil. Really it would be most correct to reckon with a varying

TABLE 25:2. Series G. Calculation of the soil constants k and C.

Slab	Loading P tons	Depression volume $V = \int y\, dA$ cm³	Contact radius r_k cm	$k = \frac{P}{V}$ kg/cm³	$C = \frac{P}{V} \sqrt{\pi\ r_k^2}$ kg/cm²	Remarks
Slab G 1	9.1	$16.5 \cdot 10^3$	325	0.55	315	
	18.4	36.4	313	0.51	280	
loading 2	27.9	59.9	299	0.47	247	
	36.7	87.2	292	0.42	218	
	45.7	125.7	284	0.36	183	
	54.9	175.5	276	0.31	153	
	61.8	230.0	272	0.27	130	
Slab G 2	9.0	$17.4 \cdot 10^3$	325	0.52	300	
	18.0	38.3	308	0.47	255	
	27.1	63.1	291	0.43	220	
	36.2	86.8	278	0.41	205	
	36.2	108.5	276	0.33	163	After loading off
	45.4	128.8	262	0.34	164	and re-loading
	54.6	174.0	248	0.31	138	
	64.0	238.1	234	0.27	111	

value of the subgrade constant from the edge of the slab towards the centre since the increased deformation towards the centre should imply that the subgrade constant there decreases. The table and the figure apparently only give the *average* subgrade constant values under the whole surface of the slab.

It must be obvious that under such conditions it is difficult to decide suitable subgrade constant values k or C for the theoretical analysis of the test slabs. According to the same principles as applied to the model slabs, the author has decided to use the two values which correspond to the loading at the commencement of crack formation in the bottom and at failure in the top. These values, introduced in Table 25:5 in the following section, have been compiled with the flexural rigidity values for the slab in Stage I and Stage II respectively according to Table 25:1.

255. Test results, treatment and theoretical analysis

255.1. *Depression measurements*

The methods used when analysing the depression and strain measurements are generally the same as in the case of the model tests (section 245.1), and the same applies to the theoretical calculations. Here however the calculations have been carried out in accordance with the theory for resilient subgrade as well as elastic subgrade. The values of the flexural rigidity of the slabs and the subgrade constants which were here used (section 254), are introduced in Table 25:5.

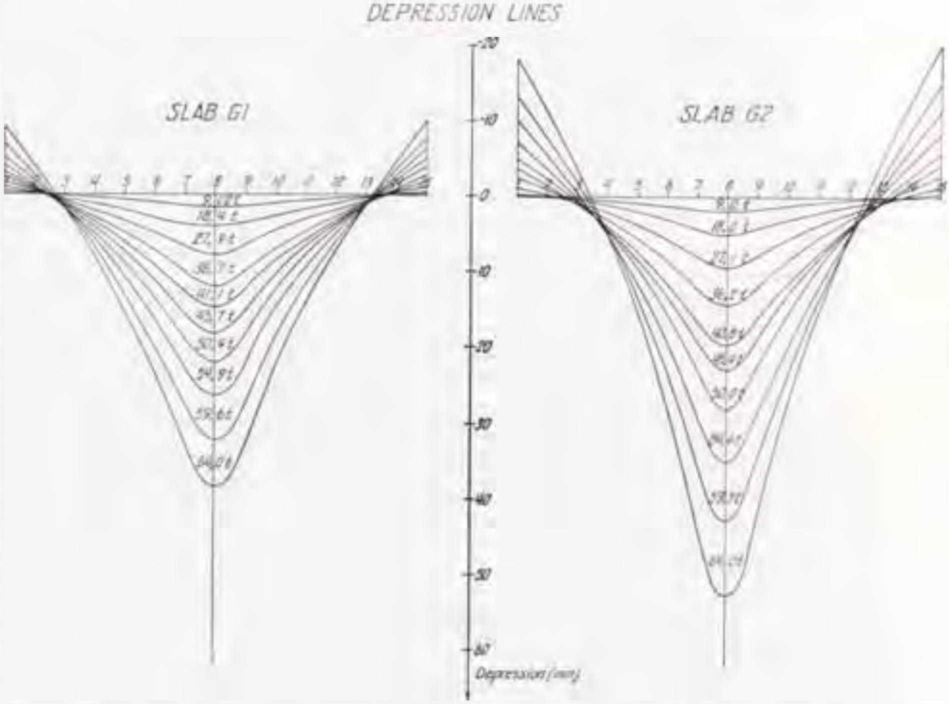

Fig. 25:16. The depression lines for one of the measuring diameters on both the test slabs. Only part of the loading steps is shown.

The result of the depression measurements can be shown through depression lines over the deformation of the diameters. The depression lines for some of the loading steps on both slabs are shown in Fig. 25:16. Also here there is a considerable lifting of the slab edges. It is also shown that the depression figure for a higher load becomes relatively more pointed and that the edge lifts more and more. This is seen even more clearly in Fig. 25:17 where some of the depression lines for slab G2 are drawn in on various scales so that they have all the same centre depression (so-called linear anamorphy). The reason for this alteration in the curves is obviously the fact that during loading the slab alters its elastic properties especially in the centre section where the stresses are greatest and where the first crack formation in the concrete tension zone and later on yielding in the reinforcement cause an increasingly weaker flexural rigidity. It can be seen from the figure that it is the curvature in the actual centre zone which relatively speaking alters most while the curvature otherwise appears to be comparatively constant.

This can be seen even more clearly in Fig. 25:18 which shows the

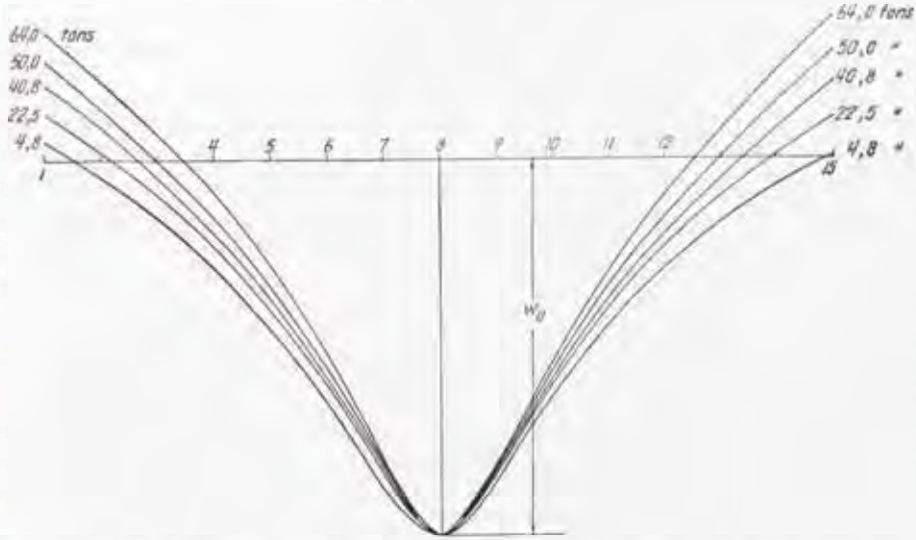

Fig. 25:17. The depression lines for some of the loading steps on the slab G2 drawn on different scales with equal centre depression values (linear anamorphy). The curves show clearly how the curvature of the slab in the centre increases with increased load.

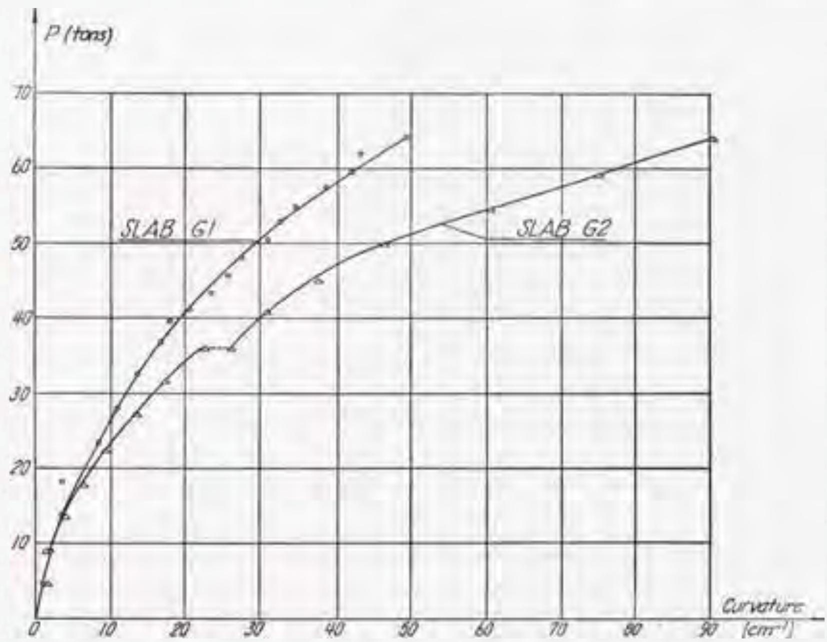

Fig. 25:18. Curves showing the curvature in the centre of slabs G1 and G2. The curvature values have been calculated from the depression values of the five measuring points nearest the centre. (See Fig. 24:7).

curvature of the centre point; the curvature values have been calculated according to the methods shown in Fig. 24:7 from the depression values of the five measuring points nearest the centre, whereby the depression line through these points is assumed to be a fourth grade parabola. The figure shows how curvature in the centre increases rapidly with increased loading; it is however apparent here as in the case of the model tests that increase in curvature takes place along an even curve without any discontinuity or sudden alterations in gradient. Something like that may otherwise be expected at the commencement of crack formation in the concrete and at the yield point in the reinforcement, analogous with that obtained in the testing of the detail test beams (Fig. 25:14).

Neither does the depression at the centre point show any tendencies whatsoever to discontinuity as it develops. The curves concerning the centre depression as well as the corresponding theoretical curves are shown in Fig. 25:28 in the summary Section 255:4.

In Fig. 25:19 the depression lines (average values for the four radii) for two low and two high loads have been compared with the corresponding theoretical depression lines for resilient and elastic subgrade respectively. The last-mentioned curves have not been taken out to the edge of the slab since no theoretical values apply in this case; the curves are drawn according to the theoretical curve for a slab of infinite extent (fig. 22:5), which, it has earlier been shown, can also be applied for slabs of finite dimensions except in the neighbourhood of the edge (see 224).

When deciding which of the subgrade theories lies closest to the tests, one should primarily study the low loading curves which correspond to an uncracked slab with a relatively high flexural rigidity (Stage I). Fig. 25:19 shows however that both the theories give approximately equally good agreement. As far as the higher loads are concerned then comparison with the tests is naturally rather less reliable depending on the varying flexural rigidity of the slab and variations in the subgrade constant. Nor it is possible to show the advantage of one of the theories over the other. Both the theories appear to give relatively satisfactory agreement and the closer relationship with one or the other of them depends on the size of the load; these conditions are clearly shown by the curves concerning the depression in the centre in Fig. 25:28. Nor it is possible to utilize deformation nearer the edge when discussing the applicability of both of the theories, since the theory for elastic subgrade does not give any values for deformation in the neighbourhood of the edge. Apart from this is should be pointed out that the theories assume that in the event of the edge lifting then the subgrade exerts a tension on the slab while the test slab in reality releases contact with the subgrade altogether.

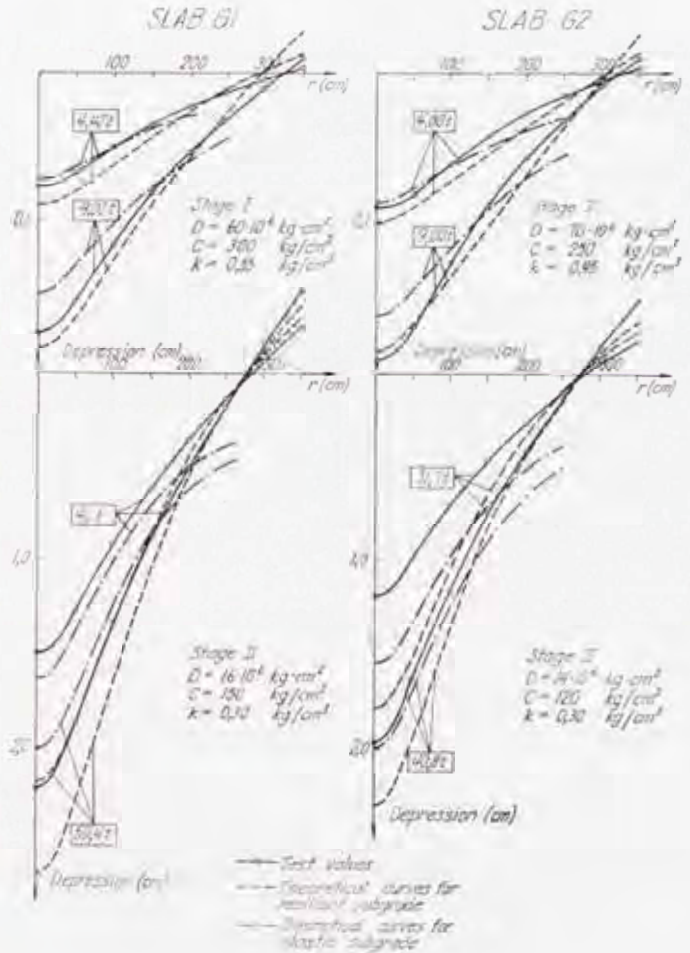

Fig. 25:19. Experimental and theoretical depression lines at some of the loading steps for slabs G1 and G2. The test curves represent the average depression for the four gauges at the same distance from the centre. The theoretical curves for resilient subgrade are calculated according to Fig. 22:13 and 22:8; in this connection the diagram in the last-mentioned figure has been used to correct the influence of load distribution. The theoretical curves for elastic subgrade are calculated according to Fig. 22:5; the diagram on this figure applies to slabs of infinite dimensions but can also be used for slabs of finite dimensions except in the neighbourhood of the edge; the theoretical curves have therefore not been continued to the edge of the slab. The constant values for the slab and the subgrade used for calculation (according to Table 22:5) are shown beside the various curves.

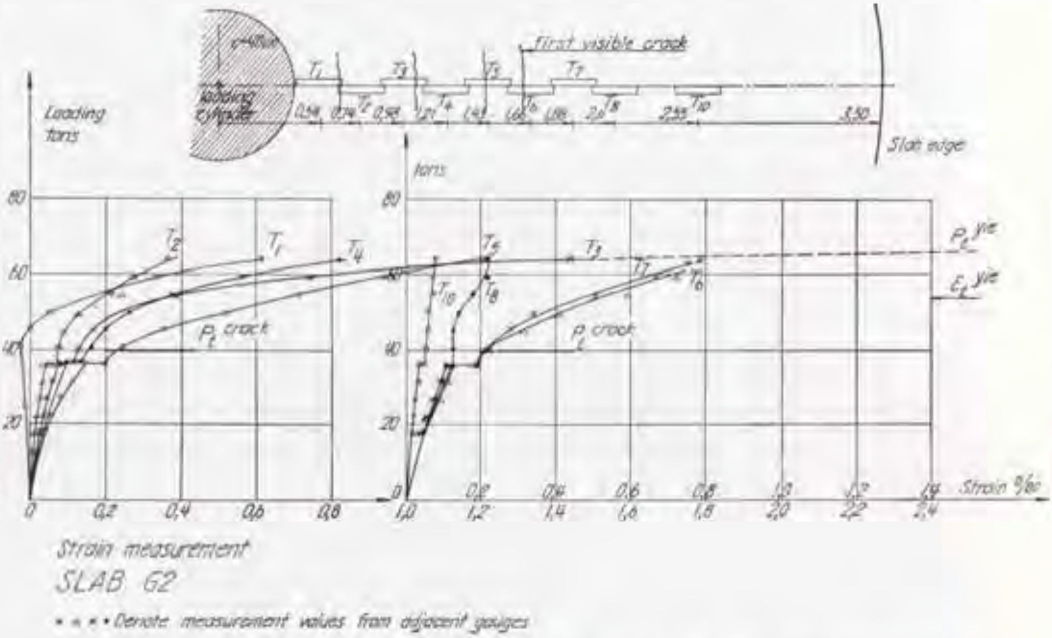

Fig. 25:20. Result of the strain measurements on slab G2. The zero position of the relationship curves and the curve lines for the three first loading steps for the gauges T_2, T_3, T_4, T_6, T_8 and T_{10} are estimated from the following measurement values and from the residual values during off-loading, while the strain gauges concerned during these first loading steps were faultily fitted. All the curves have been evened out slightly with respect to occasional irregularities. Above the curves there is a sketch showing the location of the strain gauges with the cracks marked in, and from the curve for gauge T_6 which was located over the first crack, as well as for the adjacent gauge T_5, it can be assumed that the first crack occurred at approx. 40 tons. From the exterpolated curve for T_3 it is found that the loading at yield point in the top reinforcement must lie at about 66 tons (yield strain according to the detail tests is approx. 2.4 ‰).

255.2. *Strain measurements. Moment and ultimate load*

The moment in the centre of the slabs can in the usual way be estimated from the curvature in the centre point (Fig. 25:18) by comparison with the corresponding measurements on the detail tests according to the method shown in Fig. 24:22. The curves obtained in this way with the relationship between the load and the moment at the centre point are shown in Fig. 25:28 in the summary Section 255:4, and in these moment diagrams the theoretically calculated relationship lines have also been drawn in. From the moment diagram the loading value at the concrete tension failure and yield point in the bottom P_b^{cr} and P_b^{yie} respectively can be calculated as loading values at the corresponding crack and ultimate moment according to the detail tests, Table 25:1.

The loads causing crack formation and attaining yield point in the top P_t^{cr} and P_t^{yie} respectively can be estimated in the same way as in the model tests through analyses of the depression and strain measurements.

In the case of the slab G 1 where no strain measurements were carried out the ultimate load could be accurately calculated from the discontinuities in the depression measurements in the points nearest the annular crack (see Fig. 24:24). The observations are summarized in Table 25:3.

In the case of slab G 2 strain measurements were carried out along one of the radii of the slab. The measurement results are summarized in Fig. 25:20. Crack formation corresponds to a sudden deviation in the strain curves; determination is however rather unreliable just concerning the *first* crack corresponding to the load P_t^{cr}, since the movements of the strain gauges were interfered with by the off-loading to zero shortly before the crack load was obtained. Comparison has also been carried out with the corresponding value of the strain in the detail tests (see Table 25:1). This later method alone has been used for the determination of the final ultimate load at yield point in the top reinforcement P_t^{yie} The strain measurements on the slab according to Fig. 25:20 only went up to the loading step of 64 tons at which load the strain did not fully reach the value which, according to the detail tests in Table 25:1, corresponded to yield point strain. By exterpolation one can estimate the load P_t^{yie} with a fair degree of reliability to approx. 66 tons according to what is shown in Fig. 25:20. The result of the ultimate load determinations is shown in Table 25:3. It should be pointed out that the strain measurements on slab G 2 were only carried out along one radius and that the ultimate load determinations with respect to this and with respect to the indirect determination through comparison with the results from the detail tests appear to be considerably less reliable than the corresponding determinations for the slab G 1.

The strain measurements also give a certain idea of the *moment distribution along the slab radius*. When analysing the measurements in this respect certain corrections must be made in the readings during the three first loading steps. Certain of the strain gauges were fitted faultily in point of fact so that from the beginning they were not resting on the measuring points. This was not discovered before the end of the three first loading steps and the gauges in question did thus not give any usable measurements for these loading steps. In these cases fairly correct zero load basic values can be estimated from the measurement values for on and off-loading which were carried out at the loading step of 36.2 tons and thereby it is assumed that the residual strain after off-loading is of the same magnitude as the increase in strain values

TABLE 25:3. Series G. Centre loading on test slabs. Failure in top surface P_f. The values marked show the assumed load values for failure in the top surface.

Slab, loading case	Load in tons at first crack according to							Load at yield in top-reinf. according to strain gauges	Load at stamp-out failure
	visual observation	dial gauge beside crack at radius					strain measurement		
		E	W	N	S	average value			
G 1									
Loading 1									38.9
Loading 2	54.9	52.6	51.5	52.2	52.0	**52**			64.0
G 2	45.4						approx. **40**[1])	approx. **66**[2])	68.5[3])

[1]) The value is rather unreliable due to the fact that the movements of the strain gauges were disturbed by the off-loading and re-loading after a load of 36.2 tons (see Fig. 25:20). Comparison has also been made with the strain measurements during the detail tests, see 254:1.

[2]) The value is estimated by comparison with the strain measurements during the detail tests, see 254:1.

[3]) The value can have been influenced by the shear reinforcement which was placed in the centre zone of slab G 2. Comparison with the corresponding load on slab G 1 appears to show, however, that the shear reinforcement had practically no effect.

between the off-loading at 36.2 tons and reloading to the same load (see Fig. 25:20).

The strain values with these corrections included have been made up for some of the loading steps into strain curves in Fig. 25:21; the strain curves for the higher loading steps are drawn with relatively free relationship to the measuring values since the increase in strain for the various gauges occur very unevenly after crack formation has commenced in the top surface of the slab. By comparing the strain values according to these curves with the curves showing the relationship between the moment and the strain in the detail test beam experiments (the detail test beams with top reinforcement in the tension side, see Fig. 25:14), it should be possible to obtain a fairly good idea of the distribution of moment. A calculation of this type has been carried out for some of the loading steps and the result is shown in Fig. 25:21. Here the corresponding theoretical curves, calculated for resilient and elastic subgrade have also been marked in. The figure shows relatively good agreement between the test and theory for both the lowest loads P_1 and P_2 which roughly correspond to the commencement of crack formation and the yield point in the bottom (Stage I and Stage II); both the subgrade hypotheses here have acceptable agreement concerning the maximum negative moment value while the theoretical curve for the elastic subgrade shows the best

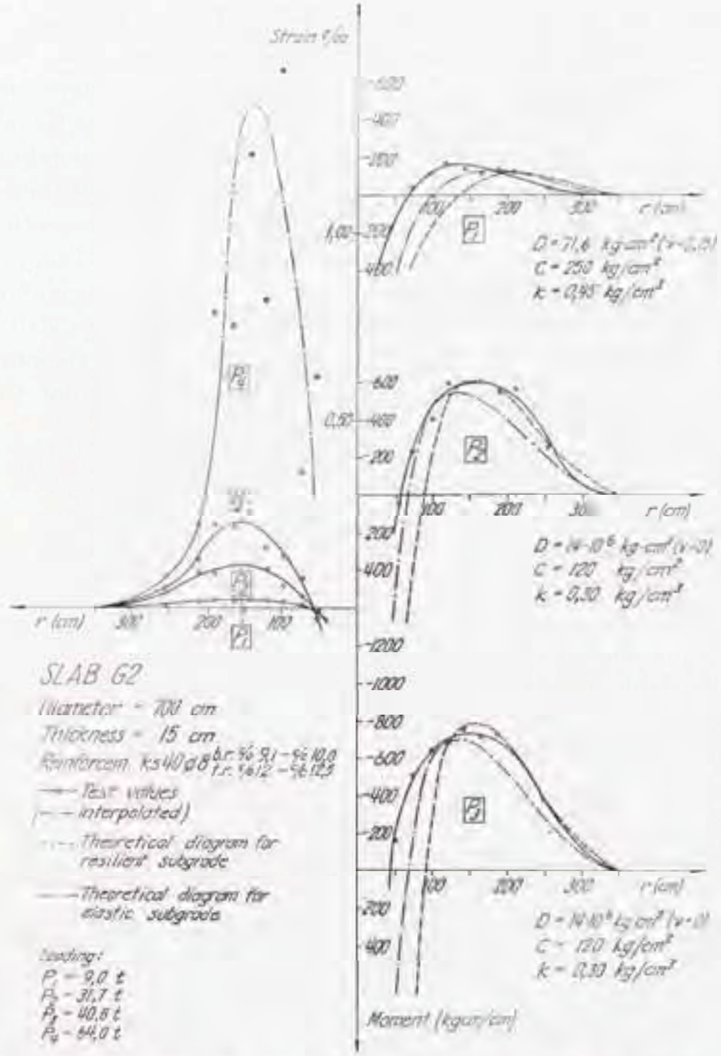

Fig. 25:21. The strain curves and the corresponding moment distribution curves obtained from the strain measurements at some loading steps for slab G2. The moment curves have been obtained from the strain curves by comparison with the strain measurements from the detail tests (see Fig. 25:14). The figures also show the corresponding moment distribution curves according to the theory for resilient subgrade and elastic subgrade respectively. The moment curves for the first-mentioned theory have been obtained according to Fig. 22:14 and 22:9, whereby the diagrams in the last-mentioned figure have been used to estimate the correction due to distributed load. The moment curves according to the theory for elastic subgrade have been obtained according to Fig. 22:7 which applies to slabs of infinite extent but certain corrections have been made for the influence of the free edge analogous with that shown by the moment curves according to Fig. 22:14 for slabs of finite dimension on resilient subgrade. The constant values for the slab and the subgrade used are shown beside the various curves.

relationship to the test curve on the whole. Also at the load $P_3 = 40$ tons, corresponding to the commencement of crack formation in the top surface, agreement between the test and theoretical curves is good, something which was hardly to be expected. At this load the slab has actually gone into a yield stage in the centre and the corresponding result from the model slabs shows that the elasticity theory is not then applicable, not even to the parts of the slab lying outside the centre section. The fact that this case shows good agreement between test and theory appears to depend on the fact that the load in question does not lie so far above the load at the commencement of yield in the centre of the slab so that the yield zone should be of relatively limited extent and therefore does not influence the moment distribution so much further out from the centre of the slab.

255.3. *The soil pressure measurements*

As has already been mentioned, the pressure cells which were cast into the slab G 1 were still in the experimental stage and the results have therefore been quite difficult to interpret. Some of the gauges were damaged by moisture, probably in connection with casting, and did not give any usable measuring values. Some of the gauges which functioned were not designed for such large pressures as those that actually occurred and therefore they gave no measuring values at higher loading. The result of the pressure measurements with the slab G 1 must therefore be judged as being altogether too unreliable to be able to use in a discussion concerning the properties of the subgrade material.[1])

The pressure measurements in the case of the slab G 2 have given more satisfactory results. The gauges have here been located in pairs beside each other and it was therefore possible to judge the reliability of the measurements obtained. The result of the measurements is shown in Fig. 25:22. It is undeniable that certain of the adjacent gauges in many cases show relatively deviating values but the deviations are generally smaller in the case of higher pressures. The deviations can naturally depend on local unevenness in the soil itself, the occurrence of stones under the gauges or similar factors. In one case a gauge showed so very much higher values compared with an adjacent gauge that the readings from this gauge have been excluded. The gauges located nearest the centre have not registered the pressure during the higher loading steps which has apparently depended on the fact that the wire has slackened altogether too much under these high pressures. The pressure increase in the various measuring points appears to have had quite a linear form

[1]) The measuring values are shown in the result supplement, Section 93.

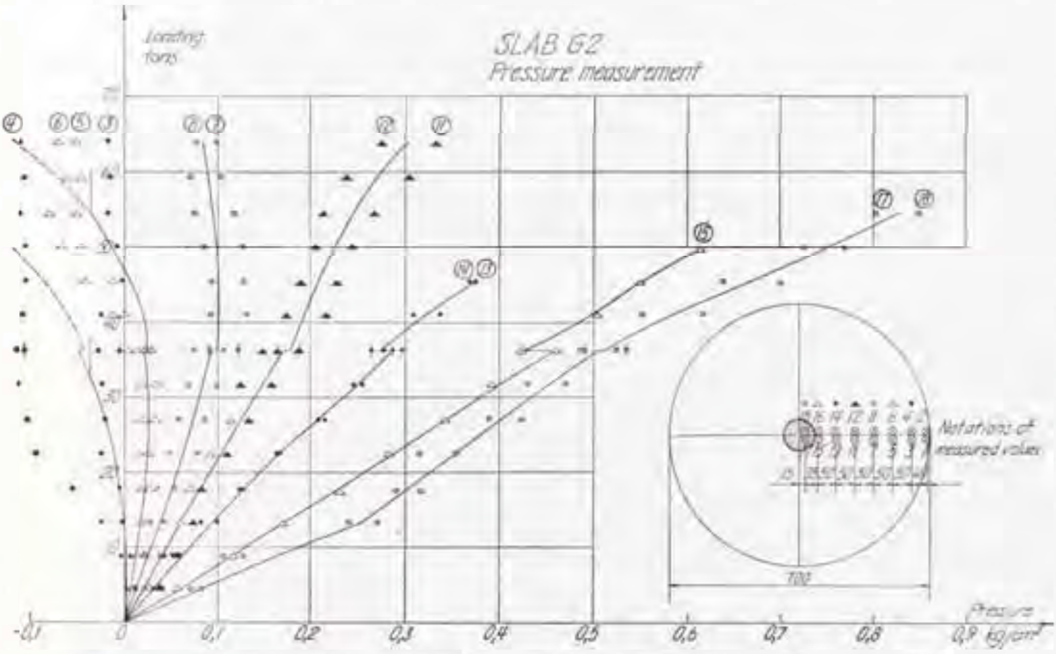

Fig. 25:22. The relationship between the total load and the measured pressure at the various measuring points for the test slab G 2. The relationship curves have been evened out with respect to occasional irregularities. Two pressure gauges were placed at each measuring point and both the measuring results are marked in on the diagram (with the exception of the gauge pair 15—16 where the results from gauge 16 have been eliminated since this gauge showed unreasonably high results). The sketch beside the curves shows the location of the gauges.

if one neglects local deviations which appear to depend to a great extent on the imperfection of the general apparatus used, more particularly the displacement already mentioned in the frequency generator scale (Section 253:2) and the difficulty in finding the exact resonance position for the natural frequency of the wire. The unevenness is particularly prevalent for the pressure gauges placed nearest the edge where the pressure from the subgrade is very small and any possible interruptions have the largest influence. Due to the counter-resilience of the subgrade when the edge of the slab lifts, the measuring values of these edge gauges will be negative; the largest negative value should roughly correspond to the pressure of the weight of the slab 0,036 kg/cm². The fact that some of the gauges registered higher negative values depends on the fact that they, as already mentioned, were subjected to a more or less powerful initial pressure when being fitted. The measuring values have been equalized by drawing relationship curves as shown in Fig. 25:22 and the measuring

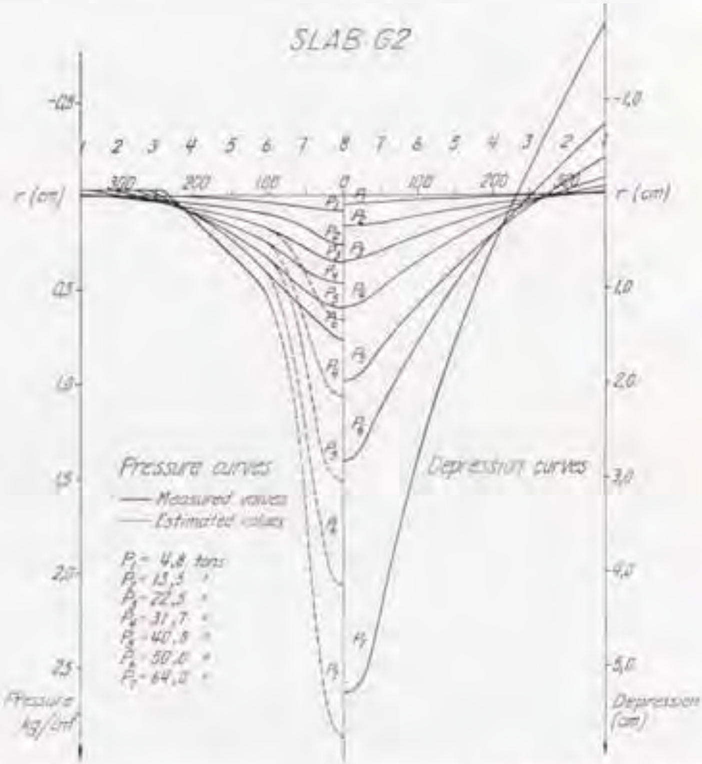

Fig. 25:23. The pressure distribution curves compared with the depression lines for the same radius on slab G2. The figure also includes some of the estimated pressure distribution curves for higher loading steps which give the correct pressure volume.

values equalized in this way have generally been used for further analysis.

When inserting the pressure curves in Fig. 25:22 equalization has also been carried out with respect to the fact that evenly running curves concerning pressure distribution along the radius of the slab would be obtained. Fig. 25:23 shows these pressure distribution curves for some of the loading steps and for comparison the depression lines for the same radius and the same loading steps have been inserted in the figure. It can be seen that the pressure curves for the lower loading steps have a considerably steeper gradient than the corresponding depression curves, while this is *not* the case for the higher loading steps.

This fact is shown even more clearly in Fig. 25: 24 where some of the curves in Fig. 25:23 are drawn linearly anamorphised. With respect to the form of the depression lines a steeper gradient would almost have been expected also on the pressure distribution curves for the higher load

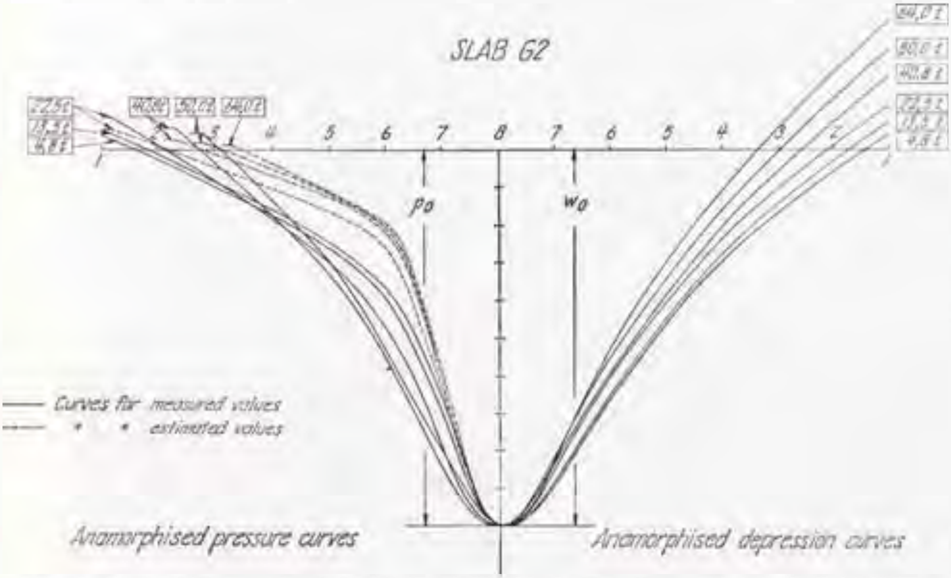

Fig. 25:24. The pressure and depression curves in Fig. 25:24 marked in with equal peak values (linearly anamorphised). Part of the estimated pressure curves with the correct pressure volume has also been marked in, (broken lines).

steps. This gives reason to suspect that the measuring values for the higher load steps are unreliable. Another condition which indicates the same thing is that the curves showing the relationship according to Fig. 25:22 between the pressure and the loading for the central gauges have a linear form or, particularly in the case of the centre gauge, the curves even show a steeper gradient with an increased load while instead it was to be expected that the curves in similarity with the corresponding depression curves should have shown a lower gradient with an increased load.

The pressure gauges were placed in pairs under the indicating dials along one of the radii (se Fig. 25:5). It is thus possible to study directly the relationship between depression and soil pressure in the various measuring points and these relationship curves have been marked in on Fig. 25:25. The figure shows very clearly that one cannot count with the relationship corresponding to a resilient subgrade since in this case the inclination of all the curves would have agreed. This figure also points out that the centre pressure gauges showed excessively low values at higher loadings since all the curves show a common tendency to an increased gradient for the measuring points nearer the centre with the exception of just the upper parts of the curves for both the centre gauges where there is a marked decrease in the gradient.

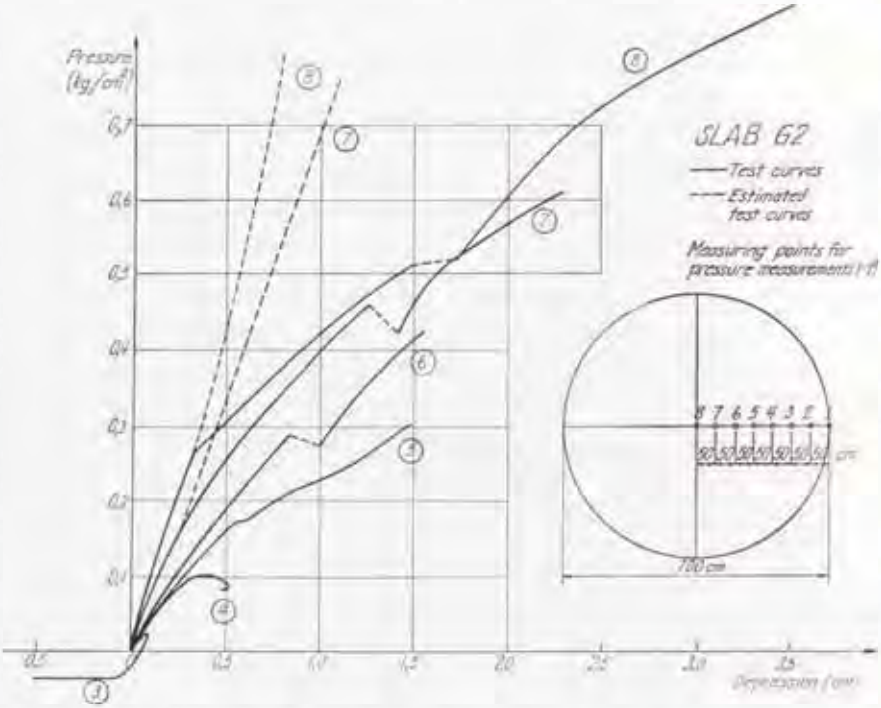

Fig. 25:25. The relationship curves between the depression and the pressure at the various measuring points along the radius for slab G2. The relationship curves for both the highest loading steps, if the estimated values for the correct pressure volume are used, have been marked in as broken lines.

The reliability of the measurement results can be checked by calculating the soil pressure volume, V_p for the various loading steps since, according to the condition of equilibrium, this is

$$P = V_p = \int^{A} p_s \, dA$$

Since, however, pressure measurements have only been carried out under one of the radii of the slab and since the depression measurements show that the various slab radii have slightly different depressions and therefore may have slightly different pressures, one cannot use the measuring results directly. The average pressures under the four radii have instead been estimated with the help of the relationship curves in Fig. 25:25 between the depression and the pressure or for the measuring points furthest out by exterpolation. The pressure volume has been calculated from these average pressures in the same way as the depression volume whereby the

TABLE 25:4. Series G, test slab G 2. Result of pressure volume calculation from the soil pressure gauges under the slab.

The average pressure estimated from the average depression values has been used for calculating purposes.

Loading		Pressure volume V_p tons	V_p/P
Load no.	Load P tons		
1	4.8	5.1	1.06
2	9.0	9.1	1.01
3	13.5	13.3	0.99
4	18.0	16.5	0.92
5	22.5	19.2	0.85
6	27.1	22.4	0.83
7	31.7	25.2	0.80
8	36.2	28.8	0.80
17	40.8	30.8	0.76
18	45.4	32.8	0.72
19	50.0	35.1	0.70
20	54.6	38.0	0.70

"negative" pressure under the lifting edge is assumed to be limited to the pressure exerted by the slab itself 0.036 kg/cm².

The result of the pressure volume calculation is shown in Table 25:4. One can see that the agreement between the loading and the pressure volume for the lowest loads is very good but for higher loads it becomes poore and poorer. The suspicion expressed previously that the pressure gauges nearest the centre show excessively low values at higher loads appears to be quite correct. The author has attempted to carry out a rough estimation of the correct pressure distribution curves with correct pressure volume for some of the higher loading steps in the following way. One assumes that the outer six (or in the case of the higher loading steps five) pressure gauges give the correct values so that the outer part of the pressure distribution curve is correct. The form of the curve in the centre zone is assumed relatively speaking to agree with the form of the curve for the lower loading steps with a correct pressure volume and one can thus estimate the relationship between the pressure values in the inner measuring points. These pressure values are proportioned in such a way that the pressure volume is correct. Some pressure curves obtained in this way are shown in Fig. 25:23 and 25:24. These show a perfectly reasonable form of curve and have considerably higher pressure values in the centre than the corresponding measuring values.

In a discussion of the test results compared with the theories according to both the subgrade hypotheses one should primarily utilize the pressure measurements from the lower loading steps where the pressure volume is correct. One also has the advantage that the slab is, generally speaking,

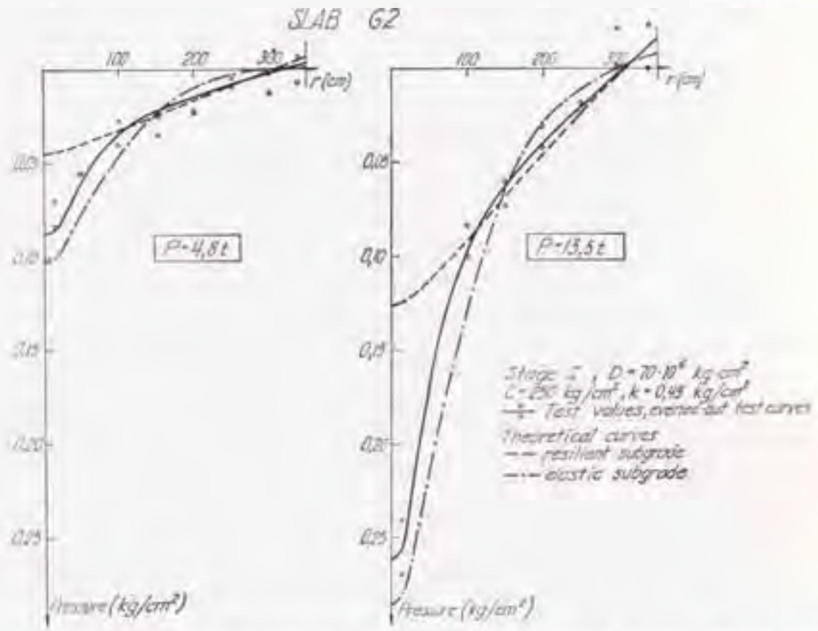

Fig. 25:26. The pressure measurement values and the theoretical pressure curves at loads of 4.8 tons and 13.5 tons for slab G2. The theoretical curves for resilient subgrade have been obtained from the corresponding depression curves in Fig. 25:19. The pressure curves for elastic subgrade have been obtained according to Fig. 22:10. The constant values for the slab and the subgrade according to Stage I have been used.

uncracked and in Stage I whereby in judging the result one does not need to pay any respect to the complication of varying flexural rigidity in the slab.

In Fig. 25:26 the pressure measurement values for some of the loading steps with a low load have been compared with the theoretical pressure distribution curves according to the theory for elastic subgrade and resilient subgrade respectively. The constant values for the slab and the subgrade according to Stage I have been used; the values used are introduced in Table 25:5 in the following section and are also shown in the figure. As the figure shows, the measuring values indubitably exhibit the best agreement with the theory curve for elastic subgrade and it is obvious that the pressure in the neighbourhood of the centre of the slab cannot be even approximately estimated according to the theory for resilient subgrade.

In Fig. 25:27 in the same way the test values and the theoretical curves have been marked in for a load corresponding to yield point in the bottom reinforcement and a load in the neighbourhood of the ultimate load at yield point in the top reinforcement respectively. The theoretical curves

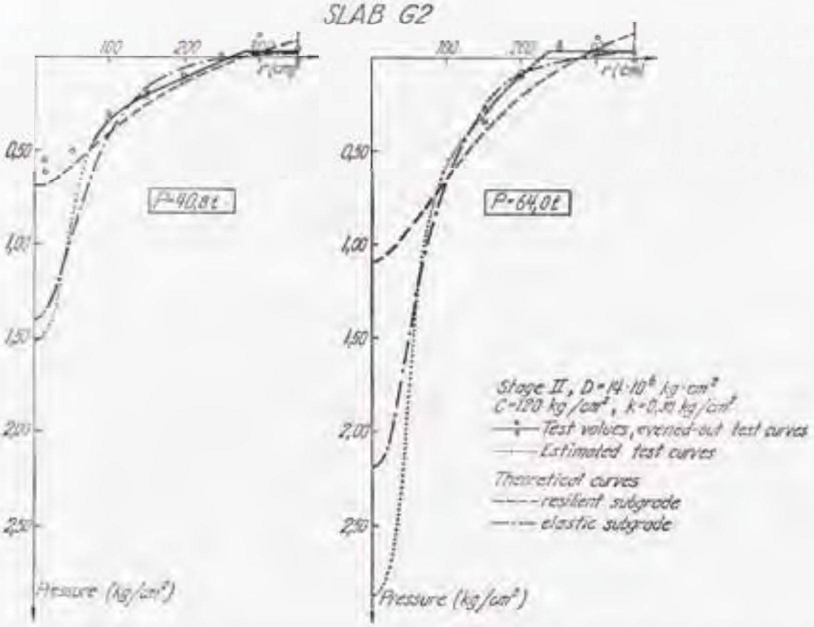

Fig. 25:27. The pressure measurement values the and theoretical pressure curves at loads of 40.8 tons and 64.0 tons for slab G2. The estimated pressure distribution curves with the correct pressure volume have also been included. The theoretical curves are calculated according to Fig. 25:26 for the constant values of the slab and the subgrade according to Stage II.

have been calculated for the flexural rigidity of the slab at Stage II and the soil constants for loads in the neighbourhood of the ultimate load (see Table 25:5 and Fig. 25:27). In the diagram the estimated "test curves" with the correct pressure volume have also been marked in. When judging the result according to the figure due respect should be taken to the influence of the varying flexural rigidity of the slab and the varying subgrade constant, as well as the difficulty in selecting suitable constant values. Most important of all it should be pointed out that the estimation of the pressure distribution curve is very unreliable concerning both the form of the curve and the individual pressure values. The purely formal comparatively good agreement between the estimated test curves and the theoretical curves for elastic subgrade should thus in itself not be given too much importance, but the figures show in any case nothing that appears to dispute the correctness of the result which was more indubitably shown in the previous Fig. 25:26, namely that the subgrade pressure can fairly well be estimated according to the theory for elastic subgrade.

255.4. *Conclusion and discussion*

The test results and the corresponding theoretical calculations have been put together in Table 25:5. Data for both the slabs and the constants for the slab and the subgrade for low and high load used for the theoretical calculations have also been introduced in this table.

The calculations and comparisons between test and theory have been carried out for loading at the commencement of crack formation P_b^{cr} and at the yield point P_b^{yie} in the bottom under the loading centre as well as for the first crack in the top P_t^{cr} and for the double-reinforced slab G 2 for final failure due to yield in the top reinforcement P_t^{yie}. The first two loads have been estimated from the relationship curves between the loading and the moment in the loading centre (see Fig. 25:28) while the later loads in the case of failure in the top have been estimated from the crack formation and strain measurements in the top surface (see Table 25:3). The test values for depression and soil pressure (slab G 2) in the centre for the loads in question have been obtained from the corresponding test curves according to Fig. 25:28. The centre soil pressure values for the slab G 2 have, in the case of the higher loading steps, been obtained from the pressure distribution curves in Fig. 25:23 estimated from the pressure volume calculations; the curve in Fig. 25:28 and the corresponding values of the centre pressure in the table must thus be considered as being *very* unreliable.

No corrections for membrane stress influence have been introduced in this case in the ultimate loads. A rough calculation of the correction values according to (23:44) shows that the correction in the case of the crack load P_t^{cr} only goes up to a few tenths of a percent and is thus completely insignificant. At the yield load P_t^{yie} on slab G 2 the correction is considerably greater but here must be added the earlier discussed influence on the flexural rigidity of the widespread crack formation in the case of the double-reinforced slabs which reduce the influence of the membrane tension and make the correction value exceptionally unreliable; the correction here may go up to between 2 and 5 tons.

The corresponding theoretical loading values have been calculated from the moment diagram in Fig. 22:7 and 22:9 respectively concerning the loads at top surface failure according to the theory for resilient subgrade, a correction has been carried out for the influence of a finite slab radius according to Fig. 22:14. The loads have been calculated for the moments at corresponding failure as determined from the detail tests (Table 25:2); the moment values have been introduced into the result Table 25:5. Comparison between test and theory shows for the two lowest loads at crack formation and yield point in the bottom that agreement is very

TABLE 25:5. Series G. Centre loading on test slabs. Comparison between test results and theory.
Diameter 7.00 m, thickness 15 cm, load distribution radius $c = 40$ cm.
The theoretical values have been calculated according to the theory for resilient subgrade (index k) as well as elastic subgrade (index e).

Series G, slab no	1					2				
DATA FOR THE TEST SLABS										
Thickness h_0, approx cm	15					15				
Reinforcement, Ks 40 ⌀ 8										
bottom reinforcement	e/e 9.1—e/e 10.6					e/e 9.1—e/e 10.0				
top reinforcement	—					e/e 12 —e/e 12.5				
Flexural rigidity Ei kgcm²/cm										
Stage I	$60 \cdot 10^8$					$70 \cdot 10^8$				
Stage II	$16 \cdot 10^8$					$14 \cdot 10^8$				
Resilience constant k kg/cm³										
for low loading (Stage I)	0.55					0.45				
for high loading (Stage II)	0.30					0.30				
Soil modulus C kg/cm²										
for low loading (Stage I)	300					250				
for high loading (Stage II)	150					120				
Elastic radius of rigidity l cm										
for low loading	$l_k = 103$ $l_e = 74$					$l_k = 112$ $l_e = 83$				
for high loading	86 60					83 62				
Relative load distribution $\alpha = \frac{c}{l}$										
for low loading	$\alpha_k = 0.39$ $\alpha_e = 0.54$					$\alpha_k = 0.36$ $\alpha_e = 0.48$				
for high loading	0.47 0.67					0.48 0.65				
Ultimate moment kgcm/cm										
at bottom concrete failure m_{cr}	940					900				
at bottom reinforcement yield m_{yie}	3300					2900				
at top concrete failure m'_{cr}	950					680				
at top reinforcement yield m'_{yie}	—					1620				
RESULT: F from tests; T_e from elast. subg. theory; T_k from resil. subg. theory	F	T_k	F/T_k	T_e	F/T_e	F	T_k	F/T_k	T_e	F/T_e
Loads in tons										
at bottom crack P_b^{cr}	8	6.6	1.21	8.0	1.00	8	6.1	1.31	7.2	1.11
at bottom reinforcement yield P_b^{yie}	42	29.7	1.41	38.4	1.09	33	26.6	1.24	32.6	1.01
at top crack P_t^{cr}	52	52.1	1.00	53.5	0.97	40	35.4	1.13	38.2	1.05
at top reinforcement yield P_t^{yie}						66	84.3	0.78	91.0	0.73
Depression in cm										
at test load P_b^{cr}	0.18	0.16	1.12	0.13	1.38	0.15	0.166	0.90	0.143	1.05
at test load P_b^{yie}	1.56	2.23	0.70	1.67	0.94	1.27	1.87	0.68	1.61	0.79
at test load P_t^{cr}	2.33	2.76	0.85	2.07	1.12	1.92	2.26	0.85	1.96	0.98
at test load P_t^{yie}						5.72	3.74	1.53	3.23	1.77
Pressure under loading centre, kg/cm²										
for test load P_b^{cr}						0.150	0.075	2.00	0.170	0.88
for test load P_b^{yie}						1.14	0.560	2.04	1.13	1.01
for test load P_t^{cr}						1.48	0.755	1.96	1.37	1.08
for test load P_t^{yie}						2.88	1.25	2.30	2.27	1.26

good between the test loads and the loads according to the theories for elastic subgrade and rather less good according to the theory for resilient subgrade. At the load P_t^{cr} at crack formation in the top the agreement is good according to both the theories, which in this case give almost the same result. The reasons for this good agreement, as opposed to the corresponding results from the model tests, have earlier been discussed in connection with the moment distribution curves in Fig. 25:21. It can, however, be pointed out that agreement is considerably less good at the higher ultimate load P_t^{yie} at the reinforcement yield point in the top of slab G 2. At this higher load the plastic zone in the centre of the slab is more extended and the properties of the slab deviate considerably from the conditions for the elasticity theory.

The theoretical values for depression in the centre have been calculated according to the diagram in Fig. 22:8 b and 22:13 for resilient subgrade and 22:11 for elastic subgrade. Agreement with the test values is relatively good according to both the theories; in general the theory for elastic subgrade gives a little better result. Agreement in the case of the highest load for the slab G 2 is, however, less good; this can depend on the fact that at this load the slab has extensive crack formation in the top and that this deformation which, to a large extent, is caused by "negative deflection", should almost be calculated on the basis of the lower modulus of elasticity for Stage II in the case of negative deflection (see Table 25:1).

Finally the theoretical values for the centre soil pressure on slab G 2, calculated according to Fig. 22:10, have been compared with the test values. Agreement is poor according to the theory for resilient subgrade and good according to the theory for elastic subgrade with the reservations for unreliability in the calculated test values for higher loading which has already been pointed out above.

It may be mentioned that the flexural rigidity of the slab and the subgrade constants have been inserted with a Stage I value when calculating the lowest load and Stage II value for the other loads.

The comparisons discussed above between moment, depression and subgrade pressure in the loading centre according to tests and theories are further illustrated by the diagrams over the magnitudes in question shown in Fig. 25:28. Even here it can be seen that the theoretical curves according to the elastic subgrade hypothesis on the whole show closer agreement with the test curves. Otherwise concerning the general form of the test curves reference is made to the discussion of the corresponding curves for the model tests in Section 245:5.

When judging the results in their entirety one must pay due attention

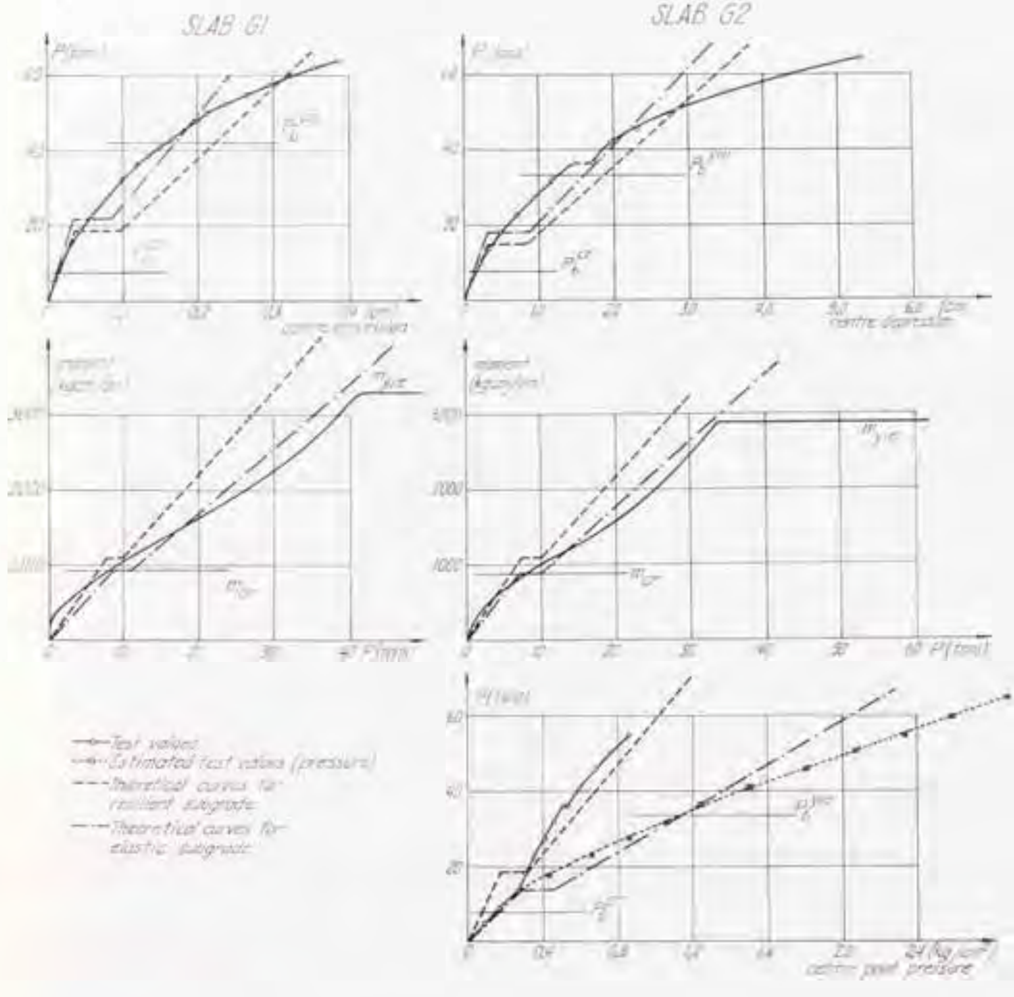

Fig. 25:28. Depression, moment and (for slab G2) subgrade pressure in the centre of the slab for slabs G1 and G2 according to test and theory. The test curves of the centre moment have been obtained by comparison with the curvature graphs for the slab and the detail tests according to the method illustrated in Fig. 24:22. The theoretical curves for resilient subgrade have been calculated according to Fig. 22:8 b and 22:13 and for elastic subgrade according to Fig. 22:10 concerning subgrade pressure and according to Fig. 22:11 concerning depression. The calculation has been carried out with the constants for the slab and the subgrade according to Stage I (with $\nu = 0{,}15$) and Stage II ($\nu = 0$).

to the influence on the theoretical calculations of the degree of unreliability of the constants for the slab and the subgrade and also pay respect to the accuracy with which the test values can be obtained. In this considerations reference is made to the corresponding discussion for the model tests in Section 245:5. Here shall only be added the fact that the subgrade constant k or C in this test series with slabs on natural clay subgrade is considerably more unreliable to determine and varies much more with loading than corresponding subgrade constant in model tests. One other fact that applies here is that the theoretical subgrade pressure value is influenced rather more than the theoretical value for depressions by the unreliability of the constants and that the expression for the subgrade pressure and depression according to the theory for elastic subgrade is somewhat more influenced by the unreliability in the constant values than the corresponding expression according to the theory for resilient subgrade.

It can thus be said that the limits for reasonable deviation between theory and test in this test series should be made rather wider than in the case of the model tests. With respect to this one can sum up by saying that the agreement reached between test and theory on the whole is as good as may be expected. The tests have possibly not given completely unanimous answers to the question as to which of the two subgrade theories best corresponds to the actual soil properties, and as far as both depression and moment are concerned, both the theories show acceptable agreement with the test results. The soil pressure measurements, particularly the measurements at the lower loading steps, which can be judged as being fairly reliable, show however a considerably better agreement with the theoretical pressure distribution according to the hypothesis for elastic subgrade. Perhaps a reminder is in order here that it is just concerning *the subgrade pressure* that both the hypotheses differ most. The fact that the result just concerning subgrade pressure shows good agreement with the theory for elastic subgrade should thus be a strong argument supporting the view that this theory is better when describing the properties of the clay subgrade of the type in question.

It should finally be pointed out that in the case of these slabs good agreement was obtained between the tests and theoretical loads for the beginning of crack formation in the top P_t^{cr}. This opposes the corresponding results from the model tests which showed that generally speaking it was not possible to apply the elasticity theory for moment calculations after a plastic stage had been attained in the slab. With the slabs in the G-series, however, the loads causing cracks P_t^{cr} in question do not lie far above the loads P_b^{yw}, corresponding to the yield point in the centre of the slab, so that the plastic zone in these cases should be so limited that it only has an insignificant affect on the moment distribution further out from the centre. At a higher load (P_t^{grie} for the G 2 slab) with a more extended plastic zone then the agreement between test and theory is considerably poorer, and the general conclusion from the model tests concerning the application of the elasticity theory can thus not be considered to have been shown to be wrong by the tests discussed here.

26. General Viewpoints on the Application of the Elasticity Theory Concerning Reinforced Concrete Pavements

The theoretical presentation in Section 22, summarized in Section 225, is based on the assumption that the concrete pavement functions as a complete elastic-isotropic slab on an ideal-elastic subgrade which functions either as a resilient bed or as an elastic-isotropic and semi-infinite medium.

Concerning the current problem of a reinforced concrete pavement on natural soil it is obvious that the assumptions made for these theories are satisfied only to a very slight extent. The reinforced slab can only be considered to be more or less elastic and isotropic when it is in a completely uncracked stage; as soon as the loading becomes so great that the slab begins to function as a *reinforced* unit then, due to the formation of cracks and the alteration in the direction of moment, its properties vary in a high degree with loading and with the distance from the loading centre. A subgrade of natural soil has properties which, to an even smaller extent, can be designated as being ideal-elastic.

The possibilities of applying the theory, in spite of this, to *reinforced* slabs have been studied with the help of model tests (series M), where a subgrade of wood fibre board has been shown to have properties which correspond relatively well to those of the theoretical resilient bed. The test results concerning *depression* show that the deformation occurring in the case of loads corresponding to the yield point in the bottom reinforcement can be calculated fairly well according to the elasticity theory if the flexural rigidity of the slab is determined on the basis of the secant modulus at the yield point, and that a corresponding calculation can also be used concerning the deformation in the case of even higher loads, generally up to the final ultimate load with crack formation (or reinforcement yielding respectively) in the upper surface, in spite of the fact that the section of the slab around the loading point has started to assume a plastic stage. Concerning the *moment* in the slab a corresponding calculation gives a satisfactory result only up to the load which corresponds to the yield point in the bottom. In the case of higher loads it is generally *not* possible to use the elasticity theory for calculation of moment or ultimate loads.

The full scale tests carried out (series G) have been specially analyzed in order to determine *the properties of the soil.* Even if a completely clear result has not been obtained, soil pressure measurements show in general that natural soil corresponds best to the hypothesis concerning elastic subgrade. Concerning depression and moment then suppositions concerning the soil in accordance with both the hypotheses give a comparatively good result. Concerning other possibilities of applying the elasticity theory to the tests in series G the same results have been arrived at as in the case of the tests in series M.

Summarizing, the conclusion can thus be reached that the elasticity theory can very well be applied to reinforced concrete pavements for the calculation of deformation and moment (loads) as long as the slab remains in the elastic stage. The deformation can be calculated fairly well in the same way even in the case of loading beyond this stage. In the calculation, the flexural rigidity of the slab should be estimated as the secant modulus at the yield point. Theoretical calculations of the flexural rigidity show that the calculation according to stage II with $n = 15$ gives good results.

For calculation of the definite ultimate load P_t at failure in the top surface, the elasticity theory is *not* suitable.

The natural soil (in any case the clay soil used for the tests in question) appears to function approximately as an elastic subgrade.

Further test results are shown and discussed in Part 5 which concerns field tests carried out in connection with concrete pavement work on airfields.

3. The Ultimate Strength Theory for Reinforced Concrete Pavements

31. Principles and Assumptions. Literary Review

It has already been pointed out that the assumptions made in the elasticity theory concerning a completely elastic, homogeneous and isotropic slab are very imperfectly satisfied when applying the theory to a reinforced concrete pavement. This applies already in stage II since the elastic properties change the whole time during the crack formation in the slab, and it is obvious that in the failure stage, when the reinforcement has started to yield, the assumptions of the elasticity theory have been completely abandoned.

The test results in accordance with the previous section have, however, shown that the elasticity theory can be used quite well for the calculation of moment and stresses in the slab up to the load which corresponds to yield point in the bottom reinforcement under the loading centre. In the case of loading considerably exceeding this, when the yield in the central zone begins to extend, the elasticity theory does not, on the other hand, give any idea of the increasing stress, and the negative moment, which finally results in circular cracks in the top surface (or top reinforcement yield in the case of top reinforced slabs), cannot be calculated according to the elasticity theory.

It can be discussed as to which condition in the slab is to be the basis for a structural design of the concrete pavement, i. e. which load shall be considered to be the ultimate load for the slab in practice. Some research workers maintain that this load should be stipulated at yield point in the reinforcement under the centre of the load and also maintain that loading exceeding this level produces detrimental permanent deformation in the bottom surface. The safety factor can in this case, however, be placed very low, 1.0 or insignificantly higher [78].[1]

The tests referred to in the previous section clearly show, however, that an ultimate load defined in this way does not produce any failure deformation whatsoever; the depression and curvature figures for the loading centre continue evenly with increased loading without any special deviations. In this connection, a comparison can be made with

[1]) So also the handbook Bygg, part II [54].

the quite different behaviour in this respect of the simply supported detail test beams where the transition between the various stages in the deflection of the beam is clearly marked on the curve showing the relationship between the load and the curvature, and where the curvature increases in a practically unlimited way without any further load increase as soon as the reinforcement yield point is reached. Using a definition as above of the ultimate load, nor any influence on the ultimate load is obtained from a higher or lower tensile strength in the concrete, nor from any existing top reinforcement, factors which are undoubtedly significant for the strength of the slab.

A more definite idea of the actual load-bearing capacity of the slab is obtained if one associates the definition of ultimate load with the occurrence of failure phenomena on the *top surface* of the slab and defines the ultimate load for single-reinforced slabs to be that load at which the first circular crack appears in the top surface or, in the case of double-reinforced slabs, to be that load when the reinforcement in the top surface reaches the yield point. A connection is thus established with the ultimate load definition which was adopted for slabs by K. W. JOHANSSEN in his yield line theory [31] and which has been adopted for other statically indeterminate problems in the case of the so-called ultimate strength methods. It should, however, be pointed out that the ultimate load in the case of slabs on soil as opposed to the above-mentioned types of structures does not correspond to definite collapse, if by that is meant the condition in which the supporting properties of the structure are completely broken down. Collapse according to this definition is first reached by the load which actually causes stamping-out around the loading plate. It is, however, obvious that this last-mentioned load cannot be adopted as a basis for a calculation of the safety for failure of the slab since, in the case of loading beyond the crack formation or top surface yield point stage respectively, there are rapidly increasing permanent deformations with increased crack formation in the top of the slab. A check should of course be carried out to insure that stamping-out collapse does not occur at a lower load than that corresponding to crack formation (or reinforcement yield respectively) in the top surface. This definite collapse load is treated in Section 333 in connection with the test analysis.

The author thus considers that the *ultimate load for a reinforced pavement* should be defined as that *load causing top surface crack formation or yield in any existing top reinforcement.* The safety factor in the case of such an ultimate load definition should naturally be selected to be higher than if the ultimate load corresponds to the yield point in the bottom surface but it should be pointed out that there is no cata-

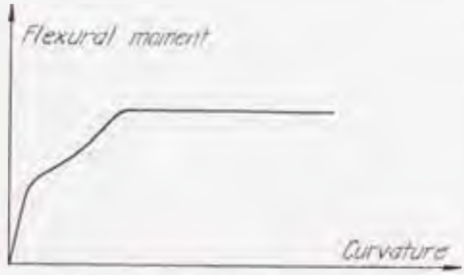

Fig. 31:1. The relationship between the flexural moment and the flexural deformation (curvature) for a simply supported slab strip of reinforced concrete (detail test beam).

strophe failure at the ultimate load defined above and not even at the stamp-out failure stage. It is obvious that this ultimate load can *not* be calculated in accordance with the methods defined by the elasticity theory which has been treated in the previous part of this paper.

The function of the slab after the yield point has been reached in the reinforcement under the loading centre can be discussed on the basis of flexural deformation of a similarly reinforced and simply supported concrete slab strip of the same type as the so-called detail tests. Fig. 31:1 shows the well-known relationship between the moment and the curvature in the case of such a simply supported slab strip; this showing that the slab behaves in a practically ideal-plastic way after the moment has reached the value which corresponds to the yield point in the reinforcement, i. e. the deformation increases unlimitedly without increasing moment. It can be assumed that the curve showing this connection can be applied also to the relationship between curvature and moment in the reinforced concrete pavement slab on soil. In the case of a low load, the slab functions more or less according to the elasticity theory and a moment distribution is obtained as shown in Fig. 22:7 or 22:9 with a marked peak under the loading surface (see Fig. 31:2), at least if the relative load distribution is not very extended. In the stage of the loading where the moment peak reaches the value corresponding to the yield point in the reinforcement under the loading centre, then this begins to yield and the moment can thus not increase further. In the case of further increased loading, then the yield in the reinforcement must extend to an increasingly larger zone primarily in radial sections (yield lines) since the elastic moment in these sections decreases more slowly than the moment in the tangential sections. The appearance of the moment diagram is thus completely changed and the peak is thus decapitated as shown in Fig. 31:2. By a simple equilibrium consideration of a wedge-shaped element, limited by two radial and

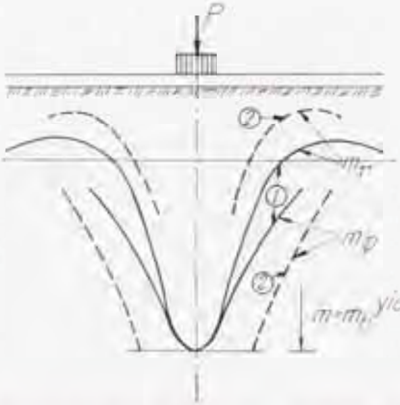

Fig. 31:2. The assumed moment distribution in a reinforced concrete slab on elastic subgrade due to a concentrated load before (1) and after (2) the yield point has been reached in the bottom reinforcement under the loading centre. The broken lines represent a supposed moment in the still elastic zones of the slab in stage 2 as above.

one tangential line, it may be seen that this moment re-distribution must influence also the moment in the parts of the slab which are still elastic, thus also the radial moment which results in tension stresses in the top of the slab and which, when these stresses reach the tension strength for concrete (or the yield strength for the top reinforcement in the case of double-reinforced slabs), cause the circular crack (failure line), which defines the ultimate load.

The conditions in the slab round the loading surface are thus on the whole analogous with the conditions assumed to exist in cross-reinforced slabs according to the yield line theory of K. W. Johanssen [31]. The slab is cracked along radial cracks in the bottom, *positive failure lines* and the failure zone is limited by a circular crack in the top corresponding to a *negative failure line*. In the continued treatment of this failure case, the author will apply the general methods of the yield line theory. In the case of a slab on soil, however, there is a serious complication concerning comparison with a free-lying, cross-reinforced concrete slab. Such a slab is only subjected to external loading from traffic and resting loads or from the support reactions determined by the equilibrium conditions, and the loads are not influenced by the prevailing deformation of the slab. A slab on soil, on the other hand, is also loaded by the soil pressure operating on it from below, and this pressure depends on the deformation of the slab and the elastic properties of the soil. These magnitudes cannot be calculated according to the equilibrium equations in the yield line theory.

The author considers that it is possible to calculate the soil pressure from the results of the elasticity theory in spite of the fact that in this stage of failure the slab is partially in a plastic state. The tests referred to in the previous part show, however, that the deformation of the slab and the soil pressure can be estimated fairly correctly according to the elasticity theory also at loads exceeding the load corresponding to the yield point in the bottom under the loading centre. The reason for this is that the zone in the neighbourhood of the load which is in a plastic state, is relatively limited so that the deformation of the slab is still largely determined by its elastic properties within the slab sections in elastic state.

On the basis of these assumptions, the author has, in the previously mentioned reports from Chalmers University of Technology, Department of Structural Engineering, Gothenburg [35, 36, 37, 38], expressed the outline of an ultimate strength theory for reinforced concrete slabs on soil and he has also prepared certain ultimate load formulae which are, however, partially based on faulty assumptions.[1]) These formulae of the author have been cited and discussed in some papers by JOHANSEN [32, 33, 34] as well as in a paper by BERNELL [8].[2]) The formulae have also been used by PERSSON [56] in the study of the problem concerning a load on an ice-floe. In this problem the slab can hardly be considered to have the properties of a *reinforced* concrete slab. According to tests by JOHANSEN [34] one can, however, reckon on the fact that the radial cracks even in the case of a plain concrete pavement have a certain property to admit moment due to the arching affect and friction against the soil, so that the method adopted should thus be also applicable for the calculation of the strength of a plain concrete pavement.

In this Part 3 of the work, the author will attempt to develop and discuss the ultimate strength method for reinforced concrete slabs on soil according to the principles laid out above and thereby to treat the simplest case where the loading is applied so far from the free edges of the slab that these do not interfere with the failure procedure. The method will be applied on tests in the earlier treated test series M and G and also on further tests in a later Part 5.

In another later part, Part 4, the more complicated case with a load on a free edge or a joint will be treated.

---

[1]) See note on page 185.

[2]) In this paper BERNELL has also suggested certain modifications of the formulae produced by the author. These would appear, however, to be even more faulty. See note on page 185.

32. Theory for Load on the Interior of a Slab

321. Loading with a circularly distributed single load

321.1 *The equilibrium equations*

A reinforced concrete pavement on soil with comparatively large dimensions is loaded by means of a concentrated load which is distributed over a circular surface with radius c, and the load is assumed to act fairly far from the free edges of the slab. The slab is considered at the phase when the circular crack in the top is just occurring. The flexural moment in the circular cross-section corresponding to the position of the crack and the radius of which can be denoted r_0, can then be assumed, to be constant and identical with the negative ultimate moment m'.

In order to be able to treat the problem in a fairly simple way the following assumptions have been made, the correctness of which will be discussed later:

a) Within the zone inside the circular failure crack, yield has occurred in the reinforcement along radial cracks in the bottom at least out to the failure circle, i. e. the circular crack in the top, whereby the moment along the whole length of a radial crack can be considered constant and identical with the positive ultimate moment (yield moment) m (Fig. 32:1).

b) The pressure from the subgrade p_s, which depends upon the co-ordinating properties of the subgrade and the slab, has a distribution which, within the zone in question inside the failure crack, can be approximated to a cone with peak value $= p_0$ and base radius $= t$ (see Fig. 32:1).

One can then produce the equilibrium equations for an element of the slab which is limited by two radial cracks and part of the circular crack in the top (see the figure), and then obtain a projection equation and an equation for the moment round the middle point:

$$\left.\begin{aligned}
&\text{Proj.: } \frac{P}{2\pi}\,d\varphi = \frac{1}{2}\,r_0^2\,d\varphi\,\frac{1}{3}\,\frac{r_0}{t}\,p_0 + \frac{1}{2}\,r_0^2\,d\varphi\;p_0\left(1-\frac{r_0}{t}\right) + \bar{q}\,r_0\,d\varphi \\
&\text{Mom.: } \frac{P}{2\pi}\,d\varphi\,\frac{2\,c}{3} = \frac{1}{2}\,r_0^2\,d\varphi\,\frac{1}{3}\,\frac{r_0}{t}\,p_0\,\frac{3}{4}\,\frac{2}{3}\,r_0 + \frac{1}{2}\,r_0^2 d\varphi\;p_0\left(1-\frac{r_0}{t}\right)\frac{2}{3}\,r_0 - \\
&\qquad\qquad - m\,r_0\,d\varphi - m'\,r_0\,d\varphi + \bar{q}\,r_0\,d\varphi\,r_0
\end{aligned}\right\}\quad (32{:}1)$$

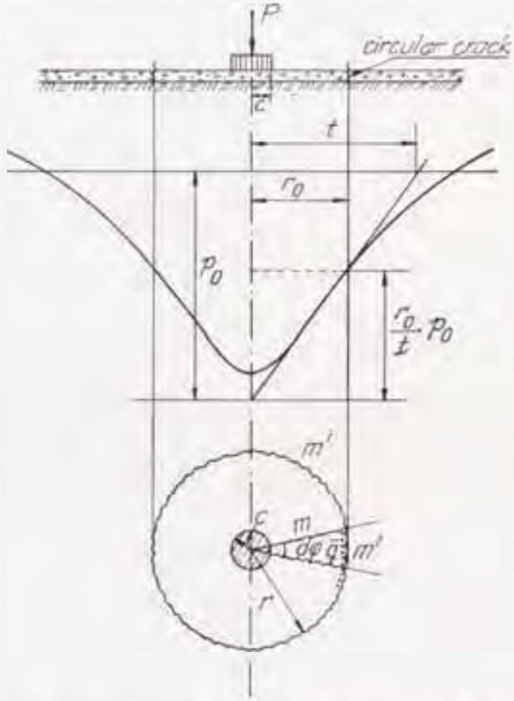

Fig. 32:1. Failure line figure for slab on soil and the assumed soil pressure distribution under the slab. The pressure distribution may be assumed to have a form represented by a straight line between the peak value and the position of the circular crack.

Here $\bar{q}$ means the shear force along the circular section. This can be calculated from the equilibrium equations for a small ring-shaped element according to Fig. 32:2. The moment in the circular section surface a—a beside the circular crack can also be described as being identical with the negative ultimate moment m', since this value is a maximum value for the negative moment. An equation for the moment round a—a gives

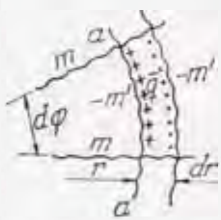

Fig. 32:2. Calculation of the shear force $\bar{q}$ in the circular crack. $\bar{q}$ is calculated from a moment equation for an element between the circular crack and a circular section a—a at a distance dr from the circular crack.

$$m'\,dr\,d\varphi + m\,dr\,d\varphi = \bar{q}\,r_0\,dr\,d\varphi$$

$$\bar{q} = \frac{m + m'}{r_0} \qquad (32:2)^{1)}$$

If this expression for q is inserted in the original equilibrium equations (32:1) we obtain after simplification

$$\left.\begin{aligned} \frac{P}{2\pi} &= \frac{1}{2}\,p_0\,r_0^2 - \frac{1}{3}\,p_0\,r_0^2\,\frac{r_0}{t} + m + m' \\ \frac{P}{\pi}\,\frac{c}{3} &= \frac{1}{3}\,p_0\,r_0^3 - \frac{1}{4}\,p_0\,r_0^3\,\frac{r_0}{t} \end{aligned}\right\} \qquad (32:3)$$

From this an expression for the ultimate moment is obtained

$$m + m' = \frac{P}{2\pi} - \frac{1}{2}\,p_0\,r_0^2\left(1 - \frac{2}{3}\,\frac{r_0}{t}\right) \qquad (32:3\,\text{a})$$

or, if $\frac{r_0}{t}$ is eliminated between the equations (32:3)

$$m + m' = \frac{P}{2\pi}\left(1 - \frac{8}{9}\,\frac{c}{r_0}\right) - \frac{1}{18}\,p_0\,r_0^2 \qquad (32:3\,\text{b})$$

this equation being more convenient to use in certain cases. The radius of the crack r_0 can be determined from the second of the equations (32:3)

$$p_0\,r_0^2\left(1 - \frac{3}{4}\,\frac{r_0}{t}\right) = \frac{P}{\pi}\,\frac{c}{r_0} \qquad (32:3\,\text{c})$$

If the ultimate load or the ultimate moment are to be calculated from these equations it is essential to know p_0 and t, i. e. the size and distribution of the subgrade pressure.

321:2. *Estimating the subgrade pressure*

The equilibrium equation derived above have been arrived at on the assumption that the centre zone of the slab is in a plastic state. Such a simple supposition cannot, as pointed out in the introduction, be made concerning the subgrade pressure. This is decided by the deformation of the slab and the elastic properties of the soil, and it is

1) This formula is generally derived by JOHANSEN [31].

obvious that certain changes occur in connection with the attainment of the yield point in the centre zone of the slab.

As has already been pointed out, however, this plastic zone is of a comparatively local character and the slab still functions on the whole as an elastic slab. One can therefore risk making the assumption that the soil pressure can still, at least approximately, be estimated on the basis of the elasticity theory. The tests referred to in Part 2 show that this assumption is fairly correct. If the slab is comparatively thin in relation to its size, it is thereby correct to use the theory for a slab of infinite dimensions.

The simplification has been made above that the pressure volume form can be approximated to a cone. In accordance with the assumptions made here it should thus be possible to estimate the position of the generatrix of the cone with the help of the curves for the distribution of soil pressure according to the elasticity theory. Independent of the fact as to whether the subgrade is assumed to be resilient or elastic, the soil pressure is proportional to the loading P on the slab (see the formulae in Table 22:1 or Fig. 22:6 and 22:8 respectively), and the height of the pressure cone can be described under the general form

$$p_0 = \gamma \cdot \frac{P}{l^2} \tag{32:4}$$

where

γ = a constant which can be estimated from the theoretical pressure curve
l = the elastic radius of stiffness according to equation (22:23) or (22:51)

If the expression (32:4) is inserted in the equations (32:3 a, b and c) one thus obtains the general formula for the ultimate load

$$m + m' = \frac{P}{2\pi}\left[1 - \pi\gamma\left(\frac{r_0}{l}\right)^2\left(1 - \frac{2}{3}\frac{r_0}{l}\right)\right] \tag{32:5 a}$$

or

$$m + m' = \frac{P}{2\pi}\left[1 - \frac{8}{9}\frac{c}{r_0} - \gamma\,\frac{\pi}{9}\left(\frac{r_0}{l}\right)^2\right] \tag{32:5 b}$$

where the radius of the crack circle

$$\frac{r_0}{l} = \sqrt[3]{\frac{\dfrac{c}{l}}{\gamma\,\pi\left(1 - \dfrac{3}{4}\dfrac{r_0}{l}\right)}} \tag{32:5 c}$$

When calculating according to the formulae (32:5) the values of t and γ are first estimated from the theoretical pressure curve. Then $\frac{r_0}{t}$ is calculated by successive approximation from the equation (32:5 c) after which $m + m'$ (or P) is obtained from (32:5 a) or (32:5 b)[1]. It is, however, generally better to use the equation (32:5 b) than (32:5 a) since this is less sensitive to a lower degree of accuracy in the determination of $\frac{r_0}{t}$.

Calculations in accordance with this have been carried out for both the types of soil under consideration.

---

[1]) According to earlier outlines for the ultimate load theory [35, 37, 38], the author has determined the radius of the failure crack r_0 purely mathematically from the condition that equation (32: 3) shall give the maximum value of $(m + m')$, and in this case only the peak value γ for the soil pressure cone was inserted. It should thus be possible according to this method to be able to *calculate* the t-value, which means that the distribution of soil pressure should follow the stated maximum condition — an obviously illogical thought.

The error of margin in the calculation method is also clarified, if one calculates t and r_0 by this means, since by derivation of the equation (32:3 a) one obtains

$$t = r_0$$

which is a completely illogical value with respect both to the distribution of soil pressure and the position of the crack.

BERNELL suggests in the article mentioned earlier [8] as an "improvement" of the author's formulae, that the radius of the crack should be taken as being constant and identical with the position of the negative maximum moment according to the elasticity theory (in the concentrated load case) and thus assumes that the moment curve according to the *elasticity theory* should still be applicable within a zone of the slab where the theory otherwise assumes a *completely plastic stage*. In accordance with this, in the equation (32:3) he puts

$$r_0 = 1.9\, l_k \text{ for resilient subgrade}$$

$$r_0 = 2.0\, l_e \text{ for elastic subgrade}$$

With such a supposition one for instance obtains:

$$t \approx 0.8\, r_0 \text{ where } c = 0.2$$

$$t \approx 0.9\, r_0 \text{ where } c = 0.5$$

thus even more illogical values, which correspond to *negative* soil pressure at the circular crack.

As shown later (325:3), the form of the soil pressure distribution, however, has only a comparatively slight influence on the final result from the ultimate load formula (32:5), so that the formulae which are based on assumptions which themselves are principally completely faulty, can however give ultimate load values which only comparatively insignificantly deviate from the result of the correct formulae.

One should not confuse the points mentioned above with the maximum principle in JOHANSEN's yield line theory [31] which, correctly applied to an energy equation for the slab within the circular crack in this case, gives exactly the same formulae as (32:5). See 324.

321.3. *Resilient subgrade*

In the case of resilient subgrade, the depression curve has the same form as the subgrade pressure distribution curve

$$p_s = k \cdot w$$

where w is the ordinate for the depression function according to Fig. 22:8, page 53. With the help of the curves for various load distributions in this figure the most closely agreeing pressure cone generatrices have been drawn in, whereby due respect has been taken in general to that part of the curve in question which lies within the crack radius r_0. The corresponding values of γ and t have been read off and inserted in equation (32:5) and the result is shown in Table 32:1. The table values are compiled in a diagrammatic form in Fig. 32:3 and 32:14.

For small values of the load distribution it is possible to write out a simplified approximate ultimate load formula if, in the root expression in equation (32:5), one inserts suitably selected values for $\frac{r_0}{t}$ and γ. In this way one obtains

$$\frac{r_0}{l_k} \approx 1.6 \sqrt[3]{a_k}$$

and

$$m + m' = \frac{P}{2\pi} (1 - 0.66 \sqrt[3]{a_k^2}) \tag{32:6}$$

TABLE 32:1. Ultimate moment values according to (32:5) with a single load on the interior of a slab on *resilient subgrade*. Values according to the approximate formula (32:6) are also shown.

Load distribution $a = \frac{c}{l}$	Estimated soil pressure distribution γ	$\frac{t}{l}$	Crack radius $\frac{r_0}{l}$	$\frac{m+m'}{P}$	$\frac{m+m'}{P}$ according to formula (32:6)
0	0	0	0	0.159	0.159
0,05	0.128	3.60	0.52	0.1465	0.145
0.1	0.129	3.20	0.66	0.1345	0.136
0.2	0.128	2.95	0.86	0.1207	0.123
0.3	0.126	2.80	1.01	0.1101	0.112
0.5	0.123	2.70	1.25	0.0921	0.093
0.7	0.116	2.75	1.48	0.0780	0.077
1.0	0.108	2.90	1.75	0.0600	0.054
1.3	0.098	3.10	2.02	0.0459	0.034
1.6	0.087	3.35	2.29	0.0350	
2.0	0.072	3.65	2.71	0.0254	
2.5	0.058	4.05	3.26	0.0164	
3.0	0.045	4.50	3.97	0.0129	

where as earlier

$$a_k = \frac{c}{l_k}; \quad l_k = \sqrt[4]{\frac{D}{k}}$$

The values calculated in (32:6) have also been introduced in Table 32:1. The table shows that this formula gives outstandingly good agreement with the exact calculation for load distribution up to approx. $a_k = 0.7$, thus for most of the cases normally occurring.

321.4. *Elastic subgrade*

In the same way as earlier the most closely agreeing pressure cone generatrices are drawn in with the basis of the pressure curves in Fig. 22:6. Here the pressure curves are, however, less linear and the effect of the load distribution is greater than that in the case of resilient subgrade so that it is more difficult to determine the correct position on the agreeing straight lines. Table 32:2 shows the selected values of γ and t as well as the corresponding ultimate moment values $\frac{m + m'}{P}$. The table values are summarized in the diagram in Fig. 32:3 and Fig. 32:14.

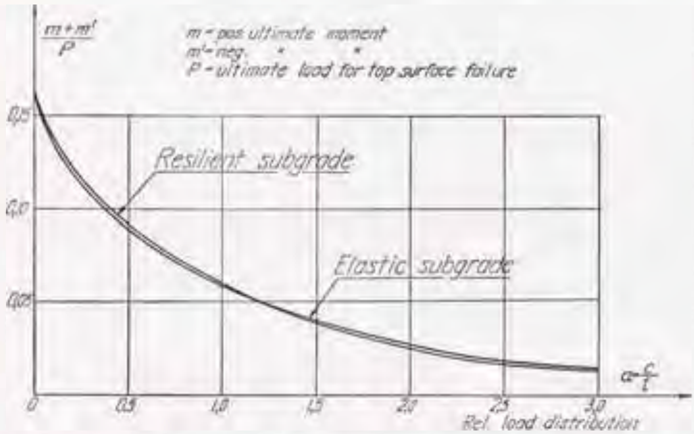

Fig. 32:3. The relationship between the ultimate moment and the relative load distribution with a single load on the interior of a slab on resilient and elastic subgrade respectively. Notice the surprisingly insignificant difference between both the relationship curves. It should be pointed out, however, that the l-value and thereby the value of the relative load distribution $\alpha = \frac{c}{l}$ is *not* the same for both the types of subgrade.

The curves are shown on more finely lined graph paper in Fig. 32:14, page 215 together with the corresponding curves for the case of twin loading. The constants involved are also explained there.

TABLE 32:2. Ultimate moment values according to (32:5) with a single load on the interior of a slab on *elastic subgrade*. Values according to the approximate formula (32:7) are also shown.

Load distribution	Estimated soil pressure distribution		Crack radius		$\frac{m+m'}{P}$ according to formula (32:7)
$a = \frac{c}{l}$	γ	$\frac{t}{l}$	$\frac{r_a}{l}$	$\frac{m+m'}{P}$	
0			0	0.159	0.159
0.05	0.190	1.40	0.48	0.1424	0.144
0.1	0.188	1.50	0.63	0.1325	0.135
0.2	0.182	1.60	0.83	0.1181	0.119
0.3	0.173	1.70	1.00	0.1070	0.108
0.5	0.156	1.95	1.25	0.0891	0.088
0.7	0.140	2.15	1.49	0.0754	0.070
1.0	0.120	2.45	1.81	0.0592	0.046
1.3	0.102	2.80	2.10	0.0466	
1.6	0.088	3.10	2.40	0.0367	
2.0	0.072	3.50	2.82	0.0272	
2.5	0.057	4.00	3.34	0.0179	
3.0	0.043	4.55	4.07	0.0152	

In the same way as in the case for resilient soil, one can find a simplified approximate failure formula for small values of the load distribution:

$$m + m' = \frac{P}{2\pi}\left(1 - 0.71\sqrt[3]{a_e^2}\right) \tag{32:7}$$

where

$$a_e = \frac{c}{l_e}; \quad l_e = \sqrt[3]{\frac{2D}{C}}$$

The values according to this formula have been introduced in Table 22:2. This gives good approximation for load distribution up to approx. $a_e = 0.6$.

322. Loading with twin load

When calculating according to the elasticity theory, the loading case with a twin load on two circular surfaces can be superimposed from the curves for the single load, as earlier discussed. This procedure cannot be used in the ultimate load method since, in the case of a twin load, one obtains a failure line figure of a completely different form than that in the case of a single load. As shown by the model tests carried out with twin loading (see Fig. 32:4), the failure crack will circumscribe both the loading points, at least in such cases where there is not an altogether too great distance between them.

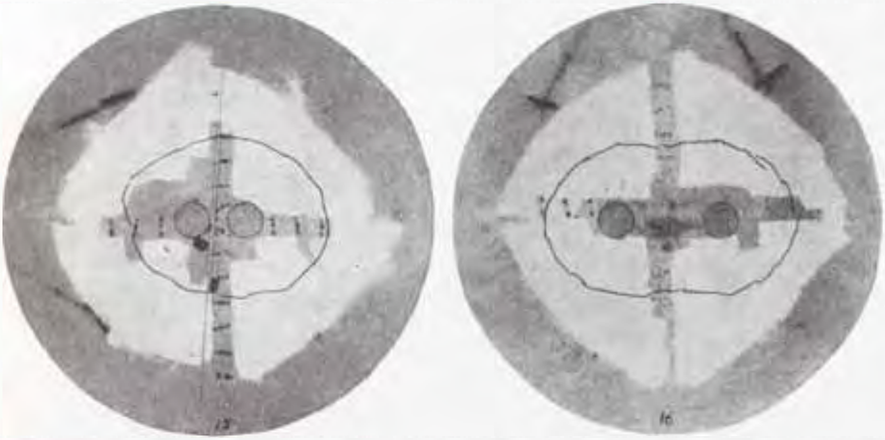

Fig. 32:4. Cracks in the top of the model slabs with twin loading, slabs MII:15 and 16. The load surfaces are marked in on the pictures. On slab 15 with the loading surfaces relatively close to each other the failure ring is elliptical. In the case of slab 16, it consists largely of two semi-circles with rather concave connecting cracks; the semi-circles appear to have their centres roughly at the loading centres.

It appears to be hardly possible to arrive at the correct failure line figure in the case of a double load merely by calculation, particularly when one takes into consideration the fact that the subgrade pressure depends on the failure line figure. When the loading points are close to each other one should get a roughly elliptical failure crack in the top while in the case of loading points at a greater distance from each other the failure crack more and more assumes the form of two separate circles. This is clearly shown by Fig. 32:4 which shows crack formation in the top of the two model slabs with twin loads.

It is thus necessary to assume a simplified failure line figure, and the author has chosen a figure which gives a negative failure crack in the top surface in the form of two semi-circles around the loading centres and straight lines between these semi-circles and in the bottom surface radial yield cracks to the semi-circles and a yield line between the centre points (see Fig. 32:5). A discussion follows later concerning the faults made when using such an approximation.

The pressure from the subgrade is estimated as before on the basis of the pressure distribution curves from the elasticity theory. In Fig. 32:6 such pressure curves are shown for twin loading with varying distances between the loading centres calculated with the help of the pressure curves for a single load. The corresponding pressure volume has, analogous with the case of a single load, been approximated through half-cones outside the loading areas and flat surfaces within the

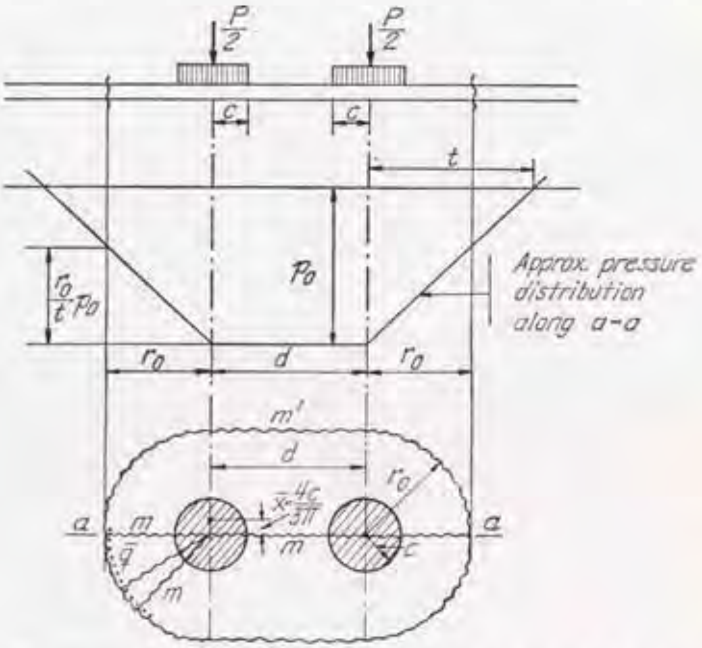

Fig. 32:5. The assumed failure line figure and pressure distribution in the case of a slab carrying a twin load.

zone between them, see Fig. 32:5. The apex of the half-cones appears, according to the pressure curves in Fig. 32:6, to be somewhat displaced inside the loading centres and their basic surfaces do not appear to be completely circular. In the approximate calculation now carried out the half-cones, however, are assumed to be circular with their apexes exactly under the loading centres.

The failure line figure as such permits the expression of three equilibrium equations, for example a projection equation of the complete failure line figure as well as two moment equations, for example one round the centre axes for half the failure figure and one round a diameter for either of the failure semi-circles. The problem is thus over-decided, this depending on the fact that the position and appearance of the failure figure have been fixed. One should therefore select the equations which are least influenced by the form of the failure line figure, and these appear to be the projection equation over the complete failure figure and the moment equation round the axes of symmetry.

With the assumptions thus made, the form of the equations (notations in accordance with Fig. 32:5) is as follows

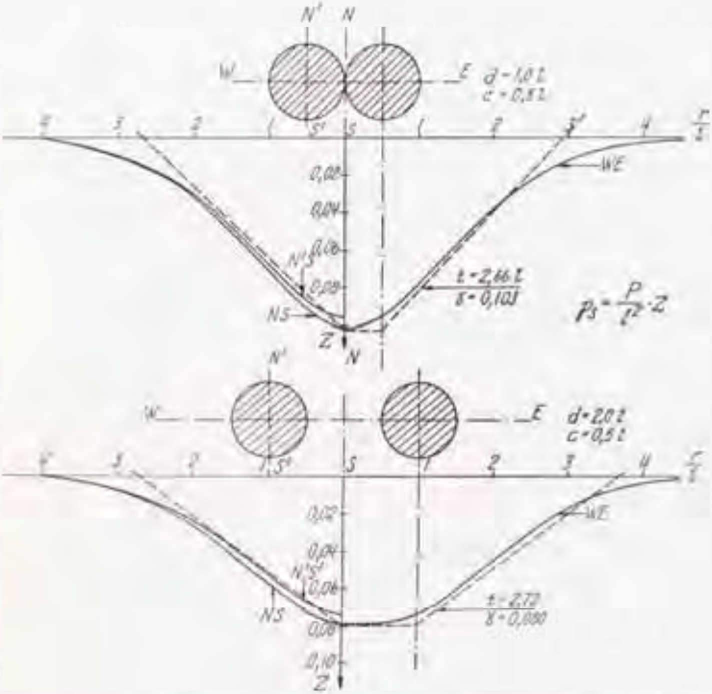

Fig. 32:6. The theoretical pressure distribution curves according to the elasticity theory for a slab on resilient subgrade, carrying a twin load with a load distribution $c = 0.5\ l$ and a distance between the loading centres of $d = l$ and $d = 2\ l$ respectively. By the use of the theoretical pressure curve (depression curve) in Fig. 22:8 a as an influence line, the pressure distribution curves for the line of symmetry between the loading centre (WE) and for the line of symmetry NS at right-angles to it as well as the diameters through the loading centres $N'S'$ have been marked in. The straight lines best agreeing to these curves obviously do not coincide completely so that a suitable average generatrix corresponding to the approximate pressure volume must be selected. This has been inserted in the figure (broken line) and the corresponding t- and γ-values have been read off.

$$\left.\begin{aligned}
&\text{Proj.: } P = \pi r_0^2 p_0 \left(1 - \frac{r_0}{t}\right) + \frac{1}{3}\,\pi r_0^2\, p_0 \frac{r_0}{t} + 2\, r_0\, d\, p_0 \left(1 - \frac{1}{2}\frac{r_0}{t}\right) + 2\,\pi\, r_0\, \bar{q}\\
&\text{Mom.: } \frac{P}{2}\frac{4\,c}{3\,\pi} = \frac{1}{2}\pi r_0^2 p_0 \left(1 - \frac{r_0}{t}\right)\frac{4\, r_0}{3\,\pi} + \frac{1}{3}\frac{1}{2}\pi r_0^2 p_0 \frac{r_0}{t}\frac{4\, r_0}{3\,\pi}\frac{3}{4} +\\
&+ r_0\, d\, p_0 \left(1 - \frac{r_0}{t}\right)\frac{r_0}{2} + \frac{1}{2} r_0\, d\, p_0 \frac{r_0}{t}\frac{r_0}{2}\frac{2}{3} + \pi\, r_0\, \bar{q}\,\frac{2\, r_0}{\pi} - 2\, r_0 (m + m') - d\,(m + m')
\end{aligned}\right\}\quad (32:8)$$

where, in accordance with (32:2), one can put

$$\bar{q} = \frac{m + m'}{r_0}$$

An insertion is here made, as before, of the expression for the maximum soil pressure

$$p_0 = \gamma \cdot \frac{P}{l^2}$$

and one thus gets the ultimate moment formulae after due simplifying.

$$\left.\begin{aligned} m + m' &= \frac{P}{2\pi} \left\{ 1 - \pi\,\gamma \left(\frac{r_0}{l}\right)^2 \left[\left(1 - \frac{2}{3}\,\frac{r_0}{t}\right) + \frac{2}{\pi}\,\frac{d}{r_0} \left(1 - \frac{1}{2}\,\frac{r_0}{t}\right) \right] \right\} \\ \frac{r_0}{l} &= \sqrt{\frac{1 + \frac{4}{3}\,\frac{c}{d}}{2\,\pi\,\gamma \left[\left(1 - \frac{2}{3}\,\frac{r_0}{t}\right) + \frac{1}{\pi}\,\frac{d}{r_0} \left(1 - \frac{1}{2}\,\frac{r_0}{t}\right) + \frac{2}{3}\,\frac{r_0}{d} \left(1 - \frac{3}{4}\,\frac{r_0}{t}\right) \right]}} \end{aligned}\right\} \quad (32{:}9)$$

From these equations the ultimate moment is calculated in the same way as in the case of the single load; thus a calculation is first made through successive approximation (rapid convergence) of the crack radius $\frac{r_0}{l}$ from the second equation and this value is then inserted in the first equation. The values of γ and t are estimated from the pressure curves of the elasticity theory of the type exemplified in Fig. 32:6. Due respect should here be taken to the pressure distribution both along the axis of symmetry through the loading centre as well as the opposed axes of symmetry at right angles and the diameter through the loading centre (see Fig. 32:6), while the t- and γ-values are calculated as suitably selected average values for the straight lines which agree best with the parts of the pressure distribution curves mentioned which fall within the annular crack. Values of t and γ estimated in this way for various distances between the loading centres and various relative load distributions are introduced in Tables 32:3 and 32:4. The mean values can easily be interpolated.

With the help of equations (32:9) and the soil pressure constants in the tables, the author has calculated the values of the ultimate moments for both the types of soil with various relative load distributions and various distances between the loading centres. The result is shown by Tables 32:3 and 32:4 and is shown diagrammatically in Fig. 32:14 in the summarizing Section 326.

TABLE 32:3. Ultimate moment values according to equation (32:9) with *twin loading* on the interior of a slab on *resilient subgrade*.

The soil pressure constants t and γ are estimated in accordance with the method given in Fig. 32:6.

$\frac{d}{l}$	$a=\frac{c}{l}$	Soil pressure constants		Crack radius	$\frac{m+m'}{P}$
		$\frac{t}{l}$	γ	$\frac{r_0}{l}$	
0.5	0	2.45	0.123	0.86	0.1107
	0.1	2.50	0.121	0.96	0.1023
	0.3	2.58	0.116	1.16	0.0878
1.0	0	2.52	0.110	1.00	0.0910
	0.1	2.55	0.108	1.08	0.0850
	0.3	2.62	0.105	1.22	0.0737
	0.5	2.66	0.103	1.36	0.0632
1.5	0	2.58	0.097	1.08	0.0785
	0.1	2.60	0.095	1.15	0.0738
	0.3	2.65	0.093	1.28	0.0644
	0.5	2.69	0.091	1.40	0.0557
	0.7	2.75	0.089	1.52	0.0474
2.0	0	2.63	0.085	1.16	0.0699
	0.1	2.65	0.084	1.22	0.0658
	0.3	2.68	0.082	1.34	0.0579
	0.5	2.72	0.080	1.45	0.0505
	0.7	2.78	0.077	1.58	0.0438
	1.0	2.89	0.072	1.79	0.0350
2.5	0	2.67	0.075	1.23	0.0635
	0.1	2.68	0.074	1.29	0.0600
	0.3	2.71	0.073	1.39	0.0529
	0.5	2.75	0.071	1.50	0.0465
	0.7	2.82	0.068	1.63	0.0408
	1.0	2.94	0.063	1.84	0.0333
	1.25	3.04	0.058	2.07	0.0285

323. Loading surfaces of arbitrary form

The simplified failure line figure used in treatment of the case of twin loading in the previous section, can naturally be applied also in the case of other types of load distribution with non-circular load surfaces which have considerably larger extents along one of axes than the other. For example very decidedly oval loading surfaces from single wheels, twin wheel loads with oval loading surfaces or loads divided over four adjacent wheels can be mentioned; these examples are shown in Fig. 32:7. In all cases occurring in practice, the loading surface would appear to be double symmetrical.

All such cases may be treated in exactly the same way as in the case of twin loading in 322, and one obtains corresponding equilibrium equations, if, in the equations (32:8) is inserted the "quarter load surface"

TABLE 32:4. Ultimate moment values according to equation (32:9) with *twin loading* on the interior of a slab on *elastic subgrade*.

The soil pressure constants t and γ are estimated in accordance with the method given n Fig. 32:6.

$\frac{d}{l}$	$a=\frac{c}{l}$	Soil pressure constants		Crack radius	$\frac{m+m'}{P}$
		$\frac{t}{l}$	γ	$\frac{r_0}{l}$	
0.5	0	1.70	0.155	0.82	0.1084
	0.1	1.75	0.152	0.94	0.0908
	0.3	1.85	0.147	1.14	0.0845
1.0	0	1.87	0.130	0.97	0.0891
	0.1	1.92	0.128	1.06	0.0828
	0.3	2.00	0.123	1.22	0.0716
	0.5	2.09	0.117	1.39	0.0617
1.5	0	1.96	0.112	1.07	0.0768
	0.1	2.00	0.110	1.14	0.0719
	0.3	2.08	0.105	1.29	0.0630
	0.5	2.18	0.099	1.46	0.0552
	0.7	2.30	0.093	1.62	0.0480
2.0	0	2.05	0.096	1.16	0.0685
	0.1	2.08	0.094	1.23	0.0645
	0.3	2.16	0.090	1.37	0.0570
	0.5	2.27	0.085	1.52	0.0504
	0.7	2.40	0.080	1.66	0.0442
	1.0	2.65	0.072	1.89	0.0362
2.5	0	2.13	0.085	1.21	0.0618
	0.1	2.16	0.083	1.28	0.0585
	0.3	2.23	0.080	1.41	0.0519
	0.5	2.34	0.076	1.54	0.0459
	0.7	2.48	0.072	1.67	0.0403
	1.0	2.69	0.066	1.88	0.0328
	1.25	2.79	0.059	2.19	0.0293

centre of gravity distance $\bar{x}$ (see Fig. 32:7) instead of the corresponding centre of gravity distance $\frac{4c}{3\pi}$ in the case of two circular loading surfaces (see Fig. 32:5). The load centre distance d should then, in an analogous manner, correspond to the distance between the centres of gravity of the quarter load surfaces along the longer loading axis of symmetry (see Fig. 32:7).

It is thus possible to calculate the ultimate moment values in the case of a load distributed over an arbitrary (double symmetrical) loading surface according to the formulae (32:9) and diagram 32:14 if putting

$c = 2.36\,\bar{x}$, where $\bar{x}$ is the quarter loading surface centre of gravity distance to the long axis of symmetry

$d =$ the centre of gravity distance of the load halves along the long axis of symmetry

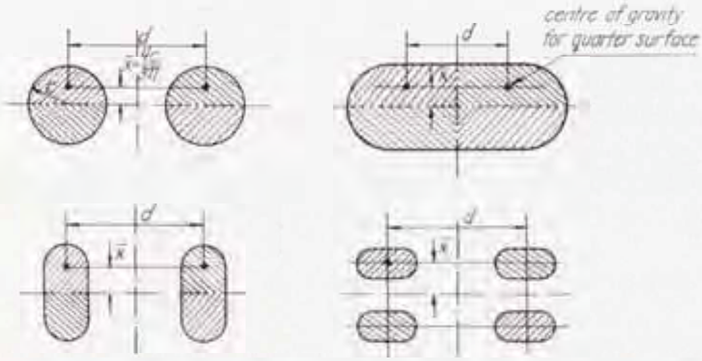

Fig. 32:7. Examples of different loading surfaces that can be treated according to the twin loading theories. $\bar{x}$ shows the distance from the centre of gravity of the quarter surface to the longer axis of symmetry.

The soil pressure constants t and γ may be estimated to the same values as for a circular double load with the c and d values as above, and they can be thus obtained from the Tables 32:3 and 32:4.

In cases where the "ovality" of the loading surface is small it is possible instead to reckon with the formulae and the diagram for a circular single load in which cases c is selected as the average radius.

324. Load placed between joints

When building runway pavements in practice, it is generally essential from working purposes to divide up the runway into longitudinal strips, separated by *longitudinal joints*, the distance between these being decided by the width of the machines used, usually 3 to 5 metres. The design of these joints will be touched upon later; often for technical reasons it is desirable to avoid the reinforcement going through the joints, and in any case, the continuity of the concrete is broken. In its normal form, the longitudinal joint can thus not transfer negative nor often positive moment but, on the other hand, shear forces through tongue and groove or dowels.

The affect of these joints on the load-bearing capacity of the pavement must be taken into consideration. In the cases where a load is exactly over or close to a joint, there is obviously a more dangerous loading case than those in which the load stands far from the joint; this case of loading will be covered in Part 4. But even in the case where the load is standing between two joints, these can influence the failure line figure unless the distance between them is altogether too large.

Fig. 32:8

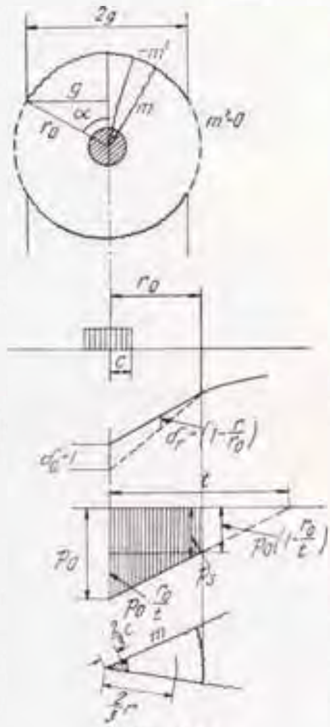

Fig. 32:9

Fig. 32:8. Failure line figure, if the load is resting exactly between two moment-free joints.

Fig. 32:9. The assumed failure line figure and soil pressure distribution in the case of a load between two joints. The figure also shows the virtual deformation of the slab, for which the energy equations in 324 are made up.

Fig. 32:8 shows such a case. The negative failure line runs into and coincides with the joints and if these are assumed to be free of moment (or in any case lack top reinforcement going through the joint) the negative failure line will thus be free of moment on the stretches where it coincides with the joints. The failure line thus also loses its circular form.

The case can be treated in a fairly simple way, assuming that the negative failure line is still circular and applying an energy equation. The fact that the joints cut off arcs from the circular failure line is neglected: in other words an assumption is made that these follow the circle line along the moment-free contact stretches (see Fig. 32:9). It is also assumed that the soil pressure distribution is not influenced by the joints and it is thus possible, as usually, to consider the soil pressure as being conically distributed with a peak value and a base radius which can be estimated from the pressure curves for the *elastic* slab of infinite dimensions.

In the state of failure, the slab is given a virtual deformation between the circular crack and the centre $\delta_r = \left(1 - \frac{r}{r_0}\right)$. With the notations in Fig. 32:9 and otherwise analogous with 321 and Fig. 32:1 one gets

strain energy

$$A_i = 4\, r_0\, \alpha\, m' \frac{1}{r_0} + 2\,\pi\, r_0\, m \frac{1}{r_0}; \quad \sin\alpha = \frac{g}{r_0}$$

applied energy

$$A_a = P\left(1 - \frac{2}{3}\frac{c}{r_0}\right) - \pi\, r_0^2\, p_0 \left(1 - \frac{r_0}{l}\right)\frac{1}{3} - \frac{1}{3}\pi\, r_0^2\, p_0 \frac{r_0}{l}\frac{1}{2}$$

Putting as usual

$$p_0 = \gamma \frac{P}{l^2}$$

one gets after simplification, since the energy expressions shall be equal

$$2\,\pi\left(m + \frac{2\,\alpha}{\pi}\, m'\right) = P\left[1 - \frac{2}{3}\frac{c}{r_0} - \frac{\pi}{3}\gamma\left(\frac{r_0}{l}\right)^2\left(1 - \frac{1}{2}\frac{r_0}{l}\right)\right] \qquad (32:10$$

The failure line radius r_0 is calculated according to the maximum principle,[1]) so that $\frac{dP}{dr_0} = 0$. One then gets

$$4\frac{d\alpha}{dr_0}\, m' = P\left[\frac{2}{3}\frac{c}{r_0^2} - \frac{\pi}{3}\gamma\frac{r_0}{l^2}\left(2 - \frac{3}{2}\frac{r_0}{l}\right)\right]$$

where

$$\frac{d\alpha}{dr_0}\cos\alpha = -\frac{g}{r_0^2}; \quad \frac{d\alpha}{dr_0} = -\frac{g}{r_0^2\cos\alpha} = -\frac{\operatorname{tg}\alpha}{r_0}$$

This equation can be simplified together with (32:10) and can be re-written in a form analogous with the previous ultimate load formulae

[1]) See Johansen [31], page 72

$$\left.\begin{aligned} m + \frac{2\alpha}{\pi}\, m' &= \frac{P}{2\pi}\left[1 - \frac{2}{3}\,\frac{c}{r_0} - \frac{\pi}{3}\,\gamma\,\left(\frac{r_0}{l}\right)^2\left(1 - \frac{1}{2}\,\frac{r_0}{l}\right)\right] \\ \frac{r_0}{l} &= \sqrt[3]{\frac{\frac{c}{l} + 6\,\frac{r_0}{l}\,\operatorname{tg}\alpha\,\frac{m'}{P}}{\pi\,\gamma\left(1 - \frac{3}{4}\,\frac{r_0}{l}\right)}}\,; \qquad \sin\alpha = \frac{g}{r_0} \end{aligned}\right\} \tag{32:11}$$

where r_0 as usual is calculated by trial and error with successive approximation.[1])

The formulae (32:11) have been used for the calculation of the ultimate moment values $\frac{m}{P}$ for several differing joint intervals $2\,g$ and several values for load distribution $\frac{c}{l}$, where the ultimate moment relation $m : m' = 2$. In this connection the values of γ and t have been chosen as earlier in order to obtain the best possible relationship to the theoretical pressure curve (according to Fig. 22:6) within the crack radius r_0 (which in this case is considerably greater than in the "uninterrupted" case). The result is shown in Table 32:5 and, as comparison, the corresponding ultimate moment values for the "uninterrupted" failure line figure have also been introduced into the table.

It is obvious that the affect of the joints on the value of the ultimate moment studied here is *very insignificant* in the cases shown in the table. An insignificant decrease in the ultimate load is obtained with decreased distance between the joints but greater distance between the joints gives an ultimate load which is higher than the normal case — this showing that the uninterrupted failure line figure which lies completely between the joints in the latter case is more dangerous. Smaller distances between joints than those examined would not appear to occur in practice and neither would lower values of $m : m'$ — higher values have obviously even less influence.

The failure radius r_0, on the other hand, is greatly influenced by adjacent joints; these apparently draw the negative failure line towards them.

---

[1]) The usual case of loading without joints can obviously also be treated through the energy equation in the same way whereby in equation (32:10) one gets $(m + m')$ in the left side. When derivating for the calculation of $\frac{r_0}{l}$, one gets an expression identical with that earlier derived (32:5 c), and by elimination with (32:10) one gets the expression (32:5 a).

TABLE 32:5. Load between moment-free longitudinal joints, distance between joints $= 2\,g$. Crack radii and ultimate moment values $\frac{m}{P}$ according to the formula (32:11) with the ultimate moment relationship $m : m' = 2$, elastic subgrade.

The marked values at $g = \infty$ represent "normal values" with an uninfluenced failure line according to Table 32:2.

Relative load distribution $\frac{c}{l}$	Relative distance between joints $\frac{g}{l}$	Crack radius $\frac{r_a}{l}$	$\frac{m}{P}$ for $m : m' = 2$
0.3	∞	**1.00**	**0.071**
	1.5	1.715	0.070
	1.8	1.98	0.064
0.5	∞	**1.25**	**0.059**
	1.6	1.88	0.063
	1.8	2.02	0.058
	2.0	2.16	0.055
0.8	∞	**1.60**	**0.045**
	1.6	1.99	0.050
	1.8	2.08	0.049
	2.0	2.20	0.046

It is thus possible to establish that in normal cases, it is not necessary to consider any weakening influence from longitudinal joints when designing the pavement in the zone between the joints.

325. Discussion of the ultimate load formulae

325.1. *General*

When deriving the ultimate load formulae we have made a number of assumptions which require closer discussion. In all cases of loading these are:

a) The reinforcement has yielded along the radial cracks at least out to the circular failure crack so that the moment in these cracks can be assumed to be constantly identical with the positive ultimate moment m.

b) The soil pressure decreases linearly from the centre out to the circular crack.

c) The soil pressure can be estimated with the help of the pressure distribution curves obtained according to the elasticity theory.

Apart from these, further simplifications were assumed in the case of twin loading concerning the form of the failure line figure and pressure volume, and the correctness of these assumptions requires further investigation.

From these, the assumptions concerning the soil pressure distribution according to b) and c) can be discussed simultaneously, whereby examination should be made of the influence of the form of the pressure distribution curve in general.

325.2. *Moment distribution in radial cracks*

As has been maintained in the introduction, the assumption of a plastic state takes place successively from the loading centre and outwards. In this connection the moment curves are altered the whole time in such a way that the moment peak under the loading centre is decapitated. Also the moment distribution in the zones further out in the slab which have not yet been affected by the plastic state are obviously influenced. It is therefore not obvious that the plastification in the radial cracks has reached the zones of the slab, where the negative moment maximum is present, before the circular failure crack appears there. This concerns primarily the relationship between the positive and the negative ultimate moments; in such cases when the concrete has a low flexural strength, it appears conceivable that the failure crack occurs at an earlier stage.

This problem obviously applies in general only for single-reinforced slabs, in which the moment in the circular failure crack decreases to *zero* as soon as the crack appears; the ultimate load must thus be calculated for the conditions immediately *before* crack formation. In the case of double-reinforced slabs it can be presumed both that the negative ultimate moment m' is considerably higher than in the case of a slab without top reinforcement and that a considerably larger tension in the top is necessary before the reinforcement there yields, this also implying a greater extent for the plastic state in the bottom. Finally in this case one gets a "genuine" failure line in the circular crack with a *constant* moment after the yield point in the top reinforcement is reached.

The author has not been able to find any method of arriving at the moment curves by calculation in the cases where the plastification along the radial cracks has only partly taken place. Fig. 32:10 appears to show the approximate appearance of the moment distribution in the radial sections in such a case; it is not possible to assume that the moment curve is of a directly similar form to the elastic moment curve with a "decapitated" top since the curve on the whole appears to alter its form even outside the limits of the plastic zone.

One can, however, arrive at some idea of the influence on the ultimate load value of such an incomplete plastification by assuming a curve form as shown in Fig. 32:10 and inserting by way of trial various values for the "plastic zone limit" r_p and the tangential moment $\varkappa\, m$ at the circular failure crack, and thereby approximate the outer "elastic" part of the

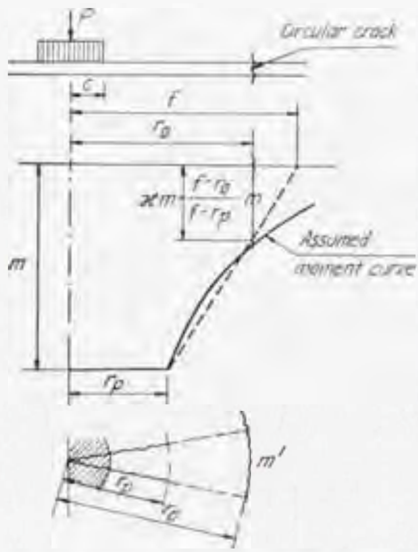

Fig. 32:10. Assumed moment distribution in the radial sections in the case of incomplete plastification. Up to the distance r_p from the centre, plastification is complete and the moment in the radial section = the ultimate moment m, outside this limit, the moment decreases along a curve which is assumed to be replaceable by a straight line (shown as a broken line in the figure).

moment curve with a straight line according to the figure with "zero-point distance" f. Thus in the case of a single load, the equilibrium equations have the form

$$\left.\begin{aligned} \frac{P}{2\pi} &= \frac{1}{2}\,p_0\,r_0^2 - \frac{1}{3}\,p_0\,r_0^2\,\frac{r_0}{t} + \bar{q}\,r_0 \\ \frac{P}{\pi}\,\frac{c}{3} &= \frac{1}{3}\,p_0\,r_0^3 - \frac{1}{4}\,p_0\,r_0^3\,\frac{r_0}{t} - m\,r_p - m\,\frac{1+\varkappa}{2}\,(r_0 - r_p) - m'\,r_0 + \bar{q}\,r_0^2 \end{aligned}\right\} \quad (32:12)$$

where, according to Fig. 32:10

$$\varkappa = \frac{f - r_0}{f - r_p} \quad (32:13)$$

The shear force q in the circular failure crack is calculated analogous with the expression (32:2) and becomes

$$\bar{q} = \frac{\varkappa\,m + m'}{r_0} \quad (32:14)$$

After insertion in (32:12) and simplification one gets

$$\left.\begin{aligned}\frac{P}{2\pi} &= \frac{1}{2}\,p_0\,r_0^2\left(1-\frac{2}{3}\,\frac{r_0}{l}\right)+\varkappa m+m' \\ \frac{P}{\pi}\,\frac{c}{3} &= \frac{1}{3}\,p_0\,r_0^3\left(1-\frac{3}{4}\,\frac{r_0}{l}\right)-\frac{1}{2}\,m\,(1-\varkappa)\,(r_0+r_p)\end{aligned}\right\}$$

If the expression (32:4) is inserted here for the peak pressure p_0, one finally gets

$$\left.\begin{aligned}\varkappa m+m' &= \frac{P}{2\pi}\left[1-\pi\,\gamma\left(\frac{r_0}{l}\right)^2\left(1-\frac{2}{3}\,\frac{r_0}{l}\right)\right] \\ \frac{r_0}{l} &= \sqrt[3]{\frac{1}{\gamma\left(1-\frac{3}{4}\,\frac{r_0}{l}\right)}\left[\frac{1}{\pi}\,\frac{c}{l}+\frac{3}{2}\,\frac{m}{P}\,\frac{r_0+r_p}{l}(1-\varkappa)\right]}\end{aligned}\right\} \quad (32:15)$$

analogous with the ultimate load formula (32:5). Calculation is carried out through trial and error of $\frac{r_0}{l}$ from the last equation, after which the ultimate moment can be calculated from the first equation.

These expressions can be used to examine the influence of a limited plastic state in the radial cracks and the result of the calculations are summarized in Table 32:6. The examinations has been carried out thoroughly for resilient subgrade, relative load distribution $c = 0.5\,l$ and a relationship $m : m' = 4$, whereby calculations have been carried out for increasing values on the plastic stage limit and a value of $f = 3.5\,l$, which was judged to be reasonable based on the elastic moment curves. The result shows that the ultimate moment value $\frac{m + m'}{P}$ is influenced to an obviously small extent by the fact that the plastification in the radial cracks is incomplete and even such a limited plastification as $r_p = 0.4\,l$ which implies that less than a quarter of the radial crack has yielded, gives a variation in the ultimate moment value with only approx. 15 % from the value at the complete plastification. Supplementary calculations show that the value of f and the moment relationship $m : m'$ influence the ultimate moment value $\frac{m + m'}{P}$ to a very insignificant extent. Also with other values of load distribution one obtains similar results, namely that the influence of the incomplete plastification is

TABLE 32:6. The influence of incomplete plastification in the radial cracks; resilient subgrade.

Calculations carried out according to equation (32:15); pressure volume constants t and φ according to Table 32:1. Comparison values according to Table 32:1 marked.

Relative load distribution $a=\frac{c}{l}$	$m:m'$	Moment distribution in radial cracks $\frac{f}{l}$	$\frac{r_p}{l}$	Crack radius $\frac{r_0}{l}$	$\frac{m+m'}{P}$	Remarks
0.5			$r_p=r_0$	1.26	**0.092**	Complete plastification
	4	2.5	0.4	1.75	0.108	
			0.6	1.73	0.103	
			0.8	1.68	0.099	
			1.0	1.57	0.095	
			1.2	1.36	0.093	
			1.26	1.26	0.092	
		3.0	0.6	1.55	0.099	
	2	2.5	0.6	1.58	0.101	
0.1			$r_p=r_0$	0.66	**0.135**	Complete plastification
	4	2.5	0.3	1.03	0.143	
			0.6	0.86	0.135	
1.0			$r_p=r_0$	1.75	**0.060**	Complete plastification
	4	3.0	0.8	2.16	0.067	

insignificant. The crack radius value $\frac{r_0}{l}$, on the other hand, is more influenced by the incomplete plastification and it appears from the table that one obtains a practically constant higher value which does not decrease to the "normal" value until the plastification is practically complete.

A corresponding examination concerning several cases of twin loading has shown that the effect of an incomplete plastification in such cases is even less significant. This naturally depends upon the fact that the incomplete plastification in the radial cracks in the case of twin loading covers a relatively smaller part of the complete failure figure since the zone between the loads can always be assumed to be in the plastic state completely.

The discussion in this section thus shows that the influence on the ultimate load of incomplete plastification in the radial cracks in the bottom is generally insignificant. It should thus be possible to calculate according to the ultimate load formulae (32:5) and (32:9) respectively and the corresponding tables as well as the diagram in Fig. 32:14, even if yield in the radial cracks should not have reached the circular crack when this appears.

325.3. *The influence of the subgrade pressure volume form*

If we discuss the case of single loading to begin with, the pressure volume in the theory presented is assumed to have the form of a cone, the generatrices of which have been drawn in guided by the elasticity theory pressure distribution curves. Apart from the approximation implied by the assumed linear pressure distribution, then the relationship to the elasticity theory is naturally unreliable since also the pressure distribution should be influenced by the assumption of a plastic state in the neighbourhood of the loading point, at least to a certain extent. There is however, an even greater degree of unreliability in the devations between the properties of the assumed ideal subgrade material (resilient or elastic soil respectively) and the actual types of soil occurring in practice, and these conditions make the choice of the magnitude and distribution of the soil pressure one of the most uncertain factors on the whole when calculating according to the ultimate load formulae presented, (32:5) and (32:9).

If, to start with, the pressure distribution is still assumed to approximate a straight line, it is possible to study the influence of the deviations between the assumed pressure volume and the actual pressure volume by varying the constants γ and t in the ultimate load formula (32:5), see Fig. 32:1. When judging reasonable deviations in this respect, one must always remember that the magnitude of the pressure volume must be constant the whole time and identical with the external loading. An increase in the peak value constant γ of the pressure cone must thus imply a decrease in its base radius t and vice versa.

An idea of the influence of such variations in the pressure distribution can be obtained in the simplest way by making comparisons between the ultimate moment values in both the Tables 32:1 and 32:2 or according to both the curves in Fig. 32:3, which apply for resilient and elastic soil material respectively. The values according to these tables and curves have, as a matter of fact, been obtained from the same ultimate load formula (32:5) but with greatly different values of t and γ, significant for both the theoretical types of subgrade. These can be said to represent two extreme types of pressure distribution, both of course with the correct pressure volume but otherwise of a greatly different character, particularly at small and moderate load distribution (see the corresponding theoretical pressure curves in Fig. 22:8 and Fig. 22:6 respectively). Some pairs of values for the same load distribution according to both the tables are summarized in Table 32:7. In spite of the very large variations in γ and t, which thus represent different types of pressure distribution, the difference in the ultimate moment value $(m + m')$ is particularly small; even the crack radius value is only influenced to a slight extent.

TABLE 32:7. Comparison between ultimate moment values calculated from the ultimate moment formula (32:5) for some values of relative load distribution α with subbase modulus constants γ and t for resilient as well as elastic soil (upper and lower values respectively).

$\alpha = \frac{c}{l}$	Soil pressure constants		Crack radius	Ultimate moment
	γ	$\frac{t}{l}$	$\frac{r_0}{l}$	$\frac{m+m'}{P}$
0.1	0.129 0.188	3.20 1.50	0.66 0.63	0.135 0.133
0.5	0.123 0.156	2.70 1.05	1.26 1.25	0.092 0.089
1.0	0.108 0.120	2.90 2.45	1.75 1.81	0.060 0.059

By comparing the ultimate moment values for twin loading in the same way as shown in Tables 32:3 and 32:4 it is seen that the influence of variations in the values of t and γ also in this case is very insignificant. Concerning the pressure volume in the case of twin load, there is also the supplementary assumption concerning the apex positions of the half-cones (see Fig. 32:5 and 32:6); this question is discussed later.

It is thus obvious that the position of the pressure cone generatrix does not need to be decided with a particularly great accuracy and that even very considerable deviations between assumed and actual values of the soil pressure constants do not influence the ultimate load value by more than a few percent. There remains to discuss the influence of the fact that the actual pressure distribution deviates to a more or less great extent from the assumed linear form. It is probable that this must be of lesser significance since such great variations in the assumed linear pressure distribution as above have shown such a small influence on the ultimate load value.

In order to take the matter to its conclusion here follows an investigation in this respect concerning the single load case, assuming that the actual pressure distribution curve can be composed of a linear section and a peak parabola as shown in Fig. 32:11. This approximation can be made to agree very well with the actual curve form within the zone in question inside the crack radius if the constants t, γ and $\varkappa$ are chosen in a suitable way. $\varkappa$ represents the height of the peak parabola and since this should be assumed to form a tangent with the straight part of the curve, then the height in the "circumscribed" point triangle corresponds to $2\,\varkappa$. See Fig. 32:11.

The equilibrium equations have the same form as 32:1 and 32:3, if corrections are made for a wedge-shaped element ΔP of the negative

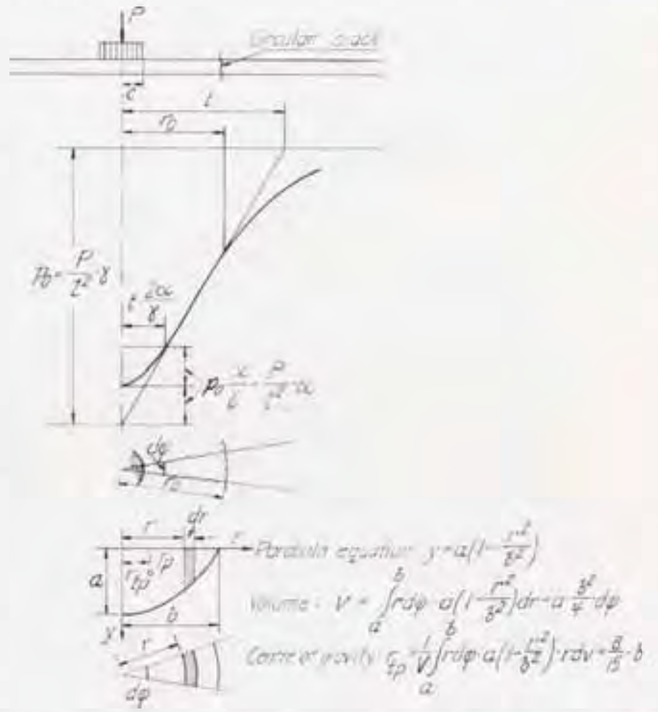

Fig. 32:11. A more accurate agreement with the actual soil pressure distribution for a single load can be attained by replacing the pressure curve with a top parabola and a straight line. The figure also shows the calculation of the volume and position of centre of gravity for a wedge-shaped element of the top paraboloid.

pressure volume between the paraboloid and the cone and the moment ΔM of this pressure volume wedge around the centre. Thus is obtained analogous with (32:3).

$$\left.\begin{aligned} \frac{P}{2\pi} &= \frac{1}{2}\, p_0\, r_0^2 \left(1 - \frac{2}{3}\,\frac{r_0}{t}\right) - \Delta P + m + m' \\ \frac{P}{\pi}\,\frac{c}{3} &= \frac{1}{3}\, p_0\, r_0^3 \left(1 - \frac{3}{4}\,\frac{r_0}{t}\right) - \Delta M \end{aligned}\right\}$$

where ΔP and ΔM with notation according to fig. 32:11 become

$$\left.\begin{aligned} \Delta P &= \frac{1}{3}\, p_0\, t^2 \left(\frac{\alpha}{\gamma}\right)^3 \\ \Delta M &= \frac{4}{15}\, p_0\, t^3 \left(\frac{\alpha}{\gamma}\right)^4 \end{aligned}\right\}$$

After simplification as before and the insertion of

$$p_0 = \frac{P}{l^2} \cdot \gamma$$

the yield formulae (32:5) receive the form

$$\left.\begin{aligned} m + m' &= \frac{P}{2\pi}\left[1 - \pi\gamma\left(\frac{r_0}{l}\right)^2\left(1 - \frac{2}{3}\frac{r_0}{t}\right) + \frac{2\pi}{3}\varkappa\left(\frac{\varkappa}{\gamma}\right)^2\left(\frac{t}{l}\right)^2\right] \\ \frac{r_0}{l} &= \sqrt[3]{\frac{\dfrac{1}{\pi}\dfrac{c}{l} + \dfrac{4}{5}\varkappa\left(\dfrac{\varkappa}{\gamma}\right)^3\left(\dfrac{t}{l}\right)^3}{\gamma\left(1 - \dfrac{3}{4}\dfrac{r_0}{t}\right)}} \end{aligned}\right\} \quad (32:16)$$

The last term in the first of the equations and in the numerator under the root in the second of the equations can be considered as being a correction to the original ultimate load formula (32:5). Table 32:8 shows the values of the ultimate moments for several values of load distribution calculated according to formula (32:16), compiled together with the corresponding values according to Tables 32:1 and 32:2 obtained through (32:5). It should be pointed out that the same values of t and γ have not been used here as in the corresponding calculations according to the formula (32:5). The straight line has here been inserted with the best possible agreement with the pressure curve between the crack radius and the peak parabola, while earlier the straight line was, as far

TABLE 32:8. Ultimate moment values calculated according to equation (32:16) with a soil pressure distribution of a peak parabola and a straight line.

The table also shows comparison values calculated according to equation (32:5) with the pressure distribution curve approximated to a straight line only.

Type of subgrade	Load distribution $u = \frac{c}{l}$	Estimated soil pressure distribution γ	$\frac{t}{l}$	$\varkappa$	Crack radius $\frac{r_0}{l}$	$\frac{m+m'}{P}$	$\frac{m+m'}{P}$ according to equ. (32:5)
Resilient	0.1	0.142	2.20	0.018	0.665	0.1347	0.1345
	0.5	0.129	2.60	0.015	1.245	0.0915	0.0921
	1.0	0.113	2.80	0.017	1.740	0.0598	0.0600
	2.0	0.079	3.45	0.016	2.690	0.0244	0.0254
Elastic	0.1	0.186	1.60	0.005	0.623	0.1324	0.1325
	0.5	0.160	1.95	0.015	1.240	0.0885	0.0891
	1.0	0.125	2.40	0.016	1.800	0.0584	0.0592
	2.0	0.078	3.40	0.016	2.760	0.0254	0.0272

as possible, selected in agreement with the whole of the theoretical pressure curve up to the crack radius.

The differences between the ultimate moment values, obtained from both the formulae, are particularly insignificant. Attention should also be paid to the good agreement between the values for the same load distribution for the both subgrade hypotheses in spite of the great differences in the soil pressure constants. There is thus no reason for using the more accurate but more complicated formula.

By summarizing, it can be said from the result of the investigations in this section that the method used to approximate the pressure curve with a straight line and to determine this from the elastic pressure distribution curves is acceptable, and that the variations from the assumed pressure distribution curves that can occur have a small influence on the ultimate moment value.

325.4. *The position of the centre points of the failure semi-circles and the soil pressure cones in the case of twin loading.*

When arriving at the ultimate moment formula for twin loading the centre points of the failure semi-circles and soil pressure cone points were assumed to coincide with both the loading circle centres (or, in the case of arbitrary loading surfaces, with the centres of gravity of the loading surface halves). It was pointed out, however, that the points of the pressure half-cones appeared to be rather displaced inwards relative to the loading centres (see Fig. 32:5 and 32:6). If it is assumed that such is the case, but that the centres of the failure semi-circles and its cone points still coincide then the failure line figure assumes an appearance as shown in Fig. 32:12. The equilibrium equations have the same form as before if one merely replaces the loading centre distance d by the failure circle centre distance s, whereby the failure formula (32:9) then receives the form

$$\left.\begin{aligned} m + m' &= \frac{P}{2\pi}\left\{1 - \pi\gamma\left(\frac{r_0}{l}\right)^2\left[\left(1 - \frac{2}{3}\,\frac{r_0}{t}\right) + \frac{2}{\pi}\,\frac{s}{r_0}\left(1 - \frac{1}{2}\,\frac{r_0}{t}\right)\right]\right\} \\ \frac{r_0}{l} &= \sqrt{\frac{1 + \dfrac{4}{3}\,\dfrac{c}{s}}{2\pi\gamma\left[\left(1 - \dfrac{2}{3}\,\dfrac{r_0}{t}\right) + \dfrac{1}{\pi}\,\dfrac{s}{r_0}\left(1 - \dfrac{1}{2}\,\dfrac{r_0}{t}\right) + \dfrac{2}{3}\,\dfrac{r_0}{s}\left(1 - \dfrac{3}{4}\,\dfrac{r_0}{t}\right)\right]}} \end{aligned}\right\} \quad (32{:}17)$$

These expressions have been applied for various values of load distribution and loading centre distance, whereby several values of s deviating from d have been inserted. The result is shown in Table 32:9.

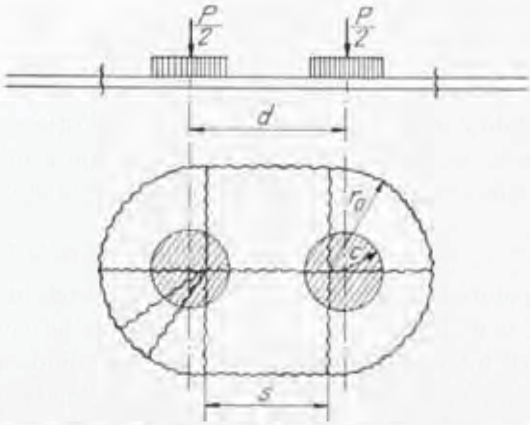

Fig. 32:12. Failure line figure for a twin load, if the loading centres and the failure circle centres are not assumed to coincide. The peaks of the pressure semi-cones (see Fig. 32:5) are assumed to lie exactly under the centres of the failure circles.

From the examples selected in the table, it may be seen that moderate deviations between the loading centre and the failure circle centre have an insignificant effect on the result of the ultimate load calculation. If, however, a loading surface is considered which deviates greatly from the circular cases, and an estimation is made of a more correct s-value

TABLE 32:9. The influence on the ultimate moment value of the differences between the assumed and the actual positions of the failure semi-circles and the centres of the pressure semi-cones at twin loading according to Fig. 32:12; in the ultimate load formula (32:9), the centres mentioned are assumed to coincide.

The table shows the ultimate moment values $\frac{m+m'}{P}$ for deviation in the values of the distance d between the loading centres and s between the centres of the failure circles. The calculation in the table are based on resilient subgrade.

$\alpha = \frac{c}{l}$	$\frac{d}{l}$	$\frac{s}{l}$	$\frac{r_a}{l}$	$\frac{m+m'}{P}$	Remarks
0.3	2	2	1.34	0.058	Value from formula (32:9)
		1.9	1.35	0.060	
		1.8	1.36	0.062	
	1	1	1.22	0.074	Value from formula (32:9)
		0.9	1.23	0.077	
0.5	2	2	1.45	0.051	Value from formula (32:9)
		1.8	1.48	0.054	
	1	1	1.36	0.063	Value from formula (32:9)
		0.9	1.37	0.066	
1.0	2	2	1.79	0.035	Value from formula (32:9)
		1.8	1.83	0.038	

with the basis of an accurate determination of the soil pressure distribution,[1]) which deviates significantly from d, then this value and equation (32:17) can of course be used for the calculation of the ultimate moment value. Unreliability in the material constants and other approximations in the calculating method mean that such accuracy in this respect is only motivated in extremely rare cases.

325.5. *The form of the failure figure in the case of twin loading*

It has been pointed out that the actual failure crack in the top surface in the case of twin loading would not appear to be composed of two semi-circles with intermediary straight lines but would rather appear to consist of a more irregular oval ring round the loads where the form depends on the distance between the loads (see Fig. 32:4). This implies alterations in the shearing force along the failure ring and the form and magnitude of the pressure volume. As far as the last-mentioned fact is concerned it appears to be practically impossible to take any respect to this from a calculating point of view; alterations in the pressure volume, on the other hand, only have a very slight influence on the ultimate moment value as already shown. Some idea may be obtained of the influence of alterations in the shearing forces along the failure line by introducing a considered concentrated shear force $\bar{Q}$ in the projection and moment equation as shown in Fig. 32:13, this representing the result both in magnitude and position of the actual shear along half the failure ring.

If the form of the subgrade pressure volume is thus approximated as earlier by means of two circular semi-cones with apex distance $= s$ and intermediate flat surfaces, and due attention is taken to the altered shearing forces in the actual failure figure as mentioned above, then the projection and moment equations analogous with equation (32:8) have the form

$$\left.\begin{aligned}
P &= \pi r_0^2 p_0 \left(1 - \frac{r_0}{t}\right) + \frac{1}{3} \pi r_0^2 p_0 \frac{r_0}{t} + 2 r_0 s p_0 \left(1 - \frac{1}{2}\frac{r_0}{t}\right) + 2\bar{Q} \\
\frac{P}{2}\frac{4c}{3\pi} &= \frac{1}{2} \pi r_0^2 p_0 \left(1 - \frac{r_0}{t}\right) \frac{4 r_0}{3\pi} + \frac{1}{3}\frac{1}{2} \pi r_0^2 p_0 \frac{r_0}{t}\frac{4 r_0}{3\pi}\frac{3}{4} + \\
&\quad + r_0 s p_0 \left(1 - \frac{r_0}{t}\right)\frac{r_0}{2} + \frac{1}{2} r_0 s p_0 \frac{r_0}{t}\frac{r_0}{2}\frac{2}{3} + \bar{Q}\bar{x} - (2 r_0 + s)(m + m')
\end{aligned}\right\}$$

These equations are otherwise not influenced at all by the fact that the

[1]) Such a soil pressure determination can be carried out for arbitrary loading surfaces with the help of the PICKET-RAY influence charts [57] but the calculation requires a great deal of work.

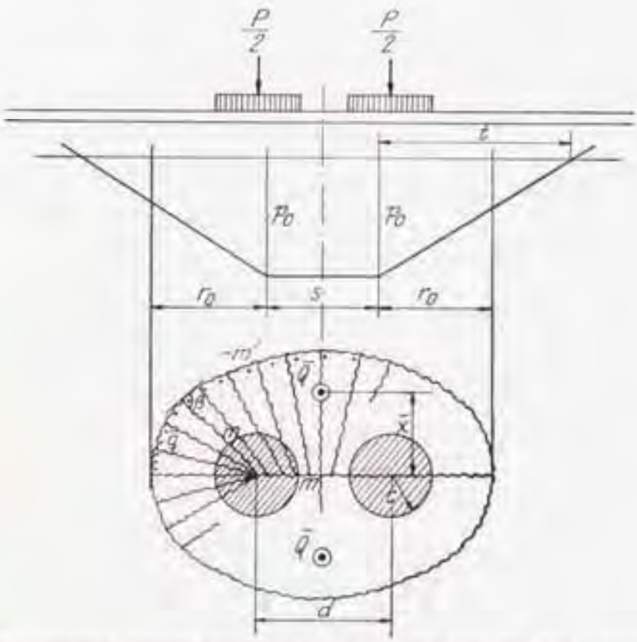

Fig. 32:13. The assumed actual failure line figure for twin loading. The concentrated loads $\overline{Q}$ are the resultant of the distributed shearing forces $\bar{q}$ along half the failure ring. The soil pressure distribution is approximated in accordance with the assumptions made earlier.

failure ring has an appearance which deviates from the earlier assumed approximate form. The resultant of the shearing forces $\overline{Q}$ can be written

$$\overline{Q} = \int_0^{\pi} \bar{q}\, ds = \int_0^{\pi} (m + m') \frac{d\varphi}{\sin^2 \beta} \tag{32:18}$$

according to Fig. 32:13, where β is the angle between the failure ring and the yield radius, whereby $\bar{q}$ is calculated fully analogous with (32:2).[1]) In the case where β is constantly $= 90^\circ$ as in the case of the formerly assumed circular failure line figure, then

$$\overline{Q} = \pi (m + m')$$

In the case of the actual failure ring, then β should not in any case vary much from 90° and one can write

$$\overline{Q} = \nu \pi (m + m') \tag{32:19}$$

where ν is somewhat < 1. The moment arm of the shearing forces resultant becomes in the case of the formerly assumed simplified failure figure $= \dfrac{2 r_0}{\pi}$. It is obvious that in the case of the actual failure ring, it

[1]) See also JOHANSEN [31], page 67.

will not be any greater deviation from this value so it can be placed

$$\bar{x} = \mu \cdot \frac{2\,r_0}{\pi} \tag{32:20}$$

where μ insignificantly differs from a value $= 1$. If these notations are introduced into the equilibrium equations, then after simplification in the same way as before one gets

$$\left.\begin{aligned} m + m' &= \frac{P}{2\,\pi}\,\frac{1}{\nu}\left\{1 - \pi\,\gamma\left(\frac{r_0}{l}\right)^2\left[\left(1 - \frac{2}{3}\,\frac{r_0}{l}\right) + \frac{2}{\pi}\,\frac{s}{r_0}\left(1 - \frac{1}{2}\,\frac{r_0}{l}\right)\right]\right\} \\ m + m' &= \frac{P}{2\,\pi}\,\frac{1}{1 + \dfrac{2\,r_0}{s}\,(1 - \mu\,\nu)}\left\{\pi\,\gamma\left(\frac{r_0}{l}\right)^2\left[\left(1 - \frac{2}{3}\,\frac{r_0}{l}\right) + \frac{4}{3}\,\frac{r_0}{s}\left(1 - \frac{3}{4}\,\frac{r_0}{l}\right)\right] - \frac{4}{3}\,\frac{c}{s}\right\} \end{aligned}\right\} (3$$

These equations can be used to estimate the influence of deviations from the approximate failure figure assumed earlier. Since the influence of a displacement of the centre points of the pressure cones has already been studied, it is sufficient here to examine the case $s = d$, i. e. that the points of pressure semi-cones coincide with the loading centre. The equations are solved by trial and error with various values of $\frac{r_0}{l}$ so that they both give the same ultimate moment $m + m'$. Investigations have been carried out in the case of resilient subgrade for both the centre distances $d = l$ and $d = 3\,l$ and for a relative load distribution $\frac{c}{l} = 0.3$, and some different combinations of ν and μ have been selected. The results are summarized in Table 32:10.

The table shows that the form of the failure ring has a small influence on the ultimate load. The investigation has certainly only included a few cases of loading distance and load distribution, but the equations show that the result appear to be the same also for other cases normally occurring.

326. Summarizing the formulae and diagrams

As shown in the previous section, in the cases where the load is far from the edge, the *ultimate moment sum* $(m + m')$ for an *ultimate load* P, corresponding to crack formation or yield in the reinforcement in a crack in the top surface round the load, can be calculated according to the formulae summarized below. It has been shown that the approximations and simplified assumptions made concerning soil pressure and

TABLE 32:10. The influence of the form of the failure figure at twin load on the ultimate moment value $\frac{m+m'}{P}$.

In the failure formula (32:9), the negative failure line is approximated by two semi-circles and intermediary straight lines (Fig. 32:5). The actual failure figure is assumed in Fig. 32:13 to be characterized by a shear force resultant $\bar{Q}$ for half negative failure figure, which can be written

$$\bar{Q} = \nu \cdot \pi \,(m + m')$$

and with the distance from the line of symmetry through the loading centres

$$\bar{x} = \mu \cdot \frac{2 r_0}{\pi}$$

The tables shows the influence on the ultimate moment value of deviating values of ν and μ from the normal values $= 1$. Calculations according to formula (32:21) for resilient subgrade (soil pressure constants t and γ according to Table 32:3) and relative load distribution $\frac{c}{l} = 0.3$.

$\frac{d}{l}$	ν	μ	$\frac{r_0}{l}$	$\frac{m+m'}{P}$	Remarks
1.0	1	1	1.220	0.074	Value from equation (32:9)
	0.9	1.0	1.303	0.074	
		1.1	1.253	0.079	
	0.8	1.0	1.392	0.074	
		1.1	1.348	0.079	
2.0	1	1	1.340	0.058	Value from equation (32:9)
	0.9	0.8	1.465	0.053	
		0.9	1.436	0.055	
		1.0	1.402	0.059	
	0.8	0.8	1.522	0.054	
		0.9	1.500	0.056	
		1.0	1.473	0.058	

failure line figures have a small influence on the ultimate moment or ultimate load values.

In the case of a *single load* with circular or almost circular extent, the following applies

$$\left.\begin{aligned} m + m' &= \frac{P}{2\pi}\left[1 - \frac{8}{9}\,\frac{c}{r_0} - \gamma\,\frac{\pi}{9}\left(\frac{r_0}{l}\right)^2\right] \\ \frac{r_0}{l} &= \sqrt[3]{\frac{\dfrac{c}{l}}{\gamma\cdot\pi\left(1 - \dfrac{3}{4}\,\dfrac{r_0}{t}\right)}} \end{aligned}\right\} \qquad (32:22)$$

where first the crack radius $\frac{r_0}{l}$ is calculated by means of successive approximation. If the relative load distribution $a = \frac{c}{l} < 0.6 - 0.7$, the following apply with excellent approximation

in the case of resilient soil

$$m + m' = \frac{P}{2\pi}(1 - 0.66\sqrt[3]{a_k^2}); \quad a_k = \frac{c}{l_k} \tag{32:23 a}$$

in the case of elastic soil

$$m + m' = \frac{P}{2\pi}(1 - 0.71\sqrt[3]{a_e^2}); \quad a_e = \frac{c}{l_e} \tag{32:23 b}$$

For a *twin load* or *an arbitrarily distributed load* with larger extent in one direction than in the other (double symmetrical loading surface) the following applies

$$\left.\begin{aligned} m + m' &= \frac{P}{2\pi}\left\{1 - \pi\gamma\left(\frac{r_0}{l}\right)^2\left[1 - \frac{2}{3}\frac{r_0}{t} + \frac{2}{\pi}\frac{d}{r_0}\left(1 - \frac{1}{2}\frac{r_0}{t}\right)\right]\right\} \\ \frac{r_0}{l} &= \sqrt{\frac{1 + 1.33\,\frac{c}{d}}{2\pi\gamma\left[\left(1 - \frac{2}{3}\frac{r_0}{t}\right) + \frac{1}{\pi}\frac{d}{r_0}\left(1 - \frac{1}{2}\frac{r_0}{t}\right) + \frac{2}{3}\frac{r_0}{d}\left(1 - \frac{3}{4}\frac{r_0}{t}\right)\right]}} \end{aligned}\right\} \tag{32:24}$$

In these equations:

m and m' = the ultimate moment per unit width for positive and negative bending of the slab respectively.

l = the elastic radius of stiffness for the slab, calculated according to the expression

$l_k = \sqrt[4]{\frac{D}{k}}$ = in the case of resilient subgrade,

$l_e = \sqrt[3]{\frac{2D}{C}}$ = in the case of elastic subgrade, where

D = flexural rigidity of slab

k, C = soil constants.

c = load distribution radius in the case of *circularly* distributed single or twin loads (or the average radius in the case of almost circular distribution)

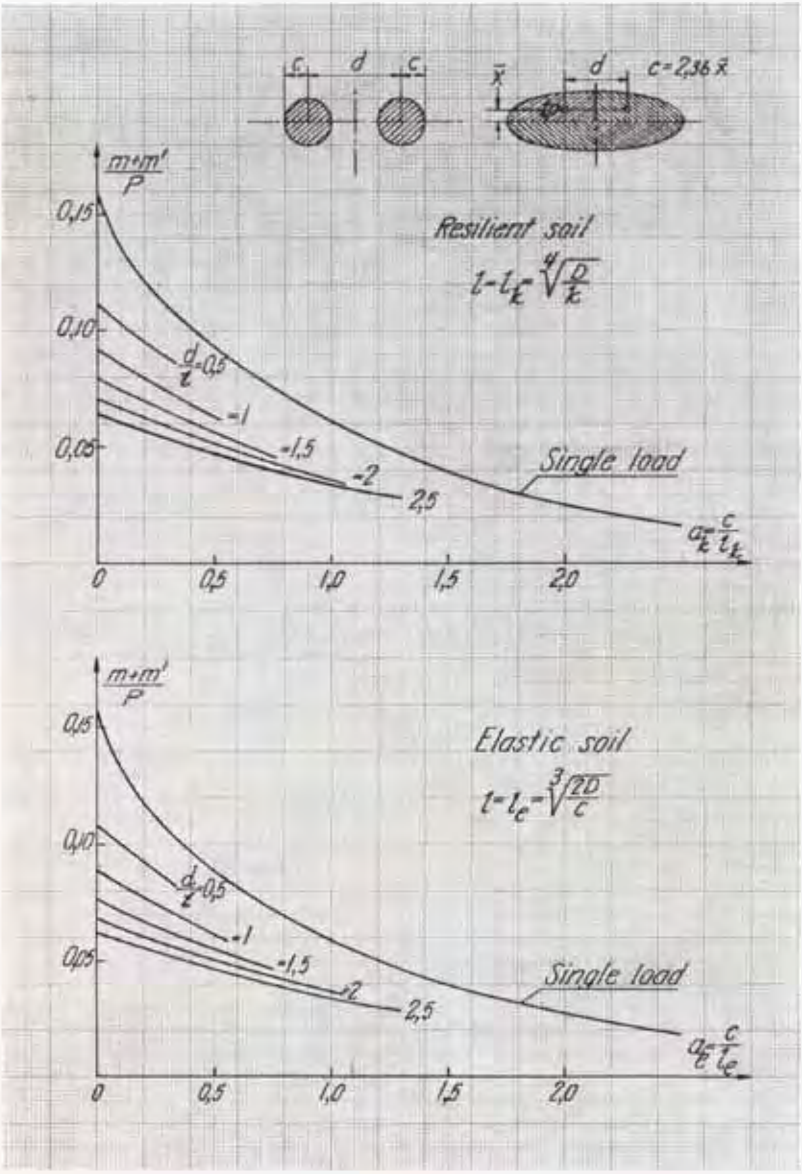

Fig. 32:14. The ultimate moment values $\frac{m + m'}{P}$ for a reinforced concrete pavement on *resilient* or *elastic subgrade*, loaded in the interior of the slab with a load P which is distributed on one or two circular loading surfaces with radius c and a distance between the loading centres of d, or has another corresponding arbitrary load distribution.

c = $2.36\,\bar{x}$, where $\bar{x}$ = the quarter surface centre of gravity distance from the long axis of symmetry on "extended" load with arbitrary loading surface

d = loading centre distance for twin load or the centre of gravity distance for loading halves in the case of other extended loads

t and γ = constants for assumed conical soil pressure distribution according to
Table 32:1 and 32:3 in the case of resilient soil
Table 32:2 and 32:4 in the case of elastic soil

The design diagram in Fig. 32:14 shows the relationship between $\frac{m + m'}{P}$ and the relative load distribution $\alpha = \frac{c}{l}$ for resilient and elastic soil with single and twin loads according to the formulae (32:22) and (32:24).

The same formulae and diagrams can normally be used if the load is standing on a section of the pavement between longitudinal joints even if these are so close (distance between joints $2\,g$ = approx. $3\,l$ - $4\,l$), that the negative failure line is influenced.

See also the summary in Section 34.

33. Application to Tests Treated Earlier, Series M and G

331. Model tests, Series M

331.1. *General*

The loading tests on the 28 model slabs, the description of which can be found in Section 24, have been discussed from the viewpoint of the elasticity theory in this earlier section. It has thereby been shown that this theory is not suitable for the calculation of loads and moment within the region of plastic state, after the yield point has been reached in the bottom reinforcement. In this section the test results concerning the ultimate load due to failure in the top surface P_t are discussed on the basis of the ultimate strength theory which was presented in the preceding section. The slabs M II 17—20 not earlier discussed will also be treated as far as dynamic loading is concerned.

331.2. *Test slabs Series M I, M II A:a and b as well as M II C, single-reinforced slabs*

Tables 33:1 and 33:2 contain the accumulated data for the single-reinforced model slabs and show the ultimate loads at failure in the top surface P_t. These values which have been corrected for the membrane tension effect, are compared with the theoretical ultimate load values calculated according to the diagram in Fig. 32:12; in some cases the correction value for the membrane effect is unreliable and has not been included in the comparison (see 245.2). The table also contains the theoretical values and the measured average values of the radius r_0 for the crack in the top.

Agreement between the theoretical values and the values obtained as a result of tests for the ultimate load is on the whole good. Agreement would appear to be less good in some cases where the difference between the theoretical crack radii and these given by tests is great. This would appear to imply that the deviations occurring in the ultimate load values depend to a certain extent on the *incomplete plastification* in the radial cracks. This problem has been treated in Section 325.2 and it was there shown that the effect of the ultimate moment value from an incomplete plastification is relatively small while the crack radius value, on the other hand, is influenced strongly. Also the differences

TABLE 33:1. Series M I, single-reinforced test slabs with single load. Ultimate loads at top surface failure according to tests and ultimate strength theory.

Series M I	test no.	1	2	3	4	5	6	7
DATA FOR THE TEST SLABS								
Total thickness h_0	cm	2.0	3.2	3.1	3.1	2.8	3.2	3.0
Resilience constant k	kg/cm³	0.27	0.13	0.32	0.053	0.34	0.54	0.16
Load distribution c	cm	5	5	5	10	10	10	20
Elastic radius of rigidity l	cm	18.5	31.6	26.8	43.5	26.6	23.0	30.6
Relative load distribution $\alpha = \frac{c}{l}$		0.28	0.16	0.19	0.23	0.38	0.43	0.65
Ultimate moment	kgcm/cm							
at bottom reinf. yield m		44	138	112	109	104	130	102
at top concrete failure m'		22	36	59	46	35	40	34
$m + m'$		66	174	171	155	139	170	136
ULTIMATE LOADS AT TOP SURFACE FAILURE								
Test results	tons							
ultimate load		0.65	1.63	1.57	1.44	1.59	1.67	1.83
membrane stress correction		0.07	(0.67)	0.09	(1.30)	0.23	0.09	0.42
corrected test load	F	0.58		1.48		1.36	1.58	1.41
Load acc. to ultimate strength theory T	tons	0.59	1.38	1.40	1.31	1.35	1.72	1.68
F/T		0.98		1.06		1.01	0.92	0.84
RADIUS FOR NEG. FAILURE CRACK r_e	cm							
Measured crack radius		35	39	36	57	38	38	58
Theoretical crack radius		18	25	23	40	30	27	44

between the assumed and actual pressure volume can contribute to a certain extent towards the deviations between the test results and the theoretical ultimate loads, as well as obviously, and perhaps primarily, the degree of unreliability in the determination of the ultimate moment. Also the unreliability in the determination of the test ultimate loads as well as the membrane stress corrections can be mentioned here.

It should be pointed out that the deviations mentioned from the conditions of the theory do not, on the whole, influence the theoretical ultimate load values to any great extent, this being shown by the discussion concerning the applicability of the ultimate load formula included in the previous section 325. The ultimate load value is, on the other hand, directly influenced by faults in the indirectly determined ultimate moment values.

331.3. *Test slabs, Series M II A:c, double-reinforced slabs.*

In the cases of the double-reinforced slabs, the ultimate loads at failure in the top surface have been determined both at the commencement of crack formation in the top surface P_t^{cr} as well as at the yield

TABLE 33:2. Series M II, sub-series A, a and b and sub-series C, single-reinforced test slabs with single load. Ultimate loads at top surface failure according to tests and ultimate strength theory.

Series M II, sub-series	:A a and b							:C
litt. test no	a:1 a 1	a:2 2	a:3 3	b:1 4	b:2 5	b:3 6	a:1 b 8	21
DATA FOR THE TEST SLABS								
Total thickness h_a cm	4.1	4.5	4.4	4.4	4.3	4.4	4.4	8.1
Resilience constant (Stage II) k kg/cm³	0.22	0.24	0.26	0.25	0.27	0.30	0.30	0.52
Load distribution c cm	20	20	20	20	20	20	20	20
Elast. rad. of rigidity (Stage II) l cm	41.4	39.8	40.0	35.6	38.7	40.0	35.6	48.2
Relative load distribution (Stage II) $a = \frac{c}{l}$	0.48	0.50	0.50	0.56	0.52	0.50	0.56	0.42
Ultimate moment kgcm/cm								
at bottom reinf. yield m	206	222	337	195	198	235	157	768
at top concrete failure m'	135	135	131	86	115	180	135	410
$m+m'$	341	357	468	281	313	415	292	1178
ULTIMATE LOADS AT TOP SURFACE FAILURE								
Test results tons								
ultimate load	4.70	4.85	4.40	2.55	4.20	6.40	5.10	15.80
membrane stress correction	1.59	0.75	0.39	0.12	0.44	1.30	1.19	1.14
corrected test load F	3.11	4.10	4.01	2.43	3.76	5.10	3.91	14.66
Load acc. to ultimate strength theory T tons	3.63	3.86	5.06	3.21	3.44	4.48	3.34	11.82
F/T	0.86	1.06	0.79	0.76	1.09	1.14	1.17	1.24
RADIUS FOR NEG. FAILURE CRACK r_0 cm								
Measured crack radius	58	69	72	75	68		64	71
Theoretical crack radius	51	50	51	47	49	50	47	56

point in the top reinforcement P_t^{gie}. The data concerning the test slabs and these ultimate load values have been collected in Table 33:3 together with the corresponding theoretical ultimate loads. As has been earlier discussed (see 245.3), concerning the membrane stress corrections noted in this table the correction values in the case of the double-reinforced slabs are very unreliable for the higher ultimate loads. This means that comparing the theoretical and the test values in these cases it is not possible to say more than that the correction values for the membrane stress effect *may* very well be of such a magnitude that agreement is good.

The lower ultimate loads at the commencement of crack formation in the top surface show very good agreement with the corresponding theoretical values. This also applies to slab M II:2, which has no reinforcement in the top and in which the tensile strength of the concrete was completely broken by the insertion of paper rings, if the ultimate load in this case is assumed to be reached, when the growth in tension

TABLE 33:3. Series M II, sub-series A:c 1 and c 2, double-reinforced slabs with single load. Ultimate loads at top surface failure according to tests and ultimate strength theory.

Series M II A	litt. / test no.	c 1:1 / 7[1])	c 1:2 / 9[2])	c 1:3 / 11	c 2:1 / 12[2])	c 2:2 / 10	c 2:3 / 13
DATA FOR THE TEST SLABS							
Total thickness h_0	cm	5.1	5.6	5.8	5.6	5.6	5.4
Resilience constant (Stage II) k	kg/cm³	0.31	0.33	0.29	0.26	0.31	0.32
Load distribution c	cm	20	20	20	20	20	20
Elast. rad. of rigidity (Stage II) l	cm	44.0	39.5	42.0	43.6	42.6	38.0
Relative load distribution $\alpha = \frac{c}{l}$		0.45	0.51	0.48	0.46	0.47	0.52
Ultimate moment	kgcm/cm						
at bottom reinf. yield m		283	269	293	418	345	260
at top concrete failure m'_{cr}		216	—[2])	164	0[2])	164	137
at top reinf. yield m'_{yie}		—[1])	~100[2])	253	—	202	220
$m + m'_{cr}$		499	—	457	418	509	397
$m + m'_{yie}$		—	369	546	—	547	480
ULTIMATE LOADS AT TOP SURFACE CONCRETE CRACK.							
Test results	tons						
ultimate load		5.95	—	4.90	5.9	6.30	4.60
membrane stress correction		0.71	—	1.04	0.89	0.74	0.28
corrected test load F		5.24	—	3.86	5.0	5.56	4.32
Load acc. to ultimate strength theory T	tons	5.15	—	4.86	4.36	5.36	4.36
F/T		1.01	—	0.79	1.14	1.04	0.99
ULTIMATE LOADS AT YIELD IN TOP REINFORCEMENT							
Test results	tons						
ultimate load		—	~ 8.4[2])	~ 7.6	—	~ 9.2	~ 8.6
membrane stress corr. (unreliable)			(6.1)	(5.3)		3.14	(8.9)
Load according to ultimate strength theory			4.00	5.80		5.75	5.25

[1]) $m'_{cr} > m'_{yie}$ — tensile strength too high, so top reinforcement is *completely without function*.

[2]) The tensile strength of the concrete broken by the insertion of cardboard rings.

values suddenly begins to increase more quickly on a strain gauge placed over such a crack indication due to a paper ring. According to the elasticity theory a slab of this type should lack load bearing capacity altogether.

Due to the unreliability in the membrane stress corrections for the higher ultimate load it is thus difficult, from these tests, to draw any definite conclusions concerning the applicability of the ultimate strength method to double-reinforced slabs concerning ultimate load due to yield in the top reinforcement. The question will be discussed in tests treated later.

331.4. *Test slabs, Series M II B:a, slabs with twin load*

Table 33:4 includes data for both the twin load slabs M II:15 and 16 as well as the comparison slab 14 with the experimentally deter-

TABLE 33:4. Series M II, sub-series B:a, slabs with twin load. Ultimate loads at top surface failure according to test and theory.

Slab 14, loaded with single load, is included in the series as a comparison slab.

Series M II:B	litt. / test no.	a:1 / 14	a:2 / 15	a:3 / 16
DATA FOR THE TEST SLABS				
Total thickness h_0	cm	5.5	5.6	5.4
Resilience constant (Stage II) k	kg/cm³	0.28	0.30[1]	0.30[1]
Load distribution c	cm	20	2 × 14	2 × 14
Elastic radius of rigidity (Stage II) l	cm	41.4	40.8	42.2
Distance between loading centres d	cm	—	42	84
Relative load distribution $\alpha = \frac{c}{l}$		0.48	0.34	0.33
Ultimate moment	kgcm/cm			
at bottom reinforcement yield m		277	299	303
at top concrete failure m'		209	218	207
$m + m'$		486	517	510
ULTIMATE LOADS AT TOP SURFACE FAILURE				
Test results	tons			
ultimate load		6.18	9.03	11.0
membrane stress correction		1.55	1.4[1]	1.7[1]
corrected test load F		4.63	7.63	9.30
Load acc. to ultimate strength theory T	tons	5.14	7.18	8.95
F/T		0.90	1.06	1.04
RADIUS FOR NEG. FAILURE CRACK	r_0 cm			
Measured crack radius		67	62	60
Theoretical crack radius		51	51	57

[1]) Interpolated between the values for the adjacent slabs.

mined ultimate loads and estimated membrane stress corrections compared with the theoretical ultimate load values calculated according to the diagram 32:14. The crack radii have also been estimated (see the crack patterns in fig. 32:4) and have been combined with theoretically calculated values. It can be confirmed that agreement between the experimentally obtained and the theoretical ultimate loads is very good. The deviations in the crack radii values can well be explained by referring this to the *incomplete plastification* in the radial cracks.

331.5. *Test slabs, Series M II B:b and c, slabs with dynamic loading*

The four model slabs in the above-mentioned sub-series have not been treated earlier. These tests were intended to show the eventual effect of repeated loading before the final ultimate load as well as the effect of a mobile load. It is obvious that repeated loading and off-loading to a load level not very far below the final ultimate load results in permanent deformations in the reinforcement in the centre of the slab if the yield point is exceeded, and also results in a more complete

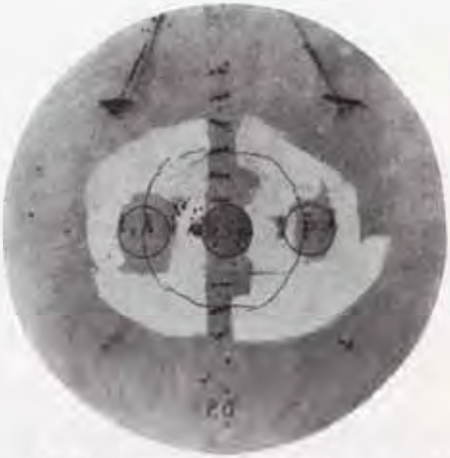

Fig. 33:1. The location of the loading and crack formation on slab MII:20. The slab was first subjected to loading at points on both sides of the centre point and at a distance of 65 cm from the centre, up to 2/3 of the ultimate load obtained by a third loading at the centre (the loading areas are marked in on the photograph and the order of loading is shown). It can be pointed out that the first two loadings were carried out, as was the intention, at points situated over the final failure ring crack and the aim of this was to find out the extent to which extensive crack formation (with yield in the bottom reinforcement) would decrease the strength of the slab concerning tension failure in the top surface. The result of the test loadings showed that this was *not* the case.

crack formation in Stage II in the bottom of the slab within zones lying further out. It may be considered in this connection that the slab under such loading would have deteriorated strength properties and a lower final ultimate load.

In an attempt to clarify these questions, the three slabs MII:17, 18 and 19 have been subjected to a pulsating load and the slab M II:20 has been subjected to loading by means of a load that was moved so that it first exerted loading on two points on each side of the centre before the slab was loaded to failure with the load in the centre (Fig. 33:1). All the data concerning the loading is shown in Table 33:5 where also the other data for the slabs as well as the theoretical and experimentally obtained ultimate loads has been compiled. The load corresponding to yield point in the bottom reinforcement has been estimated in the usual way with the help of the curvature diagrams for the centre point and has been introduced into the table; it can be pointed out that in all cases of pre-loading considerably higher loads than this were reached. The pre-loading would thus appear to have implied a relatively widespread plastic stage and permanent deformations of the slab.[1])

[1]) The complete test results concerning the tests on these slabs are to be found in the result supplement, Section 922.

TABLE 33:5. Series M II. sub-series B:b and c, slabs with dynamic loading. Ultimate loads at top surface failure according to test and ultimate strength theory.

Series M II B — load type		Pulsating load			Mobile load
	litt. / test no.	b:1 / 17	b:2 / 18	b:3 / 19	c / 20
DATA FOR TEST SLABS					
Total thickness h_s	cm	5.2	5.1	5.2	5.3
Resilience constant k	kg/cm³	0.35	0.37	0.34	0.52
Load distribution c	cm	20	20	20	20
Elast. radius of rigidity l	cm	40.8	38.2	38.8	33.7
Relative load distribution $a = \frac{c}{l}$		0.49	0.52	0.52	0.59
Ultimate moment	kgcm/cm				
at bottom reinforcement yield m		280	271	270	264
at top concrete failure m'		190	173	176	189
$m+m'$		470	444	446	453
LOADING PROCEDURE					
Loading series		4×0 to 4 t + + 1×0 to 5,5 t + ultimate load	5×0 to 6 t + + ultimate load	23×0 to 5 t + ultimate load	0 to 5 t 65 cm south centre + 0 to 5 t 65 cm north centre + + ultimate load in centre
Load at yield point in bottom reinforcement	tons	2 ÷ 2.5	approx. 3	approx. 3	approx. 3.5
ULTIMATE LOADS AT TOP SURF. FAILURE					
Test results	tons				
ultimate load		6.90	6.70	7.00	7.33
membrane stress corr.		~0.7	0.75	0.55	0.51
corrected test load F		~6.2	5.95	6.45	6.8
Load acc. to ultimate strength theory T	tons	5.05	4.88	4.90	5.33
F/T		1.23	1.22	1.31	1.27

The table shows, however, that no decrease whatsoever in the final ultimate load can be shown in any of the slabs. When comparing with the theoretical ultimate load, calculated in the usual way as for static loading, it can be shown on the contrary, that the ultimate loads for these slabs is rather higher than for most of the comparable slabs loaded with a static load. To the extent where this is not pure coincidence, one can possibly explain such an increase in ultimate load by indicating two conceivable reasons. The repeated loading gives an increased permanent compression of the subgrade board especially in the centre zone so that the subgrade pressure becomes more concentrated in this zone, and such a concentration of subgrade pressure should imply somewhat increased ultimate load. Apart from this the average flexural rigidity of the slab decreases due to the more complete plastification and through a more complete crack formation in the tension zone which takes place during pre-loading; this implies a higher value of the relative load distribution and thereby a higher ultimate load.

To the extent definite conclusions can be drawn from the few tests carried out with dynamic loading it can thus be stated that such loading does *not* imply any decrease in the bearing capacity of the slab if this is defined as the load causing failure in the top surface.

332. The Gothenburg test slabs, Series G

The loading tests on the two full-scale slabs on clay subgrade in Gothenburg (series G) are treated in Section 25, and analysis according to the elasticity theory showed that the subgrade functioned almost as elastic material. Analysis also showed that the ultimate load at crack formation in the top surface only to a slight extent exceeded the load at which yield in the bottom reinforcement commenced. The assumption of a plastic state at this load must thus have been of a very limited extent and this explains that the ultimate load value agreed fairly well with the theoretical load causing concrete failure in the top surface according to the *elasticity theory*, see Table 25:5. The higher ultimate load values for slab G 2 at top reinforcement yield, on the other hand, showed poor agreement with the elasticity theory.

Table 33:6 shows the result of the ultimate load calculations according to the ultimate strength theory compiled together with the test values and the required data for the slabs. The table shows that the agreement between the ultimate loads according to the tests and the theoretical ultimate strength is very good. This also applies to the loads causing concrete failure in the top in spite of the very incomplete plastification in the radial cracks already mentioned. This is completely in agreement with the theoretical discussion in 325.2, and Table 32:6 also shows that the ultimate load in a case such as this should lie rather lower than the theoretical load calculated according to the failure formula (32:22) (diagram 32:14), as well as that the crack radius measured is considerably greater than that theoretically calculated.

The ultimate load at yield point in top reinforcement shows very satisfactory agreement with the corresponding theoretically calculated load, particularly if respect is taken to the degree of unreliability in the determination of the ultimate load value and to the influence of

TABLE 33:6. Series G. Centre loading on test slabs. Ultimate loads at top surface failure according to test and ultimate strength theory.

The diameter of the slabs 7.00 metres, thickness approx. 15 cm. Loading surface radius c = 40 cm.

When calculating the theoretical ultimate loads the soil is assumed to function *as elastic* subgrade

Series G,	slab no.	1	2
DATA FOR TEST SLABS			
Total thickness approx h_0	cm	15	15
Reinforcement Ks 40 ⌀ 8			
bottom		c/c 9.1—c/c 10.0	c/c 9.1—c/c 10.0
top			c/c 12.0—c/c 12.5
Soil modulus C	kg/cm²	150	120
Elastic radius of rigidity l	cm	60	62
Relative load distribution $\alpha = \frac{c}{l}$		0.67	0.65
Ultimate moment	kgcm/cm		
at bottom reinforcement yield m		3300	2900
at top concrete failure m'_{cr}		950	680
at top reinforcement yield m'_{yie}		—	1620
$m + m'_{cr}$		4250	3580
$m + m'_{yie}$		—	4520
ULTIMATE LOADS AT TOP SURFACE FAILURE			
Concrete tension failure P_t^{cr}	tons		
test F		52	40
theory T		55	46
F/T		0.95	0.88
Yield in top reinforcement P_t^{yie}	tons		
test F		—	66
theory T			59
F/T			1.12
RADIUS OF NEG. FAILURE CRACK r_0	cm		
Measured crack radius		~ 150	
Theoretical crack radius		90	

the membrane stresses; the correction which is not included here, may, according to earlier estimations, be between 2 and 6 tons. As far as can be judged from this test, the ultimate strength method is thus very suitable for application to double-reinforced slabs when calculating the ultimate load due to yield in the top reinforcement.

The calculations in Table 33:6 have been carried out under the assumption that the soil functions as an elastic medium. The corresponding calculations carried out for resilient subgrade show considerably poorer agreement with the test results. Also this discussion confirms the impression obtained earlier, that the properties of the clay subgrade in question more nearly correspond to that of elastic subgrade.

333. Tests with stamping out collapse

At some of the tests, viz. those carried out with the slabs in Series MI and G, the load was increased until definite collapse was reached due to stamping-out around the loading plate. These tests are collected and analysed in Table 33:7.

The stamping-out collapse in its purest form is caused by shear-tensile rupture in a conical crack proceeding from the circumference of the loading area. The corresponding shearing stress τ_{stamp} may be estimated from the formula

$$\tau_{\text{stamp}} = \frac{P - p_s \pi (c + h_0)^2}{\pi h_0 (2c + h_0)} \cdot 1.15 \qquad (33:1)$$

where the second term in the numerator is an expression for the total counter-pressure from the subgrade against the base of the stamped-out cone, and p_s is thus the average soil pressure value under that base, which can be estimated from the soil pressure curves in Fig. 22:6 (elastic subgrade, slabs series G) or in Fig. 22:8 (resilient subgrade, slabs series MI). The factor 1.15 is placed in the expression (33: 1) in analogy with the corresponding expression for shear stress in beams, but here it may have a somewhat higher value.

The table shows the τ_{stamp}-values estimated in the way mentioned above. These values should be identical with the pure tensile strength values σ_t, and in order to analyse that, the τ_{stamp}-values have been compared with the flexural strength values σ_f taken from the corresponding detail tests. The result shows that the ratio $\sigma_f/\tau_{\text{stamp}}$ is about 1.7—2.0 with the exception of the values for the slab MI: 2, which have an exceptionally low σ_f-value, and the slab MI: 4, where the stamping-out crack coincided with a circular top crack earlier occurring near the centre. In fact this was also more or less the case with some of the other model slabs, which fact may have contributed to the somewhat low τ_{stamp}-values. This case is not, however, of any practical interest, because a stamping-out collapse is dangerous only when it arises *before* the normal ultimate load is reached due to flexural rupture in the top surface.

The values $\sigma_f/\tau_{\text{stamp}}$ in the table are perhaps somewhat greater than the normal relation between flexural strength and pure tensile strength for concrete (see Section 633). This can indicate that the oblique tensile stresses in the cone surface are not uniformly distributed and that the factor 1.15 in the equation (33: 1) is too small. Another explanation is given above.

However, judging from the tests accounted for in Table 33: 7, of

TABLE 33:7. Series M1 and G, stamping-out collapse.

The stamping-out stress τ_{stamp}, calculated according to formula (33:1), is compared with the flexural strength σ_f, which is calculated from the detail test values in Tables 24:2 and 25:1 respectively.

Test slabs, data			Stamping-out load P_{stamp}	Stamping-out stress τ_{stamp}	Flexural strength σ_f from detail tests	$\frac{\sigma_f}{\tau_{stamp}}$
Slab series no	Thickness cm	Loading area c cm	tons	kg/cm²	kg/cm²	
M1:1	2.0	5	1.19	17	33	1.9
2	3.2	5	1.77	17	22	1.3
3	3.1	5	2.37	20	37	1.8
4	3.1	10	1.89	10	29	2.9[1])
5	2.8	10	2.78	15	27	1.8
6	3.2	10	3.38	15	25	1.7
7	3.0	20	4.47	11	22	2.0
G1						
loading 1	~15	20	38.9	15	~25	~1.8
loading 2		40	64.0	13		
G2		40	68.5	14		

[1]) Stamping-out along a circular crack.

course altogether too few, the stamping-out load P_{stamp} may be roughly estimated from the expression (33: 1) if τ_{stamp} is made equal to σ_t. Inserting, in order to be quite certain as to the table results, $\tau_t = \frac{1}{2}\sigma_f$, the equation (33: 1) can be re-written thus:

$$P_{stamp} - p_s \pi (c + h_0)^2 = 0.45\, \sigma_f \pi h_0 (2c + h_0)$$

or, writing p_s according to the expression in Fig. 22: 6 A or Fig. 22: 8 A

$$P_{stamp}\left[1 - \pi\left(\frac{c + h_0}{l}\right)^2 \cdot Z_2\right] = 1.4\, \sigma_f h_0 (2c + h_0) \qquad (32:2)$$

In this expression the Z_2-value may be estimated from the pressure curves in the figures just mentioned as an average value under the stamping-out cone with a relative base radius value $\frac{c + h_0}{l}$.

34. General Viewpoints on the Application of the Ultimate Strength Theory to Reinforced Concrete Pavements

According to the viewpoints given in Section 31 the ultimate load for a reinforced pavement should be judged on the basis of the load causing commencement of crack formation in the top surface or, in the case of double-reinforced slabs, yield in the top reinforcement. An ultimate load defined in this way cannot be calculated according to the methods of the elasticity theory, this being clearly shown by the earlier analysis of the tests in series M and G according to the elasticity theory.

On the other hand, the ultimate load in question can be calculated theoretically according to the ultimate strength method, due respect being taken to the properties of the slab after the reinforcement yield point has been reached, by applying the principles of the yield line theory according to Johansen, but it is assumed that the soil pressure can still be estimated according to the elasticity theory. Under these conditions and with simplified suppositions concerning the yield line figure and the soil pressure distribution it is possible to set out relatively simple formulae for the determination of the ultimate load or the ultimate moment, summarized in 326. Examinations of the ultimate formulae show that the approximate assumptions and simplifications carried out when deriving them in general have a very small effect on the result.

The analysis of the test results from series M and G concerning the loads causing top surface failure shows that it should be possible to apply the formulae arrived at to reinforced concrete pavements. It is, however, true that in many cases there are relatively large deviations between the ultimate loads obtained from tests and according to the ultimate load theory. It has been pointed out in the test analysis, however, that the degree of unreliability is comparatively great both in the determination of the experimental ultimate loads as well as in the calculation of the theoretical loads. Particularly in the cases where the ultimate loads were estimated indirectly through comparison between the strain measurements in the main test and the detail test, as in the case of the double-reinforced slabs, then the degree of unreliability can become significant.

One condition which also contributes to a great extent towards the difficulties in the consideration of the test values, is the influence of the membrane stresses. Particularly in the model tests the membrane stresses are great and for several of these slabs with a large degree of flexural deformation at failure (particularly the double-reinforced slabs) then the membrane stress effect appears to have been of the same magnitude as the effect of the flexural stresses. The estimation which the author has attempted to make of the correction in the ultimate load value due to membrane stresses, is to be considered as being very rough, and it is clear that in the cases where the membrane stress effect is significant compared with the ultimate load value, then the ultimate load value must be judged as being very unreliable. In this respect the slabs in the full-scale series G are much more favourable and the result shows also that in these tests, too few of which alas were carried out, closer agreement with the theory has been obtained.

As far as the theoretical ultimate load values are concerned, these are calculated on the basis of the experimentally determined ultimate moment values, and it has also been maintained (in Section 245 for example) that considerable unreliability characterizes these values which were obtained indirectly through the detail tests as well as the fact that faults in the ultimate moment values have a direct influence on the theoretical ultimate load value. Apart from this there are also unreliable factors in this value due to approximations and simplifications when compiling the ultimate load formulae, even if these factors — as already mentioned above — have definitely a less significant influence than those earlier mentioned.

With respect to the points made above, the agreement between the experiments and the theory must be judged as being fully satisfactory.

The ultimate strength theory can be applied in the cases of both resilient and elastic subgrade. In the analysis of the model tests the subgrade has, as earlier, been considered as resilient while in the full scale tests the subgrade was regarded as being elastic. The calculations in the last-mentioned case according to the theory for resilient subgrade have given considerably poorer agreement with the test results.

Further tests are described and analyzed in Part 5.

The flexural rigidity values for the test slabs which were determined experimentally and used in the analysis correspond to the secant modulus at yield point in the reinforcement. The theoretical calculations of the flexural rigidity, based on Stage II and $n = 15$, have been shown to give relatively good agreement with these experimentally determined values and this method of determining the flexural rigidity in the case of pavement design should be fully acceptable.

4. Load on a Free Edge or a Joint

41. The Elasticity Theory according to Westergaard

As mentioned in the earlier literary review, as far as the author has been able to find out, only WESTERGAARD has treated the case where the loading on the pavement is placed on a free edge or a joint which cannot transfer flexural moment. WESTERGAARD starts in this connection from a case of loading with periodically repeated loading along the edge and obtains the influence of a single load by allowing the period to increase towards infinity [71]. He derives in this way an expression for the depression due to a concentrated load on the edge. Analogous with the rest of his treatment of the problem of a slab on an elastic subgrade, WESTERGAARD assumes that the subgrade behaves as a resilient layer with a modulus of subgrade reaction k.

With reference to these derivations WESTERGAARD in his earlier papers [72, 74] states formulae for the depression and the moment under a semi-circularly distributed load along a free edge (WESTERGAARD's loading case III). For the depression under the load the following expression is stated

$$w_e = \frac{1}{\sqrt{6}} \; \frac{P}{k\,l^2} \, (1 + 0.4\, r) \tag{41:1}$$

This is actually the depression under a load concentrated in a point, but the effect of small load distributions is stated to be comparatively insignificant. For the moment under the centre point of the semi-circular loading surface, WESTERGAARD quotes a formula which, after suitable re-writing, can be expressed:

$$m_e = -\,P\,(1 + 0.54\, r)\left(0.350 \cdot {}^{10}\log \frac{c}{l} - 0.032\right) \qquad (41{:}2)^{1)}$$

[1]) The derivation of this moment formula is not stated in WESTERGAARD's papers. Attempts by the author through integration of the expressions for the concentrated load in WESTERGAARD's paper [71] to arrive at the formula in question have *not* produced a result in agreement with WESTERGAARD.

In these formulae, as earlier, l = the elastic radius of rigidity, calculated from the expression

$$l = \sqrt[4]{\frac{D}{k}}$$

WESTERGAARD has also produced a diagram covering the depression and the moment of the edge load [72]. He has shown the depression in the form of level curves for the depression surface in the neighbourhood of the concentrated load, and with the help of these it is possible to obtain the depression curves parallel with and at right angles to the edge (see Fig. 41:1). Since the depression surface according to Maxwell's theorem can be considered also as an influence surface for the depression in the edge due to a load in a certain point on the slab, it is possible to use the level curves in order to obtain the depression in the edge due to concentrated loads at a varying distance from the edge, and for a load with a moderately large distribution the position of the concentrated load can be replaced by the centre of gravity position of the loading surface. The moment distribution curves of WESTERGAARD show the moment along the free edge in the case of different load distributions, whereby the load has, however, linear distribution along the edge. The values of the moment under the loading centre which can be calculated from the formula (41:2) and the values obtained from the curves just mentioned do not agree at all — the latter are almost double so large as the former. It should, however, be reminded that the load in one of the cases is semi-circularly distributed while in the other case it is linearly distributed. It should, however, be possible to assume that the moment distribution outside the load distribution zone agrees more or less with that obtained with a semi-circular distribution of the load.

In some later papers [76, 77], WESTERGAARD has derived and stated new formulae for depression and moment with loading on the interor and on the edge of a slab in such cases where the load distribution has other forms than that of a circle. The edge loading formulae are based also here on the earlier quoted original case of concentrated loading [71]. If the assumption is made, as earlier, in this paper that the pressure surface between the slab and a loading wheel is circular, then the most important types of loading surface are partly the semi-circular distribution (as WESTERGAARD treated in his original formula), applicable in the case when a loading wheel is exactly over a moment-free joint, and partly the circular distribution tangent to the edge, applicable in the case when a loading wheel is close to the edge of a pavement. For these two important cases of loading it is possible, after suitable re-writing and simplification[1]) to obtain the following formulae for depression and moment under the loading centre:

in the case of a semi-circular load:

$$w_e = \frac{1}{\sqrt{6}} \frac{P}{k\,l^2} (1 + 0.4\,\nu) \left[1 - 0.323\,(1 + 0.5\,\nu)\,\frac{c}{l}\right] \tag{41:3}$$

$$m_e = -P\,(1 + 0.5\,\nu) \left(0.489 \cdot {}^{10}\log \frac{c}{l} - 0.091 - 0.027\,\frac{c}{l}\right) \tag{41:4}$$

in the case of a circular tangent load:

$$w_e = \frac{1}{\sqrt{6}} \frac{P}{k\,l^2} (1 + 0.4\,\nu) \left[1 - 0.760\,(1 + 0.5\,\nu)\,\frac{c}{l}\right] \tag{41:5}$$

$$m_e = -P\,(1 + 0.5\,\nu) \left(0.489 \cdot {}^{10}\log \frac{c}{l} - 0.012 - 0.063\,\frac{c}{l}\right) \tag{41:6}$$

The formulae for depression[2]) (41:3) and (41:5) are in the case of load distribution equal to zero identical with the depression formula (41:1) stated earlier as applying for a concentrated load. On the other hand, the moment formula (41:4) for the semi-circular case does *not agree at all* with the earlier formula (41:2) for the same case. The formula quoted here gives moment values which are considerably higher than the corresponding values according to the earlier formula.

The formulae above take greater respect to the influence of the load distribution than the old formulae, since more terms in the series development are included, but they do not apply for other than comparatively moderate load distribution, since only terms of the first order in $\frac{c}{l}$ have been included. As a matter of fact, the terms with $\frac{c}{l}$ in the deflection

[1]) In the original formulae, the Poisson's ratio ν is included in a considerably more complicated functional relationship. Here, however, simplifications have been introduced of the same type as WESTERGAARD himself introduced in his original formula [71] for the case of edge loading and which are well applicable, for the small ν-values here concerned, within the region where the formulae apply.

[2]) WESTERGAARD also states that the depression according to (41: 3) and (41: 5) at small distances y at right angles to the edge decreases according to the formula

$$w_y = w_e \left[1 - (0{,}76 + 0{,}4\,\nu) \cdot \frac{y}{l}\right]$$

This formula has been utilized when making out the depression curves at right angles to the edge in fig. 41: 1.

formulae (41:3) and (41:5) express only the influence of the load distribution depending on the fact that the centre of gravity of the load distribution surface (the semi-circle) at an increased radius becomes an increased distance from the free edge, thus not the influence of the magnitude of the load distribution surface in itself. If the centre of gravity distance of the semi-circular load $\bar{c} = 0.425\ c$ is inserted instead of the radius c in the formula (41:3), then this formula becomes identical with (41:5).

A better idea of the influence of large load distribution can be obtained with the help of the "influence charts" for pavements quoted by Picket and Ray [57] which in the case of the edge load treated here are based directly on Westergaard's original formulae in his first paper [71]. These influence charts can be used as a help to calculate the depression and the moment in a point of the edge and in a point at a distance $\frac{l}{2}$ from the edge due to an arbitrarily distributed load with an arbitrary position within a zone of $2\,l$ from the point in question. The author has utilized this method in order to produce curves over the moment distribution along the edge as well as the depression along and at right angles to the edge in the case of various load distribution radius with semi-circular load and circular load, tangent the edge. The results are shown by Fig. 41:1 and 41:2. The curves for moment and depression in the loading centre for various values of load distribution have also been drawn in. A comparison between the values according to these curves and according to the formulae (41:3) — (41:6) show results which are completely in agreement in the case of small values of load distribution. A control with the help of the Picket-Ray influence charts of the moment distribution curves for a linear load along the edge produced by Westergaard and mentioned earlier also gives full agreement.

It is thus obvious that the original formula (41:2) for edge loading according to Westergaard [72] is, at least from a theoretical viewpoint, completely erroneous. Unfortunately it has become fairly wide spread both in design specifications and handbook literature as well as in the treatment, analyses and discussion of test results,[1]) while the new correct formulae according to [76] have attracted very slight attention.

The maximum moment of the edge loading according to the formulae (41:4) and (41:6) or the diagrams in the figures (41:2) have been compared with the moments of the load on the interior of the slab

[1]) As far as Swedish conditions are concerned, it may be mentioned as examples in this respect the Design Specifications of the Swedish Cement and Concrete Research Institute [78] and the handbook Bygg. [54] The author has himself used the erroneous formula in a report concerning loading tests on the Arlanda airport [39].

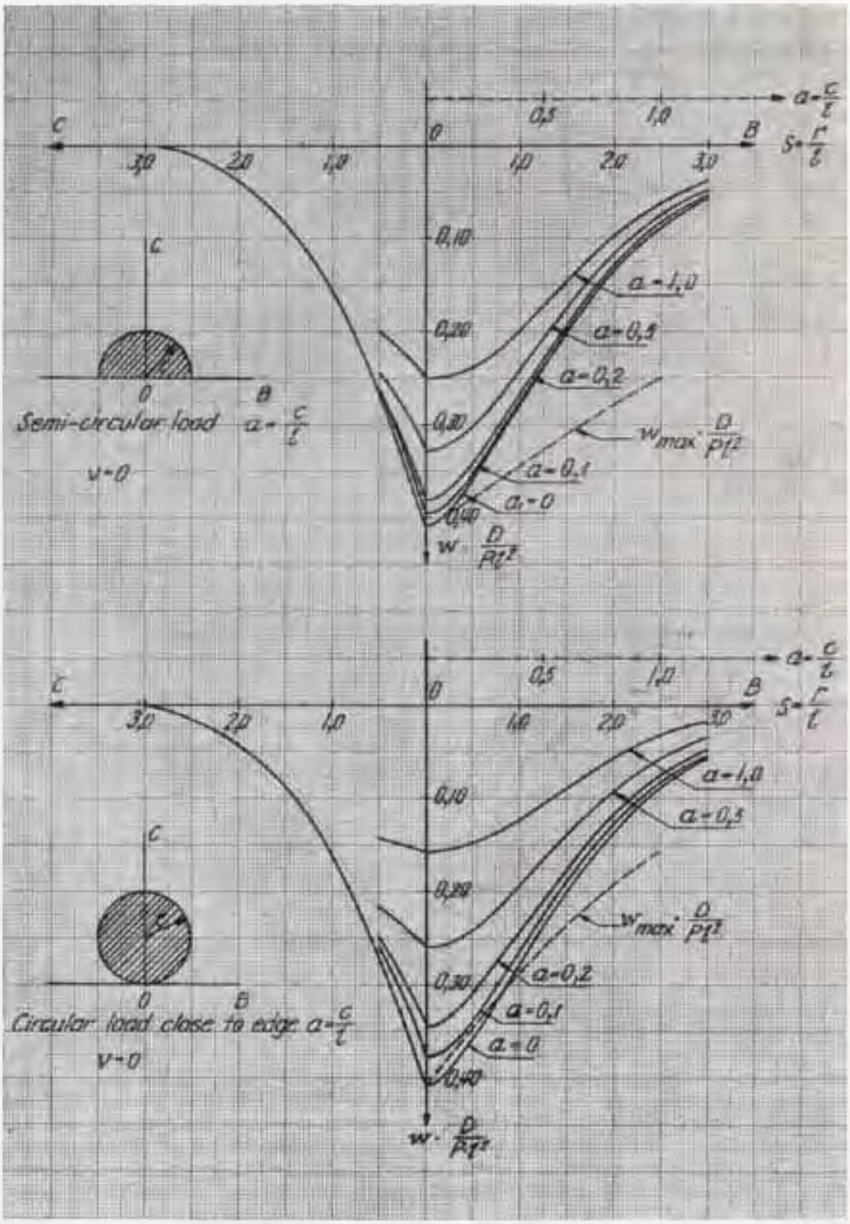

Fig. 41:1. The depression lines along and, in adjacent points, at right-angles to the free edge of a slab of semi-infinite extent subjected to a load with various types of load distribution acting on the free edge. The maximum depression under the loading centre for various extent of load distribution is also drawn in (broken lines and special co-ordinate axis). The curves apply to resilient subgrade.

The curves for a concentrated load ($a=0$) have been obtained directly from WESTERGAARDS level curves in [72] for $\nu=0$. The remaining curves have been drawn on the basis of the Pickett-Ray influence charts [57]; these apply for $\nu=0.15$, but the corresponding curves for $\nu=0$ have been estimated from the basis of the formulae (41:3) and (41:5) centre values) as well as WESTERGAARD's level curves in [72], given for $\nu=0$ and $\nu=0,25$.

TABLE 41:1. Maximum positive moment m_e of edge loading P on a slab of semi-infinite extent (with $\nu=0$) on resilient subgrade according to the formulae (41:4) and (41:6) and Fig. 41:2, compared with the corresponding moment of the load on the interior of the slab m_{int} according to Fig. 22:9.

Relative load distribution $\alpha=\frac{c}{l}$	Moment of semi-circular load on the edge m_e^{sc}	Moment of circular load tangent to the edge m_e^{tg}	Moment of load on the interior of the slab m_{int}	$\frac{m_e^{sc}}{m_{int}}$	$\frac{m_e^{tg}}{m_{int}}$
0.1	0.583 P	0.507 P	0.232 P	2.50	2.17
0.2	0.438	0.366	0.177	2.47	2.08
0.3	0.354	0.286	0.145	2.44	1.97
0.5	0.251	0.188	0.105	2.38	1.79
1.0	0.127	0.083	0.058	2.25	1.43
2.0	0.036	—	0.018	2.00	—

(according to the diagram in fig. 22:9), and the results for some values of the relative load distribution have been summarized in table 41:1.[1]) The values in the table show that the relationship between the maximum positive moments of the edge loading and of the load on the interior of the slab decrease gradually as the relative load distribution increases — in the case of the semi-circular load, the relationship is practically constant. Fig. 41:3 shows that the relationship between these moment quotas and the relative load distribution can very well be represented by straight lines. The maximum negative moment m_e^- appears, to judge by the diagrams in Fig. 41:2, to have approximately constant value independent of the load distribution, since the negative moment peak comes further from the loading centre with greater load distribution.

With the help of the diagrams in fig. 41:3, the maximum positive moments in the case of loading on a free edge can be set out in the form of the simple equations:

in the case of a semi-circularly distributed loading surface

$$m_e^+ = P\,(1+0.5\,\nu)\left(2.5-0.25\,\frac{c}{l}\right)Z_4^0 \qquad (41:7)$$

[1]) If corresponding comparisons are carried out with the edge loading moment calculated according to WESTERGAARD's original formula (41: 2) the result is obtained that the edge loading moment is approx. 1.5 times greater than the moment of the same load on the interior of the slab, i. e. the loading exactly over a joint, which cannot transfer moments (whereby half the load will form a semi-circularly distributed load on each edge of the joint) should give *smaller* stresses in the slab than the same load on the interior of the slab. Such a result appears to be completely illogical and shows thus, also in this way, that the formula in question cannot be correct.

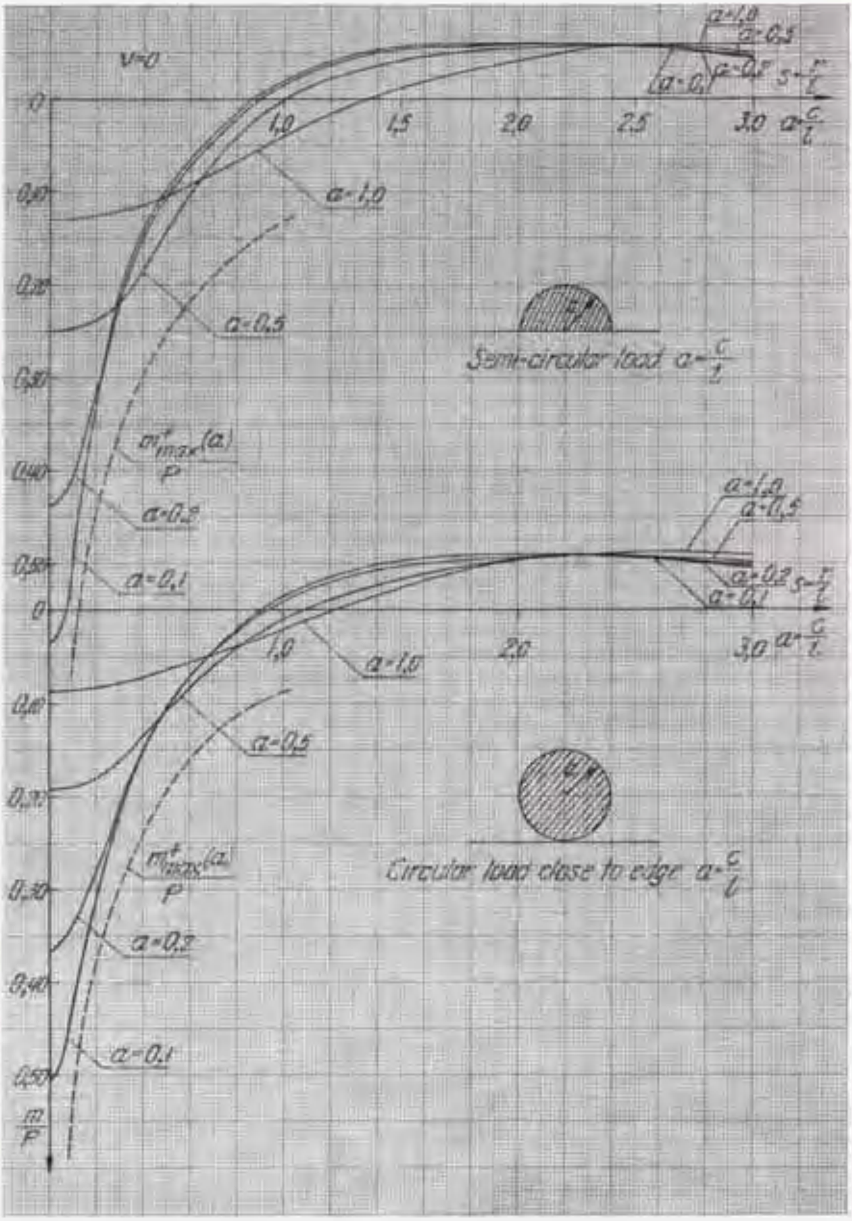

Fig. 41:2 A and B. Moment distribution curves along the free edge of a slab of semi-infinite extent with the load on the free edge. The maximum moment for various extent of load distribution is also marked in (broken lines). The curves apply to resilient subgrade and a Poisson's ratio for the slabs $\nu = 0$ (Fig. A) and $\nu = 0{,}15$ (Fig. B).

The curves for $\nu = 0{,}15$ have been drawn in directly on the basis of values in accordance

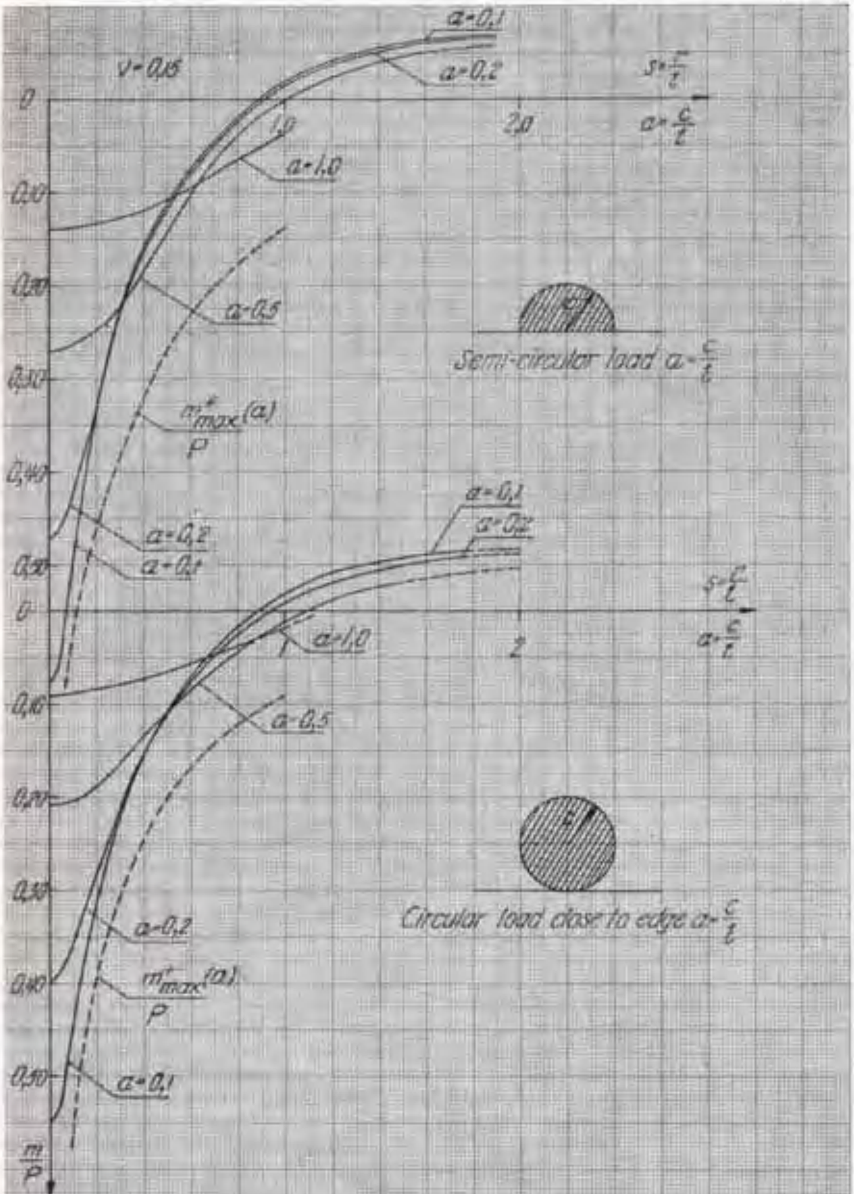

with the Pickett-Ray influence charts [57]. The corresponding curves for $\nu = 0$ have been estimated from the basis of the formulae (41:4) and (41:6) (maximum values) as well as Westergaard's moment curves for a linear load (see page 231), given for $\nu = 0$ and $\nu = 0{,}25$. These last-mentioned curves have also been utilized to obtain the moment values at a larger distance from the loading centre than that obtainable from the influence charts.

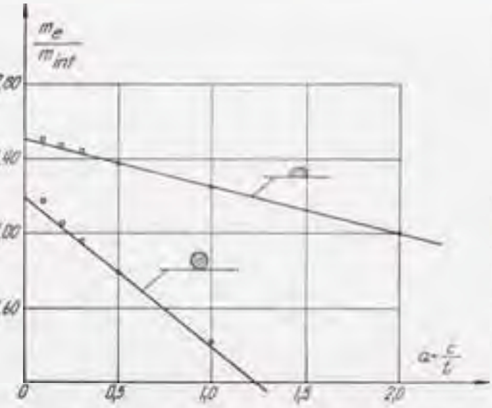

Fig. 41:3. The relationship between the moment m_e of a load on the edge and m_{int} of a load on the interior of a slab ($\nu = 0$) on resilient subgrade. The figure shows that the relationship values for various extent of load distribution $\frac{c}{l}$ can be represented by straight lines with a sufficient degree of accuracy.

in the case of a circular loading surface tangent the edge

$$m_e^+ = P\,(1 + 0.5\,\nu)\left(2.2 - 0.8\ \frac{c}{l}\right) Z_4^0 \tag{41:8}$$

where Z_4^0 is obtained from the moment diagram in Fig. 22:9, page 54 for a load on the interior of the slab. For the maximum negative moment, independent of the load distribution, can be written

$$\left.\begin{aligned} m_e^- &= -\ 0.060\ P \ \text{ when } \nu = 0 \\ m_e^- &= -\ 0.066\ P \ \text{ when } \nu = 0.15 \end{aligned}\right\} \tag{41:9}$$

It would not appear to be an altogether too wild supposition that the relationship between the moment of the edge loading and the moment of the load on the interior of the slab can be calculated in a similar way for elastic subgrade as for the type of subgrade WESTERGAARD has reckoned with, namely resilient subgrade. The formulae (41:7) to (41:9) should, according to this supposition, be of use for the calculation of the edge loading moments, whether the subgrade is resilient or elastic, whereby the values of Z_4^0 are obtained for the moment in the case of a load on the interior of the slab from the diagrams in fig. 22:7 on page 52 and fig. 22:9 on page 54 respectively, and thereby determining the relative load distribution $a = \frac{c}{l}$ from the respective l-values.

$$l_k = \sqrt[4]{\frac{D}{k}} \text{ in the case of resilient subgrade}$$

$$l_e = \sqrt[3]{\frac{2\,D}{C}} \text{ in the case of elastic subgrade}$$

WESTERGAARD has not stated the moment distribution curves or any values of the moment for the deflection at right angles to the edge of the slab. It can be assumed, however, that the negative moments in the sections in question can hardly in any case be less than the negative moments in the sections along the edge, since the edge in the first-mentioned direction carries the load with a cantilever effect. Along the edge itself there is naturally no positive moment.

The question of the correctness of the edge loading formulae according to WESTERGAARD and the relationships (41:7) to (41:9) set out here would appear to require further clarification on the basis of tests. Not much is derived, however, by a study of tests with edge loading carried out earlier, and this is due to the fact that, when analyzing the tests, the basis usually used was the original erroneous edge loading formula (41:2) for which WESTERGAARD is responsible. In the earlier mentioned test review by BERGSTRÖM and assoc. [4] those authors state that the results of edge loading tests show great deviations by comparison with the theoretical values. In some of the tests with edge loading referred to in this paper, included in a large series of loading tests with plain concrete test pavements on natural soil (the Arlington tests) by TELLER and SUTHERLAND [64] it was considered that good agreement was certainly shown with the erroneous formula, but simultaneously also with the correct moment curves stated by WESTERGAARD. Concerning later tests a series of model tests by BONE [10], which were carried out under conditions which should be similar to the theoretical conditions of WESTERGAARD, are of special interest and the results here show good agreement with the new formulae both for the semi-circular case and for the case of a tangent edge load, formulae (41:4) and (41:6).

The problem will be discussed further in connection with the following test accounts. The correctness of the suggested method for calculating the edge loading moment according to the theory for *elastic* subgrade will thereby be examined.

WESTERGAARD treats a further case of a load on a pavement, namely the case of a load on a free corner (WESTERGAARD's loading case I, see Fig. 41:4). He thereby considers the corner to be a cantilever, loaded

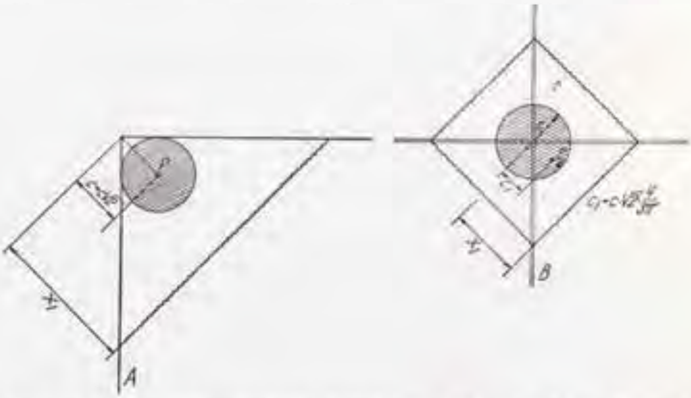

Fig. 41:4. Case of loading with circularly distributed load P on a free corner (A) and on a joint intersection (B).

from above by a circularly distributed load P tangent the corner and from below by the soil pressure, estimated from the deformation. WESTERGAARD finds in this way that the dangerous section is at the following distance from the corner

$$x_1 = 2\sqrt{c_1\, l} \tag{41:10}$$

(see Fig. 41:4) and quotes for the stresses in this section an approximate expression which can be re-written to the moment formula

$$m_e^- = -\frac{P}{2}\left[1 - \left(\frac{c_1}{l}\right)^{0,6}\right] \tag{41:11}$$

where c_1 is the centre of gravity distance of the loading surface from the corner and l is as usual the elastic radius of rigidity for resilient subgrade.

For a circular surface with $c_1 = c\sqrt{2}$ one thus obtains

$$m_e^- = -\frac{P}{2}\left[1 - 1{,}23\left(\frac{c}{l}\right)^{0,6}\right] \tag{41:12}$$

For the more usual cases, where the load P is standing on an intersection of joints which do not transfer moment, but shearing forces (Fig. 41:4), then the stresses will be greatest if P is standing exactly over the joint intersection whereby a quarter of it is loading each section of the slab. The moment in this case should be able to be expressed analogous with (41:11), if the centre of gravity distance $c_1 = 0{,}6\, c$, is inserted and one thus obtains

$$m_{fi}^- = -\frac{P}{8}\left[1 - 0.74\left(\frac{c}{l}\right)^{0,6}\right] \tag{41:13}$$

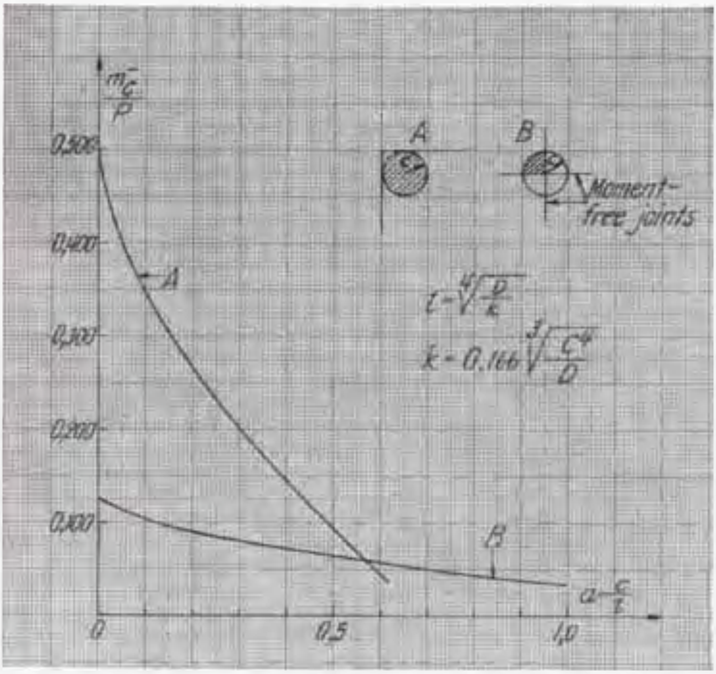

Fig. 41:5. The relations according to the equations (41:12) and (41:13) between the negative maximum moment and the load distribution with a load on a free corner and a joint intersection respectively for a slab on resilient subgrade. The relationship formula (23:4) between k and C is also shown in the figure.

No positive moments of significance occur in these cases. The negative moments according to (41:12) and (41:13) are, at least in the case of small and moderate load distribution, significant by comparison with the negative moments in other cases of loading. Fig. 41:5 shows the relationship between the moment and the load distribution, calculated according to the formulae (41:12) and (41:13). For large values of the relative load distribution the formulae would not appear to be applicable.

Loading tests with the corner loading case would appear only to have been carried out on plain concrete slabs and, according to [4] such tests show great variations when compared with the theoretical values according to the formula (41:12). The agreement is particularly poor in the case of thick slabs, this apparently depending upon the fact that such slabs, due to their rigidity, are sensitive for poor contact with the subgrade.

The author has not carried out any tests himself on reinforced pavements. With slabs of this type, which are comparatively thin, agreement with the theory could be expected to be fairly good.

42. The Ultimate Strength Theory

421. General

The expressions stated in the previous section are naturally applicable only as long as the slab functions more or less elastically, that is to say in the case of a reinforced pavement, only so long as the yield point is not yet reached in the reinforcement. In order to calculate the ultimate load, defined in the same way as in the treatment of the case of load on the interior of the slab, also here the yield line theory can be applied under the same conditions as in the previous case.

The conditions in the case of loading on a free edge are considerably more complicated than in the case of loading earlier treated. The failure line figure becomes a curve that can *not* be approximated with a semi-circle, since this would violate the equilibrium conditions. The depression "volume" and thereby the soil pressure volume become irregular in so far as the depression increases more rapidly in a direction at right angles to the edge than along the edge as the loading point is approached. This is shown both by Fig. 41:1 and by the fact that the moment along the free edge must be zero. Calculation of the soil pressure is further complicated by the fact that this irregular depression "volume" is cut by an unsymmetrically negative failure line.

In order to study the problem with reasonable calculating work and make it fairly easy to consider, it is therefore essential to introduce very simplified suppositions concerning both the form of the failure line figure and the form of the soil pressure volume. JOHANSEN has shown [31, 32], that with comparatively good approximation the curved failure lines can be replaced by lines in the form of a polygon. The simplest form that can be used in this case is the triangular form as shown in Fig. 42:1. A discussion follows later as to the magnitude of error in the case of such an approximation. The subgrade pressure is assumed to decrease linearly from the loading centre both along the edge and at right angles to it but at various rates, and between these lines the pressure volume can be approximated with plane surfaces. The pressure volume thus obtains the form of a pyramid with a triangular base (see Fig. 42:1). This approximation is naturally rather rougher than that used in the treatment of the

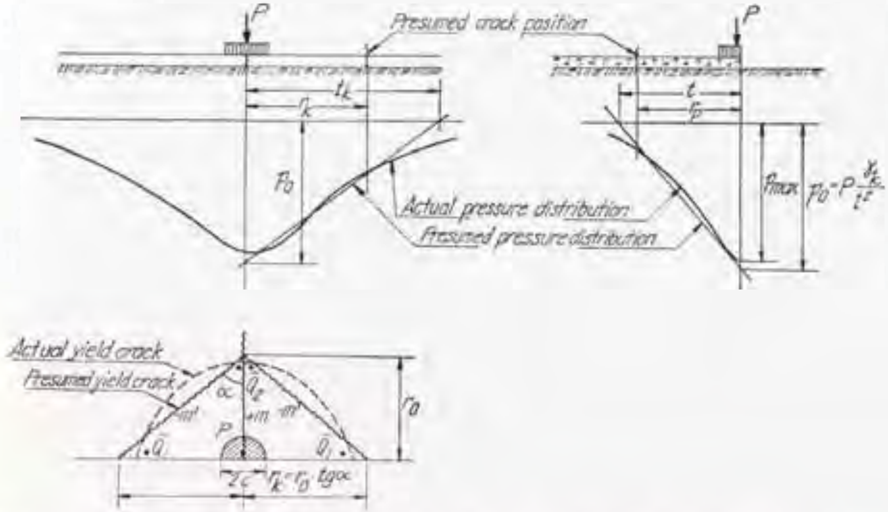

Fig. 42:1. Presumed subgrade pressure distribution and failure line figure with a semi-circular load on a free edge of a slab on soil. The probable actual pressure distribution and failure crack in the top are also drawn in.

earlier case with a load on the interior of the slab, but in that connection it has been shown that even large alterations in the form of the pressure volume have a comparatively small influence on the theoretical ultimate load value.

422. Semi-circular load on an unstrengthened edge. Loading on a joint

The first case to be treated is that where the loading is distributed along the edge in the form of a semi-circle, this case being, as earlier mentioned, applicable for loading on a moment-free joint. The slab is assumed to have the same reinforcement in both directions and this implies that the moment along the failure lines is constant and independent of the directions. The positive ultimate moment (yield moment) is denoted as earlier m and the negative moment (corresponding to the tensile strength of the concrete or the yield moment for the top reinforcement alternatively) m'. The notations are otherwise shown in Fig. 42:1. The base triangle of the soil pressure pyramid has along the edge a length of $2\,t_k$ and a height at right angles to the edge $= t$. The height of the pressure cone, corresponding to the soil pressure under the loading centre, is written $= p_0$. In the angle between the negative failure line and the free edge and the negative and positive failure lines respectively there will be found, according to JOHANSEN [31][1]), the concentrated "corner forces"

$$\bar{Q}_1 = m' \operatorname{tg} \alpha$$

$$\bar{Q}_2 = (m + m') \cot \alpha$$

The equilibrium equations used consist of a projection equation for the section of the slab inside the negative failure lines, a moment equation for this section of the slab around the free edge and a moment equation for half this section of the slab around the positive yield line. In this way one obtains the three equations:

$$\left.\begin{aligned}
&\text{(a)}\ P = r_0^2 \operatorname{tg}\alpha\, p_0 - 2\frac{r_0}{t}\, p_0 r_0 \frac{1}{2} r_0 \operatorname{tg}\alpha \frac{1}{3} - \\
&\quad - 2\frac{r_0}{t_k} \operatorname{tg}\alpha\, p_0 r_0 \operatorname{tg}\alpha \frac{1}{2} r_0 \frac{1}{3} + 2\, m' \operatorname{tg}\alpha + 2\,(m + m') \cot\alpha \\
&\text{(b)}\ P\,\frac{4\,c}{3\,\pi} = r_0^2 \operatorname{tg}\alpha\, p_0 \frac{r_0}{3} - 2\,\frac{r_0}{t}\, p_0 r_0 \frac{1}{2}\, r_0 \operatorname{tg}\alpha\, \frac{r_0}{3}\frac{3}{4}\frac{2}{3} - \\
&\quad - 2\frac{r_0}{t_k} \operatorname{tg}\alpha\, p_0 r_0 \operatorname{tg}\alpha \frac{1}{2}\frac{r_0}{3}\frac{r_0}{4} - 2\, m'\, r_0 \operatorname{tg}\alpha + 2\,(m + m')\, r_0 \cot\alpha \\
&\text{(c)}\ \frac{P}{2}\frac{4\,c}{3\,\pi} = \frac{1}{2}\, r_0^2 \operatorname{tg}\alpha\, p_0 \frac{r_0}{3} \operatorname{tg}\alpha - \frac{r_0}{t}\, p_0 \frac{r_0}{2}\, r_0 \operatorname{tg}\alpha\, \frac{1}{3}\frac{1}{4}\, r_0 \operatorname{tg}\alpha - \\
&\quad - \frac{r_0}{t_k} \operatorname{tg}\alpha\, p_0\, r_0 \operatorname{tg}\alpha\, \frac{r_0}{2}\frac{1}{3}\frac{2}{3}\frac{3}{4}\, r_0 \operatorname{tg}\alpha + m'\, r_0 \operatorname{tg}^2\alpha - (m + m')\, r_0
\end{aligned}\right\} \quad (42{:}1)$$

or after simplification

$$\left.\begin{aligned}
&\text{(a)}\ P \cot\alpha = p_0\, r_0^2 \left(1 - \frac{1}{3}\frac{r_0}{t} - \frac{1}{3}\frac{r_0}{t_k} \operatorname{tg}\alpha\right) + 2\,[m' + (m + m') \cot^2\alpha] \\
&\text{(b)}\ P \cot\alpha\, \frac{4\,c}{3\,\pi} = \frac{1}{3}\, p_0\, r_0^3 \left(1 - \frac{1}{2}\frac{r_0}{t} - \frac{1}{4}\frac{r_0}{t_k} \operatorname{tg}\alpha\right) - 2\, r_0 [m' - (m + m') \cot^2\alpha] \\
&\text{(c)}\ P \cot^2\alpha\, \frac{4\,c}{3\,\pi} = \frac{1}{3}\, p_0\, r_0^3 \left(1 - \frac{1}{4}\frac{r_0}{t} - \frac{1}{2}\frac{r_0}{t_k} \operatorname{tg}\alpha\right) + 2\, r_0 [m' - (m + m') \cot^2\alpha]
\end{aligned}\right\} \quad (42{:}2)$$

By adding the equations (b) and (c) and by adding and subtracting the equations (a) and (b) respectively one gets

[1]) JOHANSEN [31], pages 61 and 62.

$$\left.\begin{aligned}
&P\,\frac{2}{\pi}\,\frac{c}{r_0}\cot\alpha\,(1+\cot\alpha) = p_0 r_0^2\left(1-\frac{3}{8}\,\frac{r_0}{t}-\frac{3}{8}\,\frac{r_0}{t_k}\,\mathrm{tg}\,\alpha\right)\\
&P\cot\alpha\left(1+\frac{4}{3\,\pi}\,\frac{c}{r_0}\right) = \frac{4}{3}\,p_0 r_0^2\left(1-\frac{3}{8}\,\frac{r_0}{t}-\frac{5}{16}\,\frac{r_0}{t_k}\,\mathrm{tg}\,\alpha\right)+4\,(m+m')\cot^2\alpha\\
&P\cot\alpha\left(1-\frac{4}{3\,\pi}\,\frac{c}{r_0}\right) = \frac{2}{3}\,p_0 r_0^2\left(1-\frac{1}{4}\,\frac{r_0}{t}-\frac{3}{8}\,\frac{r_0}{t_k}\,\mathrm{tg}\,\alpha\right)+4\,m'
\end{aligned}\right\}\quad(42{:}3)$$

If it is assumed as earlier that the soil pressure is proportional to the load and can be expressed through the formula (see 41:3)

$$p_0 = \gamma_k\,\frac{P}{l^2} \qquad (42{:}4)$$

one gets after insertion and simplification

$$\left.\begin{aligned}
&P\,\frac{2}{\pi}\,\frac{c}{l}\,\frac{l}{r_0}\cot\alpha\,(1+\cot\alpha) = \gamma_k P\left(\frac{r_0}{l}\right)^2\left(1-\frac{3}{8}\,\frac{r_0}{t}-\frac{3}{8}\,\frac{r_0}{t_k}\,\mathrm{tg}\,\alpha\right)\\
&P\cot\alpha\left(1+\frac{4}{3\,\pi}\,\frac{c}{r_0}\right) = \frac{4}{3}\,\gamma_k P\left(\frac{r_0}{l}\right)^2\left(1-\frac{3}{8}\,\frac{r_0}{t}-\frac{5}{16}\,\frac{r_0}{t_k}\,\mathrm{tg}\,\alpha\right)+\\
&\qquad +4\,(m+m')\cot^2\alpha\\
&P\cot\alpha\left(1-\frac{4}{3\,\pi}\,\frac{c}{r_0}\right) = \frac{2}{3}\,\gamma_k P\left(\frac{r_0}{l}\right)^2\left(1-\frac{1}{4}\,\frac{r_0}{t}-\frac{3}{8}\,\frac{r_0}{t_k}\,\mathrm{tg}\,\alpha\right)+4\,m'
\end{aligned}\right\}\quad(42{:}5)$$

These formulae can finally be rewritten thus

$$\left.\begin{aligned}
&\frac{r_0}{l} = \sqrt[3]{\frac{\dfrac{2}{\pi}\,\dfrac{c}{l}\cot\alpha\,(1+\cot\alpha)}{\gamma_k\left[1-\dfrac{3}{8}\,\dfrac{r_0}{t}\left(1+\dfrac{t}{t_k}\,\mathrm{tg}\,\alpha\right)\right]}}\\
&m+m' = \frac{P}{4}\left[\left(1+\frac{4}{3\pi}\,\frac{c}{r_0}\right)\mathrm{tg}\,\alpha-\frac{4}{3}\,\gamma_k\left(\frac{r_0}{l}\right)^2\left(1-\frac{3}{8}\,\frac{r_0}{t}-\frac{5}{16}\,\frac{r_0}{t_k}\,\mathrm{tg}\,\alpha\right)\cdot\mathrm{tg}^2\alpha\right]\\
&m' = \frac{P}{4}\left[\left(1-\frac{4}{3\pi}\,\frac{c}{r_0}\right)\cot\alpha-\frac{2}{3}\,\gamma_k\left(\frac{r_0}{l}\right)^2\left(1-\frac{1}{4}\,\frac{r_0}{t}-\frac{3}{8}\,\frac{r_0}{t_k}\,\mathrm{tg}\,\alpha\right)\right]
\end{aligned}\right\}\quad(42{:}6)$$

These equations give, for every value of the angle α, certain pairs of values for m and m' expressed in terms of the ultimate load P. The relation between the ultimate moments $\frac{m}{m'}$ thus corresponds to a certain form of the failure line figure, because when the angle α is fixed, then the height of the failure line triangle r_0 is determined through the equation (42:6 a).

In order to be able to use the formulae (42:6) for calculation of the ultimate load or the ultimate moment, it is necessary to determine the constants for the soil pressure pyramid t, t_k and γ_k. According to the same principles as in the treatment of the interior load case, the result of the elasticity theory is used, thus the depression curves shown in Fig. 41:1 on page 234. It is obvious that the form of the pressure volume alters very considerably with the radius of the loading surface. By inserting the closest agreeing straight lines to the curves in Fig. 41:1 it is possible to obtain values of t_k and γ_k in the case of various distributions of the load. It is more difficult to estimate the t-values since the depression lines at right angles to the edge according to Fig. 41:1 are only obtained for the parts nearest to the edge, except for the concentrated load case ($c = 0$) since the methods used do not allow calculation of further values of the depression at right angles to the edge. It is, however, obvious that the t-value increases quite rapidly with increased load distribution. The author has attempted to complement the available curve sections from the basis of the test material available, this being shown in following sections. It is obvious that an estimation obtained in this way of the t-value is very unreliable but it should be pointed out that the form of the soil pressure volume here, as in the interior load case, has only a very weak influence on the result of the ultimate load formula. This will be further discussed later.

On the basis of the theoretical curves and the tests mentioned, the author has found that t and t_k can be estimated with sufficient accuracy from the simple relationships

$$\left.\begin{aligned} t &= 1{,}5\,l + 1{,}27\,c \\ t_k &= 3{,}0\,l + 0{,}42\,c \end{aligned}\right\} \qquad (42:7)$$

the γ_k-value is taken directly from Fig. 41:1 according to the principles quoted.

With the constants for soil pressure calculated in this way, calculations have been made for different values of load distribution $\frac{c}{l}$ and for different angles α. First of all $\frac{r_0}{l}$ was determined through successive

TABLE 42:1. Ultimate moment values according to the formula (42:6) for a semi-circularly distributed load on the free edge of a pavement.

The estimation of the subgrade pressure constants t, t_k and γ_k is based on the elasticity theory for resilient subgrade according to WESTERGAARD.

Relative load distribution	Subgrade pressure constants			Failure figure		Ultimate moment		
$\frac{c}{l}$	$\frac{t}{l}$	$\frac{t_k}{l}$	γ_k	$\alpha°$	$\frac{r_0}{l}$	$\frac{m+m'}{P}$	$\frac{m'}{P}$	$\frac{m}{m'}$
0.1	1.63	3.04	0.40	45	0.760	0.207	0.206	0.01
				50	0.697	0.249	0.172	0.45
				55	0.635	0.299	0.142	1.11
				60	0.584	0.362	0.116	2.12
				65	0.531	0.450	0.093	3.85
0.3	1.88	3.13	0.37	45	1.18	0.166	0.162	0.02
				55	0.990	0.240	0.110	1.17
				65	0.828	0.364	0.070	4.21
0.5	2.14	3.21	0.34	45	1.48	0.135	0.132	0.03
				55	1.24	0.199	0.088	1.25
				60	1.13	0.243	0.070	2.49
				65	1.04	0.302	0.054	4.56
0.7	2.39	3.30	0.32	45	1.74	0.110	0.107	0.03
				55	1.46	0.165	0.070	1.36
				60	1.34	0.202	0.055	2.70
				65	1.24	0.250	0.042	4.94
0.9	2.65	3.38	0.30	45	1.98	0.091	0.087	0.05
				55	1.66	0.137	0.056	1.45
				60	1.53	0.168	0.043	2.89
				65	1.42	0.209	0.033	5.34

approximation from the equation (42:6 a), after which the ultimate moment values can be calculated from both the other equations. Each angle corresponds, as mentioned above, to a certain value of relationship between the ultimate moments $\frac{m}{m'}$.

The result is shown in Table 42:1 and has also been represented in the form of the diagram in Fig. 42:2.

By interpolation from the diagram it is possible to draw the result in the form of a design diagram according to Fig. 42:11 which is more suitable for design calculation, this diagram being inclnded in the summary Section 427, page 270. This diagram gives in the same way as in the interior load case the relationship curves between load distribution and the moment condition $\frac{m + m'}{P}$. The figure includes such curves for different constant values of the relation $\frac{m}{m'}$, which can be

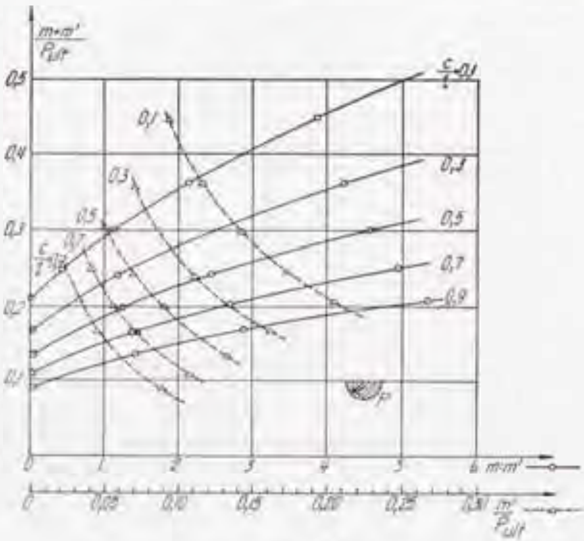

Fig. 42:2. The ultimate moment values $\frac{m+m'}{P_{\text{ult}}}$ for various relative load distribution values $\frac{c}{l}$ with a semi-circular load on a free edge of a slab on soil. The unbroken lines in the diagram represent the relationship curves for various values of the ultimate moment relation $\frac{m}{m'}$, the broken lines represent the relationship curves for various values of the negative ultimate moment $\frac{m'}{P_{\text{ult}}}$. The figure summarizes the result according to Table 42:1.

used in design purpose if the relation between the ultimate moments is known or can be obtained. In many cases with a given slab thickness and no top reinforcement, the moment m' is decided from the strength of the concrete, and to facilitate calculation in such cases, the figure also includes curves for constant negative ultimate moment m' (as also in Fig. 42:2).

In the calculations it became obvious that, particularly in the case of small load distribution, the approximate relationship

$$tg^2\,\varkappa \approx \frac{m+m'}{m'}$$

is obtained, whereby the error becomes greater with increasing values of $\frac{c}{l}$ and $\frac{m}{m'}$. If this approximate value is inserted in the equation (42:2 a), the equation can be simplified, whereby one obtains

$$m + m' = \frac{P}{4}\operatorname{tg}\alpha\left\{1 - \gamma_k\left(\frac{r_0}{l}\right)^2\left[1 - \frac{1}{3}\frac{r_0}{t}\left(1 + \frac{t}{t_k}\operatorname{tg}\alpha\right)\right]\operatorname{tg}\alpha\right\}$$

Instead of the equations (42:6 b and c) one can thus use the considerably simpler approximate formulae

$$\left.\begin{aligned} &\text{(a)}\ \frac{m + m'}{m'} = \operatorname{tg}^2\alpha \\ &\text{(b)}\ m + m' = \frac{P}{4}\operatorname{tg}\alpha\left\{1 - \gamma_k\left(\frac{r_0}{l}\right)^2\left[1 - \frac{1}{3}\frac{r_0}{t}\left(1 + \frac{t}{t_k}\operatorname{tg}\alpha\right)\right]\operatorname{tg}\alpha\right\} \end{aligned}\right\} \quad (42:8)$$

whereby, as earlier, $\frac{r_0}{l}$ is calculated according to equation (42:6 a) through successive approximation. Calculations carried out in accordance with these formulae give results which, in the case of small load distribution $\frac{c}{l}$ and small values of $m : m'$, almost exactly agree with the earlier calculations according to (42:6) and which, in the case of large values such as $\frac{c}{l} = 1.0$ and $m : m' = 5$, deviates from the earlier calculated values by only approx. 3 %. (The deviations in the failure line angle are, on the other hand, considerably greater).

These relatively convenient formulae (42:8) can thus be used for the calculation of ultimate loads or ultimate moment instead of the diagrams in fig. 42:11. See also the summary in Section 427.

423. Circular load tangent to the edge; unstrengthened edge

The above-mentioned case of loading should, as earlier mentioned, be applicable in the cases where the load is close to a free edge. It is obvious that if a wheel rolls out over an edge, if the strip of soil along the edge of the runway is loose or is at a lower level than the surface of the pavement, then a large part of the load can be transferred to a smaller surface than the normal circular contact surface. In this case it will be a transitional form between the case of loading treated earlier and that treated in this section. See 424.

The analysis of this case of loading is completely analogous with the previous presentation. Fig. 42:3 shows the failure line figure assumed. It is obvious that the three equilibrium equations (42:1) in the previous case have here a quite similar form, the only difference being that the equation (42:1 b) in the left-hand side now has the expression Pc instead

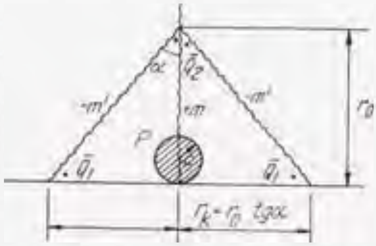

Fig. 42:3. The presumed failure line figure with a circularly distributed load tangent to the free edge of a slab on soil.

of $P\ \dfrac{4\,c}{3\,\pi}$. After simplification and combination of the three equations one then gets, analogous with (42:3)

$$\left.\begin{aligned}
&P\frac{3}{2}\frac{c}{r_0}\cot\alpha\left(1+\frac{4}{3\pi}\cot\alpha\right)=p_0\,r_0^2\left(1-\frac{3}{8}\frac{r_0}{t}-\frac{3}{8}\frac{r_0}{t_k}\,\mathrm{tg}\,\alpha\right)\\
&P\cot\alpha\left(1+\frac{c}{r_0}\right)=\frac{4}{3}p_0r_0^2\left(1-\frac{3}{8}\frac{r_0}{t}-\frac{5}{16}\frac{r_0}{t_k}\mathrm{tg}\,\alpha\right)+4\,(m+m')\cot^2\alpha\\
&P\cot\alpha\left(1-\frac{c}{r_0}\right)=\frac{2}{3}\,p_0\,r_0^2\left(1-\frac{1}{4}\frac{r_0}{t}-\frac{3}{8}\frac{r_0}{t_k}\,\mathrm{tg}\,\alpha\right)+4\,m'
\end{aligned}\right\}\quad(42{:}9)$$

and after insertion in the usual expression (42:4)

$$p_0=\gamma_k\cdot\frac{P}{l^2}$$

one gets the final formulae which are analogous to the equations (42:6)

$$\left.\begin{aligned}
&\text{(a)}\ \frac{r_0}{l}=\sqrt[3]{\frac{\dfrac{3}{2}\,\dfrac{c}{l}\,\cot\alpha\left(1+\dfrac{4}{3\pi}\cot\alpha\right)}{\gamma_k\left[1-\dfrac{3}{8}\,\dfrac{r_0}{t}\left(1+\dfrac{t}{t_k}\,\mathrm{tg}\,\alpha\right)\right]}}\\
&\text{(b)}\ m+m'=\frac{P}{4}\left[\left(1+\frac{c}{r_0}\right)\mathrm{tg}\,\alpha-\frac{4}{3}\,\gamma_k\left(\frac{r_0}{l}\right)^2\left(1-\frac{3}{8}\frac{r_0}{t}-\frac{5}{16}\frac{r_0}{t_k}\mathrm{tg}\,\alpha\right)\mathrm{tg}^2\alpha\right]\\
&\text{(c)}\ m'=\frac{P}{4}\left[\left(1-\frac{c}{r_0}\right)\cot\alpha-\frac{2}{3}\,\gamma_k\left(\frac{r_0}{l}\right)^2\left(1-\frac{1}{4}\frac{r_0}{t}-\frac{3}{8}\frac{r_0}{t_k}\,\mathrm{tg}\,\alpha\right)\right]
\end{aligned}\right\}\quad(42{:}1$$

TABLE 42:2. Ultimate moment values according to the formula (42:10) for a circularly distributed load tangent to the free edge of a pavement.

The estimation of the subgrade pressure constants t, t_k and γ_k is based on the elasticity theory for resilient subgrade according to WESTERGAARD.

Relative load distribution	Subgrade pressure constants			Failure figure		Ultimate moment		
$\frac{c}{l}$	$\frac{t}{l}$	$\frac{t_k}{l}$	γ_k	$\alpha°$	$\frac{r_0}{l}$	$\frac{m+m'}{P}$	$\frac{m'}{P}$	$\frac{m}{m'}$
0.1	1.80	3.10	0.375	45	0.936	0.199	0.182	0.094
				50	0.870	0.237	0.150	0.585
				55	0.810	0.284	0.123	1.320
				60	0.750	0.342	0.099	2.460
				65	0.690	0.422	0.078	4.390
0.3	2.40	3.30	0.32	45	1.50	0.151	0.119	0.27
				55	1.33	0.216	0.077	1.80
				65	1.12	0.381	0.044	5.98
0.5	3.00	3.50	0.27	45	1.93	0.119	0.079	0.50
				50	1.90	0.144	0.065	1.20
				55	1.68	0.166	0.046	2.58
				60	1.57	0.197	0.038	4.80
0.7	3.60	3.70	0.22	45	2.36	0.098	0.054	0.81
				55	2.06	0.138	0.029	3.83
0.9	4.20	3.90	0.175	45	2.86	0.0835	0.0390	1.14
				55	2.54	0.1140	0.0185	5.15

When estimating the values of γ_k, t_k and t, the procedure is the same as in the earlier treated case of loading and it is found that t and t_k can be estimated according to

$$\left.\begin{aligned} t &= 1{,}5\,l + 3\,c \\ t_k &= 3{,}0\,l + c \end{aligned}\right\} \qquad (42:11)$$

while γ_k is taken directly from Fig. 41:1. With the constants for the soil pressure chosen in this way, calculations have been carried out in the same way as in the previous case of loading for various values of load distribution and for various angles α. The result has been compiled in Table 42:2 and in Fig. 42:4. According to the same principles as in the earlier treated case of loading, this diagram has been utilized to present a more convenient design diagram. This is reproduced in Fig. 42:11 in the summary Section 427.

It can be pointed out that the approximate formulae (42:8) can also be applied in the case of a circular load tangent to the edge, whereby $\frac{r_0}{l}$ as usual is calculated according to (42:10 a). In this case rather

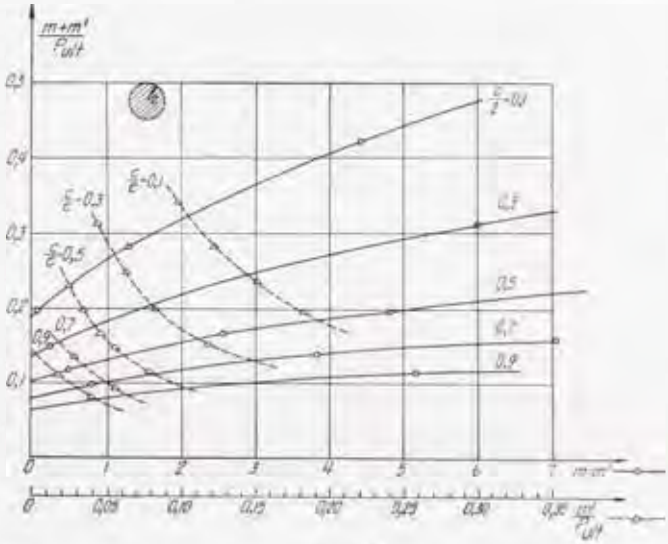

Fig. 42:4. The ultimate moment values $\frac{m+m'}{P_{\text{ult}}}$ for various relative load distribution values with a circularly distributed load tangent to a free edge of a slab on soil. The unbroken lines in the diagram represent the relationship curves for various values of the ultimate moment relation $\frac{m}{m'}$, the broken lines represent the relationship curves for various values of the negative ultimate moment $\frac{m'}{P_{\text{ult}}}$. The figure summarizes the result according to Table 42:2.

poorer agreement was reached with the more exact formulae for larger load distribution, but with moderate values of relative load distribution, this method can well be used. See also the summary in Section 427.

424. Arbitrarly distributed load, twin load

The methods used above with an approximately triangular failure figure can also, naturally, be applied for load surfaces of other forms, for example oval loading surfaces or loads from double wheels. The loading surface is assumed, according to Fig. 42:5, to be symmetrical for an axis at right angles to the edge, and half the loading surface centre of gravity distance $\bar{x}$ from the edge and $\bar{y}$ from the axis of symmetry are introduced as characteristic load distribution constants.

One can then write out general equilibrium equations of the same type as (42:1), whereby the right-hand side is completely unchanged while in the left-hand side of equation (b) and (c) $\bar{x}$ and $\bar{y}$ respectively

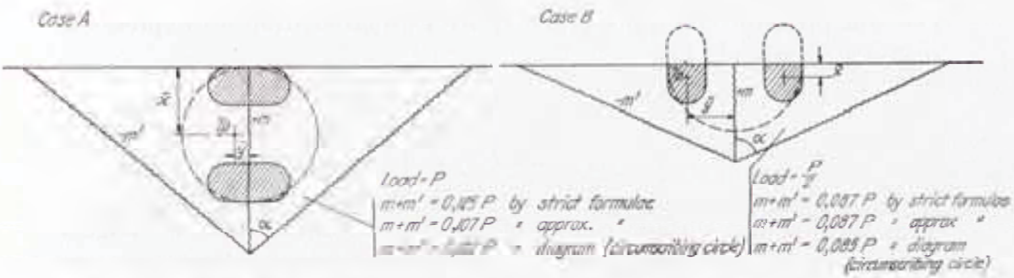

Fig. 42:5. Example of loading areas and approximate failure line figures in the cases of *non-circular* loading areas on the edge of a pavement. Instead of the loading area radius c, the loading area is characterized in such cases by the positions of the centres of gravity $\bar{x}$ and $\bar{y}$ for half the area. The figure shows as an example the oval loading areas from twin wheels with total wheel load P, exerted close to a free edge as well as over a joint (load $P/2$). The failure line triangles drawn in and the moment values stated have been calculated from the formulae (42:12) for twin wheels having pressure areas with a width of 0.5 l and the center of gravity distance of the half-areas 0.2 l with a distance between centres of 1.10 l, whereby the pavement is assumed to have an ultimate moment relationship $m : m' = 3$. As comparison, the moment calculations according to the approximate method, equations (42:8) and (42:12 a), are shown as well as calculations estimated from diagram 42:11 for the nearest corresponding circular and semi-circular areas circumscribing the actual loading area.

are inserted instead of $\dfrac{4\,c}{3\,\pi}$. One thus obtains, in the same way as in 422, the general ultimate moment formulae

$$\left.\begin{aligned}
&(\mathrm{a})\ \frac{r_0}{l} = \sqrt[3]{\frac{1{,}5 \cot \alpha \left(\dfrac{\bar{x}}{l} + \dfrac{\bar{y}}{l} \cot \alpha\right)}{\gamma_k \left[1 - \dfrac{3}{8}\,\dfrac{r_0}{t}\left(1 + \dfrac{t}{t_k}\ \mathrm{tg}\,\alpha\right)\right]}} \\
&(\mathrm{b})\ m + m' = \frac{P}{4}\left[\left(1 + \frac{\bar{x}}{r_0}\right)\mathrm{tg}\,\alpha - \frac{4}{3}\gamma_k\left(\frac{r_0}{l}\right)^2\left(1 - \frac{3}{8}\,\frac{r_0}{t} - \frac{5}{16}\,\frac{r_0}{t_k}\,\mathrm{tg}\,\alpha\right)\mathrm{tg}^2\,\alpha\right] \\
&(\mathrm{c})\ m' = \frac{P}{4}\left[\left(1 - \frac{\bar{x}}{r_0}\right)\cot \alpha - \frac{2}{3}\,\gamma_k\left(\frac{r_0}{l}\right)^2\left(1 - \frac{1}{4}\,\frac{r_0}{t} - \frac{3}{8}\,\frac{r_0}{t_k}\,\mathrm{tg}\,\alpha\right)\right]
\end{aligned}\right\} \quad (42{:}12)$$

where

$\bar{x}$ = half the load surface centre of gravity distance to the free edge
$\bar{y}$ = half the load surface centre of gravity distance to the axis of symmetry

The soil pressure constants t and t_k are estimated from an expression, analogous with (42:11)

$$\left.\begin{aligned} t &= 1{,}5\, l + 3\, \bar{x} \\ t_k &= 3{,}0\, l + \bar{x} \end{aligned}\right\} \qquad (42{:}13)$$

since the loading surface centre of gravity distance from the edge c and $\bar{x}$ respectively determines mainly the depression. For the same reason, the soil pressure pyramid height γ_k can be determined according to the diagram in Fig. 41:1 or the table 42:2 for the corresponding cases of a circular loading with radius $c = \bar{x}$.

Instead of the equations (42:12 b and c), also here the approximate formula (42:8) can be used. In normal cases and with a fairly concentrated loading surface this formula will give good agreement with the more accurate formula (42:12), but particularly in the case of larger distribution of the load at right angles to the edge, the agreement is less good. For the examples in Fig. 42:5 the moment values according to the more accurate formulae (42:12) and the approximate method above have been shown beside the figures

As long as the centre of gravity position for the load surface in question agrees fairly well with the corresponding positions for some of the earlier treated loading surfaces, the semi-circular surface and the circular surface, then the diagram in Fig. 42:11 applying for these standard cases can naturally be used for the calculation. Fig. 42:5 also shows the ultimate moment values estimated in this way, calculated for load distribution in the form of a circle or a semi-circular surface circumscribing the actual surfaces. Agreement is fairly good, even very good in example B in the figure.

Where load extension in the direction of the edge is great, for example in the case of twin wheels with large wheel interval both close to the edge, then the approximation obtained by calculating with a triangular failure line figure becomes rougher and rougher, and the use of a more accurate failure line figure as shown in Fig. 42:6 can be motivated. Purely from the point of view of principle, this particular case does not produce any difficulties if it is assumed that the positive yield lines are at right angles to the edge and the pressure volume limiting surfaces as usual are assumed to be plane between the failure lines, but a systematic treatment means a great deal of calculating work since the depression curves must be determined for every loading centre distance, for example with the Picket-Ray influence charts [57], and is difficult to account in the form of formulae and tables or diagrams. The author has therefore abstained from a more detailed treatment, since the cases in practice

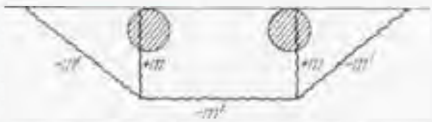

Fig. 42:6. Alternative failure line for edge loading with a great extent along the edge, for example twin loading with both the loading areas some way from each other along the edge.

where the simpler failure line figure does not give an acceptable approximation, appear to be rare.

In cases with twin loading close to the edge with a large wheel interval, it can instead be motivated to examine as to whether a failure line figure with separate failure line triangles round each loading surface will not be more dangerous.

425. Strengthened edge

The result of the analyses above, even if these are very approximate, appears to show that in the case of loading on a free edge and as a rule also on joints, there are considerably larger stresses than when the loading is on the interior of the slab. There is thus a need of local strengthening of the edge relative to the rest of the slab. This can be carried out either by thickening the edge or forming a special edge beam, or by intensifying the reinforcement in the complete edge zone. In the case of reinforced slabs, this last-mentioned method would appear to be preferable in cases where it is sufficiently effective, since it does not require any special cast-form arrangements.

Fig. 42:7 shows an edge which has been strengthened by means of an edge beam or a concentrated reinforcement band so that this gives the edge *increased* ultimate moment $= M$ and M'. The reinforcement parallel with the edge is also intensified relative to the reinforcement at right angles to the edge so that the corresponding ultimate moments become $m_e = \mu \cdot m$ and $m_e' = \mu' \cdot m'$ respectively. m and m' are thus the ultimate moments when bending at right angles to the edge. The strengthened zone is assumed to include the complete failure line figure.

When calculating the concentrated failure line corner forces, due respect must be taken to the edge beam or the intensified reinforcement. The corner forces are obtained as usual according to Johansen [31] from the equilibrium equations for triangular elements between the failure lines and the adjacent sections according to Fig. 42:8, and the failure lines and sections respectively are assumed to be step-formed in the directions of the reinforcement, whereby the ultimate moment is

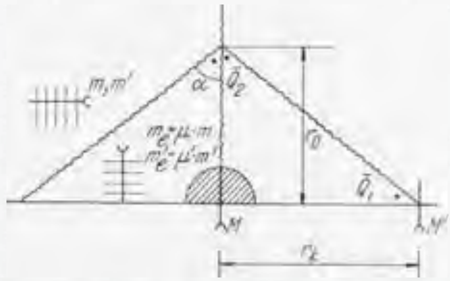

Fig. 42:7. Assumed failure line figure with the load on the free edge of a slab which is strengthened in the edge zone with extra reinforcement giving ultimate moments of $m_e = \mu\, m$ and $m_e' = \mu'\, m'$ respectively, as well as an edge beam or extra reinforcing strip in the edge giving edge moment with ultimate values M and M' respectively (for the entire edge beam). Reinforcement at right angles to the edge (or the flexural strength of the slab itself) gives ultimate moment values m and m'.

considered to be divided up into components in these directions. At the free edge the corner force is unchanged, since if the moment equations for the corresponding triangular elements in Fig. 42:8 are set out around a—a, then the components of the ultimate moment at right angles to the edge cancel out each other and one gets

$$\overline{Q}_1\, ds \sin\beta = m'\, ds \cos\beta + M' \cos\beta - M' \cos\beta$$

thus, as earlier, where $\beta \to (90^\circ - \alpha)$

$$\overline{Q}_1 = m' \operatorname{tg} \alpha \tag{42:14 a}$$

thus only dependent on the ultimate moment of bending at right angles to the edge. The corner force $\overline{Q}_2$ in the angle between the positive and negative failure lines can, according to JOHANSEN,[1]) be calculated from

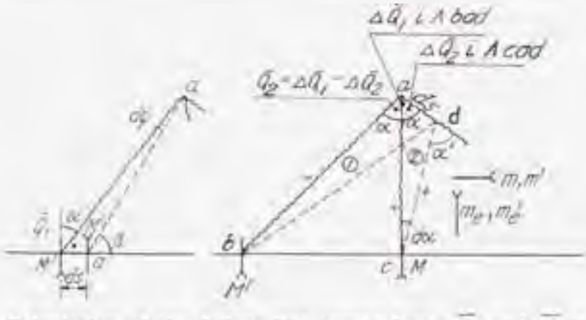

Fig. 42:8. Calculation of the failure line corner forces $\overline{Q}_1$ and $\overline{Q}_2$ in Fig. 42:7.

1) See [31], page 59.

the partial corner forces from the two triangular elements abd and adc in Fig 42:8.

$$\overline{Q}_2 = \Delta\overline{Q}_1 - \Delta\overline{Q}_2$$

When setting out the equilibrium equations for both the triangles, the edge moments M and M' will not be included, since eventual contributions from here to the ultimate moments in both the sections at the points of the triangles cancel out each other. By taking the moment of the triangle abd around bd it can be seen that $\Delta Q_1 = 0$. In a corresponding way ΔQ_2 will be found from the moment equation round dc for the triangle adc:

$$\Delta\overline{Q}_2\, ds \sin\alpha' + m\, ds \sin\alpha \sin d\alpha + m_e\, ds \cos\alpha \cos d\alpha + m'\, ds \sin\alpha \sin d\alpha + \\ + m_e' \cdot ds \cos\alpha \cos d\alpha = 0$$

which at the limiting transition gives

$$\Delta\overline{Q}_2 = -m_e \cot\alpha - m_e' \cot\alpha$$

One thus gets

$$\overline{Q}_2 = (\mu\, m + \mu'\, m') \cot\alpha \qquad (42{:}14\ \mathrm{b})^{1)}$$

Now the equilibrium equations for the section of the slab within the negative failure lines can be set out in the same way as before. One gets

$$\left.\begin{aligned}
&(\mathrm{a})\ P = p_0 r_0^2 \operatorname{tg}\alpha \left(1 - \frac{1}{3}\frac{r_0}{t} - \frac{1}{3}\frac{r_0}{t_k}\operatorname{tg}\alpha\right) + 2\, m' \operatorname{tg}\alpha + \\
&\qquad + 2\,(\mu\, m + \mu'\, m') \cot\alpha \\
&(\mathrm{b})\ P\,\frac{4c}{3\pi} = \frac{1}{3} p_0 r_0^3 \left(1 - \frac{1}{2}\frac{r_0}{t} - \frac{1}{4}\frac{r_0}{t_k}\operatorname{tg}\alpha\right)\operatorname{tg}\alpha - 2\, m' r_0 \operatorname{tg}\alpha + \\
&\qquad + 2\,(\mu\, m + \mu'\, m')\, r_0 \cot\alpha \\
&(\mathrm{c})\ \frac{P}{2}\,\frac{4c}{3\pi} = \frac{1}{2}\,\frac{1}{3}\, p_0 r_0^3 \operatorname{tg}^2\alpha \left(1 - \frac{1}{4}\frac{r_0}{t} - \frac{1}{2}\frac{r_0}{t_k}\operatorname{tg}\alpha\right) - \\
&\qquad - (\mu\, m + \mu'\, m')\, r_0 + m'\, r_0 \operatorname{tg}^2\alpha - (M + M')
\end{aligned}\right\} \quad (42{:}15)$$

These equations apply for the loading surface in Fig. 42:7 with a semicircular load distribution. In the case of other types of loading surfaces, only the left hand side in the equations (b) and (c) are altered according to the presentation in 423 and 424.

1) This result can also be obtained directly according to JOHANSEN [31], fig. 46.

If the equations are treated in the same way as earlier one gets

$$\left.\begin{aligned}
&(a)\ P\frac{2}{\pi}\frac{c}{r_0}\cot\alpha\,(1+\cot\alpha)=p_0\,r_0^2\left(1-\frac{3}{8}\frac{r_0}{t}-\frac{3}{8}\frac{r_0}{t_k}\operatorname{tg}\alpha\right)-\frac{3}{r_0}(M+M')\cot^2\alpha\\
&(b)\ P\cot\alpha\left(1+\frac{4}{3\pi}\frac{c}{r_0}\right)=\frac{4}{3}p_0\,r_0^2\left(1-\frac{3}{8}\frac{r_0}{t}-\frac{5}{16}\frac{r_0}{t_k}\operatorname{tg}\alpha\right)+4\,(\mu\,m+\mu'\,m')\cot^2\alpha\\
&(c)\ P\cot\alpha\left(1-\frac{4}{3\pi}\frac{c}{r_0}\right)=\frac{2}{3}p_0\,r_0^2\left(1-\frac{1}{4}\frac{r_0}{t}-\frac{3}{8}\frac{r_0}{t_k}\operatorname{tg}\alpha\right)+4\,m'
\end{aligned}\right\}\ (42:$$

and corresponding equations for the other types of loading surfaces. With the exception of the fact that the term $\frac{3}{r_0}(M + M')\cot^2\alpha$ in the equation (42:16 a) has been added, these equations are completely identical with the formulae (42:3), which apply to an unstrengthened edge, if in the equation (b) of these formulae, $(m + m')$ is replaced by $(\mu\,m + \mu'\,m')$.

In order to be able to continue the calculations in a fairly simple form it is assumed that also here it is possible to express the soil pressure in the same way as for the cases handled earlier, namely according to (42:4)

$$p_0 = \gamma_k \cdot \frac{P}{l^2}$$

This assumption here naturally admits even more discussion than in the earlier treated cases, since it is based on an analogy with the elasticity theory for a *constantly thick* and *unstrengthened* slab, and a strengthened edge, particularly where it is thickened, must obviously influence the depression and thereby the soil pressure. By allowing the stiffness of the strengthened edge to influence the value of the flexural rigidity of the slab D in a suitable way, this value being included in the expression for the elastic radius of rigidity l, then the expression for the maximum soil pressure may be brought into fairly good agreement with the actual conditions. When selecting a value for l, due respect should be taken to the fact that it is the rigidity in the actual edge zone which mainly determines the deformation and the soil pressure, so the flexural rigidity of the edge beam should thus be distributed over a comparatively narrow edge strip. The author finds it reasonable to assume that the width of this edge strip can be selected to be equal to the elastic radius of rigidity l; in cases where the edge strengthening covers a greater width, then only an edge zone with a width l should be taken into account when calculating. It should thus be possible to estimate the "effective" flexural rigidity D_k of the edge according to the expression

$$D_k = \frac{1}{l}\,[D_{\text{slab}}\,(l - b_k) + (EI)_k] \qquad (42:17)$$

where $(EI)_k$ is the total flexural rigidity for an edge beam (edge zone) with width b_k ($b_k \leq l$). The assumption is naturally particularly unreliable and will later be discussed on the basis of tests but, on the other hand, an error when selecting the flexural rigidity has a very small influence on the l-value.

If the assumed expression for the soil pressure p_0 is inserted, and after re-writing the equations (42:16), the final ultimate formulae for load distribution in the form of a semi-circle will become

$$\frac{r_0}{l} = \sqrt[3]{\frac{\dfrac{2}{\pi}\,\dfrac{c}{l}\,\cot\alpha\,(1 + \cot\alpha) + \dfrac{3}{l}\,\dfrac{M + M'}{P}\,\cot^2\alpha}{\gamma_k\left[1 - \dfrac{3}{8}\,\dfrac{r_0}{t}\left(1 + \dfrac{t}{t_k}\,\operatorname{tg}\alpha\right)\right]}}$$

$$\mu\,m + \mu'\,m' = \frac{P}{4}\left[\left(1 + \frac{4}{3\pi}\,\frac{c}{r_0}\right)\operatorname{tg}\alpha - \frac{4}{3}\,\gamma_k\left(\frac{r_0}{l}\right)^2\left(1 - \frac{3}{8}\,\frac{r_0}{t} - \frac{5}{16}\,\frac{r_0}{t_k}\,\operatorname{tg}\alpha\right)\operatorname{tg}^2\alpha\right]$$

$$m' = \frac{P}{4}\left[\left(1 - \frac{4}{3\pi}\,\frac{c}{r_0}\right)\cot\alpha - \frac{2}{3}\,\gamma_k\left(\frac{r_0}{l}\right)^2\left(1 - \frac{1}{4}\,\frac{r_0}{t} - \frac{3}{8}\,\frac{r_0}{t_k}\,\operatorname{tg}\alpha\right)\right]$$

(42:18)

For a circular loading surface tangent to the edge or for a loading surface of arbitrary form according to Fig. 42:5, one obtains in exactly the same way the corresponding expressions, if the first term in the denominator of the root expression in (42:18 a) is replaced by the denominator of the root expression in equations (42:10 a) and (42: 12 a), respectively, and equations (42:18 b and c) by (42:10 b and c) and (42:12 b and c) respectively.

When estimating the soil pressure constants t and t_k, the conditions are complicated again by the influence of the edge beam. This naturally influences the form of the pressure volume to a certain extent since it stiffens the slab only in the direction following the edge. Since no theoretical analysis of the elastic deflection of an edge-strengthened slab is available, and since the result of the few tests with a strengthened edge carried out, these being described in the following, do not show any significant difference in the form of the pressure volume in the case of various types of strengthening of the edge, then the author considers that the same expressions for the soil pressure constants can be used here as earlier, i. e. select t_k and t according to the equations (42:7) for the semi-circular load, (42:11) for the circular load tangent to the edge and (42:13) for an arbitrary loading surface, while γ_k is estimated from Fig. 41:1 in accordance with the same principles used earlier.

In such cases where there is no edge beam or enlarged reinforcement band, i. e. where M and $M' = 0$, the formulae will be completely identical with those for an unstrengthened edge, if $(m + m')$ in the equation (b) is merely replaced by $(\mu\, m + \mu'\, m')$. This means that in these cases, the results obtained earlier can be applied directly, as well as the diagrams, with the above-mentioned replacement of notations. In Fig. 42:11, the value of the relation $\frac{m}{m'}$, should be replaced by the expression $\left(\frac{\mu\, m + \mu'\, m'}{m'} - 1\right)$. In the usual cases where the reinforcement strengthening only concerns bottom reinforcement, then $\mu' = 1$ and the earlier result can be applied directly if m is put equal to $m_v = \mu\, m$.

Where there is an edge beam strengthening or a reinforcement band with ultimate moments M and M', then this influences the value of r_0 according to the equations (42:18). The design diagram can then not be used, but the formulae (42:18) and corresponding must be used directly. It becomes obvious, however, also here that in the case of moderate large load distribution and normal[1]) cases of edge reinforcement, then an approximate expression corresponding to (42:8 a) can be used

$$\mathrm{tg}^2\,\alpha = \frac{\mu\, m + \mu'\, m'}{m'} \tag{42:19 a}$$

whereby (42:15 a) is simplified to the ultimate moment formula analogous with (42:8 b)

$$\mu\, m + \mu'\, m' = \frac{P}{4}\,\mathrm{tg}\,\alpha \left\{1 - \gamma_k \left(\frac{r_0}{l}\right)^2 \left[1 - \frac{1}{3}\,\frac{r_0}{t}\left(1 + \frac{t}{t_k}\,\mathrm{tg}\,\alpha\right)\right] \mathrm{tg}\,\alpha\right\} \tag{42:19 b}$$

Here $\left(\frac{r_0}{l}\right)$ is inserted with the values according to (42:18 a) or a corresponding expression in the case of other loading surfaces. The agreement

[1]) By "normal" edge reinforcement, the author means a reinforcement which makes a free edge with a circular tangent load or a joint edge with a semi-circular load equally strong with the interior of the slab.

with the more exact formulae is, compared with the corresponding approximate formulae for the unreinforced edge, as good or even better.

See also the summary in Section 427.

426. A discussion of the method

426.1. *General*

There remains a discussion of the effect on the result formulae caused by the approximations which were introduced when deriving them. These imply that the failure line figure was approximated to be triangular instead of having the correct curved form, and otherwise the same assumptions were made concerning constant moment distribution in the bottom crack and the simplified soil pressure volume as in earlier treatment of the case with a load on the interior of the slab.

It should be sufficient to discuss only one of the edge loading cases treated, and here the case with a semi-circular load on an unstrengthened edge (the joint case) has been chosen as being the most important.

426.2. *The approximation of the failure line figure*

Some idea of the errors committed by using a simplified triangular failure line can be obtained by studying the simple case where the soil pressure is *constant* $= p$. In this case, according to JOHANSEN [31], the correct failure line is in the form of a segment of a circle terminating in two lines at tangents according to Fig. 42:9. If in the usual way, a moment equation is expressed for the section I of the slab round the failure line radius $\alpha - \alpha$, a moment equation round the loading centre for an element II which is limited by two radii and a section of the circular failure line, as well as a projection equation for the whole zone within the negative failure line, one obtains

$$\left.\begin{aligned}
&\frac{P}{\pi}\,\alpha\,\bar{x} = p\,\frac{1}{2}\,r_0^2\,\mathrm{tg}\,\alpha\,\frac{1}{3}\,r_0\,\mathrm{tg}\,\alpha - m\,r_0 + m'\,\mathrm{tg}\,\alpha\cdot r_0\,\mathrm{tg}\,\alpha \\
&\frac{P}{\pi}\,d\varphi\,\frac{2}{3}\,c = p\,\frac{1}{2}\,r_0^2\,d\varphi\,\frac{2}{3}\,r_0 - r_0\,d\varphi\,(m + m') + \bar{q}\,r_0^2\,d\varphi \\
&P = 2\,p\,\frac{1}{2}\,r_0^2\,\mathrm{tg}\,\alpha + p\,\frac{r_0}{2}\,(\pi - 2\,\alpha) + 2\,m'\,\mathrm{tg}\,\alpha + \bar{q}\,r_0\,(\pi - 2\,\alpha)
\end{aligned}\right\}\quad(42{:}20)$$

Here $\bar{x}$ = the moment arm for the centre of gravity for the sector of

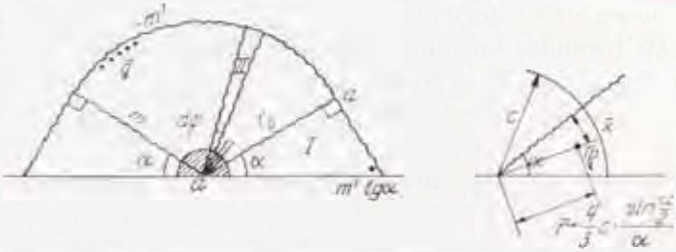

Fig. 42:9. The correct failure line (according to JOHANSEN [31]) with the load on the free edge of a slab on soil, influenced by *constant* subgrade pressure (left-hand figure). The right-hand partial figure shows the position of the centre of gravity of a sector of the semi-circularly distributed edge load.

the semi-circularly distributed load which falls on the slab section I and according to Fig. 42:9 can be written

$$\bar{x} = \bar{r} \sin \frac{\alpha}{2} = \frac{4\,c}{3\,\alpha} \sin^2 \frac{\alpha}{2} = \frac{2\,c}{3\,\alpha}\,(1 - \cos \alpha)$$

Furthermore, as usual, the shearing force along the circular failure line is

$$\bar{q} = \frac{m + m'}{r_0}$$

After insertion and simplification one obtains

$$\left.\begin{aligned} &\frac{P}{\pi}\,\frac{2\,c}{3}\,(1 - \cos \alpha) = \frac{1}{6}\,p\,r_0^3 \operatorname{tg}^2 \alpha - m\,r_0 + m'\,r_0 \operatorname{tg}^2 \alpha \\ &\frac{P}{\pi}\,\frac{2\,c}{3} = \frac{1}{3}\,p\,r_0^3 \\ &P = p\,r_0^2 \operatorname{tg} \alpha + \frac{1}{2}\,p\,r_0^2\,(\pi - 2\,\alpha) + 2\,m' \operatorname{tg} \alpha + (m + m')\,(\pi - 2\,\alpha) \end{aligned}\right\} \quad (42{:}20\text{ a})$$

If the soil pressure p is expressed in the same way as earlier from the relationship

$$p = \gamma\,\frac{P}{t^2}$$

one obtains, after inserting and re-writing the formulae

$$
\left.
\begin{aligned}
&\text{(a)}\ P\left[1-\gamma\left(\frac{r_0}{l}\right)^2\left(\frac{\pi}{2}-\varkappa+\operatorname{tg}\varkappa\right)\right]=2\,m'\operatorname{tg}\varkappa+2\,(m+m')\left(\frac{\pi}{2}-\varkappa\right)\\
&\text{(b)}\ \frac{r_0}{l}=\sqrt[3]{\frac{2}{\pi\,\gamma}\,\frac{c}{l}}\\
&\text{(c)}\ \operatorname{tg}^2\varkappa=\frac{m}{m'}-\frac{P}{m'}\,\frac{1}{3\pi}\,\frac{c}{r_0}\left(\operatorname{tg}^2\varkappa+2\cos\varkappa-2\right)\approx\frac{m}{m'}
\end{aligned}
\right\}\quad (42{:}21)
$$

From these formulae it is possible to calculate the value of the ultimate load for various values of load distribution and relationship $\frac{m}{m'}$, whereby calculation according to equation (c) is carried out through successive approximation. In this connection, the approximate value can be used as a basic value for tg $\varkappa$.

The values obtained in this way can be compared with the corresponding values obtained through an approximate failure line corresponding to that used when expressing the edge loading formulae. The formulae concerning the corresponding case of loading (semi-circularly distributed edge load), have the following form with a constant soil pressure p

$$
\left.
\begin{aligned}
&P\left[1-\gamma\left(\frac{r_0}{l}\right)^2\operatorname{tg}\varkappa\right]=2\,m'\operatorname{tg}\varkappa+2\,(m+m')\cot\varkappa\\
&\frac{r_0}{l}=\sqrt[3]{\frac{2}{\pi\,\gamma}\,\frac{c}{l}\,\cot\varkappa\,(1+\cot\varkappa)}\\
&\operatorname{tg}^2\varkappa=\frac{m+m'}{m'}-\frac{P}{m'}\,\frac{1}{3\pi}\,\frac{c}{r_0}\,(\operatorname{tg}\varkappa-1)\approx\frac{m+m'}{m'}
\end{aligned}
\right\}\quad (42{:}22)
$$

which is obtained by allowing t and t_k in the earlier formulae to proceed towards infinity.

Comparative calculations according to (42:22) and (42:21) have been carried out for several different values of load distribution $\frac{c}{l}$ and moment relation $\frac{m}{m'}$. In this connection the soil pressure constant γ has been inserted with such a value that one obtains roughly the same failure line figure (r_0-value) according to (42:22) as in the calculations according to the edge loading formula (42:6) with the same load distribution and

TABLE 42:3. Influence of the presumed form of the failure line figure.

Comparative calculations at *constant* subgrade pressure $p = \gamma \frac{P}{l^2}$ have been carried out according to formula (42:21) with an exact failure line figure according to Fig. 42:9 as well as formula (42:22) with a simplified triangular failure line figure according to Fig. 42:1 respectively for various values of the load distribution $\frac{c}{l}$ and the ultimate moment relationship $\frac{m}{m'}$. The subgrade pressure constant γ is selected so that the same failure line figure is obtained from (42:22) and when calculating the edge load moment from (42:6).

Relative load distribution $\frac{c}{l}$	$\frac{m}{m'}$	γ	$\frac{m}{P}$ from the exact formula (42:20)	$\frac{m}{P}$ from the appr. formula (42:21)	$\frac{m_{appr.}}{m_{exact}}$
0.1	1	0.30	0.158	0.147	0.93
	2	0.28	0.243	0.239	0.98
	4	0.26	0.352	0.372	1.06
0.5	1	0.19	0.103	0.101	0.98
	2	0.19	0.147	0.164	1.11
	4	0.19	0.192	0.248	1.29
0.9	1	0.15	0.071	0.073	1.03
	2	0.15	0.098	0.116	1.18
	4	0.15	0.120	0.169	1.41

moment relation, see Table 42:1. In this way the result obtained should be the best possible as compared with earlier calculations of the edge loading moments.

The results have been compiled in Table 42:3. The table shows that the errors committed by using the approximate failure line are very insignificant for normally occurring values of load distribution and moment relation; unsatisfactorily large deviations are first obtained with the simultaneous large values of load distribution and moment relation.

426.3. *Moment distribution in bottom cracks*

Even less than in the case of a load on the interior of the slab is it certain in the case of edge loading, that the positive moment along the complete bottom crack have managed to reach its yield value before top cracks have occurred. This depends upon the fact that the negative moment within the elastic state increases relatively quicker in the case of edge loading than in the case of interior loading.

The influence on the ultimate load of such an incomplete yield along bottom crack has been investigated here in exactly the same way as in the interior load case, see Section 325:2. The equilibrium equations are set out on condition that the positive moment is distributed as shown in Fig. 42:10 with a yield zone r_p and an elastic positive moment, which can approximately be assumed to decrease linearly towards a value of zero at a distance l from the loading centre, whereby the moment at the point of the failure triangle analogous with (32:13) is written

$$\varkappa\, m = \frac{l - r_0}{l - r_p} \cdot m$$

The failure line corner force $\overline{Q}_2$ in the point of the triangle is obtained here in exactly the same way as (42:14 b) to

$$\overline{Q}_2 = (\varkappa\, m + m') \cot \alpha$$

while the corner force Q_1 at the free edge according to (42:14 a) remains unchanged. The equilibrium equations, simplified and rewritten in the usual way, obtain under these conditions the form

$$\left.\begin{aligned}
\frac{r_0}{l} &= \sqrt[3]{\frac{\dfrac{2}{\pi}\,\dfrac{c}{l}\,\cot\alpha\,(1+\cot\alpha) + \dfrac{3}{2}\,\dfrac{m}{P}\,(1-\varkappa)\left(\dfrac{r_0+r_p}{l}\right)\cot^2\alpha}{\gamma_k\left[1-\dfrac{3}{8}\,\dfrac{r_0}{t}\left(1+\dfrac{t}{t_k}\,\mathrm{tg}\,\alpha\right)\right]}}\\
\varkappa\, m + m' &= \frac{P}{4}\left[\left(1+\frac{4}{3\pi}\,\frac{c}{r_0}\right)\mathrm{tg}\,\alpha - \frac{4}{3}\,\gamma_k\left(\frac{r_0}{l}\right)^2\left(1-\frac{3}{8}\,\frac{r_0}{t}-\frac{5}{16}\,\frac{r_0}{t_k}\,\mathrm{tg}\,\alpha\right)\mathrm{tg}^2\,\alpha\right]\\
m' &= \frac{P}{4}\left[\left(1-\frac{4}{3\pi}\,\frac{c}{r_0}\right)\cdot\cot\alpha - \frac{2}{3}\,\gamma_k\left(\frac{r_0}{l}\right)^2\left(1-\frac{1}{4}\,\frac{r_0}{t}-\frac{3}{8}\,\frac{r_0}{t_k}\,\mathrm{tg}\,\alpha\right)\right]
\end{aligned}\right\} \qquad (42:23)$$

These formulae have been utilized for random calculation with some different values of r_p, l and $\dfrac{m}{m'}$. When calculating $\dfrac{r_0}{l}$ successive approximation must be used and also from the beginning a suitable value of $\dfrac{m}{P}$ must be assumed. The results of the calculations shown in Table 42:4 agree with the results of the corresponding calculations in the case of an interior load in so far as the values of the ultimate load are only insignificantly influenced by an incomplete yield moment distribution in the bottom cracks, while the value of $\dfrac{r_0}{l}$ and here also α, thus the form of the failure line figure, are influenced rather more.

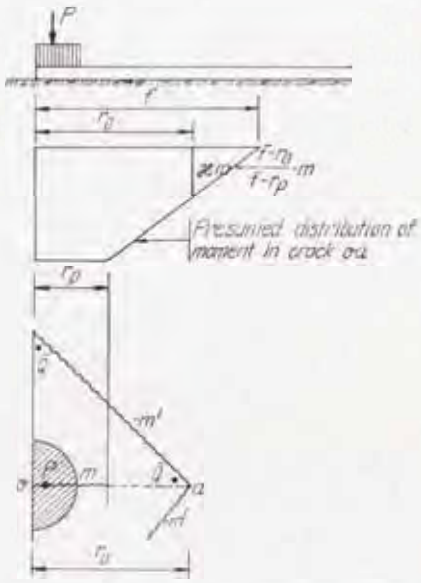

Fig. 42:10. The assumed moment distribution and the failure line figure with loading on the free edge of a slab on soil in cases where the positive moment in the crack o – a in the bottom has reached the yield value only in part of the crack (incomplete plastification).

TABLE 42:4. Influence of incomplete plastification in the positive yield crack with a semi-circular load on a free edge of a slab on soil.

The calculations are carried out according to the formulae (42:23); the soil pressure constants t, t_k and γ_k are taken from Table 42:1. The notations are as in Fig. 42:10.

$a = \frac{c}{l}$	$\frac{m}{m'}$	Moment distribution in radial crack		Crack radius	$\frac{m+m'}{P}$
		$\frac{f}{l}$	$\frac{r_p}{l}$	$\frac{r_a}{l}$	
0.5	4	2.0	$r_p = r_a$	1.06	0.287
			0.6	1.23	0.330
			0.8	1.16	0.318
			1.0	1.09	0.298
		2.5	0.6	1.16	0.315
	2	2.5	$r_p = r_a$	1.17	0.229
			0.6	1.28	0.250
0.1	4	2.5	$r_p = r_a$	0.528	0.456
			0.3	0.555	0.470
0.9	4	2.5	$r_p = r_a$	1.47	0.182
			0.8	1.57	0.205

426.4. *The distribution of soil pressure*

The influence of the deviations from the assumed soil pressure volume, i. e. the values t, t_k and γ_k, have been investigated in the same way as with the case of a load on the interior of the slab by inserting into the edge load formulae values for the soil pressure constants which deviate from the normal values. It proves here, as in the earlier treated case of loading, that the influence of this is relatively insignificant, and that particularly associated decreases of the maximum pressure γ_k and increases of the t-values or vice versa produce very small differences in the ultimate moment values.

427. Summary and discussion. Loading on a corner

From the previous treatment of the various cases of load distribution and edge strengthening it is shown that in normal cases with good approximation, the various ultimate moment formulae for *a load on a free edge* or *a moment-free joint* can be summarized thus:

$$m_e + m_e' = \frac{P}{4}\,\mathrm{tg}\,\alpha\left\{1 - \gamma_k\left(\frac{r_0}{l}\right)^2\left[1 - \frac{1}{3}\,\frac{r_0}{t}\left(1 + \frac{t}{t_k}\,\mathrm{tg}\,\alpha\right)\right]\mathrm{tg}\,\alpha\right\} \qquad (42{:}24\text{ a})$$

$$\frac{m_e + m_e'}{m'} = \mathrm{tg}^2\,\alpha \qquad (42{:}24\text{ b})$$

where $\dfrac{r_0}{l}$ is calculated through successive approximation from the expressions:

in the case of a semi-circularly distributed edge load (joint)

$$\frac{r_0}{l} = \sqrt[3]{\frac{\dfrac{2}{\pi}\,a\cot\alpha\,(1 + \cot\alpha) + \dfrac{3}{l}\,\dfrac{M + M'}{P}\cot^2\alpha}{\gamma_k\left[1 - \dfrac{3}{8}\,\dfrac{r_0}{t}\left(1 + \dfrac{t}{t_k}\,\mathrm{tg}\,\alpha\right)\right]}} \qquad (42{:}25\text{ a})$$

in the case of a circular load tangent to the edge (free edge)

$$\frac{r_0}{l} = \sqrt[3]{\frac{1.5\,a\cot\alpha\left(1 + \dfrac{4}{3\pi}\cot\alpha\right) + \dfrac{3}{l}\,\dfrac{M + M'}{P}\cot^2\alpha}{\gamma_k\left[1 - \dfrac{3}{8}\,\dfrac{r_0}{t}\left(1 + \dfrac{t}{t_k}\,\mathrm{tg}\,\alpha\right)\right]}} \qquad (42{:}25\text{ b})$$

in the case of a load distributed over an arbitrary loading surface

$$\frac{r_0}{l} = \sqrt[3]{\frac{1.5 \cot \alpha \left(\frac{\bar{x}}{l} + \frac{\bar{y}}{l} \cot \alpha\right) + \frac{3}{l} \frac{M + M'}{P} \cot^2 \alpha}{\gamma_k \left[1 - \frac{3}{8} \frac{r_0}{t} \left(1 + \frac{t}{t_k} \operatorname{tg} \alpha\right)\right]}} \qquad (42:25\text{ c})$$

where

m and m' = the ultimate moments per unit width in the slab parallel to the edge of the slab (due to bending *at right angles* to the edge)

m_e = $\mu \cdot m$ and $m_e' = \mu' \cdot m'$ = ultimate moments per unit width in the edge zone at right angles to the edge (due to enlarged reinforcement *along* the edge)

M and M' = *the total increase* in the ultimate moment due to an edge beam or a concentrated reinforcement band along the edge

l = the elastic radius of rigidity according to the formulae (42:27) in the following

a = $\frac{c}{l}$ = the relative load distribution for *a semi-circular load* or *a circular load tangent to the edge* with radius c

$\bar{x}, \bar{y}$ = centre of gravity distances to the free edge or to the axis of symmetry at right angles to the edge respectively for *half* the loading surface in the case of an *arbitrarily* distributed edge loading

t, t_k and γ_k = constants for assumed soil pressure distribution (see Fig. 42:1) according to Table 42:1 and 42:2, whereby in the case of an arbitrarily distributed load the same values may be used as for a circular load tangent to the edge with $c = \bar{x}$. t and t_k are estimated according to the formulae

$$\left.\begin{aligned} t &= 1{,}5\, l + 3\, \bar{x} \\ t_k &= 3{,}0\, l + \bar{x} \end{aligned}\right\}$$

The approximate formulae (42:24) should not be used for larger values of load distribution $a = \frac{c}{l}$ than approx. 1.0 in the case of a semi-circular load or 0.6 in the case of a circular load tangent to the edge and larger values of the moment relationship $\frac{m_k + m_k'}{m'}$ than approx. 5; in the case of smaller load distribution the formulae can however be used for considerably higher values of the moment relationship. In the case of larger load distribution the more accurate formulae according to (42:18) should be used instead and these can be written in the general form

$$\left.\begin{aligned} m_k + m_k' &= \frac{P}{4}\left[\left(1+\frac{x}{r_0}\right)\operatorname{tg}\alpha - \frac{4}{3}\gamma_k\left(\frac{r_0}{t}\right)^2\left(1-\frac{3}{8}\frac{r_0}{t}-\frac{5}{16}\frac{r_0}{t_k}\operatorname{tg}\alpha\right)\operatorname{tg}^2\alpha\right] \\ m' &= \frac{P}{4}\left[\left(1-\frac{x}{r_0}\right)\cot\alpha - \frac{2}{3}\gamma_k\left(\frac{r_0}{t}\right)^2\left(1-\frac{1}{4}\frac{r_0}{t}-\frac{3}{8}\frac{r_0}{t_k}\operatorname{tg}\alpha\right)\right] \end{aligned}\right\} \quad (42:26)$$

When using the edge loading formulae, to start with, any eventual edge beam strengthening moments M and M' should be estimated or selected and then the formulae should be used to calculate pairs of values for $(m_k + m_k')$ for various α-values, which provide alternative reinforcement possibilities. Often m' is given from the earlier design of the slab for the interior load case, and interpolation can then be used to arrive at the necessary values of the edge zone strengthening m_k and m_k'. In certain cases, the moment relationship can be determined from the beginning according to (42:24 b) (as for example for slabs with only an edge beam or an edge reinforcement band but without enlarged edge zone reinforcement), and then the formulae (42:24) can be used directly to determine $(m_k + m_k')$. In both cases it is necessary to make recalculation with more suitable values for M and M' if the result shows that, in the previous calculation, the selected edge strengthening was unsuitable.

In cases where the edge is *not* strengthened with a special edge beam or reinforcement band, so that thus $M = M' = 0$, then the result according to the ultimate moment formulae for the standard cases can be expressed through the *moment diagrams* in Fig. 42:11. These are based on the more accurate formulae (42:6) and (42:10). In many cases these diagrams can also be used for other forms of load distribution surface. This is considered then to correspond to the semi-circular or circular surface circumscribed.

In the current treatment of the edge loading cases it has been assumed that the soil behaves as a resilient bed with a constant resilience modulus k. The estimation of the soil pressure constants t, t_k and γ_k are based on WESTERGAARD's treatment of the edge loading case, this being based on the hypothesis concerning resilient subgrade. However, it would appear not to be an altogether too illogical supposition to assume that the result in this section can be applied also for soil with properties

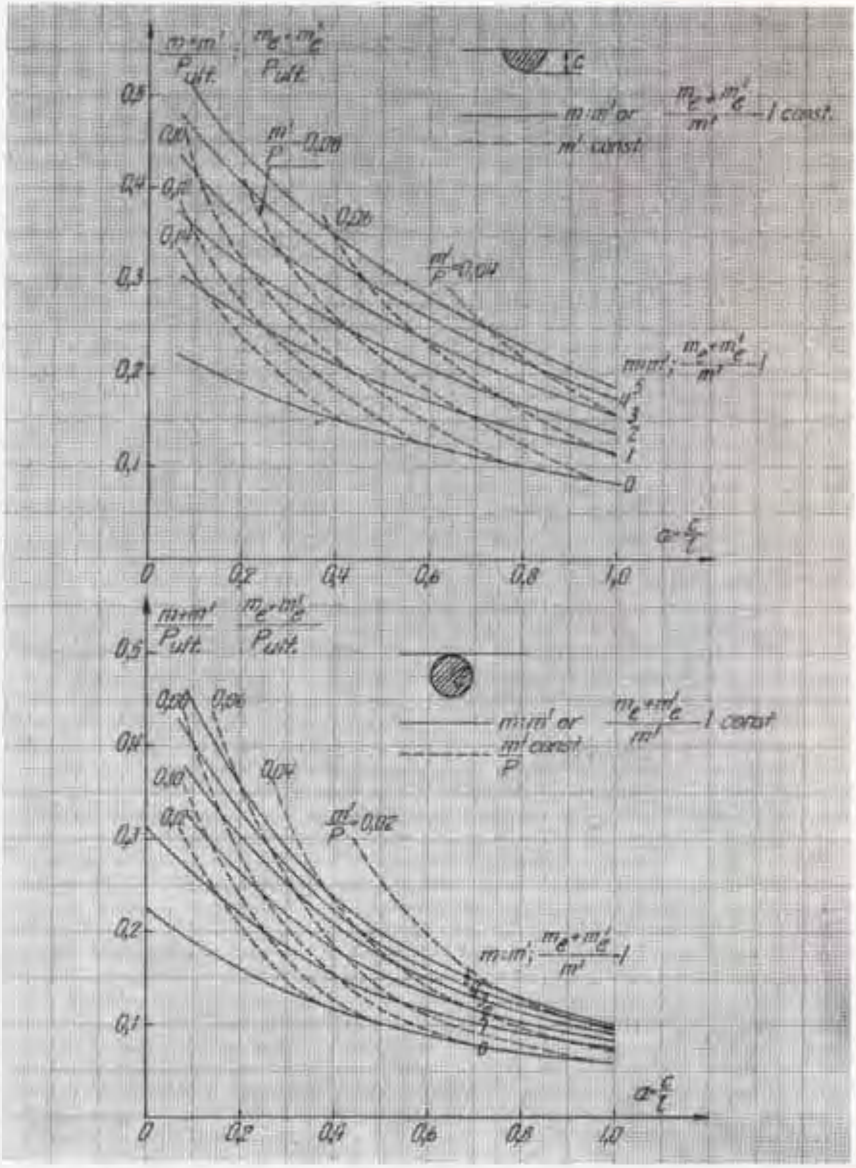

Fig. 42:11. Design diagram for a load on the free edge of a slab on soil; edge *without* edge beam or concentrated reinforcement strip. For a semi-circular load and a circular load tangent to the edge, the diagram gives the ultimate moment values of $\frac{m+m'}{P_{\text{ult}}}$ and $\frac{m_e+m_e'}{P_{\text{ult}}}$ respectively as a function of the load distribution $a=\frac{c}{l}$. Relationship curves have been drawn in for various values of the moment relationships $\frac{m}{m'}$ and $\left(\frac{m_e+m_e'}{m'}-1\right)$ respectively (unbroken lines) as well as for various values of the negative ultimate moment $\frac{m'}{P_{\text{ult}}}$ (broken lines). Here m and m' respectively denote the ultimate moments of the reinforcement at right angles to the edge (or the flexural strength of the concrete respectively), m_e and m_e' the ultimate moments in an edge zone strengthened by intensified reinforcement parallel with the edge.

corresponding to those of elastic subgrade. When treating the case of a load on the interior of the slab it has been shown that the ultimate moment expressions obtained for both the types of subgrade are identical, and that the only difference in this connection is that the soil pressure constants have different values, but that the difference in the ultimate moment values for the same relative load distribution is extremely insignificant, depending upon the slight effect of the form of soil pressure distribution (see section 325:3). The considerable difference between both the types of subgrade becomes apparent in the different values of the elastic radius of rigidity l, which results in different values of the relative load distribution. It appears probable that a corresponding argument can be applied for this edge loading case.

It should thus be possible on the basis of these assumptions to use the equations (42:24), (42:25) and (42:26) respectively as well as the diagram in Fig. 42:11 for both resilient and elastic subgrade, whereby as earlier is valid:

in the case of resilient subgrade

$$l = l_k = \sqrt[4]{\frac{D}{k}} \tag{42:27 a}$$

in the case of elastic subgrade

$$l = l_e = \sqrt[3]{\frac{2\,D}{C}} \tag{42:27 b}$$

and where the flexural rigidity of the slab at a strengthened edge is written

$$D_k = \frac{1}{l}\,[D_{\text{slab}}\,(l - b_k) + (E\,I)_k] \tag{42:27 c}$$

$(E\,I)_k$ = the total flexural rigidity of an edge beam with a width of b_k $(\leq l)$.

The investigation in section 426 has shown that the simplifications made when arriving at the ultimate formulae have a comparatively small effect on the result. It is, however, obvious that when deriving the edge loading formula, more approximations have been made and of a rougher nature than in the case of the corresponding expression for the interior load. A particularly high degree of unreliability applies to the suppositions which are necessary when treating the case of the strengthened edge. It is therefore to be recommended that a higher safety factor is adopted when using the edge loading formulae. This has comparatively small economic significance since the surfaces along the edges and joints in question only represent a small part of the pavement. For the free edge, where the difficulties in placing sufficient strengthening can sometimes become great, the necessary increase in the ultimate load can be compensated by the fact that the loading on a free edge represents a particularly exceptional case of loading, whereby just there a lower degree of safety to failure may be allowable.

Concerning the cases of *loading on a free corner* and *loading on a joint intersection* not treated earlier in this section, then the treatment in the previous Section 41 concerning the elasticity theory is applicable also from the point of view of the ultimate strength theory. The dangerous section which occurs at a distance x_1 from the edge according to the formula (41:10) (see Fig. 41:4), also corresponds to the negative failure line at the ultimate load. The formulae (41:12) and (41:13) and the corresponding diagram in Fig. 41:5 can thus be used for the calculation of the necessary negative ultimate moment m_r' at a free corner or a joint intersection, and only this negative ultimate moment influences the ultimate corner load.

The question concerning the suitable design of the strengthening at the edges and joints will be discussed in section 44.

43. The Gothenburg Tests, Series G, Edge Loading

431. Performance of tests, test procedures and the results

The tests with two full-scale slabs on clay subgrade in Gothenburg (Series G), which have been accounted in Section 25, also included a number of test loadings on free edges. When the test slab G:2 (the double-reinforced slab) was made, the reinforcement was allowed to stick out round the circumference (see Fig. 25:7), and after the slab had been tested by loading the centre, further concrete was cast all round it so that it obtained a quadratic form with dimensions 8×8 metres. One of the four sides thus obtained was left unstrengthened, one was supplied with double closer reinforcement while two were thickened and supplied with an extra reinforcement band nearest the edge. Since the newly cast edge zone was only 0.5 metres wide in the middle, the strengthenings could not be inserted over a greater width. The design of the four edges is shown in Fig. 43:1.

Casting and testing was carried out during the spring of 1946. The reinforcement used consisted of deformed bars Ks 40 from the same shipment as that used in the main tests while the concrete had the same

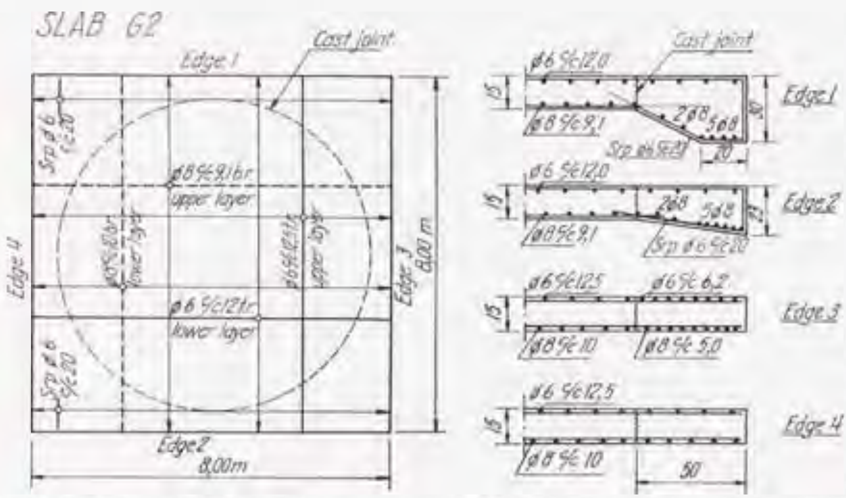

Fig. 43:1. Design of the four edges cast around slab G2. The sections are taken through the edge centre and the 50 cm wide edge units outside the cast joints also represent the cross-section of the detail test beams.

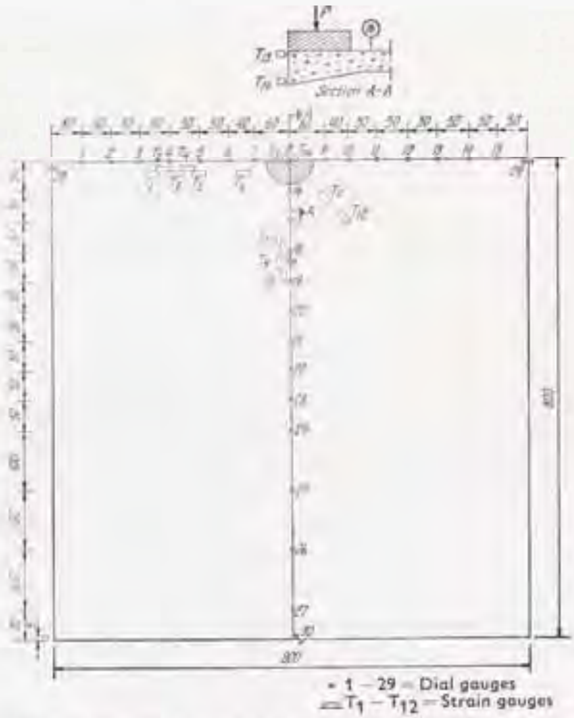

Fig. 43:2. The location, in principle, of the measuring device used for the edge loading tests. The location of the strain gauges varied somewhat between the different tests. The dial gauges 1—15 were attached to a measuring beam which ran along the edge (see Fig. 43:3), the outer ends of which were supported on the corners of the slab. The dial gauges 16—27 were attached to a measuring beam which was supported on the centre of the first measuring beam and on the opposite edge of the slab. The absolute movements of the slab edges were measured by means of the dial gauges 28, 29 and 30 which were attached to rods driven down into a long pipe which was itself driven deeply into the ground (see Fig. 25:7).

composition as in the rest of the slab (see page 136). The compressive strength, determined from eight test cubes, was 280 kg/cm² with maximum deviation of +24 and −15 kg/cm².

To use for the determination of the ultimate moment and the flexural rigidity of the edge sections, four detail test beams, with a width of 50 cm and with a section and reinforcement as in the four edges, were cast at the same time as the slab edges. See Fig. 43:1.

Loading was applied with the help of the same loading device as in the main tests (see Fig. 25:3, page 138). The loading was transferred to the edge of the slab by means of a semi-circular loading half-cylinder with a radius of 40 cm and with the centre point exactly at the centre of the edge. The load from the jack was exerted on the centre of gravity of this semi-circular surface so that it could be assumed that the loading

Fig. 43:3. Photograph showing the loading and measuring devices close to the edge centre. The jack influenced the semi-cylindrical concrete load distribution unit. Round the loading cylinder, the centre measuring beam rests with a yoke-shaped support on the centre of the edge measuring beam. The strain gauges are arranged with their points directly onto small steel plates attached by adhesive to the surface of the slab, punch marks having been made in these plates.

was uniformly distributed over the loading surface (WESTERGAARD's loading case III).

During test loading, the following measurements were carried out:

a) Depression along the edge and at right angles to the edge in the line of symmetry were measured with the help of dial gauges. These were fitted on measuring beams and were arranged in principle in the same way as in the main test, see Section 253. The ends of the measuring beams were thus supported on the slab and the movement of these ends were measured by means of dial gauges which were attached in circular bars, these bars having been driven down into pipes which themselves were 6–7 metres long and had been driven into the ground.

b) Strain measurements were made at a number of points on the top surface along both the measuring beams and along the bisector between them. Strains in the top and bottom at approximately the level of the reinforcement were measured on the side surface of the slab edge under the load. For these measurements, strain gauges were used with a measuring base of 25 cm and of the same type as used in the main tests, see Fig. 25:9, page 142.

The measuring devices and the location of the gauges are shown in principle by Fig. 43:2.[1]) The photograph in Fig. 43:3 shows the loading and test devices.

[1]) The exact gauge location in the various cases is shown by the sketches in association with the result diagrams in the result supplement, Section 93.

Fig. 43:4. Crack patterns round the loading areas at the four edges. The cracks are marked with the number of the loading step causing the crack. Stamping-out cracks are specially marked.

During the four test loadings the load was increased in steps of approx. 2 tons at intervals of about 5 minutes, the load increase generally taking 1 minute and the load was maintained constant for 2 minutes before the dial and strain gauges were read off. During the increase in load, observations were made of crack formation in the slab top surface and the side surface of the loaded edge, the cracks being marked and numbered as they were discovered. The loads causing the first crack which were visually determined in this way as well as the ultimate loads which were objectively estimated with the help of the strain measurements, are introduced in Table 43:3 in Section 433.2 concerning the test analysis.

The load was increased until total collapse occurred due to stamping-out failure which started in the casting joint in all four cases and spread round or in the neighbourhood of the load distribution plate. The stamping-out collapse occurred due to poor shear strength in the casting joint at a lower load than normal but in all the cases concerned it was.

Fig. 43:5. Photograph of the crack pattern and stamping-out failure on edge 4. The concrete load-distribution cylinder is still on the slab and the stamping-out crack is visible inside and in front of this cylinder.

however, so high that it did not influence the normal moment failure. The loads in the case of stamping-out failure are also included in Table 43:3.

The crack patterns close to the four edges are shown in Fig. 43:4. The photograph in Fig. 43:5 shows the crack formation and the stamping-out at one of the edges.

The rest of the test results are stated in connection with the result analysis and discussion in Section 433.[1])

432. Material constants for slab and subgrade

432.1. *Flexural rigidity and ultimate moment*

The four detail test beams with the same section as the edges in the main tests were all tested for positive moment, simply supported with a span of 2.40 metres and with concentrated loads at points at intervals of one third. Deformation at flexure was measured by means of a curvature gauge within the zone between the loading points, except in the case of the beam for edge 1, where the vertical deflection of the centre point was instead measured by means of dial gauges in the centre and at the supporting points. Strain gauges were also used to measure the strain values in the top and the bottom surface as well as on the edge corresponding to the outer edge of the slab and with the same location of the gauges at the "steel level" as in the main test (see Fig. 43:2).

[1]) The complete result of the depression and strain measurements are described in the result supplement, Section 93.

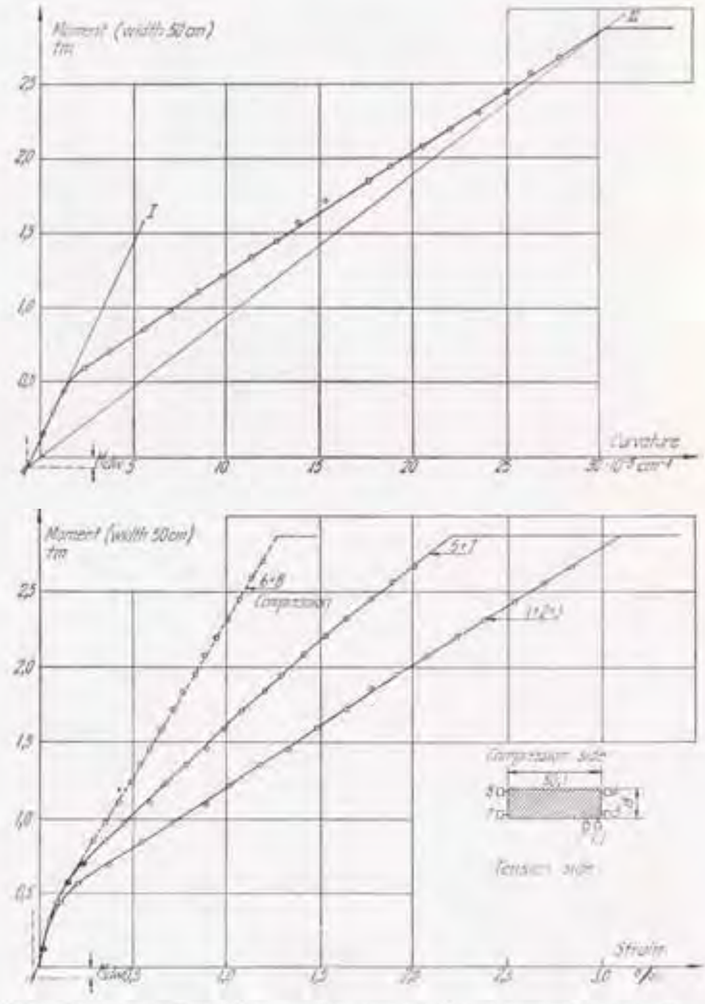

Fig. 43:6. Curvature and strain diagrams for the detail test beam belonging to edge 3. The sketch beside the strain diagram shows the location of the strain gauges in principle. The strain curves show the average value of the readings from the respective gauges. Correction for the dead-weight of the slab has been carried out by moving the origin as shown in the figure.

The results of the beam tests are summarized in Table 43:1.[1]) Fig. 43:6 shows the curvature and strain diagrams for one of the beams. The calculated values from the beam tests of the flexural rigidity in Stage I and II have been introduced in Table 43:1. Those in Stage II are calculated from the secant modulus at the yield point. For the

[1]) The tests are fully described in the form of curvature and strain diagrams in the result supplement, Section 93.

TABLE 43:1. Slab G 2. Data for edge beams according to detail tests and calculations.

Calculations of the negative ultimate moment (at yield point in the top reinforcement) are based on the test values from the negative flexure tests of the detail test beams belonging to the centre loading of slab G 2 according to Table 25:1, these values having been re-proportioned with respect to the differences in (nominal) thickness and reinforcement according to the formulae (43:1). $\bar{\sigma}_e$ is assumed $= 220$ kg/cm².

Detail test unit from edge		1	2	3	4
Section, width 50 cm				 Intensified reinf.	
Positive moment from *tests*	tonm				
at first concrete tension crack		1.05	~ 0.7	0.60	0,60
ultimate moment (reinf. yield)		4.20 to 4.50[1])	2.70 to 3.00[1])	2.95	1.75
Negative ultimate moment from *calc.* and Table 25:1	tonm	1.6	1.0	1.6	—
Flexural rigidity EI from *tests*	kgcm²				
for Stage I		—	$52 \cdot 10^8$	$28 \cdot 10^8$	$26 \cdot 10^8$
for Stage II		$33 \cdot 10^8$	$18 \cdot 10^8$	$9.6 \cdot 10^8$	$7.5 \cdot 10^8$
EI from *calculations*	kgcm²				
for Stage I ($n = 10$)		$190 \cdot 10^8$	$71 \cdot 10^8$	$34 \cdot 10^8$	$32 \cdot 10^8$
for Stage II ($n = 15$)		$35 \cdot 10^8$	$16 \cdot 10^8$	$10.8 \cdot 10^8$	$6.5 \cdot 10^8$
Curvature from *tests*	cm⁻¹				
at commenc. crack formation		—	$2.0 \cdot 10^{-5}$	$2.2 \cdot 10^{-5}$	$2.2 \cdot 10^{-5}$
at yield point		—	15 to $26 \cdot 10^{-5}$[1])	$30 \cdot 10^{-5}$	$24 \cdot 10^{-5}$
Strains from *tests*	‰				
at first concrete crack		~ 0.20	~ 0.18	~ 0.15	~ 0.15
at yield point in					
steel level, tension side		2.2	2.8	2.2	2.2
corresp. on compr. side		-0.7	-0.9	-1.3	-0.8

[1]) The two values represent the commencement and termination of yield in the reinforcement along the inclined beam surface where the various bars have different internal lever lengths.

sake of comparison the theoretical values of the flexural rigidity have also been introduced. The test result and the calculated values agree very well.

The table also includes the values of the positive ultimate moment given by the tests. In the case of the edge beams 1 and 2 part of the reinforcement was situated along the inclined surface (see Fig. 43:1) and the ultimate moment value was therefore more undecided since the upper reinforcement bars yielded first and then the other lying along the inclined surface. The both figures in the table represent the commencement and termination of yield. For a moment failure in the bottom the lower value may be used, this applying to the first yielding bar, while in the calculation according to the ultimate strength method, the higher value may be used.

All the test values have been corrected for the influence of the weight of the beam itself (see Fig. 43:6).

Since the detail beam tests only included tests with positive bending, the negative ultimate moment at the yield point in the top reinforcement must be estimated by means of theoretical calculations. The basis used here consists of the test values when testing for negative deflection of the detail tests belonging to the centre point loading test of the slab, Table 25:1.

The average value $m' = 1\,620$ kgcm/cm obtained according to Table 25:1 has thus been reproportioned for the four edge beam tests whereby, according to GRANHOLM [20, 21]

$$M_{ult} = \sigma_r^{yie} A_r h \left(1 - \frac{p}{2}\right) \tag{43:1 a}$$

where the "relative reinforcement percentage"

$$p = \frac{A_r}{bh^2} \frac{\sigma_r^{yie}}{\sigma_c} \tag{43:1 b}$$

No respect has here been taken to the influence of double reinforcement, and otherwise it has been calculated with nominal values of thickness and covering layer, etc. The values for the ultimate negative moments estimated in this way are introduced in Table 43:1. These values are naturally very unreliable, but they will only be used for estimation of the negative supplementary moment M' of the edge strengthening in ultimate load calculation, whereby unreliability in the value of M' has a very small influence on the ultimate load value.

Finally the table includes approximate values of the measured strain on the tension side of the beams at the commencement of crack formation and the strain values measured against the edge surface at the "steel level" on the tension and compression sides as well as the curvature at the yield point. These values will later be used in the main tests to estimate the loading on the respective edges P_b^{yie} in the case of yield in the bottom. In order to estimate the ultimate load P_t^{yie} due to yield in the reinforcement in the top, the corresponding strain values from the detail tests belonging to the centre loading case must be used (Table 25:1).

432.2. *Soil constants*

For the further analysis, the same values have been used for the soil constants as in the case of the centre loading, namely according to Table 25:2

for low loading: $k = 0.45\ \mathrm{kg/cm^3}$, $C = 250\ \mathrm{kg/cm^2}$

for high loading: $k = 0.30\ \mathrm{kg/cm^3}$, $C = 120\ \mathrm{kg/cm^2}$

It should be reminded that these values are calculated from the depression volume in the centre loading tests for loads which are considerably higher than those occurring during the edge loading tests. The depression and curvature at the lower ultimate loads in the case of edge loading were, however, of roughly the same magnitude as at the higher ultimate load in the case of centre loading, and from this viewpoint the soil constant values stated should be fairly correct. It should be taken into consideration, on the other hand, that the theories and the formulae for the case of edge loading are based on WESTERGAARD's assumption of resilient subgrade while the actual soil properties would appear to be closer to those of elastic subgrade, so that it would perhaps be more correct to determine the soil constant (the k-value) in connection with the actual case of loading. WESTERGAARD himself expresses the opinion that the k-value should be calculated from the depression in the case of the same loading for which it was to be used. The analysis of the depression measurements in the following section will serve to clarify this question.

433. Test results, treatment and theoretical analysis

433.1. *Depression*

The values obtained on the depression dial gauges are used, after correction for the movements of the soil attached dials, to get the depression in the measuring points, and the results are exemplified in Fig. 43:7 and 43:8.[1]) Fig. 43:7 shows the depression lines at some of the loading steps for the most powerfully strengthened and the completely unstrengthened edge while Fig. 43:8 shows the depression in the centre of the four edges. It can be seen that the influence on the depression of a local edge strengthening is comparatively insignificant.

When making a theoretical analysis of the depression measurements, respect must be taken to the edge strengthening. In the theoretical treatment in Section 425 of the strengthened edge, the author has assumed that in the calculation of the elastic radius of rigidity l for the edge zone, it is reasonable to distribute the edge beam flexural rigidity (supplementary rigidity) over a width $= l$ according to the formula (42:17). An analysis of the depression values is very suitable to verify this assumption

[1]) All the measuring values and depression curves are to be found in the result supplement, Section 93.

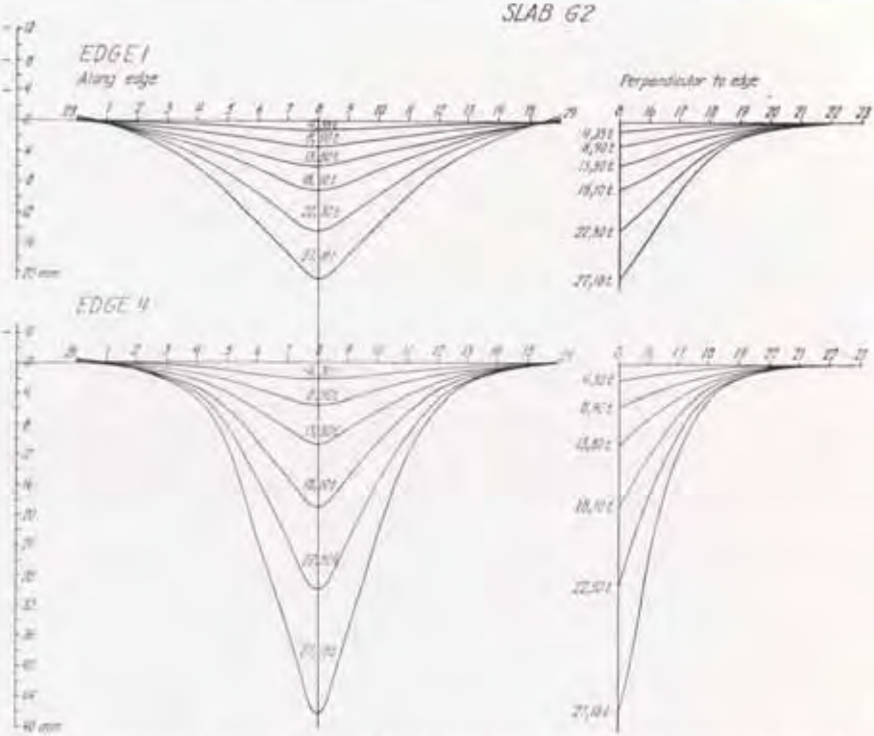

Fig. 43:7. Depression lines at some of the loading steps for the most strengthened edge 1 and the unstrengthened edge 4.

Fig. 43:8. The relationship between the load and the deflection in the centre of the four edges.

while the magnitude of l has a comparatively large effect on the theoretical depression values since it is included in the corresponding expression with a second grade factor.

The calculation of l must be carried out through successive approximation. The calculation is exemplified for edge 1. The flexural rigidity of the edge beam $(EI)_{II} = 33 \cdot 10^8$ kgcm², its width 50 cm. For the rest of the slab the flexural rigidity $D_{slab} = 14 \cdot 10^6$ kgcm²/cm applies according to the Table 25:1, page 149. One then obtains for the edge zone, if it is assumed that $l = 110$ cm,

$$D_k = \frac{1}{110}\,(14 \cdot 10^6 \cdot 60 + 33 \cdot 10^8) = 38 \cdot 10^6 \text{ kgcm}^2/\text{cm}$$

$$l = \sqrt[4]{\frac{38 \cdot 10^6}{0{,}30}} = 106 \text{ cm} \qquad \text{and so on}$$

In a corresponding way the other l-values are calculated for the edges in Stage I and Stage II. These and the corresponding relative load distributions are introduced in Table 43:2.

By the use of these constants, the theoretical depression values in the edge centre have been calculated with the help of the diagrams in Fig. 41:1 and the formula (41:3); the depression values have been calculated partly with a low load, 10 tons (Stage I), partly with loads lying in the neighbourhood of the estimated ultimate loads (see Table 43:3 below). The depression values calculated in this way have, in Table 43:2, been compared with the corresponding measured depression values, and Fig. 43:9 shows also the theoretical and practical centre depression curves for some of the edges. Fig. 43:10 finally shows a comparison of the depression lines for the loads in question, according to theory and tests, for the edge and the normal to the edge, whereby the theoretical lines have been calculated on the basis of the depression diagrams in Fig. 41:1.

The result of this analysis of the depression values shows that fairly good agreement exists between the theory and the tests. One thing that is especially prominent is the good agreement according to Fig. 43:10 between the form of the theoretical and practical depression lines. The assumption that the rigidity of the edge beam shall be distributed over a width l, when calculating the elastic radius of rigidity for the edge zone thus appears to be acceptable when calculating the deformation of the edge, and it thus appears possible to use the same method for the estimation of the soil pressure in the ultimate strength theory. The soil constant values used also appear to be fairly correct.

TABLE 43:2. Slab G 2, edge loading. Depression from tests and theory (resilient subgrade).

Size of slab 8 × 8 m, thickness 15 cm, double-reinforced. Loading area of semi-circular extent with radius $c = 40$ cm.

Constant values for soil (resilient) and interior of slab from Table 25:1 and 25:2.

$$\text{for low loading } k = 0.45 \text{ kg/cm}^3 \; D_{I} = 70 \cdot 10^8 \text{ kgcm}^2\text{/cm}$$
$$\text{for high loading } k = 0.30 \text{ kg/cm}^3 \; D_{II} = 14 \cdot 10^8 \text{ kgcm}^2\text{/cm}$$

Slab G 2, edge no.	1			2			3			4		
Section							Intensified reinf.					
DATA FOR THE EDGES												
Flex. rigid. for 50 cm width edge beam kgcm²												
Stage I	$190 \cdot 10^8$ [1]			$52 \cdot 10^8$			$28 \cdot 10^8$			$26 \cdot 10^8$		
Stage II	$33 \cdot 10^8$			$18 \cdot 10^8$			$9.6 \cdot 10^8$			$7.3 \cdot 10^8$		
Edge zone rad. of elast. rigid. l_{edge} cm												
low loading	140			117			112[1]			112[1]		
high loading	106			96			86			83		
Rel. load. distrib. $a = \frac{c}{l}$												
low loading	0.29			0.34			0.36			0.36		
high loading	0.38			0.42			0.47			0.48		
DEPRESSION {F from tests, T from theory}	F	T	F/T	F	T	F/T	F	T	F/T	F	T	F/T
Centre edge depression cm												
at 10 tons (Stage I)	0.38	0.42	0.90	0.52	0.62	0.84	0.59	0.67	0.88	0.62	0.67	0.88
at 25 tons (Stage II)[2]	2.60[2]	3.12[2]	0.83	2.40	3.10	0.78	3.75	3.75	1.00	3.77	4.00	0.94

[1]) Here is used the same value as for the interior of the slab according to Table 25:5.
[2]) For edge 1, the depression is calculated at 30 tons which is nearer the ultimate load value.

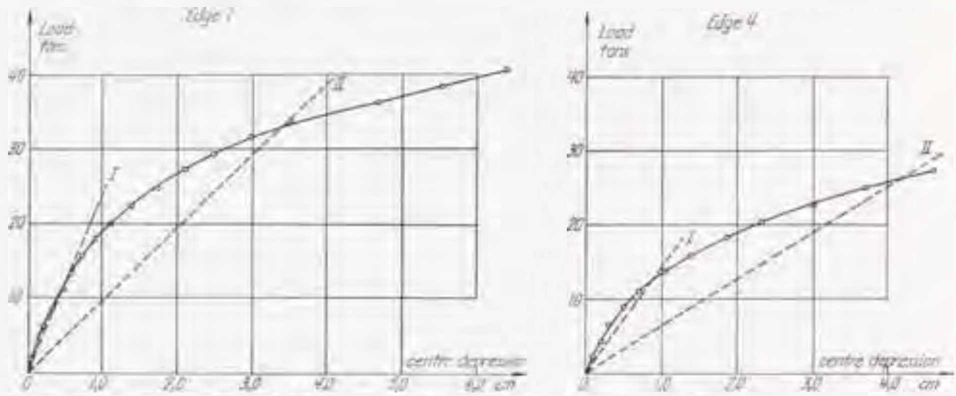

Fig. 43:9. The relationship between the load and the deflection in the edge centre according to tests and theory for loading on the edges 1 and 4. The theoretical curves are calculated according to the formula (41:3) with the constants for the slab and the subgrade in accordance with Stage I ($\nu = 0.15$) and Stage II ($\nu = 0$). For the calculation of the rigidity of the strengthened edge, the increased rigidity is assumed to be distributed over a width equal to the elastic radius of rigidity l.

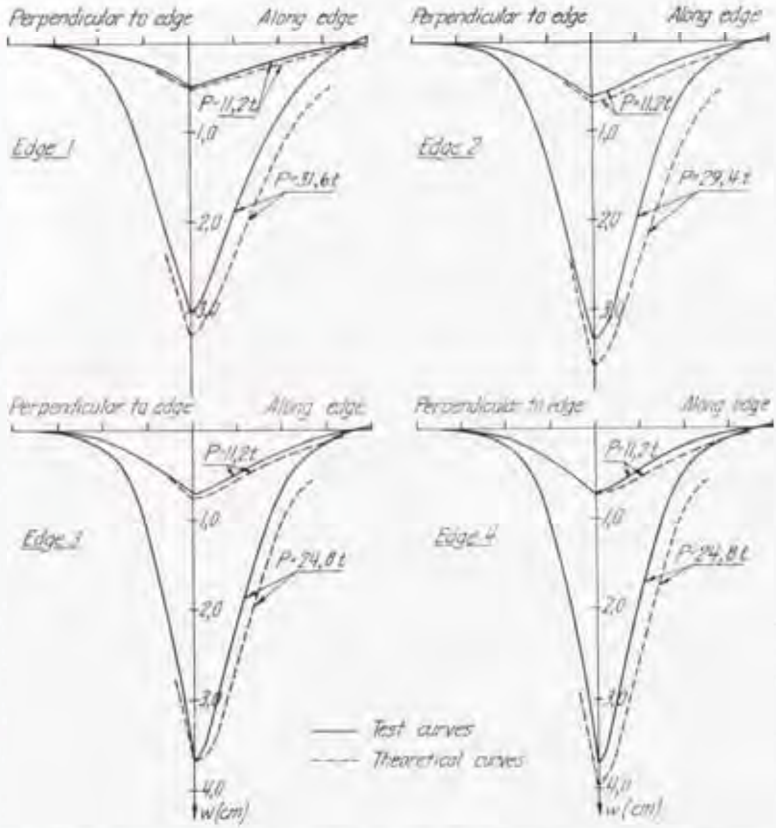

Fig. 43:10. The depression lines along the edge and perpendicular to the edge according to test and theory for some of the loading steps when loading the edges on slab G2. The theoretical depression lines have been calculated with the help of the depression diagram in Fig. 41:1 and the formula (41:3). For the lower loading step, the constants for the slab and the subgrade have been calculated according to Stage I and for the higher loading step according to Stage II, see also the caption to Fig. 43:9. Since the figure is mainly intended to show the good agreement in curve form between the theoretical and experimental depression lines, load steps have been selected to give good agreement with the theoretical centre depression. The theoretical curves actually apply to an infinitely long edge so that the theoretical curves nearest the slab edges should be relatively more depressed than the corresponding test curves. The figure also shows that this is generally the case.

433.2. *The moment and the ultimate load according to the elasticity theory*

The increase in moment and the various failure phenomena in the edges of the slab can be followed by a study of the strain measurements on the top surface of the slab and on the edge surface of the slab under the loading point. The readings of the strain gauges, compiled in Fig. 43:11, clearly marks the commencements of crack formation due to tension

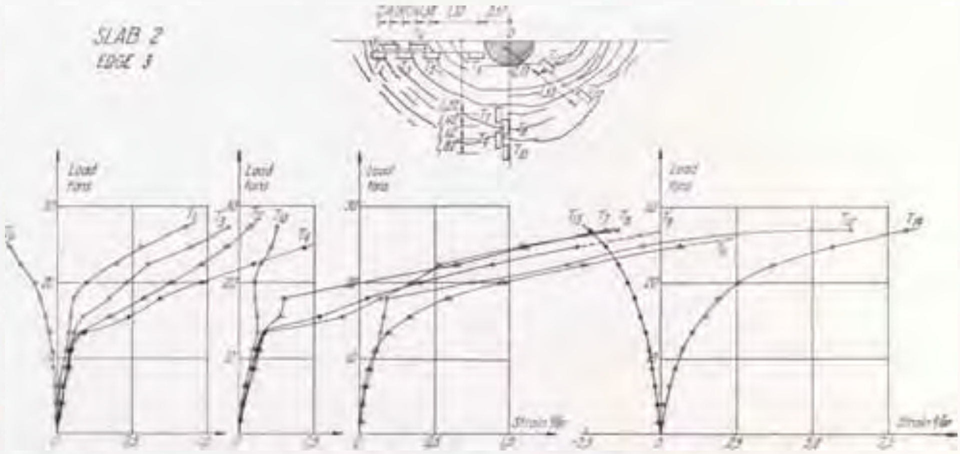

Fig. 43:11. The results of the strain measurements from the test loading of edge 3. Over the strain curves there is a sketch of the location of the gauges with the cracks marked in, and the strain curves are grouped after the location. According to the detail tests from the case of centre loading (Table 25:1), strain in the top surface at yield point is $2.4-2.5\ ^0/_{00}$ and it is found from the strain curves for the gauges T_8 and $T_{11}-T_{12}$ respectively that the corresponding ultimate load is about 26 tons. The two gauges T_{13} and T_{14} on the outside of the edge (see Fig. 43:2) can be utilized for the determination of moment and ultimate loads in the centre of the edge by comparing with the gauges located in a similar position on the detail test beams.

failure in the concrete, but the difficulties are considerably greater concerning the determination of the load when yield in the top reinforcement begins. The magnitude of the reading depends namely on the exact distance of the reinforcement from the concrete surface as well as the distribution of the cracks. The strain gauges which, for example, included two cracks between the measuring points, produced altogether excessively high readings. The estimation of the load at the commencement of yield in the bottom reinforcement and at yield in the top reinforcement are thus necessarily exceptionally unreliable.

The results of this estimation which is based on a comparison between the strain measurements in the main loading tests on the edge surfaces of the slab and in the flexural tests on the corresponding detail test beams, are shown by Table 43:3. Since no tests with negative flexure were carried out on the detail test beams belonging to the edge loading tests, then estimation of the ultimate load P_t^{yie} at yield point in the top reinforcement is derived from the detail tests belonging to the centre loading test where, according to Table 25:1 for the tests in question, a strain in the top of 2.4 to $2.5\ ^0/_{00}$ was measured at the negative moment failure. Since these measurements are not applicable to the thickened

TABLE 43:3. Slab G 2, edge loading. Loads at concrete crack formation and reinforcement yield in bottom and top surface, estimated from curvature and strain measurements, as well as visually observed crack loads and loads at stamping-out failure.

The two figures for loads estimated from the strain measurements, given in some cases, show the lowest and the highest load values judged in accordance with the various groups of gauges (see Fig. 43:2).

Critical values of curvature and strain at bottom surface failure P_b^{cr} and P_b^{yie} from Table 43:1. Critical values of strain at top yield load P_t^{yie} are taken from Table 25:1 as being 2,4-2,5 $^0/_{00}$.

Edge no.	P_b^{cr} tons			P_b^{yie} tons		P_t^{cr} tons		P_t^{yie} tons	Stamping-out failure
	Curvature measurem.	Strain measurem.	Visual	Curvature measurem.	Strain measurem.	Strain measurem.	Visual	Strain measurem.	
1	—	6 to 9	13	—	21 to 24	16 to 18	—	27 to 31	41
2	5	5	15	17	22	14	18	~25[1])	32
3	4.5	4	11	19	19 to 21	13	18	26	27
4	4	4	13	16	16 to 17	11	13	23 to 24[2])	30

[1]) *Very unreliable* value due to the fact that the strain gauge T_7 was displaced at the higher loading steps. The measurements for T_7 are exterpolated from the movement of the corresponding gauges at edge 3. The load value has also been judged from gauges T_8 and T_{16} compared with T_{10} on edge 1 at ultimate load.

[2]) The lower load value was obtained by exterpolation from the strain measurements from T_{12}.

edges, then failure in the top surface has been estimated from the basis of the strain gauges at right angles to the edge and in the bisector between the edge and the normal (see Fig. 43:2). In the loading test on edge 2, some of the strain gauges on the top indicating strains in the crack where the yielding began were displaced during the testing. The estimation of the ultimate load for this edge was therefore further complicated; the figures given in the table are based on a comparison between the readings of some of the strain gauges at this edge, which were not disarranged and the corresponding strain gauges on edge 1.

The loads at concrete tensile failure and reinforcement yield in the bottom under the loading centre can be estimated also from the curvature of the slab edge. Although no special curvature gauges were used in these tests, the curvature in the centre of the slab edge can be calculated from the differences between the depression values from the dial gauges nearest the centre. Here the five measuring points nearest the centre have been used and the curve form has been agreed in the form of 4-grade parabola (see Fig. 24:7, page 91).[1])

The curvature values obtained in this way have been compared with the curvature values according to the detail tests from edges 2, 3 and 4

[1]) The complete results of the curvature calculations are shown in the result supplement, Section 93. When calculating the centre curvature, due respect has been taken to the fact that the distances between the five measuring points were not identical, see Fig. 43:2, as opposed to Fig. 24:7.

at concrete tensile failure and reinforcement yield failure (see Table 43:1) and the P_b^{cr} and P_b^{yie} obtained in this way are shown by Table 43:3. They agree generally fairly well with the values that could be estimated from the strain measurements.

The last column in the table includes the load at which shear failure occurred at the casting joint between the original circular slab and the newly cast edges. This definite collapse, which corresponds to stamping-out failure for the interior load case, was influenced considerably in these tests by the poor shear strength in the cast joint. In all cases the loads in question, however, were above the estimated loads for top surface failure.

Analysis of the depression measurements showed that WESTERGAARD's formulae give the depression behaviour for the edges fairly correctly, in spite of the fact that these were strengthened in opposition to the conditions of the theory. In order to examine whether this is also the case when calculating the moments, the formula (41:4) and the corresponding diagram in Fig. 41:2 were used to calculate the loads P_b^{cr} and P_b^{yie} at failure in the bottom. In this connection the l values calculated earlier have been used for the calculation of the relative load distribution. The positive ultimate moments m_{cr} and m_{yie} in the case of concrete tensile failure and bottom reinforcement yield respectively have been calculated from the results of the flexural tests on the detail test beams, see Table 43:1. In the case of the thickened edges it is, of course, not correct to distribute uniformly the ultimate moment values according to the table over the beam width 50 cm. since the height of the beam and the distribution of the reinforcement vary considerably over the width. The moment can be estimated to be distributed in the same way as the flexural rigidity (moment of inertia), and the author has calculated the ultimate moment values m_e in question close to the actual edge of the slab according to the expression

$$m_e = M_{\text{beam}} \frac{i_e}{I_{\text{beam}}} \tag{43:2}$$

where, according to Fig. 43:12

M_{beam} = the total ultimate moment of the edge beam according to Table 43:1 (the *lower* values of the yield moment)

I_{beam} = the total moment of inertia of the edge beam (see Table 43:1)

i_e = the moment of inertia of the edge strip per unit width around an axis coinciding with the centre of gravity axis of the complete edge beam (see Fig. 43:12).

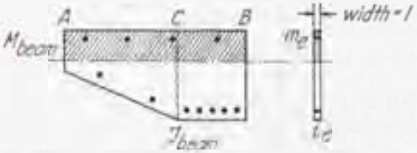

Fig. 43:12. Sections at the calculation of the moment of inertia in formula (43:2). The example shown in the figure corresponds nearest to the edge 1 in Stage II, and the "edge strip" here corresponds to beam section CB concerning reinforcement, etc.

In this way it is possible to calculate the ultimate moment values at the concrete tensile failure (Stage I, $n = 10$) and reinforcement yield (Stage II, $n = 15$) and the values are shown in Table 43:4. This method does not claim to have any high degree of correctness; for example no respect is taken to the twisting at the flexion of the unsymmetrical edges which obviously exists, nor to the actual appearance of the concrete compression zone.

The ultimate moment values used would, however, appear to be sufficiently correct to show that the theoretical ultimate loads P_b^{cr} and P_b^{yie} for the thickened edges 1 and 2, as shown in Table 43:4, show particularly poor agreement with the test loads. These have been introduced into the table with the values taken from Table 43:3, whereby the lowest and highest load values according to the various strain and curvature measurements have been included. It is obvious that WESTERGAARD's moment formulae over-estimate the strengthening properties of an edge beam to a great extent. This is also quite in accordance with what could be expected since the thickened and stiffened edge must "accumulate" a higher moment than the unthickened for which the formulae and diagrams apply. For the unthickened edges 3 and 4, agreement between the theoretical and practical results are also fully satisfactory.

Calculations have also been carried out for the soil hypothesis of elastic subgrade, whereby the formula (41:7) and the diagram 22:7 for the load on the interior of the slab have been used. The elastic radius of rigidity l_e for the stiffened edges has been calculated according to (42:27 b and c) completely analogous with the l_k-value for resilient soil. As Table 43:4 shows, quite similar results are obtained, only with some higher theoretical loading values; for the completely unstrengthened edge 4, which best agrees with the conditions of the theory, the assumption of elastic subgrade means better agreement with the test values.

The definite ultimate load P_t^{yie} due to yield in the top reinforcement in the case of strengthened edges gives even worse agreement when calcu-

TABLE 43:4. Slab G 2, edge loading. Crack and yield loads according to tests and *elasticity theory* (resilient or elastic subgrade).

Slab size 8×8 m, thickness 15 cm, double reinforcement. Load area semi-circular with radius $c = 40$ cm.

Constant values for slab and soil as shown in Table 25:5.

with low loading $k = 0{,}45$ kg/cm³; $C = 250$ kg/cm² $D = 70 \cdot 10^{8}$ kgcm²/cm
with high loading $k = 0{,}30$ kg/cm³; $C = 120$ kg/cm² $D = 14 \cdot 10^{8}$ kgcm²/cm

Slab G 2, edge	1			2			3			4		
Section							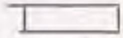 Intensified reinforcement					
DATA FOR THE EDGES (see also Table 43:2)												
Elastic radius of rigidity l cm												
$l_k = \sqrt[4]{\frac{D}{k}}$ low loading	140			117			112[1])			112[1])		
high loading	106			96			86			83		
$l_e = \sqrt[3]{\frac{2D}{C}}$ low loading	117			89			83[1])			83[1])		
high loading	89			78			67			62		
Relative load distribution $a = \frac{c}{l}$												
$a_k = \frac{c}{l_k}$ low loading	0.29			0.34			0.36			0.36		
high loading	0.38			0.42			0.47			0.48		
$a_e = \frac{c}{l_e}$ low loading	0.34			0.45			0.48			0.48		
high loading	0.45			0.51			0.60			0.65		
Ultimate moment from (43:1) kgcm/cm												
at bottom concrete failure m_{cr}	~5600			~2600			1200			1200		
at bottom reinf. yield m_{yie}	~16200			~12000			5900			3500		
at top concrete failure m_{cr}	—			—			—			680[2])		
at top reinf. yield m_{yie}	~3600			~2300			3200			1620[2])		
CRACK AND YIELD LOADS:	F	T_k	T_e	F	T_k	T_e	F	T_k	T_e	F	T_k	T_e
F from tests (Table 43:3); T_k from resil. subgr. theory; T_e from elast. subgr. theory												
Load in tons												
at bottom crack P_b^{cr}	6-9	14.4	16.5	~5	7.3	9.0	4-5	3.5	4.4	4—6	3.5	4.
at bottom reinf. yield P_b^{yie}	21-24	52.3	60.0	17-22	41.8	48.0	19-21	22.5	26.7	16	13.6	16.
at top crack P_t^{cr}	16-18	—	—	14	—	—	13	—	—	11	11.3	—
at top reinf. yield P_t^{yie}	27-31	60.0	—	~25[3])	38.3	—	26	53.4	—	23-24	27.0	—

[1]) Here the same values are taken as for the interior of the slab, see Table 25:5.
[2]) From Table 25:5.
[3]) Very unreliable value, see Table 43:3, note 1).

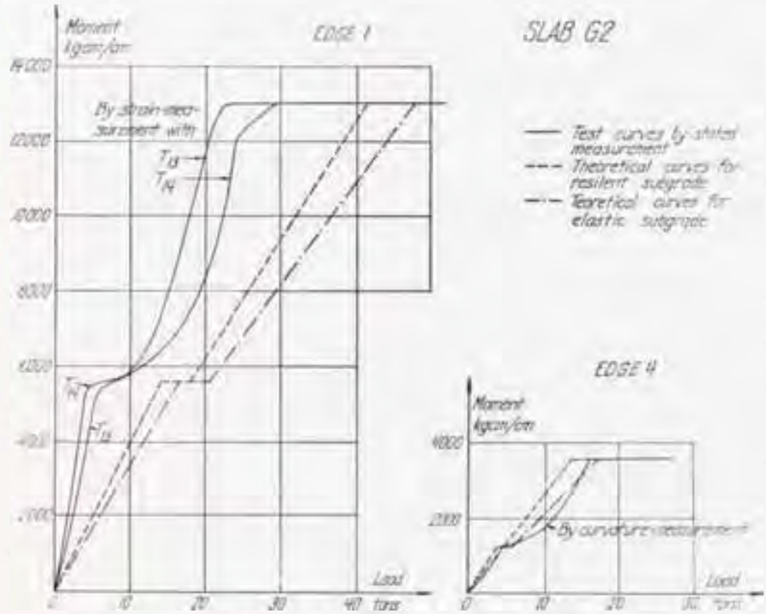

Fig. 43:13. The relationship between the load and the moment in the centre of the edge according to the tests and the elasticity theory for loading on edges 1 and 4. For the strengthened edge 1, the test curves has been obtained by comparison with the strain measurements on the outside of the slab edge and the corresponding measurements from the detail tests belonging to it (see Fig. 43:2 and 43:6 respectively), whereby the distribution of the moment over the unsymmetrical edge beam width is assumed to be proportional to the distribution of the moment of inertia. For the unstrengthened edge 4, the test curve has been obtained in the corresponding way from the curvature measurements. The theoretical relationship has been calculated for the hypotheses concerning both resilient subgrade (according to formula 41:4) and elastic subgrade (according to formula 41:7 and diagram 22:7), whereby the constants for the slab and the subgrade for both Stage I ($\nu = 0.15$) and Stage II ($\nu = 0$) have been used. See also the caption to Fig. 43:9.

lated according to the elasticity theory methods, this being shown by the last lines in the table. The theoretical values are obtained according to formula (41:9), whereby the negative ultimate moment values for the thickened edges have been calculated, on the basis of the corresponding ultimate moment values according to Table 43:1, in the same way as the positive moments have been obtained, by estimation through the formula (43:2). In this case fair agreement with the test loads was *only* obtained in the case of the completely unstrengthened edge 4.

The conditions discussed above are further clarified in Fig. 43:13 which shows the relationship curves between the load and the moment in the centre of the edge according to theory and tests for the edges 1 and 4. The test curves have been obtained according to the methods shown

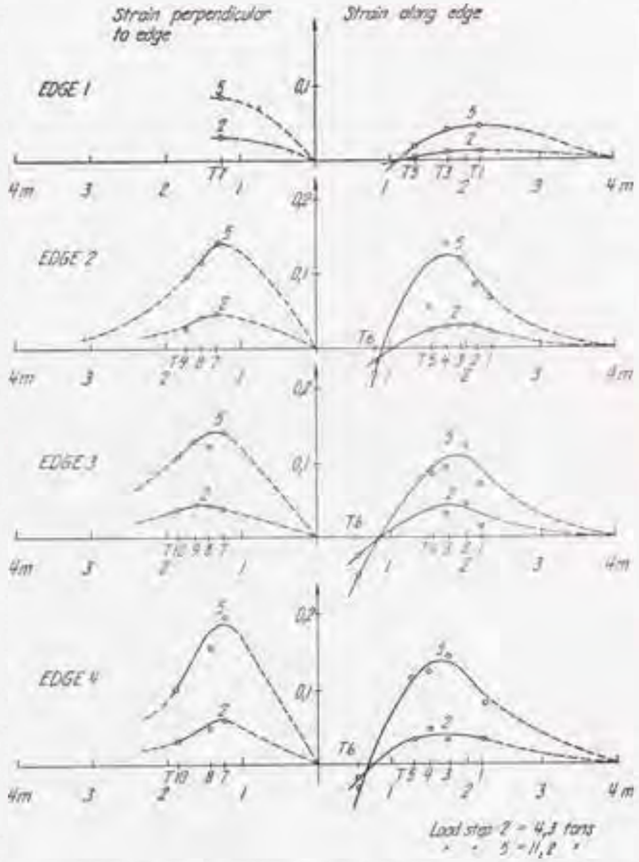

Fig. 43:14. Strain distribution at some of the loading steps for the four edge loadings along the edge and perpendicular to the edge. The slab is *uncracked* in the top surface at these loads. The results from gauges with obviously erroneous movements (fitting or function errors) have been eliminated.

in Fig. 24:22, page 108, by comparing the strain values in the slab edge surface for edge 1 and the curvature in the centre of the edge for edge 4 with the corresponding measurements obtained with the respective detail test beams, whereby the moment values for slab edge 1 have been given according to (43:2). The figures clearly show that agreement between the theory and the tests at edge 1 is quite non-existent while the agreement in the case of edge 4 is good and best for the assumption that the soil is elastic.

The strain measurements can also give a certain idea of the moment or stress distribution in the rest of the slab. In Fig. 43:14 the strain values along the edge and at right angles to the edge at some of the loading steps have been compiled for the four edges. It can be seen that the strain (and thereby the moment) increases rather more rapidly in the section at right angles to the edge than along the edge, particularly in the case of the strengthened edges but also in the case of the unstrengthened edge 4.

For the last-mentioned edge, the moment distribution along the edge from the tests has been estimated from the strain curves according to Fig. 43:14 and has been compiled together with corresponding theoretical curves which were calculated according to the diagram in Fig. 41:2. The results are shown in Fig. 43:15. Agreement is fairly good but it should be pointed out that the theoretical curve is here based on the assumption that the subgrade is resilient and it is conceivable that this perhaps less correct assumption of the soil properties can contribute towards the fact that agreement between the theory and the tests is not completely good.

433.3. *The ultimate strength theory*

It is thus obvious that the elasticity theory can *not* be used for the calculation of the effect of strengthening at the free edge. In the following it will be examined if a better result can be obtained through the ultimate strength theory.

When applying the methods in Section 425 to the test results, it should be observed that the edge reinforcement M and M' respectively in the edge loading formulae only consists of the *difference* between the ultimate moment of the edge beam and the ultimate moment of an identically wide unstrengthened edge strip. For the unstrengthened slab, the same ultimate moment values are assumed as those applying for the central parts of the slab according to Table 25:1, thus

$$m = 2\,900 \text{ kgcm/cm}$$

$$m' = 1\,600 \text{ kgcm/cm}$$

$$\frac{m}{m'} = 1.8$$

The calculation has been carried out according to the methods shown in Section 427, whereby the soil is considered to behave as both resilient and elastic subgrade. In the latter case it has been thus assumed according to 427, page 271, that the same formulae and diagrams for the ultimate load calculation can be used as for the "basic case" of resilient soil, if the value for the relative load distribution $a_e = \frac{c}{l_e}$ is used, as a consequence of the l_e-value according to (42:25 b) for elastic soil.

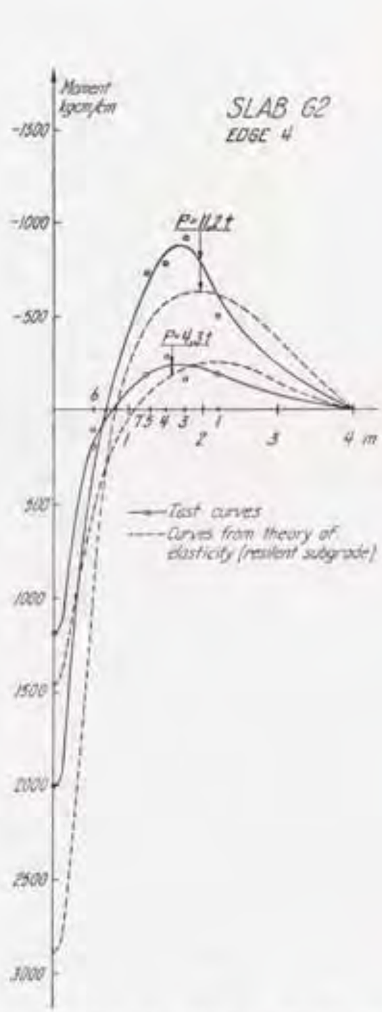

Fig. 43:15. Moment distribution along the edge according to test and theory when loading edge 4. The test curves have been obtained from the strain measurements along the slab edge, whereby the moment values with the exception of the centre value have been calculated from strain values through the relationship

$$m = \varepsilon \frac{2D}{h}$$

The theoretical curves have been calculated with the help of the diagram in Fig. 41:2 and the formula 41:4 with the constants according to Stage I for a load of $P = 4.3$ tons and according to Stage II for a load of $P = 11.2$ tons.

TABLE 43:5. Slab G 2, edge loading. Ultimate loads at yield in top reinforcement from tests and the *ultimate strength theory*.

Slab size 8 × 8 m, thickness 15 cm, double-reinforced. Load area semi-circular with radius $c = 40$ cm.

Constant values for slab and soil from Table 43:4.

Ultimate moment values for slab outside edges as shown in Table 25:1:

positive ultimate moment $m = 2900$ kgcm/cm
negative ultimate moment $m' = 1620$ kgcm/cm

at yield point for the reinforcement in question.

Slab G 2, edge	1	2	3	4
Section			 Intensified reinforcement	
DATA FOR THE EDGES (see also Table 43:2)				
Ultimate moment for entire edge beam (width 50 cm) tm				
positive M_a	4.2-4.5	2.7-3.0	2.95	1.75
negative M_a'	1.6	1.6	1.6	—
Supplementary moment for edge strengthening tm				
positive M	3.05	1.55	1.50	0
negative M'	0.80	0.19	0.79	0
$M + M'$	3.85	1.74	2.29	0
Relative load distribution $\alpha = \frac{c}{l}$ (l from Table 43:2)				
for resilient soil α_k	0.38	0.42	0.47	0.48
for elastic soil α_e	0.45	0.51	0.60	0.65
ULTIMATE LOADS at top yield P_{ℓ}^{yie}				
From tests tons	27-31	~25[1])	26	23-24
From theory tons				
for resilient soil	24.4	22.5	24.9	20.0
for elastic soil	27.0	24.9	28.9	23.9

[1]) Very unreliable value, see Table 43:3, note 1).

The result of the calculations for the four edges are shown in Table 43:5 where the theoretical values have been compiled together with the test values according to Table 43:3. Agreement is as good as can be expected with respect to the unreliability in the ultimate load determination and the approximations and simplified suppositions on which the theoretical ultimate load formulae are based. The closest agreement to the test values are obtained in accordance with the soil hypothesis of elastic subgrade.

It should be pointed out that in these tests, a certain incomplete plastification in the positive yield lines must be assumed. According to what was shown by the theoretical treatment, this should not influence the theoretical ultimate load values to any great extent although it naturally contributes to a certain degree of the unreliability in these values.

It seems to be clear, however, that the ultimate load formulae show the strengthening effect of the edge beam fairly correctly. Both the tests and the theoretical values show that this effect is surprisingly small. The best effect of the strengthening is obviously obtained for edge 3, where the edge has been given an increased ultimate moment but not such a large degree of increased rigidity.

44. Summary and General Viewpoints

The tests discussed in the previous section consist naturally of too little test material to provide basis for a definite judgement of the formulae and calculation methods presented in Section 41 and 42, as well as their applicability to free edges and joints in reinforced concrete pavements. The test results give, however, certain comparatively clear indications for this judgement, and the conclusions that can be drawn will be summarized and further discussed in this section. Further edge loading tests are described and analyzed in Part 5.

As far as can be judged in this respect, the tests have shown that the depression formulae for edge loading and the corresponding diagrams produced by WESTERGAARD can be well applied to reinforced pavements, if the flexural rigidity of the slab is calculated on the basis of Stage II. The conclusion is thus here the same as in the case of the depression due to an interior load, and the formulae and diagrams give also here a fairly good idea of the deformation even up to such high loads that the reinforcement under the loading point has assumed a plastic state; depression calculations according to the elasticity theory can thus (at least in the case of resilient soil) be used as a basis for the estimation of the distribution of soil pressure in the case of ultimate load calculations based on the yield line theory. In cases where there is an edge which has been stiffened by thickening or the insertion of reinforcement strip, then the deformation can be calculated as for a uniformly rigid edge with a rigidity corresponding to that obtained if the strengthening is assumed to be uniformly distributed over an edge zone with a width equal to the elastic radius of rigidity l.

Concerning the calculation of the moments in the loading centre in the case of a load on a free edge or a joint, then WESTERGAARD's moment formulae (41:4 and 41:6) and the corresponding diagrams in Fig. 41:2 would appear to be applicable only for an edge without local edge stiffening or, where the edge is strengthened, without the rigidity being significantly increased in this way. The assumption of the author that the relationship between the maximum moment of edge loading and interior loading has the same value, no matter whether the subgrade is resilient or elastic, would appear to be correct, and the formulae (41:7) and (41:8) based on this assumption would thus appear to be applicable in the case of both resilient and elastic soil. When designing a joint or a free edge for a reinforced pavement based on failure due to the beginning of yield in the bottom reinforcement under the loading centre, then it should be possible to use the moment formulae quoted above according to the elasticity theory only in such cases where the edge is unstrengthened or where it has not been given a significantly increased rigidity due to strengthening, for example through moderate increase of the bottom reinforcement. In the latter case, strengthening must naturally be carried out in a sufficiently wide zone of the edge so that the moment inside this zone cannot produce failure in the unstrengthened slab, and it must be known or determined how the moment decreases at a distance from the edge.[1] It should be reminded that the formulae and the diagrams for this case are based on WESTERGAARD's *later* moment formulae (41:4) and (41:6); the original moment formula (41:2) — unfortunately the one most common in handbook literature and design standards — has been shown to give erroneous results.

It is, however, the opinion of the author that the design for the case of edge loading, in the same way as for the case of interior loading, should be based on the *definite ultimate load*, which gives failure in the top through formation of cracks or yield in any top reinforcement. The reasons for this, which are developed in more detail in Section 31, apply fully also for this case of loading. Calculating an ultimate load defined in this way, it would appear, judging from the tests (and also theoretical considerations), that the elasticity theory formulae (41:9) for the negative maximum moment can only be used for unstrengthened edges on condition that the plastic state in the bottom has not been reached (or is very insignificant) at the load in question. In *all cases*, however, the ultimate strength methods according to section 42, which are based on the yield line theory (as well as the assumption that the soil pressure can be estimated according to the elasticity theory), appear to give a good idea of the definite ultimate load and of the influences of various types of edge strengthening methods.

It is certainly obvious that the conditions are worse in the case of edge loading than in the case of an interior load as far as the yield line theory assumptions concerning a completely plastification in the positive yield lines is to correspond to the behaviour in practice. This depends upon the fact that the negative moment is greater in relation to the

[1]) An investigation of this kind can be carried out to a certain extent on the basis of the PICKET-RAY influence charts [57] which also give the moment values at a distance $l/2$ from the edge.

positive moment in the case of edge loading than it is in the case of interior loading, and the negative failure crack tends therefore to occur relatively earlier before a plastification in the bottom has reached so far. Both theoretical examinations and test results show, however, that an incomplete plastification of this type in the positive yield lines influences the ultimate load to a comparatively small extent; a calculation in such cases according to the usual formulae, which assume a completely plastification, only results in a moderate increase of the ultimate load value.

The tests show that the formulae and diagrams derived according to the principles of the yield line theory can be used for both resilient and elastic subgrade; the only difference in this respect is that the relative load distribution $\alpha = \frac{c}{l}$ is calculated on the basis of the l-value for the type of subgrade in question.

The four tests on the edges on slab G2 with various types of strengthening indicates quite clearly that local strengthening is relatively ineffective. Apart from this, thickened edges imply considerable difficulties from the point of view of moulding forms and reinforcement. The simplest and most effective type of edge reinforcement consists clearly of an edge zone of more closely spaced reinforcement, possibly supplemented by a powerful reinforcement band nearest the edge. The enlarging of the reinforcement should cover an edge zone which is so wide that the failure line figure considered falls within it; the height of the failure line triangle r_0 gives an idea of the width of strengthening required.

In most cases the pavement consists of a single-reinforced slab and it is naturally simplest in this case, if, with strengthening along the edges and joints, only an increase in the bottom reinforcement can be considered satisfactory. In order to investigate the extent to which this is possible, the author has in Table 44:1 calculated comparative moment values for a single load with various load distribution, affecting partly the interior of a pavement, partly a joint (with half the load on each side of the joint) and partly close to a free edge (see fig. 44:1, cases 1—3). In the table it has been assumed that the negative ultimate moment m' in the three loading cases is identical (single-reinforced slab), and the relationship between the required positive ultimate moments in the interior of the slab m as well as on the joint and the edge m_e have been calculated and compared for various values of the negative ultimate moment.

The table shows that, in the case of a joint, there should be no difficulty whatsoever in producing the necessary strengthening by enlarging

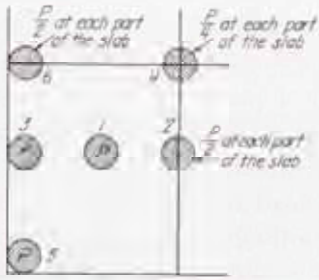

Fig. 44:1. Various loading cases for a circularly distributed load on a pavement divided up into several section by means of joints which cannot transfer moment.

the reinforcement within a zone along the joint. The necessary positive ultimate moment along the joints is in normal cases rather slightly higher than the positive ultimate moment in the interior of the slab. Concerning the free edge, the difficulties in producing the necessary strengthening in the same way can be greater. It is often necessary here to further strengthen the edge, preferably without edge thickening however, but instead, for example, through a reinforcement band along the edge or with locally inserted top reinforcement within the strengthening zone. Such a top reinforcement (or, in the case of double-reinforced pavements, intensification of the top reinforcement) has the best effect if the reinforcement is placed with the bars at right angles to the edge so that the m'-value is increased, this being easily shown by an examination with the help of the diagrams in Fig. 42:11.

TABLE 44:1. Moment values according to the ultimate strength theory for a load on the interior of a slab as well as on a joint and a free edge (cases 1, 2 and 3 respectively in Fig. 44:1). The positive ultimate moments are calculated for at the same value of the negative ultimate moment in all three cases.

The ultimate moment values are calculated according to the diagrams in Fig. 42:11.

$a=\frac{c}{l}$	$\frac{m'}{P}$	Load on centre of slab P		Load on joint edge $\frac{P}{2}$			Load on slab edge P		
		$\frac{m+m'}{P}$	$\frac{m}{P}$	$\frac{m_e+m'}{P}$	$\frac{m_e}{P}$	$\frac{m_e}{m}$	$\frac{m_e+m'}{P}$	$\frac{m_e}{P}$	$\frac{m_e}{m}$
0.2	0.06	0.118	0.058	0.138	0.078	1.34	0.362	0.302	5.20
	0.05	0.118	0.068	0.160	0.110	1.62	0.420	0.370	5.44
	0.04	0.118	0.078	0.201	0.161	2.06	0.490	0.450	5.77
0.5	0.04	0.089	0.049	0.108	0.068	1.39	0.182	0.142	2.90
	0.03	0.089	0.059	0.137	0.107	1.81	0.219	0.189	3.20
	0.02	0.089	0.069	0.202	0.182	2.64	0.258	0.238	3.45
0.9	0.03	0.064	0.034	0.066	0.036	1.06	0.097	0.067	1.98
	0.02	0.064	0.044	0.091	0.071	1.61	0.113	0.093	2.11

When judging the values in Table 44:1 and when designing the edges, one may make use of a fact which has not been considered in the table but is favourable for the edge, namely the influence of temperature decrease and shrinkage. This influence, which will be treated in Part 6, can be assumed to decrease the negative ultimate moment m' in the interior of the slab since part of the tensile strength of the concrete is engaged by the tensile stresses resulting when the slab contracts due to temperature decrease and shrinkage. Close to a free edge or a joint, which allow contraction, there are no such stresses and no reduction of m'. In this way there is a considerably higher value of m' (but *not* m'_s) for an edge and a joint than for the interior of the slab also in the case of slabs with completely unstrengthened top surface at the edge (such as single-reinforced slabs). One should also take into consideration the viewpoints mentioned earlier that loading on a free edge is a very exceptional case of loading, so that when designing the edge it may be permissable to have a lower safety factor than for the rest of the slab.

Finally, concerning the case of a load on a free corner or a joint intersection, no tests with these cases have been carried out on reinforced pavements to show the applicability of the formulae stated (41:10) and (41:11). It is, however, obvious that the ultimate load here depends *only* on the *negative* ultimate moment, while practically no positive moment occurs in this case of loading. With failure in at least single-reinforced pavements there will be no plastification whatsoever in the slab but failure will occur as soon as the flexural strength of the concrete has been exceeded, thus completely in accordance with the definition of failure given in the elasticity theory. In this case of loading it should therefore be possible to allow considerably lower safety factors than for the other cases of loading with "plastic" failure, and under such conditions no extra reinforcement is generally needed in the corners. See also the design example in Section 722.

5. Field Tests in Connection with Concrete Pavement Work on Airports

51. The Väsby Tests (Series V)

511. A review of the tests

During the years 1944 and 1945 a region at Upplands Väsby north of Stockholm which was intended for use for an Atlantic airport project, was the site of a comparatively extensive test programme with testing of pavement slabs on a full scale. The programme included mainly plain concrete slabs but was supplemented during the autumn of 1945 with a series of four reinforced slabs, A, B, C and D, carried out in accordance with a programme drawn up by the author. The slabs were designed on the basis of the earlier outline to the ultimate load method which was available at this time. The natural soil consisted of relatively loose clay down to some considerable depth.

The intention was that all four slabs were to be tested up to an ultimate load with cracks in the top surface with loading both on the centre of the slab as well as on two opposite edges. Due to the fact that the test device was not originally capable of producing a sufficiently high degree of loading, in the cases of the slabs A and B this ultimate load was not reached in the centre of the slabs. The loading device was later supplemented so that in the case of the last two slabs C and D, the complete test programme could be carried out.

The four test slabs were square, each side being 8 m. long. The slabs A and B had a nominal thickness of 14 cm, the slabs C and D 17 cm; to judge from the cut-out detail tests (see 513.1) the thickness in reality would appear to have been rather greater. All the slabs had bottom reinforcement consisting of deformed bar Ks 40; the slabs B and D were also reinforced in the top with deformed bar Ks 60, but this reinforcement appears to have finished up so far under the top surface, to judge by the cut-out detail tests, that it hardly functioned, so that all the slabs can be considered from a functional point of view to be single-reinforced. The amount of reinforcement used and the nominal positions of the reinforcement are shown in Fig. 51:1. On all the slabs, one of the edges had been strengthened in a strip with a width of 1.5 m with doubly intensified reinforcement in the bottom parallel to the edge.

The slabs were cast on a gravel subbase which, in the case of the slabs A and B was 100 cm thick, in the case of C and D 15 cm thick. The

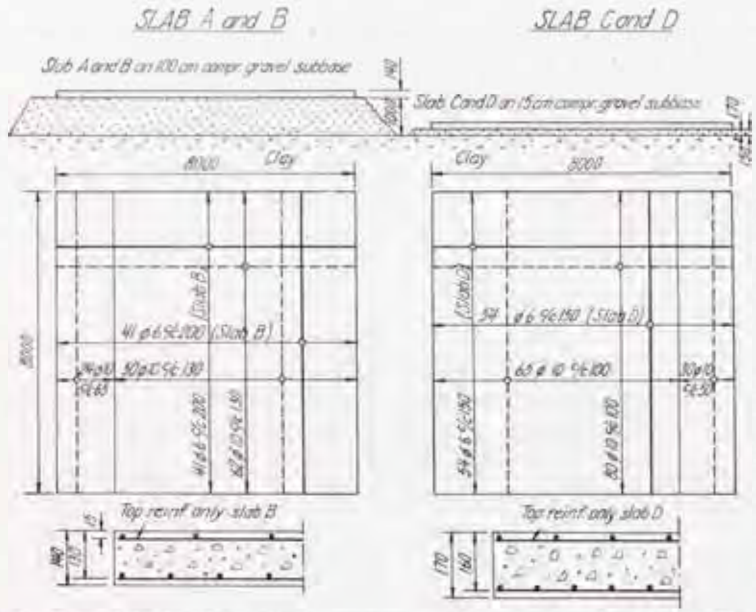

Fig. 51:1. Test slabs for Series V, dimensions, reinforcement and subbase. The figures show the *nominal* measurements; the actual thicknesses and especially the position of the reinforcement in the top deviate to a more or less greater degree from these.

layer of gravel was spread directly on the surface of the soil (see Fig. 51:1) and was compressed very carefully.

Test loading of the slabs was carried out by the Swedish State Road Institute, and the Institute has also described the tests in a report [47]. The tests have also been referred to and analyzed according to the elasticity theory by Bergström and assoc. [4] and Odemark [53]; concerning the edge loading tests, however, only by the first-mentioned and only in a summarizing way.

The test values necessary for analysis in this section have been taken directly from the Road Institute report [47].

512. Test procedure and results

Test loading was carried out with the help of a loading apparatus designed by the Swedish State Road Institute. This consisted of a system of beams laid up on trolleys which ran on rails on each side of the test surfaces. The beams were loaded with counterweights and the load was transferred to the slabs by means of a hydraulic jack fitted between the slab and the system of beams. The load distribution plate had a diameter of 80 cm. By adding extra counterweights it was possible to come up to a maximum loading of approx. 120 tons.

During the tests, measurements of the deformation of the slab were carried out by means of dial gauges, approx. 1.0 m apart, located during the centre loading tests along two lines at right angles through the loading centre parallel with the edges of the slab and, during the edge loading tests, along the edge under loading and along the line of symmetry at right angles to it. Apart from this the curvature was measured in the centre of the slab and the centre of the edge respectively, using curvature gauges in accordance with the same principle shown in Fig. 24:7, these having a measuring base of 2 m[1]).

Test loading in the *centre of the slab* was generally carried out so that the load was first increased up to the original maximum load on the loading machine, approx. 80 tons, after which unloading took place. After further counterweights had been added, in the case of slab C and D extra loading was carried out up to and beyond the failure point. The failure ring crack was noticed on slab C at 114 tons, on slab D at 101 tons. No special arrangement had been made, however, to be able to indicate the crack formation and the top surface was not dusted with white chalk, so that it is probable that the crack had actually occurred somewhat earlier. By studying the depression procedure at the measuring points in the neighbourhood of the crack it is possible to determine fairly accurately that the ultimate loads for both the slabs were

slab C approx. 100 tons
slab D approx. 90 tons

During the test loading of the *free edges*, the load distribution plate was located in the centre of the side so that it was *tangent to* the edge. Loading was carried out with only *one* increase until cracks in the top surface occurred and generally some loading steps beyond this point. The visually determined crack loads for the various edges were:

slab A: unstrengthened edge 36 tons, strengthened edge 46 tons
slab B: unstrengthened edge 40 tons, strengthened edge 54 tons
slab C: unstrengthened edge 28 – 36 tons, strengthened edge 40 tons
slab D: unstrengthened edge 32 tons, strengthened edge 42 tons

It can be pointed out that no special precaution had been carried out to indicate crack formation so that it presumably occurred at a rather

[1]) In the result supplement, Section 94, the depression values and curvature values in the centre of the slab and the centre of the edge respectively are given for all the test loading operations treated here.

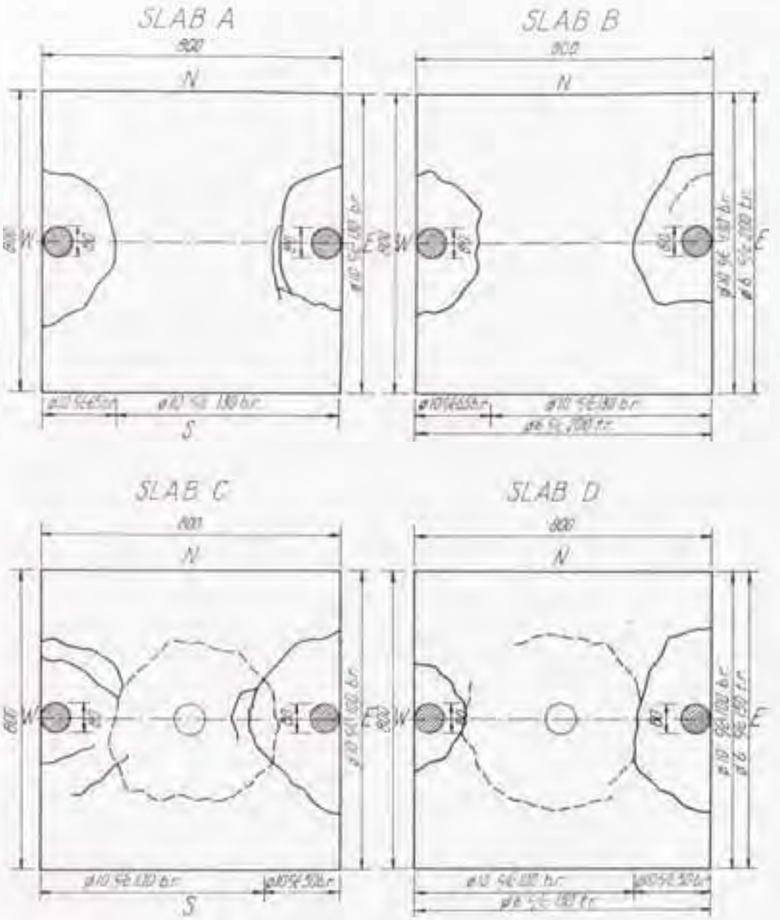

Fig. 51:2. Crack patterns when loading the slabs in Series V. The cracks which occurred in slabs C and D during the first loading on the centre of the slabs, are shown as broken lines.

lower load than the load at which the cracks were discovered. A study of the depression gauge values close to the cracks does not give any reliable results here.

Fig. 51:2 shows the crack patterns in the various cases. In slabs C and D, crack formation due to edge loading was influenced by the circular crack which had earlier occurred during test loading in the centre of the slab. The crack loads given above for edge loading of these slabs are therefore obviously altogether too low and these results, for this reason, have not been included in the ultimate load analysis. In the case of slabs A and B, as already mentioned, no cracks ocurred during the test loading of the centre of the slab.

513. Material constants for slabs and soil

513.1. *Flexural rigidity and ultimate moment*

In order to determine the flexural rigidity and the ultimate moment, special test beams were sawn out of the test slabs after these had been finally tested. According to the programme two such detail tests were to be taken out of each slab, one from each direction of the reinforcement, but by an unfortunate error, this was only done in the case of the thinner slabs A and B. It was thus not possible, unfortunately, to carry out any direct determination of the material constant values for the slabs C and D, just these slabs which were tested up to the ultimate load during centre loading. An estimation can be made by comparing with the results from the detail tests, which were sawn out of the slabs A and B. In the same way the constant values for the strengthened edges were estimated.

The four detail test beams, which had the approximate dimensions of 250×50 cm, were tested for positive moment simply supported with a span of approx. 1.90 m and with two loading points at intervals of approx. one third of the length.[1]) The deformation was measured in the usual way by the use of curvature gauges between the loading points. The test device is shown in Fig. 51:3. During the test, the beams were arranged with one end sticking out over the supporting point and after loading up to failure, the uncracked part at this end was utilized for the determination of the negative ultimate moment, whereby this part of the beam was subjected to flexure in the reversed position.

Fig. 51:4 shows the relationship between the positive moment and the curvature for the four test beams. The flexural rigidity was calculated in the way described earlier from the secant at the yield point. The summarized results are shown in Table 51:1. This table also includes the result of the theoretical calculation of the flexural rigidity based on Stage II with completely uncracked tension zone and $n = 15$. The theoretical values agree relatively well with the test values and it should thus be possible to calculate the flexural rigidity for the slabs C and D as well as for the strengthened edges by proportioning up the test values (average values) in relationship to the theoretically calculated values. In this connection nominal values of the thickness and effective thickness (see Fig. 51:1) were presumed. The result is shown by Table 51:2.

Table 51:1 also shows the ultimate moment values for the four test beams. The positive ultimate moments have been obtained from the curves in Fig. 51:4, due attention being paid to the fact that, in the case

---

[1]) The tests were carried out by the Swedish State Testing Institute and the results are shown in certificate no. 4945, issued by the Institute in March 1949.

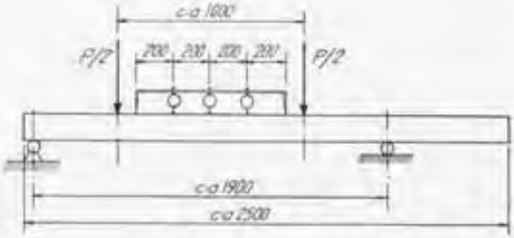

Fig. 51:3. The layout and test device for flexural testing of the detail test beams belonging to slabs A and B. The deformation was measured by means of a curvature gauge placed between the loading points. One end of the beam which projected beyond the support point, was later subjected to flexural testing in a reversed position to determine the negative ultimate moment.

of the top-reinforced beams B there is not such a distinct deviation of the curves at the transition to the failure stage. This appears to depend on the top reinforcement which, as mentioned earlier, lay comparatively deep in the slab so that in the neighbourhood of failure it would lie under the neutral layer and thus gradually be subject to an increased tension, this implying that the moment value gradually increases. For calculation of the ultimate moment in practice, it would appear most

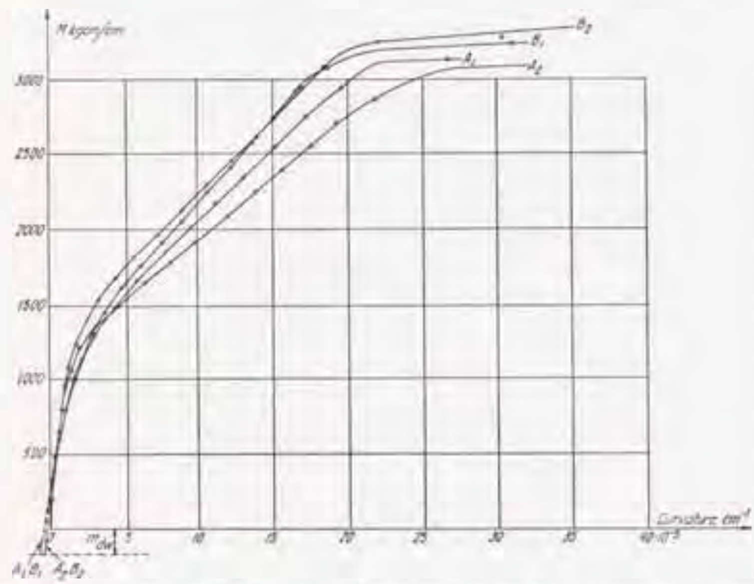

Fig. 51:4. Curvature graphs from the flexural testing of the detail tests shown in Fig. 51:3. The co-ordinate axis shown as broken lines at the bottom show the correction for the deadweight of the unit.

TABLE 51:1. Series V. Detail tests belonging to slabs A and B.

		A 1	A 2	B 1	B 2	Average value
Nominal thickness h_0	cm	14	14	14	14	14
Actual thickness	cm	14.1	15.3	14.8	15.6	
Reinforcement, bottom		⌀ 10 c/c 130 mm		⌀ 10 c/c 130 mm		
top				⌀ 6 c/c 200 mm		
Effective thickness h, nomin.	cm	12.5	11.5	12.5	11.5	12
actual		12.1	11.9	12.8	12.3	
Reinforcement percentage	%					0.5
Flexural rigidity Ei stage II	kgcm²/cm	$14 \cdot 10^6$	$12 \cdot 10^6$	$15 \cdot 10^6$	$15 \cdot 10^6$	$14 \cdot 10^6$
Theor. calc. Ei_{II}	kgcm²/cm	$11.3 \cdot 10^6$	$11.0 \cdot 10^6$	$11.7 \cdot 10^6$	$12.6 \cdot 10^6$	
Pos. ultimate moment m	kgcm/cm	3290	3230	3380	3450	3340
Neg. ultimate moment m'	kgcm/cm	1390	1690	1610	2100	1700

TABLE 51:2. Series V. Flexural rigidity and ultimate moment values for slabs and edges.

For the test slabs A and B and the unstrengthened edges on these slabs the average values from the detail test beams according to Table 51:1 have been used. For the other slabs and edges, the values in question have been estimated by calculation from proportioning of the average values for the four detail test beams A and B.

Slab or edge		Test values		Calculated values			
		Slabs and unstrengthened edges		Slabs and unstrengthened edges	Strengthened edges		Strengthene edges
		A	B	C and D	A	B	C and D
Nominal total thickness h	cm	14	14	17	14	14	17
Nominal effective thickness h_e	cm	12	12	15	12	12	15
Bottom reinforcement		⌀ 10 c/c 130		⌀ 10 c/c 100	⌀ 10 c/c 65		⌀ 10 c/c 50
Reinforcement percentage	%	0.50	0.50	0.52	1.00	1.00	1.04
Flexural rigidity Ei_{I}	kgcm²/cm	$60 \cdot 10^6$	$60 \cdot 10^6$	$103 \cdot 10^6$	$60 \cdot 10^6$	$60 \cdot 10^6$	$103 \cdot 10^6$
Flexural rigidity Ei_{II}	kgcm²/cm	$13 \cdot 10^6$	$15 \cdot 10^6$	$28 \cdot 10^6$	$22 \cdot 10^6$	$25 \cdot 10^6$	$47 \cdot 10^6$
Pos. ultimate moment m	kgcm/cm	3260	3410	5400	6300	6600	10500
Neg. ultimate moment m'	kgcm/cm	1540	1850	2500	1540	1850	2500
Moment at first concrete crack in bottom m_{cr}	kgcm/cm	1300	1300	1900	1300	1300	1900
Curvature at yield-point	cm^{-1}	~2.5	~2.3	~1.9	2.8	~2.6	~2.2

correct here to take the moment at the yield point and completely ignore the influence of the top reinforcement bars. The ultimate moment values according to the tests have been corrected for the moment due to the weight of the unit itself. The average value of the ultimate moments determined in this way have been used to obtain the corresponding values for the slabs C and D as well as for the strengthened edges by proportioning in accordance with the formulae (41:3), whereby $\bar{\sigma}_e$ is placed $= 350$ kg/cm². The calculation is shown in Table 51:2.

Table 51:1 also includes the values of the negative ultimate moment which was obtained during the testing of the uncracked end parts of the test beams, these being subjected to bending with the main reinforcement in the pressure side. The corresponding values for the slabs C and D have been calculated from the average value of the ultimate moments obtained and re-proportioned with respect to the nominal difference in thickness between the slabs A and B and the slabs C and D. The result is shown in Table 51:2.

The table also shows the values for curvature at the commencement of crack formation in the concrete tension zone and at yield point in the reinforcement, which can be estimated from the deformation curves for the detail test beams in Fig. 51:4 and which were used for the calculation of the flexural rigidity of the unstrengthened edges on slabs A and B. For the other edges, the corresponding values for curvature have been estimated in accordance with the relationship

$$\frac{1}{\varrho} = \frac{m}{E\,i}$$

513.2. *Soil constants*

The subgrade consisted, as mentioned above, of clay which was comparatively loose down to some considerable depth. It was assumed to function as an elastic subgrade.

When determining the subgrade constant, a calculation of the average depression from the centre loading tests can hardly be considered, since the depression volume under the square slabs is almost impossible to estimate. The only method remaining is to carry out an estimation from the measurement values concerning deformation and then adopt the elasticity theory. In this way both C and k values were determined in order to permit analysis of the edge loading tests to be carried out in accordance with both the subgrade hypotheses.

For the calculations (by the diagram in Fig. 22:11) the measurement values for the centre depression during the centre loading tests on the

TABLE 51:3. Series V. Determination of k- and C-values.

Calculations from the depression in the slab centre for given loads when loading in the *centre of the slab*, whereby the depression diagram in Section 225 was applied. Flexural rigidity as shown in Table 51:2.

The depression values at loading 2 are corrected for residual deformation after loading 1.

Slab A				Slab B				Slab C				Remarks
P ton	w_0 cm	C kg/cm²	k kg/cm³	P ton	w_0 cm	C kg/cm²	k kg/cm³	P ton	w_0 cm	C kg/cm²	k kg/cm³	
10	0.16	320	0.87	10	0.11	(520)	(1.78)	10	0.15	270	0.60	Stage I
20	0.37	250	0.67	20	0.30	340	1.00	20	0.34	224	0.49	
40	1.06	281	1.30	40	0.94	315	1.44	40	0.94	245	0.84	Stage II loading 1
50	1.60	220	0.90	50	1.43	240	1.00	50	1.35	202	0.64	
60	2.26	175	0.68	62	2.18	182	0.70	60	1.82	170	0.51	
72	3.31	131	0.47	—	—	—	—	76	2.92	125	0.34	
				70	3.07	133	0.45	80	2.95	131	0.36	Stage II loading 2
				78	3.81	114	0.37	102	4.43	107	0.28	
								113	6.45	71	0.16	

slabs A, B and C[1]) were used and the values of the flexural rigidity in accordance with Table 51:2. The Table 51:3 shows the result of the calculations for some of the loading steps and it becomes obvious that the value of the soil constant, estimated according to this method, decreases greatly with increased loading. This does naturally not only depend on the fact that the properties of the subgrade alter when the loading and deformation increase but also depends possibly most on the alteration in the rigidity properties of the slab at the successive crack formation in the bottom surface during increasing loading. For the calculation of the C values in the table, the flexural rigidity D has indeed been assumed to be constant, corresponding to Stage II over the complete slab.

The method used to determine the soil constant is thus particularly unreliable. Since a faulty value of the soil constant only influences the value of the relative load distribution $\alpha = \frac{c}{l}$ to a relatively slight extent, then the influence of this unreliability in the determination when cal-

[1]) See the result supplement, fig. 94:1. The depression curves in this figure have been taken from the Road Institute report [47]. This report describes the depression measurements for the two loadings which were carried out, each zeroed separately. In the test supplement fig. 94:1, which is the basis for the calculations carried out here, in accordance with the principles in 233 the deformations have been "restored to the first loading" and the value for the highest loading steps which belonged to the second loading has thus been corrected for the permanent deformation which remained after the first loading.

During the test of slab D, six loadings were carried out, the final loading after such a comparatively long interval that definite deformation values in accordance with the principle of first loading cannot be obtained for this slab.

culating the moment and the ultimate load is fortunately comparatively small.

When selecting suitable values for the subgrade constants attention should be paid to the fact that the depression values at the highest loading steps are influenced by the plastification taking place in the centre zone of the slab. It would thus appear to be most correct to estimate the subgrade constants at a load corresponding to or rather higher than the load at yield point in the bottom reinforcement. For this reason the following values were selected:

for slabs A and B: $C = 220$ kg/cm²; $k = 0.90$ kg/cm³

for slabs C and D: $C = 160$ kg/cm²; $k = 0.45$ kg/cm³

These values are estimated on the basis of the centre loading case. For the case of edge loading the subgrade constant value should possibly be determined at a lower loading, since the depression at ultimate load in this case is smaller than in the case of centre loading. With respect to the fact that the depression volume in the case of edge loading is completely different compared to that in the case of centre loading, it is not possible directly to compare the influence of the deformation on the soil constant in both the cases of loading, and there would not appear to be enough definite points to qualify the estimation of other values of the soil constants in the case of edge loading. This question is also treated in the discussion in 432.2 concerning the determination of the subgrade constant in the Gothenburg tests and also in the analysis of the depression measurements in 514.2.

514. Test results, treatment and theoretical analysis

514.1. *Loading on the centre of the slab*

Table 51:4 includes the experimentally determined loads at yield point in the bottom surface P_b^{yie} and crack in the top surface P_t for the slabs C and D together with the corresponding theoretically calculated values. The load P_b^{yie} for the slab C has been estimated in the usual way from the curvature in the centre of the slab,[1][2] compared with the theoretically calculated curvature value at yield point according to Table 51:2.

The table shows very good agreement between the test loads and the

[1] In the case of slab D, due to the irregular loading procedure mentioned in the note on page 310, it was not possible to obtain reliable curvature values and thus not possible to determine P_b^{yie}.

[2] See the result supplement, Section 94.

TABLE 51:4. Series V. Loading on centre of test slabs.
Ultimate loads from tests and theory (elasticity as well as ultimate strength theory).
Size of slabs 8×8 m. Loading area radius $c = 40$ cm.
When calculating the theoretical failure loads, the soil is assumed to be elastic subgrade.

Series V, slab		C	D
DATA FOR THE TEST SLABS			
Total thickness h_o approx.	cm	17	17
Reinforcement Ks 40			
bottom		⌀ 10 c/c 100	⌀ 10 c/c 100
top			⌀ 6 c/c 150
Flexural rigidity D	kgcm²/cm	$28 \cdot 10^6$	$28 \cdot 10^6$
Soil modulus C	kg/cm³	160	160
Elast. rad. of rigidity $l = \sqrt[3]{\frac{2D}{C}}$		70	70
Rel. load distribution $\alpha = \frac{c}{l}$		0.57	0.57
Ultimate moment	kgcm/cm		
at pos. moment m		5400	5400
at neg. moment m'		2500	2500
$m + m'$		7900	7900
RESULTS			
Load at yield in bottom reinforcement P_b^{ylc}	tons		
from tests		57	–[1]
from theory		56	
Load at failure in top concrete surface P_t	tons		
from tests		~ 100	~ 90
from elasticity theory		140	140
from ultimate strength theory		94	94

[1]) See note on page 311.

theoretical loads P_b^{ylc}. Concerning the definite ultimate loads P_t, agreement between the tests and theory is poor when calculating according to the elasticity theory but good when calculating according to the ultimate strength theory. The tests thus give the same results in all respects as those earlier obtained.

514.2. *Loading on free edges*

The results of the depression and curvature measurements on the eight edges have been applied to the WESTERGAARD edge loading formulae and the corresponding diagrams for depression and moment; the results of these calculations have been compiled in Table 51:5. The values of flexural rigidity, subgrade constants and ultimate moments, according to the previous section, which were used in the calculations, are shown in the table.

Theoretical values of the depression under the load have been calculated from the diagram in Fig. 41:1 and the formula (41:5), and the result

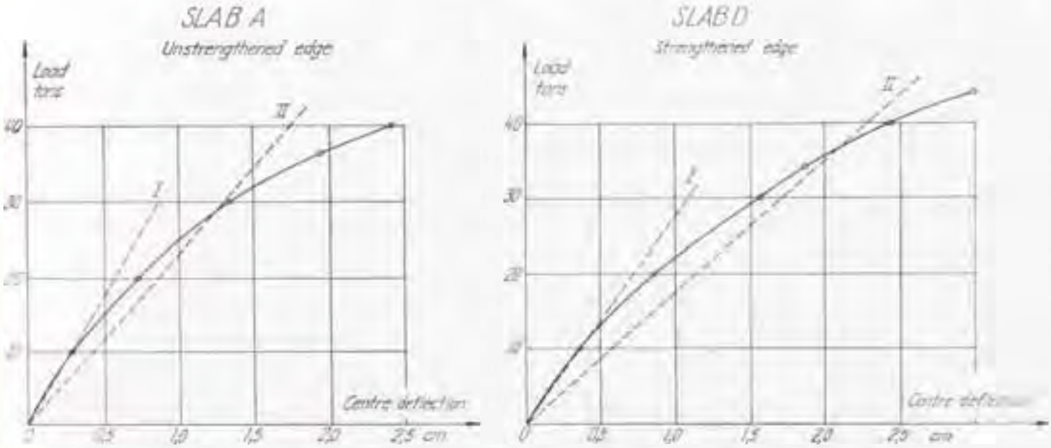

Fig. 51:5. Relationship between depression and loading in the centre of the edge from tests and theory concerning the unstrengthened edge A and the strengthened edge D. The theoretical curve lines are calculated from formula (41:5) with the constant values for the slabs and the soil according to Stage I (with $\nu = 0.15$) and Stage II (with $\nu = 0$).

has been calculated for a loading of 40 tons which is in the neighbourhood of a load corresponding to yield point in the bottom (Stage II) for the various edges. For the unstrengthened edges C and D, the deflection at 36 tons is instead calculated, since the test loading was interrupted at this lower load due to the early crack formation mentioned earlier. For some of the edges, the theoretical and experimental relationship curves between the load and the depression in the loading point have been compiled in Fig. 51:5.[1]) In these diagrams the theoretical relationship curves for a low load (stage I) have also been drawn in, whereby the constant values are obtained according to the Tables 51:2 and 51:3.

The Table 51:5 and the diagram in Fig. 51:5 show relatively good agreement between the calculated and measured depressions. The deviations reflect the unsure method when determining k-values and the fact that the soil appears to correspond more closely to an elastic subgrade while the theory and the soil constant value concern resilient subgrade. With respect to the slight influence of unreliability in the subgrade constant when calculating the moments and the ultimate loads it can be considered that the k-value has been estimated with suitable values and it can be calculated for the case of centre loading even when it concerns edge loading, i. e. WESTERGAARD's formulae for depression show fairly well the relationship between the depression due to edge load and interior load on the slab.

[1]) For all the edges, the curves of this type are shown in the result supplement, Section 94.

In order to calculate the loadings in the case of edge loading tests, which corresponds to yield point in the reinforcement, the curvature measurements in the centre of the edge have been compared with the values of curvature at the yield point obtained from the detail beam tests and the corresponding calculations according to Table 51:2. In some of the tests the increase in loading was terminated before the yield point was reached according to this estimation, and the load in question in these tests has been estimated by means of exterpolation from the curvature graphs (the estimated values have been shown in brackets in the table). On the whole the determination of the loads from the curvature in this test series must be considered as being very unsure, since the measuring values shown in the original report issued by the Road Institute were altogether too sparse (too large loading steps) to admit a completely sure determination of the edge curvature, and the corresponding curvature values at yield point used in the comparison were not, in the case of most of the edges, determined directly from the deflection tests on the detail test beams but instead were estimated by means of comparative calculations (see Section 513:1 and Table 51:2). Apart from this, some of the loads were, as mentioned above, estimated from exterpolated curvature values.

The test yield point loads estimated in this way are shown in Table 51:5 together with the corresponding theoretical load values calculated according to WESTERGAARD's moment formula (41:6) or the diagram in Fig. 41:2 and with the values of the positive ultimate moment obtained from Table 51:2. This calculation is thus based on WESTERGAARD's assumption of resilient subgrade. A corresponding calculation has also been made according to the hypothesis of elastic subgrade, based on the assumption mentioned in Section 41 that the relationship between the moments at centre and edge loading is the same for elastic subgrade as for resilient subgrade.

The agreement between the load values at yield point estimated from the tests and theoretically calculated is fairly good for most of the edges and, with respect to the unreliability mentioned in determining the test values, in any case as good as can be expected. The best agreement with the test values would appear to be when calculating according to the elastic subgrade hypothesis and it would thus appear that the method used for calculating moment for this type of subgrade should be applicable.

It is obvious that the failure load values at bottom reinforcement yield point obtained and calculated are in the immediate neighbourhood of the definite top failure (in certain cases even somewhat higher). It should thus be expected that the slab functions "elastically" right up

TABLE 51:5. Series V. Edge loading on test slabs. Depression and ultimate loads from tests and the *elasticity theory*.

Size of slabs 8 × 8 m. Circular loading area with radius $c = 40$ cm tangent to the edge. In the calculation of the theoretical depression values, the soil is assumed to be resilient (constants with index k). When calculating the ultimate loads the soil is assumed to be resilient as well as elastic (constants with index k and e respectively).

Slab series V, edge	Unstrengthened edges				Strengthened edges			
	A	B	C	D	A	B	C	D
DATA FOR THE TEST SLAB EDGES								
Total thickness, approx. cm	14	14	17	17	14	14	17	17
Reinforcement Ks 40	⌀ 10 c/c 300		⌀ 10 c/c 100		⌀ 10 c/c 150		⌀ 10 c/c 200	
Flexural rigidity D_{II} kgcm²/cm	$13 \cdot 10^8$	$15 \cdot 10^8$	$28 \cdot 10^8$	$28 \cdot 10^8$	$22 \cdot 10^8$	$25 \cdot 10^8$	$47 \cdot 10^8$	$47 \cdot 10^8$
Soil constants, high loading								
resiliance constant k kg/cm³	0.90	0.90	0.50	0.50	0.90	0.90	0.50	0.50
soil modulus C kg/cm²	220	220	160	160	220	220	160	160
Elastic radius of rigidity l cm								
$l_k = \sqrt[4]{\frac{D}{k}}$	62	64	86	86	70	72	98	98
$l_e = \sqrt[3]{\frac{2D}{C}}$	49	52	70	70	59	61	84	84
Relative load distribution $a = \frac{c}{l}$								
$a_k = \frac{c}{l_k}$	0.65	0.63	0.46	0.46	0.57	0.55	0.41	0.41
$a_e = \frac{c}{l_e}$	0.81	0.78	0.57	0.57	0.68	0.66	0.48	0.48
Ultimate moment kgcm/cm								
at bottom reinf. yield m_{yie}	3260	3410	5400	5400	6300	6600	10500	10500
at top concr. failure m'_{cr}	1540	1850	2500	2500	1540	1850	2500	2500
DEPRESSION MEASUREMENTS								
Depression at 40 tons cm								
from tests	2.29	2.11	1.61[1])	2.12[1])	2.18	1.75	2.31	2.45
from theory	2.66	2.51	2.57[1])	2.57[1])	2.16	2.05	2.31	2.31
ULTIMATE LOADS								
Load at bottom reinf. yield P_t^{yie} tons								
from tests	(40)	40	29	(33)	46	45	(48)	(47)
from elasticity theory								
resilient soil	22	23	26	26	37	38	48	48
elastic soil	29	29	32	32	45	45	53	53
Load at top concrete failure P_t tons								
from tests	36	40			46	54		
from elasticity theory	26	31			26	31		

[1]) The depression values for C and D unstrengthened apply at 36 tons which was the maximum load for these edges.

to the ultimate load and that it should thus also be possible to calculate the load at top failure by means of the elasticity theory method. The last lines in Table 51:5 show the result of a calculation of this type for the four "undisturbed" edges of slabs A and B. The theoretical values for the ultimate load have been calculated according to the formula (41:9) whereby the negative ultimate moment values have been estimated from the detail beam tests according to Table 51:1. The result is however hardly encouraging. It is particularly obvious that the effect of edge strengthening cannot be shown at all in this way while the theoretical ultimate load according to the formula (41:9) is independent of the strengthened positive ultimate moment. The test values show clearly that an increase in the ultimate load is obtained by intensifying the reinforcement in the bottom along the edge.

Apart from the high degree of unreliability in the negative ultimate moment values, the reason for the poor agreement with the elasticity theory would appear to be that, in spite of the fact that the yield point load and the final ultimate load are so close to one another, there is anyhow a levelling and a re-arrangement of moment which influences the final rupture.

This matter will therefore be examined by considering if a better result can be obtained by means of the ultimate strength methods in Section 42, in spite of the fact that the conditions for this (complete yield along the cracks in the bottom surface) cannot be satisfied so well. Since the negative ultimate moment can be taken as being equal in both directions and since the strengthened zone can be assumed to stretch itself over the complete failure figure, it is not necessary here to follow the methods in Section 425, which concern local edge strengthening, and the ultimate loads can thus be obtained with the help of the diagram in Fig. 42:11.

Calculation of the theoretical ultimate loads has been carried out for both the subgrade cases, i. e. the soil being considered both as a resilient and as an elastic subgrade. In this connection, the values of the elastic radius of rigidity l according to Table 51:5 obtained by distributing the edge beam rigidity over an edge zone with a width l, and the corresponding values of the relative load distribution according to Table 51:5, were used for the calculation in the two soil cases. The results are shown in Table 51:6, and the table shows in most of the tests remarkably good agreement between the ultimate loads obtained theoretically and experimentally. This is possibly rather surprising with respect to the fact mentioned above that yield in the bottom surface cannot have spread out so far before top failure occurred. It has, however, been shown theoretically (see section 426:3) that such incomplete plastification in

TABLE 51:6. Series V. Edge loading on test slabs. Ultimate loads at failure in the top from tests and the *ultimate strength theory*.

Size of slabs 8 × 8 m. Circular loading area with radius $c = 40$ cm tangent to the edge. In the calculation of the ultimate loads, the soil is assumed to be resilient (index k) as well as elastic (index e).

Slab series V, edge	Unstrengthened edges		Strengthened edges	
	A	B	A	B
DATA FOR THE TEST SLAB EDGES (see also Table 51:5)				
Ultimate moment kgcm/cm				
positive $m_{yir} = m$	3260	3410	6300	6600
negative $m'_{cr} = m'$	1540	1850	1540	1850
$\frac{m}{m'}$	2.10	1.85	4.10	3.55
$m + m'$	4800	5260	7840	8450
Relative load distribution $a = \frac{c}{l}$				
for resilient soil a_k	0.65	0.63	0.57	0.55
for elastic soil a_e	0.81	0.78	0.68	0.66
ULTIMATE LOADS at crack in top P_t tons				
from tests	36	40	46	54
from theory				
for resilient soil	38	50	47	57
for elastic soil	45	50	54	59

the positive yield lines influences the ultimate load value to a comparatively small extent. The theoretical examination according to table 42:4 shows that application of the usual ultimate load formulae in such cases of incomplete plastification should give ultimate load values which are rather too high. From this viewpoint, the theoretical ultimate load values calculated according to the hypothesis of elastic subgrade should perhaps be in a more correct relationship to the test loads than the loads according to the hypothesis of resilient subgrade, in spite of the fact that the last-mentioned loads show better formal agreement with the test loads.

It is however obvious that the effect of edge strengthening can be estimated quite correctly by means of the ultimate load method no matter whether the subgrade is assumed as being resilient or elastic. The result is thus here the same as in the earlier treated edge loading tests.

52. The Norrköping Tests, Summer 1948, Series N

521. Extent, performance and results

In connection with the extension of Norrköping airport in 1948, the summer of this year was used to carry out a number of loading tests on reinforced concrete pavements in accordance with a programme drawn up by the author. Tests on plain concrete pavements were also carried out simultaneously, but these will not be treated here.

The programme consisted of the testing of two reinforced test slabs C and D, 7×7 m, as well as application of test loading on two zones of newly completed taxiways c and d. All the pavements were about 16 cm thick with bottom reinforcement consisting of two-way reinforcement ⌀ 10 c/c 140 mm. One of the test slabs and one of the taxiway pavements tested were also supplied with top reinforcement ⌀ 6 c/c 250 mm, but as shown by later tests, this reinforcement was so weak that the flexural strength of the concrete itself gave a higher ultimate moment, so that also these test slabs can be considered as being only bottom-reinforced and all thus similar in principle. The taxiways tested consisted of four strips with a width of 4.125 m, separated by longitudinal joints with bottom reinforcement right through and with tongue and groove.

Fig. 52:1 shows the design of the pavement as well as a plan of the test region with the test points treated here marked in. On the separate test surfaces C and D only test loading in the centre point was carried out, on the taxiways c and d test loading was carried out partly midstrips exactly between joints, partly on the free edges which were designed with extra reinforcement and thickening (see Fig. 52:1). Apart from the points marked in on fig. 52:1, the taxiways were test loaded at a further number of points but in these cases the load was not taken up to failure in the top surface and these test loadings will not be treated here.

The reinforcement consisted of deformed bar with a yield point of approx. 4600 kg/cm². The concrete had a cement content of 285 kg/cm². Cube tests carried out showed an average 28 days compressive strength of 526 kg/cm² and standard flexural beams made showed an average flexural strength of 54 kg/cm².

At the site of the tests the subgrade consisted of clay to some considerable depth. Both the taxiway pavement and the test slabs were laid

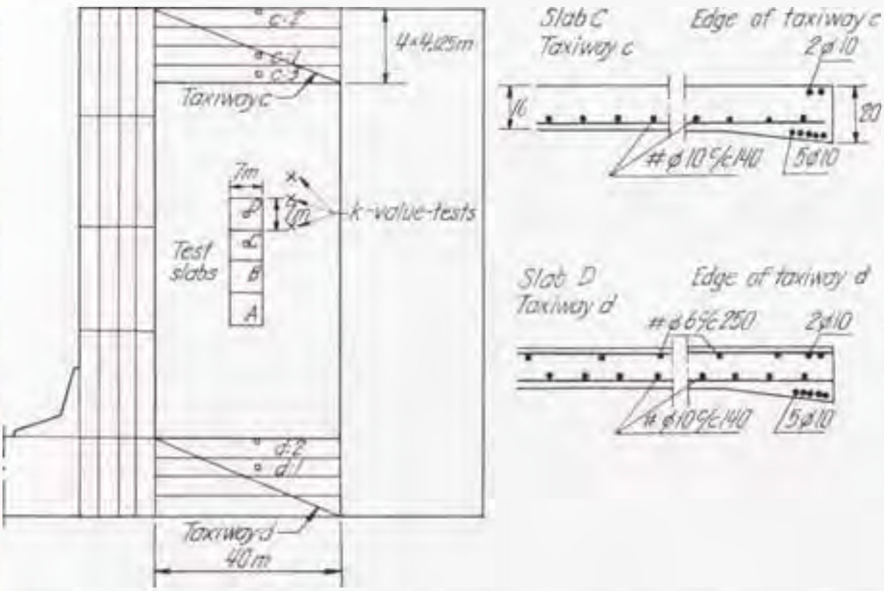

Fig. 52:1. Plan of the test zone (dispersal slab and taxiways) as well as the sections of the tested independent slabs C and D and the taxiways c and d. The test slabs A and B were unreinforced and are not discussed here. The test loading points are marked in on the plan (only tests to failure are included).

out without any special subbase. The top soil was graded off and an approx. 10 cm thick levelling layer of gravel and crushed stone was laid out and rolled with a smooth roller before the pavement was cast.

As in the case of the other investigations, special beams were made as detail tests to determine the ultimate moment and the flexural rigidity. Such beams were cast simultaneously with the casting of the pavement on the taxiways and the test slabs. The beams were 2.5 m long, their thickness and reinforcement agreeing with that of the corresponding taxiway or slab. For every testing place (independent slab or taxiway respectively) four such detail test units were made, two of which corresponding to a strip from one of the directions of the reinforcement in the pavement and two corresponding to a strip from the other direction.

The test loading was carried out in co-operation with the Swedish State Road Institute and the Stockholm Air Port Building Committee.[1])

[1]) A description of the tests concerning the individual slabs has been supplied by BERNELL [8] who was engaged in the tests representing the Stockholm Air Port Building Committee. The author has not quoted or utilized the data in this report since they have been found to be lacking in information and, to a certain extent, less correct (see also note 1, page 185).

The loading was applied with the help of the Road Institute loading apparatus which has been earlier described in connection with the description of the Väsby tests, Section 51.

The test slabs and the selected zones of the taxiways were loaded at all the test points with a circular loading plate with a diameter of 80 cm. The crack pattern plan on Fig. 52:2 shows the exact location; during the test loading of the edges, the loading plate was located with its edge 10 cm inside the free slab edge. The load was generally applied with steps of 2 tons at intervals of 3 minutes. During the test the deformation of the slab was measured by means of dial gauges placed along two directions at right angles. The curvature in the loading point was also measured with curvature gauges which, however, as opposed to most of the earlier tests, only measured the depression of the centre point over a measuring base of 40 cm.[1]) Finally the strains in the top surface of the slab were measured along the same lines as the depressions with the help of strain gauges with a measuring base of 25 cm of the same type as used in the Gothenburg tests[1]) (see Fig. 25:9).

The loading was increased directly without any intermediate off-loading to a load rather higher than the load where the circular failure crack in the top surface occurred. No visual determination of this load was made but it can in the usual way be calculated objectively from the discontinuity in the diagrams of the strain measurements. The ultimate loads thus obtained were

slab C, load on the centre		68 tons
slab D, load on the centre		50 tons
taxiway c, load on the centre	(test c:1)	50 tons[2])
taxiway d, load on the centre	(test d:1)	57 tons
taxiway c, load on the edge	(test c:2)	22 tons
taxiway c, load on the edge	(test c:3)	12 tons
taxiway d, load on the edge	(test d:2)	34 tons

[1]) The necessary results from the deflection and curvature measurements have been taken from the Road Institute test report which includes diagrams of the centre depression and centre point deformation (curvature) as well as the depression lines for two or three loading steps. The other test results (strain measurements, etc.) have been taken directly from the original protocol.

For the loading points treated here (see Fig. 52:1) the test results are shown in the form of centre depression and curvature diagrams as well as strain diagrams in the result supplement, Section 95.

[2]) As early as at 35 tons, one of the strain gauges in this test loading showed a discontinuity in its readings which could indicate a crack in the top surface. Since the strain was here only approx. 0.07 ‰ and since the subsequent strain increase went relatively slowly, this possible crack has *not* been considered as being a failure crack.

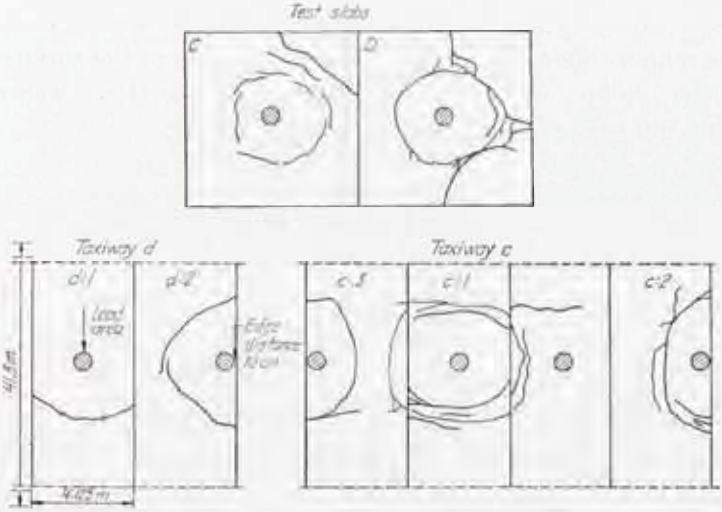

Fig. 52:2. Crack patterns after testing the independent test slabs C and D and the taxiways c and d with the loading areas marked (diameter 80 cm).

During the loading tests c:2 and c:3 on the opposite edges of taxiway c, both the depression and the strain increased very rapidly already at the beginning, about twice as rapidly as on the equally strong edge of taxiway d, test d:2 (in test c:3 even more rapidly). The explanation of this must be that the edges of this taxiway were not in contact with the soil from the beginning and this caused large extra strains in the taxiway and too low ultimate loads. The results of the test loading on the edges of taxiway c have therefore not been included in the test analysis.

The appearance of the top surface cracks is shown in Fig. 52:2 which also shows the location of the loading areas. During the two test loading procedures c:1 and d:1 on the taxiways exactly between longitudinal joints a failure line figure was obtained which went into the joints, i. e. the type of failure which has been treated in theory in Section 324. By comparison with the failure circles on the independent slabs C and D (with the same thickness and reinforcement) it can be seen that the crack radius here is larger and the failure figure is oval; at test point d:1 only half the failure figure has come up.

Another interesting observation to be made from a study of the ultimate loads is that the tests on the *double-reinforced* taxiway c results in *lower* ultimate loads than the corresponding tests on the *single-reinforced* taxiway d. This could show that the top reinforcement, which is too weak to increase the negative ultimate moment, should even have an unfavourable effect which in such a case should depend on the fact that the reinforcement causes fine shrinkage cracks in the surface which function as failure indications. The corresponding effect was *not* obtained in the case of the independent slabs.

522. **Material constants for slabs and soil**

522.1. *Flexural rigidity and ultimate moment*

The above-mentioned detail test beams were tested at the Swedish State Testing Institute according to a programme made up by the author. Of the beams from each testing place, two were tested with the bottom surface (main reinforcement) in the tension zone (positive moment) and two with the top surface in the tension zone (negative moment). The beams were tested simply supported with concentrated loads applied from above at points separated by a distance corresponding to one quarter of the length.[1]) During the test the deflection was measured in the centre point of the beams and 40 cm on each side of the centre point by means of dial gauges on both edges of the beam. The curvature of the centre section has been calculated from these measurements. This calculation is naturally considerably less reliable than the corresponding measurement by means of curvature gauges, the result from the highest loading steps being particularly unreliable, the deflection here being measured by means of rods graduated in millimetres. From the curvature diagrams obtained in this way, the flexural rigidity in Stage II (secant modulus values at yield point) and the ultimate moment have been obtained in the usual way.[2]) The ultimate moment values are particularly relatively unreliable, partly depending upon the unreliability in the curvature measurements mentioned above and partly relying on the fact that the moment increases slowly even after the yield point in the bottom reinforcement has obviously been reached. The ultimate moments have been determined at the yield point of the reinforcing bars and in the estimation of this value, measurements of the development of the largest cracks have also served as a guide.[2]) In all the calculations, corrections have been made for the moment due to the deadweight of the unit.

The result of the detail beam tests is compiled in Table 52:1 where the average values from the beam tests are included. The thickness of

[1]) The test results are shown in the Swedish State Testing Institute certificate no. 26546 of January 31st 1949. The results here have been obtained by the analysis of this test protocol. See the note below.

[2]) Diagrams of the centre depression and curvature as well as the development of the largest cracks are shown in the result supplement, Section 95.

TABLE 52:1. Series N. Detail tests.

Test beams with a length of 250 cm, nominal thickness $h_0 = 16$ cm, and effective height $h = 13{,}5$ cm.

Each result shown in the table is the average value of *two* tests.

Detail test from slab and taxiway respectively	C	D	c	d	Average value
Ultimate moment kgcm/cm					
pos. moment m	3520	3630	3620	3790	3600
neg. moment m'	1810	2060	1780	1700	1800
Flexural rigidity at yield point Ei kgcm²/cm	$19 \cdot 10^8$	$23 \cdot 10^8$	$24 \cdot 10^8$	$26 \cdot 10^8$	$23 \cdot 10^8$
Curvature at yield point cm^{-1}	$18 \cdot 10^{-3}$	$15 \cdot 10^{-3}$	$14.5 \cdot 10^{-3}$	$15 \cdot 10^{-3}$	$15.5 \cdot 10^{-3}$

the test beams was about 16 cm and the effective height at the bottom reinforcement was about 13.5 cm but these values varied somewhat. Since it was not possible to carry out any direct measurements of thickness on the test surfaces, and it can be assumed that the variation in thickness is as great as it was in the detail test beams, it has been considered most correct, in the continued analysis of all the tests, to calculate with the average values from the results of all the detail tests; the variations in the results between the various detail test beams can give an idea of the spread in the constant values for the slab.

The table also includes the values of curvature at the yield point estimated from the test curves. The average value has been used for the estimation of the load P_b^{yie} at yield point in the bottom surface in the main tests.

522.2. *Soil constants*

Since there was not any possibility to calculate the depression volume, the subgrade constants were estimated in the same way as with Series V on the basis of the depression values in the case of centre loading according to the elasticity theory. Table 52:2 shows the results of such C-value calculations for several different loading steps in the neighbourhood of P_b^{yie} and P_t from centre loading tests on the four slabs; for slab d, which was also studied concerning the case of edge loading, the k-values have also been calculated. As comparison, the calculations have been made also for loads of 15 tons whereby the corresponding flexural rigidity value in Stage I has been estimated from the detail tests as an average value from the various tests.

In accordance with the principles discussed in 513.2 for the determination of the subgrade constant for the Series V, the following values are selected for the continued test analysis:

TABLE 52:2. Series N. Determination of soil constant values.

Calculations from the depression in the slab centre under centre loading with the given loads, whereby the depression diagram in Section 225 has been applied.

For calculation the values of the flexural rigidity from the detail tests were used:

$$\text{Stage I:} \quad D_{\text{I}} = 110 \cdot 10^{9} \text{ kgcm}^2/\text{cm}$$
$$\text{Stage II:} \quad D_{\text{II}} = 23 \cdot 10^{9} \text{ kgcm}^2/\text{cm}$$

Load tons	Slab C		Slab D		Taxiway c		Taxiway d			Remark
	w_0 cm	C kg/cm²	w_0 cm	C kg/cm²	w_0 cm	C kg/cm²	w_0 cm	C kg/cm²	k kg/cm²	
15	0.264	210	0.300	179	0.272	197	0.225	258	0.56	Stage I
40	1.15	200	1.52	140	1.20	190	0.94	260	0.99	Stage II
50	1.76	150	2.60	88	1.76	150	1.30	230	0.83	Stage II
60	2.76	105	—	—	2.37	130	1.74	190	0.67	Stage II

Slab C: $C = 150$ kg/cm²

D: $C = 90$ kg/cm²

c: $C = 150$ kg/cm²

d: $C = 200$ kg/cm²; $k = 0.70$ kg/cm³

The considerable differences between the subgrade constant values for the adjacent and similar slabs C and D should be noticed. This shows that very large local variations in the properties of the subgrade can occur.

523. Test results, treatment and theoretical analysis

523.1. *Loading on the centre of the slab*

The failure load at yield point in the bottom surface P_b^{yie} for the four test loadings on the centre of the slabs (and the taxiways respectively) were estimated in the usual way with the help of the curvature diagrams for the loading point compared with the corresponding curvature values according to the detail tests, see Table 52:1. The ultimate loads at failure in the top surface P_t^{cr}, determined through analysis of the strain measurements, have been given earlier. These test values have been compared with the corresponding theoretically calculated values and the results are shown in Table 52:3. The table also includes the required data for the test slabs. When calculating according to the elasticity theory, the subgrade is considered to function as an elastic subgrade.

Concerning the load at bottom reinforcement yield P_b^{yie}, the agreement between the test values and the values calculated in accordance

TABLE 52:3. Series N. Loading on centre of test slabs.

Ultimate loads from tests and according to *elasticity theory* (elastic soil) as well as *ultimate strength theory*.

Thickness of slabs, nominally 16 cm. Loading area circular with radius $c = 40$ cm.

Test area type		Independent slabs		Taxiways	
Notation		C	D	c 1	d 1
DATA FOR THE TEST AREAS					
Reinforcement		Double	Single	Double	Single
Flexural rigidity Ei_{11}	kgcm²/cm	$23 \cdot 10^8$			
Soil constant C	kg/cm³	150	90	150	200
Calculation constants					
Elast. radius of rigidity l_e	cm	67	80	67	61
Rel. load distribution $\alpha_e = \frac{c}{l_e}$		0.60	0.50	0.60	0.66
Ultimate moment	kgcm/cm				
at bottom reinf. yield m_{yir}		3600			
at top concrete failure m'_{cr}		1800			
$m + m'$		5400			
RESULTS					
Ultimate load at bottom yield P_t^{yir}	tons				
from tests		38	33	30	39
from elast. theory		38	34	38	41
Ultimate load at top crack P_t^{cr}	tons				
from tests		68	50	50	57
from *elasticity theory*		100	98	100	100
from *ultimate strength theory*		66	60	66	70

with *the elasticity theory* is satisfactory. The differences in the test values from slabs C and D, for which slabs comparatively similar test data are valid, give an idea of the spread, and a further impression of this can be obtained by considering the ultimate moment values from the detail tests according to Table 52:1. For the taxiways c and d which had also comparatively similar test data, the variation in the ultimate load values appear to be even greater and the theoretical values are even higher than the test values. Concerning the load at failure in the top surface P_t^{cr}, the theoretical values according to *the elasticity theory* lie much higher than the test values, and the tests thus confirm earlier conclusions that the elasticity theory is not suitable in this case.

The theoretical loads according to *the ultimate load theory* lie, in the case of the independent slabs C and D, between the widely spread test values, while the theoretical loads for the taxiways c and d are considerably higher than the test loads. For calculating purposes, *no* respect has been taken to the effect of the joints, since according to the theoretical treatment of this case in Section 324, the effect of the joints on the ultimate load would appear to be very small.

Concerning the *independent* test slabs, agreement between test and theory (with the obvious exception of P_t^{cr} according to the elasticity theory) is thus as good as can be expected with respect to the spread shown by both the similar tests. For the *taxiways*, on the other hand, the theoretical loads all the way through are higher than the test loads. The reason for this can naturally be referred to some extent to the influence of the joints, but appear mainly to depend on the *extra stresses* of the tension forces due to shrinkage and also decrease in temperature that can have occurred in the taxiways which were 40 m long. An influence of this type can be said to absorb part of the ultimate moment values, and with a reasonable reduction of the value $(m + m')$ from this viewpoint, good agreement may be reached. These questions will be treated in a later Section 64. The subgrade constant values for the taxiways can possibly also have been estimated as having excessively high values, this appearing probable by comparison with the subgrade constant value for the adjacent independent slabs. The reason also in this case can be the above-mentioned effect of shrinkage and temperature which produces a certain membrane stress effect in the slab and thereby decreases the depression.

523.2. *Test loading on the edge of the taxiway*

As already mentioned, test loadings on the edge of the taxiway c gave unreliable results and only the test loading d:2 is discussed here. Since the taxiway edges are thickened and strengthened (see Fig. 42:1) and no detail test beams of a corresponding type have been made and tested, it is thus not possible to estimate the load P_b^{yie} for bottom surface failure.

The required data for edge strengthening has been estimated theoretically by proportioning from the corresponding test values for the unreinforced slab according to the detail tests. In this connection the supplementary stiffening of the edge consists of a beam as shown in Fig. 52:3 which contains a reinforcement strip along the edge. It is thus possible in this way according to (43:1) ($\bar{\sigma}_c = 400$ kg/cm²) to obtain the *supplementary moment* of the edge beam.

$$M = 14 \cdot 3600 \frac{5}{1} \frac{17}{13.5} \frac{1 - 0.070}{1 - 0.024} = 3.0 \cdot 10^5 \text{ kgcm}$$

as well as the *total flexural rigidity* of the edge beam

$$(E\,I)_{\text{beam}} = 23 \cdot 10^6 \frac{15500}{98} = 36 \cdot 10^8 \text{ kgcm}^2$$

Fig. 52:3. Section of the edge beam of the taxiways. The supplementary ultimate moment M is calculated for the beam section AB with only *supplementary* reinforcement while the flexural rigidity $E\,I_{\text{beam}}$ is calculated for the entire edge beam AC with all the reinforcement included.

where the denominator and the numerator in the fraction consist of the theoretical values of the moment of inertia for the complete edge member and slab respectively, calculated for Stage II and $n = 15$ (see Fig. 52:3). For negative deflection, the supplementary moment $M' = 0$ is considered, since yield in the top surface is considered to exist because the concrete cracks and the weak top reinforcement thereby has no significance.

With the use of these values and with the methods otherwise shown by the theoretical treatment of the strengthened edge in Section 425, the results of the test loading d:2 have been analyzed according to the ultimate strength theory. The results are shown in Table 52:4 and this table also includes the required data for the edge. The values of the elastic radius of rigidity l have here been calculated according to the earlier applied principle that the supplementary stiffness of the edge beam is distributed over an edge strip with a width l. The table also includes the values of the centre depression in the edge according to tests and the elasticity theory (resilient subgrade) compared with each other, and agreement is relatively good. This confirms that the subgrade constant values here used are fairly correct and that the method of estimating the flexural rigidity of the edge can be used.

The theoretical ultimate loads have been calculated with the constants according to both the subgrade hypotheses. Agreement with the test values is best for the assumption that the subgrade is resilient but the theoretical loads in both cases are considerably higher than the test loads.

It should be pointed out however that there can be a considerable influence due to shrinkage and temperature also here. These factors reduce the ultimate moment sum $(m_e + m_e')$ along the edge, this directly influencing the ultimate load. See also more concerning this in Section 64.

It should also be necessary in this case to count on very incomplete plastification in the yield crack in the bottom surface. A rough estimation of the curvature of the edge beam at the yield point from the theoretical values of the ultimate moment and flexural rigidity for the edge

TABLE 52:4. Series N. Loading on slab edge d 2.

Ultimate loads from tests and the *ultimate strength theory* (elastic and resilient soil).

Loading area circular with radius $c = 40$ cm, placed with its edge 10 *cm inside* the edge of the taxiway. The thickness of the taxiway is nominally 16 cm, data as shown in Table 52:3.

Edge strengthened as shown in Fig. 52:1. Edge beam data:

extra flexural rigidity $D_{beam} = 24 \cdot 10^8$ kgcm²

extra ultimate moment $M = 3{,}0$ tm; $M' = 0$

Taxiway d, loading point		d 2
DATA ON TEST SURFACE		
Reinforcement		Single reinf.
Flexural rigidity in edge zone D_{edge}	kgcm²	
for elastic subgrade		$53 \cdot 10^8$
for resilient subgrade		$49 \cdot 10^8$
Soil constants		
soil modulus C	kg/cm²	200
resilience constant k	kg/cm³	0.70
Elast. radius of rigidity l_{edge}	cm	
for elastic subgrade l_e		81
for resilient subgrade l_k		92
Relative load distribution $a = \frac{c}{l}$		
for elastic subgrade a_e		0.62
for resilient subgrade a_k		0.54
ULTIMATE LOAD at failure in top surface P_t		
Ultimate load from test	tons	34
Ultimate load from ultimate strength theory	tons	
for elastic subgrade		46
for resilient subgrade		41
DEPRESSION at ultimate load		
From tests	cm	1.20
From theory (resil. soil)	cm	1.40

beam shown on the previous page, shows by comparison with the curvature measurements during the edge loading test that bottom reinforcement yield point in the edge beam itself has hardly been reached at the load for failure in the top surface. This should imply that the moments in the thinner slab further in from the edge are considerably lower than the yield moment. Under such conditions, strictly speaking, it should not be possible to apply the ultimate strength method and, respect being taken to the above-mentioned effect of temperature and shrinkage, it is almost surprising that the ultimate loads calculated from the ultimate strength method do not lie even further above the test loads. It can be definitely stated that the edge strengthening in this case is unsuitably designed so that its effect cannot be fully utilized.

Problems of a similar type will be treated further in connection with the analysis of the tests in the following section.

53. The Arlanda Tests 1953 (Series A)

531. General. Review of tests carried out earlier and tests treated here

After the authorities for various reasons had abandoned the suggestion to situate the planned Atlantic Airport for Stockholm at Upplands Väsby (see Section 51), it was decided in 1949 to locate the airport at a place close to Halmsjön 40 km north of Stockholm where *Arlanda airport* is now being built. The subgrade conditions at this place were considerably more favourable than in the case of other alternatives earlier examined, since there was natural gravel subgrade or good possibilities through the use of grading to produce a subgrade of compressed gravel for the runways. In general it was therefore possible from the *point of view of load-carrying* to select the alternatives of runways with asphalt pavement or concrete pavement, it was however considered from the *point of view of maintenance* and with the introduction into service of jet-propelled aircraft to be most suitable with concrete runway pavements.

The problem for this airport was thus partly different to the earlier problem, since the subgrade here largely consisted of well compressed gravel with a very high value for the subgrade constants (k- or C-value). From the point of view of load-carrying, it was not essential to have *reinforced* concrete pavements but it was considered valuable from economical aspects to find out whether a reinforced pavement would be more advantageous than an unreinforced. It was also essential in this connection to study the subgrade and examine the applicability of the calculating methods to subgrade conditions of this type.

For this purpose, loading tests were carried out during 1948—1949 on four test slabs resting on a gravel subbase which was specially prepared and compressed for the tests. The test programme was made up in cooperation with the author. Of the slabs used, one was unreinforced 35 cm thick and the others had bottom reinforcement and were 18 and 14 cm thick respectively. Testing was carried out by the Swedish State Road Institute and the tests have been accounted for in a report from the Road Institute [48] as well as in papers by Odemark [53] and Bernell [8].

The tests were however so far unsuccessful as visible failure in the top surface of the reinforced slabs was not obtained during the first testing occasion in the summer of 1948 since the loading apparatus had too small a capacity (maximum 100 tons). It was not until the following spring when the loading possibilities had been developed, that failure with visible cracks was obtained at very much higher loading values. A closer examination of the strain measurements on the top surface which were made simultaneously, shows however, that unreasonably high concrete strain values were obtained, thus:

slab 12:	visible failure crack	155 tons,	strain 0.30 ‰
slab 13:		140 tons,	0.46 ‰
slab 14:		100 tons,	0.44 ‰,

and in the case of all three slabs there were evenly increasing strain values during the complete loading procedure without any sign of such sudden strain increases which are usually found when a crack appears in the top surface. This, as well as the study in other respects of the strain measurements, shows that the slabs must have been cracked already before the last loading, and if the strain values at concrete tension failure obtained by testing the corresponding detail test beams[1]) are compared, it is possible to estimate that the crack formation in the top surface must have occurred in the neighbourhood of the maximum loading to 100 tons during the summer of 1948 without the failure cracks being discovered. Attempts to apply the ultimate strength theory to these tests also show that the theoretical ultimate loads should be in the neighbourhood of this load.

The test results from the 1948—1949 Arlanda tests would appear however, for the reasons explained, to be altogether too unreliable to be analyzed at least from the point of view of the ultimate strength method. BERNELL [8] has analyzed the tests from the viewpoint of the elasticity theory in agreement with the methods given by the present writer, and has hereby shown good agreement with the theory, if the soil is assumed to function as an elastic subgrade.

During the summer of 1953, the paving work on the first of the Arlanda airport runways, the east-west runway, was commenced. The completely prepared runway subbase consisted in its eastern part of a cutting in a gravel ridge, in its central part of an approx. 3 m thick bank of gravel from the ridge and in its western part of an approx. 1 m thick bank of gravel from the ridge, very carefully laid out and compressed.

On the basis of k-value determinations directly on the ground which had earlier been carried out on the runway subbase by the Swedish State Road Institute, it was possible to come to the conclusion that the

[1]) Swedish State Testing Institute certificate no 27702

runway from the point of view of load-carrying needed a concrete pavement on its outer parts, while the centre part of the runway had such a good load-carrying capacity that it could stand up to the assumed wheel load pressure (45 tons) without the help of any rigid pavement. But, due to the reasons explained earlier, it was desired to have a concrete pavement also on this part of the runway.

Since the tests earlier carried out on test pavements, as mentioned above, could not be considered to be completely sucessful, and since it was also desirable to study certain other problems from an experimental point of view, problems that were not sufficiently theoretically investigated at this time, such as the design of joints and free edges, it was considered suitable to carry out new loading tests on test pavements on the runway subbase. Tests were thereby planned so that they would be able to supply direct information for the following design work concerning the concrete pavement.

A special problem was presented in the design of the pavement on the centre part of the runway with 3 m thick gravel subbase with, as mentioned, such a high load-carrying capacity that the surface could on the whole accept wheel loading pressures of 45 tons without any rigid surface layer. The pavement in this case only needs to satisfy demands of an even, maintenance-free surface, but does not need to have, in itself, load-carrying capacity and flexural rigidity, and the ideal pavement in this case would, in point of fact, be a thin but tough membrane with a hard surface. A concrete pavement nearest corresponding to this ideal consists of a thin slab with a relatively powerful reinforcement in the centre, i. e. mid-depth reinforcement. When loading such a slab, fine tension cracks occur in the concrete at relatively low loading, after which the slab functions as a reinforced slab with an effective depth similar to half the total thickness *both* for the positive and negative moments. Since there was no practical experience whatsoever of such thin slabs on good subgrade, it was decided to carry out loading tests on a thin test slab, laid on the section in question of the runway. The slab was arranged so that tests could also be carried out on moment-free joints.

In order to obtain reliable data for pavement design on the rather lower load-carrying outer parts of the runway, test loading was also carried out on a "normal" test pavement with bottom reinforcement, this being laid on the one metre bank in the western section of the runway.

The joint edges must be designed so that shear forces occurring under loading close to the edge can be transferred. If the joints, as being of the usual design with tongue and groove, are calculated in accordance with, for example, the methods suggested by WÄSTLUND-BERGSTRÖM [78], it is doubtful if a normal tongue and groove joint has sufficient strength in the case of the relatively small slab thickness in question here. The test programme therefore also included loading tests close to joints, whereby tongue and groove joints as well as other designs of joint edges were tested.

In agreement with the viewpoints given above, the test programme thus included two test pavements consisting each of three sections separated by joints without dowels or through reinforcement, but with the capacity to transfer shear forces. The slabs were designed and tested in accordance with the following test programme:

I. Test area I, 16 cm thick with bottom reinforcement, subgrade of soil with average load-carrying properties. (1 m thick gravel subbase).
   a) Loading on centre of slab (test 2).
   b) Loading exactly over the two joints which were strengthened in different ways (tests 1 and 3).

II. Test area II, thin slab on very good soil (3 m thick subbase). Slab thickness 8 cm, mid-depth reinforcement with *two* types of reinforcement mesh.
   a) Loading on the slab centre on two of the sections with different reinforcement (tests 9 and 10).
   b) Loading exactly over a joint (test 8).
   c) Loading on the free edges of the outer sections with different reinforcement (tests 14 and 15). This programme point was not planned from the beginning, so that the loaded edges were completely unstrengthened.

III. Special testing of the joint design, whereby the joint edges on both the test areas were designed in three different ways, partly with normal tongue and groove joints, partly with two types of "saw-tooth" joints (tests 4—7 and 11—13 respectively). The test loading was carried out with the loading area tangent to the joint.

The design of the test slabs and the location of the loading points in the various test loading experiments are shown in Fig. 53:1.

532. Test slabs, test devices and test procedure

The dimensions, thickness and reinforcement of the test pavements are shown in Fig. 53:1. The joints between the three sections of the slab in each test area were designed to be moment-free without any through reinforcement; one of the joints was strengthened in such a way that the mesh parallel with the joint was twice as intensive on both sides of the joint over a width which was calculated to cover the yield figure, while

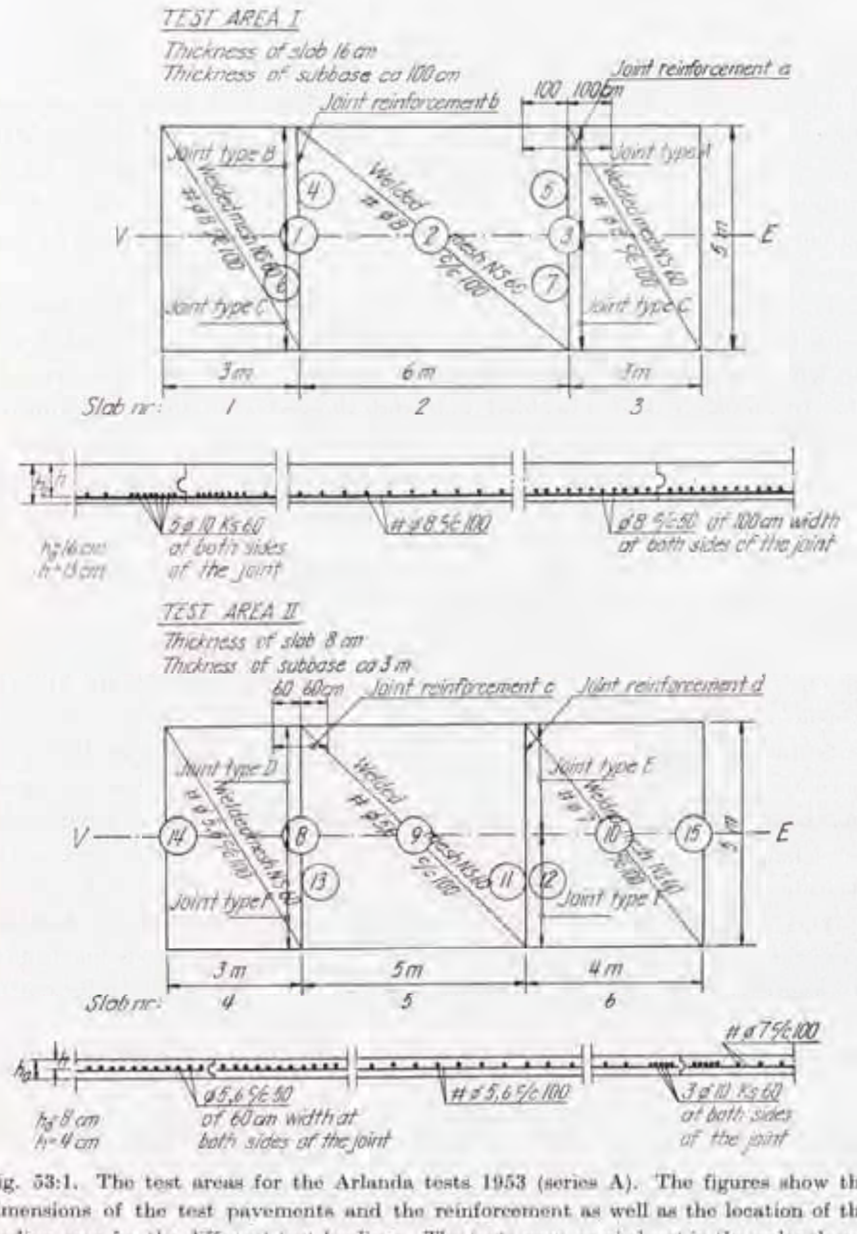

Fig. 53:1. The test areas for the Arlanda tests 1953 (series A). The figures show the dimensions of the test pavements and the reinforcement as well as the location of the loading area for the different test loadings. The tests were carried out in the order shown by the numbers.

the other joint was strengthened by a reinforcement strip of deformed bars Ks 60 on each side of the joint.

Both the test areas were laid on suitable places on the respective parts on the runway, after the subbase of the runway was levelled by using the thinnest possible layer of sand which was rolled. The concrete was cast directly on the subbase surface and was vibrated with a vibrator bridge. The reinforcement consisted of welded reinforcement mesh of cold-drawn wire with the specified quality corresponding to Ns 60 (0.2-limit = 6000 kg/cm²). A 7-day flexural strength of 35 kg/cm² was specified for the concrete.

The strength of the reinforcement was checked by means of tension tests both on the wire before the reinforcement mesh was welded and on wires clipped out of the welded fabric sheet. For the 8 mm wire on the 16 cm slab, the unwelded material showed a 0.2-limit of approx. 7000 kg/cm² and an ultimate strength of approx. 8000 kg/cm² with very even values but on the welded material there was very uneven ultimate strength values between approx. 6000 and 8000 kg/cm². For the wire on the 8 cm slab, both from the 5.6 mm mesh and the 7 mm mesh, the unwelded material showed a 0.2-limit of approx. 6000 kg/cm² and an ultimate strength of 7700—7800 kg/cm² and on the welded material, the values for the ultimate strength varied between approx. 7000 and 8000 kg/cm². The 0.2-limit was not determined on the welded wire but the tensile strain at failure point was very uneven and, in some cases, was outstandingly low.[1]) The uneven and less good values from the mesh wire tests were explained by the manufacturer, saying that the mesh had been manufactured with a great deal of urgency so that a less suitable wire had been used and there had possibly been faulty settings on the welding machines.

The strength of the concrete was checked by means of standard flexural beams; three for each slab section. The flexural strength gave an average value of 42 kg/cm² (maximum deviation approx. 6 kg/cm²).[1])

Simultaneously with the test pavements, 40 cm wide detail test beams were made for use in flexure tests when determining the ultimate moment and the flexural rigidity. For the test area I one pair of such beams were made and for test area II two pairs of beams were made with the same thickness and reinforcement as the test slabs in question, whereby the reinforcement in each pair of detail tests was taken from both directions of the same wire fabric sheet which had been used as reinforcement in the respective test areas (slab sections).

Loading was exerted on the various testing points with the help of

[1]) The full results of the mesh tests and the concrete tests are shown in the result supplement, Section 96.

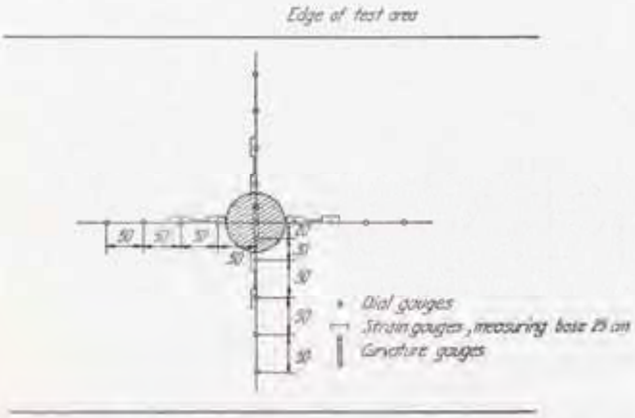

Fig. 53:2. An example of the location of the measuring instruments for the test loadings shown in Fig. 53:1.

the Swedish Road Institute loading apparatus (see 512). The diameter of the loading distribution plate was 80 cm. Between this and the test slab surface, a pressure-equalizing wood fibre board was laid. The loading device permitted a loading with a maximum of 124 tons. On the edge loading tests 14 and 15, the loading plate was located so that it projected about 10 cm outside the edge of the test slab.

The depression of the slab at various points was measured with the Road Institute measuring device by means of dial gauges fitted in measuring beams, which were supported at large distance from the loading point. Measurements were carried out along two directions at right angles through the loading centre in points at a distance of 50 cm. The curvature of the centre was also measured by, in common with the Norrköping tests, measuring its relative depression over a measuring base of 40 cm. The strain values in the top surface of the slab were measured along the measuring radii with strain gauges having a measuring base of 25 cm (see Fig. 25:9). An example of normal gauge location is shown in Fig. 53:2.[1])

Concerning the special measurements carried out in the investigation of the joint edge design, see the account of these tests in Section 536.

Testing was carried out in the same order as the numbering of the test points in Fig. 53:1. The load was applied in steps of generally speaking 5 tons. In the tests on the thin slab, repeated loading and unloading was generally carried out at 45 tons and at the top load as well as in some of

[1]) Complete results in the form of diagrams of the centre depression values and curvature values as well as strain values are shown in the result supplement, Section 96. The location of the strain gauges in the various tests is marked in on the respective diagrams.

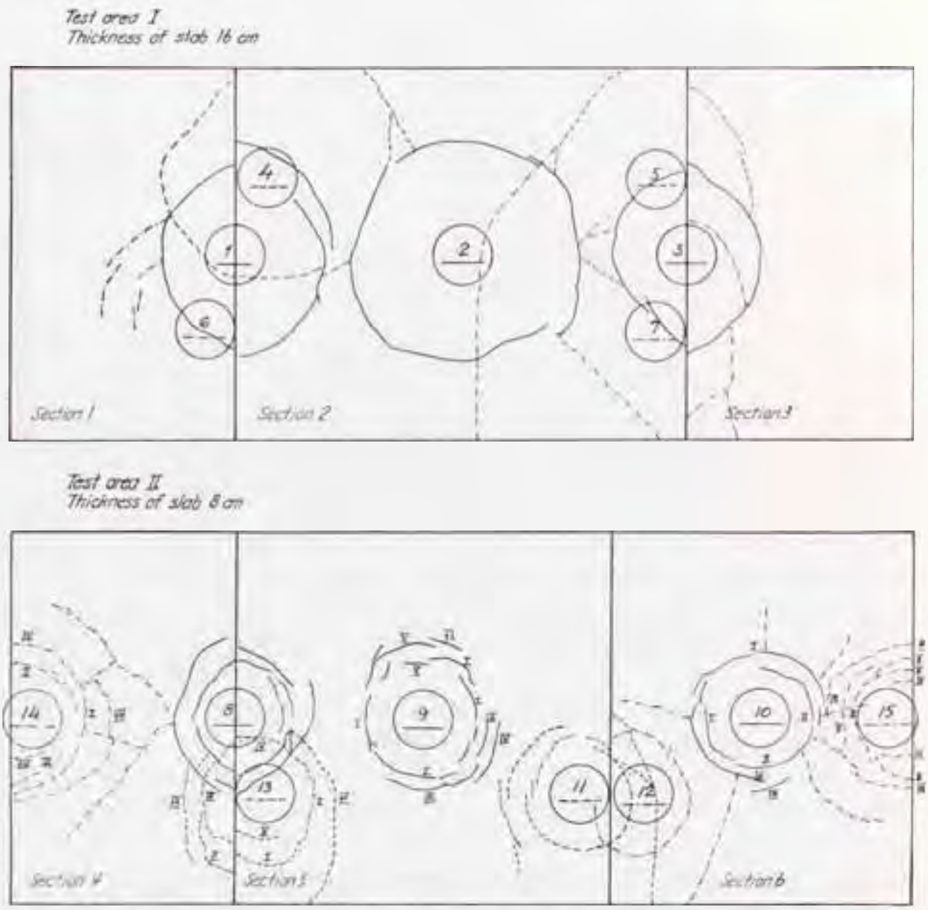

Fig. 53:3. The crack patterns after the test loading of the test areas I and II. The position of the loading area for the different tests is marked in and under the number of the test is shown how the crack lines are marked. The Roman numerals show the order in which the cracks appeared.

the tests also at other loading steps. In this connection off-loading was carried out in one step and the renewed loading in steps of generally 10 tons.

During the higher loading steps, the surface of the slab was inspected thoroughly and any cracks were marked in. The crack patterns for both the test areas are shown in Fig. 53:3. This figure also shows that the crack patterns round some of the loading points merge with each other. This is especially the case with loading close to a joint, and when judging the results from these tests concerning ultimate loads or stresses in the slab, respect must be taken to the fact that the test loading was carried out on zones of the slab which were already cracked. The main aim of the test loadings in question, that of studying the effect of the joint itself, were not however influenced by crack formation.

The result of the depression and strain measurements, as well as the other test results, are shown and discussed in Sections 534—536.

533. Material constants for the slabs and the soil

533.1. *Flexural rigidity and ultimate moment*

The detail test beams which had dimensions of 250×40 cm, were tested at the Swedish State Testing Institute in accordance with a programme made up by the author. The beams were flexurally tested for positive moment simply supported in the same way as the detail test in the V series as shown in Fig. 51:3, thus with one end projecting over the support, and the flexural deformation and, in the case of the 8 cm beams, also the strain measurements on the tension and depression sides were measured over a distance between the loading points. After this first test up to yield point, the uncracked parts of the beam at the projecting end were utilized for deflection tests in the reversed positions; in the case of the 16 cm beams failure tests were only carried out without curvature measurements, while in the case of the 8 cm beams all the measurements of curvature and strains were carried out as in the first test. In some cases, contrary to the test programme, the last-mentioned flexural test was carried out with the beam in the same position as during the first test.

The results of the ultimate moment determinations are compiled in Table 53:1. The values show comparatively great variations, particularly in the case of the 16 cm slab, which are shown by the separate test values in the table. This must obviously depend on the earlier mentioned defects in the reinforcement mesh, so that failure in some cases occurs far below the yield point of the mesh wire. It should be pointed out that in the case of the 8 cm slab, there was no principle difference between the values of positive and negative bending, while the section is fully symmetrical with mid-depth reforcement, and in the table the positive and negative ultimate moments have been considered as being identical.

The curvature measurements give the usual relationship diagrams between the moment and curvature, from which the flexural rigidity of the test slabs can be estimated. Concerning the thin 8 cm slab it is obvious that the flexural rigidity at the transition to Stage II decreases to a great extent, while the reinforcement is mid-depth, and the thickness of the slab at crack formation decreases from the total 8 cm to the effective 4 cm. Deformation (and also strain) therefore increase rapidly after the

TABLE 53:1. Series A. Results of tests on the detail test beams.

The table includes ultimate moment values from *all* the flexural tests with the average values marked, as well as the average values of the other results.

Detail test from test area slab section		I 2	II 5[3])	II 6[3])
Total thickness h_a, nominal	cm	16	8	8
Effective thickness h, nominal	cm	13	4	4
Reinforcement mesh Ns 60		▭ 8 c/c 100	▭ 5.6 c/c 100	▭ 7 c/c 100
Moment at concrete tension failure m_{cr}	kgcm/cm			
measured values		1070 1070	430 374 459 425	294 362 294 233
average values		**1070**	**450**	**295**
Neg. ultimate moment m'	kgcm/cm	**1270**[1])	660 610	860 (490)[2])
Pos. ultimate moment $m_{g\ddot{u}}$ measured values	kgcm/cm	3000 3340 4090	610 760	(340)[2]) (250)[2])
average values		**3500**	**660**[3])	**860**[3])
Curvature $\frac{1}{\varrho}$	cm^{-1}			
at concrete tension failure		$1.1 \cdot 10^{-5}$		
at yield point		$30 \cdot 10^{-5}$	$\sim 130 \cdot 10^{-5}$	$\sim 130 \cdot 10^{-5}$
Strain at concrete tension failure	‰		0.13–0.20	0.09–0.13
Flexural rigidity Ei from *tests*	$kgcm^2/cm$			
at concrete tension failure (Stage I)		$\sim 100 \cdot 10^8$	$\sim 13 \cdot 10^8$	$\sim 13 \cdot 10^8$
at yield point		$12 \cdot 10^8$	$\sim 0.5 \cdot 10^8$	$\sim 0.5 \cdot 10^8$
Flexural rigidity Ei from *calculations* stage II, $n=15$	$kgcm^2/cm$	$11 \cdot 10^8$	$0.50 \cdot 10^8$	$0.65 \cdot 10^8$

[1]) Through an error only one test with negative flexure was carried out.
[2]) Failure due to ripped mesh wire close to the weld crossing.
[3]) The thin mid-depth reinforced slabs have the same resistence for positive and negative flexure.

first crack has occurred but the gauge readings are influenced by the positions of the cracks and the number of cracks as well as by how rapidly the depth of the crack increases. The test values after crack formation are therefore unreliable, and judgement of the procedure is also made more difficult by the fact that, for some of the beams, repeated loading and off-loading was carried out and that, in the case of many of the beams, loading was not continued until the definite yield point in reinforcement had been attained. In Fig. 53:4 the relationship between the moment and the curvature is as far as possible represented in the form of an average curve of the test results obtained from the various detail tests (off-loading is not included here),[1]) and it can be seen that

[1]) The various test curves, also from the detail tests on the 16 cm slab, are shown in the result supplement, Section 96.

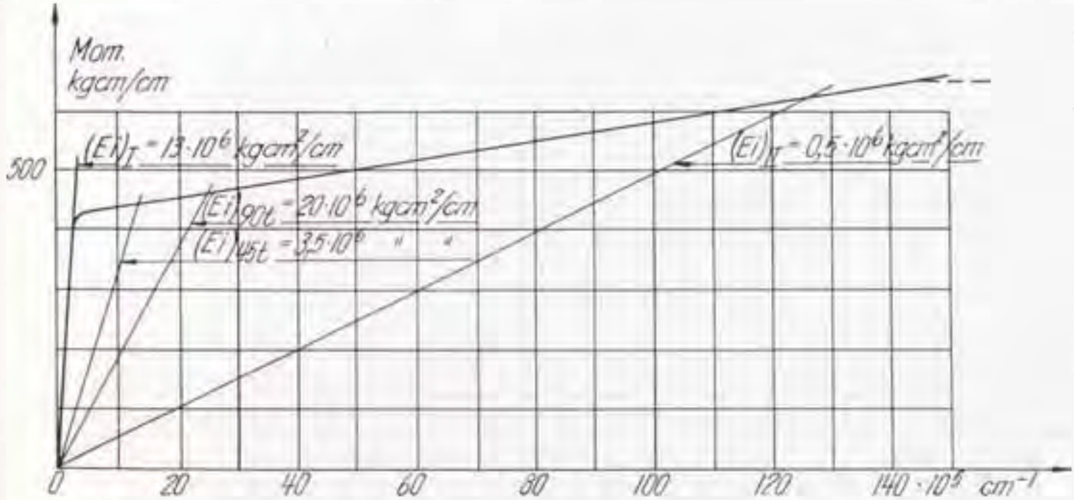

Fig. 53:4. Average curve for the moment-curvature relationship for the 8 cm slab, estimated from the detail tests. The *Ei* values used in the test analysis are shown beside the corresponding secants.

the curvature increases almost instantaneously as soon as the first crack has occurred. Yield does not occur until very large values of curvature have been attained.

Table 53:1 gives the estimated flexural rigidity values for uncracked sections and at yield point. The corresponding curvature values have also been introduced into the table. The test values of the flexural rigidity have been compared in the table with the theoretically calculated values of the flexural rigidity in Stage II ($n = 15$), and showing good agreement with the test values.

It is however obvious that in the case of test loading on the 8 cm test pavement, the deformations by no means reached the level which, according to the detail tests, must correspond to the flexural rigidity values at Stage II, and since the test loading of the slab is to be considered as a first loading of the same character as the flexural tests on the detail beams, a considerably higher *Ei*-value must be used in the test analysis. On the other hand, a runway pavement of this type will gradually pass over into Stage II with a completely developed crack formation and thereby attain a flexural rigidity which corresponds to the values calculated above. In practical design it would thus appear to be most correct to base calculations on an *Ei*-value in accordance with Stage II as above. These questions are also discussed in connection with the *C*-value calculations below as well as the analysis of the test results in Section 535.

The strain measurements in the detail tests on the thinner slab show that the strain increases in a practically unlimited way after tension failure in the concrete. The strain values at concrete tension failure have also been introduced into the table.[1])

533.2. *Soil constants*

The soil constants are determined in the same way as for the other field tests from the centre depression of the test slabs under loading on the centre of the slab sections.

For the test area I (16 cm) the depression values from test loading 2 were thus utilized and the values of the flexural rigidity of the slab necessary for the calculation were taken from Table 53:1. The results of the C-value calculations for Stage I and II are shown in Table 53:2.

For the test area II (8 cm) the depression values from the test loadings 9 (section II:5) and 10 (section II:6) were utilized. When calculating respect must be taken to the fact that the deformation of the slab at higher loading by no means corresponds to the flexural rigidity values for Stage II as shown in Table 53:1. The Ei-value for a certain load and depression has instead been selected so that it corresponds to the secant modulus at the curvature measured at the corresponding load (see Fig. 53:4). The Ei-values estimated in this way and the calculated C-values are shown in Table 53:2.

If, in the calculation of the C-value, other Ei-values are selected there will be a practically unchanged value of C. Even such extreme values as the theoretically calculated Stage II values, as shown in Table 53:1, give results which hardly deviate. This is also shown by a calculation of the depression by using these values of Ei. Thus according to Fig.

TABLE 53:2. Series A. Determination of the soil modulus C from depression values obtained from the test loadings on the centre of the sections.

Calculations in accordance with the depression diagram in Fig. 22:5, the values of flexural rigidity being estimated with the help of the detail tests in Table 53:1.

Slab I, test 2				Slab II, tests 9 and 10, average values			
P ton	w cm	D kgcm²/cm	C kg/cm³	P ton	w cm	D kgcm²/cm	C kg/cm³
15	0.068	$100 \cdot 10^8$	1500	20	0.088	$13 \cdot 10^8$	2900
90	1.27	$12 \cdot 10^8$	700	45	0.25	$3.5 \cdot 10^8$	2700
				90	0.60	$2.0 \cdot 10^8$	2300

[1]) The strain curves for the various detail test slabs are included in the test supplement, Section 96.

22:5 and with the C-values according to Table 53:2, if Ei is put as being equal to $0.5 \cdot 10^6$ kgcm²/cm (section II:9) one gets:

$$P = 45 \text{ tons}; \quad l = \sqrt[3]{\frac{2 \cdot 0.50 \cdot 10^6}{2700}} = 7.2 \text{ cm}; \quad \frac{c}{l} = 5.55$$

$$w_0 = \frac{45 \cdot 10^3 \cdot 7.2^2}{0.5 \cdot 10^6} \, 0.058 = 0.27 \text{ cm} \text{ — according to test } 0.25 \text{ cm}$$

$$P = 90 \text{ tons}; \quad l = \sqrt[3]{\frac{2 \cdot 0.50 \cdot 10^6}{2300}} = 7.6 \text{ cm}; \quad \frac{c}{l} = 5.30$$

$$w_0 = \frac{90 \cdot 10^3 \cdot 7.6^2}{0.5 \, 10^6} \, 0.061 = 0.64 \text{ cm} \text{ — according to test } 0.63 \text{ cm}$$

thus particularly good agreement.

The calculation of the C-value is thus, in cases such as this with very large relative load distribution, almost completely independent of the correct selection of the flexural rigidity. It is also obvious that the C-value is here much more independent of the loading than in earlier calculations of the same type where the varying rigidity conditions of the slab have a greater influence.

Further control of the C-value is obtained by making a comparison between the depression lines in theory and practice in Fig. 53:10 page 353. Calculations with other Ei-values show that also the theoretical depression lines are practically independent of the value for the flexural rigidity.

534. The 16 cm test pavement. Test results, treatment and theoretical analysis

534.1. *Test results*

In the loading tests on the various loading points of the 16 cm test area I, the load was increased until failure occurred in the top surface and then generally some loading steps beyond this point.

The results of the depression measurements have been compiled in the form of depression lines, of which some examples are shown in Fig. 53:5.[1]) Apart from the measurements with the load in the centre of the slab (test 2) and over the joint (test 3) one of the tests with loading

[1]) Test results of the depression and strain measurements for all the tests are shown in the result supplement, Section 96, in the form of depression and curvature diagrams for the loading points as well as strain diagrams.

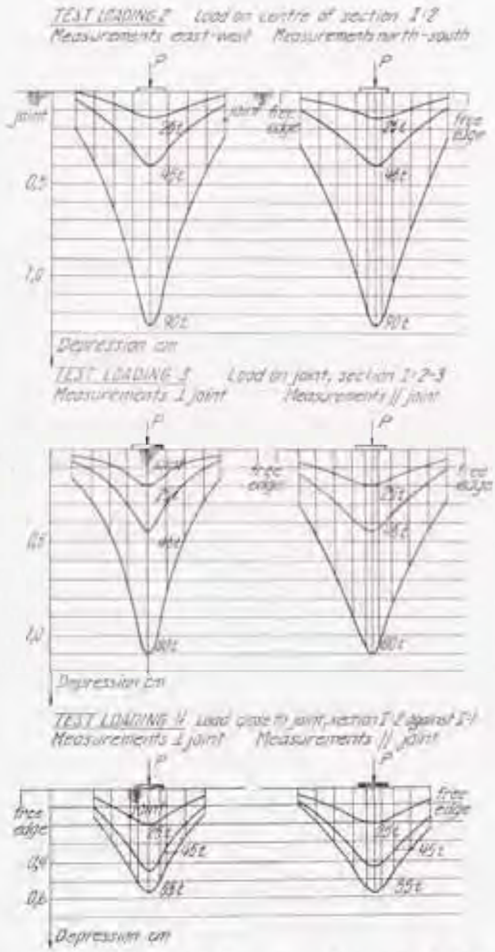

Fig. 53:5. Depression lines for some loading steps for part of the tests on slab I. The result from one of the joint edge tests is also included (test 4), and it is remarkable how slight an effect the joint appears to have on the form of the depression lines.

beside a joint (test 4) has also been included for comparison, this test being included in the examination of the joint edge design. The joint edge tests are otherwise described in Section 536.

From the strain measurements[1]) on the top surface, load at failure in the top surface P_t can be determined in the usual way. The ultimate loads determined in this way are shown in Table 53:3.

Otherwise it is possible as usual to get some idea of the moments and stresses in the loading point by studying the curvature of the slab at this point. The curvature values have been calculated from the deforma-

[1]) See note [1]), page 341.

TABLE 53:3. Series A, 16 cm test area I. Result of test loadings.
Loads at failure in top as well as at crack formation and yield in bottom, according to test results from strain measurements (P_t) and curvature measurements (P_b^{cr}, P_b^{yie}).

Test no.	Location of load	Load at failure in top P_t tons	Load at concrete failure in bottom P_b^{cr} tons	Load at yield in bottom P_b^{yie} tons
2	On centre of slab 2	95	13	90
1	On joint 1-2, b	60-65	—	$>P_t$
3	On joint 2-3, a	80	—	$>P_t$

tion of the centre point on a measuring base of 40 cm on the basis of only the deformation of the centre point over this distance, but with this short measuring base-line, the method should give sufficiently accurate results.[1]) By comparing the curvature values for the centre point as usual with the corresponding measurements on the detail tests, it is possible to determine the loads for concrete tension failure P_b^{cra} and reinforcement yield P_b^{yie} in the bottom surface for loading on the centre of the slab.

In order to determine in the same way the load P_b when testing the strengthened joints where there are no corresponding detail tests, a theoretical estimation of the ultimate moment and flexural rigidity for these joint edges must be carried out by proportioning in the usual way from the results of the detail tests corresponding to the unstrengthened slab. In this way (see the corresponding calculations on page 326, $\bar{\sigma}_c$ is assumed to be = 300 kg/cm²) one obtains:

Joint 2—3, strengthening a, mesh ⌀ 80 c/c 50 mm

$$m_{yie} = 3500 \cdot 2 \frac{1 - 0.09}{1 - 0.045} = 6600 \text{ kgcm/cm}$$

$$Ei_{11} = 12 \cdot 10^6 \frac{137}{80} = 20 \cdot 10^6 \text{ kgcm}^2\text{/cm}$$

$$\frac{1}{\varrho_{yie}} = \frac{6600}{20 \cdot 10^6} = 33 \cdot 10^{-5} \text{ cm}^{-1}$$

Joint 1—2, edge strengthening b, reinforcement strip 5 ⌀ 10 Ks 60 approx. 26 cm wide.

For the entire edge beam with $b = 25$ cm, the following apply:

$$M_{0_{yie}} = 25 \cdot 3500 \frac{1.65}{0.38} \frac{1 - 0.19}{1 - 0.045} = 3.2 \cdot 10^5 \text{ kgcm}$$

[1]) See note [1]), page 341.

$$E\,I_{\text{beam}} = 12 \cdot 10^{6}\ \frac{5700}{80} = 8{,}5 \cdot 10^{8}\ \text{kgcm}^{2}$$

$$\frac{1}{\varrho_{yie}} = \frac{3{,}2 \cdot 10^{5}}{8{,}5 \cdot 10^{8}} = 38 \cdot 10^{-5}\ \text{cm}^{-1}$$

If the curvature values estimated in this way are compared with the curvature graphs for the loading point, it can be seen that yield failure in the bottom is never reached in the joint loading tests, i. e. $P_t < P_b^{yie}$. Edge strengthening is thus in both cases so far unsuitably designed that it is not fully utilized when failure in the slab occurs due to crack formation in the top surface. The P_b^{yie}-values estimated are shown in Table 53:3.

534.2. *Load on the centre of the slab (test 2), theoretical analysis*

To judge by the load values in the result Table 53:3 it is clear that the centrally-loaded slab section at definite crack failure in the top surface has just reached yield point in the bottom surface. The slab should therefore on the whole follow the elasticity theory right up to the ultimate load.

Calculations which are based on the theory for elastic subgrade, compared with the test results in Table 53:4 also show that there is good agreement between theory and test results. This also concerns the load P_t at failure in the top surface. It should however be pointed out that the ultimate moment values from the detail tests shown in Table 53:1 and on which the ultimate load values in Table 53:4 are based, are very unreliable and show great spread. The negative ultimate moment value has been obtained from only *one* test.

Calculation of the final ultimate load P_t has also been carried out in accordance with the *ultimate strength theory* and the table shows that agreement with the test values is also here very good.

It thus appears as far as can be judged on the basis of the unreliable ultimate moment values, as if the ultimate load calculation can be carried out on the basis of either the elasticity theory or the ultimate strength theory. This obviously depends on the fact that with the moment distribution for this comparatively extensive relative load distribution and with the ultimate moment values in question, negative moment failure is obtained at almost the same load as the load at which the yield point in the reinforcement under the loading centre is reached. In the case of large relative distribution the "elastic" moment curve is otherwise already so evened out that it approximately satisfies the

TABLE 53:4. Series A, 16 cm test area I. Loading on centre of section, test 2.

Loads at crack formation and yield in bottom and at failure in top from tests as well as the elasticity theory and the ultimate strength theory.

The size of the slab section 6 × 5 m. Loading area with radius $c = 40$ cm.

The constant values for the slab and the soil from Table 53:1 and 53:2. The soil is assumed to behave as an elastic subgrade.

Slab I, section 2.	Stage	I	II
DATA FOR SLABS			
Flexural rigidity Ei	kgcm²/cm	$\sim 100 \cdot 10^8$	$12 \cdot 10^8$
Soil modulus C	kg/cm³	1500	700
Loading constants			
Elast. radius of rigidity l	cm	51	32
Rel. load distribution $a = \frac{c}{l}$		0.78	1.25
Ultimate moments	kgcm/cm		
with positive flexure m		~ 1100	3500
with negative flexure m'			1300
RESULTS			
Ultimate load at bottom failure P_b	tons		
from tests		13	90
from *elasticity theory*		~ 13	82
Ultimate load at top failure P_t	tons		
from tests			95
from *elasticity theory*			90
from *ultimate strength theory*			96

demand of the ultimate strength theory concerning constant moment in the radial cracks out to the failure ring crack, and the influence of "incomplete plastification" should thus in such cases be even smaller than usual.

534.3. *Loading on joints (tests 1 and 3), theoretical analysis*

For this case of loading it has earlier been shown (see Table 53:3) that yield point was never reached in the bottom reinforcement before top surface failure occurred. The loading procedure is thus completely within the elastic stage.

Table 53:5 shows the results of a test analysis according to the elasticity theory. Calculations have been carried out both for resilient and elastic soil, in the last-mentioned case according to the supposition made by the author in Section 41 that the relationship between the moment of centre and edge loading is similar for both the subgrade hypotheses. The k-value has thereby been calculated from the relationship formula (23:4). When calculating the flexural rigidity and the l-value for the joint b strengthened with reinforcement strip it has been assumed in the usual way that the flexural rigidity of the edge strengthening can be distributed over a width l.

TABLE 53:5. Series A, 16 cm test area I. Test loading on joints.

Theoretical analysis according to the elasticity theory and the ultimate strength theory. Loading area with radius $c=40$ cm exactly over joints.

Flexural rigidity of the unstrengthened slab $Ei_{II}=12\cdot 10^6$ kgcm²/cm and its ultimate moments $\begin{cases} m=3500 \text{ kgcm/cm} \\ m'=1300 \text{ kgcm/cm} \end{cases}$

Soil constants $C=700$ kg/cm², $k=4{,}5$ kg/cm³.

Slab I, joint strengthening Test loading no.	a 3	b 1
DATA FOR JOINTS	2–3	1–2
Strengthening along the joint	Mesh ⌀ 8 c/c 50 mm over a width of 1 m	Extra 5 ⌀ 10 Ks 60 over a width of appr. 25 cm
Flex rigid. of "edge beam" at joint b, width 25 cm, calc. value EI_{beam} kgcm²	—	$8.5\cdot 10^9$
Flex. rigid. of edge zone, width l, D_{edge} kgcm²/cm		
for resilient soil	$20\cdot 10^6$	$23\cdot 10^6$
for elastic soil	$20\cdot 10^6$	$25\cdot 10^6$
Elast. radius of rigidity l cm		
elastic soil l_e	39	42
resilient soil l_k	46	48
Relative load distribution		
elastic soil $a_e=\frac{c}{l_e}$	1.04	0.95
resilient soil $a_k=\frac{c}{l_k}$	0.87	0.88
Ultimate moment calculated for edge		
for entire edge beam b, width 25 cm, kgcm	—	$3.2\cdot 10^5$
per unit width kgcm/cm	6600	13000
RESULTS		
Ultimate load at top failure tons	80	60 à 65
Curvature in loading centre at ult. load cm⁻¹	$22-26\cdot 10^{-5}$	$11-13\cdot 10^{-5}$
ANALYSIS ACCORDING TO ELAST. THEORY		
m^+_{max} at ult. load kgcm/cm		
from tests, from curvature $m=\frac{1}{\varrho}\cdot Ei$	4400–5200	3500–4200
from theory with elastic soil	5000	4170–4520
from theory with resilient soil	6120	4810–5215
Ultimate load P_t from theory tons	44	44
Depression values at ultimate load cm		
from tests	1.12–1.23	0.53–0.69
from theory (resilient soil)	1.13	0.83–0.90
ANALYSIS ACCORDING TO ULTIMATE STRENGTH THEORY		
Ultimate load from theory		
for elastic subgrade	87	83
for resilient subgrade	75	72

The results of the calculations according to the table show that there is fairly good agreement between the experimentally estimated and theoretically calculated positive moment at the ultimate load, whereby calculation according to the assumption of elastic subgrade gives the best agreement with the test values. When judging the results, however, it should be remembered that the test values have been estimated according to the expression

$$m = \frac{1}{\varrho} Ei$$

and that the flexural rigidity Ei was thereby inserted with the Stage II-value applying at yield point while in the tests there was never any question of reaching yield point in the bottom reinforcement.

The theoretical value according to the elasticity theory, formula (41:9), for the definite ultimate load P_t agrees, on the other hand, very badly with the test values. This can depend partly on the fact that with these strengthened edges there is another distribution of the negative moment than that assumed by the theory which is based on an unstrengthened edge. It should also be remembered that the expression (41:9) for the negative maximum moment is based on the assumption of resilient subgrade, while the soil functions more nearly as elastic subgrade. A comparison between the corresponding moment values in the case of load on the centre shows that the maximum negative moment for elastic subgrade is lower than for resilient subgrade, and an analogy in this respect for the case of edge loading would thus give higher values for the theoretical ultimate load.

It has been pointed out that the conditions for the ultimate strength theory in the edge loading tests are by no means satisfied and the test analysis according to Table 53:5 shows that the positive moment in the loading point at the ultimate load is low, perhaps 50 % under the yield moment. If, in spite of this, calculations are carried out according to the ultimate strength method the result, according to the table, nevertheless shows relatively good agreement with the test value at least concerning the ultimate load on the joint with a strengthening consisting of intensified mesh in the edge zone.

If some calculations are however carried out according to the ultimate strength theory (design diagram in Fig. 42:11) on the assumption of different lower values of the positive moment than that corresponding to the ultimate moment, it will be shown that the ultimate load decreases comparatively slightly with decreased positive moment. For values otherwise applying to the joint a, the following are obtained:

$$\frac{c}{l} = 1.04; \qquad m' = 1300 \text{ kgcm}^2/\text{cm}$$

$$m{:}m' = 5; \qquad \frac{P}{2} = \frac{m + m'}{0.180} = 33.2\, m' \qquad P = 86 \text{ tons}$$

$$4 \qquad \frac{m + m'}{0.167} = 29.9\, m' \qquad 78 \text{ tons}$$

$$3 \qquad \frac{m + m'}{0.150} = 26.7\, m' \qquad 70 \text{ tons}$$

$$2 \qquad \frac{m + m'}{0.133} = 22.5\, m' \qquad 60 \text{ tons}$$

This explains that in Table 53:5 it is possible to get a theoretical ultimate load value which lies only slightly higher than the test value (on the assumption of elastic subgrade) in spite of the fact that there are such great deviations between the positive ultimate moment value used when calculating and assumed to have been completely reached in positive yield cracks, and the actual positive moment distribution. Corresponding observations have also been made concerning the Norrköping tests.

It thus appears that, at least from an estimating point of view, it is possible to use the ultimate strength theory when calculating or designing a joint or edge even if the conditions of the theory are not satisfied. The conclusion reached earlier, however, remains that the edge strengthening is faultily designed so that the extra reinforcement cannot be fully utilized. In the correct design of a joint or edge, the elasticity theory should be used to help check that the bottom reinforcement at the ultimate load attains or (from a calculating point of view) exceeds the yield point and then locate other possibly necessary reinforcement in the top surface, whereby the ultimate strength theory may be used to calculate the nesessary reinforcement.

535. The 8 cm test pavement. Test results, treatment and theoretical analysis

535.1. *Test results*

During the loading tests on the 8 cm test area II, the load was increased generally in steps up to 45 tons (corresponding to the specified maximum wheel load pressure exerted by traffic) after which repeated loading and off-loading was carried out. The load was then increased

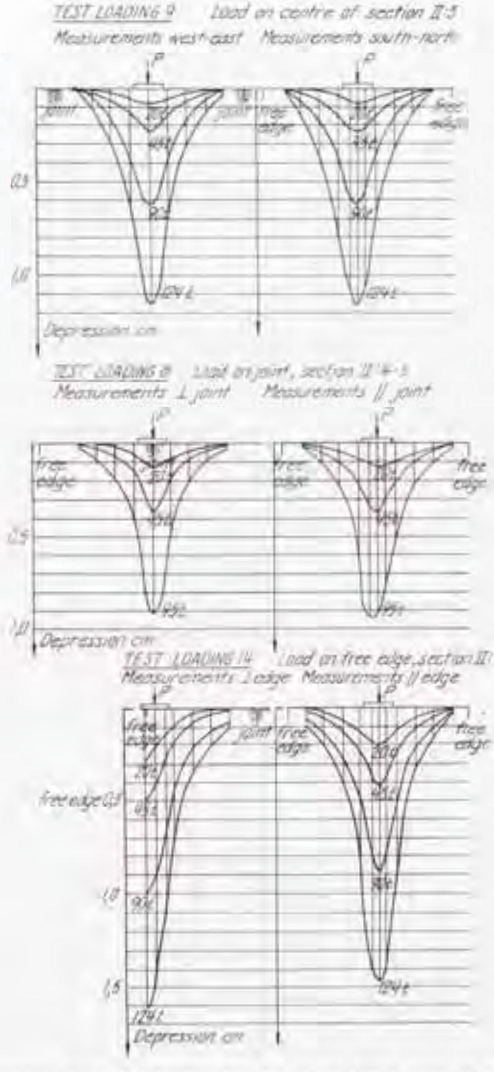

Fig. 53:6. Depression lines for some loading steps from part of the tests on slab II.

to the maximum load, generally 124 tons, where one or two loading and off-loading procedures were carried out.

The results of the depression measurements are exemplified in Fig. 53:6 which shows the depression lines for some of the loading steps with some of the test loadings, as well as in Fig. 53:7 which shows the centre depression and the curvature diagrams for test loading 10.[1])

[1]) The results of the depression and strain measurements with all the tests are shown in the test supplement, Section 96.

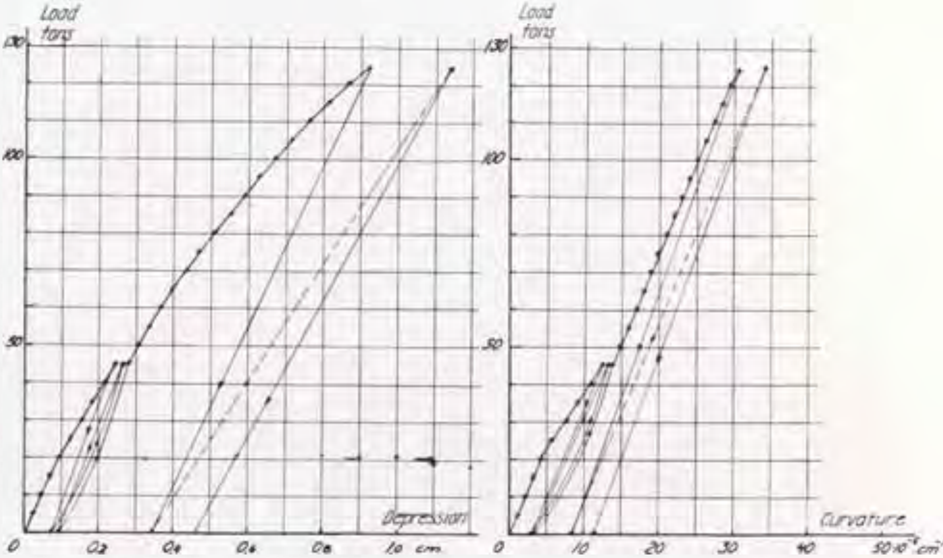

Fig. 53:7. Centre depression and curvature diagram for test loading 10 on the centre of slab section II:6.

It is obvious that the depression and curvature graphs as shown in Fig. 53:7 have a much more linear appearance than the corresponding graphs in any earlier test. This clearly depends on the fact that the variations of the rigidity of the thin slab under loading influence the depression and deformation to a very small extent, a fact that has been already discussed in connection with the determination of the soil constants. At a relatively low load in the case of most of the tests, a comparatively weak but obvious break-off point on the depression and curvature graphs (see Fig. 53:7) was obtained. This would appear to be caused by the occurrence of the first cracks in the bottom surface so that the slab goes over from Stage I to Stage II. The flexural rigidity is thereby changed to a particularly great extent in these slabs which have mid-depth reinforcement, since the effective thickness has been decreased from 8 to 4 cm (see Fig. 53:8).

As expected, circular cracks occurred in the top surface at a relatively low load. In the usual way the crack load could be determined on the basis of the strain measurements,[1]) and the crack load determined was generally rather much lower than the load where the first cracks could be observed. The crack width increased namely comparatively slowly for loading above the crack load.

[1]) See note 1), page 349.

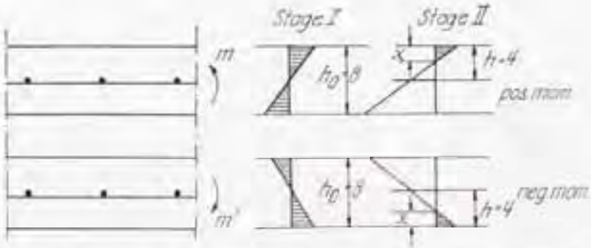

Fig. 53:8. Stress distribution in Stage I and Stage II (theoretical) in the 8 cm mid-depth reinforced slab for positive and negative moment. See also Fig. 53:9.

It should be pointed out that the occurrence of cracks in the top surface on these slabs with mid-depth reinforcement does *not* imply that the ultimate load has been reached but only implies that the slab, also for negative moment, has gone over to Stage II and functions as a reinforced concrete slab with an effective depth equal to half the total thickness (Fig. 53:8). The definite ultimate load in the meaning formerly implied is first reached when the reinforcement stresses in the annular cracks reach the yield point. In spite of the fact that the loads in these tests were generally increased up to 124 tons, thus to considerably higher maximum loads than in the case of the 16 cm slabs, no reinforcement yield was obtained in the annular cracks for any of the tests, however, as far as could be judged from the strain measurements. The same decision is arrived at by the fact that when the slab surface was inspected after the termination of the test, the cracks had closed so much that they were practically invisible.

Table 53:6 includes the loads at the first crack in the top and bottom surfaces for the various test loadings estimated as mentioned above. In order to clarify the behaviour of the slab even more, the table also includes deformation phenomena: curvature in the loading point and the measured maximum strain in the top surface at the highest test load, and from these values the maximum stresses in the reinforcement by positive and negative moment have been estimated. The slab is thereby assumed to have gone over completely to Stage II with completely cracked tension zone (see Fig. 53:8). In point of fact, the tests by no means reach this condition, which according to Table 53:1 corresponds to a curvature of approx. $130 \cdot 10^{-5}$ cm^{-1}, since the tension zone is, according to Fig. 53:9, to a large extent active, and the reinforcement stresses are thus considerably lower than those shown in the table, these values representing a theoretical upper limit.

It is thus obvious that concerning all the test loadings on the 8 cm slabs, the yield point in the reinforcement and thereby the ultimate

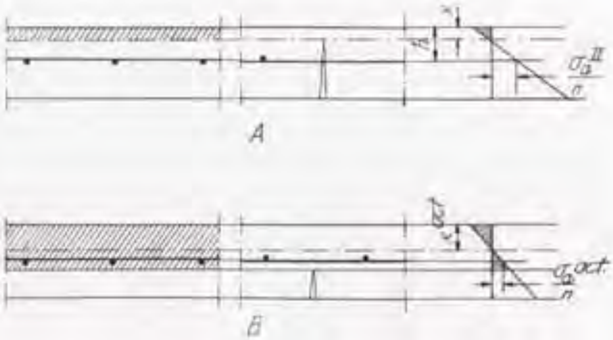

Fig. 53:9. Theoretical (A) and actual (B) stress distribution and crack formation for the 8 cm mid-depth reinforced pavement.

load of the slab was never even nearly reached. The slab functioned completely within the elastic stage and the following test analysis will therefore be completely based on the *elasticity theory*.

TABLE 53:6. Series A, 8 cm test area II. Result of test loadings.

Loads at concrete failure in top and bottom as well as estimated maximum stresses in the reinforcement at the highest loading.

Stress calculations according to Stage II (completely cracked tension zone) and $n = 15$.

Test no.	Location of load	Load at first crack in bottom P_b^{cr} tons	Load at first crack in top P_t^{cr} tons	Curvature and estimated stresses (Stage II, $n = 15$) at $P = 124$ tons (test 8, $P = 95$ tons)			
				pos. moment		neg. moment	
				$\frac{1}{\varrho}$ cm^{-1}	σ_r 1) kg/cm^2	ε_t^u/₀₀	σ_r 2) kg/cm^2
9	Centre of slab 5	22	45	$37 \cdot 10^{-5}$	2000	0.7	600
10	Centre of slab 6	20	45	$31 \cdot 10^{-5}$	1500	0.7	550
8	On joint 4–5, c (load $P = 95$ tons)	17	25	$24 \cdot 10^{-5}$	1050	1.2	900
14	On edge, slab 4	—	(15)	$36 \cdot 10^{-5}$	1900	1.8	2500
15	On edge, slab 5	—	(10)	$46 \cdot 10^{-5}$	2300	2.1	2300

1) $\sigma_r = \frac{1}{\rho}(h - x)E_r$

2) $\sigma_r = E_r\, \varepsilon_t \frac{h - x}{2h - x}$

535.2. *Theoretical analysis of the centre loading tests (tests 9 and 10)*

As early as in the calculation of the C-values in 533.2, the elasticity theory has been applied to the depression values of the slab in the case of centre loading, and the soil modulus C has thereby been calculated for several different loads so that agreement between theoretical and

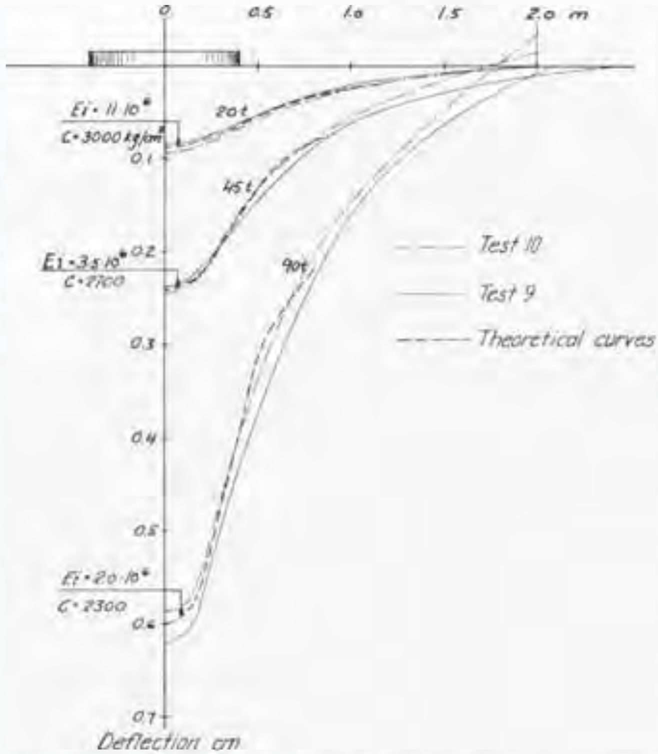

Fig. 53:10. Depression lines from test loadings 9 and 10 on the centre of the slab sections II:5 and II:6, 8 cm mid-depth reinforced slab, from tests and the elasticity theory (elastic soil). The theoretical curves are calculated in accordance with the diagram in Fig. 22:5 and with the values for the constants for slab and soil shown beside the respective curves.

experimental centre depression has been obtained. In these calculations those secant values of the flexural rigidity were used, which can be estimated from the curvature values under the loading centre for the loads in question, if it is assumed that the relationship curve $M - \frac{1}{\varrho}$ of the test slab agrees with that of the detail test beams (Fig. 53:4). The fact that the theoretical and measured depression lines also show good agreement is demonstrated by Fig. 53:10. However, practically the same depression values are obtained in the centre and also the depression lines are in fairly good agreement for other values of the flexural rigidity. As shown in 533.2 it is even possible to use the very low theoretically calculated Ei-values in Stage II without the agreement being very much poorer. On the whole the theoretical deflection values appear to be practically independent of the value of flexural rigidity used for the slab.

Since no actual ultimate loads were reached in these tests, the test results are analyzed instead in such a way that the moments theoretically calculated (for elastic subgrade) and experimentally estimated (from curvature values) are compared for loads of 20, 45 and 90 tons. The results are shown in Table 53:7 and the table also includes the calculation data for the slab sections. As a value for flexural rigidity for the higher loading steps has been used, in the same way as mentioned above, partly the *Ei*-values which, according to the detail tests and Table 53:2, corresponds to the curvature of the slab in the loading centre (columns 2 and 3) and should nearest represent the *actual* flexural rigidity of the slab at the load in question; and partly the theoretically calculated *Ei*-values for Stage II and $n = 15$ (column 4—7), which represent a *theoretical* but by no means attained final stage for the slab. The subgrade is assumed to function as elastic subgrade with the *C*-values calculated according to Table 53:2.

With this thin slab very large values of the relative load distribution are obtained, particularly with the theoretical flexural rigidity values in columns 4—7 in the table. The moment according to the elasticity theory has been obtained from the diagrams in Fig. 22: 7, where, however, the negative moment values for the extended load distribution values in the columns 4—7 can not be obtained (the calculation which form the basis for the moment curves in Fig. 22: 7 have not been carried out for larger values of relative load distribution than 3). Concerning the test values of the moment in the table, the positive moments have been estimated from the curvature in the loading centre and the negative moments from comparison between the values of the strain in the top surface and the strain measurements in the detail beam tests.[1] With respect to the fact that the measuring length for the strain gauges in both cases was different (25 and 40 cm respectively) and that the moment distribution and crack formation was not comparable, together with the fact that the vast spread between the different detail test beam results (see the moment values in Table 53: 1), this method of estimating the negative moments in the slab must be considered as being *very* unreliable.

The table shows that agreement between these theoretically calculated and experimentally estimated moment values under these conditions is good.

One fact of particular interest is that the agreement concerning the positive moments is approximately as good whether the "actual" *Ei*-values according to columns 2 and 3 are used or the theoretical values according to columns 4—7. This obviously applies in the same way

[1]) See the result supplement, Section 96.

TABLE 53:7. Series A, 8 cm test area II: 5 and 6. Test loadings 9 and 10 on the centre of the sections.

Test results and theoretical analysis according to the elasticity theory (elastic soil).
Loading area with radius $c = 40$ cm.

Slab A II, Stage	I		II							
			Ei from detail tests corresponding to curvature				Ei theoretically calculated from Stage II and $n=15$			
Column	1		2		3		4	5	6	7
Loading tons	20		45		90		45		90	
Slab II, section	5 and 6		5 and 6		5 and 6		5	6	5	6
DATA FOR SLAB SECTION										
Flexural rigidity Ei kgcm²/cm	$13 \cdot 10^6$		$3.5 \cdot 10^6$		$2.0 \cdot 10^6$		$0.50 \cdot 10^6$	$0.65 \cdot 10^6$	$0.50 \cdot 10^6$	$0.65 \cdot 10^6$
Soil modulus C kg/cm²	2900		2700		2300		2700	2700	2300	2300
Elast. radius of rigidity l cm	20.8		13.7		12.0		7.2	7.8	7.6	8.3
Rel. load distribution $a = \frac{c}{l}$	1.90		2.92		3.33		5.56	5.13	5.26	4.82
TEST RESULTS, slab section	5	6	5	6	5	6	5	6	5	6
Curvature in loading centre $\frac{1}{\varrho}$ cm⁻¹	$3.7 \cdot 10^{-6}$	$4.1 \cdot 10^{-6}$	$12 \cdot 10^{-5}$	$12 \cdot 10^{-5}$	$26 \cdot 10^{-5}$	$23 \cdot 10^{-5}$	$12 \cdot 10^{-5}$	$12 \cdot 10^{-5}$	$26 \cdot 10^{-5}$	$23 \cdot 10^{-5}$
Max. strain ε_t ‰	0.049	0.043	0.14	0.14	0.46	0.48				
ANALYSIS OF RESULTS, elast. theory										
Moment in loading centre $m^{+}{}_{max}$ kgcm/cm										
from tests $m = \frac{1}{\varrho} Ei$	470	530	420	420	520	460	60	78	130	150
from theory	460		405		550		50	63	120	153
Max. neg. moment $m^{-}{}_{max}$ kgcm/cm										
from main tests and detail tests	100-170		300-400		350-450					
from theory	170		280		~400					

concerning the moments as earlier shown concerning the depression values that the result in this respect is almost completely independent of the value of the flexural rigidity of the slab. Columns 1 and 4—7 represent a type of "theoretical" loading procedure: after the flexural strength in the concrete is reached, the slab cracks in the tension zone and goes over completely to Stage II with $h = 4$ cm (see Fig. 53: 8). The flexural rigidity thereby diminishes to a great extent and the moments decrease suddenly, and then with continued loading increase roughly proportionally to the loading. In point of fact the procedure goes on instead according to columns 1 and 2—4, corresponding to the detail beam testing according to Fig. 53: 4. The crack formation through the tension zone and the transition to Stage II proceeds successively (see Fig. 53: 9); the flexural rigidity decreases then comparatively slowly and the moment remains constant or increases slowly. The actual stresses in the reinforcement are, as earlier mentioned, *lower* than the theoretical stresses. Since it is probable that the repeated loading and off-loading occurring in practice as a result of traffic gradually give the slab a crack formation which corresponds to Stage II, then it should be quite correct when designing to calculate with the flexural rigidity and the moment and stresses which theoretically correspond to this stage.

Concerning the negative moments, agreement between the theory and the tests according to Table 53: 7 is as good as can be expected with respect to the unreliable test values mentioned above. The extent to which the negative moments change when the slab goes over completely to Stage II cannot be verified theoretically at these large values of load distribution. To judge from the test results and the theoretical moment curves, it would appear however as if the magnitude of the negative moment has no significance when designing a slab such as this where the reinforcement is of the mid-depth type.

The calculations in Table 53: 7 are based on the supposition that the subgrade functions as an elastic subgrade. Calculations of the moments according to the hypothesis of resilient subgrade give much poorer agreement with the test results, particularly with the flexural rigidity values in column 4—7, Stage II.

The test results and the discussion thus mean that when designing a mid-depth reinforced slab of this type, the flexural rigidity of the slab and the stresses in the reinforcement should be calculated on the basis of the assumption that the slab has completely gone over into stage II. The maximum stress is calculated from the moment under the loading centre according to the elasticity theory and on the assumption that the subgrade functions as an elastic subgrade.

535.3 *Analysis of the test loadings on joints and free edges*

It is not possible to analyse the loading tests on the joint c and on the free edges according to the same method as used above for the tests concerning centre loading since the formulae and the diagrams for the cases of edge loading in section 44 do not apply for the large values of relative load distribution concerned here. The formulae (41:7) and (41:8) for the relationship $m_{edge} : m_{centre}$ have not been verified for larger values of $\frac{c}{l}$ than 1.0 for edge loading at a tangent and 2.0 for joint loading, and the corresponding relationship curves in Fig. 41:3 show an unmistakable tendency to deviate upwards from the straight line in the case of increased load distribution.

In order to give some idea of the conditions prevailing with these large values of relative load distribution, Table 53:8 compares the moment values estimated from the test results (curvature) in the joint and edge loading tests with the corresponding theoretical moments when loading on *the interior* of a similarly reinforced slab. The flexural rigidity is thereby estimated by theoretical calculations according to Stage II and $n = 15$; as far as the slab strips along the joint with their strengthening are concerned there are no detail beam tests made for direct determination of the flexural rigidity. When estimating the curvature and moment for the edge loading tests 14 and 15, respect must be taken to the fact that the slab was not in contact with the subgrade when loading was commenced, this being clearly shown by the large initial deformation shown by the depression and curvature diagrams.[1]) The curvature values have been corrected as far as possible for this by exterpolating the corresponding diagram lines to zero loading, and the curvature thus obtained at a load of zero is taken as the initial value, but the condition in question naturally contributes to increasing the unreliability of the result.

As comparison the table also includes the corresponding calculations for the centre loading tests 9 and 10, which can give an idea of the accuracy and spread in agreement between the tests and theory.

The results according to the table give values of the relationship between the positive moments of joint loading or edge loading on one side and centre loading on the other, which by comparison with Fig. 41: 3 and Table 41: 1 appear reasonable. When judging the result, it should be remembered that the load area in the case of edge loading projected 10 cm over the edge of the slab. This thus corresponds actually to a rather more concentrated load than that reckoned with, i. e.

[1]) See the result supplement, Section 96.

TABLE 53:8. Series A, 8 cm test area II. Comparison between moments in the slab due to a load of 90 tons on the centre of the slab and on a joint or a free edge.
Loading area with radius $c=40$ cm.
Soil modulus $C=2300$ kg/cm², elastic subgrade.

Slab A II.		test no.	9	10	8	14	15
Position of load, 90 tons			centre of section		joint	free edge	
DATA FOR SLAB SECTION OR JOINT			5	6	4 – 5	4	6
Reinforcement mesh			5.6 c/c 100	7 c/c 100	5.6 c/c 50	5.6 c/c 100	
Flexural rigidity		kgcm²/cm	$0.50 \cdot 10^8$	$0.65 \cdot 10^8$	$0.82 \cdot 10^8$	$0.50 \cdot 10^8$	$0.65 \cdot 10^8$
Elast. radius of rigidity l		cm	7.6	8.3	8.9	7.6	8.3
Rel. load distribution $\frac{c}{l}$			5.25	4.82	4.50	5.25	4.82
RESULTS							
Curvature in load centre $\frac{1}{\varrho}$		cm⁻¹	$26 \cdot 10^{-5}$	$23 \cdot 10^{-5}$	$23 \cdot 10^{-5}$	$29 \cdot 10^{-5}$	$32 \cdot 10^{-5}$
Max. strain in top surface $\varepsilon_{t\max}$		‰	0.46	0.48	1.3	1.8	2.1
ANALYSIS OF RESULTS							
Moment in load centre $m^{+}_{\max} = \frac{1}{\varrho} Ei$		kgcm/cm	130	150	185	145	205
Max neg. moment $m^{-}_{\max} = \frac{\varepsilon_t^{\max}}{2h-x} Ei$		kgcm/cm	35	49	170	135	205
Moment from theory with load on centre of a similar section $m^{\text{theor}}_{\text{centre}}$		kgcm/cm	120	153	195	120	155
$m_{\text{centre}} : m^{\text{theor.}}_{\text{centre}}$			1.10	0.98			
$m_{\text{joint}} : m^{\text{theor.}}_{\text{centre}}$					0.95		
$m_{\text{edge}} : m^{\text{theor.}}_{\text{centre}}$						1.20	1.30

rather larger values of the centre loading moment and rather smaller values for the moment relationship.

On the basis of the curves in Fig. 41:3 or Table 41:1, in the case of large values for load distribution, one can obviously state

$$m^{+}_{\text{joint}} < 1.0\, m^{+}_{\text{centre}};\ m^{+}_{\text{edge}} < 1.4\, m^{+}_{\text{centre}}$$

The results according to Table 53:8 remain within these limits. It is clear that the case of loading on a joint has not given larger positive moment in the slab than the load on the interior of the slab and that the load on a free edge has only given comparatively slight increase in the positive moment.

Concerning the negative moment, a theoretical analysis of the test results is even more difficult and the formulae (41:9) cannot be used at all to give an idea of the moments at these large load distribution values. The negative moments according to the tests can be estimated from the maximum strain values (see the table) in the same way as the positive moments from the curvature in the centre, according to the expression

$$\frac{1}{\varrho} = \frac{\varepsilon_r}{h - x} = \frac{\varepsilon_t}{2h - x}$$

where ε_r is the strain in the reinforcement and ε_t is the measured strain in the top surface. If the negative moments estimated according to the table are compared with the corresponding positive moments, it is found that they are no higher than approximately the same magnitude, and the same result is arrived at if the corresponding stresses in the table 53: 6 are compared. The negative moments thus lack all significance for design purposes, since the strength of the slab for positive and negative moment is the same.

535.4. *Discussion of the test results. General viewpoints concerning the the thin mid-depth reinforced pavement.*

The tests and theory have shown that the moment and stresses in the pavement reinforcement are small compared with the yield point (0.2-limit). For the wheel load of 45 tons assumed here, the safety factor concerning the attainment of the yield point in the case of centre loading is 8—9, even if the theoretical values of flexural rigidity are used. According to the normal viewpoints concerning designing, a slab such as this may be considered as being robustly overdimensioned, and a normal procedure in such cases would be to decrease the dimensions. A decrease of the reinforcement or the thickness of the slab (this latter being hardly advisable from the point of view of construction) also implies, however, a change in the flexural rigidity and thereby the moment. In order to clarify the influence of this, the stresses have been calculated for a number of different designs of pavement with various slab thickness and reinforcement. On the basis of the dimensions for slab section 5, the thickness has partly been varied with the reinforcement unchanged, and the reinforcement has partly been varied with unchanged thickness, in addition to which the thickness has been varied with a constant reinforcement percentage (the same as in slab 5). The subgrade modulus has been assumed as being equal to 2300 kg/cm² and the flexural rigidity and stresses have been calculated as being in stage II with $n = 15$.

Table 53:9 shows that in this example, a decrease of slab thickness or reinforcement only decreases the stresses even further. Increase of slab thickness implies considerably increased stresses while modifications of the reinforcement influence the stresses only to a very small extent.

The reason for this is obviously that, with these pavement having

TABLE 53:9. Theoretically calculated stresses in the reinforcement due to a load of 45 tons with a load distribution $c = 40$ cm on a thin mid-depth reinforced slab, Stage II. $n = 15$. Soil modulus $C = 2300$ kg/cm³.

	Thickness h_0 cm	Reinforcement cm²/m	Flexural rigidity EI_{II} kgcm²/cm	Max. pos. moment	Reinforcement stress at 45 tons kg/cm²
Reinforcement const.	15	∅ 5.8 c/c 100 = 2.65	$2.03 \cdot 10^8$	$6.7 \cdot 10^{-3}\,P$	1680
	12		1.25	4.1	1290
	10		0.83	2.5	940
	8		0.51	1.3	630
	6		0.26	0.7	450
Thickness const.	8	∅ 8 c/c 100 = 5.03	$0.78 \cdot 10^8$	$2.1 \cdot 10^{-3}\,P$	540
		∅ 7 = 3.85	0.65	1.8	590
		∅ 5.8 = 2.65	0.51	1.4	670
		∅ 5 = 1.96	0.40	1.0	630
		∅ 4 = 1.26	0.27	0.6	580
Reinforcement percentage const.	15	4.96		$10.2 \cdot 10^{-3}\,P$	1400
	12	3.97		5.8	1260
	10	3.31		3.0	950
	8	2.65		1.3	630
	6	1.99		0.5	450

such a low degree of flexural rigidity, the subgrade with its good bearing capacity carries practically the whole load directly under the load distribution plate and the slab only functions to a very small extent with distributing the pressure and influencing the deformation. The soil is thus deformed on the whole in the same way as if the load had rested directly on the soil, and the slab is forced to follow the soil. The radius of curvature in the loading centre is largely independent of the slab thickness, and thus the stresses in the slab are less, the thinner the slab is.

Stresses due to traffic loading are thus very small no matter what dimensions the slab has. The slab must however also admit the stresses due to temperature variations and shrinkage. In this connection it should be calculated that the reinforcement admits all the normal stress resulting from similar temperature decrease and shrinkage. In practice the influence from this often becomes dominating when calculating the required reinforcement. These questions are treated in more detail in Part 6.

With respect to that shown above, i. e. that the stresses caused by traffic loading are always very low for slabs of this type, it is obvious that the cases of loading with a load on a joint or a free edge do not need to cause any trouble. The rather higher traffic loading stresses which result in the last-mentioned case of loading are still relatively very small.

and besides the stresses due to temperature and shrinkage on edges and joints often fade out. It should thus not be necessary to strengthen the edges or joints in any way for this type of slab.

Further viewpoints on the thin mid-depth reinforced slab and its design are expressed in Part 7.

536. Examination of joint design

536.1. *Test arrangement and measuring devices*

Although the closer consideration of joints and joint effects lies outside the framework for this paper it can be of certain interest to supply a short description of the joint tests which were carried out in connection with the Arlanda test programme.

The intention with this part of the test programme was to study types of joint which function more effectively than the usual tongue and groove joint, since this can be assumed to have insufficient strength in the case of these thin slabs. In the case of tongue and groove joints, joint failure occurs roughly as shown in Fig. 53:11 A with a stamp-out failure under the groove, whereby hardly half the section of the thickness is operative. By designing the joints in such a way as to connect together the joint edges in a suitable way along their entire height, it should be possible to get stamp-out failure to go through the complete thickness as shown in Fig. 53:11 B.

In accordance with this programme, the joints between the sections in the test areas I and II were designed in such a way that half the length of each joint consisted of a normal tongue and groove joint while the other half was designed as "saw-tooth joint" of two different types in accordance with the last-mentioned principle. The design and descriptions of the various types of joint are shown by Fig. 53:12. Fig. 53:1 shows where the different joint types were located. On both slabs, joints of all three

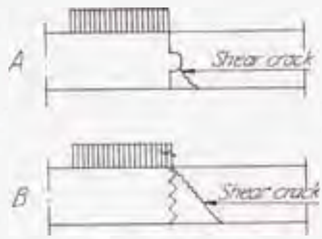

Fig. 53:11. Stamping-out failure for different types of joint. Fig. A shows the failure on a normal tongue and groove joint while Fig. B shows the failure on a joint where the slabs are joined over the entire height.

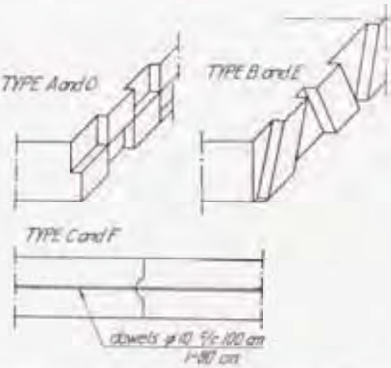

Fig. 53:12. The three types of joint edge tested. The principal design was similar for 16 cm and 8 cm test slabs. The types A and D as well as B and E represent "sawtooth" joints where the edges are held together over their entire height. The tongue and groove joint shown at C and F was fitted with very sparsely distributed and weak dowels, which were only intended to prevent the slab sections from sliding apart but did *not* have any significance for the transfer of shearing forces or moment.

types were incorporated, suitably dimensioned for the slab thickness in question.

During testing the load distribution area was located so that it was tangent to the joint, whereby the largest possible shear force was obtained in the joint. The placing of the load is otherwise shown in the result Table 53:10. During loading the horizontal and vertical displacements between the joint edges were measured by means of dial gauges and strain gauges as shown in Fig. 53:13[1])

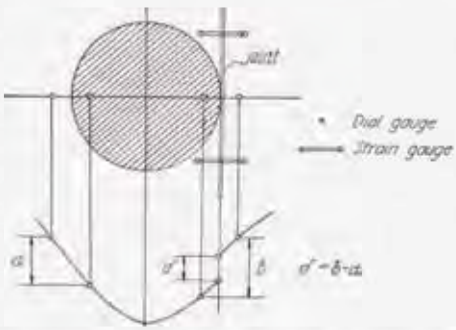

Fig. 53:13. Measuring devices and the location of the loading area for the joint tests.

[1]) Apart from this the joint tests were used to carry out the same measurements of deformations and strains as in the case of the other loading tests. The depression, curvature and strain diagrams are shown in the result supplement, Section 96.

TABLE 53:10. Test series A:III. Testing the design of the joint edge.

Test No.	Slab thick-ness cm	Joint type	Location of load	Max loading tons	Horizontal joint displ. cm		Vertical joint displ. cm	
					45 tons	Max. load	45 tons	Max. load
4	16	B	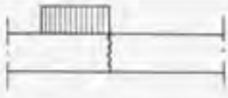	95	0.008	0	0	0.08
5		A	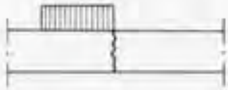	95	0.017	0.023	—	—
6		C	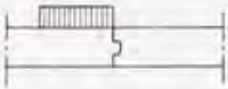	100	0.025	0.043	0	0.06
7		C	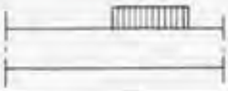	100	0.027	0.036	0	0.07
11	8	F	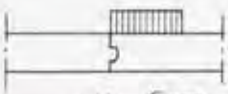	124	0.018	0	—	—
12		F	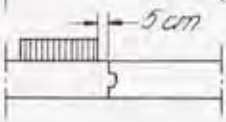	124	0.012	0.022	—	—
13		F	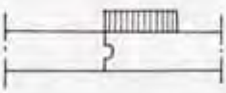	124	0.017	0.024	0.02	0.08
No shear failure in any of tests								

536.2 *The test results*

No shear failure in the joints was obtained by any of the test loadings. On the test area I *all* the types of joint were tested with maximum loads of 95—100 tons. On the test area II only the tongue and groove joints were tested with maximum loads of 124 tons; since these did not give rise to failure, it was considered unnecessary to test the other types of joint which were less suitable from other viewpoints. Instead one of the tongue and groove joints was tested on both sides of the joint whereby in test 12 an attempt was made to induce a failure in the upper "tongue" of the groove. The load was therefore located a small distance from the joint so that eventual shear crack would not be prevented by the loading from the load distribution plate.

Table 53:10 shows the result from the various test loadings, whereby the position of the load as well as the horizontal and vertical load displacement for 45 tons and the maximum load are shown. It can also be pointed out that cracks occurred transversely over the joint tongues in the top surface on the joint types A, B, D and F (saw-tooth joints), this clearly depending on the fact that the joint edges had become too much bonded together.

The test showed that all the types of joint gave more than sufficient strength concerning shear failure and that the joint deformations in all cases were very insignificant. Since the sawtooth joints are difficult to cast and design and since, at least in the models here used, do not allow dilatation, there does not appear to be any reason to cease using the usual tongue and groove joints. This type of joint appears to have sufficient shear strength even in the case of very thin slabs. With such slabs, which are only used on soil which has a high load-bearing capacity, such a large part of the load is carried directly by the subgrade, that the shear force transmission over the joint is insignificant.

6. Influence of Temperature and Shrinkage

61. General Review. Calculation of Stresses

611. Various reasons causing stresses in concrete pavements

In the previous presentation in this paper, the influence on reinforced concrete pavements of only the wheel load stresses has been studied.

There are, however, also other causes of stress in the pavement. Among these may be mentioned:

a) Temperature variation in the pavement.

b) Shrinkage and swelling in the concrete as the result of processes associated with the hardening procedure or under the influence of a varying degree of moisture.

c) Unevenness in the subbase and settling in the soil.

The factors mentioned under point c) above give in many cases the largest stresses in the pavement, stresses of a type that can result in serious damage. Reference can here be made to the cases in tests earlier referred to, where there have been zones with poor contact, a so-called "miss", under the pavement. It is, however, impossible to take any respect to such conditions when working out calculations; for the calculations it is necessary to assume an even and homogeneous subbase. As far as resisting the influence of unevenness in the subgrade is concerned, however, the reinforced slabs, as a rule, would appear to be much more advantageous than the considerably thicker and more rigid plain concrete slabs since, due to the lower degree of flexural rigidity, the reinforced slab is much more able to follow any existing unevenness in the soil without such large stresses resulting. On the other hand it can naturally be pointed out that a more rigid slab has better properties concerning the bridging over of very localized soil unevenness.

The other factors resulting in stresses in the slab mentioned above, namely temperature variations as well as shrinkage and swelling, are much easier to get at from a calculating point of view and they can be treated in a similar way. The cause of stresses occurring in the concrete is that the deformations produced by the factors mentioned are prevented by the fact that the slab is more or less locked for different reasons. Increases in temperature and swelling thereby result in compressive stresses, temperature decreases and shrinkage result in tensile stresses.

612. Stresses in pavements with joints

In normal cases attempts are made to limit the temperature and shrinkage stresses by dividing up the pavement at suitable distances through joints, which allow a certain amount of movement between adjacent slab edges. When calculating the stresses, each particular part of the pavement between such joints can be considered to be a unit, the movements of which are determined by its own weight and by the friction against the soil.

When studying these conditions it is simplest to divide up the influence of temperature and shrinkage into two parts:

1. *Uniform temperature variations* (average temperature variation), including shrinkage or swelling. Due to the fact that movement is partially prevented by the friction of the pavement against the soil, the result is a constant strain over the complete cross section, corresponding to a *normal force* in the pavement. Dangerous stresses from a designing point of view gives thereby only the *tensile force* N_t due to temperature decrease and shrinkage.

2. *Temperature variations* (or shrinkage respectively) through the slab, caused by rapid heating up or cooling off of the top surface, result in temperature differences between the top and bottom of the slab. An influence of this type tends to produce warping in the slab, this being completely or partially prevented by the weight of the slab itself and the contact with the soil, the result being a corresponding flexural moment m_t. In principle, m_t can be positive or negative (a positive warping moment however caused by a heated top surface cannot reasonably occur simultaneously with a tensile force N_t of uniform temperature decrease), but in practice the positive m_t has the greatest significance. Rapid heating due to sunshine on the top surface can result in considerable differences in temperature between the top and bottom surfaces, while a corresponding cooling of the top surface always proceeds less rapidly and is not so intensive.

The resulting influences of temperature and shrinkage, the tensile force N_t and the warping moment m_t can be estimated theoretically. Calculation of the tensile force is based on the frictional effect between the pavement and the soil, and estimation of the warping moment is based on calculations and experimental determinations of the temperature distribution throughout the slab. An excellent presentation of the theories and the methods of calculation as well as a review of literature and research within this field has been supplied by BERGSTRÖM

[6], and the calculating methods, adopted for practical application, are summarized in the Swedish Cement and Concrete Research Institute (CBI) design specifications for concrete pavements [78].

In accordance with the principles stated and the papers mentioned, the tensile force N_t, caused by the friction against the soil due to the contraction of the slab can be written

$$N_t = 2.4\, h_0 \cdot f_s \left(\frac{L}{2} - \frac{x}{3}\right) \qquad (61{:}1)$$

where

f_s = the coefficient of friction between the pavement and the soil

L, h_0 = the length of the pavement between joints allowing contraction, and its thickness respectively

x = a distance nearest the centre of the pavement, where the movement due to temperature decrease is so small that friction is not fully achieved, sliding tests having shown that this requires movements exceeding approx. 1.5 mm.

With the normal assumption concerning temperature decrease (according to [78]) and with a reasonable addition for movement due to shrinkage, then the values of x are obtained between approx. 4–5 m, i. e. the term $\frac{x}{3}$ in the equation (61:1) can generally be neglected compared with $\frac{L}{2}$ if the length of the sections in question are fairly large, as normally used in reinforced concrete pavements. It is then possible (as always on the safe side) to write

$$N_t = 1.2\, h_0\, f_s\, L \qquad (61{:}2)$$

N_t is obtained in t/m if h and L are expressed in m.

The coefficient of friction f_s can be estimated from sliding tests with slabs or from the measurements of the movements and forces in the free end of pavements actually constructed. The CBI design specifications based on earlier American tests [41], give the values of f_s as 2–3, depending on the thickness of the slab. Later American experience and tests [3] show that these values are fairly high and that a value $f_s = 1.5$ is always on the safe side, and the latest recommended practice [1, 3] suggest a value $f_s = 1.5$ for fully developed friction in normal cases (sand or gravel subbase).

The stresses due to the warping moment m_t for a plain concrete slab can be written as

$$\sigma_{mt} = \frac{E}{1-\nu} \alpha \Delta T_m \qquad (61{:}3\text{ a})$$

where ΔT_m is the difference between the average temperature in the slab and the temperature in the surface in question. According to [6], in the case of slab thicknesses between approx. 10 and 30 cm, it is possible to reckon with a temperature difference ΔT_m in the bottom surface of approx. 4° C when heating up the top, and 1.5—2° C in the top surface when cooling the top. With a reasonable value of the slab elasticity modulus E and a temperature coefficient $\alpha = 10^{-5}$ this formula (61:3 a) will thus give as the most dangerous tensile stresses from warping for a *plain concrete* slab:

$$\left.\begin{aligned} \sigma^b_{mt} &= \text{approx. } 14 \text{ kg/cm}^2 \text{ in the bottom} \\ \sigma^t_{mt} &= \text{approx. } 7 \text{ kg/cm}^2 \text{ in the top} \end{aligned}\right\} \qquad (61{:}3\text{ b})$$

these being largely independent of the slab thickness. The *second* top surface value may also apply to a *single-reinforced slab.*

In earlier discussion of the concrete pavement problem, the elasticity theory has, as mentioned (see 21), always been the basis, and the calculating methods have been primarily aimed at plain concrete pavements. The method for calculating the temperature influence has always been to estimate, as above, the *supplementary stresses* of temperature and shrinkage, which can be superimposed on the wheel load stresses when designing a pavement, whereby the most dangerous combination of stresses may not be allowed to reach failure (flexural concrete strength).

In the case of reinforced pavements and particularly when applying the ultimate strength theory, it is essential to carry out a more accurate study of how the stresses of wheel load and of temperature and shrinkage are combined in practice. It is obvious, at least in the application of the ultimate strength theory, that these stresses cannot be directly superimposed. These conditions of special interest for this investigation are treated in Sections 62 and 63.

613. **Jointless, so-called continuous reinforced pavements**

Conditions are completely different, however, in the type of pavement which is *entirely without* movable transverse joints, or where these joints are some considerable distance from each other. Pavements of this type are usually called *continuous* (continuously reinforced) *pavements.*

Characteristic for this type of pavement is the fact that the slab, due to its great length between joints, can be considered as being completely locked concerning gliding movement due to uniform temperature variation and shrinkage. The slab has thus *absolutely no* length variation over at least some distance between the joints. The result of this is that even with moderate temperature decrease together with shrinkage, there will be tension cracks right through the pavement, and the cracked parts must be held together by reinforcement, which must then absorb all the stresses due to temperature and shrinkage. In order to prevent the cracks first occurring from widening, the reinforcement must be designed so that the yield point is not exceeded. Instead, in such a case, with further temperature decrease and shrinkage, even more and closely spaced cracks will occur, and by the use of well-distributed reinforcement with good bonding properties (deformed bar or welded mesh of tightly spaced type) then the crack formation becomes so closely spaced and the cracks themselves become so fine that they are completely without significance.

Due to the closely-spaced crack formation thus caused, the flexural rigidity of the slab for moment in both directions is so small that the warping effect due to uniform temperature distribution can be neglected. Respect need thus only be taken to uniform temperature decrease.

In order to determine the required reinforcement in a continuous pavement with respect to the influence of temperature and shrinkage, the condition above is used as a basis, i. e. the fact that the reinforcement in the cracks may not exceed the yield point (0.2-limit). If a section of the slab between two cracks as shown in Fig. 61:1 is considered from this point of view, then the reinforcement should be designed so that the tensile stress σ_r^{cr} in the reinforcement in the crack is lower than the yield point value, when the concrete in the central zone between the cracks just reaches the tensile strength σ_t. Further falls in temperature then give a new crack instead of increasing the reinforcement stress in the old cracks (whereby the stress there instead *decreases*).

The total maximum tensile force N_t can thus be written

$$N_t = \sigma_r^{cr} A_r = \sigma_t A_c + \sigma_r^0 A_r \tag{61:4 a}$$

or with

$$\frac{A_r}{A_c} = \mu$$

$$\sigma_r^{cr} = \frac{1}{\mu} \sigma_t + \sigma_r^0 \tag{61:4 b}$$

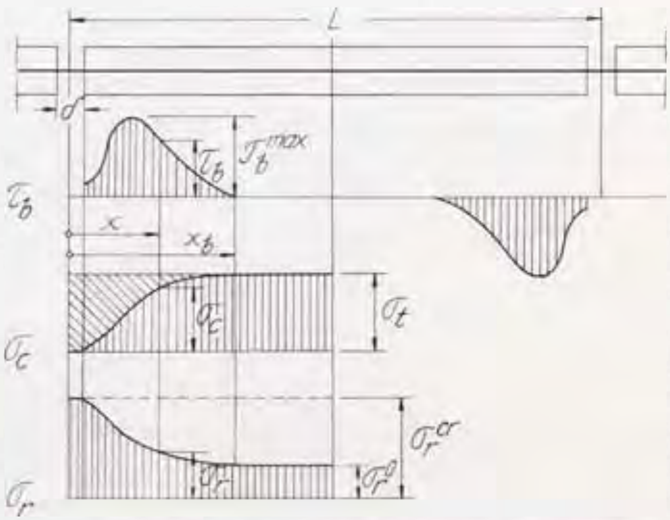

Fig. 61:1. Assumed distribution of bond stress τ_b between the concrete and the reinforcement along the distance between two cracks in a continuous reinforced pavement as well as the corresponding stresses σ_c in the concrete and σ_r in the reinforcement. Bond is assumed to be completely transferred over a stretch x_b nearest the cracks. The diagonally shaded surface over the σ_c diagram corresponds to the expression in brackets in the final formulae (61:11) and (61:12) for the crack width δ and the crack distance L.

where σ_r^0 is the stress in the reinforcement in the central zone between the cracks. If it is further assumed that the bond stresses between the steel and the concrete as shown in Fig. 61:1 are transferred on to a stretch x_b nearest the cracks, which is less than half the distance between the cracks, then midway between the cracks there is a zone where no slip occurs between the steel and the concrete; this assumption will be discussed later. The resulting strain due to stress, temperature increase T (the coefficient of length extension α is assumed to be the same for concrete and steel) as well as shrinkage ε_{sh} of the concrete itself will then be similar for concrete and steel (see Fig. 61:2):

$$\alpha T + \varepsilon_{sh} - \varepsilon_t^{ult} = \alpha T - \frac{\sigma_r^0}{E_r}$$

or

$$\sigma_r^0 = E_r (\varepsilon_t^{ult} - \varepsilon_{sh}) \tag{61:5}$$

where ε_t^{ult} is the ultimate strain of the concrete at the tensile strength σ_t. If (61:4) and (61:5) are combined, the result is

Fig. 61:2. Schematic presentation of the deformation on a unit length midway between the cracks in the pavement shown in Fig. 61:1. The original condition is represented by I, while II shows the condition if the steel and the concrete are permitted to be freely deformed under the influence of temperature decrease T and shrinkage ε_{sh} in the concrete. III corresponds to the actual condition in the co-operating section, whereby it is assumed that there is no internal slip between the concrete and the reinforcement.

$$\sigma_r^{cr} = \frac{1}{\mu}\ \sigma_t + E_r\,(\varepsilon_t^{\text{ult}} - \varepsilon_{sh}) \tag{61:6 a}$$

or

$$\sigma_r^{cr} = \sigma_t\left(\frac{1}{\mu} + n\right) - \varepsilon_{sh}\,E_r \tag{61:6 b}$$

whereby as usual

$$\varepsilon_t^{\text{ult}} = \frac{\sigma_t}{E_c} = n\ \frac{\sigma_t}{E_r}$$

with suitably selected value of $n = \dfrac{E_r}{E_c}$ (comparatively high, since the concrete is assumed to have reached the tensile strength stage).

The required minimum reinforcement to absorb the effect of temperature and shrinkage can thus be calculated according to (61:6), if σ_r^{cr} is written as σ_{yie} equal to the yield point of the steel:

$$\mu_{\min} = \frac{\sigma_t}{\sigma_{yie} - E_r\,(\varepsilon_t^{\text{ult}} - \varepsilon_{sh})} \tag{61:7 a}$$

The strain values in the denominator are difficult to state but it should in any case be certain that $\varepsilon_{sh} > \varepsilon_t^{\text{ult}}$. Always on the safe side, these values may be assumed to be similar and the reinforcement can be calculated from

$$\mu_{\min} = \frac{\sigma_t}{\sigma_{yie}} \tag{61:7 b}$$

The corresponding value of the tensile force N_t due to temperature and shrinkage, also with another reinforcement percentage $> \mu_{\min}$, can be written with the same simplification as

$$N_t \approx h_0 \, \sigma_t \quad \text{per unit width} \tag{61:8}$$

It should be pointed out that these expressions, even the "more exact" according to (61:6), are *completely* independent of the temperature T; it is only assumed that the influence of temperature and shrinkage is so great that the tensile strength in the concrete has been reached. The expression thus also applies for *only* shrinkage.

In cases where the length of the runway between the movable transverse joints is so great that the tensile force N_t, calculated according to (61:2), is *greater* than the value according to (61:8), then the pavement must be considered as being continuous and calculations must be carried out in accordance with the methods quoted. This thus happens if the distance between the joints

$$L > \frac{10 \, \sigma_t}{1.2 \, f_s} \text{ metres } (\sigma_t \text{ in kg/cm}^2)$$

If it is assumed that $f_s = 1.5$ and $\sigma_t = 30$ kg/cm², then a "limiting length" $L \approx 170$ m is arrived at. With a distance between the joints exceeding or in the neighbourhood of this value, then movable transverse joints are *only* detrimental and result in very large joint movements. Considerably shorter distances between joints should thus be selected or a *completely* joint-free continuous pavement should be designed.

The expression for $\mu_{\min}$ according to (61:6 b) was quoted as early as 1933 by Vetter [69], who has also shown how to estimate the distance between the cracks, whereby he assumed that the bond has a constant distribution, but he does not appear to have mastered the occurrence of cracks of finite width and the factors influencing this width of the cracks.[1]) The author will discuss these problems below and also make more general assumptions concerning the distribution of the bond stress.

If the alteration in length of the reinforcement and the concrete ΔL is studied over the complete distance L between two cracks in Fig. 61:1, in the case of a completely arbitrary stress distribution it is possible to write

[1]) Vetter's expression has been quoted and developed by Zuk [79], who has also stated some expressions for the crack width.

$$\left.\begin{aligned} \Delta L_{\text{steel}} &= 0 = \alpha\, T\, L - 2 \int\limits_0^{\frac{L}{2}} \frac{\sigma_r}{E_r}\, dx \\ \Delta L_{\text{concr}} &= \delta = \alpha\, T\, L + \varepsilon_{sh}\, L - 2 \int\limits_0^{\frac{L}{2}} \frac{\sigma_c}{E_c}\, dx \end{aligned}\right\} \qquad (61:9)$$

where the relationship between the stresses in the reinforcement and the concrete σ_r and σ_c respectively in an arbitrary section is, analogous with (61:4)

$$\sigma_r + \frac{1}{\mu}\, \sigma_c = \sigma_r^{cr} = \text{constant} \qquad (61:10)$$

If the equations (61:9) are subtracted the result is

$$\delta = \varepsilon_{sh}\, L + 2 \int\limits_0^{\frac{L}{2}} \left(\frac{\sigma_r}{E_r} - \frac{\sigma_c}{E_c} \right) dx$$

or, respect being taken to the assumption that the bond stress is transferred on a certain distance x_b nearest the crack, while the stresses on the centre part are constant, σ_r^0 and σ_t respectively

$$\delta = L \left(\varepsilon_{sh} + \frac{\sigma_r^0}{E_r} - \frac{\sigma_t}{E_c} \right) - 2\, x_b \left(\frac{\sigma_r^0}{E_r} - \frac{\sigma_t}{E_c} \right) + 2 \int\limits_0^{x_b} \left(\frac{\sigma_r}{E_r} - \frac{\sigma_c}{E_c} \right) dx$$

The first bracket is similar to 0 according to (61:5). If σ_r^0 and σ_r are eliminated through the equations (61:4) and (61:10), the result will be after simplification

$$\delta = \frac{2}{E_r} \left(\frac{1}{\mu} + n \right) \left(\sigma_t\, x_b - \int\limits_0^{x_b} \sigma_c\, dx \right) \qquad (61:11)$$

If this expression is inserted in the last of the equations (61:9), the result is

$$L = \frac{2}{\mu\, E_r \left(\alpha\, T + \varepsilon_{sh} - \dfrac{\sigma_t}{E_c} \right)} \left(\sigma_t\, x_b - \int\limits_0^{x_b} \sigma_c\, dx \right) \qquad (61:12\text{ a})$$

which, in the same way as (61:7) can, with sufficient accuracy, be written

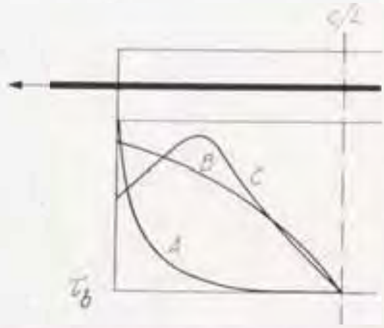

Fig. 61:3. Various assumptions concerning the distribution of bond stress between the reinforcement and the concrete in a *tensile test*. The curves show schematically the results of:

A — GRANHOLM [23] and BERNANDER [7] on the basis of theoretical calculations according to the elasticity theory.
B — BERNANDER [7] from tests.
C — KUUSKOSKI [42] from tests. Similar test curves have also been obtained by PARLAND [55].

$$L = \frac{2}{\mu\, E_r\, \alpha\, T} \left(\sigma_t\, x_b - \int_0^{x_b} \sigma_c\, dx \right) \qquad (61{:}12\ \mathrm{b})$$

x_b and σ_c in the equations (61:11) and (61:12) can be calculated if the distribution of the bond stress τ_b is known since the following applies generally (see fig. 61:1)

$$\sigma_c\, A_c = p \int_0^x \tau_b\, dx \qquad (61{:}13)$$

or over the *complete* bond stretch x_b

$$\sigma_t\, A_c = p \int_0^{x_b} \tau_b\, dx \qquad (61{:}14)$$

where p is the total circumference of the reinforcement area. The expression with the integral in brackets in (61:11) and (61:12) means in point of fact the area outside the stress curve σ_c in fig. 61:1 and can thus easily be calculated, if the stress distribution is known.

Knowledge concerning maximum values of the bond stress and its distribution is incomplete. Theoretical calculations based on the elasticity theory and carried out by GRANHOLM [23] or BERNANDER [7] show that the bond stress decreases very steeply from the crack and inwards (Fig. 61:3). In actual practice the conditions are considerably more irregular. In the case of deformed bar the result is, as shown by experiments with tensile tests on reinforcement embedded in a concrete unit carried out for example by KUUSKOSKI [42], BERNANDER [7] and

Parland [55], plastic deformation or crushing in the contact surfaces between steel and concrete, and considerably more uniform distribution curves occur (Fig. 61:3), while in the case of smooth bars bonding ceases altogether and will be substituted by pure friction in the parts nearest the crack. Reinforcement mesh (of smooth wire) gives a mainly discontinuous bond anchorage in the cross wire welding points. The tests referred to here are, however, aimed at the conditions in the tension zone for beams under flexure, and the test units have generally much shorter length and considerably higher reinforcement percentage than what will correspond to the conditions in continuous concrete pavements. In order to clarify the conditions in this case even more, it would appear to be necessary to have tests carried out specially prepared for this purpose.

For the aim in question, namely to give a general idea of the distance between the cracks and the crack width as well as the factors influencing these, it would appear to be sufficient to examine some simple cases of assumed bond stress distribution. Here cases are studied with constant and triangular stress distribution over the bond stretch x_b as shown in Fig. 61:4; the actual bond stress in the case of deformed bar would appear to have a distribution lying somewhere between both these extreme cases.

For these cases, equations (61:14) and (61:12) give the following expressions for *deformed bar* (or smooth bar):

with uniform distribution as shown in Fig. 61:4 A

$$\left.\begin{aligned} x_b &= \frac{\sigma_t A_c}{\tau_b^{\max} p} = \frac{\sigma_t}{\tau_b^{\max}} \frac{\varnothing}{4\mu} \\ L &= \frac{\sigma_t}{\mu E_r \alpha T} x_b \\ \delta &= \frac{\sigma_t}{E_r}\left(\frac{1}{\mu} + n\right) x_b \end{aligned}\right\} \qquad (61:15\text{ a})$$

with triangular distribution as shown in Fig. 61:4 B

$$\left.\begin{aligned} x_b &= 2\frac{\sigma_t A_c}{\tau_b^{\max} p} = \frac{\sigma_t}{\tau_b^{\max}} \frac{\varnothing}{2\mu} \\ L &= \frac{2}{3} \frac{\sigma_t}{\mu E_r \alpha T} x_b \\ \delta &= \frac{2}{3} \frac{\sigma_t}{E_r}\left(\frac{1}{\mu} + n\right) x_b \end{aligned}\right\} \qquad (61:15\text{ b})$$

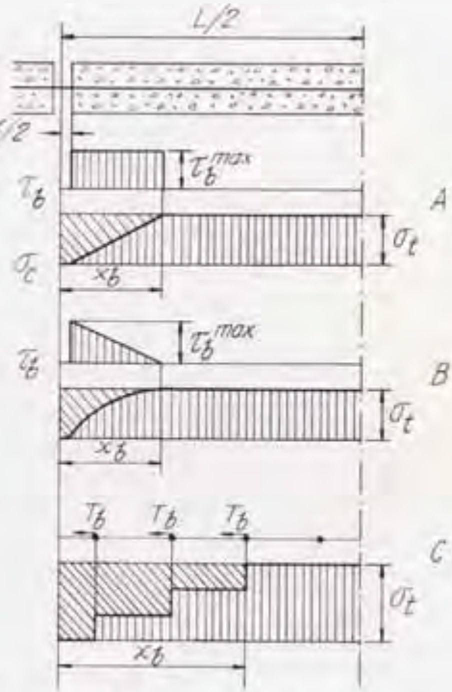

Fig. 61:4. Stress in the concrete between two cracks in a continuous reinforced pavement with several simple cases of assumed distribution of bond stress between the concrete and the reinforcement. Cases A and B represent extreme cases of distribution with smooth or deformed bar, case C shows the distribution with welded mesh reinforcement (smooth wire) if it can be assumed that all bond anchorage is transferred through the cross wire welding points (in the case of the figure three cross wires). The diagonally shaded areas represent the brackets in the equations (61:11) and (61:12).

where ⌀ is the diameter of the reinforcing bars. It can be generally shown that other conceivable cases of stress distribution give similar expressions to those above with the numerical coefficients between the values in (61:15 a) and (61:15 b). In the expression for δ, it is also possible to neglect n compared with $\frac{1}{\mu}$ and thus the expression for crack width can generally be written

$$\delta \approx (1.0 \div 1.3)\,\frac{\sigma_t^2\,A_r}{E_r\,\tau_b^{\max}\,p}\,\frac{1}{\mu^2} = (1.0 \div 1.3)\,\frac{\sigma_t^2}{\tau_b^{\max}}\,\frac{\varnothing}{4\,\mu^2\,E_r} \quad (61{:}15\text{ c})$$

Where the reinforcement consists of *welded mesh*, made up of smooth, cold-drawn wire it can be assumed that the bond, at least in the crack condition, is transferred mainly through the welded cross wires nearest the crack. The bond stress distribution between concrete and reinforcement will then be step-formed as shown in Fig. 61:4 C and if it is assumed that the bond stress is transferred through m cross wires with a spacing d and that the cracks occur in the spacing centre, the result is:

$$\left.\begin{aligned} x_b &= \left(m - \frac{1}{2}\right) d \\ L &= \frac{\sigma_t}{\mu\, E_r\, \alpha\, T}\, m\, d \\ \delta &= \frac{\sigma_t}{E_r} \left(\frac{1}{\mu} + n\right) m\, d \end{aligned}\right\} \qquad (61{:}16\ \mathrm{a})$$

In normal cases, the bond stress would appear to be transferred through 2—3 cross wires. With the simplification used earlier it is thus possible to write an expression for the crack width with mesh reinforcement as

$$\delta \approx (2-3) \frac{\sigma_t}{E_r} \frac{d}{\mu} \qquad (61{:}16\ \mathrm{b})$$

It should be pointed out that the expressions for the crack width are completely independent of the temperature difference T. This applies naturally only concerning the maximum crack width just before the occurrence of a new crack.

The formulae above are applied to a normal case of continuous pavement occurring in practice. The following values are adopted:

$\sigma_t \;= 30$ kg/cm² (note: pure tension)
$\sigma_{yie} = 6000$ kg/cm² (mesh Ns 60 or deformed bar Ks 60)
$T \;= 50\,^\circ$C, $\alpha = 10^{-5}$

which appear to be fairly representative values for a normal pavement.

The required reinforcement percentage μ will then be, according to (61:7)

$$\mu > \frac{30}{6000} = 0.5\ \%$$

It is particularly interesting to study the bond stretch x_b relative to the distance L between the cracks. The formulae (61:15) and (61:16) give generally, with a reinforcement percentage $\mu = 0.5\ \%$

with uniform τ_b-distribution $x_b = 0.18\,L$

with triangular τ_b-distribution $x_b = 0.27\,L$

with mesh with τ_b-distribution on

two cross wires $L = 2 \cdot 5.7\,d$; $x_b = 0.13\,L$

three cross wires $L = 3 \cdot 5.7\,d$; $x_b = 0.15\,L$

It is obvious from these calculations that, *completely* independent of the bond distribution and the maximum bond stress, the bond between the reinforcement and the concrete in normal cases always transfers on a stretch considerably shorter than half the distance between the cracks. The assumption made when deriving the formula (61:7) for the calculation of the required reinforcement percentage, namely that the bond stress is equal to zero on some stretch midway between the cracks, must thus be correct. It is also clear that a new crack between two earlier cracks can occur anywhere on this relatively long stretch where $\tau_b = 0$ (see Fig. 61:1). Generally speaking the distance between cracks obtained should be *shorter* than that expected from the formulae (61:15) and (61:16); these formulae represent the *largest possible* distance between cracks (and also crack width).

With some different values of $\tau_b^{\max}$ for the example of a slab with a thickness $h_0 = 10$ cm and reinforcement $\varnothing$ 8 c/c 100 ($\mu = 0.5\,\%$) the following crack data are obtained

$\tau_b = 50$ kg/cm²	$L = 135-180$ cm	$\delta = 0.7-0.9$ mm
$\tau_b = 100$ kg/cm²	$L = 68-90$ cm	$\delta = 0.35-0.45$ mm
$\tau_b = 150$ kg/cm²	$L = 45-60$ cm	$\delta = 0.23-0.30$ mm

and with reinforcement wire fabric with a mesh width between the transverse wires of 10 cm and longitudinal wires of $\varnothing$ 8 c/c 100 ($\mu = 0.5\,\%$)

$$L = 120-150 \text{ cm} \qquad \delta = 0.6-0.9 \text{ mm}$$

It is obvious that the reinforcement must have a *good* bonding property in order to obtain a sufficiently small crack width (maximum 0.3–0.4 mm would appear to be acceptable). With concrete of the good quality used for pavements, it should be possible to count on sufficiently high values for the bond ($\tau_b^{\max} = 150-200$ kg/cm²) to obtain satisfactory crack formation if the reinforcement consists of deformed bar. Smooth bar, on the other hand, cannot be used for continuous pavements. Smooth wire mesh would not appear to give acceptable crack width either; in such cases mesh made of deformed wire may be preferred.

In the discussion above, respect has only been taken to the behaviour of the pavement with prevented *contraction* due to lowered temperature and shrinkage. With considerable temperature increase, large compressive forces are obtained in the pavement and the risk for blow-up can occur. According to both theoretical examinations of Zuk [79] and the experiences of American test pavements, this risk would appear to be practically non-existent. These examinations carried out by Zuk also showed neither blow-up phenomena nor other unfavourable movements either in horizontal or vertical curves in a continuous pavement.

Up till now only the influences of temperature and shrinkage have been considered and no respect has been taken to the function of the pavement under traffic wheel load. When judging this, it must be remembered that the pavement is so cracked through, at least transversally, that its possible capacity to absorb positive or negative moment depends on whether the reinforcement is designed so that it also functions as structural reinforcement taking flexure. From this viewpoint it would appear to be most correct to have the reinforcement in the neighbourhood of the centre plane of the concrete so that it can function as tensile reinforcement for both positive and negative moment according to the principles applied to the thin slabs belonging to the Arlanda tests (Section 535). This requires however very good and even subgrade or subbase to be able to design the slabs so thinly that the pavement will be economical in practice. In the case of soil with a lower load-carrying capacity, then the effective slab thickness may be increased by displacing the reinforcement rather downwards (larger effective depth for positive moment) or by using double reinforcement. The stress in the continuous longitudinal reinforcement due to wheel load (as well as the required transverse reinforcement) can be calculated in the usual way on the basis of the elasticity theory. It may also be possible to make the main part of the wheel load stress to be taken up by bottom reinforcement transversely across the runway but the function of the slab in this case is difficult to analyze theoretically.[1])

[1]) According to an analysis by Zuk [79] the runway which is cracked through transversely is considered to be flexurally rigid in transverse direction (with the uncracked section according to Stage I), while in longitudinal direction the transverse cracks between the strips only transmit shear forces. In order to solve this problem, Zuk has been forced to introduce new and unknown k-values for the force transmission between the strips. The problem in this form would appear to be treated in a more complete way according to the methods quoted by Granholm for the groove-and-tongue boarded floor [24] or according to the strip method presented by Kärrholm [43]. Only utilizing the flexural strength of the concrete according to Zuk will give the design of uneconomically thick slabs, but the same viewpoint can naturally be used also for slabs with transverse flexural reinforcement. The viewpoint as such, however, appears to be unnecessarily conservative since a certain moment-transferring effect in the transverse cracks may always be presumed since the continuous reinforcement also functions as flexural reinforcement.

The question as to how the stresses of temperature and shrinkage in the continuous reinforcement are to be combined with traffic loading stresses requires also a closer consideration. The most convenient way would appear to be to add up directly the stresses caused by the respective influences and make sure that the resulting stress falls short of the yield point by the necessary margin of safety. It is however obvious that if the pavement is subjected to wheel load just when it is subjected to the maximum stresses of temperature and shrinkage in the stage just before the occurrence of a new crack, then new cracks will occur which reduce the stresses in the reinforcement. According to this viewpoint it should thus be sufficient to check the longitudinal continuous reinforcement for temperature and shrinkage as well as for traffic loading *separately*.

These and many other unanswered questions concerning the continuous concrete pavement can hardly be judged and solved otherwise than on the basis of tests. To a large extent the detail problems can best be studied by means of model tests on slab strips subjected to tension.[1]) Finally the function of the continuous pavement must be judged, however, on test roads subjected to normal traffic or, preferably, special test traffic. Experiences from such test roads mainly American (see Section 71) show generally that the pavement functions well and that the necessary reinforcement can be calculated according to the methods given.

Then, both the theoretical calculations and the experiences from work carried out show that in the case of continuous pavements, a reinforcement percentage so high as 0.5 % or even rather higher must be reckoned with in the case of normal qualities of concrete and reinforcing steel. This shows that the type of pavement in question would appear to be economically advantageous only if the thickness of the slab can be maintained at a fairly low level. The type of thin pavement with mid-depth reinforcement which was tested during the Arlanda test series (Section 535) would appear to be suitable for continuous pavements.

The theoretical analysis indicates, however, further possibilities of reducing the necessary reinforcement. As shown by (61:7), the reinforcing steel used should have the highest possible yield point, and the new Swedish type of cold-drawn deformed bar (Kam 90) would appear to be excel-

---

[1]) The only tests of this type found by the author has been carried out by GUTZWILLER and WALING [25] but provide a poor basis for the verification of analysis and formulae in this section, because the test slabs were designed with crack indications right through which gave cracks at pre-determined distances from each other right from the beginning of testing.

lent as reinforcement in continuous pavements. From the same viewpoints, concrete with the lowest possible tensile strength should be used. This can hardly be effected, however, by a considerable decrease in the cement content since the demand for resistance to wear and resistance to frost would appear to make essential the use of high grade concrete. Other steps should be used in an attempt to decrease the tensile strength, for example suitable concrete composition or certain additives. A further point worth consideration is that of producing closely spaced crack indications transversely simultaneously with the casting, or to examine the possibility of producing a high degree of shrinkage in the concrete at a low age, when the tensile strength is low, by the use of certain suitable additives, since this means according to (61:12 a) the occurrence of closely spaced and non-dangerous crack formation permitting the use of decreased reinforcement according to (61:7 a).

62. Effect of Temperature and Shrinkage on the Ultimate Moment and the Ultimate Load in a Reinforced Concrete Pavement

The effects of temperature and shrinkage previously discussed, the tensile force N_t and the moment m_t, do not form any "external" loading. They are only caused by the fact that the deformations in the pavement are prevented since the possibility of movement in the slab is limited. If these "locked" deformations can be released, then the stresses caused by them also disappear.

This argument can be used concerning a study of the effect of temperature and shrinkage in combination with the external loading due to traffic. If we assume that the pavement is subjected to a tensile force N_t or a positive moment m_t due to the temperature, giving rise to tensile stresses in the reinforcement, and that the pavement is then subjected to an increasing external loading, it is obvious that the stresses caused by this are added to the temperature stresses, only as long as the reinforcement has not reached its yield point. As soon as this stress in the reinforcement is reached, then the tensile strain corresponding to the effect of the temperature is released without any further increase in stress, and thereby the phenomenon discussed above occurs, namely that the temperature effect completely disappears. This discussion implies that temperature and shrinkage do not influence the value of the positive ultimate moment m_{yie}.

The situation concerning the negative ultimate moment is, however, completely different concerning a pavement with no top reinforcement. In such a case a typical brittle failure occurs at the moment the flexural strength limit of the concrete is reached, and after the negative failure line has thus occurred, the ultimate moment decreases to zero. The tensile stresses occurring in the pavement due to temperature and shrinkage (in this case a combination of N_t and negative m_t can be considered), reduce the tensile strength available to take up the negative moment from the wheel load and this thus decreases the negative ultimate moment to the same extent.

In this case the superimposition principle applies up to the brittle failure point, and, apart from the insignificant effect of the reinforcement,

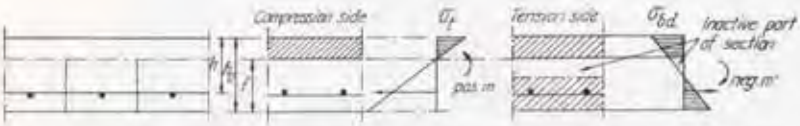

Fig. 62:1. Section of single-reinforced slab under the influence of a mobile wheel load. The section is assumed to be first loaded by the positive moment m which gives tension cracks in the reinforced side (crack depth f) and then by the negative moment m'. That part of the section under tension which is within the crack depth f is thereby inactive. The circumstances are accentuated even further if the section is simultaneously loaded with tensile force.

the flexural strength can thus be written as for an unreinforced section

$$\sigma_f = \omega \frac{N_t}{h_0} + \sigma^t_{mt} + \frac{6\ m'}{h_0^2} \tag{62:1}$$

where the factor ω has been introduced in order to correct for the difference in ultimate values between the pure tensile strength of $\frac{N_t}{h_0}$ and the flexural strength σ_f, calculated in accordance with Navier's principle with linear stress distribution. σ^t_{mt} is the flexural stress in the top surface due to the negative warping moment m_t according to (61:3). Thus, according to equation (62:1),

$$m' = \frac{h_0^2}{6} \left[\sigma_f - \left(\sigma^t_{mt} + \omega \frac{N_t}{h_0} \right) \right] \tag{62:2}$$

which implies that, when designing, the flexural strength σ_f of the concrete must be reduced with respect to the tension stresses of temperature and shrinkage when calculating the negative ultimate moment m'.

Here, however, there is a complication when applying this to practical conditions with mobile wheel loads. It can be considered that the complete pavement, due to the mobile moment loading, gradually develops a crack formation which stretches up from the bottom surface towards the neutral layer. In slab sections influenced by negative moment this crack formation will generally extend into the functional tension zone (see Fig. 62:1). This situation naturally occurs also if there is no influence of temperature and shrinkage, but should be even further accented if there is such an effect, since the significance of the tension zone then increases. The problem has been studied in a practical case in connection with the model tests, namely for slab MII:20 where the ultimate load occurred after the slab had been earlier loaded at two points just over the final negative failure crack (see Fig. 33:1) and in this test there was no apparent effect of this pre-crack or pre-deflection phenomenon. It thus appears probable from this test, that this effect can be ignored and the negative ultimate moment can be calculated according to the expression (62:2).

In the case of a double-reinforced pavement, the conditions are different. Since here a *completely* cracked-through section must be reckoned with, then the tensile force N_t must be completely admitted by the bottom and top reinforcement. On the other hand, the negative moment failure in this case depends on the yield in the top reinforcement and the same cancelling-out of the temperature effect may occur as in the case of positive ultimate moment. In the case of a double-reinforced pavement, it should thus not be necessary to pay respect to the influence of temperature and shrinkage when calculating either the positive or negative ultimate moments. The reinforcement, on the other hand, should be able to admit the tensile force N_t alone with the required degree of safety. This design condition agrees in fact with that reached in Section 613 concerning the continuous reinforced pavements.

These conditions which are discussed purely theoretically in this section need, however, further clarification and confirmation through tests. In the next section the author will describe tests of this type which were planned in order to illustrate directly the influence of combinations of tensile forces and flexure for positive and negative moment loading of a single-reinforced slab.

63. Tests with Flexure and Tension on Concrete Slabs

631. Definition of problem and test programme

The investigation which was planned for the experimental study of the combination of tensile and flexural forces on concrete slabs should attempt to clarify the following questions in agreement with the hypotheses and discussions in the previous section:

I. The influence of tension in combination with flexure due to positive moment (tensile stresses in the reinforcement).

II. The effect of tension in combination with flexure due to negative moment, the possibility in this case of applying the equation (62:1) and the magnitude of the factor ω in this equation.

III. The influence of a "pre-deflection" with crack formation due to positive moment on a flexural loading due to negative moment with or without the combination of tension.

Literary studies in connection with the planning of these tests showed that the problem of simultaneous tension and flexure of concrete has been handled very sparsely earlier both experimentally and theoretically. It was therefore considered suitable to extend the test programme to include a more general investigation of the loading cases of pure tension as well as combined flexure and tension of concrete. The programme was therefore made more extensive and more detailed measurements were planned than were originally necessary for the examination of the more special problem within the scope of this paper.

The author intends to take up this larger problem by itself in connection with a detailed analysis not yet carried out of the very extensive test material that the tension-flexure tests resulted in. Within the framework of this paper, some rather more limited and reviewable results are accounted, these being aimed directly at the questions concerned with the design of concrete pavements according to the ultimate strength theory.

The tests were carried out as loading tests with combined tension (with constant strain) and flexure on strips of concrete. All the test units were made with a width of 20 cm and a total thickness of approx.

5 cm, length approx. 1 m. The investigation was divided up into three test series in agreement with the programme questions above:

Series I. Reinforced slab strips, tension simultaneous with positive moment (the reinforcement in the tension zone). Reinforcement of 2 ⌀ 6 Ks 40. Within each group of four test units, one was tested with flexure alone up to failure, two with a tensile force of approx. 1000 or 2000 kg as well as a flexural moment up to failure, and the fourth, with only tension to failure. The last-mentioned test unit was not reinforced.

Series II. Unreinforced slab strips, tension together with moment. Four test units in each group were tested in accordance with the same programme as that applying to Series I.

Series III. Reinforced slab strips, which were first subjected to a so-called pre-deflection of positive moment and then tested to failure with negative moment and tension. The various groups of test units were supplied with two types of reinforcement, 2 ⌀ 6 and 2 ⌀ 4, and were tested with a tensile force $N = 0$, 1000, 1500, 2000 kg. The test units within each group were tested with the same tensile force, but the pre-deflection (curvature during pre-deflection) was varied or double tests were carried out with the same pre-deflection; in normal cases pre-deflection was carried out with a positive moment, which gave a completely cracked-through tension zone in stage II. Apart from this, each group included an unreinforced control unit which was tested only for tension.

632. Test units, test devices and test procedure

The test units for the tension-flexure tests were designed in accordance with Fig. 63:1. In each group of four test units, one was designed as a pure tension test (always unreinforced), and these test units were cast with a narrower centre section in order to insure failure crack in the centre zone. A total of 104 test beams were manufactured, some of which were unsuccessful for various reasons during casting, managing or testing.

The test beams were cast four at a time in the same mould with a masonite bottom and intermediary walls of U-beams, and from the same batch three standard test cube units and three standard deflection beams were also manufactured The concrete maintained 480 kg/m^3 cement with the proportions cement:gravel:sand:water = 1:2.35:1.40:0.4. The consistency was maintained at approx. 12 VB°.

As shown in Fig. 63:1, the test units were designed with narrowed ends. As a support and for the application of the tensile force, transverse pins

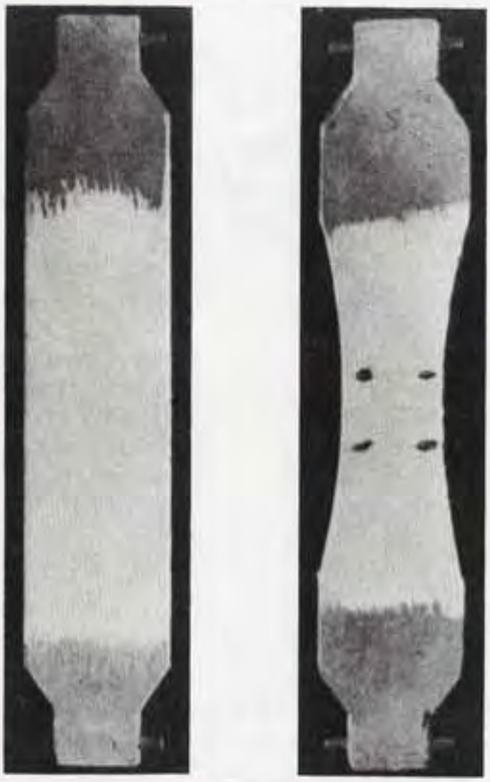

Fig. 63:1. Test units for the tension-flexure tests. The normal test units according to the left-hand illustration were made both reinforced (series I and III) and unreinforced (series II). The right-hand illustration shows a test unit for pure tension testing (always unreinforced), of which one was included in each casting group of four units.

The narrowed ends of the test units have cast-in transverse pins consisting of 20 mm shaft steel, this serving as a support and a means of applying the tensile force. See Fig. 63:2.

consisting of 20 mm shaft steel were cast in, and since these were fitted in recesses in the mould sides of U- beams, fairly good force centration could be relied upon. The transverse pins were anchored in the ends of the test units with the help of three brackets according to Fig. 63:2. There was no direct anchoring between the support pins and the reinforcement.

The transverse pins were attached to the support block as shown in Fig. 63:2, where the load transfer was applied through the medium of ball bearings. The support blocks were fitted in the tension heads of the testing machine used. Since the testing machine applied forces in such a way that the lower tension head is screwed downwards, a constant strain in the test unit is maintained, thus in principle the same

Fig. 63:2. Support block, used both as support and to transfer tensile force to the test units during the tension-flexure tests. The block was attached to the tension head in the test machine through the bolt on the right (see also Fig. 63:4). The force was transferred to the test unit support through two shafts at right-angles, carried in ball bearings, the Cardan suspension of which gave freedom from support moment in all directions. The last shaft consisted of the test unit support pin, shown on the figure with its three anchoring brackets.

force transference as that obtained due to the tensile force caused by temperature.

The flexural moment was transferred to the test units through a screw jack which was placed between the pillars of the machine and a load-distributing beam, which transferred the flexural force by means of two loading rollers against the test slab strip (see Fig. 63:3 and 63:4). The load was measured by means of a ring dynamometer as shown in Fig. 24:14.

Testing was carried out in principle by first applying a tensile force, this implying that the beam got a constant strain. Any eventual moment due to eccentric attachment could be compensated for by the suitable application of flexural force. After the tensile force had reached its intended value, the beam was bent to failure.

During the testing, measurements were made of the flexural deformation between the loading points by means of a curvature gauge. The strain values were also measured with a pair of strain gauges on each side. Fig. 63:3 and 63:4 show the test device and the location of the gauges.

After testing to failure, both parts of the beam on each side of the failure section were used for flexure tests, these being carried out in the way shown in Fig. 24:15, page 98. Only the ultimate load was measured in this case. In some of the cases one of the halves in question was too short to be used.

More detailed information about the test procedure in the three test series is supplied in the following sections in connection with a description and discussion of the results.

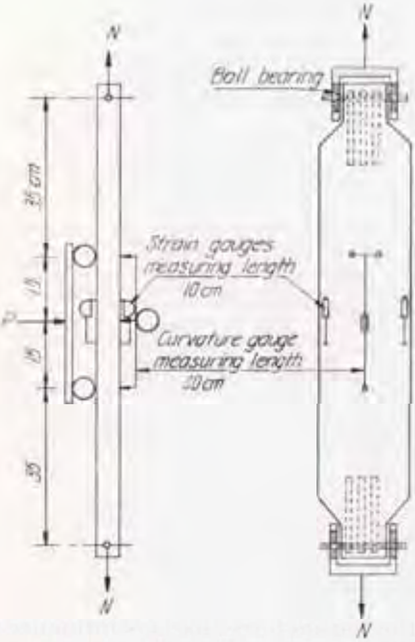

Fig. 63:3

Fig. 63:4

Fig. 63:3. Schematic sketch of the test unit and the test device used in the tension-flexure tests.

Fig. 63:4. Photograph of the test device for the tension-flexure tests with the test unit fixed in the testing machine.

633. **Test results, treatment and analysis**

633.1. *Series I, positive moment and tension.*

In the tests in Series I with tension and positive flexure of reinforced test slabs, the tension was applied completely before the flexure loading was applied. It was noticed that the tensile force began to decrease in connection with first crack formation in the tension zone, and that it later successively decreased until moment failure occurred. A further powerful reduction in tensile force then appeared. In one test (test A:3) failure suddenly occurred in connection with the appearance of the first tension crack, which in this case with the application of very large tensile force appears to depend on the fact that the residual concrete section received excessively large tensile stresses before the counteracting flexural moment had achieved any significance.

TABLE 63:1. Tension-flexure beams, series I, *reinforced* test units, test loading with *positive* moment.

All test beams reinforced with 2 ⌀ 6 Ks 40; unreinforced control test unit not included.

Test group and No.	Dimensions: Width $b = 20$ cm Reinf. 2 ⌀ 6		Flexural tests on half-beams M_{yie} at "normal thickness" $h = 5.0$ cm kgcm	Main tests			
	Total thickness h_0 cm	Eff. thickness h cm		Tension, kg: at mom. 0 N_0	Tension, kg: imm. before failure N	Flexure at failure P kg	Ult. moment M_{yie} at "normal thickness" $h = 5.0$ cm kgcm
A:1	5.20	4.65	8400	0	0	420	7900
2	5.25	4.60	10100	1000	500	562	10700
3	5.32	4.74	9300	2400	2300	144[1])	—
B:1	5.38	4.91	{8300 9300	0	0	636	11300
2	5.15	4.71	11000	1000	500	562	10400
3	5.34	4.76	10300	2600	1050	526	9700
C:1	5.30	4.85	7900	0	0	630	11400
2	5.54	5.13	7500	1000	640	628	10700
3	5.30	4.80	7700	2000	1260	658	12000

[1]) Sudden failure occurred here when the first crack in the tension zone appeared.

The test results as shown in table 63:1 confirm completely the hypothesis presented in Section 62, that the tensile force does *not* influence the positive ultimate moment. In order to be able to compare the ultimate moment values from the main tests more easily, these are re-calculated to apply to a normal height of 5 cm; the same applies to the flexural tests on the half-beams (in most cases only one of the half-beams was tested for positive moment). The spread in the ultimate moment values is certainly significant but no general tendency to decreased ultimate moment value in the case of increased tensile force can be observed. Besides, the same spread applies between the ultimate moment values from the flexural tests on the half-beams but good agreement has been reached, at least in the case of groups A and B, between the values from the main tests and the corresponding half-beam tests. In series C, however, the half-beam values lie fairly far below the corresponding values from the main tests, but the low values appear here to depend on errors in the force registration (manometer), and it is obvious that the moment values from the half-beams have approximately the same internal variations as the moment values from the corresponding main tests.

The tests in Series I thus show clearly that the positive ultimate moment m_{yie} can be calculated *without* respect to the influence of the tensile stress due to temperature and shrinkage.

633.2. *Series II, unreinforced test beams*

In Series II, which included testing with combined flexure and tension on unreinforced test beams, the test results, shown in Table 63:3, have been analyzed according to the simple superimposition formula

$$\sigma_f = \omega \frac{N}{A_c} + \frac{M}{W} \tag{63:1}$$

in agreement with formula (62:1). During the introductory test procedure, when only the tension was applied, it became obvious in most of the tests that the attachment through which the tension was applied was somewhat eccentric so that a certain flexural moment was obtained by only the tensile force (readings on curvature gauge). The formula (63:1), however, is only valid with completely centrally applied tensile force, and therefore, in the calculation of the moment M in formula (63:1), the flexural ultimate load P was corrected with that force P_0 which was found necessary, when applying flexure, to return the curvature value to zero ($M = 0$). See Table 63:2, note 1.

Otherwise, it was found out during these tests that the tension did not decrease at all or decreased only very insignificantly during the flexural procedure up to the sudden failure.

The analysis of the results according to (63:1) is shown in Table 63:2 for a factor $\omega = 1.7$. This factor is selected as an approximate average value

$$\omega = \frac{\sigma_f}{\sigma_t} \tag{a}$$

for the *pure tension* tests. The result figures of σ_f in the last column in the table show that the calculating method used gives reasonable results. There is certainly quite a large spread between the results from the different tests, even within the same group of test units from the same batch of concrete, but the spread between the pure flexural strength values from the flexural tests on the half-beams is just as large, and the agreement between σ_f according to the result analysis with the formula (63:1) and according to the flexural tests on the half-beams from the same test unit is strikingly good all the way through.

The test results thus show that with combined flexure and tension on an unreinforced concrete slab, it is possible to calculate the strength on the basis of the pure flexural strength according to the formula (62:1) or (62:2), whereby (at least in this case) it is possible to put $\omega = 1.7$. This value lies rather high in comparison with current information — for example in the CBI design specifications [78] a factor $\omega = 1.5$ is

TABLE 63:2. Tension-flexure beams, series II, *unreinforced* test units.

Test group and No.	Standard flex. beams aver. value of 3 tests σ_f kg/cm²	Dimensions in failure section cm		Flexural tests on half-beams σ_f kg/cm²	Main tests			Analysis from equ. (63:1)		
					Load at failure		Flexure at $M=0$ P_0 kg	Formal stresses[1]) kg/cm²		$\sigma_f = \omega\,\sigma_N + \sigma_M$ $\omega = 1.7$
		h_0	b		Tension N kg	Flexure P kg		σ_N	σ_M	
A:1	30	5.20	20	33, 35	0	174		0	33.8	33
2		5.20	20	31	1000	88	9	9.6	15.3	32
3		5.10	20	38, 43	1960	66	34	19.1	6.4	39
4		5.20	20	45, 45	2700	0		26.0	0	44
B:1	37	5.40	20	35, 37	0	185		0	33.5	33
2		5.25	20	42, 45	1000	163	13	9.5	28.6	45
3		5.35	20	46, 46	2000	90	35	18.7	10.1	42
4		5.30	13.5	34	1700	0		23.8	0	40
C:1	41	5.10	20	49	0	252		0	50.9	51
2		5.30	20	46	1000	175	9	9.4	31.6	47
3		5.35	20	46	2500	54	32	23.4	4.0	44
4		5.35	13.5	39	1900	0		26.3	0	45
D:1	36	5.10	20	42, 40	0	190		0	38.4	38
2		5.15	20	39, 38	1000	120	17	9.7	20.3	37
3		5.25	20	37	2000	70	37	19.1	6.3	39
4		5.20	13.7	37	1500	0		21.0	0	36
E:1	38	5.40	20	41, 43	0	211		0	38.0	38
2		5.37	20	41, 37	1000	130	14	9.3	21.1	37
3		5.35	20	44	2020	85	39	18.9	8.4	41
4		5.30	13.7	38	1490	0		20.5	0	35

[1]) $\sigma_N = \frac{N}{A} = \frac{N}{b\,h_0}$; $\sigma_M = \frac{M}{W} = 17.5\,(P - P_0)\,\frac{6}{b\,h_0^2}$

stipulated – and the value would appear to vary to a great extent depending on the thickness of the slab, the composition of the concrete, etc. On the other hand it can be correct in the case in question to select a comparatively high value of ω with respect to the fact that the estimation of the tensile force due to temperature and shrinkage is very unreliable.

633.3. *Series III, reinforced pre-deflected test beams, negative moment and tension.*

The tests in Series III, which was the most extensive of the test series, were intended to be similar to the conditions for negative moment loading of a cross-section of a single-reinforced pavement which had earlier been subjected to positive moment loading due to a mobile load and thereby developed cracks in the bottom through the reinforced zone. For this reason, the single-reinforced test beams in this series were subjected, after being fitted in the test machine, to a *positive* "pre-deflection" of a flexural single force in the centre, which caused crack formation in the reinforced side and through the whole tension zone. Then the beam was tested for failure with tensile force simultaneously with the usual flexure loading from the opposite side, this causing a *negative* moment.

With certain of the first tests carried out with a large tensile force (N approx. 2000 kg) it became obvious that eccentricity due to the pre-cracking had become so great that failure occurred due to this tensile force before its full value had been reached and flexure had been applied; in this way many of the tests became unsuccessful. By compensating the deflection due to this eccentricity under the application of tension by means of a flexural force which maintained the curvature at zero the whole time, this undesired case of failure was avoided in later tests.

In most of the tests a "normal" pre-deflection was applied with crack formation throughout the complete tension zone if Stage II is assumed. This type of crack formation would appear to be the type to be expected after some considerable time of normal traffic on a single-reinforced pavement, designed with a reasonable margin of safety (1.7—2, see Part 7).

On the whole it is these tests with "normal" pre-deflection which are described in Table 63:3, and the depth of the crack formation zone in pre-deflection has been checked partly through visual observation (with a magnifying glass) and measurement, partly through the calculation of the position of the neutral layer from the curvature measurements carried out during the pre-deflection. These values agree comparatively well, and agreement with the theoretically calculated position of the neutral layer is also good (see the table, note 1).

It is remarkable that the failure crack in the main test with negative flexure in a large number of tests occurred *beside* the pre-crack (see Table 63:3). This implies that pre-cracking on the whole lacks significance for strength at negative flexure. The test analysis in Table 63:3 confirms this conclusion. The flexural strength σ_f has here been calculated according to the formula (63:1) as for a homogeneous section *without* respect being taken to the pre-cracks, and the result shows fully reasonable values, where *no* influence of the pre-cracks can be traced. As in the case of the preceding test Series II, spread is certainly large, but if comparison is made between the formal calculation of the σ_f-values and the flexural tests on the corresponding non-cracked half-beams, as well as the result of the pure tension tests included in each group (whereby the flexural tests on the corresponding half-beams have

TABLE 63:3. Tension-flexure beams, series III, reinforced test units with *positive pre-flexure*, test-loading with *negative* moment. The table also includes unreinforced tension tests.

Test group	Reinforcement Tensile force N_0 at $M=0$	Standard flexure beams, aver. value of 3 tests σ_f kg/cm²	Tensions tests: Pure tension σ_t kg/cm²	Tensions tests: Flexural tests on half-beams σ_f kg/cm²	Main tests: Dimen. in failure section $b=20$ cm h_0 cm	Main tests: Flexural tests on half-beams σ_f kg/cm²	Pre-flexure: Max. curvature 10^{-3}cm^{-1}	Pre-flexure: Crack-depth[1] f/h_0 meas.	Pre-flexure: Crack-depth[1] f/h_0 from ε	Load at failure: Tension force N kg	Load at failure: Flexural force P kg	Flexural force P_0 kg at $M=0$	Formal stresses[2] σ_N	Formal stresses[2] σ_M	$\omega \cdot \sigma_t$ ($\omega=1.7$)	$\sigma_f = \omega\,\sigma_N + \sigma_M$ ($\omega=1.7$)	Remark U = Failure crack beside pre-crack KF = More powerful pre-flexure with reinf. yield
A:1	2 ⌀ 6	33	24	38	5.36	43, 41	11		0.64	0	235	—	0	42.9	41	43	U
2	$\mu \approx 0.50$ %				5.33	41, 37	44		0.69	0	216		0	39.9		40	U, KF
3	$N_0=0$				5.37	31, 48	44		0.69	0	222		0	40.4		40	KF
Ba:1	2 ⌀ 6	25	23	40	5.48	43, 48	24	0.65	0.62	930	171	14	8.5	27.4	39	42	U
2	$\mu \approx 0.50$ %				5.35	38, 43	58	0.82	0.77	960	150	34	9.0	21.3		37	KF
Bb	$N_0=1000$	36	23	40, 41	5.39	46, 44	21	0.73	0.78	925	176	22	8.6	27.8	39	42	U
Bc		30	24	35, 45	5.36	43	18	0.70	0.69	1010	158	22	9.4	24.8	41	41	
Ca:1	2 ⌀ 6	33	24	40, 35	5.38	41	18	0.72	0.71	1900	82	51	17.6	5.7	41	36	U
2	$\mu \approx 0.50$ %				5.35	49, 48	22	0.76	0.62	1950	101	62	18.2	7.2		38	U
Cb	$N_0=2000$	38	24	37, 38	5.35	43, 45			0.74	1450	141	54	13.6	15.9	41	39	U
Da	2 ⌀ 4	32	22	36, 36	5.40	41	19	0.77		0	227	—	0	40.8	37	41	
Db	$\mu \approx 0.25$ % $N_0=0$	33	25	—	5.50	45	15	0.78	(0.69)	0	237	—	0	41.1	43	41	
Ea	2 ⌀ 4	37	21	34	5.23	41	18		0.70	960	145	24	9.2	23.2	36	39	U
Eb	$\mu \approx 0.25$ % $N_0=1000$		24	39	5.34	45, 45	18	0.80		980	199	49	9.2	27.6	41	43	
Ec		35	30	37, 43	5.21	46, 41	18	0.79	0.74	940	166	32	9.0	25.9	51	41	U
F	2 ⌀ 4 $\mu \approx 0.25$ % $N_0=1500$		26	44	5.18	49, 48	18	0.80	0.75	1470	126	40	14.2	16.8	44	41	

[1]) When calculating for stage II, $n=15$, at 2 ⌀ 6, $f/h_0=0.69$ is obtained
at 2 ⌀ 4, $f/h_0=0.77$ is obtained

[2]) $\sigma_N = \dfrac{N}{20\,h_0}$; $\sigma_M = 17.5\,(P-P_0)\,\dfrac{6}{20\,h_0^2}$

also been taken into consideration), fully acceptable agreement is reached in practically all cases, and also here the value of 1.7 for the factor ω in the equation (63:1) appears to be fairly correct.

A number of tests was also carried out with test beams which were subjected to more powerful preflexure, whereby the positive deflection was taken so far that strain values were obtained in the reinforcement quite a long way in the yield zone. Some of these tests, particularly with test units with the more powerful reinforcement 2 ⌀ 6 and with no or comparatively small tensile force, gave exactly the same result as those discussed above, these being shown in the table (the pre-deflection magnitude is shown by the curvature value and the depth of the crack zone). Other tests of this type — and this applies particularly to the tests with large tensile force and weak reinforcement, 2 ⌀ 4 (reinforcement percentage $\mu \approx 0{,}25$ %), — show, on the other hand, decrease in strength compared with the earlier mentioned tests, in most cases, however, comparatively moderate. In special tests with the largest tension (1500—2000 kg) sudden failure occurred in many cases when only tension or a very low moment loading was acting. It should be pointed out, however, that for these test units a normal tensile force due to temperature would only correspond to 500—600 kg (see formula (61:2)).

The author thus finds that in normal cases of single-reinforced pavement design, the strength for *negative* moment loading can be estimated *without* respect being taken to pre-cracking phenomena, and thus the formulae (62:1) or (62:2) can be applied when calculating the negative ultimate moment.

64. Summary and Application on Field Tests

The treatment of the influence of temperature and shrinkage on concrete pavements in this Part 6 is comparatively short and is primarily intended to show how respect can be taken to the above-mentioned influences when applying the ultimate strength methods for calculating reinforced concrete pavements, as developed earlier in this paper. In the description in Section 63 of the tests carried out with the application of combined tension and flexure, generally speaking only those results are shown which are significant for the problems concerned in this connection.

The influence of decreased temperature and shrinkage can be assumed to correspond to the stresses in the pavement from a tensile force N_t according to the formula (61:1) and a warping moment m_t giving rise to flexural stresses σ_{mt} according to the formula (61:3 a). In the case of normal single-reinforced pavements with transverse joints at a fairly large distance from each other, these stresses can be summarized as follows:

$$\left.\begin{array}{l} N_t = 1.2\, h_0\, f_s\, L \ \text{ tons/m, if} \begin{cases} h_0 = \text{slab thickness in m} \\ L = \text{joint distance in m} \\ f_s = 1.5 \text{ in normal cases} \end{cases} \\ \sigma^t_{mt} = 7 \ \text{kg/cm}^2 \ \text{tensile stress in top} \end{array}\right\} \qquad (64{:}1)$$

The most dangerous cases of loading occur when the effect of temperature decrease and shrinkage as mentioned above take place at the same time as wheel load stresses.

As shown by theoretical consideration and tests carries out on test units used for simultaneous flexure and tension, when designing a single-reinforced concrete pavement according to the *ultimate strength method* no respect needs to be taken to the influence of temperature and shrinkage when calculating the positive ultimate moment m_{yie}, while when calculating the negative ultimate moment m' the flexural strength of the concrete must be decreased by the stresses due to temperature and shrinkage according to (64: 1). The above-mentioned tests carried out on test units which, before being subjected to ultimate loading with negative moment have been subjected to pre-deflection with crack formation due to positive moment, show that in normal cases and with a not altogether too small reinforcement percentage ($\mu >$ approx. 0.3 %), the influence of the pre-cracking phenomenon (see Fig. 62:1) can be neglected and the negative ultimate moment can be calculated as for an uncracked section.

The ultimate moment values for single-reinforced concrete pavements can thus be calculated as follows:

$$\left.\begin{aligned} &m = \text{the ultimate moment of the reinforced section} \\ &m'_{\text{red}} = \frac{h_0^2}{6}\left[\sigma_f - \left(\sigma^t_{mt} + 1.7\,\frac{N_t}{h_u}\right)\right] = m' - \Delta\, m'_t \end{aligned}\right\} \qquad (64{:}2)$$

where σ_f is the flexural strength of the concrete slab and the remaining magnitudes are decided in accordance with (64:1). The factor $\omega = 1.7$ has been obtained from the tests according to Section 63 and should be on the safe side.

When calculating the ultimate load according to the formulae and the diagrams for the *ultimate strength method*, the moment sum ($m + m'_{\text{red}}$) according to (64: 2) shall be used. It should be pointed out, however, in this connection that the influence of the normal force and thereby also the negative ultimate moment according to (64: 2) is in most cases different in directions along and across the pavement. The lowest value of the moment sum may be taken, however, when designing the interior of the pavement. Beside the edges and the joints which have the possibility to move, the effect of the temperature will be zero in a direction at right angles to the edge, this meaning that when designing edges and joints, the negative ultimate moment m' does not need to be reduced but only m'_c. This circumstance decreases the necessity of strengthening the edges and joints.

In the Norrköping tests, described in Section 52, test loading was carried out on finished taxiways, and it was pointed out in the discussion of the results from these tests that the influence of temperature and shrinkage on these 40 m long taxiways could be significant and could partially explain the comparatively poor agreement between the ultimate loads in test and theory. An estimation of this will be carried out in accordance with the methods summarized above.

Since the tests were carried out during the summer at normal temperatures, it can be assumed that there was no apparent effect of warping. On the other hand a comparatively moderate temperature decrease of, for example 5° C, together with probable shrinkage which can be assumed to correspond to a temperature decrease of at least 10° C, produced quite sufficient movement to give fully developed friction under the larger part of the taxiway. The normal stress of this can thus be estimated in accordance with (64: 1) and, with $f_s = 2.5$ the result is

$$L = 40 \text{ m}, \; h_0 = 16 \text{ cm}$$

$$N_t = 1.2 \cdot 0.16 \cdot 2.5 \cdot 40 = 19 \text{ tons/m}$$

This corresponds to a tensile stress

$$\sigma_N = \frac{19 \cdot 10^3}{16 \cdot 100} = 12 \text{ kg/cm}^2$$

which gives a reduction of the negative ultimate moment, which according to (64:2) can be estimated to be

$$\Delta m_t' = \frac{16^2}{6} \, 1.7 \cdot 12 \approx 900 \text{ kgcm/cm}$$

With reasonable assumptions concerning temperature and shrinkage, there may thus be a very considerable reduction of m' which, according to the detail tests (Table 52: 1), was equal to 1800 kgcm/cm.

Due respect being taken to this not improbable decrease in negative ultimate moment, when calculating ultimate loads for the taxiways c and d with the data according to Table 52:3, the following results were obtained:

a) Load on the centre of the section, test c:1 and d:1 (see Table 52: 3)

$$m = 3600 \text{ kgcm/cm}; \; m_{\text{red}}' = 1800 - 900 = 900 \text{ kgcm/cm}$$

From the diagram in fig. 32:14:

Test c:1; $\dfrac{c}{l} = 0.60$; $P_t = \dfrac{4500}{0.081} = 55$ tons — according to the tests 50 tons

Test d:1; $\dfrac{c}{l} = 0.66$; $P_t = \dfrac{4500}{0.077} = 58$ tons — according to the tests 57 tons

b) Load on the edge of the taxiway, test d:2 (see Table 52:4):

$$m = m_e = 3600 \text{ kgcm/cm}$$

$$m_e' = 900 \text{ kgcm/cm}; \; m' = 1800 \text{ kgcm/cm}$$

In addition to this an edge beam according to Table 52:4

According to the formulae in 427 the ultimate load will be:

$P_t = 39$ tons — according to the tests 34 tons.

The agreement between the ultimate load according to theory and tests is here considerably better than the result according to the Tables 52:3 and 52:4, where the theoretical ultimate load values have been calculated without respect to the probable influence of temperature and shrinkage. This influence can obviously be significant in the case of the large section lengths in question.

When carrying out calculations according to the *elasticity theory*, the stresses caused by temperature and shrinkage according to (64:1) are added, in accordance with the superimposition principle, to the stresses caused by wheel load.

On pavements without transverse joints, the so-called *continuous reinforced pavements*, with respect to temperature and shrinkage a longitudinal reinforcement is required with a reinforcement percentage μ according to

$$\mu > \frac{\sigma_t}{\sigma_{yie}} \tag{64:3}$$

where

σ_t = the strength of the concrete towards *pure* tension

σ_{yie} = the yield point of the steel

This reinforcement does not appear to require intensification with respect to traffic loading. The crack width δ can thus be judged by estimation according to theoretical analysis:

with deformed bar reinforcement

$$\delta = (1.0 \div 1.3)\,\frac{\sigma_t^2}{\tau_b^{\max}}\,\frac{\varnothing}{4\,\mu^2\,E_r} \tag{64:4 a}$$

where

$\tau_b^{\max}$ = the maximum bonding strength

$\varnothing$ = the diameter of the reinforcing bars (deformed bar),

with mesh reinforcement (of smooth wire)

$$\delta = (2 \div 3)\,\frac{\sigma_t}{E_r}\,\frac{d}{\mu} \tag{64:4 b}$$

where

d = mesh width between cross wires.

Further viewpoints concerning the effect of temperature and shrinkage when designing concrete pavements are included in Section 72.

7. Practical Viewpoints on Reinforced Concrete Pavements. Design Methods

71. General Viewpoints. Some Experiences from Pavement Work Carried out

When the thought of building airport runway pavements of concrete with a relatively powerful structurally active bottom reinforcement was originally put forward in connection with the introductory discussions in 1944 concerning an airport near Stockholm for the heavy Atlantic traffic, the idea was primarily to find a type of pavement which would have sufficient load-carrying capacity for the heavy wheel loads and the very poor soil properties concerned in the Väsby project which was then topical. The closer examination of this type of structure which followed, the results of which are presented in this book, soon showed however that there were many advantages apart from increased load-carrying capacity with this new type of structure, which was called "*structurally reinforced concrete pavement*" as opposed to the earlier used plain or slightly crack-reinforced types of concrete pavement, also if the properties of the soil did not make such a pavement essential from the point of view of load-carrying. Comparative economical calculations which have been carried out for many airport projects have shown that the type of pavement generally means good economy; this question will be further discussed in Section 73. Apart from this, considerable technical and constructional advantages appear to be present with the use of structurally reinforced pavements in comparison with the often very thick unreinforced concrete pavements otherwise essential. Perhaps the greatest advantage is the fact that with structurally reinforced pavements the distance between the transverse joints can be made fairly large — it is these transverse joints which, in the case of concrete pavements, have been the most troublesome constructional part and that which has been least able to stand up to traffic.

After this new type of pavement had been brought forward in connection with the preliminary presentation of the earliest test results, quite a lot of airport pavements of this type have been built in Sweden. In many cases the author himself has had the opportunity to apply directly the theoretical methods of calculation and test results then available to the designing problem in question. This was the case in the extension of Norrköping airport in 1948 where also some of the taxiways were used as objects for test loading (see section 52) and where moreover precise studies of working methods were carried out. Another case is the first built east-west runway at Arlanda airport where the result of the test loading, as shown in Section 53, was directly used in the suggested design of the runway pavement to be built. Apart from this, the author's calculation methods have been applied to the design of pavements on many military airfields. In other cases structurally reinforced pavements built have been designed on the basis of the elasticity theory method, whereby the methods developed by WESTERGAARD and HOGG for *plain* concrete pavements have been applied with suitable modifications [54, 78]. The test material described in this paper is, as a matter of fact, the first to show that it is really correct to apply this theory also to *reinforced* conrete pavements within the elastic stage and with suitably selected material constant values for the slab and the soil.

As a matter of fact structurally reinforced pavements would appear now to have become the normal type of pavement in Sweden for runways on airfields with heavy traffic. As far as the author has been able to determine, this type of pavement on the whole has shown itself to be very good in practice.

From a constructional point of view, the first reinforced pavements at Norrköpings airport showed certain problems which are associated with the reinforced structure.[1]) Trials were carried out there with, for example, double-reinforcement which showed that there were great difficulties in its use. Also the through reinforcement at the longitudinal joints which was specified for this pavement in order to make the joints transfer moment, proved difficult to insert from the point of view of constructional technique. In some later projects, after more was known about the function of the joints, the through reinforcement was completely disposed with; this was the case for the first time with the abovementioned first constructed runway at Arlanda. On the whole the problems from a constructional point of view now appear to have been solved, at least concerning pavements with only bottom reinforcement.

Also from the functional viewpoint, the reinforced pavements have come up to expectations. An inspection carried out by BERGSTRÖM and ÖRBOM[2]) during 1953 and 1954 on some airfield pavements of

[1]) A description of the studies of constructural technique during the work carried out at Norrköping has been supplied by BERNELL in a typed report in 1948 from Kungliga Väg- och Vattenbyggnadsstyrelsen (Royal Swedish Board of Roads and Waterways).

[2]) The report of the inspection as far as crack formation and joint damage is concerned is unpublished, but the inspectors have willingly placed their observations in this matter at the disposal of the author.

concrete showed that crack formation and joint damage was very moderate for the pavements which had been built on the structural reinforcement design. Concerning the above-mentioned first runway at Arlanda airport, this was so far unsuccessful since during grading work the runway was given excessive inclinations and lateral slopes; it was therefore condemned from the point of view of aircraft safety and will be relaid during the extension work now being carried out. No complaints have however been made concerning the pavement, and during an inspection carried out in December 1959, it was found that the pavement was in good condition. It is true that during the six years since it was built there has only been very occasional aircraft traffic, but during the last two years in connection with the extension of the new runways, there has been very intensive traffic with heavy trucks with rear axle pressures of up to 20 tons. Of course the wheel loads for which the pavement was designed have by no means been reached, but on the other hand the loading area from the truck wheels is more concentrated and great dynamic forces must have occurred. During the inspection in question it was found that crack formation was very slight, and comparison with the crack charts made out during the inspections immediately after the completion show that most of the cracks occurred as early as during the building period. There was no significant separation in the *completely* reinforcement-free longitudinal joints in spite of the fact that the runway was not provided with any edge strips whatsoever which could have had an anchoring effect in this respect.

In an other field of use where concrete pavements occur, namely roads, the structurally reinforced type of concrete pavement, on the other hand, hardly seems to have been used at all in practice. A very suitable study object for this field of use is the private stretch of road which was laid in 1957 by Skånska Cementaktiebolagets factory in Hellekis between the lime quarries and the cement factory, this road being built with structurally reinforced pavement. This road is particularly interesting since it has perhaps the most intensive traffic of any road in Sweden with a continuous stream of limestone-loaded special trucks with about 21 tons rear axle pressure. It is also interesting from the point of view that it was the first modern road in Sweden which was built in one operation, i. e. the pavement was laid as soon as the subbase was completed [40][1]). The pavement consisted of a 14 cm thick concrete slab with bottom reinforcement of welded wire fabric made of cold-drawn steel. This was laid out directly from rolls, which made it difficult to get the mesh to lie flat in its correct position during casting. The

[1]) A detailed description of the building of this road is included in Svenska Vägföreningens Tidskrift, Volume 8, 1948, and in Cement- och Betong, Volume 6, 1947.

distance between the transverse joints was 24 m, and the pavement was designed according to the ultimate strength method for a wheel pressure of 10,5 tons with a certain dynamic supplement and for an factor of safety of approx 1,6 concerning failure through crack formation in the top. During the whole time the road has been in use, traffic has been extremely intensive with an average frequency of approx. 100 trucks per day in each direction, running in one direction fully loaded the whole time and often with an overload of 10 %. Due to certain crack formation and surface damage, a careful inspection was made of the pavement during the year 1954, an inspection in which the author had an opportunity to take part [22, 40]. It could thereby be determined rather definitely that the damage was of comparatively moderate extent and did not diminish the function of the road in any way, and it was also found that at least the most serious crack damage most probably depended on unevenness in the subgrade (culvert and old embankment crossings, etc.) as well as insufficient drainage and disposal of water from the edges of the road, this causing washed-out subgrade at some places. Moreover, unevenness in the position of the reinforcement caused by the unsuitable system used for laying it, may have caused some crack formation.

It appears to the author that the mainly good experience from this road with its exceptionally hard traffic should be utilized when projecting public roads in Sweden. The rapid development in traffic towards greater intensity and increasing wheel load have resulted in the fact that the existing concrete pavements of unreinforced or crack-reinforced type do not stand up to the stresses, and this has caused a sort of concrete pavement crisis concerning roads. It is possible that the structurally reinforced pavement can contribute to a solution of the problem. In any case the experiences available can well motivate that this type of pavement should be thoroughly tested under normal road conditions together with other types of pavement. On the whole in Sweden, there appears to be a lack of tests concerning running of traffic on special test road stretches. In view of the gigantic development programme at present planned for Swedish roads, such rational traffic tests with comparisons between pavements of different types would appear to be *absolutely necessary*.

It would appear to be eminently desirable to try to find possibilities of giving concrete, with its durability and light surface, its leading place again among pavement material. Instead of this, the tendency within road building technique just now would appear to be that the load-carrying capacity of the subbase itself is being increased and the pavement is being made of a non rigid asphalt covering. But even with such a type of subbase, and obviously with a good natural subgrade, replacement of the soft pavement by a concrete pavement could be considered, namely a concrete pavement of the type consisting of thin, powerfully mid-depth reinforced slab which was the subject of experiments during the Arlanda tests (Section 53). This type of pavement came forward during the projection of the Arlanda runway just because of the fact that the runway subgrade had sufficient load-carrying capacity to withstand the stipulated wheel load without any rigid pavement, but that a concrete pavement was desired in any case because of the other advantages of this type of pavement material. The idea was that the pavement should function as a reinforced concrete slab with an effective depth equal to half the total thickness for both positive and negative wheel load moments which, in this case, are of roughly the same magnitude. Fine tension cracks thereby occur both in the top and the bottom surface and the slab will take a very low degree of flexural rigidity, i. e. it functions on the whole as a non-rigid pavement. Wheel load stresses are very low, in practice the thinner the slab is the lower they become, this being shown in Table 53: 9.

The good results shown from the 1953 tests at Arlanda (see Section 535) prompted the author to come forward with a suggestion that about 1/3 of the runway in question should be designed with this thin type of pavement. As the result of doubts from the authorities responsible for the building, a test stretch of only 80 m was however built. This test stretch was obviously too small to provide experience of constructional technique during the building work, and the contractors found that there were considerable difficulties in producing such a thin pavement. In this case the same machines and the same technique were used as for the building of the thicker pavement on the rest of the runway, and there is no reason to believe that, with working technique and equipment directly suited for this task, there should be any special difficulties in producing perhaps even thinner pavements than the 8 cm slab used here. It should be pointed out that it is not necessary to set up any great demands concerning tolerances in the thickness or the position of the reinforcement, this being shown by Table 53: 9.

During the above-mentioned inspection of the old runway at Arlanda, the 8 cm slab in the test pavement showed crack formation within the loaded section completely in accordance with predictions, thus with only very fine cracks in the surface. No cracks had opened or caused any other surface damage. In the sections which had not been subjected to loading there were no visible cracks whatsoever. The pavement was also in very good condition otherwise.

Tests, calculations and experience available up to date,[1]) thus show that the thin slab with mid-depth reinforcement is a suitable type of pavement, also for roads, in such cases where a subbase with uniform and high load-carrying capacity exists or can be produced fairly simply. There is no doubt that the type of pavement is economical with suitable working technique (see also Section 73). Also from a technical viewpoint, a thin pavement with mid-depth reinforcement has advantages compared with a more rigid pavement in the cases good soil conditions make possible free selection. According to the results shown by tests and theory the stresses on joints and free edges are comparatively small, and these details can be designed in a simpler way than with a more rigid pavement. The tensile forces due to temperature decrease are small and the stresses due to un-uniform temperatures are negligible with a thin slab so that the dilatation joints can be placed at *large* distances; particularly for road pavements it would be a great advantage to be able to have the transverse joints, which are troublesome from a constructional and traffic point of view, at large distances from each other and the joints can then be given a better and more costly design. Apart from this, the less rigid pavement should be able to follow settling in the subgrade better without cracking — this advantage should be particularly obvious by comparison with normal plain or crack-reinforced road pavements. On the other hand a thin slab has obviously a poorer capacity to bridge over very localized unevenness in the subgrade, for example in the levelling layer, without suffering from deformation at such places. There is, however, no risk that the pavement will crack right through in such cases, something which can often happen with a more rigid pavement. Whether damage of one or the other type is most troublesome can only be decided by traffic tests. On the whole only rational tests on test roads can provide the basis for a general judgement concerning the suitability of the thin, mid-depth reinforced concrete pavements for road pavement purposes in various cases. It appears to the author that this should be worth an careful examination.

The thin, mid-depth reinforced pavement should also provide the possibility, in a fairly economical way, to carry out pavement projects of the type which are usually called continuously reinforced pavements (better name: continuous reinforced pavements). This type of pavement is designed completely without transverse joints or with transverse

---

[1]) Similar types of thin, reinforced pavements were also included among the pavements in a test road project at Oxten in England, and a 5-year report from 1955 by LOE [46] shows that these pavements, apart from certain joint damages, exhibit good condition with closely spaced, hair-fine cracks.

joints at very large distances from each other (see 613), and a powerful reinforcement is necessary to hold together and closely space the cracks occurring due to the particularly intense effect of temperature decrease and shrinkage caused by the fact that, due to its lack of joints, the pavement must be considered as being completely locked to the subgrade. It is obvious that a pavement of this type combining the large advantages of a concrete surface with the jointlessness of asphalt pavement must be regarded as almost ideal from the point of view of road-building engineers; the joints in the traditional concrete pavement are still, no matter how it is designed, its weakest element from the point of view of design, traffic and maintenance. The continuous reinforced concrete pavement has recently been the object of great interest particularly in the United States and during the last ten years many test roads with pavements of this type have been built and studied thoroughly. A committee report from the American Concrete Institute [2] gives a good review of the experiences and results from these test roads and detailed reports are available from many of the projects in question (see, for example, [16, 45, 67, 68]). In practically all cases there is very good experience from about 10 years function with normal traffic (20 years in one case [16]); the pavements are generally in good condition with close crack formation consisting of fine and completely harmless cracks. A couple of test stretches have also been made in Sweden with this type of pavement; a project of this type (Ängelholm) has just been completed; another (Törnevalla), completed in 1953, has shown too intensive crack formation, according to the Swedish State Road Institute report [44], apparently depending on too weak reinforcement. This type of pavement requires, unfortunately, a comparatively high percentage of reinforcement. Theoretical considerations (see Section 613) show that in normal cases a reinforcement percentage with a minimum value of 0.5 % or rather higher must be reckoned with, and experience from the American test roads appear to confirm the correctness of this figure. With the pavement thicknesses of 7"—10" used in the United States, this implies an excessively large amount of reinforcement which from the point of view of economy would appear to prohibit the use of this type of pavement altogether. The question comes into an entirely different light, however, in cases where the load-carrying capacity of the subbase permits designing the pavement as a thin mid-depth reinforced concrete slab; with a slab thickness of about 8 cm, the amount of steel needed for the continuous design is comparatively moderate. Attention should also be paid to the possibilities of displacing the reinforcement downwards or designing it as double reinforcement to strengthen the concrete slab without requiring to thicken it so much. The possibilities of reducing the required reinforcement by using even higher grade reinforcement (type Kam 90) or by reducing the tensile strength of the concrete in other ways have been discussed earlier. This and other questions concerning the continuous reinforced pavement, which were mentioned in Section 613, require extensive research, and it would appear to be a matter of the greatest interest on the whole if this type of pavement with its extensive technical advantages is made the object of continued and intensive investigations.

72. Design of Reinforced Concrete Pavements

721. General principles

In design calculations for reinforced concrete pavements it is obviously possible, as for all reinforced concrete structures, to adopt *either* methods according to the *elasticity theory* and base the strength demands on the permissible stresses, *or* to use the *ultimate strength method* based on the plasticity theory — as far as the slab is concerned the yield line theory — and determine the load-carrying capacity with a suitable safety factor.

When designing in accordance with the *elasticity theory* it is possible, in agreement with the theories and the test results in this paper, to calculate the maximum stresses that occur due to wheel load, temperature and shrinkage and make sure that the most dangerous combination of these stresses does not exceed the permissible stresses, which in this case may be determined for the positive moment in relationship to the yield point of the reinforcement and for the negative moment in relationship to the flexural strength of the concrete (with single-reinforced pavements) with a very small safety factor. When calculating wheel load stresses, the formulae and the diagrams in Section 225 can be adopted for the case of loading on the interior and the formulae and diagrams in Section 41 for the edge loading case, while the stresses caused by temperature and shrinkage can be estimated as described in Section 64. Tests show that the flexural rigidity of the slab can thereby be estimated theoretically on the basis of stage II with an inactive tension zone and $n = 15$. Otherwise, the principles given in the design specifications from the Swedish Cement and Concrete Institute (CBI) [78] can be applied.[1] The elasticity theory, however, would not appear to apply for strengthened edges or joints.

In accordance with the viewpoints earlier presented in this paper, the

[1] These specifications [78] quote, as earlier pointed out (see Section 64), the stresses of edge loading with a faulty formula. Apart from this the expressions given for the negative maximum moment only apply for small values of the relative load distribution and the instructions concerning the calculation of flexural rigidity appear to be vague. The suggested safety factor against failure in the top surface (tensile strength in concrete) would appear to the author to be rather on the low side.

author would like to point out, however, that the *ultimate strength theory* gives a more correct idea of the load-carrying capacity of a reinforced concrete pavement and thus considers that designing should be carried out in agreement with this method, whereby a higher margin of safety should of course be adopted. The ultimate strength method has also the advantage that it can be used also for designing strengthened edges and joints. The method to be used when designing a normal, structurally bottom-reinforced concrete pavement is described in more detail in the following Section 722.

For thin mid-depth reinforced pavements of the Arlanda type, the elasticity theory should always be used in design calculations for the reasons shown in the account of the tests. This method is explained in more detail in Section 723.

722. Design of structurally reinforced concrete pavements according to the ultimate strength theory

722.1. *Principles and loading assumptions.*

The specifications given below for designing reinforced concrete pavements are based on the ultimate strength method as it is presented in this paper from theory and tests. The flexural rigidity of the pavement is assumed to be calculated in accordance with Stage II with a completely inactive tension zone and $n = 15$, the soil being assumed to act as an elastic subgrade with a known soil modulus C.

The pavement is to be calculated for *wheel load* in combination with effect of *temperature decrease and shrinkage*, this giving the desired *safety factor* aginst ultimate load. It is generally possible to write

$$s\,P = f(m + m') \tag{72:1}$$

where

P = the most dangerous loading from wheel load.

$f(m + m')$ is a function relationship depending on the extent and the form of the loading area as well as the flexural rigidity of the slab D and the soil modulus C, collected together in the magnitude

$$\text{elastic radius of rigidity } l = \sqrt[3]{\frac{2\,D}{C}}$$

m = the ultimate moment of the slab per unit width for positive flexure, calculated on the basis of the reinforcement yield point σ_{yie} ($\sigma_{0,2}$).

m' = the ultimate moment of the slab for negative flexure, for single-reinforced slabs calculated on the basis of the flexural strength of the slab σ_f. Following the suggestion of the so-called Flexure-Tension Committee [63], the flexural strength σ_f^{stand} checked on standard flexure beams, shall be reduced by 10 %. In the cases in question m' is also *reduced* for the effect of *temperature* and shrinkage according to section 64. It is thus possible to calculate

$$\left.\begin{aligned} m'_{\text{red}} &= m' - \Delta m'_t \\ m' &= 0.9\, \sigma_f^{\text{stand}} \frac{h_0^2}{6} \\ \Delta m'_t &= \left(\sigma^t_{mt} + 1.7 \frac{N_t}{h_0}\right) \frac{h_0^2}{6} \end{aligned}\right\} \tag{72:2}$$

where σ^t_{mt} and N_t are estimated from (64:1).

s = safety factor for failure due to crack formation in the top surface.

The reinforcement thus determined should naturally, in the cases where cracks may occur right through, be able to absorb all the tension N_t alone without yielding. The reinforcement A_a should thus be checked for

$$\frac{N_t}{A_a} < \sigma_{yie}$$

Moreover, the slab thickness h_0 chosen or determined must be controlled for stamping-out collapse according to Section 333 and the result must fulfil the condition

$$P_{\text{stamp}} \geq s \cdot P \tag{72: 3}$$

where

P_{stamp} = stamping-out load calculated from formula (33: 2).

This failure case can be dangerous only if the wheel load is great in relation to the load distribution area.

722.2. *The safety factor.*

It is a difficult question to decide the value to be given to the safety factor s. The test material in this paper has not been aimed at clarifying questions of this type. This requires the results from tests with running traffic on test roads together with experience from normal traffic on paved roads and runways and from repair work on any failure cracks occurred. Only some general viewpoints will therefore be presented here.

It is obvious that the safety factor in this case should be selected considerably higher than when calculating from the elasticity theory. In the latter case, the ultimate load is assumed to be reached at yield point in the bottom reinforcement, whereas the definition of failure according to the ultimate strength method assumes that the reinforcement has actually yielded to a certain extent. In order to avoid permanent deformations with *normal loads* a safety factor of 1.6–2.0 may be enough. On the other hand it can be pointed out that the load-carrying capacity of the slab is by no means exhausted even at failure point in accordance with the definitions adopted here. Failure in this meaning is first obtained at stamping-out, and this case of failure does not imply any risk of catastrophe either but only more or less extensive material damage. In this case it is possible, without risk of catastrophe, to adopt the principle in accordance with which the safety factor is to be determined from the condition that the costs of the pavement together with the repair costs of any possible failures shall be a minimum.

Due respect must also be taken to the frequency of the heaviest wheel load for which the pavement is designed as well as to the intensity and the composition of other traffic. It would thus appear motivated to adopt a considerably lower safety factor when designing for wheel load for example from an aircraft, which only uses an airport in exceptional cases, while higher safety factors can be motivated for example on taxiways on airfields with uniform frequent and heavy traffic, as for military airfields used for squadrons of heavy types of aircraft. Extensive investigation of this problem has been carried out by the United States military air force authorities [50, 58]. An example of a pavement, where a very high frequency of just the heaviest type of traffic for which it is designed should motivate a higher safety factor, is the Hällekis road mentioned earlier [22].

With consideration to the fact that the loading case of wheel load together with maximum effect of temperature and shrinkage for which design has been carried out is to be considered as exceptional, it can however be motivated to allow a certain reduction of the otherwise necessary safety factor. According to the Swedish Concrete Specifications, a decrease of safety factor by 30 % is permissible with stress combinations of this type. A reduction as large as this would not appear to be applicable in the pavement case, since at least the temperature and shrinkage stresses of friction are normally frequent.

Thus, in every special case an attempt should be made to judge the necessary value of the safety factor with due respect to the traffic conditions and other conditions prevailing. By way of guidance, a safety factor of 1.6 to 2.0 in normal cases would appear to be reasonable.

722.3. *Dynamic loading effect.*

One condition which has not been mentioned in the discussion of the safety factor is the occurrence of dynamic loading effect, which in the cases in question can instead be added as a percentual dynamic supplement to the traffic loading. This question is not yet investigated to any great extent; only a few general viewpoints of importance when judging this factor are given here.

Extensive tests and experience from military airfields in the United States [58] show that in the centre sections of the runways, where take-off and landing movements occur, there will be no dynamic loading effect at all but instead, in certain cases, the wheel load can be even reduced since the wings carry part of the load. On the other hand a lesser dynamic loading supplement of the magnitude of 10—15 % would appear to be motivated at the ends of the runways and on the taxiways and disposal slabs where the aircraft taxi slowly or stand still with the engines running.

As far as road pavements are concerned, the dynamic effect from traffic is of considerably greater significance and depends primarily on the unevenness in the surface of the pavement. Even with good pavements a certain degree of unevenness must be reckoned on, this giving impact supplements of between 20 and 40 %, and on pavements in rather poorer condition values of up to 100 % would not appear to be unreasonable.

722.4. *The soil modulus C.*

When designing a pavement it is necessary to know the soil modulus C. The difficulties in determining this very inconstant soil factor have earlier been discussed (Section 233).

The most reliable method of determining the C-value is to carry out loading tests on pavement test slabs on a full scale, and this method has been discussed in some detail in Section 233. With extensive pavement works where the correct designing is of great economic significance, this method — even if expensive — is well worth carrying out.

For less accurate demands, it is possible to estimate C on the basis of loading tests with small rigid slabs directly on the soil surface, so-called k-value determinations, whereby the diameter is usually 80 cm. According to the known relationship between the load P and the depression w the following is obtained:

$$C = \frac{P}{2\,R\,w} \qquad (72{:}4)$$

where R = the radius of the slab. This method is very suitable for routine examinations, for example in cases where variations in the properties of the soil are examined along some considerable road distance. See also [78].

With pavements on a strengthening subbase and where it is desirable to compare the effect of various types of subbase layers under the pavement, it is possible to quote the properties of the "composite" soil with an average modulus C_{ae}, which can be calculated in accordance with the methods given by ODEMARK [53, 54].

In many cases it is essential to use hand-book information[1]) and a general knowledge of the types of soil in order to estimate a reasonable soil modulus value at least preliminarily; this can otherwise be motivated if it only concerns a pavement of a comparatively small extent. In such cases a *low* C-value on the safe side should be selected; it is advantageous to know that the influence of the C-value on the calculation is comparatively small.

As a very general guidance for such an estimation, merely giving the magnitude of the C-value, may be mentioned:

Gravel, closely compacted	1000—2000 kg/cm²
Sand, closely compacted	500—1000 kg/cm²
Sand, loosely compacted	100—200 kg/cm²
Clay	20—200 kg/cm²

722.5. *Constructonal design. Joints.*

Normally pavements of this type are designed with *single-reinforcement* in bottom. Along the free edges it can sometimes become essential to place certain top reinforcement as strengthening. The concrete should have a high flexural strength, at least $\sigma_f = 40$ kg/cm² — in most of the pavement work carried out for airfields a standard beam flexural strength $\sigma_f^{\text{stand}} \geqq 48$ kg/cm² has been specified.

For constructional reasons, wider pavements for runways or taxiways must be cast in strips (sections), separated by longitudinal joints at a distance from each other which is determined by the width of the working machine (usually 5—7.5 m). The longitudinal joints can, as shown in Fig. 72:1, be designed in one of two alternatives:

a) Reinforcement in bottom through the joint which transfers the positive moment. The joint reinforcement is usually designed as junction bars between the reinforcement on both sides of the joint

[1]) See, for example, the Swedish hand-book BYGG, volume II [54], section 338:224, page 786.

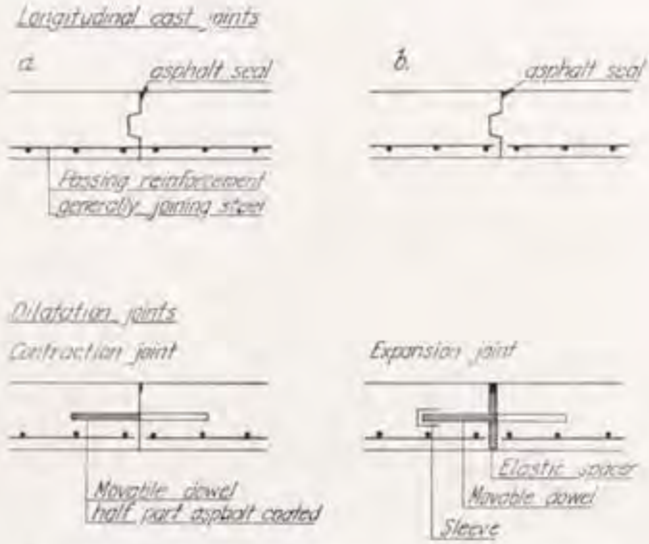

Fig. 72:1. Various types of joints in reinforced pavements.

and should then be designed with a 40 % increased area and length = double the normal junction length. Tongue and groove transfers the shear forces. The joints in this case do not weaken the pavement (see 324) and do not need to be specially calculated.

b) Completely moment-free joints without through reinforcement but with tongue and groove, which transfers shear forces. The joint edges must in this case often be strengthened (see Section 424) whereby certain intensified reinforcement close to the joint is usually sufficient.

The type of longitudinal joint to be selected depends on a comparison in costs between the troublesome working procedures for a) and the generally rather greater consumption of steel in b).

In order to avoid excessively large temperature stresses caused by friction, the runway is divided up by transverse joints designed as *dilatation joints*, which allow for movement due to temperature and shrinkage. The distance between these joints L completely determines the magnitude of the frictional forces and when selecting the distance between joints the costs and the disadvantages to traffic caused by more frequent joints must be weighed up against the costs for increased dimensions which result from the decreased negative ultimate moment with a large distance between joints; the normal joint distance may be 25 – 40 m. Two joint types of this sort occur, namely *contraction joints*, which only allow contraction on adjacent slabs, and *expansion joints* which also allow increase in length. Fig. 72:1 shows example of suitable joint design. It would appear to be advisable to design each third joint as an expansion joint. It should be pointed out that the longitudinal joints of type b) also function as contraction joints while, when using joints as shown at a), longitudinal contraction joints must also be arranged at the same minimum distance from each other as they have along the pavement.

If possible free edges and joint edges should be designed without thickening; the required strengthening should primarily be reached by intensifying the reinforcement.

The pavement is usually laid out directly on the soil or subbase after the surface has been levelled with a thin compressed layer of fine sand. In order to decrease friction between the runway and the soil and in order to obtain a better casting surface downwards, in many examples of constructional work paper has been laid out on the pavement base before casting. With the normal procedure of casting directly on to the surface of the sand, the author will recommend that the total thickness h_0 is reduced by 1 cm when calculating m', since the lower casting surface will be somewhat uneven and mixed up with sand.

Before casting, all the reinforcement should be laid out on the pavement base and fitted accurately at its correct height on clamps of concrete.

722.6. *Calculation methods.*

The calculation procedure when designing a single-reinforced pavement is shown by the examples below. References to the required formulae and diagrams have been specially marked, and some of the points in the calculations have been supplied with more general commentaries in the form of notes.

A. Loading due to single wheels

1. *Calculation conditions*

Load: Wheel load $P = 20$ tons from single wheel, tyre pressure $p = 6$ kg/cm²
No dynamic loading supplement is added

Soil modulus C is assumed to be $= 100$ kg/cm² (normal clay soil)

Pavement thickness h_0 is selected $= 16$ cm
reinforcement covering layer $= 3$ cm
max. distance between joints $L = 50$ m

Note

If the thickness selected shows itself to be less suitable (for example gives an excessively low or high reinforcement percentage) the calculation must be carried out again with another value. Calculations are often carried out for different values of h_0, after which an economic comparison is made. The same thing applies concerning the selection of the distance between joints L.

Material: reinforcement of welded wire fabric Ns 50, concrete with $\sigma_f^{\text{stand}} = 48$ kg/cm².

The safety factor is selected as being 1.8 (see 722.2).

2. *Negative ultimate moment and temperature effect*

Note

When calculating the negative ultimate moment the author recommends that the total thickness h_0 is decreased with, by example 1 cm, if the slab is cast directly on the sand base. The reason is that in this case a somewhat uneven bottom surface must be reckoned with.

The negative ultimate moment with a thickness reduction of 1 cm becomes

$$m' = 0.9 \cdot 48 \; \frac{15^2}{6} = 1620 \text{ kgcm/cm} \quad \text{according to} \quad \textbf{formula (72:2)}$$

Reduction for temperature stresses: if the soil friction f_s is taken as being 1.5, the result is

$$N_t = 1.2 \cdot 0.16 \cdot 1.5 \cdot 50 = 14.4 \text{ t/m}$$

$$\sigma^t_{mt} \approx 7 \text{ kg/cm}^2 \quad \text{according to} \quad \textbf{formula (64:1)}$$

$$\Delta m_t = \frac{15^2}{6}\left(7 + 1.7 \cdot \frac{144}{15}\right) = 870 \text{ kgcm/cm according to} \quad \textbf{formula (72:2)}$$

$$m'_{\text{red}} = 1620 - 870 = 750 \text{ kgcm/cm}$$

3. *Designing the interior of the slab*

31. Load distribution and radius of rigidity

The load is assumed to be circularly distributed

$$\text{Loading radius } c = \sqrt{\frac{20 \cdot 10^3}{6 \cdot \pi}} = 32.5 \text{ cm}$$

When calculating the flexural rigidity of the slab it is assumed that $\mu = 0.3\ \%$, reinforcement of $\varnothing$ 6–7, h = 12.3 cm (average value).

The flexural rigidity can be estimated in a simple way with the help of **fig. 72:2**

$$D = \frac{2.1 \cdot 10^6}{15} \; \frac{12.3^3}{12} \; 0.37 = 8.0 \cdot 10^6 \text{ kgcm}^2\text{/cm}$$

Note

After the required reinforcement has then been calculated in 33, μ is altered where necessary, and recalculation is carried out from here onwards.

$$\text{Elastic radius of rigidity } l = \sqrt[3]{\frac{2 \cdot 8.0 \cdot 10^6}{100}} = 54 \text{ cm in accordance with } \textbf{formula (72:1)}$$

$$\text{Relative load distribution } \alpha = \frac{c}{l} = \frac{32.5}{54} = 0.60$$

32. Ultimate moment

In accordance with the design diagram **fig. 32:14 B**

is

$$\frac{m + m'}{P_{\text{ult}}} = 0.081 \quad \text{for} \quad \frac{c}{l} = 0.60$$

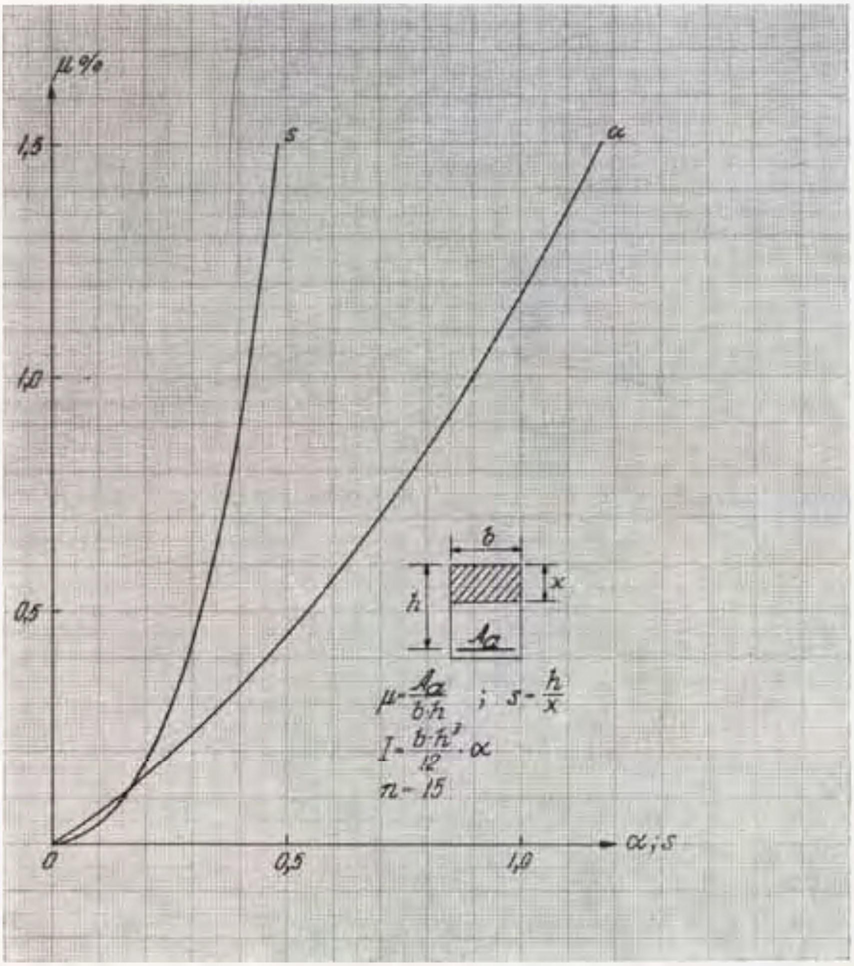

Fig. 72:2. Diagram for the calculation of section values for single-reinforced concrete slabs in Stage II ($n = 15$).

If $P_{\text{ult}} = s\,P$ and $m' = m'_{\text{red}}$ are inserted, then

$$(m + m')_{\text{req}} = 1.8 \cdot 20 \cdot 10^3 \cdot 0.081 = 2900 \text{ kgcm/cm}$$

$$m_{\text{req}} = 2900 - 750 = 2150 \text{ kgcm/cm}$$

33. Reinforcement

The required reinforcement can suitably be calculated in accordance with the n-free method, for example according to GRANHOLM [21], page 183, whereby $\sigma_r = \sigma_{0.2} = 5000$ kg/cm², $\bar{\sigma}_c = 200$ kg/cm², thus:

$$\frac{1}{\bar{m}} = \frac{12.6^2}{2150}\,200 = 15; \quad c = 1.035$$

$$A_r = \frac{2150 \cdot 100}{12.6 \cdot 5000}\,1.035 = 3.6 \text{ cm}^2/\text{m}$$

Note

Here the effective depth is taken down to the *bottom* reinforcement layer, which is placed *along* the runway. In the upper layer it should be possible to select the same reinforcement in spite of the lesser depth, motivated by the lower temperature effect and thereby higher value of m' in this direction, on condition that the longitudinal joints are made reinforcement-free. Otherwise, closer spaced reinforcement is inserted in the upper reinforcement layer

The reinforcement corresponds to $\mu = 0.29\,\%$, which *agrees* so *well* with the assumption made according to 31 that no recalculation need be carried out.

Control of the stress in the reinforcement due to temperature and shrinkage, if a through crack appears, gives

$$\sigma_r^{cr} = \frac{N_t}{A_r} = \frac{14.4 \cdot 10^3}{3.6} = 4000 \text{ kg/cm}^2 < \sigma_{0.2}$$

Thus, select for example the reinforcement

⌀ 6.8 c/c 100 mm, Ns 50

34. Control for stamping-out

The selected slab thickness $h_0 = 16$ cm shall be controlled for stamping-out according to **formula (33:2)**

whereby the factor Z_2 for the average soil pressure under the loading area can be estimated according to the diagram **fig: 22:6**

$$\frac{c}{l} = 0.60; \quad \frac{c+h_0}{l} = 0.89; \quad Z_2 \approx 0.10$$

$$P_{\text{stamp}}\,[1 - \pi \cdot 0.89^2 \cdot 0.10] = 1.4 \cdot 0.9 \cdot 48 \cdot 16\,(2 \cdot 32.5 + 16)$$

$$P_{\text{stamp}} = 105\,000 \text{ kg} > s \cdot P$$

4. *Designing the joints*

The joints are made moment-free *without* through reinforcement. The edge zone is strengthened with intensified reinforcement if necessary.

41. Load distribution and radius of rigidity

With the joint case the load is $P_{\text{ult}} = 1.8 \cdot \dfrac{20}{2} = 18$ tons, distributed over a semi-circle with radius $c = 32.5$ cm. Assume $\mu = 0.35\,\%$ (somewhat increased joint reinforcement)

$$D = \frac{2.1 \cdot 10^6}{15} \cdot \frac{12.3^3}{12} \cdot 0.42 = 9.1 \cdot 10^8 \text{ kgcm}^2/\text{cm}$$

$$l = \sqrt[3]{\frac{2 \cdot 9.1 \cdot 10^8}{100}} = 57 \text{ cm}$$

$$\frac{c}{l} = 0.57$$

42. Ultimate moment

According to 2, if it is assumed that no top reinforcement is necessary, then

$m' = 1620$ kgcm/cm at right angles to the joint

$m'_e = 750$ kgcm/cm along the joint

Note

Since the joint here is designed *without* through reinforcement, then there is no effect of temperature in the direction at right angles to the joint and an unreduced m'-value can thus be reckoned with.

In accordance with the designing diagram **fig. 42:11 A**

$$\frac{m'}{P} = \frac{1620}{18 \cdot 10^3} = 0.09 \quad \text{and} \quad \frac{c}{l} = 0.57$$

$$\frac{m_e + m'_e}{P_{\text{ult}}} = 0.175$$

$$(m_e + m'_e)_{\text{req}} = 18 \cdot 10^3 \cdot 0.175 = 3150 \text{ kgcm/cm}$$

$$m_e = 3150 - 750 = 2400 \text{ kgcm/cm}$$

33. Reinforcement

$$\frac{1}{m} = \frac{12.6^2}{2400} 200 = 13 \qquad A_r = \frac{2400 \cdot 100}{12.6 \cdot 5000} 1.042 = 4.0 \text{ cm}^2/\text{m}$$

This corresponds to $\mu \approx 0.33\%$, no recalculation.

The difference compared with the normal reinforcement in the centre of the section is insignificant. Over a width which approximately corresponds to the height of the failure line triangle $\frac{r_0}{l} \approx 1.3 - 1.5$ (see table 42:1), i. e. approx. 1 m, the difference corresponds to a reinforcement with a cross section of approx. 0.4 cm^2. This reinforcement can simplest be added in the form of a pair of extra edge wires, for example

joint reinforcement extra edge wires 2 ⌀ 6.8

Note

If instead the longitudinal joints had been in the form of joints with through reinforcement (junction bars) as shown in Fig. 72: 1, alternative a), then no special calculation of the joints had been necessary. The junction bars are given an area, if they consist of Ks 60

$$A_r^{\text{joint}} = 1.40 \cdot 3.6 \cdot \frac{50}{60} = 4.2 \text{ cm}^2/\text{m},$$

for example ⌀ 12 c/c 250, length $2 \cdot 35 \cdot 1.2 = 85$ cm

5. *Designing the free edges*

51. Load distribution and radius of rigidity

The free edges are designed for circularly distributed load tangent to the edge.

Here it is assumed that $\mu = 0.90\%$

$$D = \frac{12.3^3}{12} \cdot \frac{2.1 \cdot 10^6}{15} 0.84 = 18.2 \cdot 10^6 \text{ kgcm}^2/\text{cm}$$

$$l = \sqrt[3]{\frac{2 \cdot 18.2 \cdot 10^6}{100}} = 71 \text{ cm}$$

$$\frac{c}{l} = 0.46$$

52. Ultimate moment

In the same way as when designing the joints, the design diagram gives **fig. 42:11 B**

$$\frac{m'}{P} = \frac{1620}{36 \cdot 10^3} = 0.045 \quad \text{and} \quad \frac{c}{l} = 0.46$$

$$\frac{m_e + m_e'}{P_{\text{ult}}} = 0.187$$

$$(m_e + m_e')_{\text{req}} = 36 \cdot 10^3 \cdot 0.187 = 6750 \text{ kgcm/cm}$$

$$m_e = 6750 - 750 = 6000 \text{ kgcm/cm}$$

This corresponds to rather more than double the moment in the interior. It can here be suitable to insert double edge mesh as well as *extra* reinforcement strip along the edge.

In this case, for the edge mesh reinforcement according to GRANHOLM [21] page 55

$$\varnothing\, 6.8\, \text{c/c}\, 50 = 7.25\, \text{cm}^2/\text{m};\ \mu = \frac{7.25}{12.6} = 0.57\ \%;\ \ p = 0.57\, \frac{5000}{100 \cdot 200} = 0.14$$

$$m = \frac{1}{100} \cdot 7.25 \cdot 5000 \cdot 12.6 \left(1 - \frac{0.14}{2}\right) = 4250 \text{ kgcm/cm}$$

A comparison with the value calculated above can make an estimation of an edge strip moment of $M = 2.0$ tm reasonable

Then, in accordance with **the formulae (42:24 b) and (42:25 b)**

$$\text{tg}^2\, \alpha = \frac{4250 + 750}{1620} = 3.1$$

$$\frac{r_a}{l} = \sqrt[3]{\frac{1.5 \cdot 0.46 \cdot 0.568\, (1 + 0.425 \cdot 0.568) + \dfrac{3}{71} \cdot \dfrac{2 \cdot 10^3}{36 \cdot 10^3}\, \dfrac{1}{3.1}}{0.28 \left[1 - \dfrac{3}{8}\, \dfrac{r_a}{l}\, \dfrac{1}{2.88} \left(1 + \dfrac{2.88}{3.46} \cdot 1.76\right)\right]}} = \sqrt[3]{\frac{0.559}{0.28 \left(1 - 0.321\, \dfrac{r_a}{l}\right)}}$$

By successive approximation (rapid convergence) is obtained

$$\frac{r_a}{l} = 1.60$$

and then, in accordance with **the formula (42:24 a)**

$$m_e + m_e' = \frac{P}{4}\, 1.76 \left\{1 - 0.28 \cdot 1.60^2 \left[1 - \frac{1}{3}\, \frac{1.60}{2.88} \left(1 + \frac{2.88}{3.46}\, 1.76\right)\right] 1.76\right\} = 0.139\, P$$

With selected values for m_e and m_e'

$$P = \frac{4250 + 750}{0.139} = 36 \text{ ton}$$

is obtained, this agreeing with the actual value and the value assumed above $P_{\text{ult}} = 36$ tons. It is thus possible to select $M = 2.0$ tm.

With an active concrete width for the edge strip $\approx 3 \cdot h_0$ one obtains, if the edge strip reinforcement consists of deformed bar Ks 60

$$\frac{1}{\overline{m}} = \frac{3 \cdot 16 \cdot 12.6^2}{2 \cdot 10^5} \cdot 200 = 7.5 \qquad A_r = \frac{2 \cdot 10^5}{12.6 \cdot 6000} \cdot 1.077 = 2.8 \text{ cm}^2$$

Control of the edge zone flexural rigidity: over a width of $l = 71$cm

$$A_r^{\text{edge}} = 2.8 + 0.71 \cdot 7.25 = 7.95 \text{ cm}^2 \quad , \quad \mu = \frac{7.95}{71 \cdot 12.6} = 0.90\ \%$$

This corresponds to the assumed value and no recalculation is necessary.

It is thus possible to select for example

edge reinforcement ⌀ 6.8 c/c 50 mm Ns50 + 2 ⌀ 14 Ks 60

Note

Obviously the case of loading on a free edge can also be regarded as being such a rare case of loading that the safety factor can be reduced considerably. From this viewpoint it can be unnecessary to have any edge strengthening beyond that inserted along the joints.

6. *Control of joint intersections*

Note

With this case of loading with the loading area over a joint intersection, the calculation according to 427 agrees with the *elasticity theory* (Section 41). With respect to the fact that in the case of failure in the top there are practically no stresses at all in the reinforcement, then a considerably lower safety factor is satisfactory, equal to that otherwise prescribed for calculation according to the elasticity theory (se section 44). A safety factor of approx. 1.3—1.4 would appear to be quite sufficient in any case.

In accordance with the diagram **fig. 41:4**

$$k = 0.166 \sqrt[3]{\frac{100^4}{8 \cdot 10^6}} = 0.38$$

$$l_k = \sqrt[4]{\frac{8 \cdot 10^6}{0.38}} = 68 \text{ cm}; \ \alpha_k = \frac{c}{l_k} = 0.48$$

$$\frac{m^-}{P} = 0.06 \qquad m^-_{\beta} = 0.06 \cdot 20 \cdot 10^3 = 1200 \text{ kgcm/cm}$$

Safety factor $s = \dfrac{1620}{1200} = 1.35$

which would appear to be quite sufficient.

B. Loading from an aircraft undercarriage with tandem twin wheels.

1. *Calculation conditions*

The same runway is to be checked for an aircraff load with a wheel loading $= 40$ tons, distributed over tandem twin wheels with four loading areas as shown in Fig. 72:3. Tyre pressure $p = 7$ kg/cm².

Loading radius for the four loading areas $c = \sqrt{\dfrac{40 \cdot 10^3}{4 \cdot 7 \cdot \pi}} = 21.3$ cm.

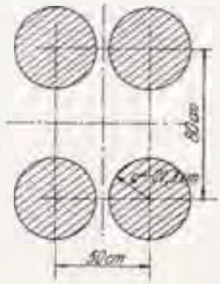

Fig. 72:3

2. *Load on the interior of the slab*

The ultimate load is calculated in accordance with **diagram in fig. 32:14**

$$\bar{x} = 25 \text{ cm} \qquad c = 2.36 \ \bar{x} = 59 \text{ cm}$$

$$d = 80 \text{ cm}$$

According to A 31 is $l = 54$ cm. Thus

$$\frac{c}{l} = 1.09; \quad \frac{d}{l} = 1.48$$

$$\frac{m + m'}{P_{\text{ult}}} = 0.037$$

With $m + m' = 2900$ kgcm/cm according to A 32, then

$$P_{\text{ult}} = \frac{2900}{0.037} = 78.5 \text{ tons}$$

Safety factor $s = \dfrac{78.5}{40} = 2$

3. *Load on a longitudinal joint* (*Fig.* 72:4)

According to A 42, the joint edges are designed so that

$$m_e + m_e' = 2900 \text{ kgcm/cm}$$

$$m' = 1620 \text{ kgcm/cm}$$

and with an extra reinforcement $2 \varnothing 6.8 = 0.72 \text{ cm}^2$, which all gives

$$\mu = 0.33 + \frac{0.72 \cdot 100}{3 \cdot 16 \cdot 12.6} = 0.45 \ \%$$

$$p = 0.45 \cdot 10^{-2} \cdot \frac{5000}{200} = 0.11$$

$$M = 0.72 \cdot 5000 \cdot 12.6 \left(1 - \frac{0.11}{2}\right) = 0.43 \cdot 10^5 \text{ kgcm}$$

according to [21]

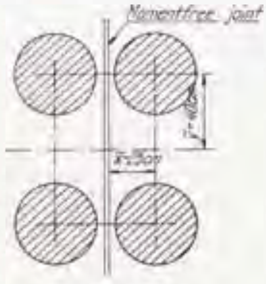

Fig. 72:4

With the load located as shown in the figure and $l = 57$ cm according to A 41 then

$$\frac{\bar{x}}{l} = \frac{25}{57} = 0.44; \quad \frac{\bar{y}}{l} = \frac{40}{57} = 0.70$$

The soil reaction pressure constants can be estimated thus:

$$\left.\begin{aligned} t \;&= 1.5\,l + 3 \cdot 0.44\,l = 2.81\,l \\ t_k &= 3.0\,l + 0.44\,l \quad\; = 3.44\,l \\ \gamma_k &= 0.29 \end{aligned}\right\} \qquad \textbf{according to 427}$$

The ultimate load $\frac{P}{2}$ is calculated according **to 427, formulae (42:25 c) and (42:26)** (the approximate formula (42:24 a) cannot be used here since the load distribution is too large) by trial and error and successive approximation.

Assume $\quad \mathrm{tg}^2\,\alpha = 2.9 \qquad \frac{P}{2} = 50$ tons

$$\left\{\begin{aligned}
&\frac{r_a}{l} = 1.90;\; \frac{r_a}{l} = \sqrt[3]{\frac{1.5 \cdot 0.59\,(0.44 + 0.70 \cdot 0.59) + \dfrac{3}{57}\,\dfrac{0.44 \cdot 10^5}{50 \cdot 10^3}\,\dfrac{1}{2.9}}{0.29\left[1 - \dfrac{3}{8} \cdot \dfrac{1.90}{2.81}\left(1 + \dfrac{2.81}{3.44}\,1.7\right)\right]}} = 1.88 \\
&2900 = \frac{1}{4}\,\frac{P}{2}\left\{\left(1 + \frac{0.44}{1.88}\right) 1.7 - \frac{4}{3}\,0.29 \cdot 1.88^2\left[\left(1 - \frac{3}{8}\,\frac{1.88}{2.81} - \right.\right.\right. \\
&\qquad \left.\left.\left. - \frac{5}{16}\,\frac{1.88}{3.44} \cdot 1.7\right) \cdot 2.9\right]\right\} = 0.0383\,P; \quad P = 76 \text{ ton} \\
&1620 = \frac{1}{4}\,\frac{P}{2}\left\{\left(1 - \frac{0.44}{1.88}\right) 0.59 - \frac{2}{3}\,0.29 \cdot 1.88^2\left[\left(1 - \frac{1}{4}\,\frac{1.88}{2.81} - \right.\right.\right. \\
&\qquad \left.\left.\left. - \frac{3}{8} \cdot \frac{1.88}{3.44} \cdot 1.7\right)\right]\right\} = 0.0156\,P; \qquad P = 104 \text{ ton}
\end{aligned}\right.$$

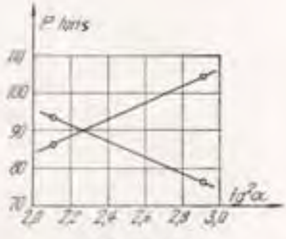

Fig. 72:5

Assume $\quad tg^2\,\alpha = 2.1 \qquad \frac{P}{2} = 50$ tons

In the same way the following are obtained

$$\begin{cases} \dfrac{r_0}{l} = 2.02 & \\ 2900 = 0.0313\,P; & P = 93 \text{ tons} \\ 1620 = 0.0189\,P; & P = 86 \text{ tons} \end{cases}$$

By interpolation between these values, for example as shown in Fig. 72:5, the following at last are obtained

$$P = 90 \text{ tons} \qquad tg^2\,\alpha = 2.25$$

If these values are checked by means of the formulae above, then

$$\begin{cases} \dfrac{r_0}{l} = 1.99 & \\ 2900 = 0.0321\,P; & P = 90 \text{ tons} \\ 1620 = 0.0180\,P; & P = 90 \text{ tons} \end{cases}$$

Thus

$$P_{\text{ult}} = 90 \text{ tons}; \qquad s = \frac{90}{40} = 2.2$$

4. *Load on a transverse joint.*

With the load located as shown in Fig. 72:6, in the same way as above, the following are obtained:

$$\frac{x}{l} = \frac{40}{57} = 0.70 \qquad \frac{y}{l} = \frac{25}{57} = 0.44$$

$$\left.\begin{aligned} t &= 1.5\,l + 3 \cdot 0.70\,l = 3.60\,l \\ t_k &= 3.0\,l + 0.70\,l \quad = 3.70\,l \\ \gamma_k &= 0.22 \end{aligned}\right\}$$

With the same procedure as before, the result will be

$$P_{\text{ult}} = 79 \text{ tons} \qquad s = \frac{79}{40} = 2$$

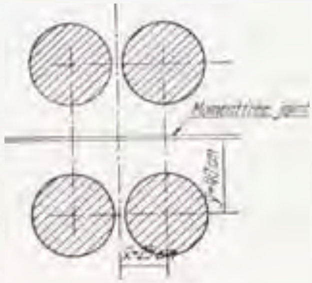

Fig. 72:6

5. *Load on a free edge.*

According to A 52 the following apply to the free edge

$$m_e + m_e' = 5000 \text{ kgcm/cm}$$

$$m' = 1620 \text{ kgcm/cm}$$

$$M = 2.0 \cdot 10^5 \text{ kgcm}$$

With the load located as shown in Fig. 72:7 in the same way as above, since $l = 71$ cm, according to A 51 the following are obtained

$$\frac{\bar{x}}{l} = \frac{46.3}{71} = 0.65 \qquad \frac{\bar{y}}{l} = \frac{40}{71} = 0.56,$$

and the ultimate load is obtained after the calculating procedure as above

$$P_{\text{ult}} = 69 \text{ tons} \qquad s = \frac{69}{40} = 1.7$$

This safety factor is rather lower than that for which the rest of the runway has been designed, but with respect to the fact that this case of loading is particularly exceptional then the result may be accepted.

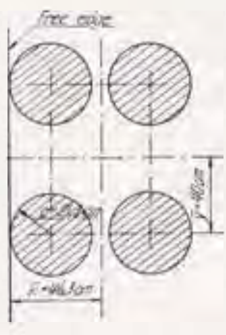

Fig. 72:7

The result of the calculations under B thus show that the loading of an aircraft undercarriage with a load of 40 tons, distributed over four loading areas, does *not* produce a more dangerous case of loading than a single load of 20 tons; as a matter of fact the safety factor with a load on the interior of the runway and on the joints is *higher* with the larger load than with the smaller. This result is, on the whole, generally applicable when comparing the effect of loads from single and combined loading areas.

723. Viewpoints on the design of structurally mid-depth reinforced pavements (including continuous reinforced pavements)

723.1. *Principles and loading assumptions.*

The type of pavement considered here would appear to be economical only in such cases where the soil itself or the subbase has such a good load-carrying capacity that a rigid pavement is not necessary from the point of view of load-carrying, and the pavement can then be made very thin. This demands a high value for the soil modulus, usually at least 500—1000 kg/cm².

The viewpoints in this Section 723 are primarily concerned with thin mid-depth reinforced pavements with dilatation joints, that is to say pavements of the type included in the Arlanda tests. It should, however, on the whole also apply to jointless, so-called continuous reinforced pavements. Since there appears to be a lack of tests and practical experience from these types of pavement, then these viewpoints should be considered more in the form of guidance for continued tests than as specifications for practical design.

This type of pavement thus consists of a relatively thin concrete slab with reinforcement in the centre plane. The calculating methods are based on the *elasticity theory*, whereby the pavement, under the effect of flexural loading, can be considered as a reinforced concrete slab with an effective thickness equal to half the total thickness. The flexural rigidity is calculated for this effective depth in accordance with Stage II and with $n = 15$.

Pavements of this type *with dilatation joints* are designed for the condition that the stresses in the reinforcement due to wheel load together with temperature and shrinkage give the required safety concerning the yield point σ_r^{yie}

$$\sigma_r = s\,\sigma_r^{\text{traffic}} + \sigma_r^{\text{temp}} \leq \sigma_r^{yie} \qquad (72{:}5)$$

where

$\sigma_r^{\text{traffic}}$ = the reinforcement stress due to the largest wheel load occurring according to the *elasticity theory*.

σ_r^{temp} = the reinforcement stress due to temperature and shrinkage, whereby it must be assumed that the whole of the normal stress N_t is taken up in the *reinforcement* A_r in the crack section while the influence of warping in this case is negligible, since the flexural rigidity of the slab is very small and the crack spacing is small. Thus

$$\sigma_r^{\text{temp}} = \frac{N_t}{A_r} \tag{72:6}$$

where N_t is calculated according to (64:1).

s = the safety factor for wheel load.

Continuous reinforced pavements may be designed for the condition concerning the reinforcement stress *longitudinally* (see Section 613) that the stress contributions corresponding to the terms in the equation (72:5) do not separately exceed the yield point:

$$\left.\begin{array}{r}\sigma^{\text{temp}}\\ s\ \sigma^{\text{traffic}}\end{array}\right\} \leqq \sigma_r^{\text{yie}} \tag{72:7}$$

Generally the influence of temperature and shrinkage is thereby the deciding factor, and the longitudinal reinforcement can thus be selected in accordance with the condition (64:3), whereby an addition of 20 % for "hyper-strength" in concrete may be reasonable. If the strength for pure tension σ_t is estimated from $\omega = \sigma_f/\sigma_t = 1.7$, according to the test results in Section 63, thus the reinforcement can be calculated from

$$\mu \geqq 0.7 \cdot \frac{\sigma_f}{\sigma^{yie}} \tag{72:8}$$

after which the wheel load stresses must be checked in accordance with the elasticity theory. *Transversely* the design is completely in accordance with (72:5). Moreover *crack formation* is checked according to 64, formula (64:4).

When selecting the safety factor s for wheel load stresses a relatively high value should be taken for these types of pavement compared with that which is otherwise recommended when designing in accordance with the elasticity theory. The author suggests a safety factor = 1.8—2. This is mainly motivated by the fact that the influence of very local unevenness in the subgrade, for example in the levelling layer, gives under wheel load a comparatively large supplement to the reinforcement stress, because a slab of this type has only a very limited capacity to bridge over such local unevenness in the soil in the way that a more rigid slab can do. An extra increase in the safety factor can also be motivated by the fact that the variations in thickness or position of reinforcement result in larger percentual deviations than in the case of a thick slab; Table 53:9 shows however that such variations in the dimensions have a relatively small effect on the stresses.

Concerning possible dynamic effect, the same viewpoints apply as for the bottom-reinforced slabs. A dynamic loading effect however is of less significance with this type of slab, since the wheel load stresses on the whole here are small.

The soil reaction pressure is large; maximum soil reaction pressure can be estimated according to the elasticity theory, the diagram in Fig. 22:6 B. A check must be carried out to insure that this pressure is lower than the failure strength of the soil itself with a satisfactory margin of safety.

723.2. *Design.*

Pavements of this type should be constructed with a relatively thin slab of 6—10 cm thickness and with mid-depth reinforcement. The stresses are usually lower the thinner the slab is made. From the point of view of construction, however, it may not be possible to use less reinforcement than approx. ∅ 5 c/c 100 mm, and this reinforcement is suggested as being the specified minimum.

Since the reinforcement located in the centre plane of the slab serves as flexural reinforcement for both positive and negative moments, then no high demands are made on the concrete from the point of view of strength. On the contrary, it is an advantage to have a low flexural concrete strength which implies closer crack distribution and, concerning the joint-free type, also a lower normal force N_t due to temperature (see (61:8)). The demands made concerning resistance to wear and resistance to frost would generally appear, however, to demand the use of fairly high quality concrete. The reinforcement used should be the type with good bonding, deformed bar or wire fabric with small mesh spacing and preferably made of deformed wire.

It should be an advantage with this type of concrete pavement to increase the distance between the transverse joints considerably, up to perhaps 60—80 m, which can be made without sacrificing the demand for good economy. The desire to increase the distance between the joints more and more shows the way to the continuous design with no transverse joints whatsoever.

Concerning the joints and the design of the joints in the cases in question, the same viewpoints and principles apply as those described in connection with the pavement with bottom-reinforcement. No slab thickening or even strengthening of the reinforcement along the joints is necessary with this type of slab. On the free edges, a certain increase in the reinforcement can possibly be actual.

With this type of pavement, it is not necessary to make any strict demands for accuracy concerning the thickness or the position of the reinforcement, since this — as shown earlier — has a very small influence on the stresses in the slab.

723.3. *Calculation methods.*

The calculating procedure when designing a thin pavement is shown by the examples below, in which references to the required formulae and diagrams have been marked.

A. Pavement with transverse joints

1. *Calculation conditions*

Loading: wheel load 40 tons from single wheel, tyre pressure $p = 8$ kg/cm²

Soil modulus C assumed $= 700$ kg/cm³

(sandy soil, comparatively well packed, permissible soil reaction pressure approx. 8 kg/cm²)

Pavement thickness h_a is selected $= 8$ cm

max. distance between joints $L = 50$ m

Material: reinforcement of welded mesh Ns 60 with $\sigma_{0.2} = 6000$ kg/cm²

2. *Design*

21. Load distribution — calculation analogous with **722:6 A 31**

$$c = \sqrt{\frac{40 \cdot 10^3}{\pi \cdot 8}} = 40 \text{ cm}$$

Assume that the necessary reinforcement is ⌀ 6 c/c 100 = 2.8 cm²/m

$$\mu = \frac{2.8}{4} = 0.70\,\% \qquad Ei = \frac{4^3}{12} \cdot 0.70\,\frac{2.1 \cdot 10^6}{15} = 0.52 \cdot 10^6 \text{ kgcm}^2/\text{cm}$$

$$l = \sqrt[3]{\frac{2 \cdot 0.52 \cdot 10^6}{700}} = 11.4 \text{ cm}; \quad \frac{c}{l} = \frac{40}{11.4} = 3.50$$

22. Stress control

The influence of *wheel load* is calculated according to the **diagram fig. 22:7**

$$m^{\text{traffic}} = 0.0052 \cdot 40 \cdot 10^3 = 208 \text{ kgcm/cm}$$

The stress according to Stage II

$$x = 0.36 \cdot 4 = 1.44 \text{ cm according to}$$ **fig. 72:2**

$$\sigma^{\text{traffic}} = \frac{208 \cdot 100}{2.8 \left(4 - \frac{1.44}{3}\right)} = 2100 \text{ kg/cm}^2$$

The influence of *temperature* is calculated according to **formula (64:1)**

$$N_t = 1.2 \cdot 0.08 \cdot 1.5 \cdot 50 = 7.2 \text{ t/m}$$

$$\sigma^{\text{temp.}} = \frac{7.2 \cdot 10^3}{2.8} = 2500 \text{ kg/cm}^2$$

Design criterium according to **formula (72:5)**
gives, if the safety factor is put as = 1.8

$$\sigma_r = 1.8 \cdot 2100 + 2500 \approx 6000 \text{ kg/cm}^2$$

The assumed reinforcement can be accepted.

23. Control of soil reaction pressure
According to the diagram **fig. 22:6 B**

$$p_s^{\max} = \frac{40 \cdot 10^3}{11.4^2} \cdot 0.026 = 8 \text{ kg/cm}^2$$

which is permissible in this case.

24. Reinforcement

Alternative 1, reinforcement-free longitudinal joints (Fig. 72:1, alternative b). In this case the temperature stress transversely is very small and minimum reinforcement can be used.

Reinforcement: mesh Ns 60 ⌀ 6 c/c 100 longitudinally
⌀ 5 c/c 100 transversely

Alternative 2 doweled longitudinal joints (Fig. 72:1, alternative a). The joint dowels are calculated only for temperature. With a 50 m wide runway, if deformed steel *Ks* 60 is used, then the following is obtained

$$A_r^{\text{dowel}} = \frac{1.4 \cdot 7.2 \cdot 10^3}{6000} = 1.7 \text{ cm}^2/\text{m} - \varnothing\ 8 \text{ c/c } 300 \text{ mm}$$

Reinforcement: mesh Ns 60 ⌀ 6 c/c 100 in both directions
longitudinal joints with Ks 60 ⌀ 8 c/c 300 mm

B. Continuous reinforced pavement

1. *Calculation conditions*

Loading and *soil* the same as in A

Pavement selected 8 cm thick, completely *without* transverse joints

Material: reinforcement of cold-drawn deformed bars Kam 90 with $\sigma_{0.2} = 9000$ kg/cm²
concrete with $\sigma_f^{\text{stand}} = 48$ kg/cm²

2. *Design*

21. Longitudinal reinforcement

The reinforcement is estimated from **formula 72:8**

$$\mu_{\min} = 0.7 \cdot \frac{48}{9000} = 0.38\ \%$$

Select, for example, reinforcement ⌀ 6 c/c 90 mm

The crack width can be estimated according to **formula 64:4 a**

$$\delta \approx (1.0 \div 1.3)\ \frac{30^2}{120} \cdot \frac{0.6 \cdot 100^2}{4 \cdot 0.40^2 \cdot 2.1 \cdot 10^6} \approx 0.03 \div 0.04 \text{ cm},$$

whereby the maximum bond stress has been assumed to be $\tau_b^{\max} = 120$ kg/cm².

This crack width may be accepted. The longitudinal reinforcement thus will be

Kam 90, ⌀ 6 c/c 90 mm

22. Control for wheel load stress.

In accordance with A2, wheel load alone gives a stress in the longitudinal reinforcement of $\sigma^{\text{traffic}} = 2000$ kg/cm².

23. Transverse reinforcement

The calculation here agrees completely with the calculations under A, and the design criterium is adopted according to **formula 72:5**

Different results are thus obtained also here if the longitudinal joints are designed with or without through reinforcement.

73. Economical Viewpoints

In order finally to clarify to some extent the economical advantages to be derived from the types of pavement treated in this paper, the author has devoted this section of the paper to some cost calculations for pavements according to various alternatives as applied to some practical pavement problems. Comparisons are made between the thick, unreinforced pavement, the normal, bottom-reinforced pavement and (in suitable cases) the thin, mid-depth reinforced pavements, and the cases treated concern pavements for airfield runways, partly on very poor soil, partly on good soil, as well as pavements for roads of the highway type. The comparisons only concern the cost of the concrete slab itself. The calculations are carried out in a simple way on the basis of unit-prices, these in their turn being calculated from a summary of the costs for pavement work carried out for the Swedish Air Force during the years 1956—59; the prices applied consist of "balanced" average values for unit-prices from a large number of work. These unit-prices as well as other conditions for the calculation are shown in Table 73:1, which gives the result of the cost calculations.

Judging by the cost figures in the table, the unreinforced pavement is *particularly* unfavourable from the economical point of view. This applies to the cases with both bad and good soil, in the latter case it is even more accented. The cost for the structurally bottom reinforced pavements are about 55—70 % of the costs for the unreinforced pavements. The lowest price is arrived at for the thin, mid-depth reinforced pavements with joints, while the joint-less continuous pavements are a little more expensive.

It is, however, obviously clear that the result of cost calculations of this type must be judged with a great deal of caution. The unit-prices, where it is possible to fix such prices at all, depend to a great extent on periodical alterations in the price of raw material and labour costs as well as on local conditions and the extent, planning and organization of the work; it is characteristic in this respect that the collocation of cost specifications from which the unit-prices in Table 73:1 have been derived, show variations in total costs for similar pavements of up to almost 80 %. However, it is on the basis of simple calculations of this

Table 73: 1. Estimated costs for various types of pavement for airfields and roads.

Calculations carried out in accordance with the directions given and examples quoted in Section 72. Calculating method and safety factors:

for plain concrete pavements: elasticity theory	$s = 1.0$
(for wheel load only	$s = 1.25$)
for bottom-reinforced pavements: ultimate load theory	$s = 1.70$
for mid-depth reinforced pavements: elasticity theory	
wheel load	$s = 1.80$
temperature	$s = 1.0$

Unit prices for cost estimation:

Mould, adjusting subbase, casting, compressing and levelling of concrete	5: 50 Sw. Cr./m²
Cost of concrete	70: 00 Sw. Cr./m³
Reinforcement cost (welded wire fabric Ns 60)	1: 00 Sw. Cr./kg
Joint costs:	
longitudinal joint	0: 50 Sw. Cr./m²
angle alteration joint (unreinforced slab, c/c 5 m)	5: 00 Sw. Cr./m
contraction joint	16: 50 Sw. Cr./m
expansion joint, c/c 80–100 m	20: 00 Sw. Cr./m

Type of pavement, loading, C-value	Distance between transverse joints m	Total thickness h_0 cm	Reinforcement kg/m²	Cost Sw. Cr./m²
AIRFIELD PAVEMENT, loading 60 tons, ⌀ 90 cm				
C = 150 kg/cm²				
Plain concrete pavement	25	50	—	42: 50
Bottom-reinforced pavement	40	18	12.4	31: 45
		20	10.5	30: 95
		22	8.9	30: 80
C = 1 000 kg/cm²				
Plain concrete pavement	25	41	—	36: 30
Bottom-reinforced pavement	40	14	4.70	20: 90
		12	4.20	19: 10
Mid-depth reinforced pavement	40	8	3.15	15: 10
	80	8	4.25	16: 10
Continuous pavement	∞	8	5.20	16: 80
ROAD PAVEMENT, loading 5 tons with 80 % dynamic. suppl, ⌀ 40 cm.				
C = 1 000 kg/cm²				
Plain concrete pavement	25	18	—	20: 10
Mid-depth reinforced pavement	40	8	3.60	15: 65
	80	8	4.55	16: 40
Continuous pavement	∞	8	5.20	16: 80

type that the designer must judge the most economical type of structure, and even comparatively large internal variations between the various unit-prices only have a comparatively small effect on the relationship from an economical point of view between the types of pavement compared.

One condition which has a more marked effect on the final result of a cost comparison, is the selection of the safety factor for the various types of pavement. Particularly difficult here is the selection of the internal relationship between the safety factors when calculating the various types of slab in accordance with the elasticity theory and with the ultimate strength theory respectively. In the examples shown in the table, the safety factors have been selected in accordance with the general viewpoints presented in Section 72. A definite idea of the essential safety factor in various cases can, however, only be obtained on the basis of experience from test roads and from normal traffic on roads with pavements of the types in question. The same applies to another question which has equally large economic significance for the pavement, namely the maintenance and repair costs and the lifetime of the pavement on the whole. The only thing that can be said here is that damage due to crack formation and other causes should probably be less extensive in the case of thin reinforced pavements than in the case of thick unreinforced pavements. The limited experience available from pavements actually built also show this tendency.

It is thus obvious that the new types of reinforced pavements, for which calculating methods have been presented in this thesis, can imply large economic profit concerning constructional costs. As far as can be judged from tests carried out on test pavements and from the limited experience from pavements actually constructed, these types of pavement function well from a technical viewpoint. It is however essential to obtain further experience from traffic tests on experimental stretches and from pavements works, particularly in the scope of road-building, to get answers to the many questions not yet solved concerning the practical use of structurally reinforced concrete pavements.

8. Summary and Bibliography

81. Summary

This thesis concerns the results of an investigation concerning manner of function and calculating methods for concrete pavements on airfields and roads with flexurally rigid active so-called *structural reinforcement*.

The *Introduction* (*Part 1*) gives a review of the problem. The enormous development of road and air traffic in recent decades has shown that the unreinforced or weakly crack-reinforced concrete pavements hitherto used have insufficient load-carrying capacity, and this makes efforts to find other types of design essential. It is then obviously convenient to let the large positive flexural moment under the loading wheel be taken up by a fairly heavy reinforcement in the bottom of the pavement. It is then also suitable to utilize the property of the reinforced concrete slab for levelling the moments during yield in the reinforcement, and the slab can thereby be treated in accordance with the principle presented by K. W. Johansen in his yield line theory [31].

In *Part 2* the behaviour of the reinforced concrete pavement within the elastic stage is studied.

In Sections 21 and 22 there is a presentation of the elasticity theory for slabs on elastic subgrade primarily in connection with methods quoted by Holl [29, 30]. It is thereby assumed that the soil behaves both as a resilient bed, a so-called *resilient subgrade*, and also as an elastic semi-infinite medium, an *elastic subgrade*. Primarily the infinitely extended slab is treated, but also slabs with finite extent are discussed and certain results are deduced. The results of the theoretical treatment are summarized in 225 in the form of formulae and diagrams concerning depression, soil reaction pressure and flexural moment both in the loading centre and in points outside the loading area.

In the following Sections 22 to 25 a description is given of tests carried out in the form of model tests within the laboratory of the Department of Structural Engineering and of full scale tests under laboratory conditions. Section 23 concerns the difficulties encountered in test analysis particularly concerning the determination of the flexural rigidity of the reinforced slab as well as the subgrade constants for the natural soil. A theory is also presented for the estimation of the influence on the ultimate load of the membrane stresses in tests with the thin model slabs. Section 24 describes the extensive series of tests on model slabs which were intended to provide the basis for a systematic study of the problem of reinforced pavement slabs. The test slabs were 2—8 cm thick and rested on a bed of porous wood fibre board, and during the test series variations were performed concerning the hardness of the subgrade, the thickness of the slabs, the strength of the concrete, the amount of reinforcement and the conditions of loading (single loading, twin loading, mobile load and repeated loading). Section 25 contains a description of loading tests on two full scale slabs, these tests having been carried out under laboratory conditions on clay soil in Gothenburg. During these tests accurate measurements were also made of the pressure between the slab and the soil by means of pressure cells of acoustic type.

The results from the tests were analyzed according to the elasticity theory, and good agreement has been proved between the test results and the theory concerning depression and soil reaction pressure as well as concerning flexural moment, in the latter case however only below yield point in the bottom reinforcement. In the case of higher amount of loading it was obvious that the elasticity theory can *not* be applied in this respect; agreement was thus very poor between the ultimate test loads at crack formation (or at yield point in the reinforcment for double-reinforced slabs) in the top surface and the corresponding calculated loads from the elasticity theory.

Part 3 concerns the reinforced concrete pavement from the viewpoint of the yield line theory, and an ultimate strength method is presented for the calculation of the load-carrying capacity of the pavement which, according to the opinion of the author, should be assumed to be equal to the load that gives rise to cracks in the top surface for a single-reinforced slab and yield in the top reinforcement for a double-reinforced slab. It was hereby assumed with reference to the results from the tests in Part 2, that the soil reaction pressure can be estimated according to the elasticity theory also if the slab has come into the yield stage and functions according to the yield line theory.

In accordance with these principles a study is made in Section 32 of loading on the interior of a slab with single load, twin load and load distributed over arbitrary areas. A discussion of the influence of the simplifications and approximations introduced when deriving the ultimate load formulae shows that such approximations lack significance on the whole. In Section 326 there is a summary of formulae and diagrams for the design of reinforced pavements in accordance with the ultimate strength theory.

In Section 33 the theoretical results thus derived are applied to the laboratory tests which have earlier been treated in accordance with the elasticity theory. The analysis shows that agreement between theory and test is as good as the unreliable test conditions allow.

Part 4 concerns the cases of loading where the load is operating on a free edge or on a joint which cannot transfer flexural moment.

In Section 41 is given a review of the results by WESTERGAARD applicable to this case on the basis of the elasticity theory, and these results are summarized in diagrams showing depression and moment caused by a semi-circular load or a circularly distributed load on a free edge or on a corner (joint intersection).

Section 42 deals with the loading cases in question from the viewpoint of the ultimate strength theory with the same assumptions concerning the soil reaction pressure as those made when treating the case with the load on the interior of the slab, and formulae are hereby derived for the calculation of ultimate loads and ultimate moments in the case of loading on a free edge when the load is semi-circularly distributed, circularly distributed or has an arbitrary load distribution area. The influence of various types of edge strengthening (thickening or extra reinforcement) has also been observed. The results of the theoretical treatment are summarized in 427 in the form of formulae and diagrams for the design of free edges and joints for reinforced concrete pavements.

Section 43 describes the tests with load on free edges carried out on one of the two full scale slabs which were made and tested on clay soil in Gothenburg. The slab was originally circular, but after the testing with a load in the centre was finished, it was completed to a square form by casting all around, and the four edges were designed with various types of thickening and with strengthened reinforcement. The results of the four test loadings show relatively good agreement in the test analysis with the elasticity theory concerning deformation, and agreement is also good within the elastic stage concerning the moments for the unstrengthened edge. Concerning moments and loads for the strengthened edges as well as the ultimate loads for all four edges at definite failure due to crack formation in the top, agreement with the elasticity theory is very poor. In these last-mentioned cases, however, the ultimate strength theory gives results which agree rather well.

A summary of viewpoints concerning this case of loading and general viewpoints concerning arrangement of edge and joint reinforcement are presented in Section 44.

Part 5 describes three series of field tests which were carried out in connection with planned work at various airfields. These tests have been carried out in co-operation with the Swedish State Road Institute and the Stockholm Airport Building Committee.

Section 51 concerns tests with a series of test slabs which were laid out in connection with preliminary investigations for a projected airfield at Upplands Väsby. Section 52 concerns a series of tests carried out in connection with the extension of Norrköping airfield in 1948. In both these series of tests, the test slabs were carried out with the same thickness and with the same design as it was planned to use for the future pavement work. During the Norrköping tests, experiments were also carried out directly on a pair of completed taxiway pavements. Test loadings were made both on the centre and on the edges of the test slabs. The results of the tests have been analyzed both according to the elasticity theory and according to the ultimate strength theory, and the results give further confirmation to the theories and calculating methods presented earlier.

Section 53 contains a description of a series of loading tests carried out on two test pavements which were laid out on the final subbase for the first planned east-west runway at Arlanda airfield. One of these test pavements was reinforced in the bottom in the normal way. The other which was laid out on a part of the runway where the subbase and the soil had a particularly good load-carrying capacity, had the form of a very thin structure with a slab thickness of 8 cm and with the reinforcement in mid-depth position. This type of pavement was intended to be a replacement for a non-rigid asphalt pavement which, from the point of view of load-carrying, had been satisfactory on this part of the runway. Both the test surfaces were loaded in the centre as well as on and beside the joints, which were arranged in the test surfaces, and also (concerning the thin pavements) on the free edges. An analysis of the test results concerning the thicker pavement showed that the conditions for the ultimate strength theory with this very good subgrade was only partially satisfied and that the reinforcement yield in the bottom cracks, which is a condition for the applicability of the yield line theory, only occurred to a very small extent with loading on the centre of the slab and did not occur at all with loading on the joints. In spite of this, however, the ultimate strength theory gives relatively good agreement with the test values. As far as the thin mid-depth reinforced test pavements were concerned, the results of the test loadings showed that even in the case of the highest load, 124 tons, the stresses in the reinforcement had not come anyway near the yield point and that the stresses in the pavement on the whole were very small. Analysis of the test results according to the elasticity theory showed good agreement. It is obvious that such thin slabs should be designed completely in accordance with the elasticity theory. A closer theoretical investigation of the stresses in thin slabs of this type shows that the stresses become less the thinner the slab is made and that the load-carrying capacity of the soil itself takes up the wheel load to a great extent.

A number of test loadings were carried out on the two test pavements also with the loading area close to the joints, the edges in contact being designed in different ways. The results showed that the usual tongue and groove joints always give satisfactory transference of shear forces.

Part 6 includes a study of the influence of temperature variation and shrinkage on the reinforced concrete pavements. Section 61 gives a review of the general methods of calculating the stresses due to temperature and shrinkage in normal pavements with joints. The author has also made an attempt to produce a theory for the calculation of the necessary reinforcement and the crack formation in joint-less, so-called continuous reinforced pavements.

In Sections 62 and 63 there are discussions of the special problems that occur from the influence of temperature and shrinkage in reinforced pavements when these are calculated in accordance with the ultimate strength theory, and on the basis of three series of tests carried out with combined tension and flexure on unreinforced and reinforced concrete slab strips it appears probable that the positive ultimate moment is not influenced at all by temperature decrease and shrinkage, while the negative ultimate moment can be calculated for a reduced flexural stress where part of the tensile strength of the concrete is taken up by the tensile and flexural stresses caused by temperature and shrinkage. This section also concerns a discussion of the problems associated with the fact that a single-reinforced slab subjected to traffic from mobile loads becomes gradually cracked right through from the bottom up to the neutral layer at positive flexure and that part of this cracked cross-section falls within the tension zone at negative flexure. Tests with tension-flexure beams appear to show that in normal cases of tension and reinforcement, this effect has no influence on the negative ultimate moment calculated in the way mentioned above.

The results of the theoretical and experimental investigations in this part are summarized in Section 64.

In the concluding *Part 7*, Section 71 contains a review of the experiences from pavement work already carried out with structurally reinforced pavements, mainly in Sweden. Several airfield pavements have been built in accordance with the principles and partly on the basis of the calculating methods presented in this paper, and it has been found that these pavements have functioned well during the time they have been in use. As far as road pavements are concerned the methods have not been adopted, however, with the exception of a private motor truck transport road at Skånska Cement AB factory in Hällekis, and this road has functioned relatively well under the exceptionally hard traffic to which it is subjected. In the scope of road pavements, further tests must be carried out with experimental roads. In this connection the thin, mid-depth reinforced type of pavement as used in the Arlanda tests ought to be tried out, also designed as a completely joint-less continuous pavement. This last-mentioned type of pavement on American test roads has been shown to give very good experiences; in these cases, however, relatively thick and also heavy reinforced slabs have been used. It would appear probable that thin slabs on a good subbase in certain cases would provide a suitable and economically advantageous design for concrete pavements on roads.

In Section 72 the author has presented suggestions for designing specifications and calculating methods for structurally reinforced pavements. For the bottom-reinforced type of pavements, these suggestions are based on the conclusions and results reached in this thesis, namely:

a) The reinforced concrete pavement functions as an elastic slab up to yield point in the reinforcement, but even at loads exceeding this, the soil reaction pressure can be estimated in accordance with the elasticity theory. The flexural rigidity of the slab can be calculated on the basis of Stage II and $n = 15$.

b) The pavement can be assumed to have reached its ultimate load when the top surface shows the first crack. For the positive moments under the loading surface, the slab has thereby reached the plastic stage with yield in the reinforcement, and the behaviour of the slab can be judged from the yield line theory. The safety factor for this ultimate load should be selected fairly high, for example from $1.7-2$ in normal cases.

c) The influence of temperature and shrinkage concerning the positive ultimate moment is zero, while concerning the negative ultimate moment it corresponds to a reduction in the flexural strength of the concrete.

For the thin, mid-depth reinforced slabs, the suggestions for designing specifications are based on the elasticity theory.

Section 73, finally, shows by means of comparative cost calculations that the new types of reinforced concrete pavements from an economical point of view are vastly superior to the unreinforced pavements.

82. References

1. ACI. Committee (FINNEY, E. A. and others). Recommended Practice for Design of Concrete Pavements. ACI Journ. 1958 Vol. 30, No 1.
2. ACI. Committee 325 (LINDSAY, J. D. and others). Continuous Reinforcement in Highway Pavements. ACI Journ. 1958 Vol. 30, No 6.
3. ACI. Committee 325 (LINDSAY, J. D. and others). Design Considerations for Concrete Pavement Reinforcement for Crack Control. ACI Journ. 1956 Vol. 28, No 4.
4. BERGSTRÖM, S. G., FROMÉN, E. and LINDERHOLM, S. Investigation of Wheel Load Stresses in Concrete Pavements. Cement- och Betonginstitutet, Handl. No 13, Sthlm 1949.
5. BERGSTRÖM, S. G. Stämpelbelastade, cirkulära plattor på elastiskt underlag. Cement- och Betonginstitutet, Medd. No 6 Sthlm 1946. Also published in Betong 1946, No 1.
6. BERGSTRÖM, S. G. Temperature Stresses in Concrete Pavements. Cement och Betong-institutet, Handl. No. 14, Sthlm 1950.
7. BERNANDER, K. G. Något om samverkan mellan högvärdig armering och betong. CTH Inst. för Byggnadsteknik, Göteborg 1955. Duplicated report.
8. BERNELL, L. Brottförloppet i statiskt armerade betongbeläggningar. Betong 1952, No. 2.
9. ACI. Committee 325 (BISHOP, I. A. and others). Prestressed Pavement — A World View of its Status. ACI Journ. 1959 Vol. 30, No. 8.
10. BONE, E. P. New Formulas for Stresses in Concrete Pavements of Airfields, Discussion. ASCE Proc. 1948, Vol. 74.
11. BOROWICKA, B. H. Influence of Rigidity of a Circular Foundation Slab on the Distribution of Pressure over the Contact Surface. Int. Conf. Soil Mech., Cambridge, Mass., Proc. 1936, Vol. 2.
12. BOROWICKA, B. H. Druckverteilung unter elastischen Platten. Ing.-Archiv 1939, Vol. 10.
13. BRINCK, C. E. Förspända betongbeläggningar, Sv. Vägfören. Tidskr. 1959, No. 6.
14. BURMISTER, D. M. The Theory of Stresses and Displacements in Layered Systems and Applications to the Design of Airport Runways. HRB Proc. 1943.
15. BURMISTER, D. M. The General Theory of Stresses and Displacements in Layered Systems. Journ. Appl. Physics, 1945, Vol. 16, Febr., March, May.
16. CASHELL H. D. and TESKE, W. E. Continuous Reinforcement in Concrete Pavements. HRB Proc. 1955, Vol. 34.
17. DØLPHER-LARSEN, E. Equilibrium of a Thin Plate Resting on a Semiinfinite Elastic Solid. Bygningsstatiske Medd. 1956, No. 1.
18. FISHER, LEE and MILLARCK. Research and its Application to Road Construction. Inst. Civ. Eng. Proc. 1959, Vol. 12.
19. FÖPPL, A & L. Drang und Zwang, Teil I, Berlin 1941.
20. GRANHOLM, HJ. En ny beräkningsmetod för armerad betong. CTH Handl. No. 38. Göteborg, 1944.

21. Granholm, Hj. Allmän teori för beräkning av armerad betong med särskild hänsyn till betongens och armeringens egenskaper i brottstadiet. CTH Handl. No. 209, Göteborg 1959.

22. Granholm, Hj. and Losberg, A. Besiktning av betongväg. CTH, Inst. för Byggnadsteknik, Göteborg 1954. Stencilled report.

23. Granholm, Hj. Om sammansatta balkar och pelare med särskild hänsyn till spikade träkonstruktioner. CTH Handl. No 88, Göteborg 1949.

24. Granholm, Hj. Om lastfördelning mellan balkar med särskild hänsyn till farbaneplattans inverkan. Betong 1936, No. 4.

25. Gutzwiller, M. I. and Waling, I. L. Laboratory Study of Pavements Continuously Reinforced with Deformed Bars. ACI Journ. 1959, Vol. 31, No. 3.

26. Habel, A. Die auf dem elastisch-isotropen Halbraum aufruhende zentralsymmetrisch belastete elastische Kreisplatte. Bauing. 1937, Vol. 18.

27. Hertz, H. Über das Gleichgewicht schwimmender elastischer Platten. Ann. d. Ph. u. Ch. 1884, Vol. 22.

28. Hogg, A. H. A. Equilibrium of a Thin Plate, Symmetrically Loaded, Resting on an Elastic Foundation of Infinite Depth. Phil. Mag. March 1938, Ser. 7, Vol. 25.

29. Holl, D. L. Thin Plates on Elastic Foundations. Proc. 5th Int. Cong. Appl. Mech. Cambridge, Mass., 1938.

30. Holl, D. L. Equilibrium of a Thin Plate, Symmetrically Loaded, on a Flexible Subgrade. Iowa State Coll. Journ. of Science, July 1938, Vol. 12, No. 4.

31. Johansen, K. W. Brudlinjeteorier, Khvn 1943.

32. Johansen, K. W. Pladeformler, Khvn 1946.

33. Johansen, K. W. Plader paa Jord. Dansk Vejtidsskrift 1949 No. 8.

34. Johansen, K. W. Slabs on Soil. DTH, Lab. for Bygningsteknik, Med. No. 4. Khvn 1955.

35. Johansson (Losberg), A. Försök med armerade betongplattor på elastiskt underlag. Betong 1947 No. 3.

36. Johansson (Losberg), A. Undersökning rörande armerade betongplattor för startbanor vid flygplatser. Rapport No. 1, provbelastning av en 15 cm betongplatta på lergrund i Göteborg. CTH Institutionen för Byggnadsteknik, Göteborg 1945. Stencilled report.

37. Johansson (Losberg), A. Undersökning rörande armerade betongplattor för startbanor vid flygplatser. Rapport No. 2, modellförsök med betongplattor på underlag av porös träfiberplatta med last på plattans mitt. CTH Institutionen för Byggnadsteknik, Göteborg 1946. Stencilled report.

38. Johansson (Losberg), A. Undersökning rörande armerade betongplattor för startbanor vid flygplatser. Rapport No. 3, provbelastning av dubbelarmerad betongplatta på lergrund i Göteborg. CTH Institutionen för Byggnadsteknik, Göteborg 1948. Stencilled report.

39. Johansson (Losberg), A. Armerade betongbeläggningar för Halmsjöflygplatsens Ö-V-bana. CTH Institutionen för Byggnadsteknik, Göteborg 1953. Stencilled report.

40. Johansson (Losberg), A. Betongväg för tung trafik vid Hällekis Cementfabrik — en intressant provväg. Sv. Vägfören. Tidskrift 1954, h. 6.

41. Kelley, E. F. Application of the Results of Research to the Structural Design of Concrete Pavements. Public Roads, July, Aug. 1939. Also published in Journ. ACI June 1939.

42. Kuuskoski, V. Über die Haftung zwischen Beton und Stahl. Stat. Tekn. Forskningsinst. Publ. No. 19. Helsinki 1950.

43. KÄRRHOLM, G. Parallelogram Plates Analysed by Strip Method. Diss. CTH, Göteborg 1956.

44. LILJA, B. Försök med beläggningar av cement-betong på riksväg 1 vid Törnevalla 1953. Statens Väginstitut, Specialrapport 12, Sthlm 1959.

45. LINDSAY, J. D. Ten-Year Report on the Illinois Continuously Reinforced Pavement. HRB. 1959, Bull. 214.

LOSBERG, A. see JOHANSSON, A.

46. LOE, L. A. The Performance during the First Five Years of the Experimental Concrete Road at Oxton, Nottinghamshire. Proc. Inst. of Civ. Eng. Part 2, 1955 Vol. 4 No. 1.

47. VON MATERN, N. and ODEMARK, N. Redogörelse för belastningsförsök på det föreslagna flygfältet vid Väsby under hösten 1945. Statens Väginstitut, Stencilled Report, Sthlm 1946.

48. VON MATERN, N. and ODEMARK, N. Belastningsförsök på Storflygplatsen vid Halmsjön 1948—1949. Statens Väginstitut, typed Report, Sthlm 1952.

49. MC LACHLAN, N. W. Bessel Functions for Engineers. London 1946.

50. MELLINGER, F. M., SALE, J. P. and WALKEN, T. R. Heavy Wheel Load on Concrete Airfield Pavements. HRB Proc. 1957, Vol. 36.

51. MELVILLE, P. L. Review of French and British Procedures in the Design of Prestressed Pavements. HRB 1958, Bull. 179.

52. NADAI, A. Die elastischen Platten, Berlin 1925.

53. ODEMARK, N. Undersökning av elasticitetsegenskaperna hos olika jordarter samt teori för beräkning av beläggningar enligt elasticitetsteorin. Statens Väginstitut Medd. No. 77, Sthlm 1949.

54. ODEMARK, N. Betongbeläggningar. Handboken Bygg band II, Section 338:2. Sthlm 1959.

55. PARLAND, H. Inelasticity of Bond Between Steel and Concrete. RILEM 1957 Papers Vol. 2 (stencilled).

56. PERSSON, B. Beständighet och bärighet hos ett istäcke. Sv. Vägfören. Tidskr. 1948, No. 8.

57. PICKETT, G. and RAY, G. K. Influence Charts for Concrete Pavements. ASCE Trans. 1951, Vol. 116.

58. SALE, J. P. and HUTCHINSON, R. L. Development of Rigid Pavement Design for Military Airfields. ASCE Proc. 1959, Vol. 85, No. AT3.

59. SCHLEICHER, F. Zur Theorie des Baugrundes. Bauing. 1926, H. 48.

60. SCHLEICHER, F. Platten auf elasticher Unterlage. Berlin 1925.

61. SCHLEICHER, F. Senkungsmittelwert und Ähnlichkeitsbedingunge für Platten und Balken auf isotoper elastischer Unterlage. Zeitschr. ang. Math. u. Mech. 1928, Vol. 8.

62. SPARKES, F. N. The Structural Design of Concrete Roads. Mag. Concr. Research 1954, Vol. 6, No. 17.

63. Svenska Cementföreningen, Committee Report. Böjdragfastheten hos betongbeläggningar. Svenska Cementföreningens Tekn. Medd. No. 12, 1953.

64. TELLER, L. W. and SUTHERLAND, E. C. The Structural Design of Concrete Pavements. Public Roads 1935, Vol. 16, No. 8, 9, 10, 1936, Vol. 17, No. 7, 8, 1943, Vol. 23, No. 8.

65. TIMOSHENKO, S. Theory of Elasticity. New York and London 1934.

66. TIMOSHENKO, S. Theory of Plates and Shells. New York 1940.

67. TREMPER, B. Continuously-Reinforced Concrete Pavement in California after Eight Years Service. HRB 1959, Bull. 214.

68. Van Breemen, W. Ten-Year Report on Experimental Continuously-Reinforced Concrete Pavements in New-Jersey, HRB 1959, Bull. 214.
69. Vetter, C. P. Stresses in Reinforced Concrete Due to Volume Changes, Trans. ASCE 1933, Vol. 98.
70. Watson, G. Theory of Bessel Function. Cambridge 1922.
71. Westergaard, H. M. Om beregning av Plader paa elastisk underlag med særlig henblikk paa spørgsmaalet om spændinger i betonveje. Ingeniøren 1923, Vol. 32.
72. Westergaard, H. M. Stresses in Concrete Pavements Computed by Theoretical Analysis. Publ. Roads 1926–27, Vol. 7.
73. Westergaard, H. M. Mechanics of Progressive Cracking in Concrete Pavements. Public Roads 1929/30, Vol. 10.
74. Westergaard, H. M. Analytical Tools for Judging Results of Structural Tests of Concrete Pavements. Public Roads 1933/34, Vol. 14.
75. Westergaard, H. M. Stresses in Concrete Runways of Airports. HRB, Proc. 1939.
76. Westergaard, H. M. New Formulas for Stresses in Concrete Pavements of Airfields. ASCE Proc. 1947.
77. Westergaard, H. M. Stress Concentrations in Plates Loaded over Small Areas. ASCE Trans. 1943, Vol. 108.
78. Wästlund, G. and Bergström, S. G. Preliminärt förslag till dimensioneringsföreskrifter för flygfältsbeläggningar av betong. Cement- och Betonginstitutet, Sthlm 1947. Stencilled report.
79. Zuk, W. Analysis of Special Problems in Continuously-Reinforced Concrete Pavements. HRB 1959, Bull. 214.